



Special Issue Reprint

The Friedmann Cosmology

A Century Later

Edited by Galina L. Klimchitskaya, Vladimir M. Mostepanenko
and Sergey V. Sushkov

mdpi.com/journal/universe



The Friedmann Cosmology: A Century Later

The Friedmann Cosmology: A Century Later

**Galina L. Klimchitskaya
Vladimir M. Mostepanenko
Sergey V. Sushkov**



Basel • Beijing • Wuhan • Barcelona • Belgrade • Novi Sad • Cluj • Manchester

Editors

Galina L. Klimchitskaya
Department of Astrophysics
Pulkovo Observatory of the
Russian Academy of Sciences
St. Petersburg
Russia

Vladimir M. Mostepanenko
Department of Astrophysics
Pulkovo Observatory of the
Russian Academy of Sciences
St. Petersburg
Russia

Sergey V. Sushkov
Department of Relativity
Theory and Gravity
Kazan Federal University
Kazan
Russia

Editorial Office

MDPI AG
Grosspeteranlage 5
4052 Basel, Switzerland

This is a reprint of articles from the Special Issue published online in the open access journal *Universe* (ISSN 2218-1997) (available at: www.mdpi.com/journal/universe/special_issues/713E1ZFOKQ).

For citation purposes, cite each article independently as indicated on the article page online and as indicated below:

Lastname, A.A.; Lastname, B.B. Article Title. <i>Journal Name</i> Year , <i>Volume Number</i> , Page Range.
--

ISBN 978-3-7258-2282-9 (Hbk)

ISBN 978-3-7258-2281-2 (PDF)

doi.org/10.3390/books978-3-7258-2281-2

© 2024 by the authors. Articles in this book are Open Access and distributed under the Creative Commons Attribution (CC BY) license. The book as a whole is distributed by MDPI under the terms and conditions of the Creative Commons Attribution-NonCommercial-NoDerivs (CC BY-NC-ND) license.

Contents

Preface	vii
Galina L. Klimchitskaya, Vladimir M. Mostepanenko and Sergey V. Sushkov Centenary of Alexander Friedmann’s Prediction of Universe Expansion and the Prospects of Modern Cosmology Reprinted from: <i>Universe</i> 2024 , <i>10</i> , 329, doi:10.3390/universe10080329	1
Andrey A. Grib and Yuri V. Pavlov Particles of Negative and Zero Energy in Black Holes and Cosmological Models Reprinted from: <i>Universe</i> 2023 , <i>9</i> , 217, doi:10.3390/universe9050217	13
Kirill A. Bronnikov, Pavel E. Kashargin and Sergey V. Sushkov Possible Wormholes in a Friedmann Universe Reprinted from: <i>Universe</i> 2023 , <i>9</i> , 465, doi:10.3390/universe9110465	23
Sergei D. Odintsov, Simone D’Onofrio and Tanmoy Paul Entropic Inflation in Presence of Scalar Field Reprinted from: <i>Universe</i> 2023 , <i>10</i> , 4, doi:10.3390/universe10010004	44
Vinicius Guilherme Oliveira, Gil de Oliveira Neto and Ilya L. Shapiro Kantowski–Sachs Model with a Running Cosmological Constant and Radiation Reprinted from: <i>Universe</i> 2024 , <i>10</i> , 83, doi:10.3390/universe10020083	62
Alexander Kamenshchik and Polina Petriakova Regular Friedmann Universes and Matter Transformations Reprinted from: <i>Universe</i> 2024 , <i>10</i> , 137, doi:10.3390/universe10030137	79
Andrey A. Grib and Yuri V. Pavlov On Phase Transitions during Collisions Near the Horizon of Black Holes Reprinted from: <i>Universe</i> 2024 , <i>10</i> , 131, doi:10.3390/universe10030131	92
Bijan Saha Spinor Field in FLRW Cosmology Reprinted from: <i>Universe</i> 2023 , <i>9</i> , 243, doi:10.3390/universe9050243	101
Laur Järv and Piret Kuusk Conventionalism, Cosmology and Teleparallel Gravity Reprinted from: <i>Universe</i> 2023 , <i>10</i> , 1, doi:10.3390/universe10010001	113
Sultan Saburov and Sergei V. Ketov Improved Model of Primordial Black Hole Formation after Starobinsky Inflation Reprinted from: <i>Universe</i> 2023 , <i>9</i> , 323, doi:10.3390/universe9070323	128
Júlio C. Fabris, Felipe T. Falciano, Luiz F. Guimarães and Nelson Pinto-Neto On the Possibility of a Static Universe Reprinted from: <i>Universe</i> 2024 , <i>10</i> , 92, doi:10.3390/universe10020092	138
Vijay Singh, Siwaphiwe Jokweni and Aroonkumar Beesham FLRW Transit Cosmological Model in $f(R, T)$ Gravity Reprinted from: <i>Universe</i> 2024 , <i>10</i> , 272, doi:10.3390/universe10070272	149
Alexander Balakin and Amir Shakirzyanov An Isotropic Cosmological Model with Aetherically Active Axionic Dark Matter Reprinted from: <i>Universe</i> 2024 , <i>10</i> , 74, doi:10.3390/universe10020074	167

Arkady A. Popov, Sergey G. Rubin and Alexander S. Sakharov Primordial Black Holes from Spatially Varying Cosmological Constant Induced by Field Fluctuations in Extra Dimensions Reprinted from: <i>Universe</i> 2024 , <i>10</i> , 166, doi:10.3390/universe10040166	181
Alexandre V. Ivanchik, Oleg A. Kurichin and Vlad Yu. Yurchenko Neutrino at Different Epochs of the Friedmann Universe Reprinted from: <i>Universe</i> 2024 , <i>10</i> , 169, doi:10.3390/universe10040169	199
Salvatore Capozziello, Giuseppe Sarracino and Giulia De Somma A Critical Discussion on the H_0 Tension [†] Reprinted from: <i>Universe</i> 2024 , <i>10</i> , 140, doi:10.3390/universe10030140	218
Galina L. Klimchitskaya and Vladimir M. Mostepanenko The Nature of Dark Energy and Constraints on Its Hypothetical Constituents from Force Measurements Reprinted from: <i>Universe</i> 2024 , <i>10</i> , 119, doi:10.3390/universe10030119	249
Mikhail Piotrovich, Serguei Krasnikov, Stanislava Buliga and Tinatin Natsvlishvili Search for Wormhole Candidates: Accreting Wormholes with Monopole Magnetic Fields Reprinted from: <i>Universe</i> 2024 , <i>10</i> , 108, doi:10.3390/universe10030108	266
Vladimir M. Mostepanenko Prediction of the Expansion of the Universe Made by Alexander Friedmann and the Effect of Particle Creation in Cosmology Reprinted from: <i>Universe</i> 2024 , <i>10</i> , 84, doi:10.3390/universe10020084	277
Victor Berezin and Inna Ivanova Conformally Invariant Gravity and Gravitating Mirages Reprinted from: <i>Universe</i> 2024 , <i>10</i> , 147, doi:10.3390/universe10030147	302
Alexander D. Dolgov, Lyubov A. Panasenko and Vladimir A. Bochko Graviton to Photon Conversion in Curved Space-Time and External Magnetic Field Reprinted from: <i>Universe</i> 2023 , <i>10</i> , 7, doi:10.3390/universe10010007	314
Laszlo Jenkovszky, Yurii Andreevich Kurochkin, N. D. Shaikovskaya and Vladimir Olegovich Soloviev Nonrelativistic Quantum Mechanical Problem for the Cornell Potential in Lobachevsky Space Reprinted from: <i>Universe</i> 2024 , <i>10</i> , 76, doi:10.3390/universe10020076	344
Ugo Moschella The Spectral Condition, Plane Waves, and Harmonic Analysis in de Sitter and Anti-de Sitter Quantum Field Theories Reprinted from: <i>Universe</i> 2024 , <i>10</i> , 199, doi:10.3390/universe10050199	353
Giampiero Esposito DeWitt Boundary Condition in One-Loop Quantum Cosmology Reprinted from: <i>Universe</i> 2023 , <i>9</i> , 187, doi:10.3390/universe9040187	374
Natalia Gorobey, Alexander Lukyanenko and Alexander V. Goltsev No-Boundary Wave Functional and Own Mass of the Universe Reprinted from: <i>Universe</i> 2024 , <i>10</i> , 101, doi:10.3390/universe10020101	388

Preface

This reprint, containing articles published in the Special Issue of the *Journal Universe*, is devoted to the centenary of Alexander Friedmann's prediction of the universe's expansion. This prediction was made by him in 1922 for the case of the closed universe and in 1924 for the open universe on the basis of Einstein's general theory of relativity. Later, it was confirmed experimentally and became the basis of modern cosmology. In a broader context, one may say that Friedmann's prediction of the expansion of the universe radically changed our picture of the world, as compared with all previous epochs, and marked the beginning of the new era in understanding of the world around us. The present reprint contains both research and review articles devoted to all aspects of expanding the universe, including the problem of its origin from the cosmological singularity, inflationary stage of the universe's evolution, cosmological scenario of the hot universe, modern stage of the universe's expansion, astrophysics of expanding the universe, acceleration of the universe's expansion, dark matter, and dark energy. Several unresolved problems and planned experiments are also discussed in this reprint.

Galina L. Klimchitskaya, Vladimir M. Mostepanenko, and Sergey V. Sushkov
Editors

Editorial

Centenary of Alexander Friedmann's Prediction of Universe Expansion and the Prospects of Modern Cosmology

Galina L. Klimchitskaya ^{1,2}, Vladimir M. Mostepanenko ^{1,2,3,*} and Sergey V. Sushkov ³

¹ Central Astronomical Observatory, Pulkovo of the Russian Academy of Sciences, 196140 Saint Petersburg, Russia; g.klimchitskaya@gmail.com

² Peter the Great Saint Petersburg Polytechnic University, 195251 Saint Petersburg, Russia

³ Kazan Federal University, 420008 Kazan, Russia; sergey_sushkov@mail.ru

* Correspondence: vmostepa@gmail.com

Abstract: In this Editorial to the Special Issue “The Friedmann Cosmology: A Century Later”, we consider an outstanding character of Friedmann’s prediction of Universe expansion, which laid the foundation of modern cosmology. The list of the main discoveries made in cosmology during the last one hundred years is followed by a formulation of the standard cosmological model. The articles contributing to the Special Issue are considered in relation to this model, and to several alternative theoretical approaches. Special attention is paid to unresolved problems, such as the nature of dark matter and dark energy, Hubble tension and the pre-inflationary stage of the Universe evolution. The conclusion is made that astrophysics and cosmology are on the threshold of new fundamental discoveries.

1. Introduction

In this Editorial to the Special Issue “The Friedmann Cosmology: A Century Later”, we analyze the role played by the fact that our Universe is expanding in the modern picture of the World, briefly list the main discoveries made in cosmology and astrophysics of the expanding Universe during the last 100 years, and characterize the topics of the contributing articles. Special attention is paid to the main unresolved problems and different approaches to their resolution.

Alexander Friedmann made his famous prediction that the Universe expands with time, starting from a point called the cosmological singularity, in his article [1] published in 1922 for the case of finite space volume. In 1924, he obtained the same result [2] for the Universe possessing an infinitely large spatial volume, which is the case for our Universe according to modern astronomical observations. Friedmann obtained his results by solving Einstein’s equations of the general theory of relativity with no additional assumption that the obtained model of the Universe should be static. In this way, he acted as a mathematician by looking for what is contained in the fundamental equations of the general theory of relativity, whether or not this is in agreement with the concepts of Ptolemy, Copernicus, and Newton, who believed that the Universe is static. Note that in the article [1] the author name was written as A. Friedman, but Albert Einstein, in his note [3] (which he later recognized as mathematically mistaken), cited [1] as written by A. Friedmann. In the second article on cosmology [2], Alexander Friedmann used just this version of his name in the Latin alphabet, which became commonly accepted over a century.

Before Friedmann, the cosmological solutions to Einstein’s equations with the cosmological constant were obtained by Einstein himself [4] (the static solution) and de Sitter [5] (the empty Universe). However, it was Friedmann who demonstrated that, for the homogeneous and isotropic space, even in the presence of an additional cosmological term in Einstein’s equations, the static solution arises in only one exceptional case.

Friedmann’s papers [1,2] laid the foundation of modern cosmology. Although during the first years after publication his results were unnoticed, they were later rediscovered



Citation: Klimchitskaya, G.L.; Mostepanenko, V.M.; Sushkov, S.V. Centenary of Alexander Friedmann’s Prediction of Universe Expansion and the Prospects of Modern Cosmology. *Universe* **2024**, *10*, 329. <https://doi.org/10.3390/universe10080329>

Received: 21 June 2024

Revised: 30 July 2024

Accepted: 6 August 2024

Published: 16 August 2024



Copyright: © 2024 by the authors. Licensee MDPI, Basel, Switzerland. This article is an open access article distributed under the terms and conditions of the Creative Commons Attribution (CC BY) license (<https://creativecommons.org/licenses/by/4.0/>).

by Lemaître [6], Robertson [7], and Walker [8]. More importantly, the Universe expansion should manifest itself as moving of all galaxies away from an observer on the Earth, leading to the redshift of light emitted by them. This effect was systematically studied by Lemaître [6] and Hubble [9] as an experimental confirmation of the Universe expansion.

In the next decades, the development of modern cosmology was marked by a formation of the theory of the Hot Universe, which is also often called the Big Bang Universe, developed by Gamov [10]. In the framework of this theory, Gamov and his collaborators explained the origin of physical elements in the process of primordial nucleosynthesis [11] (see also the modern review [12]). A big success of the theory of the Hot Universe was the prediction [13], and subsequent discovery in 1965 [14], of the relic radiation or cosmic microwave background radiation. This discovery can be considered as a final confirmation of the Big Bang theory and, in particular, of the Friedmann prediction that the initial state of the Universe evolution is the cosmological singularity. Later on, a lot of papers have been published about the properties of relic radiation and its interaction with electrons and the intergalactic medium (see Refs. [15–19] for reviews). On the theoretical side, it was shown [20,21] that any solution of Einstein's equations describing the Big Bang possesses the initial singularity.

The theory of the Hot Universe does not describe the very early stages of its evolution below and just after the Planck time, where the quantum effects come into play. Thus, an application of the standard general theory of relativity to the period down to cosmological singularity results in serious problems. One of them, called the horizon problem, states that at Planck time the Universe should consist of about 10^{89} causally disconnected parts, in contradiction with the fact that the relic radiation has the same temperature in all points and in all directions.

The problems in the description of the evolution of the Universe near the cosmological singularity were partially solved by the model of inflation proposed in the beginning of 1980s. According to this model, the initial expansion of the Universe goes on exponentially fast. This happens under the influence of either the so-called inflaton scalar field [22–28] or the vacuum polarization effects of quantized fields [29,30]. According to the model of inflation, the usual elementary particles were created during the period of reheating after the end of the exponentially fast expansion, when the inflaton field oscillated near the minimum of its potential [28,31,32]. The theory of reheating is based on the effect of the exponential growth of the number of boson pairs created from vacuum by the periodic in time fields [33,34]. It was elaborated on by many authors [35–46].

One more great discovery in the physics of the expanding Universe was made in 1998, when two groups of researchers [47,48] working with the redshift data of supernovae in binary systems arrived to the conclusion that the expansion of the Universe is accelerating. This result could be explained by the existence of a new form of matter, which constitutes of approximately 68% of the Universe energy and was called dark energy. As opposed to usual and dark matter, dark energy is characterized by negative pressure (see Ref. [49] for a review). There are many models of dark energy proposed in the literature, describing it using the cosmological constant [50], classical scalar field called a quintessence [51,52], scalar-tensor gravity [53–55], and hypothetical elementary particles, whose properties depend on the density of matter in the environment [56–58].

2. The Standard Cosmological Model

Friedmann's seminal works [1,2] and further developments described in the previous section lie into the basis of the Λ CDM model, which is the standard model of contemporary cosmology (see, for example, Ref. [59]). Here, Λ is the cosmological constant, and the abbreviation CDM for the cold dark matter means that this form of matter, which contributes approximately 28% of the Universe's energy, is assumed to consist of non-relativistic particles (e.g., of axions [60,61]). This model assumes that the general theory of relativity is the correct theory of gravity on cosmological scales, and the space-time geometry of the homogeneous and isotropic expanding Universe is described by the Friedmann metric (see

Section 2 of Ref. [62] belonging to this Special Issue, where the Friedmann equations and their solutions possessing the cosmological singularity are presented and discussed in the cases of closed, open, and quasi-Euclidean spaces).

As a result, the Λ CDM cosmological model provides a reasonably good account of (i) the existence and structure of the cosmic microwave background; (ii) the large-scale structure in the distribution of galaxies; (iii) the observed abundances of hydrogen (including deuterium), helium, and lithium; and (iv) the accelerating expansion of the Universe, observed in the light from distant galaxies and supernovae.

The Λ CDM model became the leading cosmological model following the observations of accelerating expansion in 1998 [47,48], and was quickly supported by other observations. Thus, in 2000, the BOOMERanG microwave background experiment measured the total (matter–energy) density to be close to 100% of the critical one [63], whereas in 2001, the 2dFGRS galaxy redshift survey measured the matter density to be near 25% [64]. The large difference between these values supports a positive value of Λ describing the dark energy. Much more precise spacecraft measurements of the microwave background from WMAP in 2003–2010 [65] and Planck in 2013–2015 [66,67] have strongly supported the standard cosmological model, and pinned down the values of its parameters, most of which are now constrained below 1 percent uncertainty.

The enormous success of observational cosmology, achieved in the last 30 years, especially the final results of the cosmic Planck mission that appeared in 2018, have successfully confirmed those previously put forward and developed cosmological theoretical ideas about the history of the Universe as its passage in the past through the stage of the hot Big Bang (including primary cosmological nucleosynthesis, recombination and generating anisotropy and polarization of the cosmic microwave background radiation). Also, it was proved that the Universe had a cold quasi-de Sitter (inflation) epoch, during which spatial inhomogeneities of the matter distribution were formed due to the quantum gravitational effects. In fact, galaxies and all compact objects were formed from these primordial inhomogeneities. Moreover, the physical properties of the effective sort of matter, which supported the inflation on the earlier epochs of the Universe evolution, are similar from the qualitative point of view to the properties of the dark energy in the late-time Universe (it seems to be reasonable to indicate this cosmic substratum as a primordial dark energy).

No less fundamental results have been achieved in astrophysics of compact relativistic objects, namely black holes and neutron stars. Specifically, the mass of the supermassive black hole in the center of our Galaxy (the object Sgr A*) was measured exactly by the motion of nearby stars around it. Next, the observational picture of the shadow of a supermassive black hole in the M87 galaxy was obtained, and the processes of merging of black holes and neutron stars in binary systems have been discovered and investigated using the gravitational (and electromagnetic, in the latter case) radiation from them. Finally, it has been observed that the velocity of gravitational waves coincides with that of light with a great accuracy.

Below, we briefly list the articles included in this jubilee Special Issue devoted to the centenary of Friedmann’s cosmology in their relation to the standard cosmological model and some research directions beyond them.

3. Current Research Topics in Cosmology

We start with several articles that are devoted to a few novel aspects of the general theory of relativity. All of them use the theoretical formalism belonging to the standard cosmological model, but deal with some nonstandard situations and exotic forms of matter. Thus, Ref. [68] considers particles of negative and zero energy, which can exist inside the horizon of a Schwarzschild black hole, and in Miln’s and Gödel’s cosmological models. The situations of this kind have already been considered previously [69–71], but here they arise in especially simple and widely used cases. Another article of this Special Issue [72] investigates the properties of traversable wormholes, which can be determined in the closed Friedmann Universe by the dust-like matter. The solutions of Einstein’s equations of such

type were considered in the literature [73–78], but some exotic kinds of matter were used as their source (e.g., the so-called phantom scalar field).

The article [79] suggests an expression for the generalized entropy depending on four parameters which contains all the known entropies considered so far (see, for example, refs. [80–83]) as particular cases. It is shown that by adding the scalar field with a power-type potential one obtains a viable model of inflation consistent with the Planck data. The next article of the Special Issue considers an isotropization of the Kantowski–Sachs cosmological model with radiation and a running cosmological constant energy density [84]. Previously this effect was investigated in the Kantowski–Sachs model without taking the running cosmological constant into account (see, e.g., refs. [85–90]). It is shown that in some cases the effect of running leads to a quicker isotropization.

Article [91] demonstrates that it is possible to construct the non-singular cosmological model for the spatially flat Friedmann Universe if taking the phantom and tachyon scalar fields into account. This is in line with previous attempts to find the non-singular cosmological models and black holes (see Refs. [92–95] for a review). Another article [96] investigates the phase transitions of the physics of elementary particles, which can occur during the collisions of particles near the horizons of black holes. Specifically, the transition between quark–gluon plasma and hadrons, the electroweak and the grand unification phase transitions are considered [28,97–99]. The back reaction of the energy density of phase transitions on the space-time metric is investigated. One more article [100] studies the evolution of the Friedmann cosmological model under an impact of the nonlinear spinor field.

Several articles belonging to this Special Issue deal with different non-Einsteinian theories of gravitation, including teleparallel gravity [101–103]. Strictly speaking, the formalisms used in these articles are beyond the standard cosmological model. Thus, in [104], which deals with the alternative theories of gravitation, the two variants of teleparallel gravity are considered. It is shown that the corresponding cosmological models are, in fact, the same as in Einstein’s general theory of relativity. This makes the choice between them the subject of convention [105,106].

One more article [107] published in this Special Issue is devoted to the elaboration of a new, improved model on inflation in the framework of $F(R)$ modified gravity, where R the scalar curvature of space-time. The theories of this kind are often considered in the literature (see, e.g., refs. [108–110]). They are, in fact, equivalent to the scalar–tensor theories of gravity [109,111]. It is shown that the obtained model demonstrates a very good agreement with the measurements of relic radiation. The scalar–tensor theories of the Brans–Dicke class [112–114] are also applied in another paper belonging to this Special Issue [115] for the construction of a cosmological model with a constant scale factor, which reproduces some properties of the standard cosmological model. The homogeneous isotropic cosmological model, which demonstrates a transition from the decelerated expansion in the past to the present acceleration, is constructed in ref. [116] on the basis of $F(R, T)$ modified gravity theory, where T is the trace of the stress–energy tensor of matter. The alternative theories of gravitation of this kind have often been considered in the literature in recent years [117–120].

Two more articles using the alternative theories of gravity are devoted to a new analytically solvable isotropic cosmological model [121] and to the model of primordial black holes determined by field fluctuations in extra dimensions [122]. The first of these articles [121] uses the so-called extended Einstein–aether–axion theory [123,124] and considers the homogeneous Universe filled with axionic dark matter. The second article [122] uses the formalism of $f(R)$ gravity and investigates the possibility that some supermassive black holes may originate from a collapse of the domains of dark energy with extremely high energy density, caused by the quantum fluctuations of the minimally coupled scalar field in the compacted inner space (see ref. [125] for a review on the primordial black holes).

Several further articles published in this jubilee Special Issue are devoted to the astrophysics of the Friedmann Universe. Thus, review [126] discusses the role of neutrinos at different stages of the evolution of the Friedmann Universe. This includes the impact

of neutrinos on the Universe expansion rate, its chemical and isotopic composition, the anisotropy of relic radiation, and formation of the large-scale structure. Special attention is paid to possible existence of the so-called sterile neutrinos, which are hypothetical neutrino-type particles not possessing the isospin charge and only interacting with other elementary particles gravitationally [127–130].

Article [131] is devoted to the critical discussion of tension concerning the value of the Hubble constant H_0 , which is the proportionality coefficient between the proper distance to the remote galaxy and the speed of its separation. Although, in the standard cosmological model, the value of H_0 is expressed via the main parameters of this model, different approaches to its measuring [66,132] result in the values that do not overlap, leading to a 5σ tension. The extensive literature devoted to the H_0 tension discussed in ref. [131] did not bring a resolution to this problem yet.

The physical nature of dark energy is still unknown, and there are many theoretical approaches to its understanding, which are reviewed in ref. [133]. These are the most common approach describing the dark energy by means of the cosmological constant, as well as the approaches using the concept of a quintessence and scalar–tensor modifications of the general theory of relativity, exploiting the chameleon, symmetron- and environment-dependent dilaton fields and corresponding hypothetical particles. In fact, only the description of dark energy in terms of cosmological constant is in the frames of the standard cosmological model, whereas all others are beyond it. There are many experimental tests for the hypothetical constituents of dark energy. One of them is based on measuring the Casimir force between two closely spaced macrobodies, which should be modified by the presence of dark energy. This approach already significantly strengthened the constraints on axions as the hypothetical constituents of dark matter [134–137]. In the case of dark energy, however, the problem is more complicated because the respective interaction potentials are not fixed uniquely, but are different in different models [138–140].

The theoretical aspects of wormhole solutions of Einstein’s equations are discussed in many papers (see Ref. [72] belonging to this Special Issue, mentioned above). To the present time, however, wormholes were not observed, in spite of the fact that some authors tried to find their observational features [141–144]. In this Special Issue, it was suggested [145] that one should consider the acceleration of matter into a wormhole possessing a monopole magnetic field. It is shown that the resulting spectrum is characterized by some unique features, which allow for distinguishing it from the spectrum of, e.g., a Kerr black hole.

The next group of articles published in this Special Issue is devoted to some quantum aspects of cosmology. These articles can be naturally divided into two subgroups. The first one considers the quantum effects on the background of classical curved space-time, whereas the second one deals with the quantization of gravitation, i.e., with quantum gravity. We begin with the articles belonging to the first group.

The most well-known quantum effect occurring in the expanding Friedmann Universe is the creation of particles of matter fields from the vacuum state. This effect is discussed in [62]. It is considered in comparison to similar effects occurring in an external electromagnetic field. The creation of particle–antiparticle pairs in the homogeneous isotropic models of the Universe plays the most important role in the early stages of its evolution. Thus, it plays a decisive role in the process of reheating after inflation, i.e., during the period of time when all of the standard elementary particles have been created [32]. There are different methods used in the theoretical description of the particle creation in the external gravitational field. One of them uses the concept of adiabatic particles [146,147], while another one is based on the diagonalization of the Hamiltonian of a quantized field [148–150].

One more (phenomenological) method describing the effect of particle creation in the Riemannian space-time is suggested in [151] published in this Special Issue. For this purpose, the action of an ideal fluid in Euler’s variables is used, where the conservation law for the number of particles is replaced with the creation law [152,153].

An important quantum process is the conversion of gravitons to photons and vice versa in the presence of an external magnetic field. This process was considered by several

authors in flat space-time (see, e.g., refs. [154–156]). It is, however, of much importance in applications to the relic gravitational waves produced at the inflationary stage of the Universe's evolution in the primordial magnetic field, where the space-time geometry was essentially non-Euclidean. Just this case is investigated in [157], which is included in the jubilee Special Issue, where the transformation between gravitons and photons in the presence of a magnetic field is considered in curved space-time. Next, the results obtained for an arbitrary metric are simplified for the case of the Friedmann Universe. In so doing, the gravitational waves are considered as small perturbations of the background space-time. It is shown that the conversion effect is present only if the electromagnetic wave vector is perpendicular to the magnetic field. An important conclusion is made that the effect of conversion of gravitons into photons in the primordial magnetic field cannot significantly diminish the amplitude of relic gravitational waves.

One more article of this Special Issue [158] investigates the motion of a quantum particle in the Cornell potential on the background of an open Friedmann cosmological model. This subject is of evident interest because this potential was used earlier to ensure the confinement of quarks inside both mesons and hadrons [159]. It is shown that, due to the space curvature, the Cornell potential becomes a potential well of finite depth, making both the bound and scattering states possible.

Finally, one more article devoted to the quantum effects in curved space-time considers the mathematical aspects of quantum field theory in the de Sitter and anti-de Sitter space-times [160]. In this article, it is shown that the correlation functions of quantum scalar field in Minkowski, de Sitter, and anti-de Sitter space-times have some similarities (see the previous results on this subject [161–163]).

The second subgroup of articles devoted to quantum aspects of cosmology deals with the quantization of gravitational field, i.e., with quantum gravity. It is common knowledge that, up to the present, there is no satisfactory theory of this kind, in spite of numerous attempts undertaken by many scientists over several decades to construct it (see the monographs and reviews [164–168]). At the same time, there are a few approaches, including the most famous by DeWitt [169–171], which apply the quantum theory of gravitation in the one-loop approximation to description of the Universe in terms of the wave function. Article [172] published in this Special Issue considers the DeWitt boundary condition imposed on the wave function of the Universe. The obtained results might be considered as a first step towards quantum gravity, leading to a non-singular cosmological model.

Another version of quantum gravity, called the Euclidean quantum gravity [173], is used in [174] to construct a new version of the no-boundary initial state of the Universe.

4. Conclusions

In the foregoing, we have considered the fundamental role of Alexander Friedmann's prediction of Universe expansion for modern cosmology, and briefly listed the major achievements in understanding of our Universe and its evolution made during one hundred years after this prediction. This evolution resulted in the formulation of the standard cosmological model Λ CDM, which provides a satisfactory explanation for most of the physical phenomena discovered by the modern astronomy and astrophysics. Many articles published in this Special Issue devoted to Friedmann's prediction of Universe expansion investigate some physical phenomena in the framework of this model.

Though the Λ CDM model, based on the general theory of relativity, Friedmann cosmology and the concept of the cosmological constant are sufficient to explain many available experimental and observational data, new data appear that have no explanation in the framework of this model, such as the Hubble tension and the CMB dipole anisotropy [175]. In addition, Λ CDM has no explicit physical theory for the origin and physical nature of dark matter and dark energy. As a result, it became clear that we are faced with a fundamental alternative today. Numerous attempts undertaken in order to quantitatively understand all modern cosmological discoveries, including primary dark

energy (which is found to be unstable) and dark matter, either go beyond the Standard Model of elementary particle physics, modify Einstein gravity, or use a combination of both of these approaches. It has also become timely to make the next step to the past of our Universe, and investigate possible variants of its pre-inflationary history and the artifacts remaining from them. This requires new astrophysical experiments in space and the further elaboration of quantum gravity. As seen from the above, many articles published in this jubilee Special Issue go beyond the standard cosmological model and look for the new approaches to these unresolved problems.

In the near future, one could expect new fundamental discoveries in astrophysics and cosmology that will shed additional light on the structure and evolution of our Universe.

Author Contributions: The authors have equally contributed to all aspects of the present paper. All authors have read and agreed to the published version of the manuscript.

Funding: The work of G.L.K. and V.M.M. was partially funded by the Ministry of Science and Higher Education of Russian Federation as part of the World-Class Research Center program: Advanced Digital Technologies (contract No. 075-15-2022-311 dated 20 April 2022). The research of V.M.M. was also partially carried out in accordance with the Strategic Academic Leadership Program “Priority 2030” of the Kazan Federal University. S.V.S. acknowledges partial support from the Strategic Academic Leadership Program “Priority 2030” of the Kazan Federal University.

Data Availability Statement: All references to the used data are contained in the text.

Conflicts of Interest: The authors declare no conflicts of interest.

References

1. Friedman, A.A. Über die Krümmung des Raumes. *Z. Phys.* **1922**, *10*, 377–386. [CrossRef]
2. Friedmann, A.A. Über die Möglichkeit einer Welt mit konstanter negativer Krümmung des Raumes. *Z. Phys.* **1924**, *21*, 326–332. [CrossRef]
3. Einstein, A. Bemerkung zu der Arbeit von A. Friedmann “Über die Krümmung des Raumes“. *Z. Phys.* **1922**, *11*, 326. [CrossRef]
4. Einstein, A. Kosmologische Betrachtungen zur allgemeinen Relativitätstheorie. *Sitzungsber. Königlich Preuss. Akad. Wiss.* **1917**, *6*, 142–152; Translated: Cosmological considerations in the general theory of relativity. In *The Collected Papers of Albert Einstein. Volume 6: The Berlin Years: Writings, 1914–1917 (English Translation Supplement)*; Klein, M.J., Kox, A.J., Schulman, R., Eds.; Princeton University Press: Princeton, NJ, USA, 1997; pp. 421–432.
5. de Sitter, W. On Einstein’s theory of gravitation and its astronomical consequences. First paper. *Mon. Not. R. Astron. Soc.* **1916**, *76*, 699–728. [CrossRef]
6. Lemaître, G. Un univers homogène de masse constante et de rayon croissant, rendant compte de la vitesse radiale des nébuleuses extra-galactiques. *Ann. Soc. Sci. Brux. A* **1927**, *47*, 49–59.
7. Robertson, H.P. Kinematics and world structure. *Astrophys. J.* **1935**, *82*, 284–301. [CrossRef]
8. Walker A.G. On Milne’s theory of world-structure. *Proc. Lond. Math. Soc.* **1937**, *42*, 90–127. [CrossRef]
9. Hubble, E. A relation between distance and radial velocity among extra-galactic nebulae. *Proc. Nat. Acad. Sci. USA* **1929**, *15*, 168–173. [CrossRef]
10. Gamow, G. Expanding universe and the origin of elements. *Phys. Rev.* **1946**, *70*, 572–573. [CrossRef]
11. Alpher, R.A.; Bethe, H.; Gamow, G. The Origin of Chemical Elements. *Phys. Rev.* **1948**, *73*, 803–804. [CrossRef]
12. Cyburt, R.H.; Fields, B.D.; Olive, K.A.; Yeh, T.-H. Big bang nucleosynthesis: Present status. *Rev. Mod. Phys.* **2016**, *88*, 015004. [CrossRef]
13. Alpher, R.A.; Herman, R.C. Evolution of the Universe. *Nature* **1948**, *162*, 774–775. [CrossRef]
14. Penzias, A.A.; Wilson, R.W. A Measurement of Excess Antenna Temperature at 4080 Mc/s. *Astrophys. J. Lett.* **1965**, *142*, 419–421. [CrossRef]
15. Gawiser, E.; Silk, J. The cosmic microwave background radiation. *Phys. Rep.* **2000**, *333–334*, 245–267. [CrossRef]
16. Partridge, R. B. *The Cosmic Microwave Background Radiation*; Cambridge University Press: Cambridge, UK, 1995.
17. Naselsky, P.D.; Novikov, D.I.; Novikov, I.D. *The Physics of the Cosmic Microwave Background*; Cambridge University Press: Cambridge, UK, 2006.
18. Evans, R. *The Cosmic Microwave Background: How It Changed Our Understanding of the Universe*; Springer: Cham, Switzerland, 2015.
19. Durrer, R. *The Cosmic Microwave Background*; Cambridge University Press: Cambridge, UK, 2020.
20. Hawking, S.W.; Ellis, G.F.R. The Cosmic Black-Body Radiation and the Existence of Singularities in our Universe. *Astrophys. J.* **1968**, *152*, 25–36. [CrossRef]
21. Hawking, S.W.; Penrose, R. The Singularities of Gravitational Collapse and Cosmology. *Proc. Roy. Soc. A Math. Phys. Engin. Sci.* **1970**, *314*, 529–548.

22. Guth, A.H. Inflationary universe: A possible solution to the horizon and flatness problems. *Phys. Rev. D* **1981**, *23*, 347–356. [CrossRef]
23. Guth, A.H.; Weinberg, E.J. Could the universe have recovered from a slow first-order phase transition? *Nucl. Phys. B* **1983**, *212*, 321–364. [CrossRef]
24. Guth, A.H. *The Inflationary Universe: The Quest for a New Theory of Cosmic Origins*; Basic Books: New York, NY, USA, 1997.
25. Linde, A.D. A new inflationary universe scenario: A possible solution of the horizon, flatness, homogeneity, isotropy and primordial monopole problems. *Phys. Lett. B* **1982**, *108*, 389–393. [CrossRef]
26. Albrecht, A.; Steinhardt, P.J. Cosmology for Grand Unified Theories with Radiatively Induced Symmetry Breaking. *Phys. Rev. Lett.* **1982**, *48*, 1220–1223. [CrossRef]
27. Linde, A.D. Chaotic inflation. *Phys. Lett. B* **1983**, *129*, 177–181. [CrossRef]
28. Linde, A.D. *Particle Physics and Inflationary Cosmology*; Harwood: Chur, Switzerland, 1990.
29. Mamayev, S.G.; Mostepanenko, V.M. Isotropic cosmological models determined by the vacuum quantum effects. *Zh. Eksp. Teor. Fiz.* **1980**, *78*, 20–27; Translated in *Sov. Phys. JETP* **1980**, *51*, 9–13.
30. Starobinsky, A.A. A new type of isotropic cosmological models without singularity. *Phys. Lett. A* **1980**, *91*, 99–102. [CrossRef]
31. Kofman, L.; Linde, A.; Starobinsky, A.A. Reheating after Inflation. *Phys. Rev. Lett.* **1994**, *73*, 3195–3198. [CrossRef]
32. Kofman, L.; Linde, A.D.; Starobinsky, A.A. Towards the theory of reheating after inflation. *Phys. Rev. D* **1997**, *56*, 3258–3295. [CrossRef]
33. Narozhnyi, N.B.; Nikishov, A.I. Pair production by a periodic electric field. *Zh. Eksp. Teor. Fiz.* **1973**, *65*, 862–874; Translated in *Sov. Phys. JETP* **1974**, *38*, 427–432.
34. Mostepanenko, V.M.; Frolov, V.M. Production of particles from vacuum by a uniform electric-field with periodic time-dependence. *Yad. Fiz.* **1974**, *19*, 885–896; Translated in *Sov. J. Nucl. Phys.* **1974**, *19*, 451–456.
35. Dolgov, A.D.; Kirilova, D.P. On particle creation by a time-dependent scalar field. *Yad. Fiz.* **1990**, *51*, 273–282; Translated in *Sov. J. Nucl. Phys.* **1990**, *51*, 172–177.
36. Traschen, J.H.; Brandenberger, R.H. Particle production during out-of-equilibrium phase transitions. *Phys. Rev. D* **1990**, *42*, 2491–2504. [CrossRef]
37. Boyanovsky, D.; de Vega, H.J.; Holman, R.; Lee, D.-S.; Singh, A. Dissipation via particle production in scalar field theories. *Phys. Rev. D* **1995**, *51*, 4419–4444. [CrossRef]
38. Kaiser, D.I. Post-inflation reheating in an expanding universe. *Phys. Rev. D* **1996**, *53*, 1776–1783. [CrossRef]
39. Fujisaki, H.; Kumekawa, K.; Yamaguchi, M.; Yoshimura, M. Particle production and dissipative cosmic field. *Phys. Rev. D* **1996**, *53*, 6805–6812. [CrossRef] [PubMed]
40. Kasuya, S.; Kawasaki, M. Restriction to parametric resonant decay after inflation. *Phys. Lett. B* **1996**, *388*, 686–691. [CrossRef]
41. Son, D.T. Reheating and thermalization in a simple scalar model. *Phys. Rev. D* **1996**, *54*, 3745–3761. [CrossRef]
42. Riotto, A.; Tkachev, I.I. Non-equilibrium symmetry restoration beyond one loop. *Phys. Lett. B* **1996**, *385*, 57–62. [CrossRef]
43. Allahverdi, R.; Campbell, B.A. Cosmological reheating and self-interacting final state bosons. *Phys. Lett. B* **1997**, *395*, 169–177. [CrossRef]
44. Prokopec, T.; Roos, T.G. Lattice study of classical inflaton decay. *Phys. Rev. D* **1997**, *55*, 3768–3775. [CrossRef]
45. Khlebnikov, S.; Tkachev, I. Relic gravitational waves produced after preheating. *Phys. Rev. D* **1997**, *56*, 653–660. [CrossRef]
46. Moss, I.G.; Graham, C. Particle production and reheating of the inflationary universe. *Phys. Rev. D* **2008**, *78*, 123526. [CrossRef]
47. Riess, A.G.; Filippenko, A.V.; Challis, P.; Clocchiatti, A.; Diercks, A.; Garnavich, P.M.; Gilliland, R.L.; Hogan, C.J.; Jha, S.; Kirshner, R.P.; et al. Observational evidence from supernovae for an accelerating universe and a cosmological constant. *Astron. J.* **1998**, *116*, 1009–1038. [CrossRef]
48. Perlmutter, S.; Aldering, G.; Goldhaber, G.; Knop, R.A.; Nugent, P.; Castro, P.G.; Deustua, S.; Fabbro, S.; Goobar, A.; Groom, D.E.; et al. Measurements of Ω and Λ from 42 high-redshift supernovae. *Astrophys. J.* **1999**, *517*, 565–586. [CrossRef]
49. Frieman, J.A.; Turner, M.S.; Huterer, D. Dark energy and the accelerating universe. *Annu. Rev. Astron. Astrophys.* **2008**, *46*, 385–432. [CrossRef]
50. Peebles, P.J.E.; Ratra, B. The cosmological constant and dark energy. *Rev. Mod. Phys.* **2003**, *75*, 559–606. [CrossRef]
51. Chiba, T.; De Felice, A.; Tsujikawa, S. Observational constraints on quintessence: Thawing, tracker, and scaling models. *Phys. Rev. D* **2013**, *87*, 083505. [CrossRef]
52. Tsujikawa, S. Quintessence: A review. *Class. Quant. Grav.* **2013**, *30*, 214003. [CrossRef]
53. Joyce, A.; Lombriser, L.; Schmidt, F. Dark energy vs. modified gravity. *Ann. Rev. Nucl. Part. Sci.* **2016**, *66*, 95–122. [CrossRef]
54. Fujii, Y.; Maeda, K.-i. *The Scalar-Tensor Theory of Gravitation*; Cambridge University Press: Cambridge, UK, 2003.
55. Quiros, I. Selected topics in scalar-tensor theories and beyond. *Int. J. Mod. Phys. D* **2019**, *28*, 1930012. [CrossRef]
56. Khoury, J.; Weltman, A. Chameleon Fields: Awaiting Surprises for Tests of Gravity in Space. *Phys. Rev. Lett.* **2004**, *93*, 171104. [CrossRef]
57. Hinterbichler, K.; Khoury, J.; Levy, A.; Matas, A. Symmetron cosmology. *Phys. Rev. D* **2011**, *84*, 103521. [CrossRef]
58. Brax, P.; Fischer, H.; Käding, C.; Pitschmann, M. The environment dependent dilaton in the laboratory and the solar system. *Eur. Phys. J. C* **2022**, *82*, 934. [CrossRef]
59. Deruelle, N.; Uzan, J.-P.; de Forcrand-Millard, P. *Relativity in Modern Physics*; Oxford University Press: Oxford, UK, 2018.
60. Weinberg, S. A New Light Boson? *Phys. Rev. Lett.* **1978**, *40*, 223–226. [CrossRef]

61. Wilczek, F. Problem of Strong P and T Invariance in the Presence of Instantons. *Phys. Rev. Lett.* **1978**, *40*, 279–283. [CrossRef]
62. Mostepanenko, V.M. Prediction of the Expansion of the Universe Made by Alexander Friedmann and the Effect of Particle Creation in Cosmology. *Universe* **2024**, *10*, 84. [CrossRef]
63. de Bernardis, P.; Ade, P.A.R.; Bock, J.J.; Bond, J.R.; Borrill, J.; Boscaleri, A.; Coble, K.; Crill, B.P.; De Gasperis, G.; Farese, P.C.; et al. A Flat Universe from High-Resolution Maps of the Cosmic Microwave Background Radiation. *Nature* **2020**, *404*, 955–959. [CrossRef]
64. Colless, M.; Dalton, G.B.; Maddox, S.J.; Sutherland, W.J.; Norberg, P.; Cole, S.; Bland-Hawthorn, J.; Bridges, T.J.; Cannon, R.D.; Collins, C.A.; et al. The 2dF Galaxy Redshift Survey: Spectra and redshifts. *Mon. Not. R. Astron. Soc.* **2001**, *328*, 1039–1063. [CrossRef]
65. Bennett, C.L.; Larson, D.; Weiland, J.L.; Jarosik, N.; Hinshaw, G.; Odegard, N.; Smith, K.M.; Hill, R.S.; Gold, B.; Halpern, M.; et al. Nine-Year Wilkinson Microwave Anisotropy Probe (WMAP) Observations: Final Maps and Results. *Astrophys. J. Suppl.* **2013**, *208*, 20. [CrossRef]
66. Aghanim, N.; Akrami, Y.; Ashdown, M.; Ashdown, M.; Aumont, J.; Baccigalupi, C.; Ballardini, M.; Banday, A.J.; Barreiro, R.B.; Bartolo, N.; et al. Planck Collaboration. Planck 2018 results. VI. Cosmological parameters. *Astron. Astrophys.* **2020**, *641*, A6.
67. Tristram, M.; Banday, A.J.; Douspis, M.; Garrido, X.; Górski, K.M.; Henrot-Versillé, S.; Hergt, L.T.; Ilić, S.; Keskitalo, R.; Lagache, G.; et al. Cosmological parameters derived from the final Planck data release (PR4). *Astron. Astrophys.* **2024**, *682*, A37. [CrossRef]
68. Grib, A.A.; Pavlov, Y.V. Particles of Negative and Zero Energy in Black Holes and Cosmological Models. *Universe* **2023**, *9*, 217. [CrossRef]
69. Penrose, R. Gravitational collapse: The role of general relativity. *Riv. Nuovo C* **1969**, *1*, 252–276.
70. Penrose, R.; Floyd, R.M. Extraction of rotational energy from a black hole. *Nat. Phys. Sci.* **1971**, *229*, 177–179. [CrossRef]
71. Toporensky, A.V.; Zaslavskii, O.B. Zero-momentum trajectories inside a black hole and high energy particle collisions. *J. Cosmol. Astropart. Phys.* **2019**, *12*, 063. [CrossRef]
72. Bronnikov, K.A.; Kashargin, P.E.; Sushkov, S.V. Possible Wormholes in a Friedmann Universe. *Universe* **2023**, *9*, 465. [CrossRef]
73. Bronnikov, K.A. Scalar-tensor theory and scalar charge. *Acta Phys. Pol. B* **1973**, *4*, 251–266.
74. Ellis, H.G. Ether flow through a drainhole-A particle model in general relativity. *J. Math. Phys.* **1973**, *14*, 104–118. [CrossRef]
75. Ellis, H.G. The evolving, flowless drainhole: A nongravitating-particle model in general relativity theory. *Gen. Relat. Gravit.* **1979**, *10*, 105–123. [CrossRef]
76. Clément, G. A class of wormhole solutions to higher dimensional general relativity. *Gen. Rel. Grav.* **1984**, *16*, 131–138. [CrossRef]
77. Clément, G. Axisymmetric regular multiwormhole solutions in five-dimensional general relativity. *Gen. Rel. Grav.* **1984**, *16*, 477–489. [CrossRef]
78. Morris, M.S.; Thorne, K.S. Wormholes in spacetime and their use for interstellar travel: A tool for teaching general relativity. *Am. J. Phys.* **1988**, *56*, 395–412. [CrossRef]
79. Odintsov, S.D.; D’Onofrio, S.; Paul, T. Entropic Inflation in Presence of Scalar Field. *Universe* **2024**, *10*, 4. [CrossRef]
80. Bekenstein, J.D. Black holes and entropy. *Phys. Rev. D* **1973**, *7*, 2333–2346. [CrossRef]
81. Tsallis, C. Possible Generalization of Boltzmann-Gibbs Statistics. *J. Statist. Phys.* **1988**, *52*, 479–487. [CrossRef]
82. Jahromi, A.S.; Moosavi, S.A.; Moradpour, H.; Graça, J.P.M.; Lobo, I.P.; Salako, I.G.; Jawad, A. Generalized entropy formalism and a new holographic dark energy model. *Phys. Lett. B* **2018**, *780*, 21–24. [CrossRef]
83. Majhi, A. Non-extensive Statistical Mechanics and Black Hole Entropy from Quantum Geometry. *Phys. Lett. B* **2017**, *775*, 32–36. [CrossRef]
84. Oliveira, V.G.; de Oliveira Neto, G.; Shapiro, I.L. Kantowski-Sachs Model with a Running Cosmological Constant and Radiation. *Universe* **2024**, *10*, 83. [CrossRef]
85. Jacobs, K.C. Spatially homogeneous and euclidean cosmological models with shear. *Astrophys. J.* **1968**, *153*, 661–678. [CrossRef]
86. Weber, E. Kantowski-Sachs cosmological models approaching isotropy. *J. Math. Phys.* **1984**, *25*, 3279–3285. [CrossRef]
87. Grøn, Ø. Transition of a Kantowski-Sachs cosmological model into an inflationary era. *J. Math. Phys.* **1986**, *27*, 1490–1491. [CrossRef]
88. Vargas Moniz, P. Kantowski-Sachs universes and the cosmic no hair conjecture. *Phys. Rev. D* **1993**, *47*, 4315–4321. [CrossRef] [PubMed]
89. Byland, S.; Scialom, D. Evolution of the Bianchi I, The Bianchi III and the Kantowski-Sachs universe: Isotropization and inflation. *Phys. Rev. D* **1998**, *57*, 6065–6074. [CrossRef]
90. Parisi, L.; Radicella, N.; Vilasi, G. Kantowski-Sachs Universes sourced by a Skyrme fluid. *Phys. Rev. D* **2015**, *91*, 063533. [CrossRef]
91. Kamenshchik, A.; Petriakova, P. Regular Friedmann Universes and Matter Transformations. *Universe* **2024**, *10*, 137. [CrossRef]
92. Creminelli, P.; Nicolis, A.; Trincherini, E. Galilean Genesis: An Alternative to inflation. *J. Cosmol. Astropart. Phys.* **2010**, *2010*, 021. [CrossRef]
93. Easson, D.; Sawicki, I.; Vikman, A. G-bounce. *J. Cosmol. Astropart. Phys.* **2011**, *11*, 021. [CrossRef]
94. Spallucci, E.; Smailagic, A. Regular black holes from from semi-classical down to Planckian size. *Int. J. Mod. Phys. D* **2017**, *26*, 1730013. [CrossRef]
95. Sebastiani, L.; Zerbini, S. Some remarks on non-singular spherically symmetric space-times. *Astronomy* **2022**, *1*, 99–125. [CrossRef]
96. Grib, A.A.; Pavlov, Y.V. On Phase Transitions during Collisions near the Horizon of Black Holes. *Universe* **2024**, *10*, 131. [CrossRef]
97. Kolb, E.W.; Turner, M.S. *The Early Universe*; Addison-Wesley: Redwood City, CA, USA, 1990.

98. Pasechnik, R.; Šumbera, M. Phenomenological review on quark-gluon plasma: Concepts vs. observations. *Universe* **2017**, *3*, 7. [CrossRef]
99. Gorbunov, D.S.; Rubakov, V.A. *Introduction to the Theory of the Early Universe: Hot Big Bang Theory*; World Scientific: Singapore, 2018.
100. Saha, B. Spinor Field in FLRW Cosmology. *Universe* **2023**, *9*, 243. [CrossRef]
101. De Andrade, V.C.; Guillen, L.C.T.; Pereira, J.G. Gravitational energy momentum density in teleparallel gravity. *Phys. Rev. Lett.* **2000**, *84*, 4533–4536. [CrossRef] [PubMed]
102. Awad, A.; El Hanafy, W.; Nashed, G.G.L.; Odintsov, S.D.; Oikonomou, V.K. Constant-roll inflation in $f(T)$ teleparallel gravity. *J. Cosmol. Astropart. Phys.* **2018**, *7*, 026. [CrossRef]
103. Krššák, M.; van den Hoogen, R.J.; Pereira, J.G.; Böhmer, C.G.; Coley, A.A. Teleparallel theories of gravity: Illuminating a fully invariant approach. *Class. Quantum Grav.* **2019**, *36*, 183001. [CrossRef]
104. Järv, L.; Kuusk, P. Conventionalism, Cosmology and Teleparallel Gravity. *Universe* **2024**, *10*, 1. [CrossRef]
105. Beltrán Jiménez, J.; Heisenberg, L.; Koivisto, T. Coincident General Relativity. *Phys. Rev. D* **2018**, *98*, 044048. [CrossRef]
106. Capozziello, S.; De Falco, V.; Ferrara, C. Comparing equivalent gravities: Common features and differences. *Eur. Phys. J. C* **2022**, *82*, 865. [CrossRef]
107. Saburov, S.; Ketov, S.V. Improved Model of Primordial Black Hole Formation after Starobinsky Inflation. *Universe* **2023**, *9*, 323. [CrossRef]
108. Appleby, S.A.; Battye, R.A.; Starobinsky, A.A. Curing singularities in cosmological evolution of $F(R)$ gravity. *J. Cosmol. Astropart. Phys.* **2010**, *6*, 5. [CrossRef]
109. Sotiriou, T.P.; Faraoni, V. $f(R)$ Theories of Gravity. *Rev. Mod. Phys.* **2010**, *82*, 451–497. [CrossRef]
110. Papanikolaou, T.; Tzerefos, C.; Basilakos, S.; Saridakis, E.N. Scalar induced gravitational waves from primordial black hole Poisson fluctuations in $f(R)$ gravity. *J. Cosmol. Astropart. Phys.* **2022**, *10*, 13. [CrossRef]
111. Chiba, T. $1/R$ gravity and scalar-tensor gravity. *Phys. Lett. B* **2003**, *575*, 1–3. [CrossRef]
112. Brans, C.; Dicke, R.H. Mach's principle and a relativistic theory of gravitation. *Phys. Rev.* **1961**, *124*, 925–935. [CrossRef]
113. Kofinas, G. The complete Brans-Dicke theories. *Ann. Phys.* **2017**, *376*, 425–435. [CrossRef]
114. Sola, J.; Gomez-Valent, A.; de Cruz Perez, J.; Moreno-Pulido, C. Brans-Dicke cosmology with a Λ -term: A possible solution to Λ CDM tensions. *Class. Quantum Grav.* **2020**, *37*, 245003.
115. Fabris, J.C.; Falciano, F.T.; Guimarães, L.F.; Pinto-Neto, N. On the Possibility of a Static Universe. *Universe* **2024**, *10*, 92. [CrossRef]
116. Singh, V.; Jokweni, S.; Beesham, A. FRLW transit cosmological model in $f(R, T)$ gravity. *Universe* **2024**, *10*, 272. [CrossRef]
117. Harko, T.; Lobo, F.S.N.; Nojiri, S.; Odintsov, S.D. $f(R, T)$ gravity. *Phys. Rev. D* **2011**, *84*, 024020. [CrossRef]
118. Tretyakov, P.V. Cosmology in modified $f(R, T)$ -gravity. *Eur. Phys. J. C* **2018**, *78*, 896. [CrossRef]
119. Rudra, P.; Giri, K. Observational constraint in $f(R, T)$ gravity from the cosmic chronometers and some standard distance measurement parameters. *Nucl. Phys. B* **2021**, *967*, 115428. [CrossRef]
120. Bouali, A.; Chaudhary, H.; Harko, T.; Lobo, F.S.N.; Ouali, T.; Pinto, M.A.S. Observational constraints and cosmological implications of scalar-tensor $f(R, T)$ gravity. *Month. Not. Roy. Astron. Soc.* **2023**, *526*, 4192–4208. [CrossRef]
121. Balakin, A.; Shakirzyanov, A. An Isotropic Cosmological Model with Aetherically Active Axionic Dark Matter. *Universe* **2024**, *10*, 74. [CrossRef]
122. Popov, A.A.; Rubin, S.G.; Sakharov, A.S. Primordial Black Holes from Spatially Varying Cosmological Constant Induced by Field Fluctuations in Extra Dimensions. *Universe* **2024**, *10*, 166. [CrossRef]
123. Jacobson, T.; Mattingly, D. Einstein-aether waves. *Phys. Rev. D* **2004**, *70*, 024003. [CrossRef]
124. Heinicke, C.; Baekler, P.; Hehl, F.W. Einstein-aether theory, violation of Lorentz invariance, and metric-affine gravity. *Phys. Rev. D* **2005**, *72*, 025012. [CrossRef]
125. Carr, B.; Kohri, K.; Sendouda, Y.; Yokoyama, J. Constraints on primordial black holes. *Rept. Prog. Phys.* **2021**, *84*, 116902. [CrossRef] [PubMed]
126. Ivanchik, A.V.; Kurichin, O.A.; Yurchenko, V.Y. Neutrino at Different Epochs of the Friedmann Universe. *Universe* **2024**, *10*, 169. [CrossRef]
127. Boyarsky, A.; Ruchayskiy, O.; Shaposhnikov, M. The Role of Sterile Neutrinos in Cosmology and Astrophysics. *Ann. Rev. Nucl. Part. Sci.* **2009**, *59*, 191–214. [CrossRef]
128. Chernikov, P.; Ivanchik, A. The influence of the effective number of active and sterile neutrinos on the determination of the values of cosmological parameters. *Astron. Lett.* **2022**, *48*, 689–701. [CrossRef]
129. Serebrov, A.; Samoilo, R.; Ivochkin, V.; Fomin, A.K.; Zinoviev, V.G.; Neustroev, P.V.; Golovtsov, V.L.; Volkov, S.S.; Chernyj, A.V.; Zharebtsov, O.M.; et al. Search for sterile neutrinos with the Neutrino-4 experiment and measurement results. *Phys. Rev. D* **2021**, *104*, 032003. [CrossRef]
130. Barinov, V.; Cleveland, B.; Danshin, S.; Ejiri, H.; Elliott, S.R.; Frekers, D.; Gavrin, V.N.; Gorbachev, V.V.; Gorbunov, D.S.; Haxton, W.C.; et al. Results from the Baksan Experiment on Sterile Transitions (BEST). *Phys. Rev. Lett.* **2022**, *128*, 232501. [CrossRef]
131. Capozziello, S.; Sarracino, G.; De Somma, G. A Critical Discussion on the H_0 Tension. *Universe* **2024**, *10*, 140. [CrossRef]
132. Riess, A.G.; Yuan, W.; Macri, L.M.; Scolnic, D.; Brout, D.; Casertano, S.; Jones, D.O.; Murakami, Y.; Anand, G.S.; Breuval, L.; et al. A Comprehensive Measurement of the Local Value of the Hubble Constant with 1 km/s/Mpc Uncertainty from the Hubble Space Telescope and the SH0ES Team. *Astrophys. J. Lett.* **2022**, *934*, L7. [CrossRef]

133. Klimchitskaya, G.L.; Mostepanenko, V.M. The Nature of Dark Energy and Constraints on Its Hypothetical Constituents from Force Measurements. *Universe* **2024**, *10*, 119. [CrossRef]
134. Klimchitskaya, G.L.; Mostepanenko, V.M. Improved constraints on the coupling constants of axion-like particles to nucleons from recent Casimir-less experiment. *Eur. Phys. J. C* **2015**, *75*, 164. [CrossRef]
135. Klimchitskaya, G.L.; Mostepanenko, V.M. Constraints on axionlike particles and non-Newtonian gravity from measuring the difference of Casimir forces. *Phys. Rev. D* **2017**, *95*, 123013. [CrossRef]
136. Klimchitskaya, G.L. Recent breakthrough and outlook in constraining the non-Newtonian gravity and axion-like particles from Casimir physics. *Eur. Phys. J. C* **2017**, *77*, 315. [CrossRef]
137. Klimchitskaya, G.L.; Kuusk, P.; Mostepanenko, V.M. Constraints on non-Newtonian gravity and axionlike particles from measuring the Casimir force in nanometer separation range. *Phys. Rev. D* **2020**, *101*, 056013. [CrossRef]
138. Brax, P.; van de Bruck, C.; Davis, A.-C.; Mota, D.F.; Shaw, D. Detecting chameleons through Casimir force measurements. *Phys. Rev. D* **2007**, *76*, 124034. [CrossRef]
139. Almasi, A.; Brax, P.; Iannuzzi, D.; Sedmik, R.I.P. Force sensor for chameleon and Casimir force experiments with parallel-plate configuration. *Phys. Rev. D* **2015**, *91*, 102002. [CrossRef]
140. Fischer, H.; Käding, C.; Sedmik, R.I.P.; Abele, H.; Brax, P.; Pitschmann, M. Search for environment-dependent dilatons. *Phys. Dark Univ.* **2024**, *43*, 101419. [CrossRef]
141. Bambi, C. Can the supermassive objects at the centers of galaxies be traversable wormholes? The first test of strong gravity for mm/sub-mm very long baseline interferometry facilities. *Phys. Rev. D* **2013**, *87*, 107501. [CrossRef]
142. Zhou, M.; Cardenas-Avendano, A.; Bambi, C.; Kleihaus, B.; Kunz, J. Search for astrophysical rotating Ellis wormholes with X-ray reflection spectroscopy. *Phys. Rev. D* **2016**, *94*, 024036. [CrossRef]
143. Tripathi, A.; Zhou, B.; Abdikamalov, A.B.; Ayzenberg, D.; Bambi, C. Search for traversable wormholes in active galactic nuclei using X-ray data. *Phys. Rev. D* **2020**, *101*, 064030. [CrossRef]
144. Paul, S.; Shaikh, R.; Banerjee, P.; Sarkar, T. Observational signatures of wormholes with thin accretion disks. *J. Cosmol. Astropart. Phys.* **2020**, *2020*, 055. [CrossRef]
145. Piotrovich, M.; Krasnikov, S.; Buliga, S.; Natsvlshvili, T. Search for Wormhole Candidates: Accreting Wormholes with Monopole Magnetic Fields. *Universe* **2024**, *10*, 108. [CrossRef]
146. Parker, L. Quantized fields and particle creation in expanding universes. I. *Phys. Rev.* **1969**, *183*, 1057–1068. [CrossRef]
147. Parker, L. Quantized fields and particle creation in expanding universes. II. *Phys. Rev. D* **1971**, *3*, 346–356. [CrossRef]
148. Grib, A.A.; Mamayev, S.G.; Mostepanenko, V.M. Particle creation from vacuum in homogeneous isotropic models of the Universe. *Gen. Relat. Gravit.* **1976**, *7*, 535–547. [CrossRef]
149. Mamayev, S.G.; Mostepanenko, V.M.; Starobinskii, A.A. Particle creation from the vacuum near a homogeneous isotropic singularity. *Zh. Eksp. Teor. Fiz.* **1976**, *70*, 1577–1591; Translated in *Sov. Phys. JETP* **1976**, *43*, 823–830.
150. Grib, A.A.; Mamayev, S.G.; Mostepanenko, V.M. Vacuum stress-energy tensor and particle creation in isotropic cosmological models. *Fortschr. Der Phys.* **1980**, *28*, 173–199. [CrossRef]
151. Berezhin, V.; Ivanova, I. Conformally Invariant Gravity and Gravitating Mirages. *Universe* **2024**, *10*, 147. [CrossRef]
152. Ray, J.R. Lagrangian Density for Perfect Fluids in General Relativity. *J. Math. Phys.* **1972**, *13*, 1451–1453. [CrossRef]
153. Berezhin, V.A. Unusual Hydrodynamics. *Int. J. Mod. Phys. A* **1987**, *2*, 1591–1615. [CrossRef]
154. Boccaletti, D.; De Sabbata, V.; Fortini, P.; Gualdi, C. Space-Time Curvature Mode Quanta. *Nuovo Cimento.* **1970**, *70*, 129–146. [CrossRef]
155. Raffelt, G.; Stodolsky, L. Mixing of the Photon with Low Mass Particles. *Phys. Rev. D* **1988**, *37*, 1237–1249. [CrossRef]
156. Dolgov, A.D.; Ejlli, D. Resonant high energy graviton to photon conversion at post recombination epoch. *Phys. Rev. D* **2013**, *87*, 104007. [CrossRef]
157. Dolgov, A.D.; Panasenko, L.A.; Bochko, V.A. Graviton to Photon Conversion in Curved Space-Time and External Magnetic Field. *Universe* **2024**, *10*, 7. [CrossRef]
158. Jenkovszky, L.; Kurochkin, Y.A.; Shaikovskaya, N.D.; Soloviev, V.O. Nonrelativistic Quantum Mechanical Problem for the Cornell Potential in Lobachevsky Space. *Universe* **2024**, *10*, 76. [CrossRef]
159. Sergeenko, M.N. Masses and widths of Resonances for the Cornell Potential. *Adv. High Energy Phys.* **2013**, *2013*, 325431. [CrossRef]
160. Moschella, U. The Spectral Condition, Plane Waves, and Harmonic Analysis in de Sitter and Anti-de Sitter Quantum Field Theories. *Universe* **2024**, *10*, 199. [CrossRef]
161. Bros, J.; Moschella, U. Two point functions and quantum fields in de Sitter universe. *Rev. Math. Phys.* **1996**, *8*, 327–392. [CrossRef]
162. Bros, J.; Epstein, H.; Moschella, U. Analyticity properties and thermal effects for general quantum field theory on de Sitter space-time. *Commun. Math. Phys.* **1998**, *196*, 535–570. [CrossRef]
163. Bros, J.; Epstein, H.; Moschella, U. Towards a general theory of quantized fields on the anti-de Sitter space-time. *Commun. Math. Phys.* **2002**, *231*, 481–528. [CrossRef]
164. Barvinsky, A.O.; Vilkovisky, G.A. The Generalized Schwinger-DeWitt Technique in Gauge Theories and Quantum Gravity. *Phys. Rep.* **1985**, *119*, 1–74. [CrossRef]
165. Green, M.B.; Schwarz, J.H.; Witten, E. *Superstring Theory. Vol. 1*; Cambridge University Press: Cambridge, UK, 1987.
166. Carlip, S. Quantum Gravity: A Progress Report. *Rep. Progr. Phys.* **2001**, *64*, 885–942. [CrossRef]
167. Rovelli, C. *Quantum Gravity*; Cambridge University Press: Cambridge, UK, 2004.

168. Kiefer, C. *Quantum Gravity*, 3rd ed.; Oxford University Press: Oxford, UK, 2012.
169. DeWitt, B.S. Quantum Theory of Gravity. I. The Canonical Theory. *Phys. Rev.* **1967**, *160*, 1113–1148; Erratum in *Phys. Rev.* **1968**, *171*, 1834. [CrossRef]
170. DeWitt, B.S. Quantum Theory of Gravity. II. The Manifestly Covariant Theory. *Phys. Rev.* **1967**, *162*, 1195–1238; Erratum in *Phys. Rev.* **1968**, *171*, 1834. [CrossRef]
171. DeWitt, B.S. Quantum Theory of Gravity. III. Applications of the Covariant Theory. *Phys. Rev.* **1967**, *162*, 1239–1255; Erratum in *Phys. Rev.* **1968**, *171*, 1834. [CrossRef]
172. Esposito, G. DeWitt Boundary Condition in One-Loop Quantum Cosmology. *Universe* **2023**, *9*, 187. [CrossRef]
173. Hartle, J.B.; Hawking, S.W.; Hertog, T. Classical universes of the no-boundary quantum state. *Phys. Rev. D* **2008**, *77*, 123537. [CrossRef]
174. Gorobey, N.; Lukyanenko, A.; Goltsev, A.V. No-Boundary Wave Functional and Own Mass of the Universe. *Universe* **2024**, *10*, 101. [CrossRef]
175. Abdalla, E.; Abellán, G.F.; Aboubrahim, A.; Agnello, A.; Akarsu, Ö.; Akrami, Y.; Alestas, G.; Aloni, D.; Amendola, L.; Anchordoqui, L.A.; et al. Cosmology Intertwined: A Review of the Particle Physics, Astrophysics, and Cosmology Associated with the Cosmological Tensions and Anomalies. *J. High Energy Astrophys.* **2022**, *34*, 49–211.

Disclaimer/Publisher’s Note: The statements, opinions and data contained in all publications are solely those of the individual author(s) and contributor(s) and not of MDPI and/or the editor(s). MDPI and/or the editor(s) disclaim responsibility for any injury to people or property resulting from any ideas, methods, instructions or products referred to in the content.

Article

Particles of Negative and Zero Energy in Black Holes and Cosmological Models

Andrey A. Grib ^{1,2}  and Yuri V. Pavlov ^{3,*} 

¹ Theoretical Physics and Astronomy Department, The Herzen University, 48 Moika, St. Petersburg 191186, Russia; andrei_grib@mail.ru

² A. Friedmann Laboratory for Theoretical Physics, St. Petersburg 191186, Russia

³ Institute of Problems in Mechanical Engineering of Russian Academy of Sciences, 61 Bolshoy, V.O., St. Petersburg 199178, Russia

* Correspondence: yuri.pavlov@mail.ru

Abstract: Particles with negative energies are considered for three different cases: inside the horizon of a Schwarzschild black hole, Milne's coordinates in flat Minkowski space–time (Milne's universe using nonsynchronous coordinates) and in the cosmological Gödel model of the rotating universe. It is shown that, differently from the Gödel model with a nondiagonal term, where it occurs that negative energies are impossible, they are present in all other cases considered in the paper. Particles with zero energy are also possible in the first two cases.

Keywords: negative energy; zero energy; black hole; Milne universe; Gödel universe



Citation: Grib, A.A.; Pavlov, Y.V. Particles of Negative and Zero Energy in Black Holes and Cosmological Models. *Universe* **2023**, *9*, 217. <https://doi.org/10.3390/universe9050217>

Academic Editors: Galina L. Klimchitskaya, Vladimir M. Mostepanenko and Sergey V. Sushkov

Received: 18 March 2023

Revised: 28 April 2023

Accepted: 28 April 2023

Published: 1 May 2023



Copyright: © 2023 by the authors. Licensee MDPI, Basel, Switzerland. This article is an open access article distributed under the terms and conditions of the Creative Commons Attribution (CC BY) license (<https://creativecommons.org/licenses/by/4.0/>).

1. Introduction

In 1922, Alexander Friedmann, in Petrograd, Russia, predicted an expansion of the Universe. Today, Friedmann's model of the Universe is called the Standard Model. Many observations confirm this model to be correct. The new world of galaxies and the stages of the Universe's evolution were discovered. New phenomena, such as black holes, relic radiation and many others, are actively investigated. Trajectories of particles with negative and zero energy are examples of such new phenomena. The possibility of relativistic particles with negative energy is important because it makes it possible to obtain large energy in interactions or decays of bodies. A simple example of this situation was proposed by R. Penrose in the case of the decays of particles in the ergospheres of rotating black holes [1,2].

It appears that in order to have negative energy of the relativistic particle with nonzero mass, one must have a very strong external field leading to large potential energy, as is the case for rotating black holes. However, it is well known that the value of the energy depends on the choice of the reference frame and the time coordinate or Killing vector in case of conserved energy. It leads to the situation whereby states with negative energies in the relativistic case occur in the case of a rotating coordinate system outside the static limit [3], where an effect analogical to the Penrose effect is found to be observable [4], and in a nonsynchronous coordinate system in cosmology [5,6].

It seems from these examples that negative energies arise in the case of the existence of nondiagonal terms in a metrical tensor (gravymagnetism), but, in this paper, we show that in the Gödel Universe, in spite of the presence of such terms, negative energies are absent. The negative energies are present in cases of the movement inside of the horizon of the Schwarzschild black hole and in Milne's universe where nondiagonal terms are present in a nonsynchronous coordinate frame.

2. Negative Energy in Nonrotating Black Hole

A nonrotating black hole of mass M in Schwarzschild coordinates is described by the metric

$$ds^2 = \left(1 - \frac{r_g}{r}\right) c^2 dt^2 - \frac{dr^2}{1 - \frac{r_g}{r}} - r^2(d\theta^2 + \sin^2\theta d\varphi^2), \tag{1}$$

where $r_g = 2GM/c^2$ is the gravitational radius of the black hole, G is the gravitational constant, and c is the light velocity. The geodesic complete space–time of the nonrotating black hole can be described in Kruskal–Szekeres coordinates, $\{u, v\} \in (-\infty, +\infty)$, which, in region $u > |v| \geq 0$, are connected with the Schwarzschild coordinate in $r > r_g$ in the following way:

$$u = \sqrt{\frac{r}{r_g} - 1} \exp\left(\frac{r}{2r_g}\right) \cosh \frac{ct}{2r_g}, \quad v = \sqrt{\frac{r}{r_g} - 1} \exp\left(\frac{r}{2r_g}\right) \sinh \frac{ct}{2r_g}. \tag{2}$$

For $r < r_g$ and $v > |u| \geq 0$, the transformation from the Schwarzschild coordinate into the Kruskal–Szekeres coordinates has the form

$$u = \sqrt{1 - \frac{r}{r_g}} \exp\left(\frac{r}{2r_g}\right) \sinh \frac{ct}{2r_g}, \quad v = \sqrt{1 - \frac{r}{r_g}} \exp\left(\frac{r}{2r_g}\right) \cosh \frac{ct}{2r_g}. \tag{3}$$

Schwarzschild coordinates are singular at $r = r_g$. Regarding their connection with Kruskal–Szekeres coordinates for other u, v , see [7], Section 31.5.

Any possible movement of physical bodies and particles must satisfy the condition $ds^2 > 0$ leading to

$$r > r_g \Rightarrow \left| \frac{dr}{dt} \right| \leq c \left(1 - \frac{r_g}{r}\right), \tag{4}$$

$$r < r_g \Rightarrow \left| \frac{dr}{dt} \right| \geq c \left(\frac{r_g}{r} - 1\right). \tag{5}$$

For $r < r_g$, the coordinate ct is space and r/c is the time coordinate.

Geodesic equations in Schwarzschild coordinates in the plane $\theta = 0$ are [8]

$$\frac{dt}{d\lambda} = \frac{r}{r - r_g} \frac{E}{c^2}, \quad \frac{d\varphi}{d\lambda} = \frac{J}{r^2}, \quad \left(\frac{dr}{d\lambda}\right)^2 = \frac{E^2}{c^2} + \frac{r_g - r}{r^3} J^2 + \frac{r_g - r}{r} m^2 c^2, \tag{6}$$

where E is the energy of a moving particle (measured by the static observer in r, θ, φ coordinates), J is the conserved projection of the particle’s angular momentum on the axis orthogonal to the plane of motion, m is the particle mass, and λ is an affine parameter on the geodesic. For massive particles, $\lambda = \tau/m$, where τ is the proper time.

In an external region of the black hole ($r > r_g$) for any physical object, the time coordinate t is always increasing and so the energy E of the particle is positive (see (6)). Inside the horizon of the black ($r < r_g$), where t is space-like ($g_{tt} < 0$), one has movement as in increasing as in decreasing t . As is seen from the first formula in (6) for a particle moving inside the horizon in the direction of a decrease in the coordinate t , the energy E of the particle will be positive, while, for increasing coordinate t , the energy E is negative. For constant t inside the black hole, $E = 0$ due to formula (6).

Surely, t inside of the black hole is space-like and E is proportional to the t -component of the momentum. Inside a black hole, one can use other reference frames and corresponding energies [9]. However, for the observer outside the black hole, the conserved E along all trajectories of the free fall is equal (see formula (88.9) in [10]) to

$$E = mc^2 \sqrt{\left(1 - \frac{r_g}{r}\right) / \left(1 - \frac{\mathbf{v}^2}{c^2}\right)}, \tag{7}$$

where v is the velocity measured by the observer at rest in the Schwarzschild coordinates. Thus, we can call E inside the black hole, following [7], the “energy at infinity”. For a discussion of other ways to determine the energy within the horizon and the movement of particles there, see, for example, the articles [9,11–13].

In Figure 1, the trajectories for radial movement with positive, zero and negative energies in Kruskal–Szekeres coordinates are represented by red, green and blue lines.

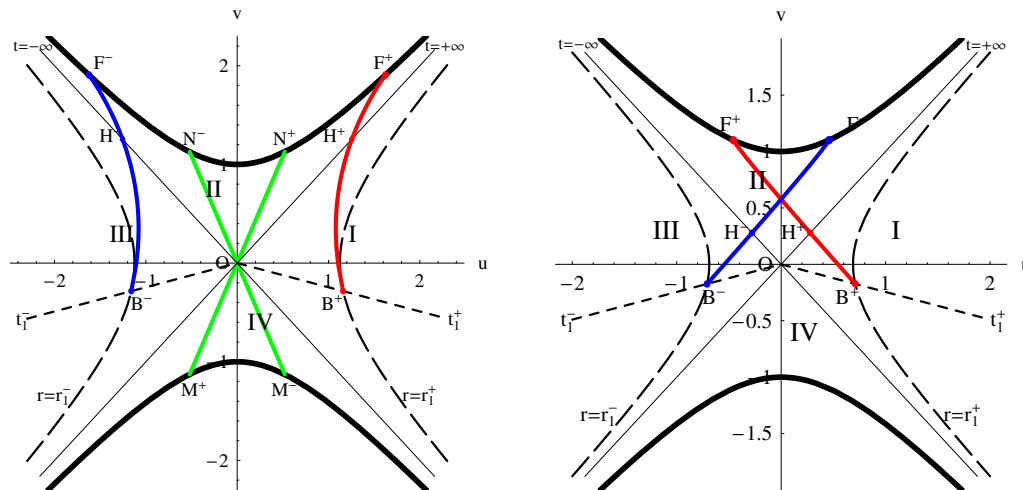


Figure 1. Trajectories of particles with positive ($B^+H^+F^+$), zero ($M^\pm ON^\pm$) and negative ($B^-H^-F^-$) energy, $t_1^\pm = \mp 0.5r_g/c$. On the left, one can see it falling from the rest at $|E| = 0.5mc^2$; on the right, $|E| = mc^2$ with the corresponding initial velocity from the point $r = 1.15r_g$. On lines ($M^\pm ON^\pm$), the coordinate $t = \pm r_g/c$.

As one can see from (2) and (3), the coordinate lines of constant t in Kruskal–Szekeres coordinates are straight lines through the origin of the coordinates. In region II, coordinate t decreases when moving from H^+ to F^+ (positive E) and increases when moving from H^- to F^- (negative value of E). Direct lines ($M^\pm ON^\pm$) correspond to constant $t = \pm r_g/c$ and therefore $E = 0$.

Let us consider the problem of the back influence of falling particles on the metric of the black hole space–time. For macroscopic bodies with 4-velocity (u^i), with the energy density ϵ and pressure p in space–time with metric g_{ik} , the energy–momentum density tensor is [10]

$$T_{ik} = (\epsilon + p)u_i u_k - p g_{ik}, \tag{8}$$

$i, k = 0, 1, 2, 3$. The trace of the energy–momentum tensor

$$T^i_i = \epsilon - 3p \tag{9}$$

is invariant and it will be negative for $\epsilon - 3p < 0$ —in particular, for dust-like matter ($p = 0$) with negative energy $\epsilon < 0$. The back influence of falling particles with negative energy will be determined by the energy–momentum tensor in the right-hand side of the Einstein equations. The notion of the existence of particles with negative energies as it is known was used by S. Hawking to predict the Hawking effect for black holes [14].

For a discussion of other ways to determine the energy within the horizon and the movement of particles there, see, for example, works

3. Negative and Zero Energies in Flat Space–Time

The geodesic line equations can be obtained for space–time with metric g_{ik} from the Lagrangian

$$L = \frac{g_{ik} dx^i dx^k}{2 d\lambda d\lambda'}, \tag{10}$$

where λ is the affine parameter on the geodesic [8]. The energy of the particle E is equal to the zero covariant component of the momentum (p_i) multiplied on the light velocity

$$p_i = \frac{\partial L}{\partial \left(\frac{dx^i}{d\lambda}\right)} = g_{ik} \frac{dx^k}{d\lambda}, \tag{11}$$

$$E = cp_0 = cg_{0k} \frac{dx^k}{d\lambda}. \tag{12}$$

Defining the affine parameter for the massive particle as $\lambda = \tau/m$, where τ is the proper time of the moving particle, one obtains

$$p_i p^i = m^2 c^2 \tag{13}$$

and the energy of the particle is

$$E = mcg_{0k} \frac{dx^k}{d\tau}. \tag{14}$$

Using notation $(\zeta^i) = (1, 0, 0, 0)$ for the translation in the time coordinate generator, one can write (12) for the energy of the particle as

$$E = c(p, \zeta). \tag{15}$$

If the metric components do not depend on the time coordinate x^0 , then ζ is the time-like Killing vector and the energy E is conserved on the geodesic. For time-like vector ζ and a massive particle, one has [15]

$$\sqrt{(\zeta, \zeta)} \leq \frac{E}{mc^2} < +\infty \tag{16}$$

and the energy (15) is positive. For space-like vector ζ , as it takes place in the ergosphere of a rotating black hole, the arbitrary positive and negative values are possible (see [15], p. 325).

Note that in spite of the invariance of the scalar product (15), the value (14) of the energy depends on the choice of the reference frame. This occurs due to the fact that by changing the reference frame in which the physical measurements are made, the observer is changing vector ζ . The analysis of the situation in a rotating coordinate system in flat space–time is provided in [3].

In Minkowski space–time in the Galilean coordinate system or any other coordinate system with $g_{00} = 1, g_{0\alpha} = 0, (\alpha = 1, 2, 3)$, the energy (12) is

$$E = c^2 \frac{dt}{d\lambda} \tag{17}$$

and it is always positive in movement “forward” in time because in the future light cone, one has $dt/d\lambda > 0$.

Consider the coordinate system in which the metric of flat space–time has the form of the metric of the expanding homogeneous isotropic Universe—the Milne universe [16]:

$$ds^2 = c^2 dt^2 - c^2 t^2 (d\chi^2 + \sinh^2 \chi d\Omega^2), \tag{18}$$

where $d\Omega^2 = d\theta^2 + \sin^2 \theta d\varphi^2$, and coordinate χ is changing from 0 to $+\infty$. In new coordinates

$$T = t \cosh \chi, \quad r = ct \sinh \chi, \quad cT > r > 0 \tag{19}$$

the interval (18) takes the form of a Minkowski interval

$$ds^2 = c^2 dT^2 - dr^2 - r^2 d\Omega^2. \tag{20}$$

This space–time with coordinate $t \geq 0, \chi \geq 0$ corresponds to the future cone in coordinates cT, r .

The radial distance between points $\chi = 0$ and χ in metric (18) is $D = ct\chi$. Taking D as the radial coordinate [17], one obtains the interval as

$$ds^2 = \left(1 - \frac{D^2}{c^2t^2}\right)c^2dt^2 + 2\frac{D}{t}dtdD - dD^2 - c^2t^2 \sinh^2\left(\frac{D}{ct}\right)d\Omega^2. \tag{21}$$

From the condition $ds^2 \geq 0$, one obtains that if D is larger than $D_s = ct$, no physical object can be at rest in coordinates t, D, θ, ϕ . The value D_s corresponds to $\chi = 1$ and it plays the role of the static limit for the rotating black hole in Boyer–Lindquist [18] coordinates.

The energy of the particle with mass m in coordinates t, D, θ, ϕ is

$$E = cg_{0k} \frac{dx^k}{d\lambda} = mc^2 \frac{dt}{d\tau} \left(1 - \frac{D^2}{c^2t^2} + \frac{D}{c^2t} \frac{dD}{dt}\right) = mc^2 \frac{dt}{d\tau} \left(1 + \chi t \frac{d\chi}{dt}\right). \tag{22}$$

From (18), one obtains, for any physical object, the inequality

$$t \left| \frac{d\chi}{dt} \right| \leq 1. \tag{23}$$

Thus, a particle can have negative energy only for $\chi > 1$, i.e., out of the static limit, if

$$\frac{d\chi}{dt} < -\frac{1}{\chi t}. \tag{24}$$

Note that the components of metric (21) depend on time and the energy (22) in general is not conserved on the geodesics. If the energy is zero, then the particle is moving noninertial according to the law

$$\frac{d\chi}{dt} = -\frac{1}{\chi t} \Leftrightarrow \chi = \sqrt{\chi_0^2 - 2 \log(t/t_0)}, \quad t \in [t_0, t_0 \exp((\chi_0^2 - 1)/2)]. \tag{25}$$

The trajectory of such movement for case $\chi_0 = 2, t_0 = 0.11$ is represented by the curve in Figure 2 in coordinates T, r (see (19)).

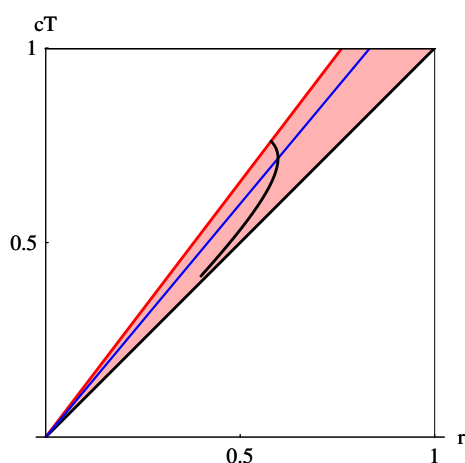


Figure 2. Possible region of movement of particle with negative and zero energies in the reference frame t, D in flat coordinate T, r .

In the event that the inertial movement trajectory in these coordinates is a straight line, the possible region of movement of particles with negative and zero energies in the reference frame t, D is defined in the coordinate T, r by conditions $1 \leq cT/r \leq \coth 1 \approx 1.313$.

Velocities of movement in coordinates T, r and t, χ satisfy condition [19]

$$t \frac{d\chi}{dt} = \frac{\frac{dr}{dT} - c \tanh \chi}{c - \frac{dr}{dT} \tanh \chi}. \tag{26}$$

Thus, for

$$\chi \tanh \chi \geq 1 \tag{27}$$

particles at rest in inertial frame T, r will have negative energies in the frame t, D . This region can be seen in Figure 2 as the region above the blue line in the red district. Zero energy of the particle at rest in T, r coordinates is possible only if the blue line is defined by the root of equation $\chi \tanh \chi = 1$, i.e., $\chi \approx 1.1997$.

Thus, one can see that for a specific choice of coordinates, one can obtain negative and zero energies for particles at rest in an inertial frame.

Note that for small distances ($D/(ct) = \chi \ll 1$), the metric (21) becomes the metric of a comoving spherical coordinate system of Minkowski space–time

$$ds^2 = c^2 dt^2 - dD^2 - D^2 d\Omega^2, \tag{28}$$

and the energy (22) will be equal to the usual energy in the inertial system of flat space–time

$$E_u = mc^2 \frac{dt}{d\tau} \approx mc^2 \frac{dT}{d\tau}, \tag{29}$$

because, for $\chi \ll 1$, one has $t \approx T$.

The decay of the body on two bodies, one with negative energy and the other with the positive energy being larger than the energy of the initial decaying one, corresponds to the Penrose process. This process occurs outside the static limit on distance $D > ct$. However, later, these two products of the decay move inside the static limit, and, during flight in the direction of the origin, where the metric is that of Minkowski space, they change their energies in such a manner that the result will be the same as in the inertial frame. In fact, due to (22)

$$E = E_u + mc^2 \chi t \frac{d\chi}{d\tau}. \tag{30}$$

Here, E_u is the energy in the reference frame t, χ , such that $g_{0i} = 0, i \neq 0$, and g_{00} does not depend on time. Thus, E_u is conserved. At the point of decay, both energies E and E_u are conserved. When body 2 with the positive energy arrives at the coordinate origin $\chi = 0$, its energy E (30) will be equal to E_u and no growth in the energy will be observed.

Body 1, with the negative energy E due to (22) after decay, will have a negative value of velocity $d\chi/dt$ larger (in absolute value) than that of body 2. This means that it will arrive at the origin before the arrival of body 2. Its energy in the origin of the coordinate frame will be also positive and the full energy of 1 and 2 will be equal to that of the decaying body. Thus, at the origin, one will not observe any effect that makes this situation similar to the situation for Kerr’s black hole.

In fact, for rotating black hole [1], as in the case of rotating coordinate system [4], the energy is conserved. In this case, when body 2 travels out of the ergosphere, far from it, body 1, with negative energy, moves further inside the horizon of the black hole or goes to infinity in case of rotating coordinates in Minkowski space. Thus, the energy of the body with positive energy, due to the conservation of the energy, will be always larger than that of the initial decaying body.

Note that the existence of states with negative energies for Milne’s metric leads to an effect similar to the Hawking effect [14] for the Schwarzschild metric. Particle creation in quantum theory will occur and the detector of particles checks them (see Section 5.3 in [20]).

This will be the creation of virtual particles (see Section 9.8 in [21]) so no change in the metric due to them can be observed.

4. Negative Energy in Gödel Universe

The metric of the Gödel cosmological model of the rotating Universe proposed in 1949 (see [22] or [23]) can be written as

$$ds^2 = c^2 dt^2 - dx_1^2 + \frac{\exp(2\sqrt{2}\omega x_1/c)}{2} dx_2^2 + 2 \exp(\sqrt{2}\omega x_1/c) c dt dx_2 - dx_3^2, \tag{31}$$

where ω is constant. Such a metric is the exact solution of Einstein’s equation with background matter as an ideal liquid without pressure and negative cosmological constant Λ

$$R_{ik} - \frac{1}{2} R g_{ik} + \Lambda g_{ik} = -8\pi \frac{G}{c^4} T_{ik}, \tag{32}$$

where

$$-\Lambda = \left(\frac{\omega}{c}\right)^2 = 4\pi \frac{G}{c^2} \rho, \quad T_{ik} = \rho c^2 u_i u_k, \tag{33}$$

$u^i = \delta_0^i$. Here, ω has the sense of the angular velocity of rotation of the vector of fluid of the background matter u^i .

Taking, instead of t, x_1, x_2 , new coordinates t', r, ϕ ,

$$\exp(\sqrt{2}\omega x_1/c) = \cosh 2r + \cos \phi \sinh 2r, \tag{34}$$

$$\omega x_2 \exp(\sqrt{2}\omega x_1/c) = \sin \phi \sinh 2r, \tag{35}$$

$$\tan \frac{1}{2} (\phi + \omega t - \sqrt{2}t') = \exp(-2r) \tan \frac{\phi}{2}, \tag{36}$$

one writes the interval (31) in the form [22,24]

$$ds^2 = 2\left(\frac{c}{\omega}\right)^2 (dt'^2 - dr^2 + (\sinh^4 r - \sinh^2 r) d\phi^2 + 2\sqrt{2} \sinh^2 r d\phi dt') - dx_3^2, \tag{37}$$

where $-\infty < t' < \infty, 0 \leq r < \infty, 0 \leq \phi < 2\pi$ and identifying $\phi = 0$ and $\phi = 2\pi$.

Now, consider the general case of space-time t', r, ϕ, z with the interval

$$ds^2 = a^2 [(dt' + \Phi(r) d\phi)^2 - dr^2 - dz^2 - R^2(r) d\phi^2], \tag{38}$$

where a is constant, $-\infty < t < \infty, 0 \leq r < \infty, -\infty < z < \infty, 0 \leq \phi \leq 2\pi$, and identifying $\phi = 0$ and $\phi = 2\pi$. Let us say $\Phi(r) > 0$ and $R(r) > 0$ for $r > 0$. For Gödel Universe $a = \sqrt{2}c/\omega, z = x_3/a$ and

$$\Phi(r) = \sqrt{2} \sinh^2 r, \quad R(r) = \sinh r \cosh r. \tag{39}$$

The metrical tensor is

$$(g_{ik}) = a^2 \begin{pmatrix} 1 & \Phi & 0 & 0 \\ \Phi & \Phi^2 - R^2 & 0 & 0 \\ 0 & 0 & -1 & 0 \\ 0 & 0 & 0 & -1 \end{pmatrix}, \tag{40}$$

$$(g^{ik}) = \frac{1}{a^2 R^2(r)} \begin{pmatrix} R^2 - \Phi^2 & \Phi & 0 & 0 \\ \Phi & -1 & 0 & 0 \\ 0 & 0 & -R^2 & 0 \\ 0 & 0 & 0 & -R^2 \end{pmatrix}, \tag{41}$$

where indexes $i, k = 0, 1, 2, 3$ correspond to t', ϕ, r, z . Note that for any $r > 0$, the metrical tensor is not degenerate $\det(g_{ik}) = -a^8 R^2(r) < 0$. The degeneration for $r = 0$ in the Gödel Universe is coordinate degeneracy. The eigenvalues of the g_{ik} tensor are

$$\begin{aligned} \lambda_{1,2} &= \frac{a^2}{2} \left(\Phi^2 - R^2 + 1 \pm \sqrt{(\Phi^2 - R^2 + 1)^2 + 4R^2} \right), \\ \lambda_{3,4} &= -a^2. \end{aligned} \tag{42}$$

For $r > 0$, one has

$$\lambda_1 \geq a^2, \quad 0 > \lambda_2 \geq -a^2 R^2. \tag{43}$$

Note that although $g_{\phi\phi}$ is positive for $\Phi(r) > R(r)$, the signature of g_{ik} for all $r > 0$ is the standard $(+, -, -, -)$.

Possible movement of particles is defined by $ds^2 \geq 0$, so, for the interval (38), one has

$$dt'^2 + (\Phi^2(r) - R^2(r))d\phi^2 + 2\Phi(r)d\phi dt' - dr^2 - dz^2 \geq 0. \tag{44}$$

It is important that for any coordinate system with interval (38), the physical body for any values of r, ϕ, z can be at rest, i.e., there is no static limit. However, in (38), there is nondiagonal term $dt'd\phi$ as in Kerr's metric. However, differently from the case of rotating coordinate system [3], there is the possibility of a change in the sign before $d\phi^2$.

From (44), one obtains

$$\left(\frac{dt'}{d\phi}\right)^2 + 2\Phi(r)\frac{dt'}{d\phi} + \Phi^2(r) - R^2(r) \geq 0. \tag{45}$$

The solution of this inequality is the union of two intervals

$$\frac{dt'}{d\phi} \in (-\infty, -(\Phi(r) + R(r))] \cup [R(r) - \Phi(r), +\infty). \tag{46}$$

Considering cases of different signs of $d\phi$, one obtains the following sets of solutions of (45):

$$d\phi \geq 0 \Rightarrow dt' \geq (R - \Phi)d\phi \vee dt' \leq -(R + \Phi)d\phi, \tag{47}$$

$$d\phi \leq 0 \Rightarrow dt' \geq -(R + \Phi)d\phi \vee dt' \leq (R - \Phi)d\phi. \tag{48}$$

These sets define light "cones" of the future and past for the metric (38). The form of these cones in cases $\Phi \ll R, \Phi = R$ and $\Phi > R$ is shown in Figure 3 for the Gödel Universe with

$$\Phi(r) > R(r) \Leftrightarrow r > r_0 = \log(1 + \sqrt{2}). \tag{49}$$

Let us find limitations on possible values of the energy of particles moving in such a Universe. The coordinate t' is dimensionless, so the "physical energy" of the particle is expressed through the time component of the momentum as

$$E = p_0 \frac{c}{a} = g_{0k} \frac{c}{a} \frac{dx^k}{d\lambda}. \tag{50}$$

For the frame with coordinates (38), the covariant t', ϕ, z components are conserved, because the components of the metric depend only on r . Thus, the conserved energy on the geodesic for the interval (38) is

$$E = ca \left(\frac{dt'}{d\lambda} + \Phi(r) \frac{d\phi}{d\lambda} \right). \tag{51}$$

From (47) and (48), for the case of movement “forward” in time, i.e., in the future light cone, one obtains

$$dt' + \Phi d\phi \geq R|d\phi|, \tag{52}$$

so

$$E \geq caR \frac{|d\phi|}{d\lambda}. \tag{53}$$

It means that for a particle moving in the future cone in the Gödel Universe, the energy is not negative.

For movement “back in time”, the energy is limited from above by

$$E \leq -caR \frac{|d\phi|}{d\lambda} \tag{54}$$

and so it can be less than or equal to zero. However, such movement physically is inconsistent. The “time machine” effect in the Gödel Universe corresponds to continuous movement in the future cone. Thus, for $r > r_0$, where $\Phi(r) > R(r)$ closed loops (they are not geodesic lines) $r = \text{const}, z = \text{const}$, called Gödel cycles, from $\phi = 0$ to $\phi = 2\pi$, are closed time-like curves [24]. Particles moving along such a cycle are moving “forward” in time but, due to the identification of values ϕ different on 2π , it occurs in the past after the whole cycle. Its energy is positive due to (53). Such a “time machine” is different from that moving in the past by the sign of the particle energy.

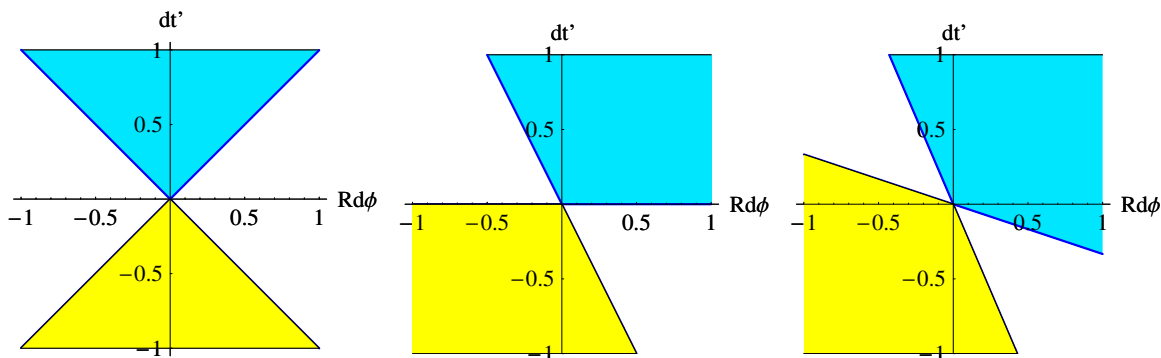


Figure 3. Light “cones” of future (blue color) and past (yellow color) for Gödel Universe in coordinates t', ϕ for cases $r = 10^{-3}$ (left), $r = r_0$ (center) and $r = 2r_0$ (right).

5. Conclusions

Three different cases are investigated concerning the possibility of the existence of particles with negative and zero energies.

1. Schwarzschild black hole of the mass M . Trajectories of particles with negative and zero energies exist inside the horizon of the black hole, which can be shown in Kruskal–Szekeres coordinates.
2. Flat space–time in Milne’s coordinates. Here, one also has the possibility of the existence of particles with negative and zero energies if a nonsynchronous system of coordinates is used.
3. Gödel cosmological model with rotation. Here, we proved that, in this model, in Gödel’s coordinates, particles with negative and zero energies do not exist.

As for observations of the discussed effects, one can say that even the well-established Penrose and Hawking effects are still not observed. However, we hope that in the future

development of observational astrophysics, one will see the consequences of the existence of negative and zero energies.

Author Contributions: A.A.G. and Y.V.P. have contributed equally to all parts of this work. All authors have read and agreed to the published version of the manuscript.

Funding: This research is supported by the Russian Science Foundation (Grant No. 22-22-00112).

Conflicts of Interest: The authors declare no conflict of interest.

References

1. Penrose, R. Gravitational collapse: The role of general relativity. *Riv. Nuovo C.* **1969**, *1*, 252–276.
2. Penrose, R.; Floyd, R.M. Extraction of rotational energy from a black hole. *Nat. Phys. Sci.* **1971**, *229*, 177–179. [CrossRef]
3. Grib, A.A.; Pavlov, Y.V. Comparison of particle properties in Kerr metric and in rotating coordinates. *Gen. Relativ. Gravit.* **2017**, *49*, 78. [CrossRef]
4. Grib, A.A.; Pavlov, Y.V. Static limit and Penrose effect in rotating reference frames. *Theor. Math. Phys.* **2019**, *200*, 1117–1125. [CrossRef]
5. Grib, A.A.; Pavlov, Y.V. Particle properties outside of the static limit in cosmology. *Int. J. Mod. Phys. A* **2020**, *35*, 2040044. [CrossRef]
6. Grib, A.A.; Pavlov, Y.V. Particles with negative energies in nonrelativistic and relativistic cases. *Symmetry* **2020**, *12*, 528. [CrossRef]
7. Misner, C.W.; Thorne, K.S.; Wheeler, J.A. *Gravitation*; Freeman: San Francisco, CA, USA, 1973.
8. Chandrasekhar, S. *The Mathematical Theory of Black Holes*; Oxford University Press: Oxford, UK, 1983.
9. Grib, A.A.; Pavlov, Y.V. Particles with negative energies in black holes. *Int. J. Mod. Phys. D* **2011**, *20*, 675–684. [CrossRef]
10. Landau, L.D.; Lifshitz, E.M. *The Classical Theory of Fields*; Pergamon Press: Oxford, UK, 1983.
11. Toporensky, A.V.; Zaslavskii, O.B. Zero-momentum trajectories inside a black hole and high energy particle collisions. *JCAP* **2019**, *12*, 063. [CrossRef]
12. Augousti, A.T.; Gusin, P.; Kuśmierz, B.; Masajada, J.; Radosz, A. On the speed of a test particle inside the Schwarzschild event horizon and other kinds of black holes. *Gen. Relativ. Gravit.* **2018**, *50*, 131. [CrossRef]
13. Radosz, A.; Gusin, P.; Augousti, A.T.; Formalik, F. Inside spherically symmetric black holes or how a uniformly accelerated particle may slow down. *Eur. Phys. J. C* **2019**, *79*, 876. [CrossRef]
14. Hawking, S.W. Particle creation by black holes. *Commun. Math. Phys.* **1975**, *43*, 199–220. [CrossRef]
15. Lightman, A.P.; Press, W.H.; Price, R.H.; Teukolsky, S.A. *Problem Book in Relativity and Gravitation*; Princeton University Press: Princeton, NJ, USA, 1979.
16. Milne, E.A. *Relativity, Gravitation and World-Structure*; Clarendon Press: Oxford, UK, 1935.
17. Ellis, G.F.R.; Rothman, T. Lost horizons. *Am. J. Phys.* **1993**, *61*, 883–893. [CrossRef]
18. Boyer, R.H.; Lindquist, R.W. Maximal analytic extension of the Kerr metric. *J. Math. Phys.* **1967**, *8*, 265–281. [CrossRef]
19. Grib, A.A.; Pavlov, Y.V. Some properties of energies in nonsynchronous reference frames in cosmology. *J. Phys. Conf. Ser.* **2021**, *2081*, 012004. [CrossRef]
20. Birrell, N.D.; Davies, P.C.W. *Quantum Fields in Curved Space*; Cambridge University Press: Cambridge, UK, 1982.
21. Grib, A.A.; Mamayev, S.G.; Mostepanenko, V.M. *Vacuum Quantum Effects in Strong Fields*; Friedmann Laboratory Publishing: St. Petersburg, Russia, 1994.
22. Gödel, K. An example of a new type of cosmological solutions of Einstein's field equations of gravitation. *Rev. Mod. Phys.* **1949**, *21*, 447–450. [CrossRef]
23. Gödel, K. *Collected Works. Volume II. Publications 1938–1974: Editor-in-chief Solomon Feferman*; Oxford University Press: Oxford, UK, 1990; Volume 2, p. 190.
24. Hawking, S.W.; Ellis, G.F.R. *The Large Scale Structure of Space-Time*; Cambridge University Press: Cambridge, UK, 1973.

Disclaimer/Publisher's Note: The statements, opinions and data contained in all publications are solely those of the individual author(s) and contributor(s) and not of MDPI and/or the editor(s). MDPI and/or the editor(s) disclaim responsibility for any injury to people or property resulting from any ideas, methods, instructions or products referred to in the content.

Possible Wormholes in a Friedmann Universe

Kirill A. Bronnikov ^{1,2,3,*} , Pavel E. Kashargin ⁴ and Sergey V. Sushkov ⁴ 

¹ Center of Gravitation and Fundamental Metrology, VNIIMS, Ozyornaya St. 46, Moscow 119361, Russia

² Institute of Gravitation and Cosmology, Peoples' Friendship University of Russia (RUDN University), Miklukho-Maklaya 6, Moscow 117198, Russia

³ Elementary Particle Physics Department, National Research Nuclear University "MEPhI", Kashirskoe Shosse 31, Moscow 115409, Russia

⁴ Institute of Physics, Kazan Federal University, Kremliovskaya St. 16a, Kazan 420008, Russia; pkashargin@mail.ru (P.E.K.); sergey_sushkov@mail.ru (S.V.S.)

* Correspondence: kb20@yandex.ru

Abstract: We study the properties of evolving wormholes able to exist in a closed Friedmann dust-filled universe and described by a particular branch of the well-known Lemaître–Tolman–Bondi solution to the Einstein equations and its generalization with a nonzero cosmological constant and an electromagnetic field. Most of the results are obtained with pure dust solutions. It is shown, in particular, that the lifetime of wormhole throats is much shorter than that of the whole wormhole region in the universe (which coincides with the lifetime of the universe as a whole), and that the density of matter near the boundary of the wormhole region is a few times smaller than the mean density of matter in the universe. Explicit examples of wormhole solutions and the corresponding numerical estimates are presented. The traversability of the wormhole under study is shown by a numerical analysis of radial null geodesics.

Keywords: wormholes; Friedmann universe; Tolman's solution; dustlike matter; general relativity



Citation: Bronnikov, K.A.; Kashargin, P.E.; Sushkov, S.V. Possible Wormholes in a Friedmann Universe. *Universe* **2023**, *9*, 465. <https://doi.org/10.3390/universe9110465>

Academic Editors: Galina L. Klimchitskaya and Vladimir M. Mostepanenko

Received: 20 September 2023
Revised: 23 October 2023
Accepted: 26 October 2023
Published: 29 October 2023



Copyright: © 2023 by the authors. Licensee MDPI, Basel, Switzerland. This article is an open access article distributed under the terms and conditions of the Creative Commons Attribution (CC BY) license (<https://creativecommons.org/licenses/by/4.0/>).

1. Introduction

A century ago, Alexander Friedmann obtained his famous models of the expanding universe [1] that amazingly remain quite relevant nowadays, after all these years of active development of the theory, experiment and observations. We are happy to submit our contribution to the journal issue dedicated to this centennial anniversary, where we discuss how a Friedmann universe may be a home for such a hypothetic and exotic kind of geometry, whose studies also possess a long and rich history, as are wormholes.

A wormhole is one of the types of strongly curved geometries, the geometry resembling a spatial tunnel between either distant regions of the same universe or different universes. Such spatial geometries within solutions to the gravitational field equations were first discussed in [2–5], but those wormholes turned out to be not traversable for subluminal particles and even photons, which were thus unable to travel from one “end of the tunnel” to the other, to say nothing on their ability to return back. The first exact solutions describing traversable wormholes seem to have appeared in [6,7] in 1973 in the framework of general relativity (GR) with a massless phantom scalar field (a hypothetic field with a wrong sign of kinetic energy) as a source. An evolving version of such scalar-vacuum solutions was also found [8], as well as examples of higher-dimensional static wormhole solutions [9,10]. Great interest in these objects has been raised by the paper of Morris and Thorne [11] (1988) who showed that a static wormhole throat considered in the framework of GR requires the existence of so-called “exotic” matter, violating the null energy condition (NEC). A phantom scalar field is a simple example of such matter.

By now, wormholes have been considered in different theories of gravity and in the presence of different kinds of matter. Thus, in [6] static, spherically symmetric wormhole solutions are presented both in GR and a class of scalar-tensor theories, with or without

an electromagnetic field. Wormholes in the Einstein–Maxwell-dilaton theory have been described in [12–15]. Other sources in GR used for wormhole construction include a Chaplygin gas [16] and various versions of phantom energy and quintessence, in particular, those with the stress–energy tensor (SET) of a perfect fluid [17–23]. It was shown [23] that static, spherically symmetric wormholes with two flat or AdS asymptotic regions are impossible in GR with any source possessing isotropic pressure, and, as a result, perfect-fluid wormholes can only contain their source in a bounded region of space surrounded by vacuum, with a thin shell on the boundary. It should also be mentioned that many authors consider wormhole models built using thin shells of exotic matter as the only (or main) source, the first of them being probably [24,25]. In [26,27], examples of static traversable wormholes are given in Einstein–Dirac–Maxwell theory, being obtained without explicitly introducing exotic matter, which means that the Dirac spinor fields themselves exhibit exotic properties [28].

The necessity of exotic matter is a basic problem of wormhole physics, at least in the case of static configurations in GR [11,29] and a broad class of scalar-tensor theories of gravity and $f(R)$ theories [30]. It is therefore natural that many authors try to replace such matter with entities appearing in various extensions of GR, and above all, it concerns static, spherically symmetric configurations. Thus, such wormhole solutions of asymptotically safe gravity were recently discussed in [31]. In brane world gravity, it has been shown that the role of exotic matter may be played by the so-called tidal contribution to the effective SET due to the influence of the bulk [32], with a number of particular examples. In Ref. [33], the most general constraints have been obtained on additional terms inherent to various modified theories of gravity, including geometric modifications, such that wormhole geometries could be constructed in such theories without exotic matter. In [34,35], particular wormhole solutions of $f(R, T)$ gravity (T being the trace of the stress–energy tensor) and some teleparallel gravity theories, respectively, were discussed, not only concerning the validity of the energy conditions, but also as a description of possible objects in galactic dark energy halos.

It turns out that rotational degrees of freedom may in principle replace exotic matter for wormhole construction. Thus, some examples of rotating cylindrically symmetric wormhole models without NEC violation have been built in the framework of GR [36–38]. The recently found static solutions [26,27] involve Dirac fields with a spin; one can also recall wormhole solutions in the Einstein–Cartan theory [39] containing no exotic matter but a nonzero torsion. Stationary rotating wormhole models with axial symmetry in GR have also been obtained [40–43]; however, the NEC is still violated in these models of rotating wormholes.

Dynamic wormholes can also exist without NEC violation, at least in a finite time interval, in configurations without static early-time or late-time asymptotic behavior. Such wormhole models in GR with cosmological-type metrics are known, being supported by electromagnetic fields described by some particular examples of nonlinear electrodynamics [44,45]. A number of dynamic wormhole models [20,46–50] were obtained by adding a time-dependent scale factor to an otherwise static metric; some others used the thin shell formalism [51]. A family of dynamic wormhole solutions to the Einstein–Maxwell-scalar equations was obtained in [52]. General properties of arbitrary dynamic wormholes are discussed in [53–55].

Overviews of various problems of wormhole physics can be found, for example, in [56,57]; see also the recent special issue of the *Universe* journal [58].

In this paper, we continue our study of possible traversable wormholes in GR sourced by such a classical and nonexotic source as dustlike matter, with or without an electromagnetic field [59,60]. For electrically neutral dust, the general dynamic spherically symmetric solution of GR was obtained by Lemaître and Tolman in 1933–1934 [61,62] and later studied by Bondi [63–66]. It is generally called the Tolman or LTB solution. The first attempt to construct a wormhole by selecting a special form of arbitrary functions in this solution was made in [59].

An extension of the LTB solution including a radial electromagnetic field was discussed in [67–72] (see also references therein), where a complete solution was achieved under some additional conditions, while in the general case, relevant integrals of the Einstein–Maxwell equations were obtained and discussed. For arbitrary electric charge distributions and arbitrary initial data, the problem was solved by Pavlov [73], and the solutions were further studied in [74]; a further extension to plane and hyperbolic symmetries of space-time were considered in [75–77]; see also references therein.

In the present study, we only consider configurations with an external magnetic (or electric) fields and electrically neutral dust; however, if there is a wormhole, its every entrance can comprise a “charge without charge” [4,5] due to electric or magnetic lines of force threading the throat. Similar models with a special choice of initial data were studied in [78,79], while here, we do not restrict the initial data but consider the possible existence of such wormholes in the cosmological context, being inscribed in Friedmann models describing a matter-dominated stage of evolution, with the possible inclusion of a cosmological constant, which then describes dark energy.

Concerning dynamic wormholes, it is necessary to recall that there are different definitions of dynamic wormhole throats, which coincide with each other for static space-times; see, e.g., [53–55,80–82]. Following papers [46–48], we here choose the simplest definition based on the properties of 3-geometry of spatial sections of space-time. This definition can in general be ambiguous due to the freedom of choosing such spatial sections (or clock synchronization), but in the problem under consideration, it looks most natural and intuitively clear.

The paper is organized as follows. In Section 2, we briefly describe the class of solutions to be studied. In Section 3, we consider the conditions for possible existence of throats and traversable wormholes. Section 4 describes a particular family of wormhole solutions with a wide enough range of parameters, to be used in Section 5 for placing them in the cosmological context. The corresponding numerical estimates are obtained in Section 6, indicating the possible existence and observable properties of such wormholes in our universe. Section 7 is a conclusion.

2. Extended LTB Solution

Let us consider a generalization of the original LTB solution [61–63], describing the dynamics of a spherically symmetric distribution of electrically neutral dustlike matter in the presence of an external (global) electric or magnetic field and a cosmological constant. Let us, for certainty, speak of a magnetic field that looks more realistic astrophysically, keeping in mind that any further results can be easily reinterpreted in terms of an electric field.

If we choose a reference frame comoving to neutral dust particles, it is consequently a geodesic reference frame for them, and the metric can be written in the synchronous form (see, e.g., [65])

$$ds^2 = d\tau^2 - e^{2\lambda(R,\tau)} dR^2 - r^2(R,\tau) d\Omega^2, \tag{1}$$

where τ is the proper time along the particle trajectories labeled by different values of the radial coordinate R , $\lambda(R, \tau)$ and $r(R, \tau)$ are functions of τ and R .

The SET of dustlike matter reads $T_\mu^{v[d]} = \rho u_\mu u^\nu$, where ρ is the energy density and u^ν the velocity four-vector. The only nonzero component of this SET in the comoving reference frame, where $(u^\nu) = (1, 0, 0, 0)$, is $T_0^{0[d]} = \rho$. For the electromagnetic field in the metric (1), the SET has the form

$$T_\mu^{v[em]} = \frac{q^2}{8\pi G r^4} \text{diag}(1, 1, -1, -1), \tag{2}$$

where q can be interpreted as an electric or magnetic charge in suitable units [83,84].

Nontrivial components of the Einstein equations with a cosmological constant Λ may be written as

$$1 + 2r\ddot{r} + \dot{r}^2 - e^{-2\lambda}r'^2 = \frac{q^2}{r^2} + \Lambda r^2, \tag{3}$$

$$1 + \dot{r}^2 + 2r\dot{r}\dot{\lambda} - e^{-2\lambda}(2rr'' + r'^2 - 2rr'\lambda') = 8\pi G\rho r^2 + \frac{q^2}{r^2} + \Lambda r^2, \tag{4}$$

$$\dot{r}' - \dot{\lambda}r' = 0, \tag{5}$$

where the dot stands for ∂/dt and the prime for ∂/dR . The conservation law for dust matter, $\nabla_\nu T_0^{[\nu d]} = 0 \Rightarrow \dot{\rho} + \rho(\dot{\lambda} + 2\dot{r}/r) = 0$, leads to

$$\rho = \frac{1}{8\pi G} \frac{F'(R)}{r^2 r'} \iff F(R) = 8\pi G \int \rho r^2 r' dR, \tag{6}$$

where $F(R)$ is an arbitrary function, which according to (6) may be said to describe the initial mass distribution. On the other hand, Equation (5) is readily integrated in τ with the result

$$e^{2\lambda} = \frac{r'^2}{1 + f(R)}, \tag{7}$$

where $f(R) > -1$ is one more arbitrary function. With (7), Equation (3) is rewritten as

$$2r\ddot{r} + \dot{r}^2 = f(R) + \frac{q^2}{r^2} + \Lambda r^2, \tag{8}$$

and its first integral is

$$\dot{r}^2 = f(R) + \frac{F(R)}{r} - \frac{q^2}{r^2} + \frac{\Lambda}{3}r^2, \tag{9}$$

where (as can be easily verified) the function $F(R)$ is the same as in Equation (6). This expression reveals the physical meaning of $f(R)$ as a function characterizing the initial radial velocity (\dot{r}) distribution of dust particles. Furthermore, if $\Lambda = 0$, only under the condition $f \geq 0$ can the particle reach large values of r , so that $f > 0$ and $f = 0$ correspond to hyperbolic and parabolic type of motion, respectively. In the case $f(R) < 0$ (elliptic motion), the particle can at most reach a radius corresponding to the condition $\dot{r} = 0$ in Equation (9). With $\Lambda \neq 0$, things are more involved, and the boundary of finite motion is shifted.

Further integration of Equation (9) with $\Lambda \neq 0$ leads to elliptic integrals. In what follows, for simplicity, we assume $\Lambda = 0$, so that only elementary functions are necessary to describe the solution (to be called for brevity the q-LTB solution). Also, in what follows we will only need the description of elliptic motion, $f < 0$. In this case, integration of Equation (9) gives

$$\pm[\tau - \tau_0(R)] = \frac{1}{h} \sqrt{-hr^2 + Fr - q^2} + \frac{F}{2h^{3/2}} \arcsin \frac{F - 2hr}{\sqrt{F^2 - 4hq^2}}, \tag{10}$$

where $h(R) := -f(R) > 0$, and $\tau_0(R)$ is one more arbitrary function that corresponds to a choice of spatial sections of our space-time, or, in other words, to clock synchronization between different dust layers with fixed values of R (Lagrangian spheres). It is easy to see that elliptic motion is possible only with $F^2 - 4hq^2 \geq 0$.

For the solution (10), there is a convenient parametric representation (see, e.g., [65,79]),

$$r = \frac{F}{2h}(1 - \Delta \cos \eta),$$

$$\pm[\tau - \tau_0] = \frac{F}{2h^{3/2}}(\eta - \Delta \sin \eta), \quad \Delta = \sqrt{1 - \frac{4hq^2}{F^2}}, \tag{11}$$

where $0 < \Delta \leq 1$, and $\Delta = 1$ corresponds to the original LTB solution without an electromagnetic field. Notably, if $q \neq 0$, hence $\Delta < 1$, the model has no singularities characterized by $r = 0$, i.e. shrinking of a Lagrangian sphere to a point. Other kinds of singularities, called shell-crossing or shell-sticking singularities, and characterized by $r' = 0$ while $F' \neq 0$ (see (6) and (18)), are not excluded.

An important special case of the LTB solution ($q = 0, \Delta = 1$) is Friedmann’s closed isotropic cosmological model with dust matter, which corresponds to the following choice of arbitrary functions [65]:

$$F(\chi) = 2a_0 \sin^3 \chi, \quad h(\chi) = \sin^2 \chi, \quad a_0 = \text{const} \tag{12}$$

(here, the radial coordinate $R = \chi$ is a “radial angle” on a 3D sphere), so that

$$r = r(\eta, \chi) = a(\eta) \sin \chi, \quad a(\eta) = a_0(1 - \cos \eta), \quad \tau = a_0(\eta - \sin \eta), \tag{13}$$

where $a(\eta)$ is the cosmological scale factor, and it is taken $\tau_0 = 0$.

3. Possible Throats

As is clear from (6), to keep the density positive, it is necessary to require $F'/r' > 0$, but it does not mean that both $F' > 0$ and $r' > 0$. Therefore, one can admit the existence of regular maximum or minimum values of r (at fixed τ), which can be interpreted as equators and throats, respectively.

As already mentioned, among different definitions of a wormhole throat in dynamic space-times, we choose the definition [46–48] according to which a throat in a space-time with the metric (1) is a regular minimum of the spherical radius $r(R, \tau)$ at a fixed value of τ (hence, a fixed spatial section of space-time). Then, as always, a wormhole is understood as a space-time region that contains a throat and extends to sufficiently large $r(R, \tau)$ on both sides from this throat. Further on, we try to build wormhole configurations based on the q-LTB solution. To carry this out, let us first of all determine the conditions characterizing a wormhole throat [60].

The 3D spatial metric of a spatial section $\tau = \text{const}$ is

$$dl_{(3)}^2 = \frac{r'^2 dR^2}{1 + f(R)} + r^2(R) d\Omega^2. \tag{14}$$

where $r(R) = r(R, \tau)|_{\tau=\text{const}}$ and the coordinate R is still arbitrary. To formulate the throat conditions, let us choose the manifestly admissible Gaussian coordinate l , measuring length in the radial direction, such that $dl = |g_{RR}|^{1/2} dR$. Then, at a throat, we must have

$$\frac{dr}{dl} = 0, \quad \frac{d^2r}{dl^2} > 0 \tag{15}$$

(for a generic minimum of r , ignoring possible high-order ones, with $d^2r/dl^2 = 0$). From the first condition, it follows that on the throat, $R = R_{\text{th}}$,

$$\frac{dr}{dl} = \sqrt{1 + f(R_{\text{th}})} = 0 \Rightarrow f(R_{\text{th}}) = -1, \quad \text{or} \quad h(R_{\text{th}}) = 1. \tag{16}$$

Thus, it is clear that only elliptic models (10) are compatible with wormhole existence. Next, to keep the metric (1) nondegenerate, it must be in general $1 + f = 1 - h > 0$, while $h = 1$ is only admissible at a particular value of R ; therefore, $R = R_{\text{th}}$ should be a maximum of $h(R)$, such that $h'(R_{\text{th}}) = 0$ and $h''(R_{\text{th}}) < 0$. Then, the second condition (15) implies

$$\left. \frac{d^2r}{dl^2} \right|_{R=R_{\text{th}}} = - \left. \frac{h'}{2r'} \right|_{R=R_{\text{th}}} > 0. \tag{17}$$

Thus, $h'(R)$ vanishes at $R = R_{th}$ together with $r'(R)$, with a finite limit of their ratio. The conditions (16) and (17) lead to restrictions on the arbitrary functions $F(R)$ and $h(R)$.

As follows from (6), the dust density tends to infinity, thus indicating a singularity, if either $r \rightarrow 0$ or $r' \rightarrow 0$, except for cases where both $r' \rightarrow 0$ and $F' \rightarrow 0$ at finite r , keeping finite the ratio F'/r' , precisely what happens at a wormhole throat. That the space-time remains regular under these circumstances can be confirmed by calculating the Kretschman scalar \mathcal{K} ,

$$\mathcal{K}(R, t) = 3\frac{F'^2}{r'^2r^4} - 8\frac{F'F}{r'r^5} + 12\frac{F^2}{r^6} + 20\frac{F'q^2}{r'r^6} - 48\frac{Fq^2}{r^7} + 56\frac{q^4}{r^8}. \tag{18}$$

Thus, at possible throats, all three derivatives— r' , F' , and h' —vanish, with finite limits of their ratios.

From (11), we obtain the following expression for the derivative r' on a constant- τ section of our space-time:

$$r' = \frac{Fh'N_1(R, \eta) + 2hF'N_2(R, \eta)}{4\Delta h^2(1 - \Delta \cos \eta)},$$

$$N_1(R, \eta) = \cos \eta - 3\Delta + 3\Delta^2(\eta \sin \eta + \cos \eta) + \Delta^3(-2 + \cos^2 \eta),$$

$$N_2(R, \eta) = -\cos \eta + 2\Delta - \Delta^2(\cos \eta + \eta \sin \eta). \tag{19}$$

At a throat $R = R_{th}$, the ratios F'/r' and h'/r' are finite and nonzero (though with different signs); r' , h' , and F' are small quantities of the same order of magnitude.

We can summarize the throat conditions as follows:

$$h = 1, \quad h' = 0, \quad h'' < 0,$$

$$F' = 0, \quad r' = 0, \quad \frac{h'}{r'} < 0, \quad \frac{F'}{r'} > 0. \tag{20}$$

Also, we have everywhere $F^2 - 4hq^2 > 0$ and $\Delta \leq 1$.

For further analysis, let us consider the limit $\lim_{R \rightarrow R_{th}} \frac{Fh'}{F'h} = -B$ such that $B = \text{const} \geq 0$.

Then, for r' near the throat, we obtain

$$r' \Big|_{R \rightarrow R_{th}} \approx \frac{F'(2N_2 - BN_1)}{4\Delta(1 - \Delta \cos \eta)} \tag{21}$$

It vanishes either if $F' = 0$ or if $N_* = 2N_2 - BN_1 = 0$. The density (6) on the throat is given by

$$\rho(R_{th}, \eta) = \frac{\Delta(1 - \Delta \cos \eta)}{2\pi Gr^2(2N_2 - BN_1)} \Big|_{R_{th}}, \tag{22}$$

and it blows up where $N_* = 2N_2 - BN_1 = 0$ while the other factors are positive ($F > 0$ by assumption). Meanwhile, N_* has different signs at the ends and the middle of the range of η :

$$N_* \Big|_{\eta=0, 2\pi} = -(1 - \Delta)^2[2 + B(1 - \Delta)] \leq 0,$$

$$N_* \Big|_{\eta=\pi} = (1 + \Delta)^2[2 + B(1 + \Delta)] > 0. \tag{23}$$

Therefore, we inevitably obtain $N_* = 0$, hence a singularity, at (at least) two values of η say, $\eta_1 < \pi$ and $\eta_2 > \pi$, for any $\Delta < 1$ ($q \neq 0$). These are so-called shell-crossing singularities forming due to $r' \rightarrow 0$, while r is finite.

In the case $q = 0, \Delta = 1$ (pure dust), we see that N_* vanishes at $\eta_{1,2} = 0, 2\pi$ and is positive at $\eta \in (0, 2\pi)$.

Thus a nonsingular evolution period for a throat $R = R_{th}$, with finite density $\rho > 0$, takes place at times $\eta_1 < \eta < \eta_2$ at which $N_* > 0$. For other Lagrangian spheres $R = \text{const}$, we obtain similar but other time limits due to R dependence of the functions F and h .

The above relations lead to general restrictions on the dust densities in the wormhole solutions. For example, consider the solution with $q = 0$ at $\eta = \pi$, that is, at maximum expansion. In this case, $r = F(R)/h(R)$, and $2N_2 = -N_1 = 8$, and according to (6), we obtain

$$\rho \Big|_{\eta=\pi} = \frac{1}{8\pi G} \frac{F'}{r^2 r'} = \frac{1}{8\pi G} \frac{F' h^4}{F^2 (F'h - Fh')} = \frac{h}{8\pi G r^2 ((1 - rh'/F'))}. \tag{24}$$

In all wormhole solutions, $h \leq 1$; furthermore, $h'/F' < 0$ near the throat, and let us suppose that this is also true at other values of R ($F' < 0$ at $r' > 0$ would give negative matter densities; while a changing sign of h' is still possible). Then, (24) leads to the simple inequality

$$\rho \leq \frac{1}{8\pi G r^2} \approx 6.8 \times 10^{26} \frac{\text{g}}{\text{cm}^3} \frac{\text{cm}^2}{r^2}. \tag{25}$$

For example, at the throat, we have $h = 1$ and $-rh'/F' = B > 0$. This inequality actually admits very large density values: thus, if the throat radius is 1 km, we have the restriction $\rho \lesssim 10^{16} \text{g/cm}^3$, a supernuclear density, which is hard to imagine with dustlike matter. We can also notice that the throat density values are diminished by large values of B .

4. A Particular Family of Wormhole Solutions

Let us select a family of LTB wormhole solutions, choosing the following simple functions of R in agreement with the requirements (20):

$$h(R) = \frac{1}{1 + R^2}, \quad F(R) = 2b(1 + R^2)^k, \quad \Rightarrow \quad \Delta = \sqrt{1 - \frac{q^2}{b^2(1 + R^2)^{2k+1}}}, \tag{26}$$

with the constants $b, k > 0$. This choice of $h(R)$ is made without loss of generality due to arbitrariness of the R coordinate (under the assumption that $h(R)$ behaves monotonically at $R > 0$ and $R < 0$), while the choice of $F(R)$ is significant. In particular, since both $h(R)$ and $F(R)$ are even functions, the wormhole is symmetric with respect to its throat $R = 0$. To describe a possible asymmetry while keeping the same form of $h(R)$, one can choose an asymmetric function $F(R)$ respecting the requirements (20), for example, replacing $1 + R^2$ in the expression for $F(R)$ with $1 + R^2 + \zeta R^3$, $\zeta = \text{const}$. Still, in what follows, we will only discuss the solutions determined by (26).

In (26), the constant b specifies a length scale, and we have

$$r(R, \eta) = b(1 + R^2)^{k+1} (1 - \Delta \cos \eta), \quad \tau - \tau_0(R) = b(1 + R^2)^{k+3/2} (\eta - \Delta \sin \eta), \tag{27}$$

$$r'(R, \eta) = \frac{bR(1 + R^2)^k (2kN_2 - N_1)}{\Delta(1 - \Delta \cos \eta)}, \tag{28}$$

with $N_{1,2}$ defined in Equation (19). The density ρ (6) and the quantity d^2r/dl^2 at $R = 0$ then read

$$\rho(R, \eta) = \frac{k\Delta}{2\pi G b^2 (1 + R^2)^{2k+3} (1 - \Delta \cos \eta) (2kN_2 - N_1)}, \tag{29}$$

$$\frac{d^2r}{dl^2} \Big|_{R=0} = \frac{\Delta(1 - \Delta \cos \eta)}{b(2kN_2 - N_1)} \Big|_{R=0}. \tag{30}$$

As already noted, different signs of the derivatives of $h(R)$ and $f(R)$, under the condition $2N_2(R, \eta) - N_1(R, \eta) > 0$, provide the fulfillment of the throat conditions (20) at $R = 0$ and, by continuity, in some its neighborhood, but the same is not guaranteed at all R and η .

The time dependence of the throat radius r_{th} and the density ρ_{th} on the throat were studied in [60]. Here, for completeness, we reproduce some figures from [60]. Thus, Figure 1 shows the time dependence of the throat radius, while the density ρ_{th} is shown in Figure 2 for $k = 1$ and different values of q , where dashed lines show the asymptotes of the function. Finite positive density values are observed for only a finite period of time $\eta \in (\eta_1, \eta_2)$ while $2N_2 - N_1 > 0$, between two singularities at which ρ and \mathcal{K} diverge. Outside this time interval, in the case $q \neq 0$, the matter density changes its sign along with d^2r/dl^2 , therefore the throat conditions hold together with the condition $\rho > 0$.

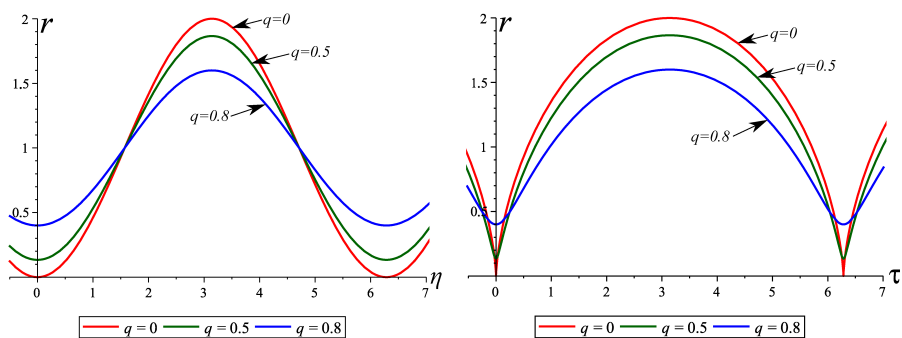


Figure 1. Time dependence of the throat radius for $q = 0, 0.5, 0.8$ in terms of η (left) and in terms of τ (right).

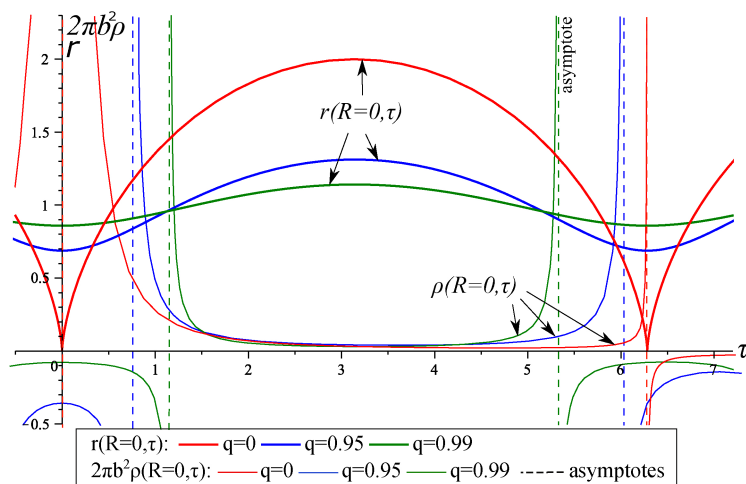


Figure 2. Time dependence of the functions $2\pi b^2\rho$ (thin lines) and $r(0, \tau)$ (thick lines) on the throat $R = 0$ for $q = 0, 0.95, 0.99$ in the model (26). Dashed lines show the asymptotes. For other values of q the plots look in a similar way.

Thus we observe a good wormhole behavior of our solution within the time interval $\eta \in (\eta_1, \eta_2)$. As the charge decreases, this interval increases; and at $q = 0$, we obtain $\eta_1 = 0, \eta_2 = 2\pi$. Outside the throat (at $R \neq 0$), the plots look almost the same, but the singularities occur at other time instants.

5. Matching to a Dust-Filled Friedmann Universe

5.1. General Observations

Now, let us look how the wormhole solution discussed above can be inscribed into the closed Friedmann isotropic space-time characterized by the relations (12) and (13). At

that, we can note [60] that to join two LTB space-time regions, characterized by different functions $F(R)$ and $h(R)$, at some hypersurface Σ corresponding to a fixed value of the radial coordinate $R = R^*$, one should first of all identify Σ as viewed from different sides. Hence, the metric tensor must be continuous on Σ . With the metric (1) it simply leads to $[r^2(R, \tau)] = 0$ (as usual, square brackets denote jumps when crossing the transition surface Σ), while by (1) $g_{\tau\tau} \equiv 1$ on both sides and does not lead to any further requirements.

Next, to avoid the emergence of a shell of matter on the junction surface Σ , according to the Darmois–Israel matching conditions [85,86], one should require continuity of the second quadratic form on Σ . When applied to the metric (1), this requirement leads to $[e^{-\lambda}g'_{\tau\tau}] = 0$ (which holds trivially due to $g_{\tau\tau} \equiv 1$) and $[e^{-\lambda}r'] = 0$. As a result, with (7) and (11), we obtain

$$[r] = 0, \quad [e^{-\lambda}r'] = 0 \Rightarrow [h] = 0, \quad [F] = 0. \tag{31}$$

Thus, to match two LTB solutions on a surface Σ ($R = R^*$), it is sufficient to identify the values of $F(R^*)$ and $h(R^*)$ in these solutions. It is important that by Equation (11), the above matching conditions hold at all times at which both solutions remain regular. Also, there is no necessity to worry about the choice of the radial coordinates on different sides of Σ because both quantities r and $e^{-\lambda}r'$ are insensitive to the choice of the coordinate R , and at reparametrizations of R the arbitrary functions $h(R)$ and $F(R)$ behave as scalars and preserve their values.

Now, let us apply the conditions (31) to the Friedmann solution (12) and (13) with $q = 0$ and an arbitrary wormhole solution described above, also putting $q = 0$, and let us specify the junction surface Σ by some values of the radial coordinates $\chi = \chi_*$ and $R = R_* > 0$ (here and henceforth, we mark by an asterisk the values of different quantities on Σ). We then obtain for the wormhole solution

$$h_* = \sin^2 \chi_*, \quad F_* = 2a_0 \sin^3 \chi_* \Rightarrow F_* = 2a_0 h_*^{3/2}. \tag{32}$$

Consider, as before, the instant of maximum expansion, $\eta = \pi$, then $r = F/h$, and according to (32), we obtain

$$F_* = r_* h_* = 2a_0 h_*^{3/2} \Rightarrow h_* = r_*^2 / (4a_0^2). \tag{33}$$

For the density, we can apply Equation (24); hence, on Σ , we have

$$\rho_* \Big|_{\eta=\pi} = \frac{h_*}{8\pi G r_*^2 (1 - r_* h'_*/F'_*)} = \frac{1}{32\pi G a_0^2 (1 - r_* h'_*/F'_*)}. \tag{34}$$

Assuming, as before, that everywhere in the wormhole solution $F'/h' < 0$, we arrive at the inequality

$$\rho_* \Big|_{\eta=\pi} < \frac{1}{32\pi G a_0^2} \approx 5.5 \times 10^{-30} \frac{\text{g}}{\text{cm}^3} \tag{35}$$

if we assume $a_0 \sim 10^{28}$ cm, approximately the size of the visible part of the universe.

On the other hand, in the Friedmann solutions (12) and (13), the matter density is

$$\rho_{\text{Fr}}(\eta) = \frac{3}{4\pi G a_0^2 (1 - \cos \eta)^3}, \quad \rho_{\text{Fr}} \Big|_{\eta=\pi} = \frac{3}{32\pi G a_0^2}. \tag{36}$$

Thus according to (35), the wormhole matter density at the junction surface Σ is not only very small, but it is even a few times smaller (by at least a factor of three) than the cosmological matter density. In other words, the wormhole region is, at least close to Σ , a region of smaller density, maybe resembling a void. This observation was made for the instant $\eta = \pi$, but it remains true at all times since the η dependence is the same for the wormhole and cosmological solutions.

Some more general observations can be made. As follows from the throat conditions (20), $h(R)$ has a maximum with $h = h_{th} = 1$, while $F(R)$ has a minimum; therefore, according to (11),

$$F(R) \geq F(0) = r_{th} \Big|_{\eta=\pi}, \tag{37}$$

where, for simplicity, $h(R)$ and $F(R)$ are assumed to be monotonic in the ranges $R > 0$ and $R < 0$. Considering, as before, the instant of maximum expansion, $\eta = \pi$, from Equations (32) and (33), we obtain at the junction surface $R = R_*$:

$$F_* = 2a_0 h_*^{3/2}, \quad r_* \Big|_{\eta=\pi} = \frac{F_*}{h_*} \Rightarrow r_* = F_*^{1/3} (2a_0)^{2/3}, \tag{38}$$

Equations (37) and (38) lead to

$$r_* \geq (2a_0)^{2/3} r_{th}^{1/3} = 7.4 \times 10^{18} \left(\frac{r_{th}}{\text{cm}} \right)^{1/3} \text{ cm}, \tag{39}$$

$$r_{th} \leq \frac{r_*^3}{(2a_0)^2} = 2.5 \times 10^{-57} \frac{r_*^3}{\text{cm}^3} \text{ cm}, \tag{40}$$

where r_{th} and r_* are taken at maximum expansion, $\eta = \pi$. We see that the length scales of the wormhole region r_* and its throat r_{th} are substantially different in cases of physical interest, $r_* \ll a_0$. Furthermore, the throat lifetime is $\Delta\tau_{th} = 2\pi r_{th}/c$, while the lifetime of the wormhole region coincides with that of the universe, $\Delta\tau_* = 2\pi a_0/c \approx 2 \times 10^{18}$ s, and thus, we have $\Delta\tau_{th} \ll \Delta\tau_*$. All these estimates (25), (35) and (39) are based on our general assumptions about the model. Numerical estimates for a specific choice of the functions $h(R)$ and $F(R)$ will be made below.

5.2. Estimates for a Particular Model

Now, to obtain further estimates, let us describe the wormhole region by Equations (26) and (27); then, the junction conditions (31) lead to

$$R_* = \cot \chi_*, \quad b = a_0 (\sin \chi_*)^{3+2k}, \tag{41}$$

which ensures matching at $R^* > 0$. Since the functions involved in (26) are even, a similar kind of matching can be applied at $R^* < 0$. The resulting composite model then consists of two closed evolving dust-filled Friedmann universes, connected by means of a wormhole, thus forming a dumbbell-like configuration, or otherwise, we can suppose that negative values of R lead to the same Friedmann universe at some different location.

Some numerical estimates are in order. Taking, as before, $a_0 \sim 10^{28}$ cm, let us also assume that the wormhole region is small as compared to the whole universe; hence, $\chi_* \ll 1$, and $\sin \chi_* \approx \chi_*$. Accordingly,

$$R_* = 1/\chi_*, \quad h_* = \chi_*^2, \quad F_* = 2b\chi_*^{-2k}, \quad b = a_0\chi_*^{2k+3}. \tag{42}$$

Note that in the wormhole solution $r(R, \eta) = b(1 + R^2)(1 - \cos \eta)$, and $R = 0$ is the throat, so $2b$ is the maximum value of the throat radius, $2b = r(0, \pi)$.

Relationships for the wormhole parameters are easily calculated. Equations (24) and (26) imply $rh'/F' = -1/k$, and we obtain for the matter density

$$\rho_{th} = \frac{c^2}{32\pi G b^2} \frac{k}{k+1} \approx 1.3 \times 10^{26} \frac{k}{k+1} \frac{\text{g}}{\text{cm}^3} \frac{\text{cm}^2}{b^2}, \tag{43}$$

$$\rho_* = \frac{c^2}{32\pi G a_0^2} \frac{k}{k+1} \approx 1.3 \times 10^{-30} \frac{k}{k+1} \frac{\text{g}}{\text{cm}^3}. \tag{44}$$

The junction conditions (41) imply

$$r_* = 2a_0 \left(\frac{b}{a_0} \right)^{1/(2k+3)} \tag{45}$$

The minimum value of r_* for given b corresponds to the limit $k \rightarrow 0$, specifically, $r_* \geq 2a_0^{2/3} b^{1/3}$ (39).

Tables 1 and 2 show some estimates of the wormhole parameters, such as the throat radius $r_{th} = 2b$, matter density ρ_{th} on the throat and the radius r_* of the whole wormhole region in the cases $k = 0.1$ and $k = 1$. The density at the junction surface does not depend on b and equals $\rho_* = 1.2 \times 10^{-31} \text{ g/cm}^3$ for $k = 0.1$, and $\rho_* = 6.7 \times 10^{-31} \text{ g/cm}^3$ for $k = 1$. We see that the wormhole region has the size of parsecs or more even for small throats. Near the throat, the density is super-nuclear for $b = 1 \text{ km}$, it is of white-dwarf order near a throat of planetary size, and reasonably small near a throat of 1 pc. At the junction, the density ρ_* is smaller than the mean cosmological density, as should be the case according to our general observations.

Table 1. Estimates of matter density ρ_{th} at the throat and the radius r_* of the wormhole region for different throat radii r_{th} , in the case $k = 0.1, \rho_* = 1.2 \times 10^{-31} \text{ g/cm}^3$.

r_{th}	r_*	$\rho_{th} [\text{g/cm}^3]$
$1.6 \times 10^{-33} \text{ cm}$ (Planck length)	$1.6 \times 10^4 \text{ km}$ (Earth)	1.9×10^{91}
1 km	$10^{21} \text{ cm} = 338 \text{ pc}$	4.9×10^{15} (nuclear density)
10 km (neutron star)	700 pc	4.8×10^{13}
$6.4 \times 10^3 \text{ km}$ (Earth)	5.1 Kpc	1.4×10^8 (white dwarf)
$2.3 \times 10^5 \text{ km}$	16 Kpc (Milky Way)	94×10^3
$695 \times 10^3 \text{ km}$ (Sun)	23 Kpc	10^4
10^7 km (super BH)	52 Kpc	49
$7 \times 10^7 \text{ km}$	96 Kpc	1 (H ₂ O)
1 pc	5.7 Mpc	5.1×10^{-12}
6.5 pc	10 Mpc (galaxy cluster)	1.9×10^{-13}
10 Kpc	100 Mpc (void)	4.8×10^{-20} (interstellar medium)

Table 2. Estimates of matter density ρ_{th} at the throat and the radius r_* of the wormhole region for different throat radii r_{th} , in the case $k = 1, \rho_* = 6.7 \times 10^{-31} \text{ g/cm}^3$.

r_{th}	r_*	$\rho_{th} [\text{g/cm}^3]$
$1.6 \times 10^{-33} \text{ cm}$ (Planck length)	$1.2 \times 10^{11} \text{ km}$	10^{92}
2 cm	16 Kpc (Milky Way)	7×10^{25}
1 km	0.14 Mpc	2.7×10^{16} (nuclear density)
10 km (neutron star)	0.2 Mpc	2.7×10^{14}
$1.6 \times 10^4 \text{ km}$	1 Mpc	10^8 (white dwarf)
$695 \times 10^3 \text{ km}$ (Sun)	2.1 Mpc	5.6×10^4
10^7 km (super BH)	3.6 Mpc	268
$1.6 \times 10^8 \text{ km}$	6.2 Mpc	1 (H ₂ O)
$1.7 \times 10^9 \text{ km}$	10 Mpc (galaxy cluster)	8.6×10^{-3}
1 pc	71 Mpc	2.8×10^{-11}
6.7 pc	100 Mpc (void)	8.6×10^{-13} (interstellar medium)

6. Wormhole Lifetime and Traversability

Now, we would like to consider the radial motion of photons in the model (26) of a dust layer, assuming that it is bounded by $|R| < R_*$ and is located between two copies of Friedmann space-time. It is clear that a photon radially falling to such a wormhole and reaching the throat has no other way than to travel further in the direction of another

universe or maybe a distant part of the same universe. The question is whether or not it will go out from the dust layer in this “other” universe rather than a singularity. In other words, whether the wormhole (or the wormhole part of space-time) is traversable.

Further on, we will consider the motion of photons under different choices of the arbitrary function $\tau_0(R)$ in the solution (11) with $\Delta = 1$ while in the Friedmann solution we fix $\tau_0 \equiv 0$. It should be noted here that for a particular LTB solution taken separately, the choice of $\tau_0(R)$ means nothing else than clock synchronization, or in other words, the choice of spatial sections of the same space-time in the same reference frame. However, in a composite model like ours, unifying two different LTB solutions, this choice is more meaningful, and different $\tau_0(R)$ corresponds to different synchronization of events in one region relative to events in the other region. Thus, fixing $\tau_0(R) \equiv 0$ in the wormhole solution, we make a physical assumption that the wormhole throat emerges simultaneously with the whole Friedmann universe, while $\tau_0(R) > 0$ means that this happens later from the viewpoint of an observer located in this universe. We will consider both options.

6.1. Radial Motion of Photons in the Case $\tau_0 = 0$

From the metric (1), it follows for null radial geodesics that

$$\frac{dR}{d\tau} = \pm \frac{\sqrt{1-h}}{|r'|}, \tag{46}$$

where the derivative $r' = r'(R, \tau)$ can be found from Equation (27):

$$r'(R, \tau) = \frac{bR(R^2 + 1)^k}{1 - \cos \eta} \left[4k + 5 - 4(k + 1) \cos \eta - (2k + 3)\eta \sin \eta - \cos^2 \eta \right]. \tag{47}$$

The plus sign in Equation (46) corresponds to the photon motion through the wormhole from $R < 0$ to $R > 0$, and the minus sign to the opposite motion. Due to the symmetry of the model, it is sufficient to consider, for example, the plus sign.

Let us calculate the time derivative of the spherical radius $r(\tau, R(\tau))$ along a light ray $R = R(\tau)$:

$$\frac{d}{d\tau} r(\tau, R(\tau)) = \frac{\partial r}{\partial \tau} + \frac{\partial r}{\partial R} \frac{dR}{d\tau} = \pm \sqrt{f + \frac{F}{r}} \pm \sqrt{1-h}, \tag{48}$$

where $R = R(\tau)$ describes the radial motion of a photon (46); the first \pm sign corresponds to the expansion (+) of the dust shells at $\eta \in (0; \pi)$ or their contraction (−) at $\eta \in (\pi; 2\pi)$; the second \pm sign corresponds to photon motion from the throat (+), or to the throat (−). It is clear that $dr/d\tau < 0$ or > 0 means convergence or divergence of light rays. Note that at the throat, $h(0) = 1$, the photons move parallel to dust particles: $dr(\tau, R(\tau))/d\tau = \partial r/\partial \tau$.

It is instructive to define an apparent horizon as the location of turning points for radial light rays, that is, the set of events where the light rays stop diverging and start to converge, or vice versa, hence,

$$\frac{d}{d\tau} r(\tau, R(\tau)) = 0. \tag{49}$$

Using Equations (27) and (48), Equation (49) is rewritten in the form

$$\cot \frac{\eta}{2} \pm R = 0, \tag{50}$$

and finally, we have the parametric equations for the apparent horizon

$$r = \frac{2^{k+1}b}{(1 - \cos \eta)^k}, \quad \tau = \frac{2^{k+3/2}b(\eta - \sin \eta)}{(1 - \cos \eta)^{k+3/2}}. \tag{51}$$

The condition (49) can be satisfied only if the terms in Equation (50) have different signs. Thus, at the expansion stage $\eta \in (0; \pi)$, there is an apparent horizon for photons moving towards the throat ($\pm R < 0$), while at the contraction stage $\eta \in (\pi; 2\pi)$, on the contrary, for photons moving from the throat ($\pm R > 0$). There are actually two apparent horizons, depending on the direction of motion.

The results of numerical integration of Equations (46) or (48) are shown in Figures 3–7. Figure 3 shows the set of null radial geodesics (blue curves) in the case $k = 0.1$, presented in the coordinates (R, τ) . The graph uses a log-10 scale for just the τ axis. The red line in the figure presents the singularity $\eta = 2\pi$. There is also a singularity at the initial time $\tau \rightarrow 0$ ($\eta \rightarrow 0$), it is not presented. The photons begin their motion at the time instant with $\tau/b = 10^{-7}$, close to the origin of the universe, and move from the region $R < 0$ to $R > 0$ through the wormhole region. The throat $R = 0$ is shown in brown and exists for a short time as compared to the universe lifetime. Some of the photons pass through the throat, others fall to the singularity instead of reaching the throat. Further on, this solution must be glued at some $R = R_*$ to the external Friedmann space-time, and the table on the right shows the correspondence between the parameter R_* and the radius r_* .

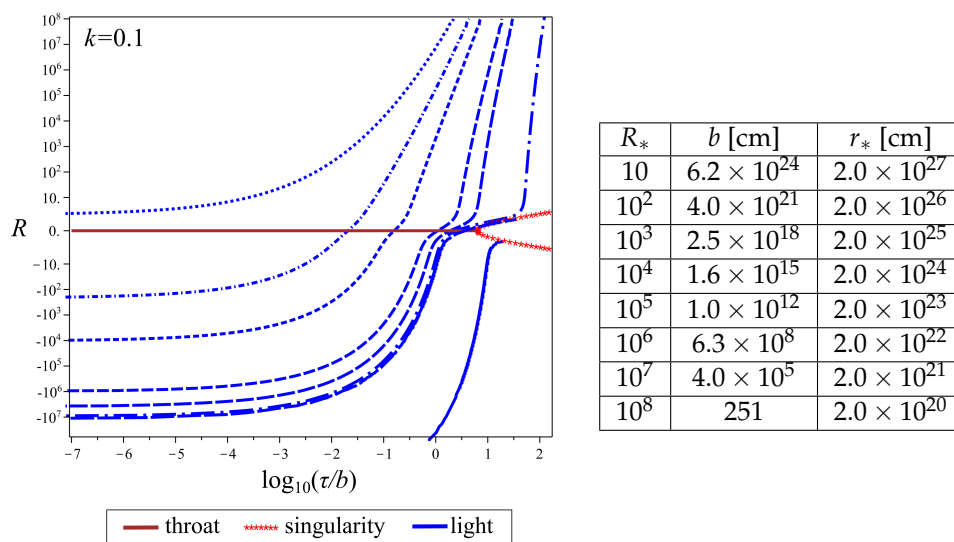


Figure 3. The figure shows the τ -dependence of the radial coordinate R of photons at their radial motion (eight blue curves). The brown horizontal line presents the throat $R = 0$; the red line depicts the singularity $\eta = 2\pi$. The table shows the correspondence between the junction coordinate $R = R_*$, the throat size b , and the radius r_* of the wormhole region. The curves from top to bottom correspond to the following initial data at the moment $\tau/b = 10^{-7}$: $R = 2.3, -198, -9.7 \times 10^3, -9.6 \times 10^5, -3.7 \times 10^6, -1.0 \times 10^7, -1.1 \times 10^7, -1.6 \times 10^{11}$.

Of greatest interest are large values of the parameter R_* (see Tables 1 and 2 above); however, for small enough $R_* = 1$ ($\chi_* = \pi/4, a_0 = 4\sqrt{2}b$), the results are qualitatively similar and more suitable for illustration. Figure 4 shows the dynamics of the throat $R = 0$ (brown curve), dust layers of the wormhole region $|R| \leq R_*$ (black point curves), the junction surfaces $R = \pm R_*$ (black curve), external Friedmann space-time $\chi \geq \chi_*$ (blue curve) in the case $R_* = 1$, presented in the coordinates $(\tau/b, r/b)$. The left panels (a) and (c) correspond to the model with $k = 0.1$; the right ones (b) and (d) correspond to that with $k = 1$. The results are presented in two scales: panels (a), (b) correspond to the usual scale; (c) and (d) correspond to an enlarged scale and clarify the dynamics at early times. The green curves correspond to photons launched on the sphere $R = -R_*$ and moving from the region $R < 0$ to $R > 0$. The geodesics in the left panels (a) and (c) are results of numerical integration in the case $k = 0.1$ with the following initial data at $R = -1$: $\tau/b = 0.64, 1.17, 1.39, 1.44, 1.45, 1.52$. The right panels (b) and (d) present geodesics with the following initial data at $R = -1$: $\tau/b = 0.172, 0.395, 0.406, 0.407, 0.414$. The matter layers begin and end

their evolution at the singularity (red line). The purple curve corresponds to the apparent horizon in the region $R > 0$.

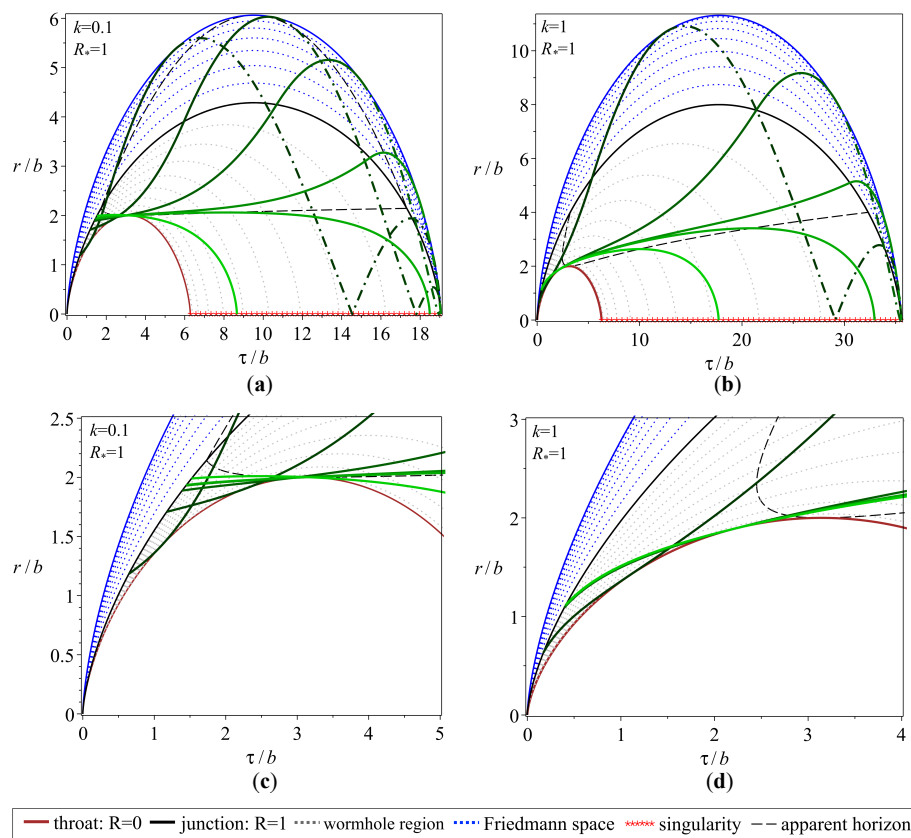


Figure 4. Illustrated are the dynamics of the throat $R = 0$ (brown curve), the junction surfaces $R = \pm R_*$ (black curve), and dust layers of the internal wormhole region $|R| \leq R_*$ (black point curves) and the external Friedmann universe $\chi \geq \chi_*$ (blue curves) in the case $R_* = 1$. Green curves correspond to photons moving from the region $R < 0$ to $R > 0$. The left figures (a,c) correspond to the model with $k = 0.1$; the right ones (b,d) correspond to that with $k = 1$. The results are presented in two scales. The top figures (a,b) correspond to the usual scale, while the bottom figures (c,d) correspond to an enlarged scale and clarify the dynamics at early times. The photons start their motion on the sphere $R = -R_*$, pass through the throat, and some of them leave the wormhole region in a finite time and move further in the Friedmann space-time. The dashed-dotted green curves correspond to the motion in the region $\chi \in (\pi/2; \pi)$ of the Friedmann universe. The red line presents the singularity $r = 0$, and the black dashed curve corresponds to the apparent horizon.

Note that to describe the motion in the (τ, r) coordinates, in fact, a set of two diagrams is required, but due to their identity, only one of them is shown. Each diagram in the figures actually depicts two identical space-time regions $R \leq 0$ and $R \geq 0$, connected by the throat $R = 0$.

Figure 5a,b show the time dependence of the radius $r(\tau, R)/b$ for photon paths (green curves) with the following parameter values: (a) $k = 0.1$, $b = 10^{12}$ cm, $R_* = 10^5$, $r_* = 2 \times 10^{23}$ cm, and (b) $k = 0.1$, $b = 1$ pc, $R_* = 937$, $r_* = 2 \times 10^{23}$ cm, respectively. Unlike the previous figure, these values b correspond to a realistic scale of the model (see Tables 1 and 2). The photons are launched on the junction surface $R = -R_*$ at different times and move from $R < 0$ to $R > 0$. Not all photons cross the throat and get to $R > 0$, and some of them reach the junction surface $R = R_*$ in finite time and enter the outer space-time. In the left panel, the photons start from $R = -R_*$ with the initial data $\tau/b = 0.026, 0.085, 0.11, 1.7$. In the right panel, the photons start from $R = -R_*$ at the

times $\tau/b = 0.14, 0.42, 0.44, 0.54$. For example, the value $\tau/b = 0.42$ cm corresponds to the time $t = \tau b/c = 1.4$ year. We can conclude that the wormhole is traversable at least during a short time of its evolution.

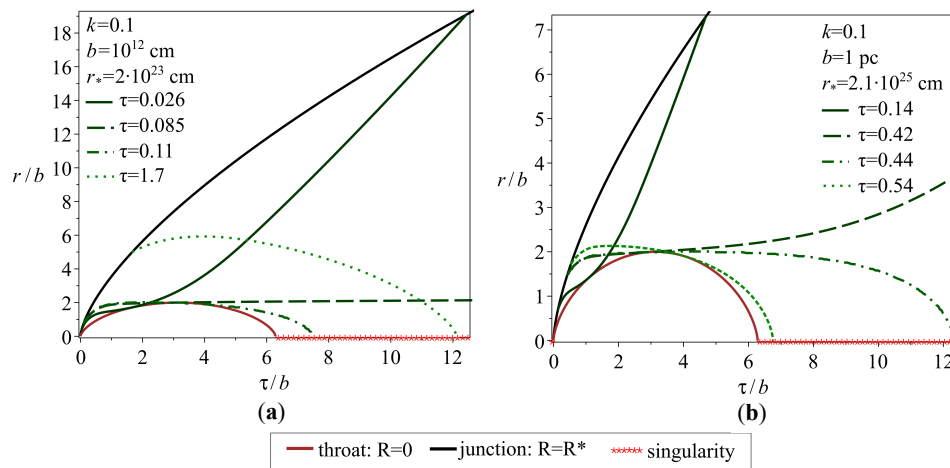


Figure 5. Dynamics of the wormhole throat $R = 0$ (brown curve), the junction surface $R = \pm R_*$ (black curve), photon trajectories (green curves) in the cases: (a) $k = 0.1, b = 10^{12}$ cm, $R_* = 10^5, r_* = 2 \times 10^{23}$ cm; (b) $k = 0.1, b = 1$ pc, $R_* = 937, r_* = 2.1 \times 10^{25}$ cm. The photons are launched on the surface $R = -R_*$ at different times: (a) $\tau/b = 0.026, 0.085, 0.11$ and 1.7 ; (b) $\tau/b = 0.14, 0.42, 0.44, 0.54$. One of the curves does not reach the throat, the rest ones pass through the throat, and two of them reach the junction surface $R = R_*$.

6.2. Radial Motion of Photons in the Case $\tau_0 \neq 0$

Now let us consider radial null geodesics in the case (27), where $\tau_0(R)$ is a nonzero even function of R . The meaning of $\tau_0(R)$ is the time τ (by the clock of an observer in Friedmann space-time) at which the dust layer corresponding to a value of the R coordinate begins to evolve. In particular, $\tau_0(0)$ is the instant at which emerges the wormhole throat $R = 0$; this $\tau_0(0)$ can take arbitrary values from the interval $0 \leq \tau_0(0) \leq \tau_{\max}$, where $\tau_{\max} = \tau|_{\eta=2\pi, R=R_*} = 2\pi b(1 + R_*^2)^{k+3/2}$ is the lifetime of the universe. Different dust layers must not collide; therefore we must have $r' \neq 0$ everywhere outside the throat. This condition is sufficient for the absence of a singularity, so that the density (6) and the Kretschmann scalar (18) are finite. Let the function $\tau_0(R)$ vanish at the boundary $R = R_*$ of the wormhole region, so that it does not affect the junction conditions.

The inequality $r' \neq 0$ is satisfied if we consider the following example of the function $\tau_0(R)$:

$$\tau_0(R) = A \left[(R_*^2 + 1)^{k+3/2} - (R^2 + 1)^{k+3/2} \right], \quad 0 \leq A \leq 2\pi b. \tag{52}$$

The derivative r' of the function $r(R, \tau)$ has the form

$$r' = \frac{R(R^2 + 1)^k}{1 - \cos \eta} \left\{ A(2k + 3) \sin \eta + b \left[4k + 5 - \cos^2 \eta - 4(k + 1) \cos \eta - (2k + 3)\eta \sin \eta \right] \right\}, \tag{53}$$

where, as can be directly verified, the expression in curly brackets is positive; hence, the condition $r' \neq 0$ is satisfied at $R > 0$ or $R < 0$, and the density ρ is everywhere finite and positive.

In this model, the lifetime of the wormhole throat remains unchanged, equal to $2\pi b$, but different values of the parameter A correspond to different emergence times of the wormhole throat (Figure 6). In particular, in the case $A = 0$, the throat begins to evolve simultaneously with all dust layers. If we assume $A = 2\pi b$, the throat collapses simultaneously with all dust layers (such fine tuning looks quite incredible but still possible in principle). Under the condition $0 < A < 2\pi b$, the throat emerges and collapses at

intermediate times during the lifetime of the universe. Smaller values of the parameter k correspond to a more compact wormhole region. Figure 6 corresponds to the case $R_* = 1$ ($a_0/b = 4\sqrt{2}$); however, realistic values of the parameters a_0 and b do not change the qualitative picture of the system dynamics.

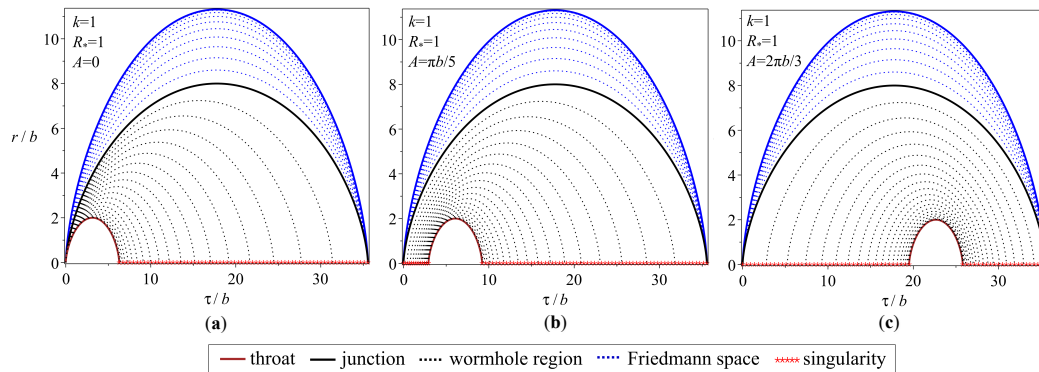


Figure 6. The figure shows the dynamics of the dust layers in the case $k = 1, R_* = 1$ for different values of the parameter A : (a) $A = 0$, (b) $A = \pi b/5$, (c) $A = 2\pi b/3$.

Obviously, there are photons passing through the wormhole in the case of a thin dust region $|R| \leq R_*$. However, as follows from the numerical estimates in Table 1, the case of a thin dust region is of little interest. As noted in the section above, the model is traversable with $\tau_0(R) = 0$ ($A = 0$). The value $A = 2\pi b$ corresponds to the case where the wormhole and the whole universe collapse simultaneously. It is quite similar to the case $A = 0$, and differs only by the direction of motion; in this case, the wormhole region is always traversable, at least for photons starting at times sufficiently close to the collapse time. Due to the continuity of the equations, the traversability is also expected for A close enough to zero or $2\pi b$.

The results of our numerical analysis are shown in Figure 7 for the case $k = 0.1, A = 2\pi b/3$ in two versions. The throat emerges and collapses at some intermediate times during the universe evolution since the parameter A significantly differs from its minimum ($A = 0$) and maximum ($A = 2\pi b$) values. Figure 7a corresponds to small enough $R_* = 1$; in this case the results are qualitatively similar and more suitable for illustration.

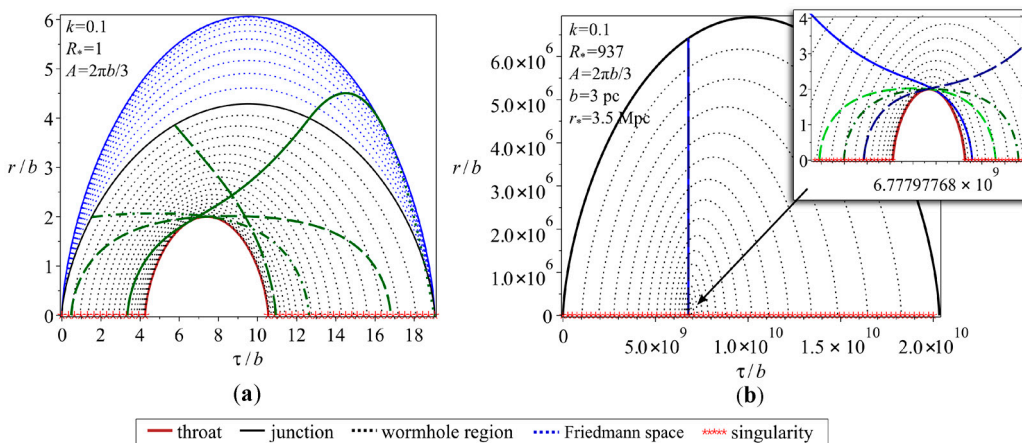


Figure 7. Dynamics of dust layers and radial photon trajectories. (a) $A = 2\pi b/3, k = 0.1, R_* = 1$. (b) $A = 2\pi b/3, k = 0.1, R_* = 937, b = 3 \text{ pc}, r_* = 3.5 \text{ Mpc}$.

Figure 7b is obtained for values more consistent with cosmic scales, namely $b = 3 \text{ pc}, r_* = 3.5 \text{ Mpc}, R_* = 937$. The inset in the right panel illustrates the behavior of the trajectories on a larger scale. In this case, there are no geodesics passing through the whole wormhole area $|R| \leq R_*$. However, the throat is halfway traversable; photons from the

universe $R < 0$ can get into the region $R > R_*$ if they are emitted close enough to the throat. The trajectories are shown in blue for photons passing through the throat and reaching $R = -R_*$ or $R = R_*$; the green color shows trajectories passing through the throat but not leaving the wormhole area.

As a result of our numerical analysis, we can conclude the following. In the general case, the wormhole region $|R| \leq R_*$ can be traversable, but only under a particular choice of the throat parameters and initial conditions. For any value of the junction surface R_* , there are always light rays passing through the wormhole, at least for A close enough to zero or $2\pi b$. If the throat emerges in the middle part of the universe lifetime, photons from the universe $R < 0$ can get into the region $R > R_*$ if emitted close enough to the throat.

6.3. Multiple Wormholes in a Multi-Universe

Schematically, an evolving dust-filled configuration with a wormhole connecting two closed Friedmann universes can be constructed as follows (see Figure 8). One takes two copies of such universes, cuts off from each universe a three-dimensional spherical region, and glues to the spherical boundaries being mouths of a dust-filled wormhole. This configuration evolves synchronously with the proper cosmic time τ , which is supposed to be the same in all regions, from the initial cosmological singularity to the final one. It is worth noting that the wormhole mouths inscribed into closed Friedmann universes are existing in the entire cosmological cycle and evolving synchronously with the universe’s evolution, i.e., growing at the expansion phase and shrinking at contraction. On the other hand, the wormhole throat situated between the two mouths is only open during a small interval of the universe’s evolution. Figure 8 shows an example where a throat appears at the moment of initial singularity, then it grows, achieves its maximum size, and after that, it shrinks and disappears. In Figure 6, one can see other examples where wormhole throats appear during cosmological evolution.

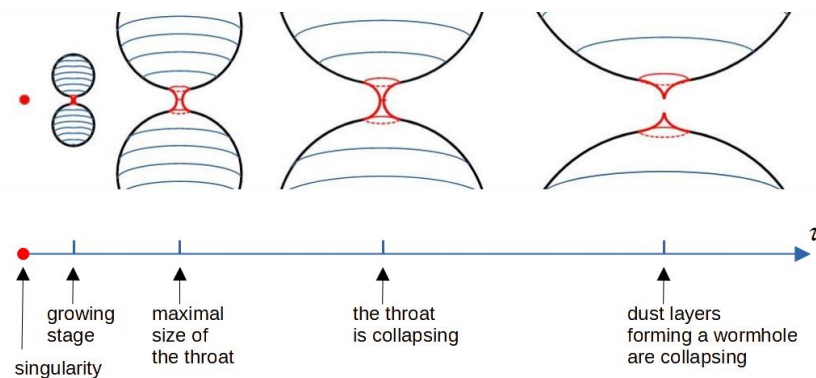


Figure 8. An evolving wormhole connecting two Friedmann universes.

The model with one dust-filled wormhole connecting two closed Friedmann universes can be naturally generalized. We can suppose that the “mother” Friedmann universe is born with multiple mouths of wormholes associated to “daughter” universes. As a result, we obtain a model of a multi-universe as a system of closed Friedmann universes connected by evolving dust-filled wormholes (see Figure 9).

Here it is necessary to stress once more that the multi-universe with multiple wormholes evolves synchronously with unified proper cosmic time τ , which is supposed to be the same in all regions. Such a high correlation between different regions can be explained if one supposes that the multi-universe is born from the quantum spacetime foam on sub-Planckian scales as a single quantum state.

One more point worth being stressed is the following. Strictly speaking, the Friedmann universe with an inscribed wormhole mouth is already neither homogeneous nor isotropic. A distant observer will see a wormhole mouth as a compact object bending photon trajectories. In addition, a wormhole mouth will introduce distortions into the

spectrum of the almost isotropic cosmic microwave background radiation. The scale of anisotropy must be proportional to an angular size of the mouth. In principle, these both effects could be potentially observable, therefore, one might verify the model of dust-filled wormholes in the Friedmann universe using astrophysical methods. Particular predictions of this kind require a further study.

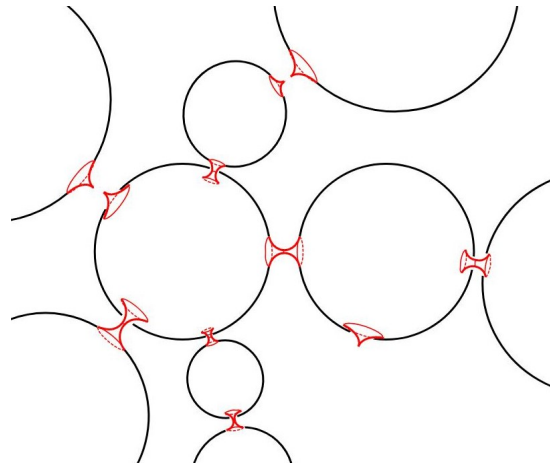


Figure 9. Multiple wormholes in the multi-universe.

7. Concluding Remarks

In this paper, we have continued our study begun in [60] and described in some detail different features of evolving wormholes able to exist in a Friedmann universe in the simplest case of purely dust solutions. However, it is evident that adding small values of the cosmological constant Λ cannot qualitatively change such local issues as the existence and properties of wormholes. Meanwhile, a nonzero Λ drastically changes the global dynamics: $\Lambda > 0$ launches a stage of accelerated expansion of the Universe, which must probably encompass the wormhole region. It is important that such wormhole regions can exist not only at a matter-dominated stage of the Universe evolution but also at its accelerated stage. In particular, examples of solutions to the Einstein equations describing wormholes in a de Sitter universe are known, and it has been noticed that such wormholes, if they existed at an inflationary stage, could greatly extend the causal connection of different parts of the universe [23].

On the other hand, the inclusion of a sufficiently small charge $q \neq 0$ also cannot strongly change the local picture of a wormhole. However, globally, the Universe cannot be precisely homogeneous and isotropic in the presence of a vector field. Also, a charge (or an effective charge due to a wormhole) on one “pole” inevitably leads to an opposite charge on the other, where the lines of force again converge. There can be a similar wormhole mouth at this other pole and one more universe beyond it, and so on. The whole picture will resemble a “churchkhela,” wonderful Georgian dessert, see Figure 10. As before, there can also be natural generalizations in the spirit of Figure 9, not to mention that some of the wormholes may connect different parts of the same universe. Possible observational signatures of such objects, in particular, concerning the properties of cosmic microwave background and cosmic magnetic fields, can be a subject of further studies. It may be of particular interest to compare the characteristics of our wormhole models with the observed parameters of cosmic voids and other local inhomogeneities in our universe.

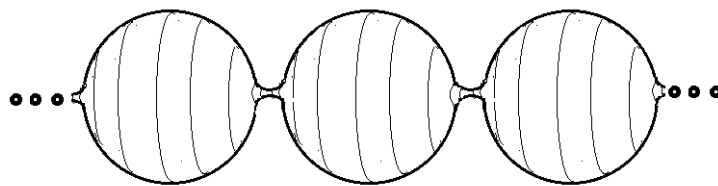


Figure 10. Multiple universes connected by magnetic wormholes.

Author Contributions: Individual contributions of authors, K.A.B., P.E.K. and S.V.S., are equal and include the following: conceptualization, methodology, formal analysis, investigation, validation, visualization, writing—original draft preparation, review and editing. All authors have read and agreed to the published version of the manuscript.

Funding: P.E.K. and S.V.S. are supported by RSF grant No. 21-12-00130. Partially, this work was conducted in the framework of the Russian Government Program of Competitive Growth of the Kazan Federal University. K.B. was supported in part by the RUDN Project No. FSSF-2023-0003, and by the Ministry of Science and Higher Education of the Russian Federation, Project “New Phenomena in Particle Physics and the Early Universe” FSWU-2023-0073.

Institutional Review Board Statement: Not applicable.

Informed Consent Statement: Not applicable.

Data Availability Statement: Not applicable.

Conflicts of Interest: The authors declare no conflict of interest.

References




1. Friedman, A. Über die Krümmung des Raumes. *Z. Phys.* **1922**, *10*, 377–386. [CrossRef]
2. Flamm, L. Beiträge zur Einsteinschen Gravitationstheorie. *Phys. Z.* **1916**, *17*, 448.
3. Einstein, A.; Rosen, N. The particle problem in the General Theory of Relativity. *Phys. Rev.* **1935**, *48*, 73–77. [CrossRef]
4. Wheeler, J.A. Geons. *Phys. Rev.* **1955**, *97*, 511–536. [CrossRef]
5. Wheeler, J.A. *Geometrodynamics*; Academic Press: New York, NY, USA, 1962; 334p.
6. Bronnikov, K.A. Scalar-tensor theory and scalar charge. *Acta Phys. Pol. B* **1973**, *4*, 251.
7. Ellis, H.G. Ether flow through a drainhole—A particle model in general relativity. *J. Math. Phys.* **1973**, *14*, 104–118. [CrossRef]
8. Ellis, H.G. The evolving, flowless drainhole: A nongravitating-particle model in general relativity theory. *Gen. Relat. Gravit.* **1979**, *10*, 105–123.
9. Clément, G. A class of wormhole solutions to higher dimensional general relativity. *Gen. Rel. Grav.* **1984**, *16*, 131–138. [CrossRef]
10. Clément, G. Axisymmetric regular multiwormhole solutions in five-dimensional general relativity. *Gen. Rel. Grav.* **1984**, *16*, 477–489. [CrossRef]
11. Morris, M.S.; Thorne, K.S. Wormholes in spacetime and their use for interstellar travel: a tool for teaching general relativity. *Am. J. Phys.* **1988**, *56*, 395. [CrossRef]
12. Bronnikov, K.A. Spherically symmetric solutions in D-dimensional dilaton gravity. *Grav. Cosmol.* **1995**, *1*, 67–78.
13. Clément, G.; Fabris, J.C.; Rodrigues, M.E. Phantom black holes in Einstein-Maxwell-dilaton theory. *Phys. Rev. D* **2009**, *79*, 064021. [CrossRef]
14. Goulart, P. Phantom wormholes in Einstein-Maxwell-dilaton theory. *Class. Quantum Grav.* **2017**, *35*, 025012. [CrossRef]
15. Huang, H.; Yang, J. Charged Ellis wormhole and black bounce. *Phys. Rev. D* **2019**, *100*, 124063. [CrossRef]
16. Lobo, F.S.N. Chaplygin traversable wormholes. *Phys. Rev. D* **2006**, *73*, 064028. [CrossRef]
17. Sushkov, S.V. Wormholes supported by a phantom energy. *Phys. Rev. D* **2005**, *71*, 043520. [CrossRef]
18. Kuhfittig, P.K.F. Conformal-symmetry wormholes supported by a perfect fluid. *New Horizons Math. Phys.* **2017**, *1*, 14–18. [CrossRef]
19. Lobo, F.S.N. Stable phantom energy traversable wormhole models. *AIP Conf. Proc.* **2006**, *861*, 936–943.
20. Kuhfittig, P.K.F. Exactly solvable wormhole and cosmological models with a barotropic equation of state. *Acta Phys. Pol. B* **2016**, *47*, 1263–1272. [CrossRef]
21. Sahoo, P.K.; Moraes, P.H.R.S.; Sahoo, P.G.R. Phantom fluid supporting traversable wormholes in alternative gravity with extra material terms. *Int. J. Mod. Phys. D* **2018**, *27*, 1950004. [CrossRef]
22. Kuhfittig, P.K.F. Static and dynamic traversable wormhole geometries satisfying the Ford-Roman constraints. *Phys. Rev. D* **2002**, *66*, 024015. [CrossRef]
23. Bronnikov, K.A.; Baleevskikh, K.A.; Skvortsova, M.V. Wormholes with fluid sources: a no-go theorem and new examples. *Phys. Rev. D* **2017**, *96*, 124039. [CrossRef]

24. Visser, M. Traversable wormholes: Some simple examples. *Phys. Rev. D* **1989**, *39*, 3182. [CrossRef]
25. Visser, M. Traversable wormholes from surgically modified Schwarzschild spacetimes. *Nucl. Phys. B* **1989**, *328*, 203–212. [CrossRef]
26. Blázquez-Salcedo, J.L.; Knoll, C.; Radu, E. Traversable wormholes in Einstein-Dirac-Maxwell theory. *Phys. Rev. Lett.* **2021**, *126*, 101102. [CrossRef]
27. Konoplya, R.A.; Zhidenko, A. Traversable wormholes in general relativity without exotic matter. *Phys. Rev. Lett.* **2022**, *128*, 091104. [CrossRef]
28. Bolokhov, S.V.; Bronnikov, K.A.; Krasnikov, S.V.; Skvortsova, M.V. A note on “Traversable wormholes in Einstein-Dirac-Maxwell theory”. *Grav. Cosmol.* **2021**, *27*, 401. [CrossRef]
29. Hochberg, D.; Visser, M. Geometric structure of the generic static traversable wormhole throat. *Phys. Rev. D* **1997**, *56*, 4745. [CrossRef]
30. Bronnikov, K.A.; Starobinsky, A.A. No realistic wormholes from ghost-free scalar-tensor phantom dark energy. *JETP Lett.* **2007**, *85*, 1–5. [CrossRef]
31. Alencar, G.; Nilton, M. Schwarzschild-like wormholes in asymptotically safe gravity. *Universe* **2021**, *7*, 332. [CrossRef]
32. Bronnikov, K.A.; Kim, S.-W. Possible wormholes in a brane world. *Phys. Rev. D* **2003**, *67*, 064027. [CrossRef]
33. Harko, T.; Lobo, F.S.N.; Mak, M.K.; Sushkov, S.V. Modified-gravity wormholes without exotic matter. *Phys. Rev. D* **2013**, *87*, 067504. [CrossRef]
34. Mustafa, G.; Maurya, S.K.; Saibal, R. On the possibility of generalized wormhole formation in the galactic halo due to dark matter using the observational data within the matter coupling gravity formalism. *Astroph. J.* **2022**, *941*, 170. [CrossRef]
35. Mustafa, G.; Hussain, I.; Atamurotov, F.; Liu, W.M. Imprints of dark matter on wormhole geometry in modified teleparallel gravity. *Eur. Phys. J. Plus* **2023**, *138*, 166. [CrossRef]
36. Bronnikov, K.A.; Krechet, V.G. Potentially observable cylindrical wormholes without exotic matter in GR. *Phys. Rev. D* **2019**, *99*, 084051. [CrossRef]
37. Bolokhov, S.V.; Bronnikov, K.A.; Skvortsova, M.V. Cylindrical wormholes: A search for viable phantom-free models in GR. *Int. J. Mod. Phys. D* **2019**, *28*, 1941008.
38. Bronnikov, K.A.; Krechet, V.G.; Oshurko, V.B. Rotating Melvin-like universes and wormholes in general relativity. *Symmetry* **2020**, *12*, 1306. [CrossRef]
39. Bronnikov, K.A.; Galiakhmetov, A.M. Wormholes and black universes without phantom fields in Einstein-Cartan theory. *Phys. Rev. D* **2016**, *94*, 124006. [CrossRef]
40. Matos, T.; Miranda, G. Exact rotating magnetic traversable wormhole satisfying the energy conditions. *Phys. Rev. D* **2019**, *99*, 124045.
41. Kashargin, P.E.; Sushkov, S.V. Slowly rotating scalar field wormholes: The second order approximation. *Phys. Rev. D* **2008**, *78*, 064071. [CrossRef]
42. Kleihaus, B.; Kunz, J. Rotating Ellis wormholes in four dimensions. *Phys. Rev. D* **2014**, *90*, 121503. [CrossRef]
43. Chew, X.Y.; Kleihaus, B.; Kunz, J. Geometry of spinning Ellis wormholes. *Phys. Rev. D* **2016**, *94*, 104031. [CrossRef]
44. Arellano, A.V.B.; Lobo, F.S.N. Evolving wormhole geometries within nonlinear electrodynamics. *Class. Quant. Grav.* **2006**, *23*, 5811–5824. [CrossRef]
45. Bronnikov, K.A. Nonlinear electrodynamics, regular black holes and wormholes. *Int. J. Mod. Phys. D* **2018**, *27*, 184105. [CrossRef]
46. Kar, S. Evolving wormholes and the energy conditions. *Phys. Rev. D* **1994**, *49*, 862. [CrossRef]
47. Kim, S.W. Cosmological model with a traversable wormhole. *Phys. Rev. D* **1996**, *53*, 6889. [CrossRef]
48. Roman, T.A. Inflating Lorentzian wormholes. *Phys. Rev. D* **1993**, *47*, 1370–1379. [CrossRef]
49. Sushkov, S.V.; Kim, S.W. Cosmological evolution of a ghost scalar field. *Gen. Relativ. Gravit.* **2004**, *36*, 1671–1678. [CrossRef]
50. Sushkov, S.V.; Zhang, Y.Z. Scalar wormholes in cosmological setting and their instability. *Phys. Rev. D* **2008**, *77*, 024042. [CrossRef]
51. Wang, A.; Letelier, P.S. Dynamic wormholes and energy conditions. *Prog. Theor. Phys.* **1995**, *94*, 137–142. [CrossRef]
52. Yang, J.; Huang, H. Trapping horizons of the evolving charged wormhole and black bounce. *Phys. Rev. D* **2021**, *104*, 084005. [CrossRef]
53. Hayward, S.A. Dynamic wormholes. *Int. J. Mod. Phys. D* **1999**, *8*, 373–382. [CrossRef]
54. Hayward, S.A. Wormhole dynamics in spherical symmetry. *Phys. Rev. D* **2009**, *79*, 124001. [CrossRef]
55. Hochberg, D.; Visser, M. Dynamic wormholes, anti-trapped surfaces, and energy conditions. *Phys. Rev. D* **1998**, *58*, 04402. [CrossRef]
56. Visser, M. *Lorentzian Wormholes: From Einstein to Hawking*; American Institute of Physics: Woodbury, NY, USA, 1995; 412p.
57. Lobo, F.S.N. Exotic solutions in General Relativity: Traversable wormholes and «warp drive» spacetimes. In *Classical and Quantum Gravity Research*; Nova Science Publishers: New York, NY, USA, 2008; pp. 1–78.
58. Bronnikov, K.A.; Sushkov, S.V. Current problems and recent advances in wormhole physics. *Universe* **2023**, *9*, 81. [CrossRef]
59. Kashargin, P.; Sushkov, S. Collapsing wormholes sustained by dustlike matter. *Universe* **2020**, *6*, 186. [CrossRef]
60. Bronnikov, K.A.; Kashargin, P.E.; Sushkov, S.V. Magnetized dusty black holes and wormholes. *Universe* **2021**, *7*, 419. [CrossRef]
61. Tolman, R. Effect of inhomogeneity on cosmological models. *Proc. Natl. Acad. Sci. USA* **1934**, *20*, 169–176. [CrossRef] [PubMed]
62. Lemaître, G. L’Univers en expansion. *Ann. SociÉTÉ Sci. Brux.* **1933**, *A53*, 51–85.
63. Bondi, H. Spherically symmetrical models in general relativity. *Mon. Not. R. Astron. Soc.* **1947**, *107*, 410; reprinted: *Gen. Rel. Grav.*, **1999**, *31*, 1783–1805. [CrossRef]

64. Christodoulou, D. Violation of cosmic censorship in the gravitational collapse of a dust cloud. *Commun. Math. Phys.* **1984**, *93*, 171–195. [CrossRef]
65. Landau, L.D.; Lifshitz, E.M. *The Classical Theory of Fields*, 4th ed.; Butterworth-Heinemann: Oxford, UK, 1987; Volume 2; 402p.
66. Bambi, C. *Black Holes: A Laboratory for Testing Strong Gravity*; Springer Nature Singapore Pte Ltd.: Singapore, 2017; 355p.
67. Markov, M.A.; Frolov, V.P. Metrics of the closed Friedman world perturbed by electric charge (to the theory of electromagnetic «Friedmons»). *Teor. Mat. Fiz.* **1970**, *3*, 3–17.
68. Bailyn, M. Oscillatory behavior of charge-matter fluids with $e/m > G^{1/2}$. *Phys. Rev. D* **1973**, *8*, 1036. [CrossRef]
69. Vickers, P.A. Charged dust spheres in general relativity. *Ann. Inst. Henri Poincaré A* **1973**, *18*, 137.
70. Ivanenko, D.D.; Krechet, V.G.; Lapchinskii, V.G. The dynamics of charged dust in the general theory of relativity. *Sov. Phys. J.* **1973**, *16*, 1675–1679. [CrossRef]
71. Khlestkov, Y.A. Three types of solutions of the Einstein-Maxwell equations. *J. Exp. Teor. Fis.* **1975**, *41*, 188.
72. Shikin, I.S. An investigation of a class of gravitational fields for a charged dustlike medium. *J. Exp. Teor. Fis.* **1975**, *40*, 215.
73. Pavlov, N.V. Charged dust spheres in the general theory of relativity I. Quadratures of Einstein's equations. *Sov. Phys. J.* **1976**, *19*, 489–495. [CrossRef]
74. Pavlov, N.V.; Bronnikov, K.A. Charged dust spheres in the general theory of relativity II. Singularities and physically permissible models. *Sov. Phys. J.* **1976**, *19*, 916–920. [CrossRef]
75. Bronnikov, K.A.; Kovalchuk, M.A. Some exact models for nonspherical collapse, I. *Gen. Rel. Grav.* **1983**, *15*, 809–822. [CrossRef]
76. Bronnikov, K.A. Some exact models for nonspherical collapse, II. *Gen. Rel. Grav.* **1983**, *15*, 823–836. [CrossRef]
77. Bronnikov, K.A.; Kovalchuk, M.A. Some exact models for nonspherical collapse, III. *Gen. Rel. Grav.* **1984**, *16*, 15–31. [CrossRef]
78. Shatskiy, A.A.; Novikov, I.D.; Kardashev, N.S. A dynamic model of the wormhole and the Multiverse model. *Uspekhi Fiz. Nauk.* **2008**, *178*, 481–488. [CrossRef]
79. Khlestkov, Y.A.; Sukhanova, L.A. Internal structure of wormholes—Geometric images of charged particles in general relativity. *Grav. Cosmol.* **2018**, *24*, 360–370. [CrossRef]
80. Maeda, H.; Harada, T.; Carr, B.J. Cosmological wormholes. *Phys. Rev. D* **2009**, *79*, 044034. [CrossRef]
81. Tomikawa, Y.; Izumi, K.; Shiromizu, T. New definition of a wormhole throat. *Phys. Rev. D* **2015**, *91*, 104008. [CrossRef]
82. Bittencourt, E.; Klippert, R.; Santos, G. Dynamical wormhole definitions confronted. *Class. Quantum Grav.* **2018**, *35*, 155009. [CrossRef]
83. Reissner, H. Über die Eigengravitation des elektrischen Feldes nach der einsteinschen Theorie. *Ann. Der Phys.* **1916**, *355*, 106–120. [CrossRef]
84. Nordström, G. On the energy of the gravitational field in Einstein's theory. *Proc. Kon. Ned. Akad. Wet.* **1918**, *20*, 1238–1245.
85. Darmois, G. Les équations de la gravitation einsteinienne. In *Mémoires des Sciences Mathématiques*; Gauthier-Villars: Paris, France, 1927; p. 58.
86. Israel, W. Singular hypersurfaces and thin shells in general relativity. *Nuovo Cim. B* **1967**, *48*, 463. [CrossRef]

Disclaimer/Publisher's Note: The statements, opinions and data contained in all publications are solely those of the individual author(s) and contributor(s) and not of MDPI and/or the editor(s). MDPI and/or the editor(s) disclaim responsibility for any injury to people or property resulting from any ideas, methods, instructions or products referred to in the content.

Entropic Inflation in Presence of Scalar Field

Sergei D. Odintsov ^{1,2} , Simone D’Onofrio ²  and Tanmoy Paul ^{3,4,*} 

¹ ICREA, Passeig Luis Companys, 23, 08010 Barcelona, Spain; odintsov@ice.csic.es

² Institute of Space Sciences (ICE, CSIC), C. Can Magrans s/n, 08193 Barcelona, Spain; donofrio@ice.csic.es

³ Department of Physics, Visva-Bharati University, Santiniketan 731235, India

⁴ Laboratory for Theoretical Cosmology, International Centre of Gravity and Cosmos, Tomsk State University of Control Systems and Radioelectronics (TUSUR), 634050 Tomsk, Russia

* Correspondence: pul.tnmy9@gmail.com

Abstract: In spirit of the recently proposed four-parameter generalized entropy of apparent horizon, we investigate inflationary cosmology where the matter field inside of the horizon is dominated by a scalar field with a power law potential (i.e., the form of ϕ^n where ϕ is the scalar field under consideration). Actually without any matter inside of the horizon, the entropic cosmology leads to a de-Sitter spacetime, or equivalently, an eternal inflation with no exit. Thus in order to achieve a viable inflation, we consider a minimally coupled scalar field inside the horizon, and moreover, with the simplest quadratic potential. It is well known that the ϕ^2 potential in standard scalar field cosmology is ruled out from inflationary perspective as it is not consistent with the recent Planck 2018 data; (here it may be mentioned that in the realm of “apparent horizon thermodynamics”, the standard scalar field cosmology is analogous to the case where the entropy of the apparent horizon is given by the Bekenstein–Hawking entropy). However, the story becomes different if the horizon entropy is of generalized entropic form, in which case, the effective energy density coming from the horizon entropy plays a significant role during the evolution of the universe. In particular, it turns out that in the context of generalized entropic cosmology, the ϕ^2 potential indeed leads to a viable inflation (according to the Planck data) with a graceful exit, and thus the potential can be made back in the scene.

Keywords: entropic cosmology; generalized entropy; apparent horizon; inflation; scalar field



Citation: Odintsov, S.D.; D’Onofrio, S.; Paul, T. Entropic Inflation in Presence of Scalar Field. *Universe* **2024**, *10*, 4. <https://doi.org/10.3390/universe10010004>

Academic Editors: Galina L. Klimchitskaya, Vladimir M. Mostepanenko and Sergey V. Sushkov

Received: 20 November 2023

Revised: 13 December 2023

Accepted: 19 December 2023

Published: 21 December 2023



Copyright: © 2023 by the authors. Licensee MDPI, Basel, Switzerland. This article is an open access article distributed under the terms and conditions of the Creative Commons Attribution (CC BY) license (<https://creativecommons.org/licenses/by/4.0/>).

1. Introduction

The growing interest in different entropy functions towards black hole thermodynamics as well as towards cosmology [1–28] leads to the proposal of generalized entropy, depending on number of parameters, which generalizes all the known and apparently different entropies (like the Bekenstein–Hawking entropy [29,30], the Tsallis entropy [31], the Rényi entropy [32], the Barrow entropy [33], the Sharma–Mittal entropy [34], the Kaniadakis entropy [35] and the Loop Quantum gravity entropy [36]) for a suitable regime of the parameters [37–40]. Such interest in entropic cosmology becomes stronger when the entropic dark energy seems to be equivalent to holographic dark energy with suitable holographic cut-offs [41]. Initially, a six-parameter dependent generalized entropy of the form

$$S_6(\alpha_{\pm}, \beta_{\pm}, \gamma_{\pm}) = \frac{1}{\alpha_+ + \alpha_-} \left[\left(1 + \frac{\alpha_+}{\beta_+} S^{\gamma_+} \right)^{\beta_+} - \left(1 + \frac{\alpha_-}{\beta_-} S^{\gamma_-} \right)^{-\beta_-} \right], \quad (1)$$

was proposed in [37], where $S = A/(4G)$ is the Bekenstein–Hawking entropy (with A being the area of the apparent horizon and G is the Newton’s gravitational constant) and $\{\alpha_{\pm}, \beta_{\pm}, \gamma_{\pm}\}$ are the parameters. However, soon after [37], a conjecture was made in [38], which stated that the minimum number of parameters required in a generalized entropy

function that can generalize all the aforementioned entropies is equal to four. In particular, the four-parameter generalization is given by

$$S_4(\alpha_{\pm}, \beta, \gamma) = \frac{1}{\gamma} \left[\left(1 + \frac{\alpha_+}{\beta} S \right)^\beta - \left(1 + \frac{\alpha_-}{\beta} S \right)^{-\beta} \right], \tag{2}$$

where $\{\alpha_{\pm}, \beta, \gamma\}$ are the parameters which are considered to be positive in order to make S_4 like a monotonic increasing function with respect to S . As a supporting argument of the conjecture, a counter example was shown in [38] by an entropy function containing less than four parameters (having three parameters, in particular) of the form

$$S_3(\alpha, \beta, \gamma) = \frac{1}{\gamma} \left[\left(1 + \frac{\alpha}{\beta} S \right)^\beta - 1 \right], \tag{3}$$

which is not able to generalize all the known entropies; particularly, S_3 does not represent Kaniadakis entropy in any situation. All the above entropies $\{S_6, S_4, S_3\}$ possesses a singularity in a different type of cosmological scenario, particularly in a bouncing context. Such diverging behaviour is common to all the known entropies (like the Tsallis entropy, the Rényi entropy, the Barrow entropy, the Sharma–Mittal entropy, the Kaniadakis entropy and the Loop Quantum gravity entropy) as well as the Bekenstein–Hawking entropy itself diverges in a bouncing scenario (at the instant of bounce). A possible explanation of this issue is given in [39], where the authors proposed a singular-free generalized entropy containing five parameters of the form

$$S_5(\alpha_{\pm}, \beta, \gamma, \epsilon) = \frac{1}{\gamma} \left[\left\{ 1 + \frac{1}{\epsilon} \tanh \left(\frac{\epsilon \alpha_+}{\beta} S \right) \right\}^\beta - \left\{ 1 + \frac{1}{\epsilon} \tanh \left(\frac{\epsilon \alpha_-}{\beta} S \right) \right\}^{-\beta} \right], \tag{4}$$

which is singular-free during the entire cosmological evolution of the universe even at a bouncing instant (in the context of bounce cosmology) and is able to generalize all the entropies known so far. According to the conjecture stated in [39], the minimum number of parameters required in a non-singular generalized entropy function that is able to generalize all the previously known entropies is equal to five. Based on universe’s evolution, in particular, whether the universe passes through a non-singular bounce (or not) during its cosmic evolution, the minimal constructions of generalized version of entropy is given by the four-parameter [38] and the five-parameter [39] generalized entropy, respectively. Various representatives of $\{S_6, S_4, S_3, S_5\}$ and their convergence to the known entropies are schematically shown in Table 1. The wide applications of the generalized entropies towards cosmology as well as towards black holes are addressed in [38,40,42–46]. Here, it also deserves mention that the microscopic interpretation of such generalized entropies were not known until recently, when some of our authors gave a statistical description of the same in microcanonical, canonical and grand-canonical ensemble [47,48].

Based on the above arguments, we will work with four-parameter generalized entropy in the present work, which contains the minimum number of parameters and also generalizes all the known entropies so far. In particular, we will concentrate on early universe cosmology with four-parameter generalized entropy, where the matter fields inside of the apparent horizon are dominated by a minimally coupled scalar field with a power law type potential. Actually, without the matter fields inside the horizon, the entropic cosmology results in a de-Sitter spacetime, or equivalently, an eternal inflation having no exit. Thus, in order to have a viable inflation, one needs to take either of the following approaches— (a) the entropic parameters vary with the cosmic expansion of the universe, or (b) by some matter fields inside the horizon. In the context of generalized entropy, the first possibility has been studied in [38], while the second approach will be examined in the present work where the matter fields are taken to be a scalar field with a power law potential. Such a form of scalar potential is motivated by the fact that the simplest ϕ^2 potential (where ϕ is

the scalar field under consideration) in standard scalar field cosmology is ruled out from inflationary perspective as it is not consistent with the recent Planck 2018 data; (note that this is particular case of FRW cosmology [49], actually in the realm of “apparent horizon thermodynamics”, the standard scalar field cosmology is analogous to the case where the entropy of the apparent horizon is given by the Bekenstein–Hawking entropy, which produces the usual Friedmann equations from the thermodynamic law of the apparent horizon). However the story becomes different if the horizon entropy is of the generalized entropic form, in which case, the effective energy density coming from the horizon entropy plays a significant role during the evolution of the universe. Motivated by this, we intend to examine the status of the ϕ^2 potential in the context of entropic inflation where the horizon entropy is given by the four-parameter generalized entropy.

Table 1. Schematic table to summarize various representatives of the generalized entropies and their convergence to the known entropies. Here, S_T = Tsallis entropy, S_B = Barrow entropy, S_R = Rényi entropy, S_{SM} = Sharma–Mittal entropy, S_K = Kaniadakis entropy and S_q = Loop Quantum gravity entropy.

S_3	$\gamma = \alpha$	S_{SM}
	$\alpha \rightarrow \infty$	S_T, S_B
	$\alpha, \beta \rightarrow 0$ with $\frac{\alpha}{\beta}$ finite	S_R
	$\beta \rightarrow \infty, \gamma = \alpha$	S_q
S_5	$\epsilon, \alpha_- \rightarrow 0, \alpha_+ = \gamma$	S_{SM}
	$\epsilon \rightarrow 0, \alpha_- = 0, \alpha_+ \rightarrow \infty, \gamma = \left(\frac{\alpha_{\pm}}{\beta}\right)^{\beta}$	S_T, S_B
	$\epsilon, \beta \rightarrow 0, \alpha_- = 0, \alpha_+ = \gamma$ with $\frac{\alpha_{\pm}}{\beta}$ finite	S_R
	$\epsilon, \alpha_- \rightarrow 0, \beta \rightarrow \infty, \alpha_+ = \gamma$	S_q
	$\epsilon \rightarrow 0, \beta \rightarrow \infty, \alpha_+ = \alpha_-$	S_K
S_4	$\alpha_- = 0, \alpha_+ = \gamma$	S_{SM}
	$\alpha_+ \rightarrow \infty, \alpha_- = 0$	S_T, S_B
	$\alpha_- = 0, \alpha_+ = \gamma, \beta \rightarrow 0$ with $\frac{\alpha_{\pm}}{\beta}$ finite	S_R
	$\beta \rightarrow \infty, \alpha_- = 0, \alpha_+ = \gamma$	S_q
	$\beta \rightarrow \infty, \alpha_+ = \alpha_-$	S_K
S_6	$\alpha_- = 0, \alpha_+ = \gamma_+ \beta_+$	S_{SM}
	$\alpha_+ = \alpha_- \rightarrow 0, \gamma_+ = \gamma_-$	S_T, S_B
	$\alpha_+, \beta_+ \rightarrow 0, \gamma_+ = 1$ with $\frac{\alpha_{\pm}}{\beta_{\pm}}$ finite	S_R
	$\beta_+ \rightarrow \infty, \alpha_- = 0, \gamma_+ = 1$	S_q
	$\beta_{\pm} \rightarrow 0, \alpha_+ = \alpha_-, \gamma_{\pm} = 1$	S_K

The paper is organized as follows: the modified Friedmann equations for four-parameter generalized entropy is discussed in Section 2. Then after giving a brief review of ϕ^n inflationary potential with the Bekenstein–Hawking entropy (i.e in standard scalar field cosmology) in Section 3, we will examine the status of the same inflationary potential with 4-parameter generalized entropy as the horizon entropy in Section 4. The paper ends with some conclusions in Section 5.

2. Modified Cosmology with Generalized Entropy

We consider a spatially flat and isotropic universe described by the Friedmann–Lemaître–Robertson–Walker (FLRW) metric

$$ds^2 = -dt^2 + a(t) \left(dr^2 + r^2 \left(d\theta^2 + \sin^2 \theta d\phi^2 \right) \right). \tag{5}$$

It can be rewritten in the following way

$$ds^2 = h_{ab} dx^a dx^b + \tilde{r}^2 \left(d\theta^2 + \sin^2 \theta d\phi^2 \right), \tag{6}$$

defining $\tilde{r}(r, t) = a(t)r$, $h_{ab} = \text{diag}(-1, a^2)$ and $x^0 = t$, $x^1 = r$. The apparent horizon is defined by $h^{ab}\partial_a\tilde{r}\partial_b\tilde{r} = 0$, which in the case of a spatially flat FLRW background has the solution [50–52]

$$r_h = \frac{1}{H}. \tag{7}$$

In this background we see that the apparent horizon is equivalent to the cosmological horizon, that is the Hubble radius. Consequently, we can define a temperature $T = |\kappa|/(2\pi)$, where κ is the surface gravity defined by [50]

$$\kappa = \frac{1}{2\sqrt{-h}}\partial_a\left(\sqrt{-h}h^{ab}\partial_b\tilde{r}\right)\Big|_{\tilde{r}=r_h}, \tag{8}$$

which can be rewritten as

$$\kappa = -\frac{1}{r_h}\left(1 - \frac{\dot{r}_h}{2Hr_h}\right), \tag{9}$$

and it leads to a temperature

$$T = \frac{1}{2\pi r_h}\left|1 - \frac{\dot{r}_h}{2Hr_h}\right|. \tag{10}$$

As in the case of the Bekenstein-Hawking entropy we can then associate a generalized entropy S_g to the apparent horizon in order to find the field equations. The first principle of thermodynamics states [51,52]

$$TdS_g = -dE + WdV, \tag{11}$$

where V is the volume of the apparent horizon, $E = \rho V$ is the total internal energy inside of the horizon and $W = \frac{1}{2}(\rho - p)$ represents the work density regarding the thermodynamic law. The right side of this equation takes the expression as follows:

$$TdS_g = -Vd\rho - \frac{1}{2}(\rho + p)dV. \tag{12}$$

To express this differential equation in terms of the apparent horizon we rewrite

$$TdS_g = T\frac{\partial S_g}{\partial S}dS = \frac{1}{G}\left|1 - \frac{\dot{r}_h}{2Hr_h}\right|\frac{\partial S_g}{\partial S}dr_h \tag{13}$$

and

$$-Vd\rho - \frac{1}{2}(\rho + p)dV = -\frac{4\pi}{3}r_h^3\left(d\rho - \dot{\rho}\frac{dr_h}{2Hr_h}\right), \tag{14}$$

where we used the conservation equation of the matter fields $\dot{\rho} + 3H(\rho + p) = 0$. At this point equating the two terms we can derive the field equation for a general dynamical apparent horizon r_h

$$\frac{\partial S_g}{\partial S}\frac{\dot{r}_h}{r_h^3} = -\frac{4\pi G}{3}\dot{\rho}, \tag{15}$$

which, for the choice of $r_h = 1/H$ along with the conservation relation of matter fields, becomes

$$\dot{H}\left(\frac{\partial S_g}{\partial S}\right) = -4\pi G(\rho + p), \tag{16}$$

which is considered to be the second Friedmann equation in the context of generalized entropic cosmology. The integration of such equation leads to the first Friedmann equation corresponding to the generalized entropy we are considering as

$$\int d(H^2) \left(\frac{\partial S_g}{\partial S} \right) = \frac{8\pi G}{3} \rho + \frac{\Lambda}{3}, \tag{17}$$

where Λ , known as the cosmological constant, appears as an integration constant. The above two equations represent the general Friedmann equations based on the apparent horizon thermodynamics for any form of horizon entropy.

For the three-parameter and the four-parameter generalized entropy, Equation (16) takes the following form:

$$\dot{H} \left\{ \frac{\alpha}{\gamma} \left(1 + \frac{\alpha}{\beta} S \right)^{\beta-1} \right\} = -4\pi G(\rho + p), \tag{18}$$

and

$$\dot{H} \left\{ \frac{1}{\gamma} \left[\alpha_+ \left(1 + \frac{\alpha_+}{\beta} S \right)^{\beta-1} + \alpha_- \left(1 + \frac{\alpha_-}{\beta} S \right)^{-\beta-1} \right] \right\} = -4\pi G(\rho + p), \tag{19}$$

respectively. Moreover the first Friedmann equation, i.e., Equation (17), yields

$$\frac{\beta GH^4}{\pi\gamma(2-\beta)} \left(\frac{\beta GH^2}{\pi\alpha} \right)^{-\beta} {}_2F_1 \left(1-\beta, 2-\beta, 3-\beta, -\frac{\beta GH^2}{\pi\alpha} \right) = \frac{8\pi G}{3} \rho + \frac{\Lambda}{3}, \tag{20}$$

for S_3 , and

$$\begin{aligned} \frac{\beta GH^4}{\pi\gamma} \left[\frac{1}{2+\beta} \left(\frac{\beta GH^2}{\pi\alpha_-} \right)^{\beta} {}_2F_1 \left(1+\beta, 2+\beta, 3+\beta, -\frac{\beta GH^2}{\pi\alpha_-} \right) \right. \\ \left. + \frac{1}{2-\beta} \left(\frac{\beta GH^2}{\pi\alpha_+} \right)^{-\beta} {}_2F_1 \left(1-\beta, 2-\beta, 3-\beta, -\frac{\beta GH^2}{\pi\alpha_+} \right) \right] = \frac{8\pi G}{3} \rho + \frac{\Lambda}{3}, \tag{21} \end{aligned}$$

for S_4 ; where ${}_2F_1$ (arguments) symbolizes the Hypergeometric function. Owing to the above equations, we may argue that the generalized entropy generates an effective energy density (along with the normal matter fields) in the Friedmann equation; for instance, the energy density coming from the S_4 is given by,

$$\begin{aligned} \rho_g = \frac{3}{8\pi G} \left\{ H^2 - \frac{\beta GH^4}{\pi\gamma} \left[\frac{1}{2+\beta} \left(\frac{\beta GH^2}{\pi\alpha_-} \right)^{\beta} {}_2F_1 \left(1+\beta, 2+\beta, 3+\beta, -\frac{\beta GH^2}{\pi\alpha_-} \right) \right. \right. \\ \left. \left. + \frac{1}{2-\beta} \left(\frac{\beta GH^2}{\pi\alpha_+} \right)^{-\beta} {}_2F_1 \left(1-\beta, 2-\beta, 3-\beta, -\frac{\beta GH^2}{\pi\alpha_+} \right) \right] \right\}, \end{aligned}$$

and consequently, Equation (21) can be written as,

$$H^2 = \frac{8\pi G}{3} (\rho + \rho_g) + \frac{\Lambda}{3}.$$

Similarly the energy density corresponding to the 3-parameter generalized entropy can be determined from Equation (20).

The energy density coming from the generalized entropy plays a significant role during the evolutionary course of the universe. However, without any matter fields inside of the horizon, Equation (19) (or Equation (18)) shows $\dot{H} = 0$ leading to $H = \text{constant}$. This argues that the entropic cosmology, in absence of matter fields, results in a de-Sitter

spacetime, or equivalently, an eternal inflation having no exit. Therefore, in order to obtain a viable inflation, one needs to incorporate either of the following possibilities—(a) the entropic parameters slowly vary with the cosmic expansion of the universe (one may see [53] where the authors studied a energy scale-varying entropic index that could lead to new physics in the early universe), or (b) some matter fields inside of the horizon. In the present work, we will concentrate on the second possibility, where the matter field is taken to be a minimally coupled scalar field with a power law potential. Such form of the scalar potential in the context of generalized entropy is well motivated, as discussed in the introduction. However before moving to the case of the generalized entropy of the apparent horizon, we will discuss the status of ϕ^n potential (from inflationary perspective) with the Bekenstein–Hawking entropy in order to understand the role of the generalized entropy during the early evolution of the universe. These are the subjects of the next sections (Moreover, the cases with varying entropic parameters, in the context of three-parameter and four-parameter generalized entropies, are addressed in Appendix A).

3. Status of ϕ^n Inflationary Potential with Bekenstein–Hawking Entropy

In this section we will investigate whether a ϕ^n type of potential, in the case where the entropy of the apparent horizon is given by the Bekenstein–Hawking entropy, can lead to a viable inflation during the early universe. As a result, the Equations (16) and (17) read as (by considering $S_g = S$)

$$H^2 = \frac{8\pi G}{3} \left\{ \frac{\dot{\phi}^2}{2} + V(\phi) \right\} \tag{22}$$

$$\dot{H} = -4\pi G \dot{\phi}^2, \tag{23}$$

respectively, and the continuity equation for the scalar field becomes

$$\ddot{\phi} + 3H\dot{\phi} + \partial_\phi V = 0. \tag{24}$$

The above equations are similar to that of in the standard scalar field cosmology—this is however expected, as the Bekenstein–Hawking entropy leads to the usual Friedmann equations in the realm of entropic cosmology. By the slow roll approximation, i.e., by assuming that the potential energy during inflation dominates all the other forms of energies, the first and second Friedmann equations become

$$H^2 = \frac{8\pi G}{3} V(\phi) \quad \text{and} \quad \dot{H} = -4\pi G \dot{\phi}^2, \tag{25}$$

respectively, and moreover, the continuity equation is approximated as,

$$\dot{\phi} = -\left(\frac{1}{3H}\right) \partial_\phi V = 0. \tag{26}$$

Consequently the slow roll parameters take the following form,

$$\epsilon(t) = \frac{3}{2} \frac{\dot{\phi}^2}{V(\phi)} \quad \text{and} \quad \eta(t) = -\sqrt{\frac{3}{8\pi G} \frac{1}{V(\phi)} \frac{\ddot{\phi}}{\dot{\phi}}}. \tag{27}$$

For the scalar potential to be of the form like $V(\phi) = V_0 \phi^n$, the dynamical equation for the scalar field from Equation (26) obtains the expression

$$\dot{\phi} \simeq -\frac{1}{3H} \partial_\phi V = -\frac{nV_0}{3} \left(\frac{8\pi G}{2} V_0\right)^{-\frac{1}{2}} \phi^{\frac{n}{2}-1}, \tag{28}$$

by using which, into Equation (27), we obtain the slow roll parameters in terms of scalar field as follows:

$$\epsilon(\phi) = \frac{n^2}{16\pi G} \phi^{-2} \quad \text{and} \quad \eta(\phi) = \frac{n(n-2)}{16\pi G} \phi^{-2}, \quad (29)$$

respectively, where both $\epsilon(\phi)$ and $\eta(\phi)$ are inversely proportional to ϕ , i.e., both of the slow roll parameters increases with the decreasing value of the scalar field. Such behaviour of $\epsilon(\phi)$ actually helps to trigger a viable inflation. In particular, a considerably large value of ϕ makes $\epsilon(\phi)$ less than unity, which confirms an accelerated stage of the universe. However as the scalar field rolls down (from a larger value to a smaller value, governing by Equation (26)), $\epsilon(\phi)$ increases, and at a certain instance of time, $\epsilon(\phi)$ becomes unity, which indicates the end of inflation. Let us consider that $\epsilon(\phi)$ becomes unity at $\phi = \phi_f$, i.e., $\epsilon(\phi_f) = 1$, which, along with Equation (29), yields the following form of ϕ_f (in terms of model parameters):

$$\phi_f^2 = \frac{n^2}{16\pi G}. \quad (30)$$

The total number of e-folds of inflationary epoch is given by

$$N_f = \int_{\phi_c}^{\phi_f} \frac{H}{\dot{\phi}} d\phi \simeq - \int_{\phi_c}^{\phi_f} \frac{3H^2}{\partial_\phi V} d\phi = - \frac{4\pi G}{n} (\phi_f^2 - \phi_c^2) = \frac{4\pi G}{n} \left(\phi_c^2 - \frac{n^2}{16\pi G} \right), \quad (31)$$

where in the last step we used the condition $\epsilon(\phi_f) = 1$. Here, ϕ_c is the scalar field at the time of horizon crossing of the CMB mode ($\sim 0.05\text{Mpc}^{-1}$ at which we are interested to determine the observable parameters). Inverting Equation (31), we immediately obtain ϕ_c in terms of N_f as,

$$\phi_c = \sqrt{\frac{n}{16\pi G} (4N_f + n)}, \quad (32)$$

so that we can then compute the slow roll parameters at the instant of horizon crossing of the CMB scale modes, and they are given by,

$$\epsilon(\phi_c) = \frac{n}{4N_f + n} \quad \text{and} \quad \eta(\phi_c) = \frac{n-2}{4N_f + n}. \quad (33)$$

These will be used to compute the spectral tilt for primordial curvature perturbation (n_s) and the tensor-to-scalar ratio (r) that are defined by

$$n_s = 1 - 6\epsilon + 2\eta \Big|_{\phi=\phi_c} \quad \text{and} \quad r = 16\epsilon \Big|_{\phi=\phi_c}, \quad (34)$$

respectively, at the horizon crossing instant. Using the expressions of $\epsilon(\phi_c)$ and $\eta(\phi_c)$ into the above equation along with a little bit of simplification yields the final forms of n_s and r as follows:

$$n_s = 1 - \frac{4(n+1)}{4N_f + n} \quad \text{and} \quad r = \frac{16n}{4N_f + n}. \quad (35)$$

Having Equation (35) in hand, we now examine the status of ϕ^n potential with the Bekenstein–Hawking entropy of the apparent horizon, in respect to the Planck 2018 data which puts a constraint on the observable indices as [54]:

$$n_s = 0.9649 \pm 0.0042 \quad \text{and} \quad r < 0.064. \quad (36)$$

It is evident from Equation (35) that both the n_s and r depend on n and N_f . In Figure 1 we plot the region of validity for the inflationary indices in the case of the Bekenstein–Hawking entropy in the n - N_f space (we will concentrate around $N_f = 60$, which is consistent with

the resolution of the horizon problem). It may be noted that we consider $n \geq 1$ in the plot, as $n < 1$ generates some singularity problem in the scalar field equation (through $\frac{\partial V}{\partial \phi}$) when the scalar field passes through $\phi = 0$. We see from this plot that the two regions barely overlaps in a small region (near at $n = 1$) far from the expected value of n_s , which can be considered statistically negligible. Therefore, in the scenario where the horizon entropy is given by the Bekenstein–Hawking entropy and the scalar field inside the horizon has a ϕ^n form of potential, there is no choice of the parameter n that provides the simultaneous agreement of $\{n_s, r\}$ with the Planck observation.

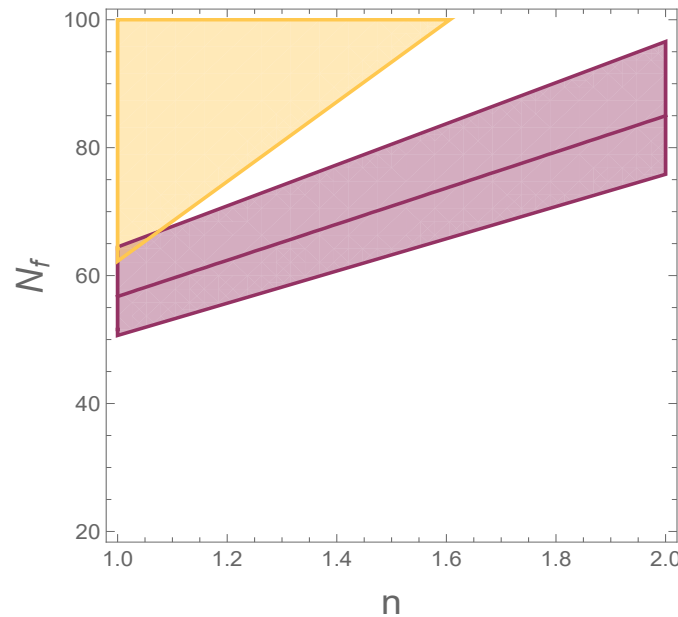


Figure 1. Region of validity for the observable indices n_s (Purple) and r (Orange) given in Equation (35) in the n - N_f space. The purple region corresponds to the constraints region of n_s while the purple line represents its central value.

4. Status of ϕ^n Inflationary Potential with Generalized Entropy

As showed in Section [3] that the simple $V(\phi) \sim \phi^2$ potential with the Bekenstein–Hawking entropy for the apparent horizon does not lead to a viable inflation from the perspective of the Planck 2018 data. However the story of the ϕ^2 inflaton potential may become different in generalized entropic cosmology, in which case, the entropic energy density arising from the generalized entropy contributes a significant role during the universe’s evolution. Thus we will investigate the status of $V(\phi) \sim \phi^2$ potential in the context of generalized entropic cosmology, where the presence of entropic energy density results in a different cosmological scenario compared to that of in the Bekenstein–Hawking entropic scenario. In particular, we will consider that the horizon entropy is of the form of four-parameter generalized entropy and the matter fields inside of the horizon is dominated by a scalar field having $V(\phi) \sim \phi^n$ potential.

For the case of four-parameter generalized entropy, the first Friedmann Equation (21), without any cosmological constant, is given by:

$$\frac{\beta GH^4}{\pi \gamma} \left[\frac{1}{2 + \beta} \left(\frac{\beta GH^2}{\pi \alpha_-} \right)^\beta 2F_1 \left(1 + \beta, 2 + \beta, 3 + \beta, -\frac{\beta GH^2}{\pi \alpha_-} \right) + \frac{1}{2 - \beta} \left(\frac{\beta GH^2}{\pi \alpha_+} \right)^{-\beta} 2F_1 \left(1 - \beta, 2 - \beta, 3 - \beta, -\frac{\beta GH^2}{\pi \alpha_+} \right) \right] = \frac{8\pi G}{3} \rho. \quad (37)$$

The cosmological constant during the early phase of the universe is suppressed compared to the inflaton energy density and, thus, one can safely neglect the Λ in studying the inflationary dynamics of the universe. Since during the inflation the typical energy scale is of order $\sim 10^{-4}M_{Pl}$ (where $M_{Pl} = 1/\sqrt{8\pi G}$ with G being the Newton's gravitational constant), we consider $GH^2 \ll 1$ during the early universe. As a consequence, we can expand the hypergeometric functions appearing in Equation (37), thanks to the relation ${}_2F_1(a, b, c, x) = 1 + \frac{ab}{c}x + O(x^2)$, leading to

$$\frac{1}{2-\beta} \frac{\beta GH^4}{\pi\gamma} \left(\frac{\beta GH^2}{\pi\alpha_+}\right)^{-\beta} \left(1 - \frac{(1-\beta)(2-\beta)\beta GH^2}{3-\beta\pi\alpha_+}\right) = \frac{8\pi G}{3}\rho, \tag{38}$$

on solving which, at the leading order in GH^2 , we obtain

$$H^2 = \left(\frac{8\pi G}{3} \frac{\gamma}{\alpha_+} \left(\frac{\beta G}{\pi\alpha_+}\right)^{\beta-1} (2-\beta)\rho\right)^{\frac{1}{2-\beta}}. \tag{39}$$

Moreover the second Friedmann Equation (16), due to $GH^2 \ll 1$, takes the following form

$$\frac{\alpha_+}{\gamma} \left(\frac{\alpha_+}{\beta} \frac{\pi}{GH^2}\right)^{\beta-1} \dot{H} = -4\pi G(\rho + p). \tag{40}$$

As mentioned earlier that we will consider a minimally coupled scalar field as the matter field inside of the horizon, for which, the corresponding energy density (ρ) and the pressure (p) are given by

$$\rho = \frac{\dot{\phi}^2}{2} + V(\phi) \quad \text{and} \quad p = \frac{\dot{\phi}^2}{2} - V(\phi), \tag{41}$$

respectively, where ϕ is the scalar field under consideration and $V(\phi)$ is its potential. Therefore, Equations (39) and (40) become

$$H^2 = \left(\frac{8\pi G}{3} \frac{\gamma}{\alpha_+} \left(\frac{\beta G}{\pi\alpha_+}\right)^{\beta-1} (2-\beta) \left\{\frac{\dot{\phi}^2}{2} + V(\phi)\right\}\right)^{\frac{1}{2-\beta}}. \tag{42}$$

and

$$\frac{\alpha_+}{\gamma} \left(\frac{\alpha_+}{\beta} \frac{\pi}{GH^2}\right)^{\beta-1} \dot{H} = -4\pi G\dot{\phi}^2. \tag{43}$$

The above two equations along with the continuity equation of the scalar field, i.e.,

$$\ddot{\phi} + 3H\dot{\phi} + \partial_\phi V = 0. \tag{44}$$

govern the cosmological dynamics in the present context. Due to the slow roll approximation during the early universe, in particular

$$\ddot{\phi} \ll H\dot{\phi} \quad \text{and} \quad \frac{\dot{\phi}^2}{2} \ll V, \tag{45}$$

Equations (42) and (43) read as

$$H^2 = \left[\frac{8\pi G}{3} \frac{\gamma}{\alpha_+} \left(\frac{\beta G}{\alpha_+\pi}\right)^{\beta-1} (2-\beta) V(\phi)\right]^{\frac{1}{2-\beta}} \tag{46}$$

$$\dot{H} = -\frac{2\pi G\gamma}{\alpha_+} \left(\frac{\beta GH^2}{\alpha_+\pi}\right)^{\beta-1} \dot{\phi}^2, \tag{47}$$

and moreover, the conservation equation is approximated as

$$\dot{\phi} \simeq -\frac{1}{3H} \partial_{\phi} V. \tag{48}$$

Therefore the first and the second slow roll parameters (defined by $\epsilon(t) = -\frac{\dot{H}}{H^2}$ and $\eta(t) = -\frac{\ddot{H}}{2H\dot{H}}$) take the following form

$$\epsilon(t) = \frac{3}{4(2-\beta)} \frac{\dot{\phi}^2}{V(\phi)} \tag{49}$$

$$\eta(t) = -\left[\frac{8\pi G}{3} \frac{\gamma}{\alpha_+} \left(\frac{\beta G}{\alpha_+ \pi} \right)^{\beta-1} (2-\beta) V(\phi) \right]^{\frac{1}{2(2-\beta)}} \left[\frac{\ddot{\phi}}{\dot{\phi}} + \frac{1-\beta}{4(2-\beta)} \frac{\partial_{\phi} V}{V(\phi)} \dot{\phi} \right], \tag{50}$$

where for the second parameter we have used Equation (48). At this stage, let us consider the power law form of the scalar potential, i.e., $V(\phi) = V_0 \phi^n$ (with V_0 and n being two positive constants). For this scalar potential, we can compute the expression of $\dot{\phi}$ from Equation (48), and is given by,

$$\dot{\phi} \simeq -\frac{V_0}{3} n A^{-\frac{1}{2(2-\beta)}} \phi^{\frac{3-2\beta}{2(2-\beta)} n - 1}, \tag{51}$$

where we have

$$A \equiv \frac{8\pi G}{3} \frac{\gamma}{\alpha_+} \left(\frac{\beta G}{\alpha_+ \pi} \right)^{\beta-1} (2-\beta) V_0. \tag{52}$$

Plugging back the above expression of $\dot{\phi}$ into Equation (49) yields the slow roll parameters in terms of ϕ as follows:

$$\epsilon(\phi) = \frac{V_0 n^2}{12(2-\beta)} A^{-\frac{1}{2-\beta}} \phi^{\frac{1-\beta}{2-\beta} n - 2} \tag{53}$$

$$\eta(\phi) = \frac{V_0}{2} n \left(\frac{7-5\beta}{4(2-\beta)} n - 1 \right) A^{-\frac{1}{2-\beta}} \phi^{\frac{1-\beta}{2-\beta} n - 2}, \tag{54}$$

where A is given above in Equation (52). It seems that the positivity of ϵ demands $\beta < 2$. Moreover the above expression of $\epsilon(\phi)$ clearly points that the model parameters (β and n) need to obey the following constraint relation, namely

$$\left(\frac{1-\beta}{2-\beta} \right) n < 2 \tag{55}$$

in order to have a successful inflation with an exit. This is because that under Condition (55), $\epsilon(\phi)$ remains less than unity for a considerably large positive value of ϕ and triggers an accelerating stage of the universe; however, as the scalar field rolls down along the potential, $\epsilon(\phi)$ increases and moves to unity at a certain value of $\phi = \phi_f$ (say) which indicates the end of inflation. Thus as a whole—owing to Condition (55)— $\epsilon(\phi)$ depends on the inverse power of ϕ , which proves to be suitable for obtaining a successful inflation with a graceful exit. The end point of inflation, i.e $\epsilon(\phi_f) = 1$, immediately leads to ϕ_f from Equation (53) as follows:

$$A^{\frac{1}{2-\beta}} \phi_f^{2-\frac{1-\beta}{2-\beta} n} = \frac{V_0 n^2}{12(2-\beta)}. \tag{56}$$

Consequently, the e-fold duration of the inflationary era is given by,

$$\int_0^{N_f} dN = \int_{t_c}^{t_f} H dt = \int_{\phi_c}^{\phi_f} \frac{H}{\dot{\phi}} d\phi, \tag{57}$$

from which, using the conservation equation, we obtain

$$N_f \simeq - \int_{\phi_c}^{\phi_f} \frac{3H^2}{\partial_\phi V} d\phi = \frac{3}{V_0 n \left(2 - \frac{1-\beta}{2-\beta} n\right)} A^{\frac{1}{2-\beta}} \left(\phi_c^{2 - \frac{1-\beta}{2-\beta} n} - \phi_f^{2 - \frac{1-\beta}{2-\beta} n} \right). \tag{58}$$

Here, ϕ_c is the scalar field at the beginning of inflation (i.e., at $N = 0$) which is considered to be the horizon-crossing instant of the large CMB scale mode ($\sim 0.05 \text{ Mpc}^{-1}$). By using Equations (56) and (58), one can easily obtain the expression for ϕ_c as follows:

$$\phi_c = \left[A^{-\frac{1}{2-\beta}} \left(\frac{nV_0}{3} \left(2 - \frac{1-\beta}{2-\beta} n\right) N_f + \frac{V_0 n^2}{12(2-\beta)} \right) \right]^{\frac{1}{2 - \frac{1-\beta}{2-\beta} n}}. \tag{59}$$

Clearly $\phi_c > \phi_f$, due to the constraint in Equation (55), as expected. Substituting the above form of ϕ_c into Equation (53) along with a little bit of simplification lead to the slow roll parameters, evaluated at the instant of horizon crossing, as

$$\epsilon(\phi_c) = \frac{n}{n + 4(2-\beta) \left(2 - \frac{1-\beta}{2-\beta} n\right) N_f} \tag{60}$$

$$\eta(\phi_c) = \frac{(7-5\beta)n - 4(2-\beta)}{n + 4(2-\beta) \left(2 - \frac{1-\beta}{2-\beta} n\right) N_f}, \tag{61}$$

respectively. Consequently, the scalar spectral index and the tensor-to-scalar ratio are obtained as

$$\begin{aligned} n_s &= 1 - 6\epsilon + 2\eta \Big|_{\phi=\phi_c} = 1 + \frac{2(4-5\beta)n - 8(2-\beta)}{n + 4(2-\beta) \left(2 - \frac{1-\beta}{2-\beta} n\right) N_f}, \\ r &= 16\epsilon \Big|_{\phi=\phi_c} = \frac{16n}{n + 4(2-\beta) \left(2 - \frac{1-\beta}{2-\beta} n\right) N_f}. \end{aligned} \tag{62}$$

Here, we compute the observable indices at the instant of horizon crossing of the large-scale CMB modes on which we are interested to corroborate the theoretical predictions with the Planck 2018 data. According to the Planck result, the n_s and r are constrained by Equation (36). From Equation (62), it may be noted that n_s and r is influenced by the entropic parameter β and that the dependence by the potential is given by the exponent n . Moreover, n_s and r also depend on the inflationary e-folding number N_f . Actually, the other entropic parameters, in particular α_\pm and γ , are packed within A (see Equation (52)) and these arise in the final expression of the observable indices through N_f . One can easily choose α_\pm and γ in such a way that N_f becomes around ≈ 60 . Therefore the important constraint that we need to take care is on the parameter β . In Figure 2 and Figure 3, we plot the region of validity of $\{n_s, r\}$ (in respect to the Planck 2018 constraint) in the β - N_f space for the case $n = 1$, and the case $n = 2$ respectively. The presence of an intersection between β and N_f (around $N_f = 60$) shows the possibility of the agreement of the four-parameter generalized entropic inflation with the Planck data. In both the figures, the gray shadowed region, corresponding to $\beta > 2$, is not acceptable since it leads to negative values of ϵ (as demonstrated after Equation (53)).

Thus as a whole, the power law inflaton potential (for $n = 1$ as well as for $n = 2$) turns out to produce a viable inflation with a graceful exit and is also consistent with the Planck data in the case where the apparent horizon has the four-parameter generalized entropy, unlike to the case of the Bekenstein–Hawking entropy, which fails to show the simultaneous compatibility of the inflationary indices with the observation.

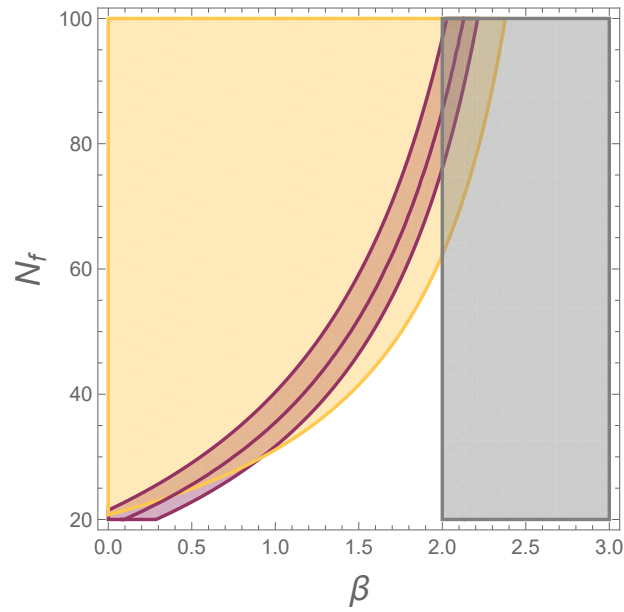


Figure 2. Region of validity of the observable indices n_s (purple) and r (orange) given in Equation (62) in respect to the Planck data. Here we take $n = 1$. The gray shadowed region, corresponding to $\beta > 2$, is not acceptable since it leads to negative values of ϵ . The purple region corresponds to the allowed region of n_s while the purple line represents its central value (i.e., $n_s = 0.9649$).

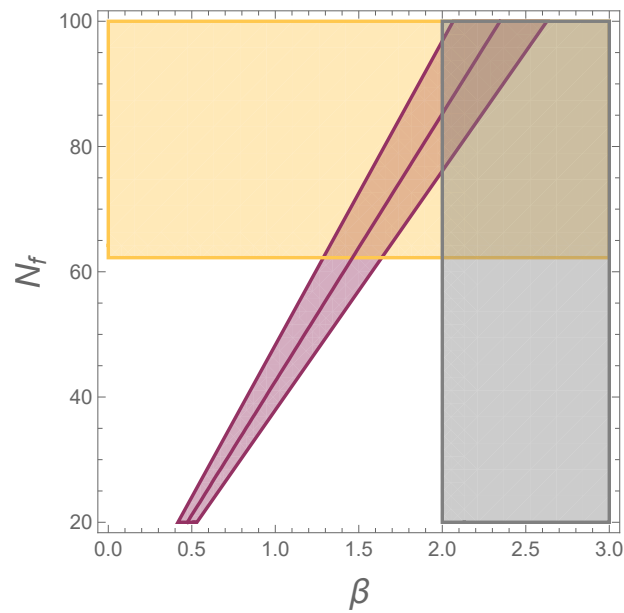


Figure 3. Region of validity of the observable indices n_s (purple) and r (orange) given in Equation (62) in respect to the Planck data. Here we take $n = 2$. The gray shadowed region, corresponding to $\beta > 2$, is not acceptable since it leads to negative values of ϵ . The purple region corresponds to the allowed region of n_s while the purple line represents its central value (i.e., $n_s = 0.9649$).

5. Conclusions

We examine the status of the simplest quadratic inflaton potential in the realm of entropic cosmology where the entropy of the apparent horizon is given by the four-parameter generalized entropy and the matter fields inside of the horizon is dominated by a minimally coupled scalar field with a ϕ^n type of potential (where ϕ is the scalar field under consideration). Actually the quadratic potential (i.e., for $n = 2$) in standard scalar field cosmology fails to produce a viable inflation, in particular, the ϕ^2 potential is not compatible with the inflationary observables based on the recent Planck 2018 data. Here, it is good to

mention that in the language of entropic cosmology, the standard scalar field cosmology is analogous to the case where the horizon has Bekenstein–Hawking entropy, which results in the usual Friedmann equations. However the story becomes different when the apparent horizon acquires the four-parameter generalized type of entropy, in which case, the entropic energy density plays a significant role during the evolutionary course of the universe. The appearance of the generalized entropy actually generates an effective energy density which modifies the Friedmann equations, and consequently the cosmic evolution of the universe, compared to the standard cosmological scenario. As a result, it turns out that with the four-parameter generalized entropy of the apparent horizon, the ϕ^2 potential results in—(1) an inflation era described by a quasi de-Sitter evolution of the Hubble parameter, which has an exit at around 55–60 e-folding number, (2) the inflationary observable quantities like the spectral index for primordial scalar perturbation and the tensor-to-scalar ratio are simultaneously compatible with the recent Planck data for suitable values of the entropic parameters, (3) for the same parameter values, the typical energy scale of the universe at the onset of inflation becomes of the order $\sim 10^{-4}$ (in Planck units). Therefore, this work clearly shows that the ϕ^2 potential can be made back into the inflationary scenario provided the apparent horizon has the four-parameter generalized type of entropy.

Regarding the four-parameter generalized entropy, a valid question may be raised about its uniqueness, in particular, whether the S_4 in Equation (2) is the unique four-parameter generalized entropy or one may construct another four-parameter entropy function that also accommodates all the known entropies. However the uniqueness property of S_4 is out of the motivation of this work, and thus we expect to study it in some future work.

Author Contributions: Conceptualization, T.P.; Methodology, T.P.; Formal analysis, S.D.; Investigation, T.P.; Writing—original draft, S.D.; Writing—review and editing, S.D.O. and T.P.; Visualization, S.D.O. and T.P.; Supervision, S.D.O. All authors have read and agreed to the published version of the manuscript.

Funding: This work was partially supported by MICINN (Spain), project PID2019-104397GB-I00 and by the program Unidad de Excelencia Maria de Maeztu CEX2020-001058-M, Spain (S.D.O). This work is funded by MCIN/AEI/10.13039/501100011033 and FSE+, reference PRE2021-098098 (S.O).

Data Availability Statement: Data are contained within the article.

Conflicts of Interest: The authors declare no conflict of interest.

Appendix A. Generalized Entropic Inflation with Varying Entropic Parameters

In this section, we will show that, beside the consideration of matter fields inside of the horizon, one can get a proper inflation (with a graceful exit) in the context of entropic cosmology by considering the entropic parameters to vary with the cosmic expansion of the universe. In particular, we will concentrate on the three-parameter and the four-parameter generalized entropy, namely the S_3 and the S_4 , where the parameter γ is considered to vary with the cosmic time. Thus $\gamma = \gamma(N)$ where N represents the e-fold number. The running behavior of γ can be described by quantum gravity as, actually, in the sector of gravity, the degrees of freedom may increase if the spacetime fluctuates at high energy scales. In the absence of matter fields inside of the apparent horizon, i.e. $\rho = p = \Lambda = 0$, and for $\gamma = \gamma(N)$, the thermodynamic law on the apparent horizon states:

$$0 = TdS_g(S, \gamma(N)) = \frac{\partial S_g}{\partial S} dS + \frac{\partial S_g}{\partial \gamma} \gamma'(N) dN, \tag{A1}$$

where a prime indicates the differentiation with respect to N , and $S_g = \{S_3, S_4\}$. Taking into account the dependence of the entropy on γ and defining $\sigma(N) \equiv \gamma'/\gamma$ we find

$$\frac{1}{S_g} \frac{\partial S_g}{\partial S} dS = \frac{\partial \ln S_g}{\partial S} dS = \sigma(N) dN, \tag{A2}$$

integrating which we find

$$S_g = \exp \left(\int_0^N \sigma(N') dN' \right). \tag{A3}$$

At this stage, we will take a certain form of $\gamma(N)$ as follows:

$$\gamma(N) = \begin{cases} \gamma_0 \exp \left(\int_N^{N_f} \sigma(N') dN' \right) & N \leq N_f \\ \gamma_0 & N > N_f \end{cases}, \quad \text{with} \quad \sigma(N) \equiv \sigma_0 + e^{-(N_f-N)}, \tag{A4}$$

where σ_0 is a constant. The second term in the expression of $\sigma(N)$ becomes effective only when $N \approx N_f$, i.e., near the end of inflation. The term $e^{-(N_f-N)}$ in the $\sigma(N)$ is actually considered to ensure an exit from inflation era and thus proves to be an useful one to make the inflationary scenario viable. In the case of the three-parameter entropy, Equation (A3) leads to the relation

$$\left(1 + \frac{\alpha\pi}{\beta GH^2} \right)^\beta - 1 = \exp \left(\int_0^N \sigma(N') dN' \right), \tag{A5}$$

which for $GH^2 \ll 1$ gives the asymptotic solution for the Hubble parameter

$$H(N) = 4\pi M_{Pl} \sqrt{\frac{\alpha}{\beta}} \left(1 + \exp \left(\int_0^N \sigma(N') dN' \right) \right)^{-\frac{1}{2\beta}}. \tag{A6}$$

In order to apply the standard inflationary analysis we compute the slow-roll parameter in terms of the e-fold parameter $\epsilon(N)$ as

$$\epsilon(N) \equiv -\frac{H'(N)}{H(N)} = \frac{1}{2\beta} \frac{\sigma(N)}{\left[1 + \exp \left(-\int_0^N \sigma(N') dN' \right) \right]}, \tag{A7}$$

and

$$\frac{\epsilon'(N)}{\epsilon(N)} = \frac{e^{-(N_f-N)}}{\sigma(N)} + \frac{\sigma(N)}{1 + \exp \left(\int_0^N \sigma(N') dN' \right)}, \tag{A8}$$

where we used the explicit expression of Equation (A4) to simplify the result. In order to impose some constraints on the model parameters we compute various observable indices such as the primordial curvature perturbation n_s and the tensor-to-scalar ratio r obtained as

$$n_s = 1 - 2\epsilon - 2\frac{\epsilon'}{\epsilon} \Big|_{N=0} \quad \text{and} \quad r = 16\epsilon \Big|_{N=0}. \tag{A9}$$

We compute these indices in the instant of horizon crossing of the large scale CMB modes, which corresponds to the beginning of inflation $N = 0$.

In the case of the three-parameter entropy with Hubble parameter of Equation (A6) along with $\sigma(N)$ defined in Equation (A4) the observable indices have the expressions

$$n_s = 1 - \left(1 + \frac{1}{2\beta} \right) (\sigma_0 + e^{-N_f}) - \frac{2}{1 + e^{N_f}\sigma_0} \quad \text{and} \quad r = \frac{4(\sigma_0 + e^{-N_f})}{\beta}. \tag{A10}$$

Since the e-fold number of inflation N_f will be taken to be $\sim 55-60$ we will neglect the terms e^{-N_f} . We can then impose an end to the inflation era with the condition

$$\epsilon(N_f) = \frac{1 + \sigma_0}{2\beta(1 + e^{-1-N_f\sigma_0})} = 1, \tag{A11}$$

from which we obtain an inter-relation between β and σ_0 that can then reduce the number of parameters inside the observable indices. This substitution gives

$$n_s = 1 - \frac{\sigma_0(2 + \sigma_0 + e^{-1-N_f\sigma_0})}{1 + \sigma_0} \quad \text{and} \quad r = \frac{8\sigma_0(1 + e^{-1-N_f\sigma_0})}{1 + \sigma_0}, \quad (\text{A12})$$

which shows that both the n_s and r depend on σ_0 and N_f . Since these observable indices are functions of only two variables we can directly check their validity in respect to the Planck 2018 data. In Figure A1 we plot the region of validity of $\{n_s, r\}$ given in Equation (A12) in σ_0 - N_f space. As we can see from Figure A1, there is no overlapped region between σ_0 , and thus the three-parameter generalized entropy with varying parameters does not provide a inflationary scenario that is compatible with the Planck data.

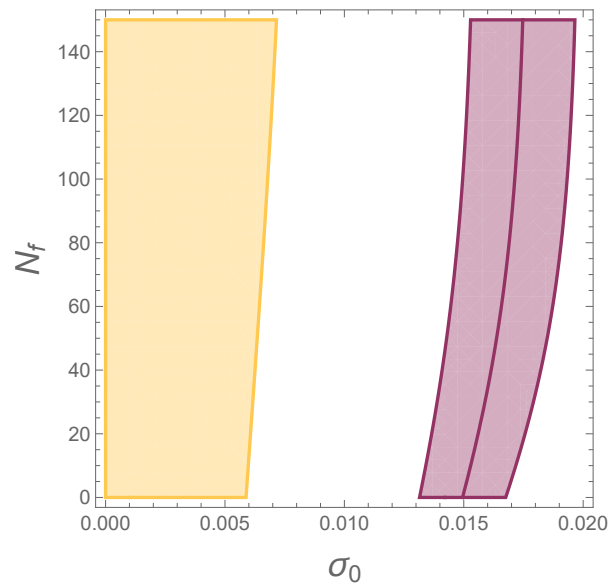


Figure A1. Region of validity for n_s (blue) and r (orange) in case of the three-parameter generalized entropy with varying parameters (by using Equation (A12)) in respect to the Planck data.

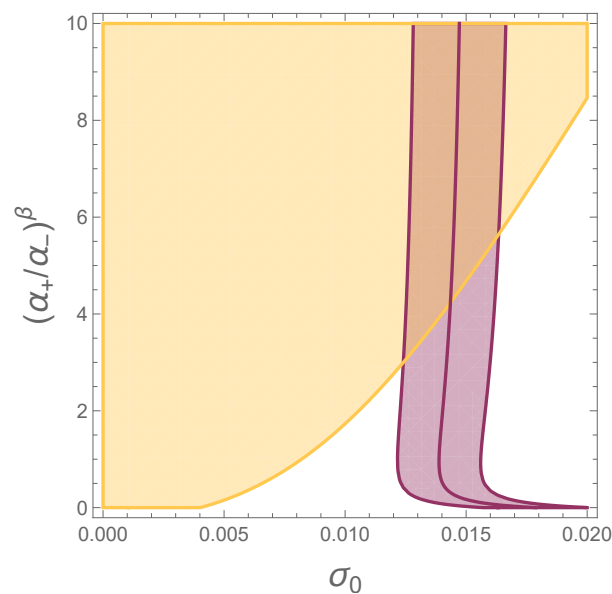


Figure A2. Region of validity for n_s (blue) and r (orange) in case of the four-parameter generalized entropy with varying parameters (by using Equations (A18) and (A19)) in respect to the Planck data. Here, we take $N_f = 58$.

In the case of the four-parameter entropy, Equation (A3) leads to

$$\left(1 + \frac{\alpha_+ \pi}{\beta GH^2}\right)^\beta - \left(1 + \frac{\alpha_- \pi}{\beta GH^2}\right)^{-\beta} = \exp\left(\int_0^N \sigma(N') dN'\right), \tag{A13}$$

in the limit $GH^2 \ll 1$ we can safely neglect the plus one in parenthesis and solve the equation for $H(N)$

$$H(N) = 4\pi M_{Pl} \sqrt{\frac{\alpha_+}{\beta}} \left[\frac{1}{2} \exp\left(\int_0^N \sigma(N') dN'\right) \left(1 + \sqrt{1 + 4\left(\frac{\alpha_+}{\alpha_-}\right)^\beta \exp\left(-2 \int_0^N \sigma(N') dN'\right)}\right) \right]^{-\frac{1}{2\beta}}. \tag{A14}$$

For this Hubble parameter the slow roll parameter is

$$\epsilon(N) = \frac{1}{2\beta} \frac{\sigma(N)}{\sqrt{1 + 4\left(\frac{\alpha_+}{\alpha_-}\right)^\beta \exp\left(-2 \int_0^N \sigma(N') dN'\right)}}, \tag{A15}$$

and

$$\frac{\epsilon'(N)}{\epsilon(N)} = \frac{e^{-(N_f-N)}}{\sigma(N)} + \frac{\sigma(N)}{1 + \frac{1}{4}\left(\frac{\alpha_+}{\alpha_-}\right)^{-\beta} \exp\left(2 \int_0^N \sigma(N') dN'\right)}. \tag{A16}$$

Again we will impose the condition on the end of inflation as

$$\epsilon(N_f) = \frac{1 + \sigma_0}{2\beta \sqrt{1 + 4\left(\frac{\alpha_+}{\alpha_-}\right)^\beta e^{-2-2N_f\sigma_0}}} = 1, \tag{A17}$$

which leads to an interrelation between the parameters $(\alpha_+/\alpha_-)^\beta$ and σ_0 . Using such a relation, we obtain the observable indices in the context of four-parameter generalized entropy with varying parameters as follows:

$$n_s = 1 - \frac{2\sigma_0 \sqrt{1 + 4\left(\frac{\alpha_+}{\alpha_-}\right)^\beta e^{-2-2N_f\sigma_0}}}{(1 + \sigma_0) \sqrt{1 + 4\left(\frac{\alpha_+}{\alpha_-}\right)^\beta}} - \frac{8\sigma_0 \left(\frac{\alpha_+}{\alpha_-}\right)^\beta}{1 + 4\left(\frac{\alpha_+}{\alpha_-}\right)^\beta}, \tag{A18}$$

and

$$r = \frac{16\sigma_0 \sqrt{1 + 4\left(\frac{\alpha_+}{\alpha_-}\right)^\beta e^{-2-2N_f\sigma_0}}}{(1 + \sigma_0) \sqrt{1 + 4\left(\frac{\alpha_+}{\alpha_-}\right)^\beta}}, \tag{A19}$$

respectively. Equations (A18) and (A19) clearly indicate that both the n_s and r depend on σ , $(\alpha_+/\alpha_-)^\beta$ and N_f . For a fixed N_f , particularly around $N_f = 55-60$, which is consistent with the resolution of the horizon problem, we find the constraints imposed for these variables in order to obtain viable inflation [54]. The validity of these constraints is shown by the intersection of the two regions in Figure A2 for $N_f = 58$.

Thus, as a whole, it turns out that in the context of entropic cosmology with varying entropic parameters, the four-parameter generalized entropy can provide a viable inflation consistent with the Planck data, unlike the three-parameter generalized entropy that fails to show the simultaneous compatibility of primordial inflationary indices with the Planck result.

References

1. Li, M. A Model of holographic dark energy. *Phys. Lett. B* **2004**, *603*, 1. [CrossRef]
2. Li, M.; Li, X.D.; Wang, S.; Wang, Y. Dark Energy. *Commun. Theor. Phys.* **2011**, *56*, 525–604. [CrossRef]
3. Wang, S.; Wang, Y.; Li, M. Holographic Dark Energy. *Phys. Rept.* **2017**, *696*, 1. [CrossRef]
4. Nojiri, S.; Odintsov, S.D. Unifying phantom inflation with late-time acceleration: Scalar phantom-non-phantom transition model and generalized holographic dark energy. *Gen. Rel. Grav.* **2006**, *38*, 1285. [CrossRef]
5. Landim, R.G. Note on interacting holographic dark energy with a Hubble-scale cutoff. *Phys. Rev. D* **2022**, *106*, 043527. [CrossRef]
6. Zhang, X. Statefinder diagnostic for holographic dark energy model. *Int. J. Mod. Phys. D* **2005**, *14*, 1597. [CrossRef]
7. Elizalde, E.; Nojiri, S.; Odintsov, S.D.; Wang, P. Dark energy: Vacuum fluctuations, the effective phantom phase, and holography. *Phys. Rev. D* **2005**, *71*, 103504. [CrossRef]
8. Ito, M. Holographic dark energy model with non-minimal coupling. *Europhys. Lett.* **2005**, *71*, 712. [CrossRef]
9. Gong, Y.G.; Wang, B.; Zhang, Y.Z. The Holographic dark energy revisited. *Phys. Rev. D* **2005**, *72*, 043510. [CrossRef]
10. Khurshudyan, M. Viscous holographic dark energy universe with Nojiri-Odintsov cut-off. *Astrophys. Space Sci.* **2016**, *361*, 392. [CrossRef]
11. Landim, R.C.G. Holographic dark energy from minimal supergravity. *Int. J. Mod. Phys. D* **2016**, *25*, 1650050. [CrossRef]
12. Ghaffari, S.; Ziaie, A.H.; Bezerra, V.B.; Moradpour, H. Inflation in the Rényi cosmology. *Mod. Phys. Lett. A* **2019**, *35*, 1950341. [CrossRef]
13. Li, M.; Lin, C.; Wang, Y. Some Issues Concerning Holographic Dark Energy. *JCAP* **2008**, *0805*, 023. [CrossRef]
14. Zhang, X.; Wu, F.Q. Constraints on holographic dark energy from Type Ia supernova observations. *Phys. Rev. D* **2005**, *72*, 043524. [CrossRef]
15. Li, M.; Li, X.D.; Wang, S.; Zhang, X. Holographic dark energy models: A comparison from the latest observational data. *JCAP* **2009**, *0906*, 036. [CrossRef]
16. Feng, C.; Wang, B.; Gong, Y.; Su, R.K. Testing the viability of the interacting holographic dark energy model by using combined observational constraints. *JCAP* **2007**, *0709*, 005. [CrossRef]
17. Lu, J.; Saridakis, E.N.; Setare, M.R.; Xu, L. Observational constraints on holographic dark energy with varying gravitational constant. *JCAP* **2010**, *1003*, 031. [CrossRef]
18. Nojiri, S.; Odintsov, S. Covariant Generalized Holographic Dark Energy and Accelerating Universe. *Eur. Phys. J. C* **2017**, *77*, 528. [CrossRef]
19. Saridakis, E.N. Barrow holographic dark energy. *Phys. Rev. D* **2020**, *102*, 123525. [CrossRef]
20. Barrow, J.D.; Basilakos, S.; Saridakis, E.N. Big Bang Nucleosynthesis constraints on Barrow entropy. *Phys. Lett. B* **2021**, *815*, 136134. [CrossRef]
21. Lymperis, A. Holographic dark energy through Loop Quantum Gravity inspired entropy. *arXiv* **2023**, arXiv:2310.01050.
22. Lymperis, A.; Basilakos, S.; Saridakis, E.N. Modified cosmology through Kaniadakis horizon entropy. *Eur. Phys. J. C* **2021**, *81*, 1037. [CrossRef]
23. Nojiri, S.; Odintsov, S.D.; Saridakis, E.N. Holographic inflation. *Phys. Lett. B* **2019**, *797*, 134829. [CrossRef]
24. Paul, T. Holographic correspondence of $F(R)$ gravity with/without matter fields. *EPL* **2019**, *127*, 20004. [CrossRef]
25. Komatsu, N. Evolution of thermodynamic quantities on cosmological horizon in $\Lambda(t)$ model. *Phys. Rev. D* **2023**, *108*, 083515. [CrossRef]
26. Luciano, G.G.; Liu, Y. Lagrangian Reconstruction of Barrow Holographic Dark Energy in Interacting Tachyon Model. *Symmetry* **2023**, *15*, 1129. [CrossRef]
27. Lambiase, G.; Luciano, G.G.; Sheykhi, A. Slow-roll inflation and growth of perturbations in Kaniadakis modification of Friedmann cosmology. *Eur. Phys. J. C* **2023**, *83*, 936. [CrossRef]
28. Nojiri, S.; Odintsov, S.D.; Paul, T.; SenGupta, S. Horizon entropy consistent with FLRW equations for general modified theories of gravity and for all EoS of the matter field. *arXiv* **2023**, arXiv:2307.05011.
29. Bekenstein, J.D. Black holes and entropy. *Phys. Rev. D* **1973**, *7*, 2333–2346. [CrossRef]
30. Hawking, S.W. Particle Creation by Black Holes. *Commun. Math. Phys.* **1975**, *43*, 199–220; Erratum in *Commun. Math. Phys.* **1976**, *46*, 206. [CrossRef]
31. Tsallis, C. Possible Generalization of Boltzmann-Gibbs Statistics. *J. Statist. Phys.* **1988**, *52*, 479–487. [CrossRef]
32. Rényi, A. *Proceedings of the Fourth Berkeley Symposium on Mathematics, Statistics and Probability*; University of California Press: Berkeley, CA, USA, 1960; pp. 547–556.
33. Barrow, J.D. The Area of a Rough Black Hole. *Phys. Lett. B* **2020**, *808*, 135643. [CrossRef] [PubMed]
34. Jahromi, A.S.; Moosavi, S.A.; Moradpour, H.; Graça, J.P.M.; Lobo, I.P.; Salako, I.G.; Jawad, A. Generalized entropy formalism and a new holographic dark energy model. *Phys. Lett. B* **2018**, *780*, 21–24. [CrossRef]
35. Kaniadakis, G. Statistical mechanics in the context of special relativity. II. *Phys. Rev. E* **2005**, *72*, 036108. [CrossRef] [PubMed]
36. Majhi, A. Non-extensive Statistical Mechanics and Black Hole Entropy from Quantum Geometry. *Phys. Lett. B* **2017**, *775*, 32–36. [CrossRef]
37. Nojiri, S.; Odintsov, S.D.; Faraoni, V. From nonextensive statistics and black hole entropy to the holographic dark universe. *Phys. Rev. D* **2022**, *105*, 044042. [CrossRef]

38. Nojiri, S.; Odintsov, S.D.; Paul, T. Early and late universe holographic cosmology from a new generalized entropy. *Phys. Lett. B* **2022**, *831*, 137189. [CrossRef]
39. Odintsov, S.D.; Paul, T. A non-singular generalized entropy and its implications on bounce cosmology. *Phys. Dark Univ.* **2023**, *39*, 101159. [CrossRef]
40. Odintsov, S.D.; Paul, T. Generalised (non-singular) entropy functions with applications to cosmology and black holes. *arXiv* **2023**, arXiv:2301.01013.
41. Nojiri, S.; Odintsov, S.D.; Paul, T. Different Faces of Generalized Holographic Dark Energy. *Symmetry* **2021**, *13*, 928. [CrossRef]
42. Nojiri, S.; Odintsov, S.D.; Paul, T. Modified cosmology from the thermodynamics of apparent horizon. *Phys. Lett. B* **2022**, *835*, 137553. [CrossRef]
43. Odintsov, S.D.; D'Onofrio, S.; Paul, T. Holographic realization from inflation to reheating in generalized entropic cosmology. *Phys. Dark Universe* **2023**, *42*, 101277. [CrossRef]
44. Nojiri, S.; Odintsov, S.D.; Faraoni, V. New Entropies, Black Holes, and Holographic Dark Energy. *Astrophysics* **2022**, *65*, 534–551. [CrossRef]
45. Bolotin, Y.L.; Yanovsky, V.V. Cosmology based on entropy. *arXiv* **2023**, arXiv:2310.10144.
46. Odintsov, S.D.; Oikonomou, V.K.; Giannakoudi, I.; Fronimos, F.P.; Lympieriadou, E.C. Recent Advances in Inflation. *Symmetry* **2023**, *15*, 1701. [CrossRef]
47. Nojiri, S.; Odintsov, S.D. Micro-canonical and canonical description for generalised entropy. *Phys. Lett. B* **2023**, *845*, 138130. [CrossRef]
48. Nojiri, S.; Odintsov, S.D.; Paul, T. Microscopic interpretation of generalized entropy. *Phys. Lett. B* **2023**, *847*, 138321. [CrossRef]
49. Friedman, A. Über die Krümmung des Raumes. *Z. Fur Phys.* **1922**, *10*, 377. [CrossRef]
50. Cai, R.G.; Kim, S.P. First law of thermodynamics and Friedmann equations of Friedmann-Robertson-Walker universe. *JHEP* **2005**, *0502*, 050. [CrossRef]
51. Akbar, M.; Cai, R.G. Thermodynamic Behavior of Friedmann Equations at Apparent Horizon of FRW Universe. *Phys. Rev. D* **2007**, *75*, 084003. [CrossRef]
52. Sanchez, L.M.; Quevedo, H. Thermodynamics of the FLRW apparent horizon. *arXiv* **2022**, arXiv:2208.05729.
53. Gennaro, S.D.; Ong, Y.C. Sign Switching Dark Energy from a Running Barrow Entropy. *Universe* **2022**, *8*, 541. [CrossRef]
54. Akrami, Y.; Arroja, F.; Ashdown, M.; Aumont, J.; Baccigalupi, C.; Ballardini, M.; Banday, A.J.; Barreiro, R.B.; Bartolo, N.; Basak, S.; et al. Planck 2018 results. X. Constraints on inflation. *Astron. Astrophys.* **2020**, *641*, A10. [CrossRef]

Disclaimer/Publisher's Note: The statements, opinions and data contained in all publications are solely those of the individual author(s) and contributor(s) and not of MDPI and/or the editor(s). MDPI and/or the editor(s) disclaim responsibility for any injury to people or property resulting from any ideas, methods, instructions or products referred to in the content.

Article

Kantowski–Sachs Model with a Running Cosmological Constant and Radiation

Vinícius Guilherme Oliveira, Gil de Oliveira Neto and Ilya L. Shapiro * 

Departamento de Física, Instituto de Ciências Exatas, Universidade Federal de Juiz de Fora, Juiz de Fora 36036-330, Brazil; vinicius.guilherme@ice.ufjf.br (V.G.O.); gilneto@fisica.ufjf.br (G.d.O.N.)

* Correspondence: ilyashapiro2003@ufjf.br

Abstract: The simplest anisotropic model of the early universe is the one with two conformal factors, which can be identified as the Kantowski–Sachs metric, or the reduced version of the Bianchi-I metric. To fit the existing observational data, it is important that the anisotropy is washed out in the early stage of the evolution. We explore the possible effects of the running cosmological constant on the dynamics of isotropy in the case of space filled by radiation.

Keywords: early universe; anisotropic models; running cosmological constant

1. Introduction

Two important theoretical challenges for the theoretical background of modern cosmology are to construct the basis for a possible variation of the equation of state of dark energy and to explain the initial conditions of the universe. One of the important aspects of the last task is to elaborate a mechanism for making the universe isotropic, at least after the initial stage of its evolution, which leaves observational traces.

The most natural candidate to be dark energy is the cosmological constant Λ (see, e.g., [1]), which has a fixed equation of state $P_\Lambda = -\rho_\Lambda$ between “pressure” and “energy density” components. If the future observational data show a deviation from this value, it may be either interpreted as a non-constant cosmological term or as the presence of a qualitatively new essence filling the universe, which may be a replacement or a complement to the cosmological constant. The non-constant cosmological term may be a consequence of the vacuum quantum effects of matter fields (see, e.g., the review [2] for a qualitative discussion and further references). The corresponding quantum contributions to the action of gravity are certainly rather complicated (e.g., necessarily non-polynomial) if expressed via curvature tensors and nonlocal form factors [3]. This explains why these terms have never been calculated with the existing quantum field theory techniques based on the weak field expansions. For the same reason, the presence of these quantum contributions cannot be ruled out. In this situation, one can rely on the phenomenological approaches, e.g., based on the assumption of quadratic decoupling in the lower-derivative sector of the gravitational effective action [4,5], or assuming and using the covariance of the effective action [6]. All these approaches converge to the IR (low-energy) running of the form

$$\rho_\Lambda(\mu) = \rho_\Lambda^0 + \frac{3\nu}{8\pi G}(\mu^2 - \mu_0^2), \quad (1)$$

where G is the Newton constant and ρ_Λ^0 is the value of the density of the cosmological constant at the fiducial value μ_0 of the scale parameter μ . The limits on the magnitude of the phenomenological parameter ν were established in [7,8] in different types of the cosmological models based on Equation (1). These limits were obtained by analyzing cosmic perturbations and making comparison with the observational data. In both cases, this analysis requires an identification of the artificial scale parameter μ of the minimal subtraction renormalization scheme with a certain physical quantity, as discussed in [3].



Citation: Oliveira, V.G.; de Oliveira Neto, G.; Shapiro, I.L. Kantowski–Sachs Model with a Running Cosmological Constant and Radiation. *Universe* **2024**, *10*, 83. <https://doi.org/10.3390/universe10020083>

Academic Editors: Galina L. Klimchitskaya, Vladimir M. Mostepanenko and Sergey V. Sushkov

Received: 15 December 2023

Revised: 16 January 2024

Accepted: 4 February 2024

Published: 8 February 2024



Copyright: © 2024 by the authors. Licensee MDPI, Basel, Switzerland. This article is an open access article distributed under the terms and conditions of the Creative Commons Attribution (CC BY) license (<https://creativecommons.org/licenses/by/4.0/>).

In the cosmological setting, some physical arguments based on quantum field theory and also the scale-setting procedure [9] hint at the identification of μ with the Hubble parameter H . On top of this, the covariance-based arguments imply that, under the derivative expansion, the effective action cannot be odd in metric derivatives. For the background cosmological metric, this gives Equation (1), and the same result follows from the assumption of quadratic IR decoupling in the beta function of ρ_Λ .

The IR running implies that there is an effective action of gravity that can be separated into the nonlocal parts responsible for the IR running of the cosmological constant, the quantum corrections to the Einstein–Hilbert term (the running of the Newton constant), and the terms which can be attributed to quantum corrections in the higher-derivative sectors. The last terms can be directly calculated (see, e.g., [10] for review and references), but are not very relevant for the late cosmology owing to the Planck suppression of the higher-derivative terms. Thus, the covariance of the effective action assumes that the lower-energy sector should satisfy certain conservation laws on its own. In this respect, the cosmological applications of Equation (1) can be separated into the models admitting the energy exchange between the vacuum and matter sectors and the ones without such an exchange. It was argued in [11–14] that the models of the first type are physically inappropriate for the late universe. On the other hand, the phenomenological limits on the parameter ν in Equation (1) derived from the metric perturbations and LSS data [7] are much stronger in these models, as was also confirmed in more recent work [15] by analyzing another set of cosmological observables (see also [16] and references therein). According to the most recent work, in the early universe (and certainly not in the later stages of the evolution) there is no suppression of the creation of particles from the vacuum [11–13], making the exchange of energy between different parts of the gravitational action less relevant. In this case, one can use the basic cosmological models based on the running [17] instead of the more complicated models of the type considered in [14].

Despite a lot of the relevant information in cosmology being obtained from linear cosmic perturbations, there is at least one special situation when one needs to perform a non-perturbative analysis. This concerns the answer to the question of why the initial stage of the universe can be described by the isotropic metric. To address this problem, one needs to start with the anisotropic model and see whether and how the isotropy is restored in a given model of gravity. Since the issue arises for the very early universe, the matter fields can be described by pure radiation, which is a dominating component in this epoch, even taking into account the symmetry restoration and the corresponding huge (compared to the present one) magnitude of the cosmological constant [1,18].

In the present work, we report on the first (at least, up to our knowledge) theoretical investigation of the effect of the running of the cosmological constant density Equation (1) on the isotropization of the early universe. For this initial work we use the simplest model including only radiation and the cosmological constant in the gravity theory based on Einstein’s GR with the running cosmological constant. It is worthwhile to explain this point in a more detailed form. Let us remember that we are discussing the very early universe, where the typical values of the Hubble parameter are greater than the masses, at least for the lightest massive particles, of the Standard Model. For smaller Hubble values, the creation of particles from the vacuum is suppressed, as was noted long ago in [11–13]. On the other hand, even for values of the Hubble parameter of the order of the electron mass, the Einstein equations tell us that the typical temperature of the CMB is huge compared to the masses of the heaviest particles of the Standard Model [5] and, probably, compared to the heaviest possible candidates for the dark matter constituents. Thus, in this regime, all kinds of matter, including baryonic and dark matter, can be regarded as having the equation of state of radiation.

The running of the Newton constant and other terms in the action of gravity are not taken into account, as they are less relevant in the given physical situation in the early universe, when the energy exchange between the vacuum and matter sectors of the action are not suppressed [15]. Finally, to explore the anisotropy we use the simplest version of

the Bianchi type I metric, which is also a version of the Kantowski–Sachs (KS) model [19]. This metric has only two conformal factors and enables one to explore the main qualitative features of the anisotropic running cosmology in the most economic and explicit way. It is worth noting that isotropization in the KS cosmological models without running was previously explored in many papers, including [20–22], where the isotropization of the metric was first discovered (see also [23–31] for further investigations in different models and [32,33] for a more complete set of references). It is worth noting the quantum mechanism of isotropization (see, e.g., [34–36]; there are also many other papers on this issue and a review in the book [37]).

The rest of this work is organized as follows. In Section 2, we formulate the background for the anisotropic running cosmology, that includes the identification of scale and derivation of the main formulas for the dynamics of the conformal factors. Let us note that the generalization to more complicated metrics, such as the general Bianchi-I, is expected to be straightforward. Section 3 reports on the numerical results for the dynamics of the conformal factors. Finally, in Section 4 we draw our first conclusions and discuss possible extensions of the present work.

2. Theoretical Background of the Anisotropic Running Cosmology

The basis of our investigation will be Einstein’s equations with the cosmological constant,

$$G_{\alpha\beta} = 8\pi G T_{\alpha\beta} + \Lambda g_{\alpha\beta}, \tag{2}$$

where $g_{\alpha\beta}$ is the metric tensor, the Newton constant G is assumed to be scale-independent, as explained above, and $\Lambda = 8\pi G\rho_\Lambda$ depends on the scale parameter μ according to Equation (1). Here, and in what follows, we adopt the units with $c = 1$ for the speed of light in a vacuum.

Consider the Kantowski–Sachs metric,

$$ds^2 = -dt^2 + a^2(t)dr^2 + b^2(t)[d\theta^2 + \sin^2\theta d\phi^2], \tag{3}$$

where r , θ , and ϕ are spherical coordinates, and $a(t)$ and $b(t)$ are the two scale factors. The growth of these functions with time characterizes the expansion of the universe. In the model (3), the radial part can expand differently to the angular parts. Since there are only two functions, this is one of the simplest possible anisotropic models. The spatial sections of this model have positive curvature.

The energy–momentum tensor for the perfect fluid is given by

$$T_{\alpha\beta} = (\rho_f + p_f)u_\alpha u_\beta + p_f g_{\alpha\beta}, \tag{4}$$

where ρ_f and p_f are, respectively, the energy density and pressure of the fluid and u_α is the four-velocity of the fluid. Since we are interested in the very early universe, the matter contents may be approximately described by radiation, so the equation of state for our perfect fluid should be

$$p_f = \frac{\rho_f}{3}. \tag{5}$$

One may identify the isotropization of metric (3) in two different ways. In a more simple way, after some time $a(t)$ would tend to $b(t)$. The second way is to see that the ratio between the scale factors tends to a constant after some time, showing that the scale factors would have the same expansion rate.

Using the KS metric (3) in the Einstein tensor on the left-hand side of Equation (2), we arrive at a system of three ordinary differential equations:

$$\frac{2\dot{a}\dot{b}}{ab} + \frac{\dot{b}^2}{b^2} + \frac{1}{b^2} = 8\pi G\rho_t, \tag{6}$$

$$2b\ddot{b} + \dot{b}^2 + 1 = -8\pi Gb^2 p_t, \tag{7}$$

$$\frac{\ddot{a}}{a} + \frac{\dot{a}\dot{b}}{ab} + \frac{\ddot{b}}{b} = -8\pi Gp_t. \tag{8}$$

In these equations, ρ_t and p_t are the total energy density and pressure, as will be detailed below.

Since there are only two variables, $a(t)$ and $b(t)$, we can restrict the consideration by Equation (6) and the difference between Equation (8) multiplied by ab^2 and Equation (7) multiplied by a . Thus, the equations which we will work with are¹

$$2b\dot{a}\dot{b} + ab^2 + a = 8\pi Gab^2\rho_t, \tag{9}$$

$$b^2\ddot{a} - ab\ddot{b} + b\dot{a}\dot{b} - ab^2 - a = 0. \tag{10}$$

To simplify notation, in what follows we use units with $8\pi G/3 = 1$. Together with $c = 1$, this means physical time t is measured in Planck units. This is certainly a very small unit, but for the very early universe this may be a useful choice. Concerning the right-hand side of Equation (2), we meet the sum of the radiation and the contribution of the variable cosmological constant Equation (1). A useful representation is using “energy density” and “pressure” of the vacuum. Then, we may arrive at the total energy density and pressure of the model, in the forms

$$\rho_t = \rho_f + \rho_\Lambda, \quad p_t = \frac{1}{3}\rho_f - \rho_\Lambda, \tag{11}$$

where we used the relation (5) for the radiation and the relation $p_\Lambda = -\rho_\Lambda$. Let us note that this relation between the “energy density” and “pressure” of the vacuum corresponds to the natural separation of the effective action of the vacuum into the cosmological constant sector, Einstein–Hilbert sector, and higher-derivative part. In the isotropic metric case, this separation, which was already mentioned in the Introduction, can be performed using global scaling. The cosmological constant and the corresponding nonlocal quantum corrections should have the same scaling, and this means the equation of state $p_\Lambda = -\rho_\Lambda$. The interested reader may find more details in [38].

The next problem is an identification of μ that would enable us to use the result in Equation (1) and then in Equation (11). We shall use the usual choice of $\mu \sim H$, and the definition of an average H suggested in [29],

$$H = \frac{1}{3} \left(\frac{\dot{a}}{a} + 2\frac{\dot{b}}{b} \right). \tag{12}$$

This choice has several advantages. In the QFT framework, the running of vacuum parameters, including the cosmological constant, corresponds to the effect of quantum matter fields on the external (classical) gravitational background. This means (see, e.g., [10] for the introduction) that one has to deal with the Feynman diagrams with external gravitational lines. As was discussed in [4,5], and numerous subsequent publications, the phenomenologically acceptable running presumes that in the cosmological constant sector there is a quadratic decoupling. Let us stress that this is a phenomenological assumption since such a decoupling was verified only in the higher-derivative sectors of the vacuum action [10] (see further references to the original works therein). In our case of an isotropic metric, there may be lines corresponding to different conformal factors. In case the magnitudes in the two terms are of the same order, it boils down to the usual identification from [4,5,9]. On the other hand, if the ratios \dot{a}/a and \dot{b}/b are very different, the choice Equation (12) guarantees that the larger version of the Hubble parameter gives a greater contribution, as required. From the phenomenological side, this definition looks natural and enables one

to implement the running Equation (1) in the anisotropic setting. The generalization to the Bianchi-I model is straightforward.

The energy conservation condition gives the equation

$$\dot{\rho}_f + \dot{\rho}_\Lambda + 3H(p_f + \rho_f + p_\Lambda + \rho_\Lambda) = 0. \tag{13}$$

In the units we use, the running corresponds to the relation

$$\rho_\Lambda = \rho_\Lambda^0 + \nu(H^2 - H_0^2). \tag{14}$$

Taking in account Equation (5), the equation of state for the cosmological constant, and the definition of the Hubble parameter (12), after some calculations we find the following energy conservation Equation (13):

$$\begin{aligned} \dot{\rho}_f a^3 b^3 + \frac{4}{3} \rho_f (\dot{a} a^2 b^3 + 2 \dot{b} a^3 b^2) + \frac{2\nu}{9} [\dot{a} \ddot{a} b^3 - \dot{a}^3 b^3 - 4 \dot{a}^3 \dot{b}^3 \\ + 4 \dot{a}^3 b \dot{b} \ddot{b} + 2 a^2 b^2 (\dot{a} \ddot{b} + \ddot{a} \dot{b}) - 2 a^2 b \dot{a} \dot{b}^2 - 2 a b^2 \dot{a}^2 \dot{b}] = 0. \end{aligned} \tag{15}$$

For the total energy density of ρ_t , and using Equation (9), we arrive at the equation

$$(18 - 4\nu) a b \dot{a} \dot{b} + (9 - 4\nu) a^2 \dot{b}^2 - \nu b^2 \dot{a}^2 + 9 a^2 = 9 a^2 b^2 (\rho_f + \rho_\Lambda^0 - \nu H_0^2). \tag{16}$$

It is worth noting that here ρ_f is the energy density of radiation, which is one of the variables that has the dynamics to be defined from the equations, and ρ_Λ^0 is the initial point of the renormalization group flow.

3. Numerical Results for the Anisotropic Metric

Solving the system of Equations (10), (15), and (16), one can explore the dynamics of the relevant functions $a(t)$, $b(t)$, and $\rho_f(t)$. Let us report on the corresponding numerical analysis.

Differently from previous work [7], we do not consider cosmic perturbations; however, the background geometry is more complicated owing to anisotropy. On the other hand, we know that the metric in the universe filled by radiation becomes isotropic in a very short time; hence, our interest concerns the very early universe. In this case, the limitations on the sign and magnitude of the parameter ν , which were established in [7] (also in [8] for another model with running cosmological constant), do not apply anymore, and hence, we can assume much greater values of ν , both positive and negative. Following this logic, we studied different cases, varying the values of the parameters, including ν , in the first place. One of our targets is the isotropization of metric (3), i.e., evaluation of the ratio b/a .

The results of the numerical analysis can be seen in the figures. Let us first summarize the general features of different models, characterized by different values of the parameter ν and different initial data. We found that for the physically relevant solutions, i.e., when the value of ν is small, both $a(t)$ and $b(t)$ always expand and that $\rho_f(t)$ always tends to zero, starting from a given initial value.

Consider the case when initially the model is strongly anisotropic, that is, we choose $b(t = 0) = 100$ and $a(t = 0) = 1$. For the numerical analysis, we used the initial values

$$\rho_\Lambda^0 = H_0 = 1, \quad \dot{a}(t = 0) = 1, \quad \rho_f(t = 0) = 2, \tag{17}$$

while the value of $\dot{b}(t = 0)$ varied. In Figures 1 and 2, we show some plots obtained by the variation of ν . One can see both $a(t)$ and $b(t)$ are rapidly growing with time, and it looks like the anisotropy does not change significantly, for all values of ν . Let us note that we took much greater values of $|\nu|$ compared to the upper bounds derived in [7,8]. There were two reasons for this. The first one was that for values of the order 10^{-6} , which are typical for models of the first type (with the exchange of energy between vacuum and matter [7]),

the plots are not visually distinguishable from the one for $\nu = 0$. The second reason was that the isotropization occurs very fast when the values of the Hubble parameter are very large. Obviously, this makes sense only assuming that the isotropization takes place in the very early universe, where typical energies are very high. This means, there is no decoupling of the highest-mass particles, providing small values of ν [4,5] and, therefore, there is no contradiction in assuming the values of order one. The same thinking concerns the sign, which was advocated as being positive in [7]. In the effective decoupling-based framework formulated in [5] (see also [2,3]), this sign is defined by the spin of the highest-mass particles in the spectrum beyond the Minimal Standard Model. And if the scale of decoupling dramatically changes, we have to take into account the possibility of fermion domination and, therefore, consider also the negative values of ν .

Following these arguments, we chose the values for the parameters, initial conditions, and the values of ν to produce the graphs demonstrating qualitative properties of the solutions. Figures 1, 2, 3 and 4 show, respectively, the time dependencies $a(t)$, $b(t)$, $\rho_f(t)$, and the ratio $b(t)/a(t)$ for four different large positive values of ν . Similarly, Figures 5–8 show the time variations of the same quantities $a(t)$, $b(t)$, $\rho_f(t)$ and $b(t)/a(t)$ for four different negative values of ν . Furthermore, Figures 9–12, illustrate the behavior of $a(t)$, $b(t)$, $\rho_f(t)$, and $b(t)/a(t)$ for four different positive and negative values of ν . Observing these plots we can see the general situation, i.e., how the running of the cosmological constant density may affect the process of isotropization. These general features are formulated in the next section.

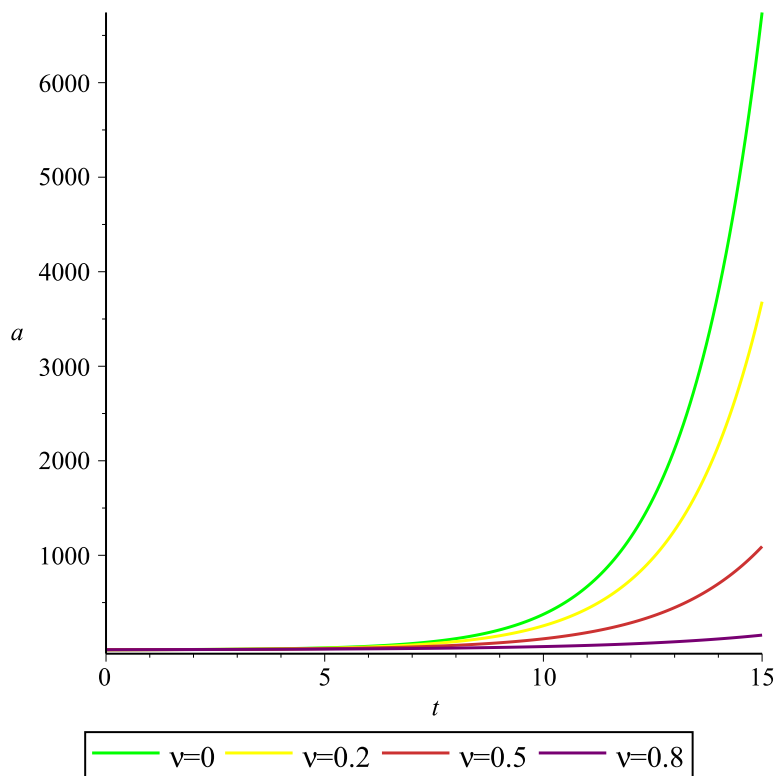


Figure 1. Variation in $a(t)$ for four different positive values of ν .

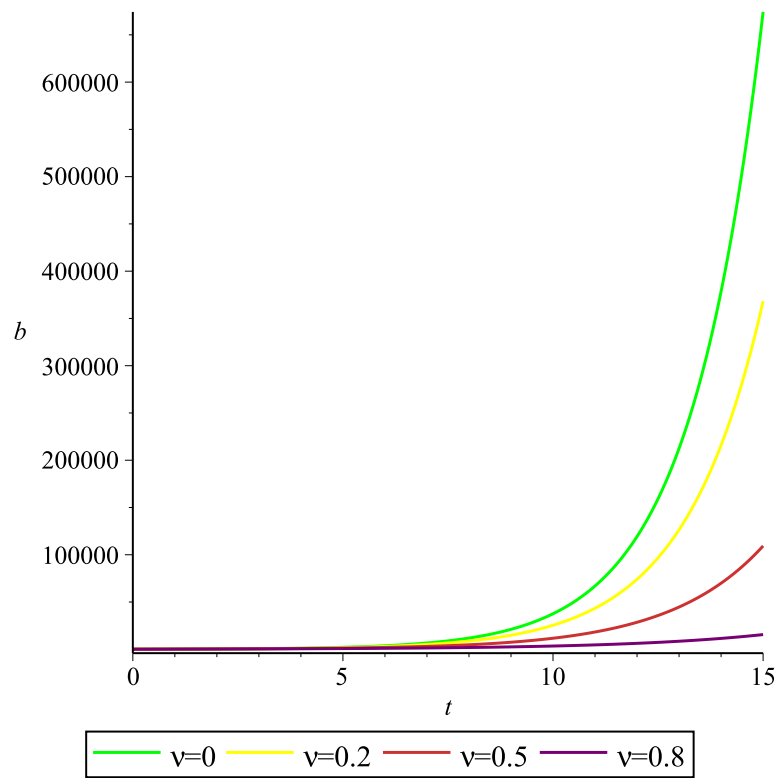


Figure 2. Variation in $b(t)$ for four different positive values of ν .

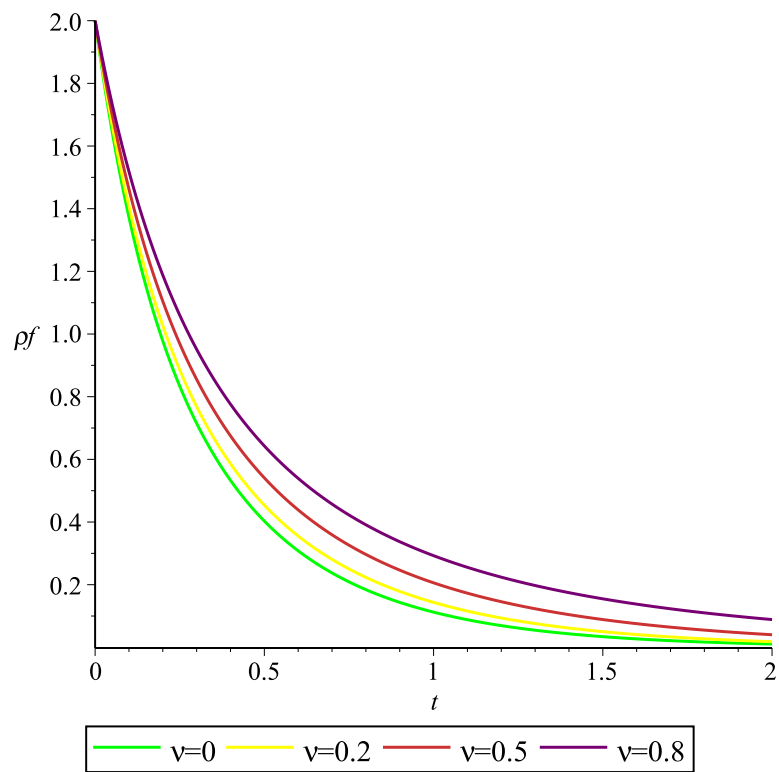


Figure 3. Variation in $\rho_f(t)$ for four different positive values of ν .

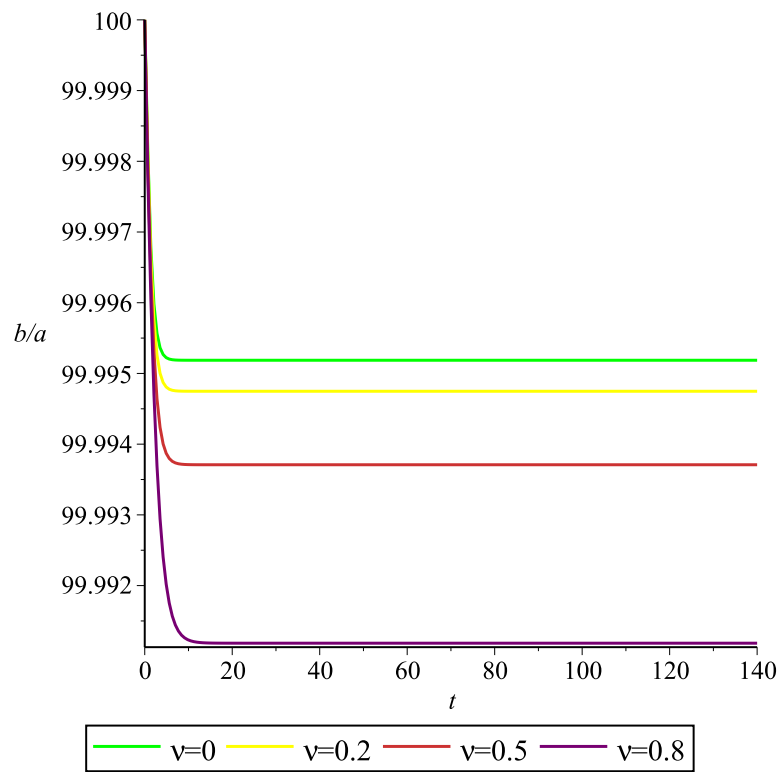


Figure 4. Variation in $b(t)/a(t)$ for four different positive values of ν .

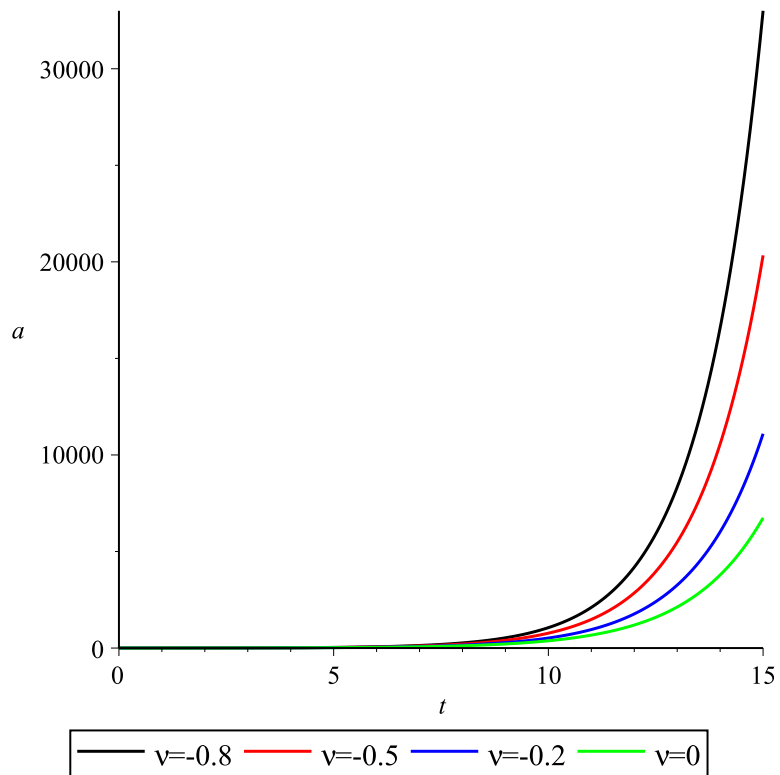


Figure 5. Variation in $a(t)$ for four different negative values of ν .

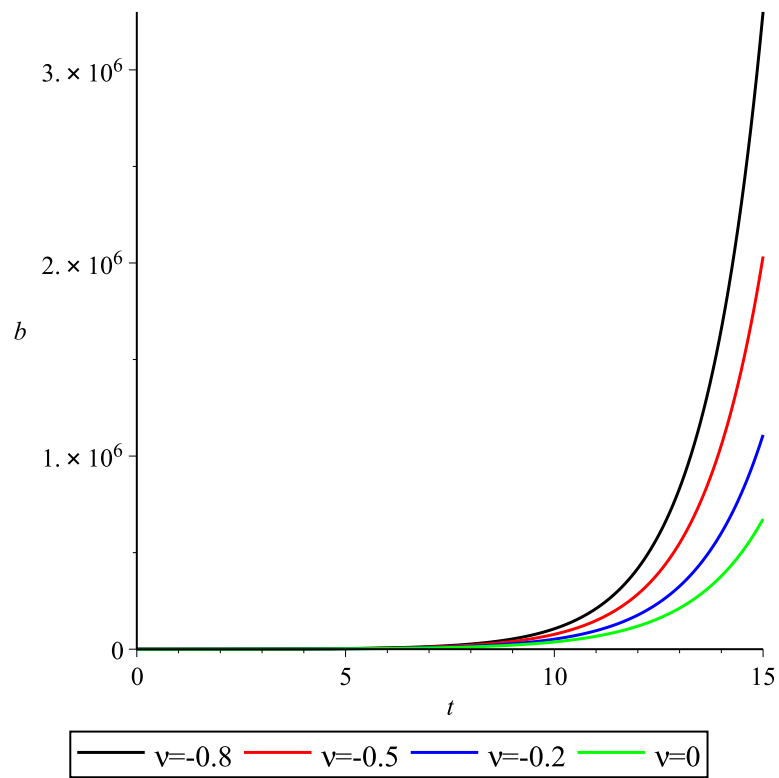


Figure 6. Variation in $b(t)$ for four different negative values of ν .

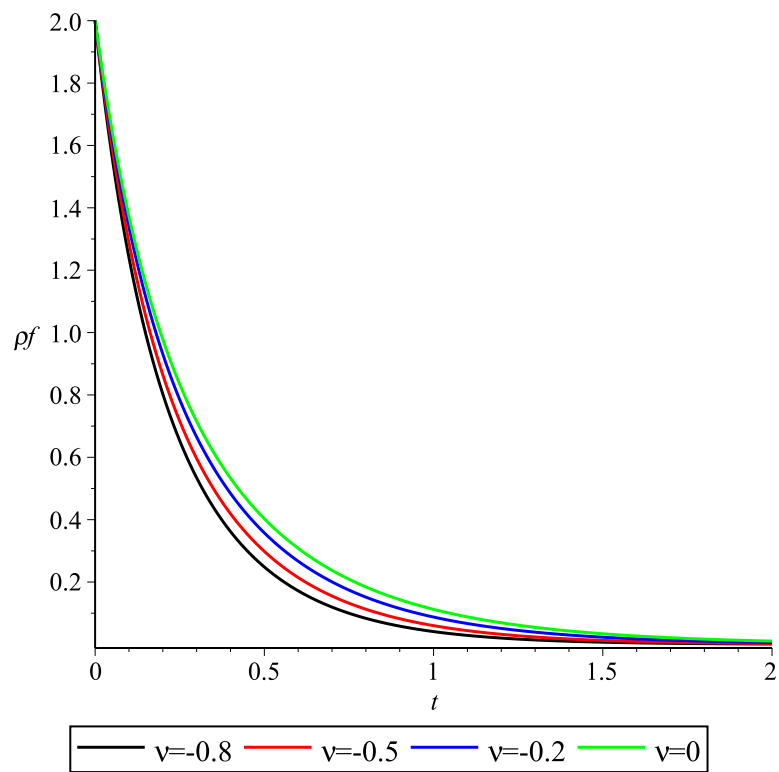


Figure 7. Variation in $\rho_f(t)$ for four different negative values of ν .

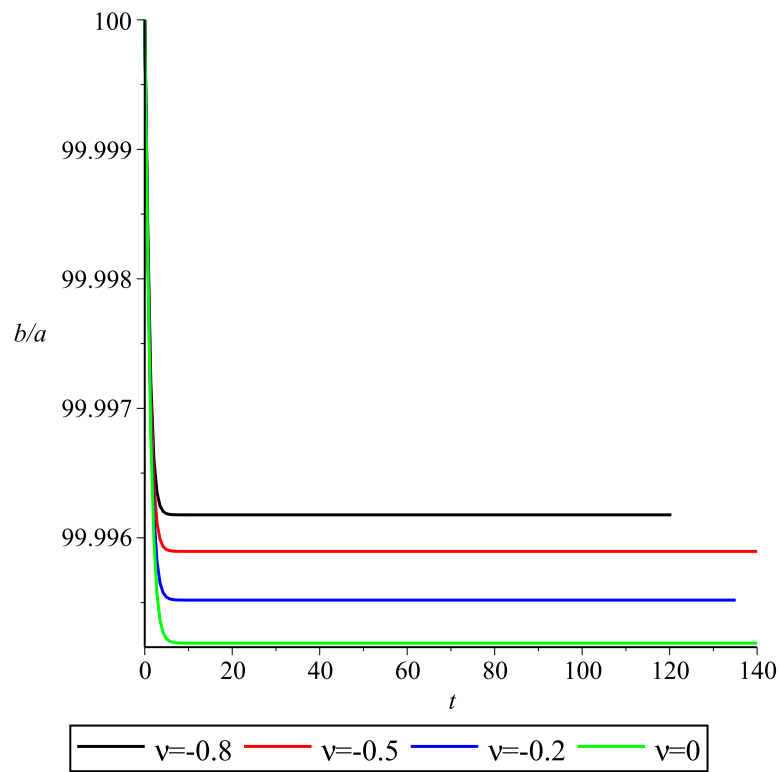


Figure 8. Variation in $b(t)/a(t)$ for four different negative values of ν .

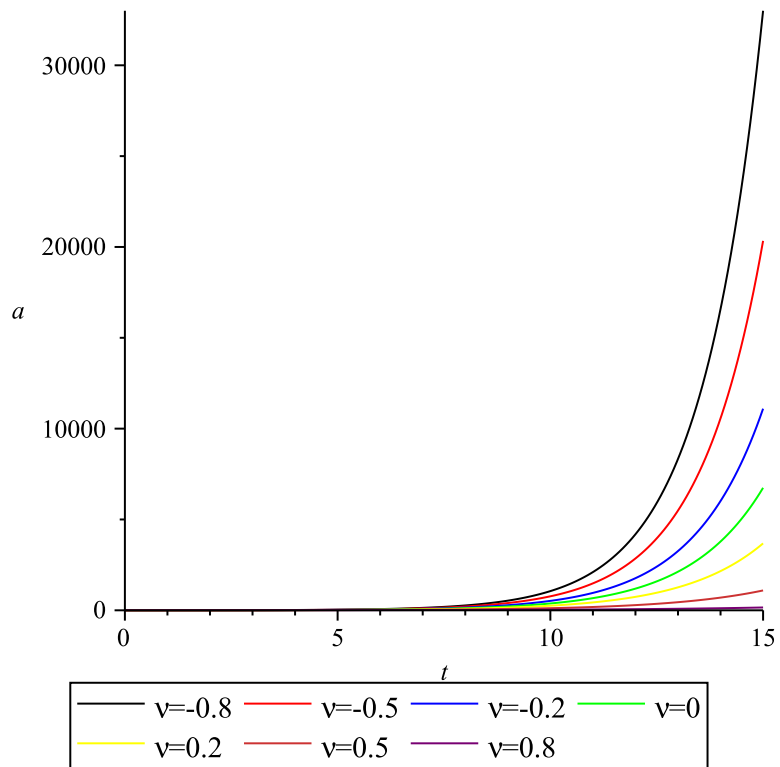


Figure 9. Variation in $a(t)$ for seven different positive and negative values of ν .

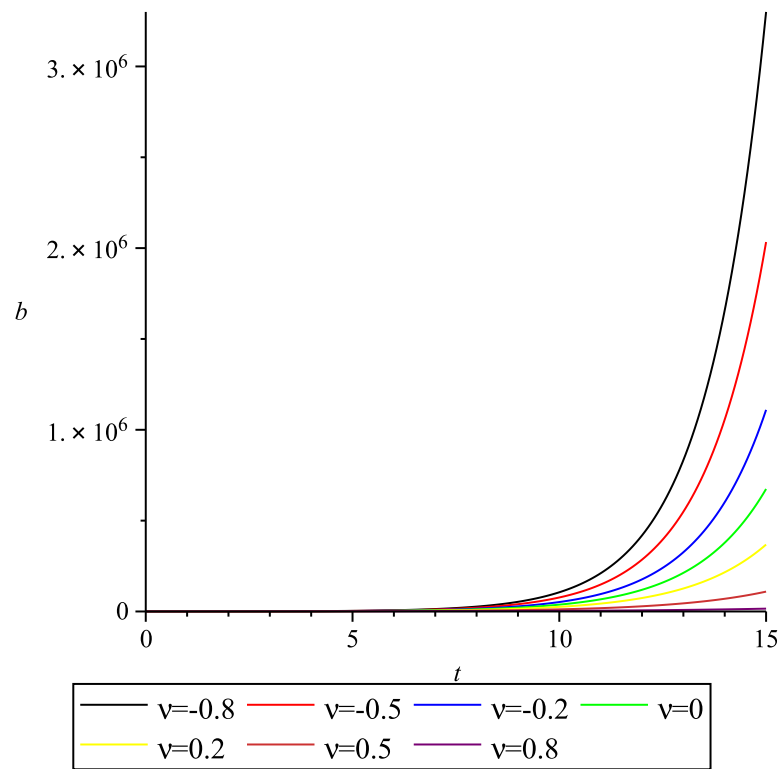


Figure 10. Variation in $b(t)$ for seven different positive and negative values of ν .

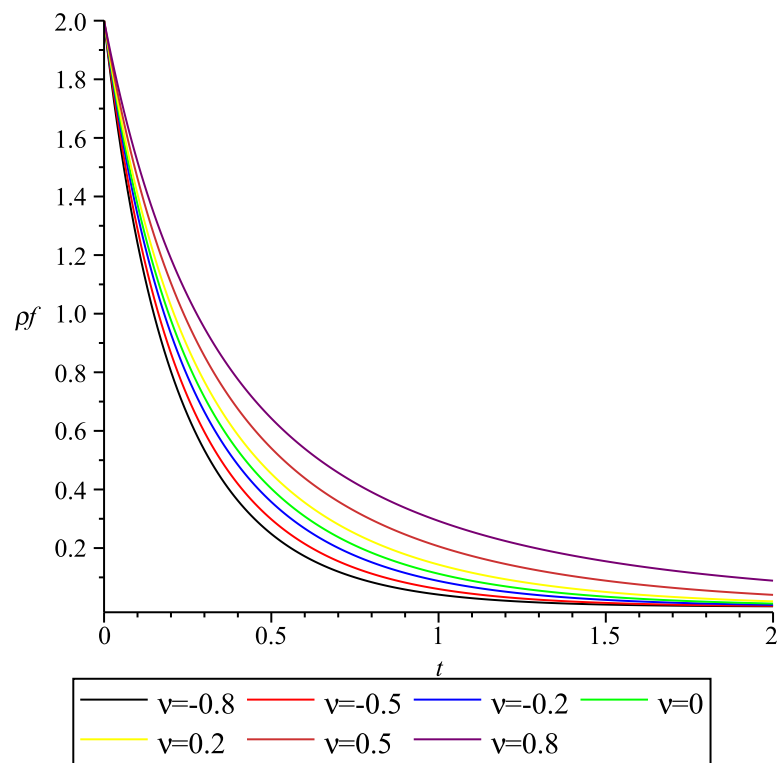


Figure 11. Variation in $\rho_f(t)$ for seven different positive and negative values of ν .

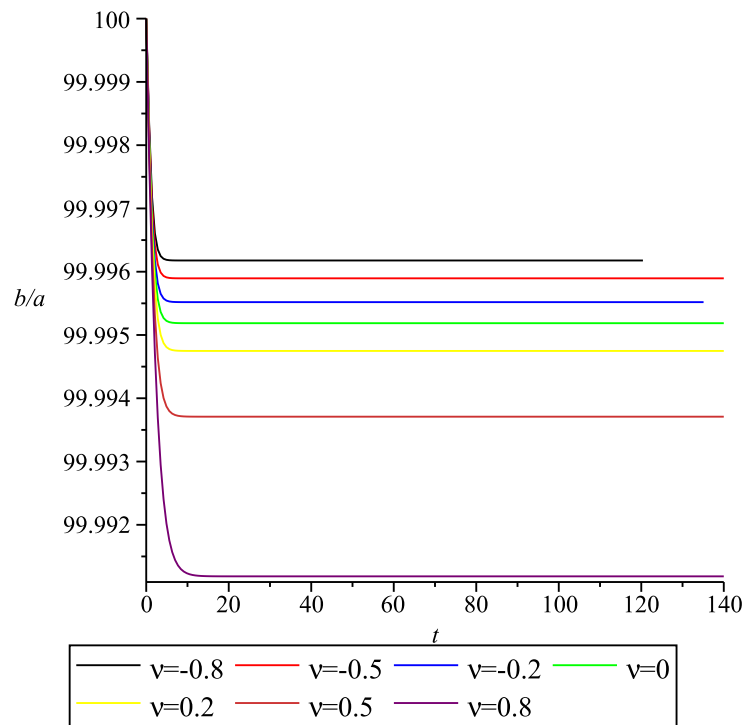


Figure 12. Variation in $b(t)/a(t)$ for seven different positive and negative values of ν .

On the basis of the numerical analysis one notes that there may be a value of ν where the tendencies related to the running stop working. As an illustration, we show this situation in Figures 13–16, corresponding to $\rho_{\Lambda}^0 = 1$ and a huge unphysical value $\nu = 8$. In this case, the term with ν in the Friedmann Equation (16) dominates over the basic term ρ_{Λ}^0 . We included these plots just to illustrate the general situation that may happen in the region of “quantum dominance”, where the running becomes very strong.

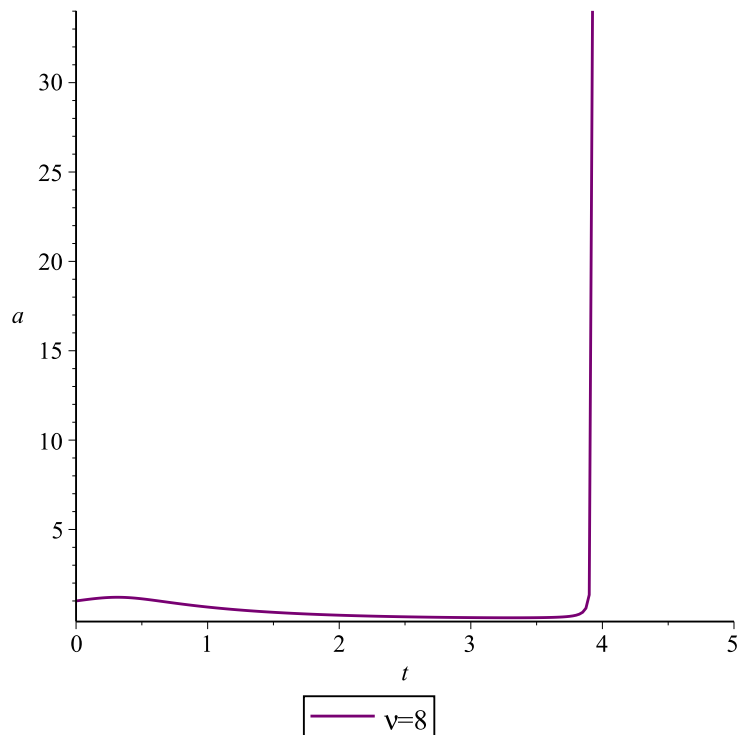


Figure 13. Variation in $a(t)$ for a large positive value of ν .

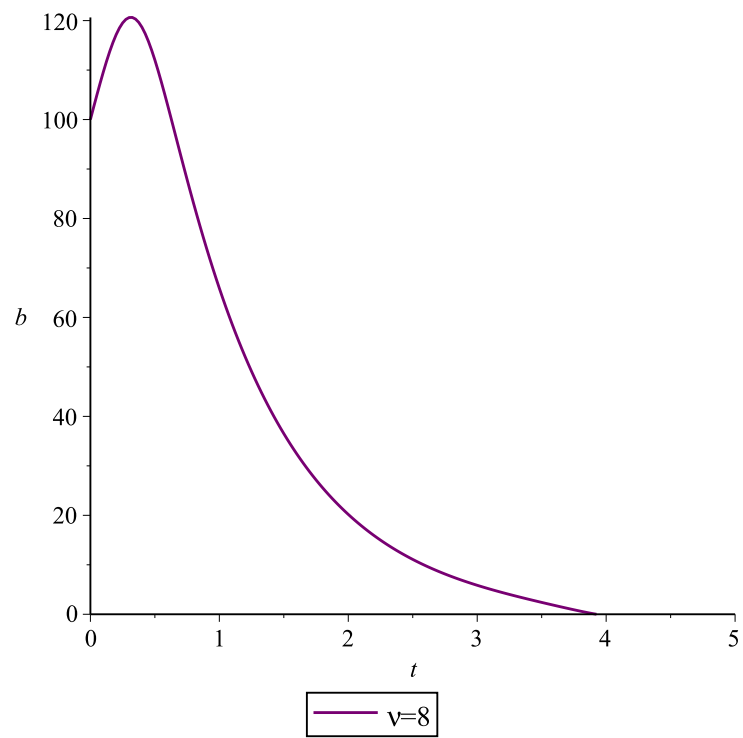


Figure 14. Variation in $b(t)$ for a large positive value of v .

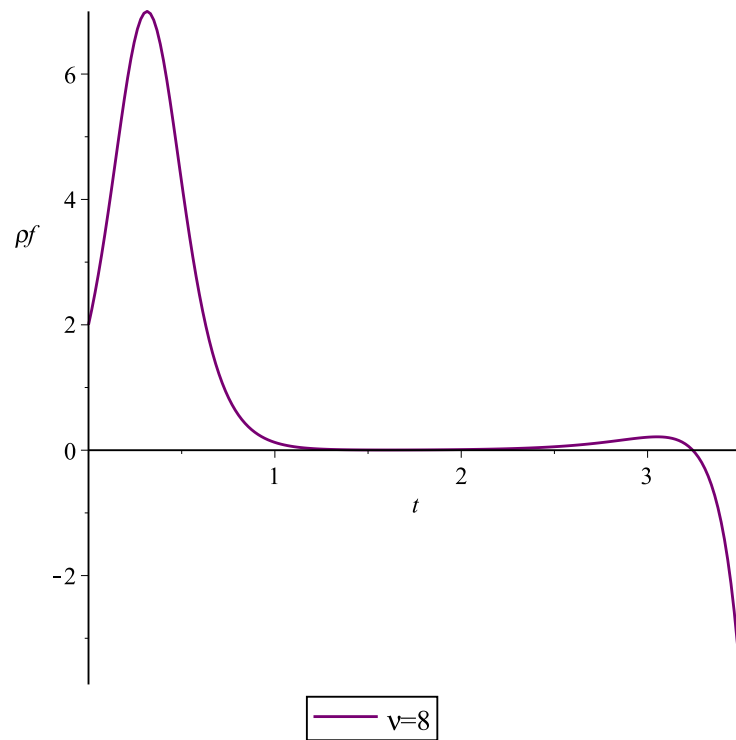


Figure 15. Variation in $\rho_f(t)$ for a large positive value of v .

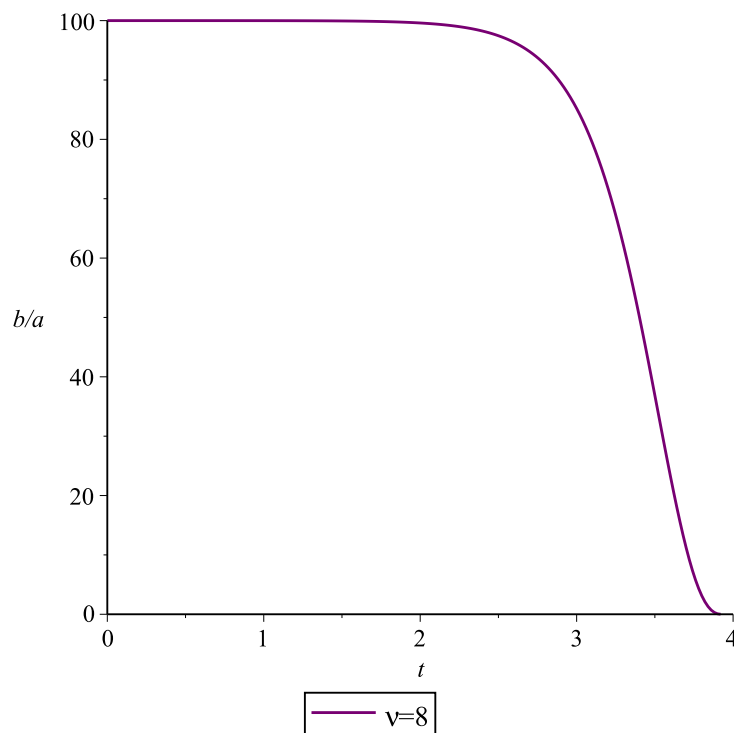


Figure 16. Variation in $b(t)/a(t)$ for a large positive value of ν .

In Figure 13, the scale factor $a(t)$ expands slowly and then the universe starts to contract. When the time gets close to $t = 4$, an exponential expansion starts and continues until it abruptly stops the expansion due to a final singularity at $t \approx 3.93$. Figure 14 shows the behavior of the second scale factor $b(t)$, which also slowly expands until it reaches a maximum value at approximately $t = 0.5$. After that, a contraction begins until it reaches a zero value and gives rise to a singularity, similar to a big crunch, at the same value of time $t \approx 3.93$. Figure 15 demonstrates $\rho(t)$ with the same values of the parameters. It is easy to see that we meet (quite naturally) a singularity at the same point. To complete this part, in Figure 16 one can observe that the ratio $b(t)/a(t)$ remains approximately constant and then begins to decrease at some point. This stage lasts until the same point, $t \approx 3.93$, when $b(t)$ goes to zero.

4. Conclusions

We have considered the effect of the running cosmological constant in the early universe on the isotropization of the KS metric. As was argued in previous publications on the running cosmology models [15] (based on the previous ideas and restrictions of [11–14]), in the early universe the running of the Newton constant is a sub-dominating effect, which can be neglected, in the leading approximation. Thus, we treated the Newton constant G as a non-running quantity.

The most important qualitative result of our work is that, different from the cosmic perturbations [7], small values of the phenomenological parameter ν do not affect the dynamics of the anisotropic conformal factors, at least in the framework of the KS metric model [19]. Taking into account the bound for ν derived from the perturbations, one could conclude that the possible running of the cosmological constant is irrelevant for the dynamics of anisotropic parameters, but this would be a misleading statement. The reason is that in the very early universe the metric becomes isotropic very fast and, therefore, the two kinds of deviation from the homogeneous and isotropic cosmology occur at distinct epochs. And, in the very early universe we can assume that the values of ν do not satisfy the aforementioned bound. Assuming that this parameter is of the order one, we can see how the running of Λ affects the isotropization.

Concerning the anisotropic model and the role of the running in isotropization of the metric, we can see that the model tends towards an isotropic configuration in the course of evolution for all values of ν which are considered. Also, one notes that for smaller values of ν , the ratio $b(t)/a(t)$ tends to a constant value quicker. On top of this, the aforementioned constant value is greater for smaller values of ν . It is worth noting that since both conformal factors depend only on time, these results do not depend on the choice of coordinates. Another conclusion one can draw from the plots in Figures 1–12 is that the smaller the value of ν , the faster the expansion of the scale factors $a(t)$ and $b(t)$. Furthermore, independent of the isotropy, the fluid density ρ_f goes to zero faster for smaller values of ν . Both tendencies hold for both positive and negative values of the parameter ν .

Finally, we conclude that the running of the cosmological constant in the model with energy exchange between the vacuum and matter (radiation, in our case) sectors describes the accelerated expansion and, for a moderate value of the phenomenological parameter ν , does not contradict very fast isotropization of the initially anisotropic model. After that, the evolution occurs in the isotropic way, except the dynamics of the cosmic perturbations, which were analyzed in detail in [8].

The last observation concerns the possible extensions and continuations of this work. Despite the KS metric results looking convincing, it would be interesting to perform the same, or maybe a more detailed analysis, for the Bianchi type I, or even more general, metric. In this respect, we note that the previous investigations of Wald [26] showed that the qualitative difference, in the case of a constant vacuum energy, is expected only starting from the Bianchi type IX metric. It would be interesting to see whether this feature holds for the running cosmological constant, maybe using the dynamical systems approach as suggested in [27].

On the other hand, since the anisotropy under discussion concerns only the very early universe, when typical energies are extremely high, it would certainly be interesting to include a consideration of the effects of higher-derivative terms, starting from R^2 . We hope to address this issue in future work.

Author Contributions: Conceptualization, V.G.O., G.d.O.N. and I.L.S.; methodology, V.G.O., G.d.O.N. and I.L.S.; validation, V.G.O., G.d.O.N. and I.L.S.; formal analysis, V.G.O., G.d.O.N. and I.L.S.; investigation, V.G.O., G.d.O.N. and I.L.S.; writing—original draft preparation, V.G.O., G.d.O.N. and I.L.S.; writing—review and editing, V.G.O., G.d.O.N. and I.L.S. All authors have read and agreed to the published version of the manuscript.

Funding: Ilya L. Shapiro acknowledges partial support from Conselho Nacional de Desenvolvimento Científico e Tecnológico—CNPq under the grant 303635/2018-5. Vinícius G. Oliveira thanks Coordenação de Aperfeiçoamento de Pessoal de Nível Superior (CAPES) for supporting his Ms. project, including this work.

Data Availability Statement: The data presented in this study are openly available in arXiv as e-Print: 2312.04723 [gr-qc].

Acknowledgments: The authors are grateful to A. Kamenshchik for useful correspondence.

Conflicts of Interest: The authors declare no conflict of interest.

Abbreviations

KS, Kantowski–Sachs

Note

¹ We have checked that any couple of the three Equations (6)–(8) provide the same solutions.

References


1. Weinberg, S. The cosmological constant problem. *Rev. Mod. Phys.* **1989**, *61*, 1. [CrossRef]
2. Shapiro, I.L. Effective action of vacuum: Semiclassical approach. *Class. Quant. Grav.* **2008**, *25*, 103001. [CrossRef]
3. Shapiro, I.L.; Solà, J. On the possible running of the cosmological “constant”. *Phys. Lett. B* **2009**, *682*, 105. [CrossRef]

4. Babic, A.; Guberina, B.; Horvat, R.; Stefancic, H. Renormalization group running of the cosmological constant and its implication for the Higgs boson mass in the standard model. *Phys. Rev. D* **2002**, *65*, 085002. [CrossRef]
5. Shapiro, I.L.; Solà, J. The scaling evolution of the cosmological constant. *J. High Energy Phys.* **2002**, *02*, 006. [CrossRef]
6. Farina, C.; Kort-Kamp, W.J.M.; Mauro, S.; Shapiro, I.L. Dynamics of the Laplace-Runge-Lenz vector in the quantum-corrected Newton gravity. *Phys. Rev. D* **2011**, *83*, 124037. [CrossRef]
7. Fabris, J.C.; Shapiro, I.L.; Solà, J. Density perturbations for running cosmological constant. *J. Cosmol. Astropart. Phys.* **2007**, *0702*, 016. [CrossRef]
8. Grande, J.; Solà, J.; Fabris, J.C.; Shapiro, I.L. Cosmic perturbations with running G and Λ . *Class. Quant. Grav.* **2010**, *27*, 105004. [CrossRef]
9. Babic, A.; Guberina, B.; Horvat, R.; Stefancic, H. Renormalization-group running cosmologies. A Scale-setting procedure. *Phys. Rev. D* **2005**, *71*, 124041. [CrossRef]
10. Buchbinder, I.L.; Shapiro, I.L. *Introduction to Quantum Field Theory with Applications to Quantum Gravity*; Oxford University Press: Oxford, UK, 2021.
11. Wang, P.; Meng, X.H. Can vacuum decay in our Universe? *Class. Quant. Grav.* **2005**, *22*, 283. [CrossRef]
12. Opher, R.; Pelinson, A. Studying the decay of the vacuum energy with the observed density fluctuation spectrum. *Phys. Rev. D* **2004**, *70*, 063529. [CrossRef]
13. Opher, R.; Pelinson, A. Decay of the vacuum energy into CMB photons. *Mon. Not. Roy. Astron. Soc.* **2005**, *362*, 167. [CrossRef]
14. Shapiro, I.L.; Solà, J.; Stefancic, H. Running G and Λ at low energies from physics at M_X : Possible cosmological and astrophysical implications. *J. Cosmol. Astropart. Phys.* **2005**, *0501*, 012. [CrossRef]
15. Agudelo Ruiz, J.A.; de Paula Netto, T.; Fabris, J.C.; Shapiro, I.L. Primordial universe with the running cosmological constant. *Eur. Phys. Journ. C* **2020**, *80*, 851. [CrossRef]
16. Basilakos, S.; Mavromatos, N.E.; Peracaula, J. Gravitational and Chiral Anomalies in the Running Vacuum Universe and Matter-Antimatter Asymmetry. *Phys. Rev. D* **2020**, *101*, 045001. [CrossRef]
17. Shapiro, I.L.; Sola, J.; Espana-Bonet, J.; Ruiz-Lapuente, P. Variable cosmological constant as a Planck scale effect. *Phys. Lett. B* **2003**, *574*, 149. [CrossRef]
18. Bludman, S.A.; Ruderman, M.A. Induced Cosmological Constant Expected above the Phase Transition Restoring the Broken Symmetry. *Phys. Rev. Lett.* **1977**, *38*, 255. [CrossRef]
19. Kantowski, R.; Sachs, R.K. Some spatially homogeneous anisotropic relativistic cosmological models. *J. Math. Phys.* **1966**, *7*, 443. [CrossRef]
20. Heckmann, O.; Schucking, E. Newtonsche und Einsteinsche Kosmologie. *Handb. Phys.* **1959**, *53*, 489.
21. Jacobs, K.C. Spatially homogeneous and euclidean cosmological models with shear. *Astrophys. J.* **1968**, *153*, 661. [CrossRef]
22. Jacobs, K.C. Cosmologies of Bianchi Type I with a Uniform Magnetic Field. *Astrophys. J.* **1969**, *155*, 379. [CrossRef]
23. Weber, E. Kantowski-Sachs cosmological models approaching isotropy. *J. Math. Phys.* **1984**, *25*, 3279. [CrossRef]
24. Grøn, Ø. Transition of a Kantowski-Sachs cosmological model into an inflationary era. *J. Math. Phys.* **1986**, *27*, 1490. [CrossRef]
25. Burd, A.B.; Barrow, J.D. Inflationary models with exponential potentials. *Nucl. Phys. B* **1988**, *308*, 929; Erratum in *Nucl. Phys. B* **1989**, *324*, 276. [CrossRef]
26. Wald, R.M. Asymptotic behavior of homogeneous cosmological models in the presence of a positive cosmological constant. *Phys. Rev. D* **1983**, *28*, 2118. [CrossRef]
27. Vargas Moniz, P. Kantowski-Sachs universes and the cosmic no hair conjecture. *Phys. Rev. D* **1993**, *47*, 4315. [CrossRef] [PubMed]
28. Byland, S.; Scialom, D. Evolution of the Bianchi I, the Bianchi III and the Kantowski-Sachs universe: Isotropization and inflation. *Phys. Rev. D* **1998**, *57*, 6065. [CrossRef]
29. Adhav, K.S.; Bansod, A.S.; Wankhade, R.P.; Ajmire, H.G. Kantowski-Sachs cosmological models with anisotropic dark energy. *Cent. Eur. J. Phys.* **2011**, *9*, 919. [CrossRef]
30. Parisi, L.; Radicella, N.; Vilasi, G. Kantowski-Sachs Universes sourced by a Skyrme fluid. *Phys. Rev. D* **2015**, *91*, 063533. [CrossRef]
31. Oliveira-Neto, G.; Canedo, D.L.; Monerat, G.A. An Anisotropic Kantowski - Sachs Universe with Radiation, Dust and a Phantom Fluid. *Braz. J. Phys.* **2022**, *52*, 130. [CrossRef]
32. Khalatnikov, I.M.; Kamenshchik, A.Y. A Generalization of the Heckmann-Schucking cosmological solution. *Phys. Lett. B* **2003**, *553*, 119. [CrossRef]
33. Casadio, R.; Kamenshchik, A.; Mavrogiannis, P.; Petriakova, P. Bianchi cosmologies, magnetic fields, and singularities. *Phys. Rev. D* **2023**, *108*, 084059. [CrossRef]
34. Zeldovich, Y.B.; Starobinsky, A.A. Particle production and vacuum polarization in an anisotropic gravitational field. *Zh. Eksp. Teor. Fiz.* **1971**, *61*, 2161.
35. Collins, C.B.; Hawking, S.W. Why is the Universe isotropic? *Astrophys. J.* **1973**, *180*, 317. [CrossRef]
36. Kofman, L.A.; Sahni, V.; Starobinsky, A.A. Anisotropic cosmological model created by quantum polarization of vacuum. *Sov. Phys. JETP* **1983**, *58*, 1090.

37. Grib, A.A.; Mamayev, S.G.; Mostepanenko, V.M. *Vacuum Quantum Effects in Strong Fields*; Friedmann Lab. Publishing: St. Petersburg, Russia, 1994.
38. Pelinson, A.M.; Shapiro, I.L. On the scaling rules for the anomaly-induced effective action of metric and electromagnetic field. *Phys. Lett. B* **2011**, *694*, 467. [CrossRef]

Disclaimer/Publisher's Note: The statements, opinions and data contained in all publications are solely those of the individual author(s) and contributor(s) and not of MDPI and/or the editor(s). MDPI and/or the editor(s) disclaim responsibility for any injury to people or property resulting from any ideas, methods, instructions or products referred to in the content.

Regular Friedmann Universes and Matter Transformations

Alexander Kamenshchik ^{1,2,*}  and Polina Petriakova ^{1,2,†} 

¹ Dipartimento di Fisica e Astronomia, Università di Bologna, Via Irnerio 46, 40126 Bologna, Italy; polina.petriakova@bo.infn.it

² I.N.F.N., Sezione di Bologna, I.S. FLAG, Viale B. Pichat 6/2, 40127 Bologna, Italy

* Correspondence: kamenshchik@bo.infn.it

† These authors contributed equally to this work.

Abstract: We apply a very simple procedure to construct non-singular cosmological models for flat Friedmann universes filled with minimally coupled scalar fields or by tachyon Born–Infeld-type fields. Remarkably, for the minimally coupled scalar field and the tachyon field, the regularity of the cosmological evolution, or in other words, the existence of bounce, implies the necessity of the transition between scalar fields with standard kinetic terms to those with phantom ones. In both cases, the potentials in the vicinity of the point of the transition have a non-analyticity of the cusp form that is characterized by the same exponent and is equal to $\frac{2}{3}$. If, in the tachyon model’s evolution, the pressure changes its sign, then another transformation of the Born–Infeld-type field occurs: the tachyon transforms into a pseudotachyon, and vice versa. We also undertake an analysis of the stability of the cosmological evolution in our models; we rely on the study of the speed of sound squared.

Keywords: Friedmann universe; regular cosmology; tachyons; scalar fields

1. Introduction

For many years, the cosmological singularity has been one of the most attractive problems in general relativity. Starting from Robertson’s seminal work [1], the initial singularity issue of Friedmann-type cosmologies was under scrutiny. Launching the singularity-to-maximal-radius-and-back cyclic evolution was already considered there. It seemed that touching the singularity did not bother him too much. Thereafter, generalization to the case of not only homogeneous and isotropic spacetimes was explored [2–5], resulting in the proof of some general theorems and the discovery of the oscillatory (BKL) approach to the cosmological initial singularity [6], also known as the Mixmaster Universe [7]. The investigation of arising (rather soft) future singularities at the finite scale factor was done further [8] and still maintains interest [9–14]. Regarding such soft future singularities, the condition of their crossing becomes important; see, e.g., [15,16]. The idea of the possible crossing of the so-called Big Bang–Big Crunch singularity appears rather counterintuitive in contrast to the crossing of the soft singularities. Thus, the desire to find models free of such singularities is understandably strong, and this direction is prevalent. However, the idea of the possible transition from a Big Crunch–Big Bang transition was also studied in some cosmological models. Let us point out here the string or pre-Big Bang scenario [17–19], wherein the accelerated expansion of the universe is driven by the kinetic energy of the dilaton field. From the cosmological singularity’s point of view, its presence is essential, since by making the transition from the string frame—where the dilaton is non-trivially coupled to gravity—to the Einstein frame, the observable evolution of the universe can be drastically changed: what looks like an expansion in one frame can look like a contraction in another one. An alternative treatment is to reformulate the theory, relying on the role of scalar fields, to define the finite variables as the scale factor shrinks to zero. That suggests a natural way to match the solutions before and after the singularity crossing and was



Citation: Kamenshchik, A.; Petriakova, P. Regular Friedmann Universes and Matter Transformations. *Universe* **2024**, *10*, 137. <https://doi.org/10.3390/universe10030137>

Academic Editor: Norma G. Sanchez

Received: 25 January 2024

Revised: 19 February 2024

Accepted: 11 March 2024

Published: 13 March 2024



Copyright: © 2024 by the authors. Licensee MDPI, Basel, Switzerland. This article is an open access article distributed under the terms and conditions of the Creative Commons Attribution (CC BY) license (<https://creativecommons.org/licenses/by/4.0/>).

inspired by superstring theories [20–22]. The importance of such features is significant in other approaches as well [23–29].

While the activity of the description of crossing a singularity in cosmology becomes intensive, attempts to find cosmological non-singular models still conserve their charm; see, e.g., [30–32]. Even more active is the search for regular black hole solutions. The study of non-singular black holes started a long time ago [33], and for recent reviews, see [34,35]. One can write down a singularity-free metric ansatz from the Schwarzschild black hole by a simple substitution of the radial coordinate r as $r \rightarrow \sqrt{r^2 + b^2}$, as was proposed by Simpson and Visser [36]. That results in the following spacetime:

$$ds^2 = \left(1 - \frac{2m}{\sqrt{r^2 + b^2}}\right) dt^2 - \left(1 - \frac{2m}{\sqrt{r^2 + b^2}}\right)^{-1} dr^2 - (r^2 + b^2) d\Omega_2^2, \quad (1)$$

where b is a parameter, and the singularity at $r = 0$ is replaced by a regular minimum of the area function at $r = 0$: a sphere of radius b . If $b > 2m$, this spacetime represents a wormhole with a throat at $r = 0$; if $b < 2m$, one has a black hole with two horizons at $r = \pm\sqrt{4m^2 - b^2}$, and the $b = 2m$ case corresponds to an extremal black hole with a single horizon at $r = 0$. At the hypersurface $r = 0$ in the black hole case, the coordinates change their temporal and spatial assignments, which corresponds to a bounce in one of the two scalar factors of the Kantowski–Sachs universe: the so-called black bounce. Afterward, a Vaidya spacetime [37], charged black-bounce spacetimes [38], and Kerr black holes [39] were “regularized” in this Simpson–Visser spirit. This one-parameter extension (1) is sustained by a phantom scalar field and a magnetic field within nonlinear electrodynamics, as was established in [40].

Generally, in the majority of works devoted to the construction of regular black holes, one can use the method that many years ago was called the “G-method” by Synge [41]; see also a recent e-print [42]. Using this method, one chooses a metric, substitutes it into the left-hand side of the Einstein equations, and then sees what happens on the right-hand side. The G-method is opposed to the “T-method”, for which one chooses the form of the matter in the right-hand side of the Einstein equations and then tries to find the metric that satisfies this system of equations by substituting it into the left-hand side. The advantage of the G-method consists of the fact that it always works (in contrast with the T-method). Unfortunately, the right-hand side of the Einstein equations that arises as the result of the application of the G-method does not always have some reasonable physical sense that can be identified with some known fields or other types of matter. The remarkable example of a regular black hole sustained by a minimally coupled phantom scalar field with an explicitly known potential was found in [43]. Some properties of this solution were studied in further detail [44], and it was also used [45] in an attempt to construct a regular rotating black hole.

Recently, Bronnikov explored [46] the regularized version of the Fisher solution [47], which has been rediscovered many times in different contexts [48–55]. One can observe an interesting transition from the standard scalar field to the phantom one there. Herein, we can note that the Friedmann cosmological models have a simpler structure than the Schwarzschild-like black holes. That gives some hope that, using an analogy with the Simpson–Visser prescription [36] in cosmology, one can obtain rather simple cosmological solutions with the matter content, which can be analyzed, at least qualitatively. Indeed, this was done in paper [44]. It was shown that when considering a non-singular metric of the flat Friedmann universe filled with a minimally coupled scalar field, one can find two interesting qualitative features of the model: First, at some moment, the standard scalar field becomes a phantom one, i.e., the kinetic term changes its sign. Second, even if we cannot find an explicit expression for the scalar field potential, we can state that it should be non-analytical, or, more precisely, it should have a cusp. Remarkably, a similar phenomenon was observed in the study of the opportunity of the so-called phantom divide line crossing [56,57], and the forms of the cusps of the potentials coincide.

As is well known, cosmological models with minimally coupled scalar fields are not the only kind of scalar field models. Some time ago, in the context of string-inspired cosmological models, the so-called tachyon fields were studied [58–62]. These tachyon fields arising in string theory [58] are not connected with the tachyon particles flying with superluminal velocities [63]. Nevertheless, we shall use the term “tachyons”, which has already become traditional in the cosmological literature. These tachyons indeed represent scalar fields with non-trivial kinetic terms of the type that was first studied by Born and Infeld [64]. It is interesting to note that the birth of Born–Infeld non-linear electrodynamics was at least in part motivated by the desire to eliminate the singularity of the electric field of a point-like electric charge. Remarkably, sharing with the linear Maxwell electrodynamics the electric–magnetic duality and the physical propagation of waves, the Born–Infeld theory manages to tame the divergence of the Coulomb self-energy [65]. Indeed, the expression for the electric field of the point-like charge Q has the form

$$\vec{E} = \frac{Q}{\sqrt{r^4 + Q^2}} \vec{e}_r. \tag{2}$$

Thus, one has regularization, which in a way reminds one to put “by hands” into the Simpson–Visser-like metrics for black holes and cosmological models. However, here in (2), the charge Q plays the role of both the source of the electric field and of the regularizing quantity. The effective density of the electric point-like charge acquires a finite radius, which is connected with the dimensional parameter b in the definition of the Born–Infeld action [64]. Later, it was discovered that this action appears as an effective action in supersymmetric theories [66,67] as well as in string theory [68]. The attempts to construct a Born–Infeld-type extension of gravity, despite not being unique and well-motivated, are under investigation; see the recent review [69].

The interest in cosmological models with tachyons was mainly connected with their possible role as a source of dark energy. However, further studies have shown that the presence of non-trivial kinetic terms in these models can imply the appearance of some very unusual properties. For example, a tachyon cosmological model with a particular potential depending on trigonometrical functions was studied, and two interesting phenomena were discovered: the self-transformation of the tachyon field into a pseudo-tachyon field and the appearance of a particular type of soft future cosmological singularity, which was called “Big Brake” in [12]. Thus, taking into account the richness of the cosmological models based on the presence of Born–Infeld-type fields, it is interesting to study regular flat Friedmann cosmological universes filled with such fields and to see what kind of effects one can observe there. This is the main goal of the present paper. Its structure is the following: in the second section, we present known results for a regular flat Friedmann universe filled with a minimally coupled scalar field [44]; in the third section, we consider a flat Friedmann universe filled with a tachyon field. The last section contains a discussion of the obtained results.

2. Regular Friedmann Universes and Scalar Fields

The well-known exact solution for a flat Friedmann universe with a massless scalar field ϕ is

$$ds^2 = dt^2 - t^{2/3} (dx_1^2 + dx_2^2 + dx_3^2), \quad \phi = \sqrt{\frac{2}{3}} \frac{1}{t}. \tag{3}$$

Hereafter, dots refer to time derivatives. Following the Simpson–Visser recipe [36], one can write down the regularized one from (3) as:

$$ds^2 = dt^2 - (t^2 + b^2)^{1/3} (dx_1^2 + dx_2^2 + dx_3^2). \tag{4}$$

A straightforward calculation provides us with the Ricci tensor components:

$$R_0^0 = \frac{2t^2 - 3b^2}{3(t^2 + b^2)^4}, \quad R_1^1 = R_2^2 = R_3^3 = -\frac{b^2}{3(t^2 + b^2)^2}, \quad (5)$$

and the Ricci scalar:

$$R = \frac{2t^2 - 6b^2}{3(t^2 + b^2)^2}. \quad (6)$$

Then, the Einstein equations immediately afford the expressions for the energy density and the isotropic pressure of matter as

$$\rho = \frac{t^2}{3(t^2 + b^2)^2}, \quad p = \frac{t^2 - 2b^2}{3(t^2 + b^2)^2}. \quad (7)$$

Considering spacetime that is filled with a spatially homogeneous scalar field with some potential $V(\phi)$, namely,

$$\rho = \frac{1}{2}\dot{\phi}^2 + V(\phi), \quad p = \frac{1}{2}\dot{\phi}^2 - V(\phi), \quad (8)$$

one can compare these expressions and gain

$$\dot{\phi} = \pm \sqrt{\frac{2}{3} \frac{\sqrt{t^2 - b^2}}{t^2 + b^2}}, \quad (9)$$

$$V = \frac{b^2}{3(t^2 + b^2)^2}. \quad (10)$$

Equation (9) can be integrated, providing the field ϕ as a function of time t . However, we are not able to invert the result and find t as an explicit function of ϕ , and thus we cannot use Equation (10) to find the explicit form of the potential in terms of the scalar field. Nonetheless, the Formulas (9) and (10) provide us with rather interesting information. One can see that the expression (9) makes sense only if $|t| \geq b$. What would happen at $|t| < b$? In this situation, the kinetic energy of ϕ changes sign, and the standard scalar field transition to a phantom one appears. Therefore, one can observe an analogous effect to that explored in [46]. The behavior in the vicinity of $t = b$ can be defined through $t = b + \tau$, $\tau \ll b$, resulting in

$$\frac{d\phi}{d\tau} = \frac{\sqrt{\tau}}{\sqrt{3b^3}}, \quad \rightarrow \quad \phi(\tau) = \phi_0 + \frac{2\tau^{3/2}}{3\sqrt{3b^3}}, \quad (11)$$

where ϕ_0 is an integration constant. Accordingly,

$$\tau = 3b \left(\frac{\phi - \phi_0}{2} \right)^{2/3}. \quad (12)$$

Replacing in the expression the potential with (12), one can find the behavior near the vicinity of the critical point, and by keeping the leading terms, we have

$$V(\phi) = \frac{1}{12b^2} \left(1 - 6 \left(\frac{\phi - \phi_0}{2} \right)^{2/3} \right). \quad (13)$$

The presence of cusp type's non-analyticity in the expression above is responsible for the transition from the standard scalar field to its phantom counterpart and vice versa.

One can also consider a slightly more general model:

$$ds^2 = dt^2 - t^{2\alpha} (dx_1^2 + dx_2^2 + dx_3^2), \tag{14}$$

in which the dynamics evolve a perfect fluid with the equation-of-state parameter as follows:

$$w = \frac{2 - 3\alpha}{3\alpha}. \tag{15}$$

This is the well-known particular solution for the flat Friedmann model with a minimally coupled scalar field and exponential potential. To eliminate the cosmological singularity, one can modify metric (14) in a Simpson–Visser spirit as

$$ds^2 = dt^2 - (t^2 + b^2)^\alpha (dx_1^2 + dx_2^2 + dx_3^2); \tag{16}$$

the corresponding Ricci tensor components are

$$R_0^0 = -\frac{3\alpha((\alpha - 1)t^2 + b^2)}{(t^2 + b^2)^2}, \quad R_1^1 = R_2^2 = R_3^3 = -\frac{\alpha((3\alpha - 1)t^2 + b^2)}{(t^2 + b^2)^2}, \tag{17}$$

and the Ricci scalar is

$$R = -\frac{6\alpha((2\alpha - 1)t^2 + b^2)}{(t^2 + b^2)^2}. \tag{18}$$

Now the expressions for energy density and pressure read

$$\rho = \frac{3\alpha^2 t^2}{(t^2 + b^2)^2}, \quad p = -\frac{\alpha((3\alpha - 2)t^2 + 2b^2)}{(t^2 + b^2)^2}, \tag{19}$$

and the corresponding expressions for the potential and the time derivative of the scalar field realizing the evolution (16) are

$$V(\phi) = \frac{\alpha((3\alpha - 1)t^2 + b^2)}{(t^2 + b^2)^2}, \quad \dot{\phi}^2 = \frac{2\alpha(t^2 - b^2)}{(t^2 + b^2)^2}. \tag{20}$$

In the absence of the regularizing parameter $b = 0$, we can get from Equation (20) the known expression for the exponential potential:

$$V(\phi) = \alpha(3\alpha - 1) \exp\left(-\sqrt{\frac{2}{\alpha}}(\phi - \phi_0)\right). \tag{21}$$

Nevertheless, if $b > 0$, one can see that, just as in the previous case, the transition from the standard scalar field to the phantom one (or vice versa) takes place. Now, we can again consider the vicinity of the instant $t = b$. Proceeding in a similar way, we obtain the following expression for the behavior of the potential in the vicinity of the cusp:

$$V(\phi) = \frac{\alpha}{4b^2} \left(3\alpha - \frac{2 \cdot 3^{2/3}}{\alpha^{1/3}} \left(\frac{\phi - \phi_0}{2} \right)^{2/3} \right). \tag{22}$$

This expression has the same non-analyticity ($\sim(\phi - \phi_0)^{2/3}$) as that seen in the expression (13), and when $\alpha = \frac{1}{3}$, these expressions coincide.

3. Regular Friedmann Universes and Tachyons

Let us now again consider a regular flat Friedmann universe with the metric (16). The expressions for the components of the Ricci tensor, Ricci scalar, energy, and pressure

are given by Equations (17)–(19). However, now the universe is filled by the tachyon (Born–Infeld-type) field with the Lagrangian [58]:

$$L = -V(T)\sqrt{1 - T_{,\mu}T^{,\mu}} \tag{23}$$

where T is the tachyon field, and the function $V(T)$ will be called the “potential” of the tachyon field. In the framework of our Friedmann model, we shall consider a spatially homogeneous tachyon field $T = T(t)$, and the Lagrangian (23) will take the simple form

$$L = -V(T)\sqrt{1 - \dot{T}^2}. \tag{24}$$

The energy density and the pressure for this field are

$$\rho = \frac{V(T)}{\sqrt{1 - \dot{T}^2}}, \quad p = -V(T)\sqrt{1 - \dot{T}^2}. \tag{25}$$

The analogue of the Klein–Gordon equation now looks as follows:

$$\frac{\ddot{T}}{1 - \dot{T}^2} + \frac{3\alpha t}{(t^2 + b^2)}\dot{T} + \frac{V_{,T}}{V} = 0. \tag{26}$$

Comparing the expressions (25) for the tachyon field with the corresponding components of the energy–momentum tensor coming from Friedmann’s equations (19), we obtain

$$T^2 = \frac{\rho + p}{\rho} = \frac{2(t^2 - b^2)}{3\alpha t^2}, \tag{27}$$

$$V(T) = \sqrt{-\rho p} = \frac{\sqrt{3\alpha^3 t^2((3\alpha - 2)t^2 + 2b^2)}}{(t^2 + b^2)^2}. \tag{28}$$

One can solve Equation (27), to find a solution

$$T(t) = T_0 \pm \sqrt{\frac{2(t^2 - b^2)}{3\alpha}} \left(1 - \frac{b}{\sqrt{t^2 - b^2}} \arctan \frac{\sqrt{t^2 - b^2}}{b} \right). \tag{29}$$

Let us note here that this solution automatically satisfies Equation (26) due to the Bianchi identities. This feature is typical for the reconstruction techniques for the potentials of both the minimally coupled and the tachyon fields; see, e.g., ref. [12] and the references therein. We cannot invert Equation (29) and find the cosmic time parameter t as a function of the tachyon field T . Thus, as a result, we cannot find an explicit form of the tachyon potential (28) as a function of T . Let us compare this situation with that of the singular cosmology for which the regularizing parameter $b = 0$. In this case, the universe expands (or contracts) following a simple power law, and Equations (27) and (28) become simpler:

$$\dot{T}^2 = \frac{\rho + p}{\rho} = \frac{2}{3\alpha}, \quad V(T) = \sqrt{-\rho p} = \frac{\sqrt{3\alpha^3(3\alpha - 2)}}{t^2}. \tag{30}$$

Integrating Equation (30), we get

$$T(t) = T_0 \pm \sqrt{\frac{2}{3\alpha}}t, \tag{31}$$

and inverting Equation (31), one obtains

$$t = \pm \sqrt{\frac{3\alpha}{2}}(T - T_0). \tag{32}$$

Substituting expression (32) into Equation (30), we find the explicit form of the tachyon potential:

$$V(T) = \frac{\sqrt{\frac{4\alpha(3\alpha - 2)}{3}}}{(T - T_0)^2}. \tag{33}$$

A tachyon model with potential (33) was considered in papers [59,60]. Such a model has a particular exact solution that describes a universe expanding according to the power law with a negative effective pressure. In our terms, it corresponds to the parameter α such that $\alpha > \frac{2}{3}$. To have a flat Friedmann universe expanding according to the power law but with positive pressure, i.e., with the parameter $\alpha < \frac{2}{3}$, one can introduce another type of the Born–Infeld-type field, which is called a “pseudotachyon” and is described by the following Lagrangian [12]:

$$L = V(T)\sqrt{\dot{T}^2 - 1}. \tag{34}$$

Furthermore, it was shown that it is possible to construct a potential of the tachyon field with the Lagrangian (24) such that the dynamics drive the universe to the point where the transformation of the tachyon field into a pseudotachyon field is unavoidable and arises in a natural way.

Let us come back to a flat Friedmann universe with metric (16) and non-singular evolution, i.e., with $b > 0$. We shall first consider the model with $\alpha > \frac{2}{3}$. In this case, the pressure is always negative, and the expression for the potential (28) is well defined. Using the obtained expression (27), one can find that

$$\sqrt{1 - \dot{T}^2} = \sqrt{1 - \frac{3}{3\alpha} + \frac{b^2}{3\alpha t^2}} \tag{35}$$

is also well defined at $\alpha > \frac{2}{3}$. However, we see that at $|t| < b$, the right-hand side of Equation (27) becomes negative. That means that at the moment in time when $t = \pm b$, we encounter the transformation of the tachyon field into the phantom tachyon field with the Lagrangian:

$$L = -V(T)\sqrt{1 + \dot{T}^2}. \tag{36}$$

Thus, the universe at $|t| > b$ is driven by the tachyon field, while at $|t| < b$, it is driven by the phantom tachyon field. Note that the transformation between these two types of Born–Infeld-type fields also occurs if $\alpha < \frac{2}{3}$.

It is interesting to look at the form of the potential in the vicinity of the point of this transition using the same method that was used in the preceding section for the analysis of the models with minimally coupled scalar fields. Straightforward calculations show that in the vicinity of the phantom–non-phantom transition point, the potential has the following behavior:

$$V = \frac{3\alpha^2}{b^2} - \frac{3\alpha(3\alpha + 1)}{b^3} \left(\frac{\alpha b}{2}\right)^{1/2} (T - T_0)^{2/3}. \tag{37}$$

Note that we again have the same exponent $\frac{2}{3}$ as in Equation (13) for the potential of the scalar field.

In the case when $\alpha < \frac{2}{3}$, we have a couple of additional particular time moments

$$t = \pm \sqrt{\frac{2}{2 - 3\alpha}} b \tag{38}$$

during which both the expression under the square root in the formula for the potential (28) and the expression under the square root for the kinetic structure (35) change their signs. This situation is exactly as described in [12], and it corresponds to the transition from the tachyon field to the pseudotachyon one. Below, Figure 1 graphically represents the transitions between different regimes in the model with $\alpha < \frac{2}{3}$. It is easy to see that for $\alpha \geq \frac{2}{3}$, the transition from tachyon to pseudotachyon is absent.

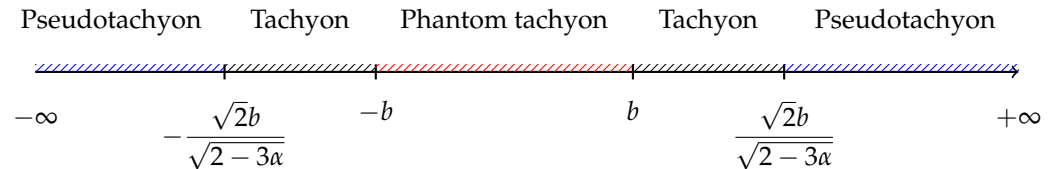


Figure 1. Possible transitions between different regimes in the tachyon model (23) with $\alpha < \frac{2}{3}$.

It is well known that cosmological solutions avoiding singularities, i.e., solutions with bounces, suffer from instability. While detailed analysis of cosmological perturbations represents a rather cumbersome task that lies beyond the scope of the present paper, we can undertake the study of the speed of sound squared for a cosmological model with the metric (16). This analysis will be relevant for both the scalar model of the preceding section and the tachyon model. We have the expressions for the time dependencies of the pressure and energy densities with respect to time; see Equations (7) and (19). Using these expressions, one can find

$$c_s^2 = \frac{dp'_{t^2}}{d\rho'_{t^2}} = \frac{(2 - 3\alpha)t^2 - 3(2 - \alpha)b^2}{3\alpha(t^2 - b^2)}. \tag{39}$$

Now we are able to study the time behavior of the speed of sound squared for models with different values of the parameter α , characterizing our cosmological evolution.

Let us start with the case $\alpha > 2$, which, in the model with the non-regularized metric, i.e., at $b = 0$, corresponds to a Friedmann universe filled with a perfect fluid with negative pressure and an equation-of-state parameter $w \leq -\frac{2}{3}$. First of all, we note that at all values of parameter α , the denominator of the expression (39) is positive at $t^2 > b^2$ and negative at $t^2 < b^2$. For $\alpha > 2$, by catching the sign of the numerator, one can easily see that

$$c_s^2 < 0 \text{ if } t^2 > b^2 \text{ or } t^2 < \frac{3(2 - \alpha)}{2 - 3\alpha} b^2, \text{ while } c_s^2 > 0 \text{ if } \frac{3(\alpha - 2)}{3\alpha - 2} b^2 < t^2 < b^2. \tag{40}$$

Then, if the time belongs to interval (40), where the speed of sound squared is positive, we may ask ourselves when c_s^2 is subluminal and when it is superluminal. A simple analysis shows that

$$c_s^2 < 1 \text{ if } \frac{3(\alpha - 2)}{3\alpha - 2} b^2 < t^2 < \frac{3(\alpha - 1)}{3\alpha - 1} b^2; \text{ and if } \frac{3(\alpha - 1)}{3\alpha - 1} b^2 < t^2 < b^2, \tag{41}$$

one has a superluminal velocity for the propagation of the perturbations.

One can consider the case $1 < \alpha \leq 2$, which matches a perfect fluid with a negative pressure with the equation-of-state parameter $-\frac{2}{3} \leq w < -\frac{1}{3}$. A similar analysis shows that $c_s^2 < 0$ at $t^2 > b^2$. The speed of sound squared is positive, subluminal, and superluminal, correspondingly, at

$$t^2 < \frac{3(\alpha - 1)}{3\alpha - 1} b^2 \text{ and } \frac{3(\alpha - 1)}{3\alpha - 1} b^2 < t^2 < b^2. \tag{42}$$

The next case is $\frac{2}{3} \leq \alpha \leq 1$, which agrees with a perfect fluid with negative pressure and equation-of-state parameter $-\frac{1}{3} \leq w \leq 0$, and $c_s^2 < 0$ at $t^2 > b^2$ and positive, but it is superluminal at $t^2 < b^2$.

The case $\frac{1}{3} \leq \alpha < \frac{2}{3}$ corresponds to a perfect fluid with positive pressure and equation-of-state parameter $0 < w \leq 1$, leading to

$$c_s^2 < 0 \text{ if } b^2 < t^2 < \frac{3(2-\alpha)}{2-3\alpha}b^2; \quad c_s^2 < 1 \text{ if } t^2 > \frac{3(2-\alpha)}{2-3\alpha}b^2, \text{ and } c_s^2 > 1 \text{ if } t^2 < b^2. \tag{43}$$

This particular case, namely $\frac{1}{3} \leq \alpha < \frac{2}{3}$, is presented graphically below in Figure 2.

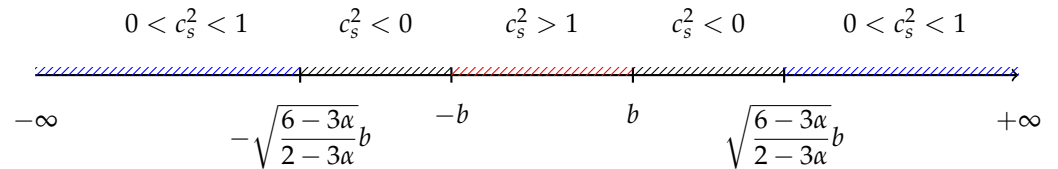


Figure 2. The corresponding squared speed of sound to the possible transformations in the tachyon model (23), which is shown in Figure 1.

Finally, in the case of $0 < \alpha < \frac{1}{3}$, suited for the equation of state with $w > 1$, we have

$$c_s^2 < 0 \text{ if } b^2 < t^2 < \frac{3(2-\alpha)}{2-3\alpha}b^2, \quad \text{and} \tag{44}$$

$$c_s^2 > 1 \text{ if } t^2 < b^2 \text{ or } \frac{3(1-\alpha)}{1-3\alpha}b^2 < t^2; \quad c_s^2 < 1 \text{ if } \frac{3(2-\alpha)}{2-3\alpha}b^2 < t^2 < \frac{3(1-\alpha)}{1-3\alpha}b^2.$$

Let us now switch off the regularization, i.e., set $b = 0$. As follows from Equation (39),

$$c_s^2 = \frac{2-3\alpha}{3\alpha}; \tag{45}$$

the speed of sound squared is positive if $\alpha < \frac{2}{3}$, i.e., if the pressure is positive, and it is subluminal if $\alpha > \frac{1}{3}$, i.e., the pressure is smaller than the energy density. We have seen that in any case, the inclusion of the parameter b and regularizing the metric introduces instabilities into the cosmological solutions. Such a situation looks rather natural. One can remember that, for example, in a very simple cosmological model of a closed Friedmann universe filled with a minimally coupled scalar field, for which the potential includes only a massive term that is quadratic in field, there are solutions with bounces, but they are actually unstable. This model was studied in detail by many authors; see, e.g., refs. [70–77]. Thus, it looks like a very challenging task to obtain a cosmological model with non-singular, stable evolution.

One can ask themselves: what can be the value of the regularizing parameter b ? As a matter of fact, because of the purely theoretical nature of our toy model, it is difficult to make some reasonable estimations. One can say only that any, even the most tiny nonzero value, of b does the job of eliminating the cosmological singularity. On the other hand, the smaller the value of b , the less distorting its effects are on other aspects of cosmological evolution. Thus, with a more complicated and realistic nonsingular cosmological model, one can hope to find a bound from above on the values of regularizing parameters when comparing the model with observational data.

4. Discussion

We applied a simple procedure for the construction of cosmological models free from singularities to flat Friedmann universes filled with minimally coupled scalar fields or by tachyon Born–Infeld-type fields. The form of the regular metric for the Friedmann universes, which we have used in the paper [44] and in the present paper, was inspired by the prescription used in the paper [36] for the construction of regular black holes. Remarkably, for both cases—the minimally coupled scalar field and the tachyon field—the regularity of the cosmological evolution, or in other words, the existence of bounce, implies the necessity of the transition between scalar fields with standard kinetic terms to those with

phantom ones. In both cases, the potentials of the minimally coupled scalar field and the tachyon in the vicinity of the point of the transition have a non-analyticity of the cusp form that is characterized by the same exponent and is equal to $\frac{2}{3}$. If in the tachyon model we choose the evolution such that the pressure changes its sign, then another transformation of the Born–Infeld-type field occurs: the tachyon transforms into a pseudotachyon, and vice versa.

It is worth noting that a transition between these two types of scalar fields was also investigated in the articles [56,57,78] in a rather different context. The starting point there was the observation that the equation of the state of effective dark energy models in the late universe can change its form across the value $w = -1$. This phenomenon is called the “crossing of the phantom divide line” in the literature. Onward, the authors of [56], inspired by [79], proposed a model wherein this effect is realized in the presence of a single scalar field; see also the earlier work [78]. For this to be achieved in [56], it was necessary to have a cusp in the potential of the scalar field, and its initial conditions needed to be chosen in a special way. Further details of this model were explored in [57]. Remarkably, the form of the cusp found in [56] coincides with that found in [44] for a minimally couple scalar field and, in the present paper, for a tachyon field. Enigmatically for us, the exponent $\frac{2}{3}$ arises everywhere.

We would like to mention some other curious facts concerning Born–Infeld-like fields. First, as was noticed in the paper [61], a cosmological model with a tachyon with constant potential exactly coincides with that based on the Chaplygin gas [80] with an equation of state $p = -A/\rho$, where A is a positive constant; see also [81–83]. An analogous observation was made in [12]: a model based on a pseudotachyon with constant potential is equivalent to a model based on a perfect fluid, which was called “anti-Chaplygin gas” and has an equation of state $p = B/\rho$, where B is a positive constant. Remarkably, an equation of state of this type was obtained from the so-called wiggly strings [84,85]. The anti-Chaplygin gas appears to be a rather convenient tool for studying future soft singularities.

Concluding the paper, we would like to say that the study of regular cosmological models free of singularities, just like the investigation of regular black holes, brings some interesting results and reveals some unusual features of General Relativity and its modifications and generalizations. However, eliminating the singularities rather often implies the appearance of some cumbersome and not quite natural types of matter. Thus, in our opinion, the idea that the singularities in General Relativity are not its drawback but its distinguishing feature, which should be accepted and for which adequate language for their treatment should be developed, is very attractive. We complete our text with a reference to an old paper by Charles Misner in which this idea was expressed in a very clear and convincing way [86]. In particular, he wrote, “We should stretch our minds, find some more acceptable set of words to describe the mathematical situation, now identified as ‘singular’, and then proceed to incorporate this singularity into our physical thinking until observational difficulties force revision on us. The concept of a true initial singularity (as distinct from an indescribable early era at extravagant but finite high densities and temperatures) can be a positive and useful element in cosmological theory”.

Author Contributions: All authors (A.K. and P.P.) contributed equally to the present work. All authors have read and agreed to the published version of the manuscript.

Funding: This research was partially supported by the INFN grant FLAG.

Data Availability Statement: Data are contained within the article.

Conflicts of Interest: The authors declare no conflicts of interest.

References

1. Robertson, H.P. Relativistic Cosmology. *Rev. Mod. Phys.* **1933**, *5*, 62–90. [CrossRef]
2. Lifshitz, E.M.; Khalatnikov, I.M. Investigations in relativistic cosmology. *Adv. Phys.* **1963**, *12*, 185–249. [CrossRef]
3. Penrose, R. *Structure of Space-Time*; W.A. Benjamin: New York, NY, USA; Amsterdam, The Netherlands, 1968.

4. Hawking, S.W.; Ellis, G.F.R. *The Large Scale Structure of Space-Time*; Cambridge University Press: Cambridge, MA, USA; New York, NY, USA, 1973.
5. Hawking, S.W.; Penrose, R. The Singularities of gravitational collapse and cosmology. *Proc. R. Soc. Lond. Ser. A* **1970**, *314*, 529–548.
6. Belinsky, V.A.; Khalatnikov, I.M.; Lifshitz, E.M. Oscillatory approach to a singular point in the relativistic cosmology. *Adv. Phys.* **1970**, *19*, 525–573. [CrossRef]
7. Misner, C.W. Mixmaster universe. *Phys. Rev. Lett.* **1969**, *22*, 1071–1074. [CrossRef]
8. Barrow, J.D.; Galloway, G.J.; Tipler, F.J. The closed-universe recollapse conjecture. *Mon. Not. R. Astron. Soc.* **1986**, *223*, 835–844. [CrossRef]
9. Barrow, J.D. Sudden Future Singularities. *Class. Quantum Gravity* **2004**, *21*, L79–L82. [CrossRef]
10. Barrow, J.D. More General Sudden Singularities. *Class. Quantum Gravity* **2004**, *21*, 5619–5622. [CrossRef]
11. Barrow, J.D.; Tsagas, C.G. New Isotropic and Anisotropic Sudden Singularities. *Class. Quantum Gravity* **2005**, *22*, 1563–1571. [CrossRef]
12. Gorini, V.; Kamenshchik, A.Y.; Moschella, U.; Pasquier, V. Tachyons, scalar fields and cosmology. *Phys. Rev. D* **2004**, *69*, 123512. [CrossRef]
13. Shtanov, Y.; Sahni, V. Unusual cosmological singularities in brane world models. *Class. Quantum Gravity* **2002**, *19*, L101–L107. [CrossRef]
14. Kamenshchik, A.Y. Quantum cosmology and late-time singularities. *Class. Quantum Gravity* **2013**, *30*, 173001. [CrossRef]
15. Fernandez-Jambrina, L.; Lazkoz, R. Geodesic behaviour of sudden future singularities. *Phys. Rev. D* **2004**, *70*, 121503. [CrossRef]
16. Keresztes, Z.; Gergely, L.; Kamenshchik, A.Y.; Gorini, V.; Polarski, D. Soft singularity crossing and transformation of matter properties. *Phys. Rev. D* **2013**, *88*, 023535. [CrossRef]
17. Gasperini, M.; Veneziano, G. Pre-big bang in string cosmology. *Astropart. Phys.* **1993**, *1*, 317–339. [CrossRef]
18. Lidsey, J.E.; Wands, D.; Copeland, E.J. Superstring cosmology. *Phys. Rep.* **2000**, *337*, 343–492. [CrossRef]
19. Gasperini, M.; Veneziano, G. The Pre-big bang scenario in string cosmology. *Phys. Rep.* **2003**, *373*, 1–212. [CrossRef]
20. Khoury, J.; Ovrut, B.A.; Steinhardt, P.J.; Turok, N. The Ekpyrotic universe: Colliding branes and the origin of the hot big bang. *Phys. Rev. D* **2001**, *64*, 123522. [CrossRef]
21. Khoury, J.; Ovrut, B.A.; Seiberg, N.; Steinhardt, P.J.; Turok, N. From big crunch to big bang. *Phys. Rev. D* **2002**, *65*, 086007. [CrossRef]
22. Khoury, J.; Steinhardt, P.J.; Turok, N. Designing cyclic universe models. *Phys. Rev. Lett.* **2004**, *92*, 031302. [CrossRef] [PubMed]
23. Kamenshchik, A.Y.; Pozdeeva, E.O.; Vernov, S.Y.; Tronconi, A.; Venturi, G. Transformations between Jordan and Einstein frames: Bounces, antigravity, and crossing singularities. *Phys. Rev. D* **2016**, *94*, 063510. [CrossRef]
24. Kamenshchik, A.Y.; Pozdeeva, E.O.; Vernov, S.Y.; Starobinsky, A.A.; Tronconi, A.; Venturi, G. Induced gravity and minimally and conformally coupled scalar fields in Bianchi-I cosmological models. *Phys. Rev. D* **2017**, *97*, 023536. [CrossRef]
25. Kamenshchik, A.Y.; Pozdeeva, E.O.; Starobinsky, A.A.; Tronconi, A.; Vardanyan, T.; Venturi, G.; Vernov, S.Y. Duality between static spherically or hyperbolically symmetric solutions and cosmological solutions in scalar-tensor gravity. *Phys. Rev. D* **2018**, *98*, 124028. [CrossRef]
26. Bars, I.; Chen, P.J.; Steinhardt, P.J.; Turok, N. Antigravity and the Big Crunch/Big Bang Transition. *Phys. Lett. B* **2012**, *715*, 278–281. [CrossRef]
27. Bars, I.; Steinhardt, P.J.; Turok, N. Sailing through the big crunch-big bang transition. *Phys. Rev. D* **2014**, *89*, 061302. [CrossRef]
28. Wetterich, C. Variable gravity Universe. *Phys. Rev. D* **2014**, *89*, 024005. [CrossRef]
29. Wetterich, C. Eternal Universe. *Phys. Rev. D* **2014**, *90*, 043520. [CrossRef]
30. Creminelli, P.; Nicolis, A.; Trincherini, E. Galilean Genesis: An Alternative to inflation. *JCAP* **2010**, *1011*, 021. [CrossRef]
31. Easson, D.; Sawicki, I.; Vikman, A. G-Bounce. *JCAP* **2011**, *11*, 021. [CrossRef]
32. Volkova, V.A.; Mironov, S.A.; Rubakov, V.A. Cosmological Scenarios with Bounce and Genesis in Horndeski Theory and Beyond. *JETP* **2019**, *129*, 553–565. [CrossRef]
33. Bardeen, J.M. Non-singular general-relativistic gravitational collapse. In Proceedings of the International Conference GR5, Tbilisi, Georgia, 9–16 September 1968; p. 174.
34. Spallucci, E.; Smailagic, A. Regular black holes from from semi-classical down to Planckian size. *Int. J. Mod. Phys. D* **2017**, *26*, 1730013. [CrossRef]
35. Sebastiani, L.; Zerbini, S. Some remarks on non-singular spherically symmetric space-times. *Astronomy* **2022**, *1*, 99–125. [CrossRef]
36. Simpson, A.; Visser, M. Black bounce to traversable wormhole. *JCAP* **2019**, *2*, 042. [CrossRef]
37. Simpson, A.; Martin-Moruno, P.; Visser, M. Vaidya spacetimes, black-bounces, and traversable wormholes. *Class. Quantum Gravity* **2019**, *36*, 145007. [CrossRef]
38. Franzin, E.; Liberati, S.; Mazza, J.; Simpson, A.; Visser, M. Charged black-bounce spacetimes. *JCAP* **2021**, *7*, 036. [CrossRef]
39. Simpson, A.; Visser, M. The eye of the storm: A regular Kerr black hole. *JCAP* **2022**, *3*, 011. [CrossRef]
40. Bronnikov, K.A.; Walia, R.K. Field sources for Simpson-Visser spacetimes. *Phys. Rev. D* **2022**, *105*, 044039. [CrossRef]
41. Synge, J.L. *Relativity: The General Theory*; North-Holland Company: Amsterdam, The Netherlands, 1960.
42. Ellis, G.F.R.; Garfinkle, D. The Synge G-Method: Cosmology, wormholes, firewalls, geometry. *arXiv* **2023**, arXiv:2311.06881.
43. Bronnikov, K.A.; Fabris, J.C. Regular phantom black holes. *Phys. Rev. Lett.* **2006**, *96*, 251101. [CrossRef] [PubMed]



44. Chataignier, L.; Kamenshchik, A.Y.; Tronconi, A.; Venturi, G. Regular black holes, universes without singularities, and phantom-scalar field transitions. *Phys. Rev. D* **2023**, *107*, 023508. [CrossRef]
45. Kamenshchik, A.; Petriakova, P. Newman-Janis algorithm's application to regular black hole models. *Phys. Rev. D* **2023**, *107*, 124020. [CrossRef]
46. Bronnikov, K.A. Black bounces, wormholes, and partly phantom scalar fields. *Phys. Rev. D* **2022**, *106*, 064029. [CrossRef]
47. Fisher, I.Z. Scalar mesostatic field with regard for gravitational effects. *Zh. Eksp. Teor. Fiz.* **1948**, *18*, 636–640.
48. Bergmann, O.; Leipnik, R. Space-Time Structure of a Static Spherically Symmetric Scalar Field. *Phys. Rev.* **1957**, *107*, 1157–1161. [CrossRef]
49. Buchdahl, H.A. Reciprocal Static Metrics and Scalar Fields in the General Theory of Relativity. *Phys. Rev.* **1959**, *115*, 1325–1328. [CrossRef]
50. Janis, A.I.; Newman, E.T.; Winicour, J. Reality of the Schwarzschild Singularity. *Phys. Rev. Lett.* **1968**, *20*, 878–880. [CrossRef]
51. Janis, A.I.; Robinson, D.C.; Winicour, J. Comments on Einstein scalar solutions. *Phys. Rev.* **1969**, *186*, 1729–1731. [CrossRef]
52. Wyman, M. Static Spherically Symmetric Scalar Fields in General Relativity. *Phys. Rev. D* **1981**, *24*, 839–841. [CrossRef]
53. Agnese, A.G.; La Camera, M. Gravitation without black holes. *Phys. Rev. D* **1985**, *31*, 1280–1286. [CrossRef]
54. Xanthopoulos, B.C.; Zannias, T. Einstein Gravity Coupled to a Massless Scalar Field in Arbitrary Space-time Dimensions. *Phys. Rev. D* **1989**, *40*, 2564–2567. [CrossRef]
55. Gaudin, M.; Gorini, V.; Kamenshchik, A.; Moschella, U.; Pasquier, V. Gravity of a static massless scalar field and a limiting Schwarzschild-like geometry. *Int. J. Mod. Phys. D* **2006**, *15*, 1387–1406. [CrossRef]
56. Andrianov, A.A.; Cannata, F.; Kamenshchik, A.Y. Smooth dynamical crossing of the phantom divide line of a scalar field in simple cosmological models. *Phys. Rev. D* **2005**, *72*, 043531. [CrossRef]
57. Cannata, F.; Kamenshchik, A.Y. Networks of cosmological histories, crossing of the phantom divide line and potentials with cusps. *Int. J. Mod. Phys. D* **2007**, *16*, 1683–1704. [CrossRef]
58. Sen, A. Rolling tachyon. *JHEP* **2002**, *4*, 048. [CrossRef]
59. Padmanabhan, T. Accelerated expansion of the universe driven by tachyonic matter. *Phys. Rev. D* **2002**, *66*, 021301. [CrossRef]
60. Feinstein, A. Power law inflation from the rolling tachyon. *Phys. Rev. D* **2002**, *66*, 063511. [CrossRef]
61. Frolov, A.V.; Kofman, L.; Starobinsky, A.A. Prospects and problems of tachyon matter cosmology. *Phys. Lett. B* **2002**, *545*, 8–16. [CrossRef]
62. Gibbons, G.W. Cosmological evolution of the rolling tachyon. *Phys. Lett. B* **2002**, *537*, 1–4. [CrossRef]
63. Feinberg, G. Possibility of faster-than-light particles. *Phys. Rev.* **1967**, *159*, 1089–1105. [CrossRef]
64. Born, M.; Infeld, L. Foundations of the new field theory. *Proc. Roy. Soc. Lond. A* **1934**, *144*, 425–451. [CrossRef]
65. Ketov, S.V. Many faces of Born-Infeld theory. *arXiv* **2001**, arXiv:hep-th/0108189.
66. Ketov, S.V. A Manifestly $N = 2$ supersymmetric Born-Infeld action. *Mod. Phys. Lett. A* **1999**, *14*, 501–510. [CrossRef]
67. Ketov, S.V. $N = 1$ and $N = 2$ supersymmetric non-Abelian Born-Infeld actions from superspace. *Phys. Lett. B* **2000**, *491*, 207–213. [CrossRef]
68. Seiberg, N.; Witten, E. String theory and noncommutative geometry. *JHEP* **1999**, *9*, 032. [CrossRef]
69. Jimenez, J.B.; Heisenberg, L.; Olmo, G.J.; Rubiera-Garcia, D. Born-Infeld inspired modifications of gravity. *Phys. Rep.* **2018**, *727*, 1–129. [CrossRef]
70. Parker, L.; Fulling, S.A. Quantized matter fields and the avoidance of singularities in general relativity. *Phys. Rev. D* **1973**, *7*, 2357–2374. [CrossRef]
71. Starobinskii, A.A. On a nonsingular isotropic cosmological model. *Sov. Astron. Lett.* **1978**, *4*, 82–84.
72. Hawking, S.W. Quantum Cosmology. Presented at the Les Houches Summer School on Theoretical Physics: Relativity, Groups and Topology, Les Houches, France, 27 June–4 August 1983; pp. 333–379.
73. Page, D.N. A Fractal Set of Perpetually Bounces Universes? *Class. Quantum Gravity* **1984**, *1*, 417–427. [CrossRef]
74. Belinskii, V.A.; Grishchuk, L.P.; Zeldovich, Y.B.; Khalatnikov, I.M. Inflationary stages in cosmological models with a scalar field. *Sov. Phys. JETP* **1985**, *62*, 195–203. [CrossRef]
75. Belinskii, V.A.; Khalatnikov, I.M. On the generality of inflationary solutions in cosmological models with a scalar field. *Sov. Phys. JETP* **1987**, *66*, 441–449.
76. Belinsky, V.A.; Ishihara, H.; Khalatnikov, I.M.; Sato, H. On the degree of generality of inflation in Friedmann cosmological models with a massive scalar field. *Prog. Theor. Phys.* **1988**, *79*, 676–684. [CrossRef]
77. Kamenshchik, A.Y.; Khalatnikov, I.M.; Toporensky, A.V. Simplest cosmological model with the scalar field. *Int. J. Mod. Phys. D* **1997**, *6*, 673–692. [CrossRef]
78. Vikman, A. Can dark energy evolve to the phantom? *Phys. Rev. D* **2005**, *71*, 023515. [CrossRef]
79. Yurov, A. Phantom scalar fields result in inflation rather than Big Rip. *arXiv* **2003**, arXiv:astro-ph/0305019.
80. Kamenshchik, A.Y.; Moschella, U.; Pasquier, V. An alternative to quintessence. *Phys. Lett. B* **2001**, *511*, 265–268. [CrossRef]
81. Fabris, J.C.; Goncalves, S.V.B.; de Souza, P.E. Density perturbations in an Universe dominated by the Chaplygin gas. *Gen. Relativ. Gravit.* **2002**, *34*, 53–63. [CrossRef]
82. Bilic, N.; Tupper, G.B.; Viollier, R.D. Unification of Dark Matter and Dark Energy: The Inhomogeneous Chaplygin Gas. *Phys. Lett. B* **2002**, *535*, 17–21. [CrossRef]

83. Bento, M.C.; Bertolami, O.; Sen, A.A. Generalized Chaplygin gas, accelerated expansion and dark energy matter unification. *Phys. Rev. D* **2002**, *66*, 043507. [CrossRef]
84. Carter, B. Duality Relation Between Charged Elastic Strings And Superconducting Cosmic Strings. *Phys. Lett. B* **1989**, *224*, 61–66. [CrossRef]
85. Vilenkin, A. Effect of Small Scale Structure on the Dynamics of Cosmic Strings. *Phys. Rev. D* **1990**, *41*, 3038–3040. [CrossRef]
86. Misner, C.W. Absolute zero of time. *Phys. Rev.* **1969**, *186*, 1328–1333. [CrossRef]

Disclaimer/Publisher’s Note: The statements, opinions and data contained in all publications are solely those of the individual author(s) and contributor(s) and not of MDPI and/or the editor(s). MDPI and/or the editor(s) disclaim responsibility for any injury to people or property resulting from any ideas, methods, instructions or products referred to in the content.

Article

On Phase Transitions during Collisions Near the Horizon of Black Holes

Andrey A. Grib ^{1,2}  and Yuri V. Pavlov ^{3,4,*} 

¹ Theoretical Physics and Astronomy Department, The Herzen University, 48 Moika, St. Petersburg 191186, Russia; andrei_grib@mail.ru

² A. Friedmann Laboratory for Theoretical Physics, St. Petersburg 191186, Russia

³ Institute of Problems in Mechanical Engineering of Russian Academy of Sciences, 61 Bolshoy, V.O., St. Petersburg 199178, Russia

⁴ N.I. Lobachevsky Institute of Mathematics and Mechanics, Kazan Federal University, Kazan 420008, Russia

* Correspondence: yuri.pavlov@mail.ru

Abstract: During particle collisions in the vicinity of the horizon of black holes, it is possible to achieve energies and temperatures corresponding to phase transitions in particle physics. It is shown that the sizes of the regions of the new phase are of the order of the Compton length for the corresponding mass scale. The lifetime is also on the order of the Compton time. It is shown that the inverse influence of the energy density in the electro-weak phase transition in collisions on the space-time metric can be neglected.

Keywords: black hole; symmetry breaking; phase transitions

1. Introduction

The works of A.A. Friedman [1,2], written 100 years ago, in which solutions were obtained for an expanding homogeneous isotropic universe [3], are the theoretical basis of the modern standard cosmological model. The discovery in 1965 of relic radiation [4,5] indicates that in the model of the expanding early Universe, there were times when the temperature of matter was so high that phase transitions predicted by the theory of elementary particles could occur. There are three such phase transitions in the standard model of particle physics [6–8]:

- (1) Between quark–gluon plasma and hadrons at the energies E of the order of 200 MeV. The corresponding temperature $T = E/k_B \approx 10^{12}$ K, where $k_B \approx 1.38 \cdot 10^{-23}$ J/K is the Boltzmann constant, may have taken place in the expanding Universe during the order of 10^{-6} s after the Big Bang.
- (2) An electro-weak phase transition at energies of the order of $E_W \approx 100$ GeV. The corresponding temperature $T_W \approx 10^{15}$ K could have taken place during the order of 10^{-12} s after the Big Bang.
- (3) The grand unification phase transition at energies.

$E_{GUT} \approx 10^{16}$ GeV. The temperature corresponding to the energy of the grand unification phase transition $T_{GUT} = E_{GUT}/k_B \approx 10^{29}$ K may not have been achieved in the early universe in models with an inflationary stage in which the heating temperature is significantly lower than T_{GUT} . In models with a radiation-dominant stage in the early Universe, the temperature T_{GUT} could be reached at times of the order of 10^{-38} s.

The study of the properties of matter at such temperatures and the phenomena at these phase transitions is of undoubted theoretical interest. Is it possible to achieve such temperatures in experiments on the Earth? The maximum high temperature for macroscopic parts of the substance is achieved at the time of nuclear explosion and can be on the order of 10^8 K. This is significantly less than the temperature of even the quark–gluon phase transition [9].



Citation: Grib, A.A.; Pavlov, Y.V. On Phase Transitions during Collisions Near the Horizon of Black Holes. *Universe* **2024**, *10*, 131. <https://doi.org/10.3390/universe10030131>

Academic Editor: Gonzalo J. Olmo

Received: 31 January 2024

Revised: 1 March 2024

Accepted: 5 March 2024

Published: 7 March 2024



Copyright: © 2024 by the authors. Licensee MDPI, Basel, Switzerland. This article is an open access article distributed under the terms and conditions of the Creative Commons Attribution (CC BY) license (<https://creativecommons.org/licenses/by/4.0/>).

The highest temperature achieved in experiments on Earth refers to microscopic quantities of matter and is obtained when heavy element nuclei collide in particle accelerators. A temperature of $4 \cdot 10^{12}$ K was obtained from a collision of gold nuclei in Brookhaven National Laboratory (United States) in 2010 [10]. In 2012, it was reported that a temperature of $5 \cdot 10^{12}$ K was reached when the lead nuclei collided at the Large Hadron Collider [11]. At such temperatures, hadron matter transforms into the quark–gluon plasma state. However, such temperatures are more than two orders of magnitude less than the temperature of the electro-weak phase transition.

Thus, macroscopic amounts of matter in the state of phase transition of elementary particle physics in laboratories on Earth cannot be obtained, and microscopic amounts can be obtained only for the phase transition in the quark–gluon plasma state.

Is it possible to observe matter at the temperatures of the phase transitions of particle physics in astrophysical processes at present? Brightly luminous accretion discs formed when matter falls into black holes have a visible temperature of hundreds of millions of Kelvin degrees [12]. As shown in our work [13], in the processes of collisions of particles near the horizon of black holes, it is possible to achieve energies in the system of the center of mass of colliding particles on the order of the energy scale of the electro-weak phase transition? A summary of these results is presented in Section 2.

Here we will consider questions about the size of the regions of the phase transition region obtained in a collision and the lifetime of such a region. To do this, in Section 3, we apply formulas for the energy density and radiation intensity of a gas of relativistic particles. The possibility of obtaining an electro-weak phase transition in a macroscopic volume during a collision in the vicinity of supermassive black holes is studied in Section 4. The influence of the matter energy–momentum tensor in the phase transition region on the space–time metric will be evaluated in Section 5.

2. The High-Energy Collisions Near the Horizon of Black Holes

The Kerr metric of a rotating black hole [14] in the Boyer–Lindquist coordinates [15] has the following form:

$$ds^2 = \frac{\rho^2 \Delta}{\Sigma^2} c^2 dt^2 - \frac{\sin^2 \theta}{\rho^2} \Sigma^2 (d\varphi - \omega dt)^2 - \frac{\rho^2}{\Delta} dr^2 - \rho^2 d\theta^2, \tag{1}$$

where

$$\rho^2 = r^2 + \frac{a^2}{c^2} \cos^2 \theta, \quad \Delta = r^2 - \frac{2GMr}{c^2} + \frac{a^2}{c^2}, \tag{2}$$

$$\Sigma^2 = \left(r^2 + \frac{a^2}{c^2} \right)^2 - \frac{a^2}{c^2} \sin^2 \theta \Delta, \quad \omega = \frac{2GMra}{\Sigma^2 c^2}, \tag{3}$$

G is the gravitational constant, c is the speed of light and M and aM are the mass and angular momentum of the black hole, respectively. We accept that $0 \leq a \leq GM/c$. The event horizon of the Kerr black hole has the radial coordinate

$$r = r_H \equiv \frac{G}{c^2} \left(M + \sqrt{M^2 - \left(\frac{ac}{G} \right)^2} \right). \tag{4}$$

According to [16], the squared energy of a collision of two particles with a mass m with the angular momenta L_1 and L_2 in the center-of-mass system, which are nonrelativistic at infinity and are freely incident on a black hole with the angular momentum aM , is given by the expression

$$\frac{E_{c.m}^2}{m^2c^4} = \frac{2}{x(x^2 - 2x + A^2)} \left[2A^2(1 + x) - 2A(l_1 + l_2) - l_1l_2(x - 2) + 2(x - 1)x^2 - \sqrt{2(A - l_2)^2 - l_2^2x + 2x^2} \sqrt{2(A - l_1)^2 - l_1^2x + 2x^2} \right], \tag{5}$$

where $x = rc^2/GM, l = Lc/GmM$ and $A = ac/GM$. Expression (5) has a singularity on the event horizon. In the general case, the limit value of the collision energy for two particles with masses m_1, m_2 , energies E_1, E_2 and angular momenta J_1, J_2 is

$$E_{c.m}^2(r \rightarrow r_H) = \frac{c^6(J_{1H}J_2 - J_2HJ_1)^2}{G^2M^2(J_{1H} - J_1)(J_{2H} - J_2)} + m_1^2c^4 \left[1 + \frac{J_{2H} - J_2}{J_{1H} - J_1} \right] + m_2^2c^4 \left[1 + \frac{J_{1H} - J_1}{J_{2H} - J_2} \right], \tag{6}$$

where $J_{nH} = 2E_n r_H / A$. If the angular momentum of one of the particles tends to J_{nH} , then the expression for the energy (6) diverges. This is the so-called Banados–Silk–West effect. Note that despite the unlimited increase in collision energy in the center of mass system, the energy that can be extracted at a large distance from a black hole cannot exceed $E_1 + E_2$ (assuming no Penrose effect [17]). This follows from the law of energy conservation.

A particle having a critical angular momentum value can travel from infinity to the event horizon of a black hole only in the case of an extremely rotating black hole $A = 1$. In other cases, particles with large angular momentum values are prevented from falling onto the horizon by the potential barrier of the effective potential. As shown in [18,19], the super high center-of-mass energy can be achieved in multiple collisions near nonextreme black holes. To reach the horizon, particles incident from infinity should have an angular momentum low in absolute value. The angular momentum of one of the particles necessary for a high-energy collision can be acquired either in multiple collisions or in the interaction with the electromagnetic field of the accretion disk. A similar effect for electrically charged black holes was discovered in [20]. Real astrophysical black holes are surrounded by matter (for example, they have an accretion disk). The possibility of particles colliding with unlimited energy near the horizon of such “dirty” black holes also takes place [21].

The value of the collision parameters corresponding to the temperature of the elementary particles phase transitions may depend on the type of black holes. In the case of Kerr black holes, the estimates for the distance from the horizon, where the collision energies required for phase transitions of elementary particles, can be achieved are given in our work [13]. So, for elementary particles with a mass m , the value of the temperature T is reached near the extreme rotating black hole at the distance

$$r - r_H \approx 2r_H \left(\frac{mc^2}{k_B T} \right)^2. \tag{7}$$

For the proton mass, the electro-weak temperature can be reached at the distance $r - r_H = 2 \times 10^{-4} r_H$. This amounts to tens of centimeters for stellar-mass black holes and hundreds of thousands of kilometers for supermassive black holes. In the mechanism of multiple collisions near the horizon of (not extreme) rotating black holes, such temperatures can be achieved at larger distances [13]. Therefore, collisions in which phase transition temperatures are reached can, in principle, occur in the vicinity of stellar-mass black holes for elementary particles and in the case of supermassive black holes for macroscopic bodies.

Next, we estimate the size of the phase transition region and the lifetime of the state with the new phase.

3. Size and Lifetime of the New Phase

The energy density of the photon gas can be calculated by the known formula: (see (63,14) in [22])

$$\varepsilon = \frac{4\sigma}{c} T^4, \tag{8}$$

where σ is the Stefan–Boltzmann constant,

$$\sigma = \frac{\pi^2 k_B^4}{60 \hbar^3 c^2} \approx 5.67 \cdot 10^{-8} \frac{\text{W}}{\text{m}^2 \cdot \text{K}^4}, \tag{9}$$

and \hbar is the reduced Planck constant. At ultra-high temperatures, other elementary particles should also contribute to the energy density of matter. Their contribution is taken into account using the factor g_{eff} , which describes the number of effective massless degrees of freedom of particles of the standard model of particle physics.

$$\varepsilon = g_{\text{eff}} \frac{\pi^2 k_B^4}{30 \hbar^3 c^3} T^4 = g_{\text{eff}} \frac{2\sigma}{c} T^4. \tag{10}$$

Under this definition, the photon’s contribution to g_{eff} is two, according to the photon’s two polarization states. In the general case, one has the following [6]

$$g_{\text{eff}} = \sum_{i=\text{bosons}} g_i \left(\frac{T_i}{T}\right)^4 + \frac{7}{8} \sum_{i=\text{fermions}} g_i \left(\frac{T_i}{T}\right)^4. \tag{11}$$

Here, it is assumed that the equilibrium temperature T_i of particles of type i may differ from T . For example, in the Universe at present the temperature of cosmic microwave background radiation is equal to 2.7 K, and estimates for the temperature of the neutrino gas give 1.95 K. Photon gas after the moment of the last collisions of the cosmological neutrinos with cosmological plasma at energies of 2–3 MeV was still heated up in the annihilation process of cosmological positrons with electrons.

The value of g_{eff} in the standard model of particle physics depends on temperature. For T in the interval $1 \text{ MeV} < T < 100 \text{ MeV}$, which takes neutrinos into account, electrons and positrons lead to $g_{\text{eff}} = 10.75$. At temperatures above 300 GeV, all standard model particles (photons, W^\pm , Z^0 bosons, eight gluons, three generations of quarks and leptons and the Higgs boson) must contribute to (10), which leads [6] to the value of $g_{\text{eff}} = 106.75$. The graph of g_{eff} , which depends on temperature, is presented in [6] on page 65, Figure 3.5.

Denoting $k_B T = mc^2$, where m is the characteristic mass scale, we obtain from (10) for the energy density of radiation of all types of particles

$$\varepsilon = g_{\text{eff}} \frac{\pi^2 m^4 c^5}{30 \hbar^3} = g_{\text{eff}} \frac{\pi^2}{30} \frac{mc^2}{l_C^3}, \tag{12}$$

where $l_C = \hbar/mc$ is the (reduced) Compton wavelength corresponding to the mass m . The pressure corresponds to a value three times less

$$p = \frac{\varepsilon}{3} = g_{\text{eff}} \frac{\pi^2}{90} \frac{mc^2}{l_C^3}. \tag{13}$$

The size R_0 of the area in which the heated drop of a new phase of matter can form after a collision is estimated from the relation

$$E_{\text{c.m.}} = \frac{4}{3} \pi R_0^3 \varepsilon, \tag{14}$$

It is assumed that the region of the new phase is a sphere with the radius R_0 . Then, one obtains

$$R_0 = \frac{l_C}{\pi} \sqrt[3]{\frac{45}{2g_{\text{eff}}} \frac{E_{\text{c.m.}}}{mc^2}}. \tag{15}$$

Assuming that the collision energy is of the order of magnitude $E_{\text{c.m.}} \sim g_{\text{eff}} mc^2$, we find that the size of the region phase transition is of the order of the Compton wavelength l_C for a particle of mass m .

Let us estimate the lifetime of a drop of a new phase formed as a result of a collision, generalizing the formula for the radiation intensity of the black body to the case of the presence of additional degrees of freedom described by the quantity g_{eff}

$$J = g_{\text{eff}} \frac{\pi^2 k_B^4}{120 \hbar^3 c^2} T^4 = \frac{g_{\text{eff}}}{2} \sigma T^4. \tag{16}$$

Let us write the energy balance equation for an infinitesimal time interval dt

$$d(\varepsilon V) = -J S dt, \tag{17}$$

where V is the volume of new phase drop and S is its surface area. When obtaining estimates by the order of magnitude, we assume that the drop is spherical, and the radius may depend on time due to expansion into the surrounding space. We also assume that during the life of a drop of a new phase, thermodynamic equilibrium takes place in it, and, therefore, we can talk about the temperature of the entire drop, the dependence of temperature on time and use formulas for the equilibrium state of the corresponding relativistic gas. Then, from (17), we obtain

$$\frac{R}{3} d\varepsilon = -(J dt + \varepsilon dR). \tag{18}$$

Using (10) and (16), we obtain the equation

$$\frac{16}{3} \frac{R}{c} \frac{dT}{T} = - \left(1 + \frac{4}{c} \frac{dR}{dt} \right) dt. \tag{19}$$

By integrating this equation, we obtain

$$T(t) = T(t_0) \exp \left[- \frac{3c}{16} \int_{t_0}^t \left(1 + \frac{4}{c} \frac{dR}{dt} \right) \frac{dt}{R} \right]. \tag{20}$$

If the drop radius does not change, i.e., $R \approx R_0 = \text{const}$, then the solution is

$$T(t) = T(t_0) \exp \left[- \frac{3}{16} \frac{c(t - t_0)}{R_0} \right]. \tag{21}$$

Thus, the temperature decreases exponentially, and the lifetime of the new phase is of the order $\tau \approx R_0/c$. Since, according to the Equation (15), the size of the new phase region is assumed to be Compton, the lifetime corresponds to Compton time $\tau_C = \hbar/(mc^2)$ for a particle of a mass m , corresponding to the phase transition energy.

Taking into account the possible expansion of the area of the new phase, the lifetime of the new phase can only decrease. Let us give formulas under the assumption of a constant expansion rate $dR/dt = v \approx \text{const}$. Then,

$$R(t) = R_0 + v(t - t_0) \tag{22}$$

and, after the integration of (19), we obtain a dependence of the temperature of the region with a new phase on the time as follows

$$T(t) = T(t_0) \left(1 + \frac{v(t - t_0)}{R_0} \right)^{-\frac{3}{16} \left(4 + \frac{c}{v} \right)}. \tag{23}$$

In the limit $v/c \rightarrow 0$, one obtains the expression (21).

Thus, the lifetime of the new phase obtained in a collision of elementary particles has the order of Compton time $\hbar/(mc^2)$ for a particle of the characteristic mass scale m . For the quark–gluon phase transition, this time is $\tau \approx 3 \cdot 10^{-24}$ s. For the electro-weak phase transition, this time is $\tau \approx 7 \cdot 10^{-27}$ s.

4. Phase Transition in Macroscopic Volume

To perform a quark–gluon or electro-weak phase transition in a macroscopic volume, it is necessary to collide with ultra-relativistic energies of macroscopic amounts of matter. When ordinary macroscopic bodies collide with such energies, the regions of the new phase can make up a macroscopic volume only if the density of the bodies is comparable to the Compton density characteristic of the phase transition of the mass m (see (12)). Only in this case, the lifetime of the new phase can significantly exceed the Compton time τ_C . Such density of matter occurs only in neutron stars. Collisions of macroscopic objects with ultra-relativistic velocities are possible in the vicinity of the horizon of extremal rotating black holes [13]. The collision of compact objects with star masses near supermassive black holes was considered in [23].

When falling towards the event horizon of a black hole, macroscopic bodies can be destroyed by tidal gravitational forces. Let us estimate the mass of black holes in which it is possible to fall to the event horizon of neutron stars without destruction by tidal forces. For evaluation, we assume that a star is destroyed if the tidal forces for the points of the center of mass and the surface exceed the force of attraction of the points of the surface to the center of the falling body. Let us assume that the falling object (neutron star) is a uniform ball of a density ρ and radius R . Also, let us consider only the nonrotating black hole and radial tidal forces. Then the condition for falling to the horizon without destruction has the form

$$\frac{2GM}{r_g^3}R < \frac{G4\pi\rho R^3}{3R^2} \tag{24}$$

or (after simple transformations)

$$M > \frac{c^3}{4G^{3/2}}\sqrt{\frac{3}{\pi\rho}}, \quad \frac{M}{M_\odot} > 1.9 \cdot 10^8 \sqrt{\frac{\rho_w}{\rho}}, \tag{25}$$

where M_\odot is the Sun mass, $\rho_w = 10^3 \text{ kg/m}^3$ is the water density. Neutron stars have the density $\rho \sim 10^{17}\text{--}10^{18} \text{ kg/m}^3$. Therefore, neutron stars fall to the horizon of black holes with a mass of $M > 20M_\odot$ without destruction. Of course, a collision with ultra-relativistic velocities of neutron stars in the vicinity of a massive black hole should be considered a very unlikely event. Estimates in [13] show that in the collision near the vicinity of the horizon of an extremal rotating black hole with a mass of $10^9 M_\odot$ at points with a radial coordinate $r_H + 7 \cdot 10^5 \text{ km}$, the maximum collision energy in the center-of-mass system can reach 100 mc^2 . In nucleon–nucleon collisions, this is the electro-weak unification energy. The masses of neutron stars range from one to three solar masses, and their radii are about 10–20 km. The gravitational radius of a black hole with a mass of 100 solar masses is approximately 300 km. Therefore, with such collision energy of two neutron stars, a black hole should form, and it will not be possible to obtain a substance in a state of an electro-weak phase transition outside the event horizon.

Thus, it is impossible to obtain the macroscopic quantities of a substance with an electro-weak phase transition with a lifetime significantly exceeding the Compton time for the electro-weak scale due to collisions in the vicinity of black holes.

5. The Influence of Spontaneous Symmetry Breaking on the Space–Time Metric

Let us consider a real scalar field with self-action [24]

$$V(\varphi) = -\frac{\mu^2}{2}\varphi^2 + \frac{\lambda^2}{4}\varphi^4 + \frac{\mu^2}{4\lambda^2}. \tag{26}$$

Here, $\mu = \tilde{\mu}c/\hbar$, $\tilde{\mu}$ is a mass parameter and λ is the dimensionless self-action constant. Stable equilibrium states of such a field are located at two points

$$\varphi = \pm\varphi_0, \quad \varphi_0 = \frac{\mu}{\lambda}. \tag{27}$$

The potential function (26) can be written as

$$V(\varphi) = \frac{\lambda^2}{4} (\varphi^2 - \varphi_0^2)^2. \tag{28}$$

Both lower states have zero energy, and the unstable equilibrium with $\varphi = 0$ has an energy density of

$$\varepsilon = \hbar c V(0) = \hbar c \frac{\mu^4}{4\lambda^2}. \tag{29}$$

Using the representation $\varphi = \varphi_0 + \chi$, one obtains

$$V(\chi) = \lambda^2 \varphi_0^2 \chi^2 + \lambda^2 \varphi_0 \chi^3 + \frac{\lambda^2}{4} \chi^4. \tag{30}$$

Thus, the mass of the χ field is $\sqrt{2}\lambda\varphi_0 = \sqrt{2}\mu$. In the case of the Higgs boson, $m_H = 125.3$ GeV, and we have

$$\varepsilon_H = \hbar c V(0) = \hbar c \frac{m_H^4 c^4}{16\hbar^4 \lambda^2} = \frac{1}{16\lambda^2} \frac{m_H c^2}{(l_C^H)^3}, \tag{31}$$

where $l_C^H = \hbar / (m_H c)$.

For the electro-weak interaction, quantum corrections lead to limitation [24]

$$\lambda \geq \alpha = \frac{e^2}{4\pi\varepsilon_0 \hbar c} \approx \frac{1}{137}, \tag{32}$$

where e is the elementary electric charge and ε_0 is the electric constant.

To estimate the inverse influence of the scalar field on the curvature of space–time, we use Einstein’s equations

$$R_{ik} - \frac{1}{2} R g_{ik} + \Lambda g_{ik} = -8\pi \frac{G}{c^4} (T_{ik}^{(0)} + T_{ik}), \tag{33}$$

where Λ is the cosmological constant, $T_{ik}^{(0)}$ is the energy–momentum tensor of the background matter. The energy–momentum tensor for a constant scalar field with minimal coupling to curvature is [25]

$$T_{ik} = g_{ik} \hbar c V(\varphi) \tag{34}$$

and is similar to the contribution of an additional cosmological constant. Upon the appearance of a non-zero cosmological constant under spontaneous symmetry breaking, this was indicated in the work [26]. Phase transition in electro-weak interactions was discussed in cosmology by Kirzhnits and Linde [27,28], Weinberg [29] and others. Estimates of changes in the value of the cosmological constant during phase transitions in the early Universe were made in work [30].

If there is only a constant scalar field and the energy–momentum tensor of the background matter is equal to zero $T_{ik}^{(0)} = 0$, then the solution to Einstein’s Equation (33) will be the de Sitter space–time. In de Sitter space, one has

$$R_{ik} = \frac{R}{4} g_{ik}, \tag{35}$$

and it follows from (33) that

$$R = 4 \left(\Lambda + l_{Pl}^2 8\pi V(\varphi) \right), \tag{36}$$

where l_{Pl} is the Planck length

$$l_{\text{Pl}} = \sqrt{\frac{G\hbar}{c^3}} = 1.6162 \cdot 10^{-35} \text{ m.} \quad (37)$$

For the electro-weak case under $\varphi = 0$, from (31), we have

$$R = 4 \left(\Lambda + \frac{\pi}{2\lambda^2} \frac{l_{\text{Pl}}^2}{(l_{\text{C}}^H)^4} \right). \quad (38)$$

For the radius of curvature, we obtain

$$r \sim \frac{(l_{\text{C}}^H)^2}{l_{\text{Pl}}} \sim 0.1 \text{ m.} \quad (39)$$

This value is many orders of magnitude greater than the Compton wavelength of the particle and the size of the region in which the phase transition occurs. It should be expected that in order for special collisions with ultra-high energy to occur, in the volumes r^3 , there must be a large number of particles falling onto the black hole. Their total mass will be much greater than the mass of the electro-weak scale. Thus, the inverse effect of energy density in the electro-weak phase transition in collisions on the space–time metric can be neglected.

6. Conclusions

An integral part of the standard model of particle physics is the mechanism of spontaneous symmetry breaking. The discovery at the Large Hadron Collider of the Higgs boson in 2012 makes us take seriously the possibility of a phase transition from one vacuum to another at high temperatures, as is the case in quantum nonrelativistic many-body theory, where the ground state plays the role of the vacuum. In our work [13], it was shown that in the processes of collisions of particles near the horizon of black holes, it is possible to achieve energies in the system of the center of mass of the order of the energy scale of the electro-weak phase transition.

In this article, we showed that the region of the phase transition in such collisions is microscopic. In the order of magnitude, the size of the region is equal to the Compton wavelength of the Higgs boson. Using formulas for black body radiation, we show that the lifetime of such region is of the order of the Compton time for the electro-weak phase transition scale.

During a phase transition, such as in the case of spontaneous symmetry breaking, the energy–momentum tensor corresponds to the emergence of an effective cosmological constant. It is shown that for phase transitions occurring during particle collisions, its influence on the space metric in the phase transition region can be neglected.

Note that despite the short time existence and microscopic volumes of a new phase of matter during an electro-weak phase transition in collisions in the vicinity of the black hole horizon, its very existence is of fundamental importance for the study of elementary particle physics in the ultra-high energy region, which is unattainable on Earth.

Author Contributions: A.A.G. and Y.V.P. have contributed equally to all parts of this work. All authors read and agreed to the published version of the manuscript.

Funding: This research received no external funding

Data Availability Statement: Data are contained within the article.

Conflicts of Interest: The authors declare no conflict of interest.

References

1. Friedmann, A.A. Über die Krümmung des Raumes. *Z. Phys.* **1922**, *10*, 377–386. [CrossRef]
2. Friedmann, A.A. Über die Möglichkeit einer Welt mit konstanter negativer Krümmung des Raumes. *Z. Phys.* **1924**, *21*, 326–332. [CrossRef]

3. Klimchitskaya, G.L.; Mostepanenko, V.M. Centenary of Alexander Friedmann's prediction of the Universe expansion and the quantum vacuum. *Physics* **2022**, *4*, 981–994. [CrossRef]
4. Penzias, A.A.; Wilson, R.W. Excess antenna temperature at 4080 Mc/s. *Astrophys. J.* **1965**, *142*, 419–421. [CrossRef]
5. Dicke, R.H.; Peebles, P.J.E.; Roll, P.G.; Wilkinson, D.T. Cosmic black-body radiation. *Astrophys. J.* **1965**, *142*, 414–419. [CrossRef]
6. Kolb, E.W.; Turner, M.S. *The Early Universe*; Addison-Wesley: Redwood City, CA, USA, 1990.
7. Linde, A. *Particle Physics and Inflationary Cosmology*; Harwood Academic Publication: New York, NY, USA, 1990.
8. Gorbunov, D.S.; Rubakov, V.A. *Introduction to the Theory of the Early Universe: Hot Big Bang Theory*; World Scientific: Singapore, 2018.
9. Pasechnik, R.; Šumbera, M. Phenomenological review on quark-gluon plasma: Concepts vs. observations. *Universe* **2017**, *3*, 7. [CrossRef]
10. Adare, A. et. al. [PHENIX Collaboration] Enhanced production of direct photons in Au + Au collisions at $\sqrt{s_{NN}} = 200$ GeV and implications for the initial temperature. *Phys. Rev. Lett.* **2010**, *104*, 132301. [CrossRef] [PubMed]
11. Chatrchyan, S. et al. [CMS Collaboration] Measurement of the pseudorapidity and centrality dependence of the transverse energy density in Pb-Pb collisions at $\sqrt{s_{NN}} = 2.76$ TeV. *Phys. Rev. Lett.* **2012**, *109*, 152303. [CrossRef] [PubMed]
12. Shapiro, S.L.; Teukolsky, S.A. *Black Holes, White Dwarfs, and Neutron Stars: The Physics of Compact Objects*; Wiley Int. Publ.: New York, NY, USA, 1983.
13. Grib, A.A.; Pavlov, Y.V. On phase transitions near black holes. *JETP Lett.* **2022**, *116*, 493–499. [CrossRef]
14. Kerr, R.P. Gravitational field of a spinning mass as an example of algebraically special metrics. *Phys. Rev. Lett.* **1963**, *11*, 237–238. [CrossRef]
15. Boyer, R.H.; Lindquist, R.W. Maximal analytic extension of the Kerr metric. *J. Math. Phys.* **1967**, *8*, 265–281. [CrossRef]
16. Banados, M.; Silk, J.; West, S.M. Kerr black holes as particle accelerators to arbitrarily high energy. *Phys. Rev. Lett.* **2009**, *103*, 111102. [CrossRef]
17. Penrose, R.; Gravitational Collapse: The Role of General Relativity. *Riv. Nuovo C.* **1969**, *1*, 252–276. Available online: <http://adsabs.harvard.edu/abs/1969NCimR...1..252P> (accessed on 30 January 2024).
18. Grib, A.A.; Pavlov, Y.V. On the collisions between particles in the vicinity of rotating black holes. *JETP Lett.* **2010**, *92*, 125–129. [CrossRef]
19. Grib, A.A.; Pavlov, Y.V. On particle collisions in the gravitational field of the Kerr black hole. *Astropart. Phys.* **2011**, *34*, 581–586. [CrossRef]
20. Zaslavskii, O.B. Acceleration of particles by nonrotating charged black holes. *JETP Lett.* **2010**, *92*, 571–574. [CrossRef]
21. Zaslavskii, O.B. Acceleration of particles as a universal property of rotating black holes. *Phys. Rev. D* **2010**, *82*, 083004. [CrossRef]
22. Landay, L.D.; Lifshitz, E.M. *Statistical Physics: Part 1*; Pergamon Press: Oxford, UK, 1980.
23. Harada, T.; Kimura, M. Collision of an object in the transition from adiabatic inspiral to plunge around a Kerr black hole. *Phys. Rev. D* **2011**, *84*, 124032. [CrossRef]
24. Okun, L.B. *Leptons and Quarks*; North-Holland: Amsterdam, The Netherlands, 1985.
25. Grib, A.A.; Mamayev, S.G.; Mostepanenko, V.M. *Vacuum Quantum Effects in Strong Fields*; Friedmann Lab. Publ.: St. Petersburg, Russia, 1994.
26. Grib, A.A. CP-noninvariance in K^0 -meson decays and nonequivalent representations in quantum field theory. *Vestn. LGU* **1967**, *22*, 50–56.
27. Kirzhnits, D.A.; Linde, A.D. Relativistic phase transitions. *Sov. Phys. JETP* **1975**, *40*, 628.
28. Kirzhnits, D.A.; Linde, A.D. Symmetry behavior in gauge theories. *Ann. Phys.* **1976**, *101*, 195–238. [CrossRef]
29. Weinberg, S. Gauge and global symmetries at high temperature. *Phys. Rev. D* **1974**, *9*, 3357–3378. [CrossRef]
30. Linde, A.D. Is the cosmological constant a constant? *JETP Lett.* **1974**, *19*, 183–184.

Disclaimer/Publisher's Note: The statements, opinions and data contained in all publications are solely those of the individual author(s) and contributor(s) and not of MDPI and/or the editor(s). MDPI and/or the editor(s) disclaim responsibility for any injury to people or property resulting from any ideas, methods, instructions or products referred to in the content.

Article

Spinor Field in FLRW Cosmology

Bijan Saha ^{1,2} 

¹ Laboratory of Information Technologies, Joint Institute for Nuclear Research, Dubna, 141980 Moscow, Russia; bijan@jinr.ru

² Institute of Physical Research and Technology, Peoples' Friendship University of Russia (RUDN University), 6 Miklukho-Maklaya Street, 117198 Moscow, Russia

Abstract: Within the scope of a Friedmann-Lemaitre-Robertson-Walker (FLRW) cosmological model we study the role of a nonlinear spinor field in the evolution of the universe. In doing so, we exploit the FLRW models given in both Cartesian and spherical coordinates. It is found that if the FLRW model is given in the spherical coordinates the energy-momentum tensor (EMT) of the spinor field possesses nontrivial non-diagonal components, which is not the case for Cartesian coordinates. These non-diagonal components do not depend on either the spinor field nonlinearity or the parameter k that defines the type of curvature of the FLRW model. The presence of such components imposes some restrictions on the spinor field. The problem is studied for open, flat and close geometries and the spinor field is used to simulate different types of sources including dark energies. Some qualitative numerical solutions are given.

Keywords: Alexander Friedmann; expanding universe; accelerated expansion; dark energy; spinor field; energy-momentum tensor



Citation: Saha, B. Spinor Field in FLRW Cosmology. *Universe* **2023**, *9*, 243. <https://doi.org/10.3390/universe9050243>

Academic Editors: Galina L. Klimchitskaya, Vladimir M. Mostepanenko and Sergey V. Sushkov

Received: 20 April 2023

Revised: 15 May 2023

Accepted: 18 May 2023

Published: 22 May 2023



Copyright: © 2023 by the author. Licensee MDPI, Basel, Switzerland. This article is an open access article distributed under the terms and conditions of the Creative Commons Attribution (CC BY) license (<https://creativecommons.org/licenses/by/4.0/>).

1. Introduction

The isotropy of cosmic microwave background (CMB) radiation, first detected by the Cosmic Background Explorer (COBE) satellite [1], and further supported by the Wilkinson Microwave Anisotropy Probe (WMAP) data [2], together with the assumption that we are not in any special position in Universe, underlines the Cosmological Principle. According to this principle we live in a homogeneous and isotropic Universe which mean all the space-time points of our Universe can be treated as the center of the Universe and all the directions are equal. Such a Universe is given by a FLRW model. The present day experimental data suggest that our Universe is indeed isotropic one and homogeneous in large scale. That is why the study of present day Universe is dominated by the FLRW model. Exact solution to the Einstein equation found by Russian mathematician A.A. Friedmann suggested that our Universe is expanding. He also observed that there can be three types of solutions: closed, flat and open [3,4]. But those days physicists believed that the Universe is static and unchanging. So Einstein dully rejected Friedmann solutions and introduced cosmological constant into the system to secure a steady solution to his equation. Recall that before Einstein the Universe was thought to be geocentric or heliocentric, which possesses center. But it was Einstein who first told that there is no specific point and any point of the space-time can be the center of the Universe, thus bringing revolutionary changes about the idea of space-time. Even he failed to accept the concept of a Universe that is changing with time. In 1929 Edwin Hubble experimentally showed that the Universe is expanding and there are many galaxies outside our milky way [5]. It buried the idea of a static Universe. Further this model was independently developed by Lemaitre [6], Robertson [7–9] and Walker [10]. So this model is also known as FLRW model. The FLRW model has not only mathematical simplicity, but also experimental support.

Thanks to its ability to simulate different kinds of matter such as perfect fluid, dark energy etc. spinor field is being used by many authors not only to describe the late time

acceleration of the expansion, but also to study the evolution of the Universe at different stages [11–17]. It was found that the spinor field is very sensitive to spacetime geometry. Depending on the concrete type of metric the spinor field may possess different types of nontrivial non-diagonal components of the energy-momentum tensor. As a result the spinor field imposes various kinds of restrictions on both the spacetime geometry and the spinor field itself [18]. Recently spinor field is used in astrophysics to see whether its specific behavior can shed any new light in the study of the objects like black hole and wormhole. Such studies were carried out within the scope of spherically symmetric [19,20] and cylindrically symmetric spacetime [21,22].

Since the present-day universe is surprisingly isotropic and the presence of nontrivial non-diagonal components of the spinor field leads to the severe restrictions on the spinor field, we have studied role of a spinor field in Friedmann-Lemaitre-Robertson-Walker (FLRW) model as well. But in those cases the space-time was given in Cartesian coordinates. In order to see influence of the coordinate transformations on spinor field some works were done by us earlier [23,24]. In this paper we will compare the results founded for FLRW model given in Cartesian and spherical coordinates and study the behavior of the spinor field under such coordinate transformations.

2. Basic Equation

Let us consider the action of the gravitational and nonlinear spinor field in the form

$$S = \int \sqrt{-g} \left[\frac{R}{2\kappa} + L_{sp} \right] d\Omega, \tag{1}$$

where $\kappa = 8\pi G$ is Einstein’s gravitational constant, R is the scalar curvature. The spinor field Lagrangian L_{sp} is given by [25]

$$L_{sp} = \frac{1}{2} \left[\bar{\psi} \gamma^\mu \nabla_\mu \psi - \nabla_\mu \bar{\psi} \gamma^\mu \psi \right] - m \bar{\psi} \psi - \lambda F(K). \tag{2}$$

Here, the nonlinear term $F(K)$ is constructed as some arbitrary functions of invariants generated from the real bilinear forms, where K takes one of the following expressions $\{I, J, I + J, I - J\}$. Here $I = S^2$ and $J = P^2$ are the invariants of bilinear spinor forms with $S = \bar{\psi} \psi$ and $P = i \bar{\psi} \gamma^5 \psi$ being the scalar and pseudo-scalar, respectively. In (2) λ is the self-coupling constant. The covariant derivatives of spinor field takes the form [25]

$$\nabla_\mu \psi = \partial_\mu \psi - \Omega_\mu \psi, \quad \nabla_\mu \bar{\psi} = \partial_\mu \bar{\psi} + \bar{\psi} \Omega_\mu, \tag{3}$$

with Ω_μ being the spinor affine connections defined by [25]

$$\Omega_\mu = \frac{1}{4} \left(\bar{\gamma}_a \gamma^\beta \partial_\mu e_\beta^{(a)} - \gamma_\rho \gamma^\beta \Gamma_{\mu\beta}^\rho \right). \tag{4}$$

In (4), $\Gamma_{\mu\alpha}^\beta$ is the Christoffel symbol and the Dirac matrices in curve and flat space-time γ and $\bar{\gamma}$ are connected to each other in the following way

$$\gamma_\beta = e_\beta^{(b)} \bar{\gamma}_b, \quad \gamma^\alpha = e_{(a)}^\alpha \bar{\gamma}^a. \tag{5}$$

Here, the tetrad vectors $e_\beta^{(b)}$ are related to the metric in the following way

$$g_{\mu\nu}(x) = e_\mu^{(a)}(x) e_\nu^{(b)}(x) \eta_{ab}, \tag{6}$$

and $e_{(a)}^\alpha$ are the inverse to $e_\mu^{(a)}(x)$:

$$e_{(a)}^\alpha e_\beta^{(a)} = \delta_\beta^\alpha, \quad e_{(a)}^\alpha e_\alpha^{(b)} = \delta_a^b. \tag{7}$$

Here, $\eta_{ab} = \text{diag}(1, -1, -1, -1)$ is the Minkowski spacetime. The γ matrices obey the following anti-commutation rules

$$\gamma_\mu \gamma_\nu + \gamma_\nu \gamma_\mu = 2g_{\mu\nu}, \quad \gamma^\mu \gamma^\nu + \gamma^\nu \gamma^\mu = 2g^{\mu\nu}. \tag{8}$$

Varying the Lagrangian (2) with respect to $\bar{\psi}$ and ψ , respectively, we obtain the following spinor field equations

$$i\gamma^\mu \nabla_\mu \psi - m\psi - \lambda \mathcal{D}\psi - i\lambda \mathcal{G} \bar{\gamma}^5 \psi = 0, \tag{9}$$

$$i\nabla_\mu \bar{\psi} \gamma^\mu + m\bar{\psi} + \lambda \mathcal{D}\bar{\psi} + i\lambda \mathcal{G} \bar{\psi} \bar{\gamma}^5 = 0, \tag{10}$$

where $\mathcal{D} = 2F_K S$, $\mathcal{G} = 2F_K P$. It can be shown that in view of the spinor field equations (9) and (10) the spinor field Lagrangian (2) can be expressed as

$$L = \lambda(2KF_K - F), \quad F_K = dF/dK.$$

In this report, we consider the spinor field that depends only on time, i.e., $\psi = \psi(t)$. In view of (3), the energy momentum tensor of the spinor field is defined in the following way [25].

$$T_\mu^\rho = \frac{i}{4} g^{\rho\nu} \left(\bar{\psi} \gamma_\mu \partial_\nu \psi + \bar{\psi} \gamma_\nu \partial_\mu \psi - \partial_\mu \bar{\psi} \gamma_\nu \psi - \partial_\nu \bar{\psi} \gamma_\mu \psi \right) - \frac{i}{4} g^{\rho\nu} \bar{\psi} \left(\gamma_\mu \Omega_\nu + \Omega_\nu \gamma_\mu + \gamma_\nu \Omega_\mu + \Omega_\mu \gamma_\nu \right) \psi - \delta_\mu^\rho L. \tag{11}$$

It should be noted that the non-diagonal components of the EMT arises thanks to the second term in (11).

The gravitational field is given by isotropic and homogeneous cosmological model proposed by Friedmann, Lemaitre, Robertson and Walker. We consider two cases when the model is given in Cartesian and spherical coordinates. We do it to show that the spinor field is even sensible to the coordinate transformations. Variation of the action (1) with respect to $g^{\mu\nu}$ leads to Einstein equation

$$G_\mu^\nu = -\kappa T_\mu^\nu. \tag{12}$$

In what follows, we consider the homogeneous and isotropic cosmological gravitational field given by FLRW model.

Case I Let us first consider the FLRW model given in Cartesian coordinates:

$$ds^2 = dt^2 - a^2(t) [dx^2 + dy^2 + dz^2], \tag{13}$$

where the scale factor $a(t)$ is a function of time only. This case was thoroughly studied in [18,26].

In view of (6) we choose the tetrad in the form

$$e_0^{(0)} = 1, \quad e_1^{(1)} = a(t), \quad e_2^{(2)} = a(t), \quad e_3^{(3)} = a(t).$$

Then, from (4) we find the following expressions for spinor affine connection

$$\Omega_0 = 0, \quad \Omega_1 = \frac{\dot{a}}{2} \bar{\gamma}^1 \bar{\gamma}^0, \quad \Omega_2 = \frac{\dot{a}}{2} \bar{\gamma}^2 \bar{\gamma}^0, \quad \Omega_3 = \frac{\dot{a}}{2} \bar{\gamma}^3 \bar{\gamma}^0. \tag{14}$$

Thanks to the fact that, in this case $\Omega_1 = \Omega_2 = \Omega_3$ the EMT of the spinor field possesses only diagonal components with [18]:

$$T_0^0 = m_{sp}S + \lambda F(K), \quad T_1^1 = T_2^2 = T_3^3 = \lambda(F(K) - 2KF_K). \tag{15}$$

The absence of non-diagonal components of the EMT leads to the fact that the spinor field does not impose any kind of restriction either on the space-time geometry or on the spinor field. The spinor field equation in this case takes the form

$$i\tilde{\gamma}^0 \left(\dot{\psi} + \frac{3}{2} \frac{\dot{a}}{a} \psi \right) - m_{sp}\psi - \lambda \mathcal{D}\psi - i\lambda \mathcal{G}\tilde{\gamma}^5\psi = 0, \tag{16}$$

$$i \left(\dot{\bar{\psi}} + \frac{3}{2} \frac{\dot{a}}{a} \bar{\psi} \right) \tilde{\gamma}^0 + m_{sp}\bar{\psi} + \lambda \mathcal{D}\bar{\psi} + i\lambda \mathcal{G}\bar{\psi}\tilde{\gamma}^5 = 0. \tag{17}$$

The foregoing system was solved exactly and given in explicit form in [18]. The Einstein field Equation (12) in this case coincide with those considered in the **case II** for $k = 0$. The Einstein equation was solved for different types on nonlinearity.

Case II Let us now consider the case when the FLRW model is given in spherical coordinates [27]:

$$ds^2 = dt^2 - a^2(t) \left[\frac{dr^2}{1 - kr^2} + r^2 d\vartheta^2 + r^2 \sin^2 \vartheta d\phi^2 \right], \tag{18}$$

with k taking the values $+1, 0$ and -1 which corresponds to a close, flat and open universe, respectively. The purpose of doing this is to show that the spinor field is not only sensitive to space-time geometry, given by different metrics, but also to coordinate transformations. In view of (6), we choose the tetrad in the form

$$e_0^{(0)} = 1, \quad e_1^{(1)} = \frac{a}{\sqrt{1 - kr^2}}, \quad e_2^{(2)} = ar, \quad e_3^{(3)} = ar \sin \vartheta.$$

Then, from (5) we find the following γ matrices

$$\gamma^0 = \tilde{\gamma}^0, \quad \gamma^1 = \frac{\sqrt{1 - kr^2}}{a} \tilde{\gamma}^1, \quad \gamma^2 = \frac{\tilde{\gamma}^2}{ar}, \quad \gamma^3 = \frac{\tilde{\gamma}^3}{ar \sin \vartheta}.$$

Further from $\gamma_\mu = g_{\mu\nu} \gamma^\nu$ one finds the γ_μ as well. From (4) in this case we find the following expressions for spinor affine connection

$$\Omega_0 = 0, \tag{19}$$

$$\Omega_1 = \frac{1}{2\sqrt{1 - kr^2}} \dot{a} \tilde{\gamma}^1 \tilde{\gamma}^0, \tag{20}$$

$$\Omega_2 = \frac{1}{2} r \dot{a} \tilde{\gamma}^2 \tilde{\gamma}^0 + \frac{1}{2} \sqrt{1 - kr^2} \tilde{\gamma}^2 \tilde{\gamma}^1, \tag{21}$$

$$\Omega_3 = \frac{1}{2} \dot{a} r \sin \vartheta \tilde{\gamma}^3 \tilde{\gamma}^0 + \frac{1}{2} \sqrt{1 - kr^2} \sin \vartheta \tilde{\gamma}^3 \tilde{\gamma}^1 + \frac{1}{2} \cos \vartheta \tilde{\gamma}^3 \tilde{\gamma}^2. \tag{22}$$

In view of (19)–(22), the spinor field equations can be written as

$$\dot{\psi} + \frac{3}{2} \frac{\dot{a}}{a} \psi + \frac{\sqrt{1 - kr^2}}{ar} \tilde{\gamma}^0 \tilde{\gamma}^1 \psi + \frac{\cot \vartheta}{2ar} \tilde{\gamma}^0 \tilde{\gamma}^2 \psi + i(m + \lambda \mathcal{D}) \tilde{\gamma}^0 \psi + \lambda \mathcal{G} \tilde{\gamma}^5 \tilde{\gamma}^0 \psi = 0, \tag{23}$$

$$\dot{\bar{\psi}} + \frac{3}{2} \frac{\dot{a}}{a} \bar{\psi} - \frac{\sqrt{1 - kr^2}}{ar} \bar{\psi} \tilde{\gamma}^0 \tilde{\gamma}^1 - \frac{\cot \vartheta}{2ar} \bar{\psi} \tilde{\gamma}^0 \tilde{\gamma}^2 - i(m + \lambda \mathcal{D}) \bar{\psi} \tilde{\gamma}^0 + \lambda \mathcal{G} \bar{\psi} \tilde{\gamma}^5 \tilde{\gamma}^0 = 0, \tag{24}$$

The solution to the spinor field equation can be given in the form [18]

$$\varphi(t) = T \exp \left(- \int_t^{t_1} A_1 d\tau \right), \tag{25}$$

where we introduce $\varphi = a^{3/2}\psi$. In the foregoing expression $T = \varphi(t_1)$ is the solution at $t = t_1$. In case of a nonzero spinor mass one can assume $\varphi(t_1) = \text{col}(e^{-imt_1}, e^{-imt_1}, e^{imt_1}, e^{imt_1})$, whereas for a massless spinor field $\varphi(t_1) = \text{col}(\varphi_1^0, \varphi_2^0, \varphi_3^0, \varphi_4^0)$ with φ_i^0 being constants. In (25) the matrix $A_1 \equiv A$ with $m = 0$ or $\mathcal{D}_1 = \mathcal{D}$, where

$$A = \begin{pmatrix} -i\mathcal{D}_1 & 0 & -\lambda\mathcal{G} & B_1 \\ 0 & -i\mathcal{D}_1 & B_1^* & -\lambda\mathcal{G} \\ \lambda\mathcal{G} & B_1 & i\mathcal{D}_1 & 0 \\ B_1^* & \lambda\mathcal{G} & 0 & i\mathcal{D}_1 \end{pmatrix} \tag{26}$$

with $\mathcal{D}_1 = (m + \lambda\mathcal{D})$, $B_1 = -\frac{\sqrt{1-kr^2}}{ar} + i\frac{\cot\vartheta}{2ar}$ and $B_1^* = -\frac{\sqrt{1-kr^2}}{ar} - i\frac{\cot\vartheta}{2ar}$. It can be shown that $\det A = (\mathcal{D}_1^2 + \lambda^2\mathcal{G}^2 - B_1B_1^*)^2$. We can choose the nonlinearity in such a way that the corresponding determinant becomes nontrivial.

In this case from (11) we find the following non-trivial components of the energy momentum tensor of the spinor field

$$T_0^0 = mS + \lambda F, \tag{27}$$

$$T_1^1 = T_2^2 = T_3^3 = -\lambda(2KF_K - F), \tag{28}$$

$$T_3^1 = \frac{a \cos \vartheta}{4\sqrt{1-kr^2}} A^0, \tag{29}$$

$$T_1^0 = \frac{\cot \vartheta}{4r\sqrt{1-kr^2}} A^3, \tag{30}$$

$$T_2^0 = -\frac{3}{4}\sqrt{1-kr^2} A^3, \tag{31}$$

$$T_3^0 = \frac{3}{4}\sqrt{1-kr^2} \sin \vartheta A^2 - \frac{1}{2} \cos \vartheta A^1. \tag{32}$$

From (27)–(32), we conclude that the diagonal components of the EMT are the same as in previous case. Moreover, in this case the energy-momentum tensor of the spinor field contains nontrivial non-diagonal components. The non-diagonal components

- do not depend on the spinor field nonlinearity;
- occur due to the spinor affine connections;
- appear depending on space-time geometry as well as the system of coordinates;
- impose restrictions on spinor field and/or space-time geometry;
- depend on the value of k which defines the type of curvature, though do not vanish ever for $k = 0$.

It should be emphasized that for a FRW model given in Cartesian coordinates the EMT have only diagonal components with all the non-diagonal one being identically zero [26]. So in this case the non-diagonal components arise as a result of coordinate transformation. Let us also note that all the cosmological space-time given by diagonal metrics such as Bianchi type VI, VI₀, V, III, I LRS – BI and FRW, possess the same diagonal components of EMT, while possess nontrivial non-diagonal elements who differ from each other for different cases [18]. Moreover non-diagonal metrics such as Bianchi type II, VIII and IX also have nontrivial non-diagonal components of EMT. Hence we see that the appearance of the non-diagonal components of the energy-momentum tensor takes place either due to coordinate transformations or space-time geometry.

The components of the EMT of the spinor field contains some spinor field invariants. To define those invariants we write the system of equations for the invariants of the spinor field

$$\dot{S}_0 + 2\mathcal{G}A_0^0 = 0, \tag{33}$$

$$\dot{P}_0 - 2(m + \mathcal{D})A_0^0 = 0, \tag{34}$$

$$\dot{A}_0^0 + 2\mathcal{G}S_0 + 2(m + \mathcal{D})P_0 + 2\frac{\sqrt{1 - kr^2}}{ar}A_0^1 + \frac{\cot \vartheta}{ar}A_0^2 = 0, \tag{35}$$

$$\dot{A}_0^1 + 2\frac{\sqrt{1 - kr^2}}{ar}A_0^0 = 0, \tag{36}$$

$$\dot{A}_0^2 + \frac{\cot \vartheta}{ar}A_0^0 = 0, \tag{37}$$

that gives the following relation between the invariants:

$$P_0^2 - S_0^2 + (A_0^0)^2 - (A_0^1)^2 - (A_0^2)^2 = C_0, \quad C_0 = \text{Const.} \tag{38}$$

In (33)–(38) the quantities with a subscript “0” are related to the normal ones as follows: $X_0 = Xa^3$. From (38) we can conclude that since C_0 is an arbitrary constant, the each term of (38) should be constant as well.

Let us recall that the Einstein tensor G_μ^ν corresponding to the metric (18) possesses only nontrivial diagonal components. Hence from (12) we obtain the following non-diagonal expressions

$$0 = T_\mu^\nu, \quad \mu \neq \nu. \tag{39}$$

In view of (29)–(32) from (39), one dully finds that

$$A^0 = 0, \quad A^3 = 0, \quad A^1 = (3/2)\sqrt{1 - kr^2} \tan \vartheta A^2. \tag{40}$$

It is worth noting that, if the FRW model given by the Cartesian coordinates the non-diagonal components of EMT are identically zero, hence relation such as (40) does not exist.

We are now ready to consider the diagonal components of the Einstein system of equations which for the metric (18) takes the form

$$2\frac{\ddot{a}}{a} + \left(\frac{\dot{a}^2}{a^2} + \frac{k}{a^2}\right) = 8\pi GT_1^1, \tag{41}$$

$$3\left(\frac{\dot{a}^2}{a^2} + \frac{k}{a^2}\right) = 8\pi GT_0^0. \tag{42}$$

The system (41) and (42) coincides the corresponding system for the FLRW metric given by cartesian coordinates in case of $k = 0$. One can solve (42) to find a , but to take into account both equations (42) and (41) it is better to combine them and rewrite (41). In view of (27) and (28) then we obtain

$$\ddot{a} = -\frac{\kappa}{6}(mS - 2\lambda F + 6\lambda KF_K)a. \tag{43}$$

The equation (43) does not contain k that defines the type of space-time curvature, hence it is true for both cases. But in order to take this very important quantity k into account we have to exploit (42) as the initial condition for \dot{a} :

$$\dot{a} = \pm\sqrt{(\kappa/3)(mS + \lambda F)a^2 - k}, \tag{44}$$

Now, we can solve (43) with the initial condition given by (44). It comes out that these equations are consistent if one takes sign “−” in (44). Alternatively, one can solve (44), but for the system to be consistent he has to check whether the result satisfies (43). Exploiting (33)–(37) it was shown that [18,26]

$$K = \frac{V_0^2}{a^6}, \quad V_0 = \text{const.}, \tag{45}$$

which is true for $K = \{J, I + J, I - J\}$ for a massless spinor field, whereas, for $K = I$ it is valid both for massless and massive spinor field. Thus, S, K , hence $F(K)$ are the functions of a . Hence given the spinor field nonlinearity the foregoing equation can be solved either analytically or numerically. The first integral of (43) takes the form

$$\dot{a} = \sqrt{\int f(a)da + C_c}, \tag{46}$$

where we define $f(a) = -\frac{\kappa}{3}(mS - 2\lambda F + 6\lambda KF_K)a$ and C_c is a constant which should be defined from (44). The solution to the equation (46) can be given in quadrature

$$\int \frac{da}{\sqrt{\int f(a)da + C_c}} = t. \tag{47}$$

In what follows we solve the system (41) and (42) numerically and in doing so we rewrite the system in the following way

$$\dot{a} = Ha, \tag{48}$$

$$\dot{H} = -\frac{3}{2}H^2 - \frac{1}{2}\frac{k}{a^2} - \frac{\kappa}{2}\lambda(2KF_K - F), \tag{49}$$

$$H^2 = \frac{\kappa}{3}(mS + \lambda F) - \frac{k}{a^2}, \tag{50}$$

where H is the Hubble constant. As one sees, in the foregoing system the first two are differential equations, whereas the third one is a constraint, which we use as the initial condition for H :

$$H = \pm \sqrt{\kappa(mS + \lambda F)/3 - k/a^2}. \tag{51}$$

Since the expression under the root must be non-negative, it imposes some restrictions on the choice of the initial value of a as well.

3. Numerical Solutions

In what follows we solve the system (48)–(50) numerically. In doing so, we consider several cases nonlinearity of the spinor field, that describes various types of sources such as perfect fluid and dark energy.

3.1. Barotropic Equation of State

It should be noted that prior to 1998, when the late time accelerated mode of expansion of the Universe was detected, perfect fluid was the most popular form of matter used to study the evolution of the Universe. But after 1998 cosmologists first considered Λ -term to explain the new phenomenon, then in analogy with perfect fluid they proposed quintessence which can be implemented by the barotropic equation of state (EoS). This equation gives a linear dependence between the pressure and energy density and was exploited by many authors [28–31]. The spinor description of perfect fluid, quintessence, Λ -term, phantom matter etc. were simulated by the nonlinear term [18,26]

$$F(S) = \lambda S^{1+W} - m_{sp}S, \quad \lambda = \text{const.}, \tag{52}$$

in the spinor field Lagrangian (2). Depending on the value of W , the Equation (52) can give rise to both perfect fluid, such as dust, radiation etc. and dark energy such as quintessence, cosmological term, phantom matter etc. For $W \in [0, 1]$, it describes a perfect fluid. The

value $W = -1$ represents a typical cosmological constant (Λ -term) [32–34], whereas $W \in [-1, -1/3]$ gives rise to a quintessence, while for $W < -1$ it ascribes a phantom matter.

Let us now solve (48)–(50) numerically for the nonlinear term given by (52). We consider both massive and massless spinor field. The values of W are taken to be $1/3, -1/2$ and -1 describing the radiation, quintessence and cosmological constant, respectively. For simplicity we set $S_0 = 1, G = 1, \lambda = 0.5$ here and in the cases to follow. We also set $m_{sp} = 0$ for a massless and $m_{sp} = 1$ for a massive spinor field.

In Figure 1 we have illustrated the evolution of the Universe filled with radiation, given by a massless spinor field. In the figures the blue solid line stands for a closed universe given by $k = 1$, red dash-dot line stands for a flat universe with $k = 0$ and black long dash line stands for an open universe with $k = -1$.

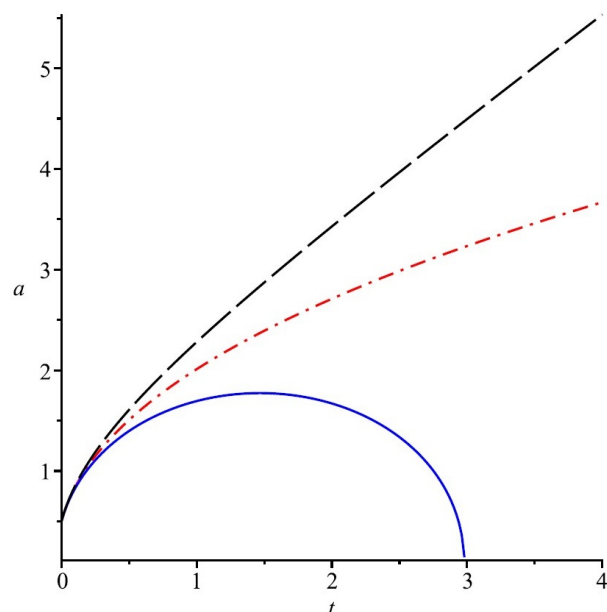


Figure 1. Evolution of the FRW Universe (scale factor a) in presence of a radiation given by a massless spinor field. Here solid blue, dash-dot red and long dash black lines correspond to $k = 1, 0, -1$, respectively.

We have also considered the case with the spinor field nonlinearity describing a quintessence ($W = -1/2$) and cosmological constant ($W = -1$). Both massive and massless spinor fields are taken into account. Since in both cases the energy density is less than the critical density, independent to the value of k we have only open type of universe. The behavior of the evolution is qualitatively same as that of in case of a modified Chaplygin gas. The corresponding figures will be similar to those in Figure 2, only the rate of expansion being much slower.

3.2. Chaplygin Gas

In order to combine two different physical concepts such as dark matter and dark energy, and thus reduce the two physical parameters in one, a rather exotic equation of state was proposed in [35] which was further generalized in the works [36,37]. It was shown that such kind of dark energy can be modeled by the massless spinor field with the nonlinearity [18]

$$F = \left(A + \lambda S^{1+\alpha} \right)^{1/(1+\alpha)}, \tag{53}$$

where A is a positive constant and $0 < \alpha \leq 1$.

We have solved (48)–(50) numerically for the nonlinear term given by (53). We consider only massless spinor field setting $m_{sp} = 0$. The parameters S_0 , G and λ were taken as in previous case. We have also set $A = 1/2$ and $\alpha = 1/3$.

As in case of quintessence and cosmological constant, the evolution of the universe filled with Chaplygin gas is qualitatively same as in case of a modified Chaplygin gas which are illustrated in Figure 2. The expansion rate in this case is higher than the previous case but slower than in the case to follow.

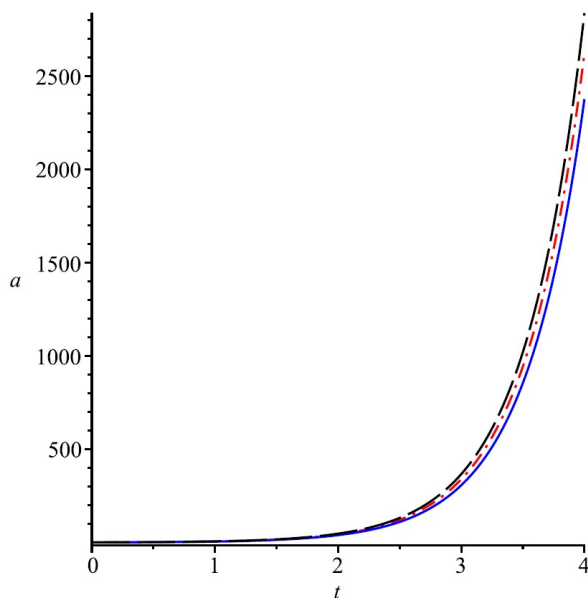


Figure 2. Evolution of the FRW Universe (scale factor a) in presence of a modified Chaplygin gas given by a massless spinor field. As one sees, due to the presence of dark energy for all values of k we have open universe. Here solid blue, dash-dot red and long dash black lines correspond to $k = 1, 0, -1$, respectively.

3.3. Modified Chaplygin Gas

Though the dark energy and the dark matter act in a completely different way, many researchers suppose that they are different manifestations of a single entity. Following such an idea a modified Chaplygin gas was introduced in [38] and was further developed in [39]. The modified Chaplygin gas can be generated by a massless spinor field with the nonlinearity given by [18]

$$F = \left[\frac{A}{1+W} + \lambda S^{(1+\alpha)(1+W)} \right]^{1/(1+\alpha)} \tag{54}$$

with W being a constant, $A > 0$ and $0 \leq \alpha \leq 1$. In fact, mathematically it is a combination of quintessence and Chaplygin gas. We have solved (48)–(50) numerically for the nonlinear term given by (54). Since we consider only massless spinor field, we set $m_{sp} = 0$. For simplicity we set S_0 , G , λ , A , and α as in previous cases. Beside that we set $W = -1/2$.

In Figure 3 we have illustrated the evolution of the universe when the universe is filled with nonlinear spinor field simulating a modified Chaplygin gas.

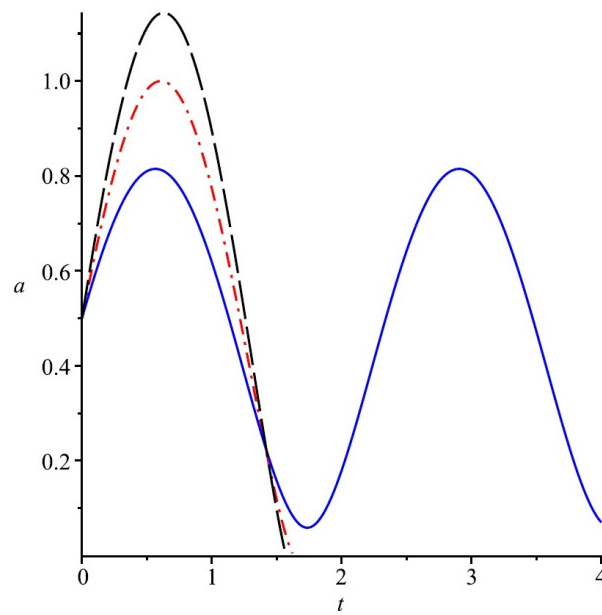


Figure 3. Evolution of the FRW Universe (scale factor a) in presence of a modified quintessence given by a massless spinor field. In this case the value of k plays definite role. Here solid blue, dash-dot red and long dash black lines correspond to $k = 1, 0, -1$, respectively.

3.4. Modified Quintessence

A modified Quintessence was proposed in order to avoid eternal acceleration of the universe. In some cases it gives cyclic universe that pops up from a Big Bang singularity, expands to some maximum value and then decreases and finally ends in Big Crunch. In some cases it might be periodic without singularity. A spinor description of a modified quintessence was proposed in [31]

$$p = W(\varepsilon - \varepsilon_{cr}), \quad W \in (-1, 0), \tag{55}$$

with ε_{cr} being some critical energy density. The model gives rise to cyclic or oscillatory universe. Setting $\varepsilon_{cr} = 0$ one obtains ordinary quintessence. As one sees from (55), the pressure is negative as long as $\varepsilon > \varepsilon_{cr}$. Since with the expansion of the universe the energy density decreases, at some moment of time ε becomes less than ε_{cr} , i.e., $\varepsilon < \varepsilon_{cr}$. This leads to the positive pressure and the contraction of the universe. It can be shown that a modified quintessence can be modeled by a spinor field nonlinearity

$$F = \lambda S^{1+W} + \frac{W}{1+W} \varepsilon_{cr}. \tag{56}$$

In this case while solving the system (48)–(50) we consider values of the parameters as in case of quintessence. For critical density we set $\varepsilon_{cr} = 1$.

In Figure 3 we have illustrated the evolution of the universe when the universe is filled with nonlinear massless spinor field simulating a modified quintessence. It should be emphasized that in this case both massless and massive the spinor field can be considered.

4. Conclusions and Discussions

Within the scope of a FLRW cosmological model we have studied the role of a nonlinear spinor field in the evolution of the universe. It is found that if the FLRW model is given in spherical coordinates the spinor field possesses nontrivial non-diagonal components of the EMT, whereas is case of Cartesian coordinates these components are trivial. Since the Einstein tensor in this case is diagonal, the presence of nontrivial non-diagonal components of the EMT imposes some restrictions on the components of spinor field. Corresponding

equations are solved and the results are graphically illustrated for the cases when the universe is filled with radiation, modified Chaplygin gas and modified quintessence.

As it was already noticed, the coordinate transformation from Cartesian to spherical coordinates gives rise to non-diagonal components of EMT that owe to spinor affine connections. This very fact suggests that the definition of spinor affine connections need if not modification then serious reconsideration. It should be noted that there were a few opinions regarding the generalization of Dirac spinor in general relativity proposed by Fock [40–42], Pauli [43], Sommerfeld [44], Wigner [45] and others. We plan to address this issue in near future.

Funding: This research received no external funding.

Institutional Review Board Statement: Not applicable.

Informed Consent Statement: Not applicable.

Data Availability Statement: No datasets were generated or analysed during the current study.

Acknowledgments: This paper has been supported by the RUDN University Strategic Academic Leadership Program.

Conflicts of Interest: The author declares no conflict of interest.

References

- Smoot, G.F.; Bennett, C.L.; Kogut, A.; Wright, E.L.; Aymon, J.; Boggess, N.W.; Cheng, E.S.; De Amici, G.; Gulkis, S.; Hauser, M.G. Structure in the COBE differential microwave radiometer first-year maps. *Astrophys. J.* **1992**, *396*, L1–L5. [CrossRef]
- Hinshaw, G.; Spergel, D.N.; Verde, L.; Hill, R.S.; Meyer, S.S.; Barnes, C.; Bennett, C.L.; Halpern, M.; Jarosik, N.; Kogut, A.; et al. First Year Wilkinson Microwave Anisotropy Probe (WMAP) Observations: Angular Power Spectrum. *Astrophys. J. Suppl. Ser.* **2003**, *148*, 135. [CrossRef]
- Friedmann, A.A. Über die Krümmung des Raumes. *Z. Phys.* **1922**, *10*, 377. [CrossRef]
- Friedmann, A.A. Über die Möglichkeit einer Welt mit konstanter negativer Krümmung des Raumes. *Z. Phys.* **1924**, *21*, 326. [CrossRef]
- Hubble, E. A relation between distance and radial velocity among extra-galactic Nebulae. *Proc. Natl. Acad. Sci. USA* **1929**, *15*, 168. [CrossRef]
- Lemaitre, G.H. l'Univers en expansion. *Annales Soc. Sci. Brux. A* **1933**, *53*, 51.
- Robertson, H.P. Kinematics and world-structure. *Astrophys. J.* **1935**, *82*, 284. [CrossRef]
- Robertson, H.P. Kinematics and world-structure II. *Astrophys. J.* **1936**, *83*, 187. [CrossRef]
- Robertson, H.P. Kinematics and world-structure III. *Astrophys. J.* **1936**, *83*, 257. [CrossRef]
- Walker, A.G. On Milne's Theory of World-Structure. *Proc. Lond. Math. Soc.* **1937**, *42*, 90–127. [CrossRef]
- Ribas, M.O.; Devecchi, F.P.; Kremer, G.M. Fermions as sources of accelerated regimes in cosmology. *Phys. Rev. D* **2005**, *72*, 123502. [CrossRef]
- Saha, B. Nonlinear spinor field in Bianchi type-I cosmology: Inflation, isotropization, and late time acceleration. *Phys. Rev. D* **2006**, *74*, 124030. [CrossRef]
- Saha, B.; Rikhvitsky, V.S. Nonlinear spinor fields in anisotropic Universe filled with viscous fluid: Exact solutions and qualitative analysis. *Phys. Part. Nucl.* **2009**, *40*, 612. [CrossRef]
- Fabbri, L. A Discussion on Dirac Field Theory, No-Go Theorems and Renormalizability. *Int. J. Theor. Phys.* **2013**, *52*, 634. [CrossRef]
- Fabbri, L. Conformal gravity with the most general ELKO matter. *Phys. Rev. D* **2012**, *85*, 047502. [CrossRef]
- Vignolo, S.; Fabbri, L.; Cianci, R. Dirac spinors in Bianchi-I $f(R)$ -cosmology with torsion. *J. Math. Phys.* **2011**, *52*, 112502. [CrossRef]
- Popławski, N. Nonsingular, big-bounce cosmology from spinor-torsion coupling. *Phys. Rev. D* **2012**, *85*, 107502. [CrossRef]
- Saha, B. Spinor field nonlinearity and space-time geometry. *Phys. Part. Nucl.* **2018**, *49*, 146. [CrossRef]
- Saha, B. Spinor fields in spherically symmetric space-time. *Eur. Phys. J. Plus* **2018**, *133*, 461. [CrossRef]
- Bronnikov, K.A.; Rybakov, Y.P.; Saha, B. Spinor fields in spherical symmetry: Einstein-Dirac and other space-times. *Eur. Phys. J. Plus* **2020**, *135*, 124. [CrossRef]
- Saha, B. Spinors in cylindrically symmetric space-time. *Universe* **2020**, *6*, 152. [CrossRef]
- Saha, B. Time-dependent Spinor field in a static cylindrically symmetric space-time. *Eur. Phys. J. Plus* **2022**, *137*, 1063. [CrossRef]
- Saha, B.; Zakharov, E.I.; Rikhvitsky, V.S. Spinor field in a spherically symmetric Friedmann Universe. *Discret. Cont. Mod. Appl. Comput. Sci.* **2020**, *28*, 132.
- Gavrilov, A.S.; Saha, B.; Rikhvitsky, V.S. Applying Friedmann models to describe the evolution of the Universe based on data from the SAI Supernovae Catalog. *Discret. Cont. Mod. Appl. Comput. Sci.* **2020**, *28*, 120. [CrossRef]
- Saha, B. Spinor field in Bianchi type-I Universe: Regular solutions. *Phys. Rev. D* **2001**, *64*, 123501. [CrossRef]

26. Saha, B. Spinor model of a perfect fluid and their applications in Bianchi type-I and FRW models. *Astrophys. Space Sci.* **2011**, *331*, 243. [CrossRef]
27. Narlikar, J.V. *Introduction to Relativity*; Cambridge University Press: New York, NY, USA, 2010.
28. Caldwell, R.R. A phantom menace? Cosmological consequences of a dark energy component with super-negative equation of state. *Phys. Lett. B* **2002**, *545*, 23. [CrossRef]
29. Sahni, V.; Starobinsky, A.A. The case for a positive cosmological Λ term. *Int. J. Mod. Phys. D* **2000**, *9*, 373. [CrossRef]
30. Zlatev, I.; Wang, L.; Steinhardt, P.J. Quintessence, Cosmic Coincidence, and the Cosmological Constant. *Phys. Rev. Lett.* **1999**, *82*, 896. [CrossRef]
31. Saha, B. Anisotropic cosmological models with perfect fluid and dark energy reexamined. *Int. J. Theor. Phys.* **2006**, *45*, 983. [CrossRef]
32. Padmanabhan, T. Cosmological constant—The weight of the vacuum. *Phys. Rep.* **2003**, *380*, 235. [CrossRef]
33. Sahni, V. Dark Matter and Dark Energy. *Lect. Notes Phys.* **2004**, *653*, 141.
34. Saha, B. Anisotropic cosmological models with a perfect fluid and a Λ term. *Astrophys. Space Sci.* **2006**, *302*, 83. [CrossRef]
35. Kamenshchik, A.Y.; Moschella, U.; Pasquier, V. An alternative to quintessence. *Phys. Lett. B* **2001**, *511*, 265. [CrossRef]
36. Bilic, N.; Tupper, G.B.; Viollier, R.D. Unification of Dark Matter and Dark Energy: The Inhomogeneous Chaplygin Gas. *Phys. Lett. B* **2002**, *353*, 17. [CrossRef]
37. Bento, M.C.; Bertolami, O.; Sen, A.A. Generalized Chaplygin Gas, Accelerated Expansion and Dark Energy-Matter Unification. *Phys. Rev. D* **2002**, *66*, 043507. [CrossRef]
38. Benaoum, H.B. Accelerated Universe from Modified Chaplygin Gas and Tachyonic Fluid. *Universe* **2022**, *8*, 340. [CrossRef]
39. Benaoum, H.B. Modified Chaplygin Gas Cosmology. *Adv. High Energy Phys.* **2012**, *2012*, 357802. [CrossRef]
40. Fock, V. Geometrization of Dirac theory of electrons. *Z. Phys.* **1929**, *57*, 261. [CrossRef]
41. Fock, V.; Iwanenko, D. Quantun linear geometry and parallel transfer. *C. R. Acad.* **1929**, *188*, 1470.
42. Fock, V.; Ivanenko, D. On a possible geometric interpretation of relativistic quantun theory. *Z. Phys.* **1929**, *54*, 798. [CrossRef]
43. Pauli, W. Über die formulierung der naturgesetze mit füng homogenen koordinaten. *Ann. Phys.* **1933**, *5*, 337. [CrossRef]
44. Mitskievich, N.V. *Physical Fields in General Theory of Relativity*; Nauka: Moscow, Russian, 1969.
45. Wigner, E.P. Eine Bemerkung zu Einsteins neuer Formulierung des allgemeinen Relativit tsprinzips. In *Part I: Particles and Fields. Part II: Foundations of Quantum Mechanics*; Wightman, A.S., Ed.; The Scientific Papers, Volume A/3; Springer: Berlin/Heidelberg, Germany, 1997.

Disclaimer/Publisher's Note: The statements, opinions and data contained in all publications are solely those of the individual author(s) and contributor(s) and not of MDPI and/or the editor(s). MDPI and/or the editor(s) disclaim responsibility for any injury to people or property resulting from any ideas, methods, instructions or products referred to in the content.

Conventionalism, Cosmology and Teleparallel Gravity

Laur Järv  and Piret Kuusk *

Laboratory of Theoretical Physics, Institute of Physics, University of Tartu, W. Ostwaldi 1, 50411 Tartu, Estonia; laur.jarv@ut.ee

* Correspondence: piret.kuusk@ut.ee

Abstract: We consider homogeneous and isotropic cosmological models in the framework of three geometrical theories of gravitation. In Einstein's general relativity, they are given in terms of the curvature of the Levi-Civita connection in torsion-free metric spacetimes; in the teleparallel equivalent of general relativity, they are given in terms of the torsion of flat metric spacetimes; and in the symmetric teleparallel equivalent of general relativity, they are given in terms of the nonmetricity of flat torsion-free spacetimes. We argue that although these three formulations seem to be different, the corresponding cosmological models are in fact equivalent and their choice is conventional.

Keywords: philosophy of spacetime; Friedmann cosmology; teleparallel gravity; symmetric teleparallel gravity

1. Introduction

At present, the Λ CDM model is considered as the most adequate large-scale description of the visible universe. It is based on the Friedmann solution of equations of Einstein's general relativity (GR) with cosmological constant Λ , which is considered to describe hypothetical dark energy, and also contains hypothetical dark matter. The essential parameters of the model can be estimated from observations with ever-improving precision.

However, not everybody acknowledges the success of the Λ CDM model as there are several observational results that are difficult to accommodate in it [1]. The hypothetical dark energy was introduced to explain a totally unexpected discovery of accelerating expansion of the universe during the last 6 billion years. The equally hypothetical dark matter was introduced to explain the observed rotation velocities of stars in galaxies, and is also required to give an account of structure formation and gravitational lensing. However, particles of dark matter have up to now never been observed and they cannot be identified with any particles from the standard model of particle physics.

There are several directions to understand the situation. Physicists who are used to investigating different theories of gravitation are inclined to modify the Einstein general relativity for obtaining predictions close to observations without using hypothetical entities. Philosophers of physics are eager to spot the roots of difficulties in the standard model of cosmology. We are not going to give an overview of the modified theories of gravitation since there is already a wealth of literature on that topic [2,3]. Instead, we will discuss some features of current cosmological models that raise questions. We shall proceed from a recent paper [4], which claims that the standard model of cosmology is in a great part conventional. Conventionalism in physics tries to separate those parts of theories that do not describe real properties of objects under consideration but are simply definitions or conventions that can be replaced by different ones, as far as observational results are retained. The idea was implicitly presented by Duhem [5], elaborated by Poincaré [6] and explained in detail by Popper [7].

The present paper considers the contemporary standard model of cosmology from the point of view of conventionalism, putting focus upon the alternative geometric formulations. We consider theories where gravitation is given not in terms of curvature of



Citation: Järv, L.; Kuusk, P. Conventionalism, Cosmology and Teleparallel Gravity. *Universe* **2024**, *10*, 1. <https://doi.org/10.3390/universe10010001>

Academic Editors: Galina L. Klimchitskaya, Vladimir M. Mostepanenko and Sergey V. Sushkov

Received: 6 November 2023

Revised: 13 December 2023

Accepted: 14 December 2023

Published: 19 December 2023



Copyright: © 2023 by the authors. Licensee MDPI, Basel, Switzerland. This article is an open access article distributed under the terms and conditions of the Creative Commons Attribution (CC BY) license (<https://creativecommons.org/licenses/by/4.0/>).

the connection as in general relativity (GR), but in terms of torsion or nonmetricity of the connection. If the curvature and nonmetricity of the corresponding connection are taken to vanish, but the torsion is not, it is known as the teleparallel equivalent of general relativity (TEGR) [8,9]. If the curvature and torsion of the connection are taken to vanish, we obtain the Symmetric teleparallel equivalent of general relativity (STEGR) [10]. The Lagrangians of these three theories differ only by a total derivative term, so their local equations of motion coincide, and one can envision a geometric trinity of gravity [11,12]. A reader interested in the mathematical details of teleparallel theories can refer to reviews like [13,14]. Let us mention that an analogous set of equivalences can be also shown in the nonrelativistic case [15,16], as well as in extended $f(R)$ -type case [17], or including both torsion and nonmetricity simultaneously [18].

The paper is structured as follows. In Section 2, we briefly review the paper by Merritt [4], where the conventions of Λ CDM cosmology are compared with those characterized by Popper [7]. Then, we discuss problems of theoretical and interpretational equivalence in physics as presented by Weatherall [19], Dürr [20] and Coffey [21]. In Section 3, we flesh out how the spatially flat Friedmann Λ CDM model is described in GR, TEGR and STEGR. At the end, Section 4 is devoted to a discussion that summarizes the results and outlines some avenues beyond Λ CDM which deserve a closer look.

2. Conventionalism in Physics and Cosmology

2.1. Merritt on Conventions in the Λ CDM Model

Merritt [4] proceeds from Popper's idea that science as distinct from non-science can be characterized by its falsifiability: universal statements of theory can be logically contradicted by an intersubjective singular existential statement. Popper was worried that if scientific theories contain conventions that can be freely changed, their criterion of falsifiability cannot be applied. He indicates that a conventionalist can use at least two strategies for preventing falsifiability: (i) introducing ad hoc hypotheses that explain potentially falsifying observations, (ii) changing some ostensive definitions that change the content of the theory.

The first strategy is explicitly used for proposing the dark matter hypothesis. In order to explain the difference in observed rotation velocities of stars in galaxies and galaxies in clusters of galaxies in comparison with theoretical predictions using known theories of gravity and observed masses, it was proposed to assume existence of additional quantities of non-luminous matter, dubbed dark matter. However, the essence and physical properties of dark matter remain mysterious.

Less explicit is the role of introducing hypothetical dark energy for explaining the observed accelerating expansion of the universe. The simplest way to explain it is to complement the Einstein equations of gravitation with a cosmological constant term. It does not change the general interpretation of the theory, but allows cosmological solutions which conform with observations. However, a more detailed interpretation of the cosmological constant is ambiguous [22]. It can be considered as a homogeneous and isotropic perfect fluid, but then its pressure must be negative with an absolute value equal to its energy density. In a sense, the cosmological constant is referred to as a new type of perfect fluid.

In both cases, hypothetical entities are introduced for explaining specific observational evidence. Up to now, these entities defy additional observational conformations or refutations. However, they seem to be a solid part of the received view of the universe. As Merritt concludes: "rather than conceive of dark matter and dark energy as postulates invoked in response to falsifying observations—cosmologists interpret those same observations as tantamount to the discovery of dark matter and dark energy".

2.2. A Peculiar Feature of Cosmological Science

In cosmological science, there is no possibility to provide experiments or to compare observations of different scenarios. There is only one visible universe and our efforts attempt to find its description. Popper is interested not only in possibilities to falsify a

theory, but even more in finding satisfactory theories. He admits that the aim is in fact not achievable: “Science does not rest on a solid bedrock. The bold structure of its theories rises, as it were, above a swamp. The piles are driven down from above into the swamp, but not down to any natural or ‘given’ base, and if we stop driving the piles deeper, it is not because we have reached firm ground. We simply stop when we are satisfied that the piles are firm enough to carry the structure, at least for the time being” [7] (ch.5, sec. 30). In fact, he does not deny that some piles may be conventional, i.e., changeable, although this may be an obstacle to possible falsification of the theory.

In what follows, we argue that there is yet another basic property of the theory of the Friedmann cosmology that can be freely chosen: the geometric framework, a curved torsion-free metric spacetime or a metric spacetime with torsion and flat connections or a flat torsion-free spacetime with nonmetricity. This follows from the fact that the corresponding Lagrangians differ only by boundary terms that vanish in Friedmann cosmology, and local equations of motion can be transformed into each other. This is reminiscent of the geometric conventionality presented by Poincaré [6]: an infinite Euclidean background can be transformed into a finite non-Euclidean background by introducing universal distorting forces. Poincaré concluded that corresponding sets of geometric axioms are just conventions for allowing us to choose a mathematical framework to be applied. The choice is not determined by experiments or observations, although it must be in line with their results.

2.3. Empirical Equivalence and Theoretical Equivalence

Although GR, TEGR and STEGR are locally empirically equivalent, this does not mean that they are equivalent in all aspects. There may be other important differences in the theories that do not affect experimental or observational results. Theories may include concepts and theoretical terms that are essentially different; they may attribute different structures to the world, etc. It follows that empirically equivalent but theoretically inequivalent theories may contain conventional parts.

Theoretical equivalence as distinct from empirical equivalence can be described using a formal approach [23], but there are also other ways to consider it. For instance, Coffey [21] proposed that theoretical equivalence of empirically equivalent theories means that they agree on what the physical world is fundamentally like [21]. Note that this is not the view of Poincaré’s geometric conventionalism. A short review of different possibilities to introduce theoretical equivalence was recently presented by Weatherall [19]. He admits that empirical equivalence is a necessary condition for two theories to be theoretically equivalent, but need not be a sufficient one.

Dürr [20] considers the case of a theory T together with an empirically equivalent but incompatible alternative account T' of relevant data. Then, T and T' are not simply different representations of the same theory, since they assert contradictory facts about the world. Dürr indicates two ways for this to occur. Firstly, the same mathematical equations can obtain different interpretations, e.g., GR formalism is usually interpreted geometrically, but can also be interpreted field-theoretically, as presented by Feynman [24] and Weinberg [25]. If the inequivalent interpretations are considered to be sufficient for theoretical inequivalence, then we have here two distinct theories of gravitation, although usually physicists consider them to be equivalent with respect to their physical content. Secondly, T and T' can have distinct equations, as in the case of Dirac–von Neumann and Bohmian quantum mechanics, which clearly are two distinct theories, although empirically equivalent.

TEGR and GR describe the underlying spacetime differently although empirically equivalently; in TEGR, mathematical formalism is interpreted as describing a flat spacetime with a non-vanishing torsion, and in GR, the related formalism is interpreted as describing a curved spacetime with a vanishing torsion. In TEGR, the inertial and gravitational forces are described separately, distinct from GR, where they are united via the principle of equivalence. It follows that TEGR and GR are not interpretationally equivalent. At the

same time, the symmetric teleparallel connection endowed with nonmetricity but lacking curvature and torsion arises in STEGR as a Stueckelberg field for diffeomorphisms, meaning it is just a gauge field, i.e., yet another aspect open for interpretation.

Knox [26] argues that if we accept spacetime functionalism, i.e., take into account only those features of the physical world that are functionally relevant in producing empirical evidence, then GR and TEGR can be considered as postulating the same spacetime ontology, since they pick out the same inertial reference frames for gravitational and non-gravitational physics (the limitations of this approach are pointed out by Read and Menon [27]). In Knox’s opinion, GR and TEGR are empirically and ontologically equivalent, and they ought to be considered rather as different formulations of the same physics and not two different theories. Her complicated deliberations demonstrate that identity of theories is not an easy problem. Recently, Wolf and Read [28] investigated isolated gravitational systems and systems with boundaries and argued that in this respect, GR and TEGR are equivalent.

If we admit that GR, TEGR and also STEGR can be considered as having equivalent physical content, then we can choose their geometric framework and consider it as conventional. We will return to these issues in Section 4.

3. Friedmann Cosmology in Different Formulations of General Relativity

3.1. Geometric Preliminaries

To back up and illustrate the discussion, we introduce some maths. In differential geometry, general metric-affine spacetimes are described by two quantities that are in principle independent: the metric $g_{\mu\nu}$, which encodes distances and angles, and the connection $\Gamma^\lambda_{\sigma\rho}$, which defines parallel transport and covariant derivatives, e.g.,

$$\nabla_\mu \mathcal{T}^\lambda_\nu = \partial_\mu \mathcal{T}^\lambda_\nu + \Gamma^\lambda_{\alpha\mu} \mathcal{T}^\alpha_\nu - \Gamma^\alpha_{\nu\mu} \mathcal{T}^\lambda_\alpha. \tag{1}$$

The generic affine connection can be decomposed into three parts,

$$\Gamma^\lambda_{\mu\nu} = \left\{ \begin{matrix} \lambda \\ \mu\nu \end{matrix} \right\} + K^\lambda_{\mu\nu} + L^\lambda_{\mu\nu}, \tag{2}$$

where the Christoffel symbols of the Levi-Civita connection depend on the metric $g_{\mu\nu}$,

$$\left\{ \begin{matrix} \lambda \\ \mu\nu \end{matrix} \right\} \equiv \frac{1}{2} g^{\lambda\beta} (\partial_\mu g_{\beta\nu} + \partial_\nu g_{\beta\mu} - \partial_\beta g_{\mu\nu}), \tag{3}$$

while contortion

$$K^\lambda_{\mu\nu} \equiv \frac{1}{2} g^{\lambda\beta} (T_{\mu\beta\nu} + T_{\nu\beta\mu} - T_{\beta\mu\nu}), \tag{4}$$

and disformation

$$L^\lambda_{\mu\nu} \equiv -\frac{1}{2} g^{\lambda\beta} (Q_{\mu\beta\nu} + Q_{\nu\beta\mu} + Q_{\beta\mu\nu}) \tag{5}$$

encode the independent aspect of the connection. The last two quantities are defined via torsion (antisymmetric)

$$T^\lambda_{\mu\nu} \equiv \Gamma^\lambda_{\nu\mu} - \Gamma^\lambda_{\mu\nu} \tag{6}$$

and nonmetricity (symmetric)

$$Q_{\rho\mu\nu} \equiv \nabla_\rho g_{\mu\nu} = \partial_\rho g_{\mu\nu} - \Gamma^\beta_{\mu\rho} g_{\beta\nu} - \Gamma^\beta_{\nu\rho} g_{\mu\beta}. \tag{7}$$

Note that torsion and nonmetricity, as well as curvature

$$R^\sigma_{\rho\mu\nu} \equiv \partial_\mu \Gamma^\sigma_{\nu\rho} - \partial_\nu \Gamma^\sigma_{\mu\rho} + \Gamma^\alpha_{\nu\rho} \Gamma^\sigma_{\mu\alpha} - \Gamma^\alpha_{\mu\rho} \Gamma^\sigma_{\nu\alpha} \tag{8}$$

and its contractions $R_{\mu\nu} = R^\rho_{\mu\rho\nu}$, $R = g^{\mu\nu} R_{\mu\nu}$, are strictly speaking all properties of the connection.

Friedmann cosmology is based on the cosmological principle which expects that at sufficiently large scales, the Universe is homogeneous and isotropic in space, i.e., it is characterised by the Killing vectors of translations ζ_{T_i} and rotations ζ_{R_i} , given in spherical coordinates as

$$\zeta_{T_x}^\mu = \left(0 \quad \chi \sin \theta \cos \phi \quad \frac{\chi}{r} \cos \theta \cos \phi \quad -\frac{\chi}{r} \frac{\sin \phi}{\sin \theta} \right), \quad (9a)$$

$$\zeta_{T_y}^\mu = \left(0 \quad \chi \sin \theta \sin \phi \quad \frac{\chi}{r} \cos \theta \sin \phi \quad \frac{\chi}{r} \frac{\cos \phi}{\sin \theta} \right), \quad (9b)$$

$$\zeta_{T_z}^\mu = \left(0 \quad \chi \cos \theta \quad -\frac{\chi}{r} \sin \theta \quad 0 \right), \quad (9c)$$

$$\zeta_{R_x}^\mu = \left(0 \quad 0 \quad \sin \phi \quad \frac{\cos \phi}{\tan \theta} \right), \quad (9d)$$

$$\zeta_{R_y}^\mu = \left(0 \quad 0 \quad -\cos \phi \quad \frac{\sin \phi}{\tan \theta} \right), \quad (9e)$$

$$\zeta_{R_z}^\mu = \left(0 \quad 0 \quad 0 \quad -1 \right), \quad (9f)$$

where $\chi = \sqrt{1 - kr^2}$ describes the curvature of the 3D space. The symmetry is obeyed when the Lie derivatives of the metric and affine connection along these vectors vanish [29],

$$\mathcal{L}_\zeta g_{\mu\nu} = 0, \quad \mathcal{L}_\zeta \Gamma^\lambda{}_{\mu\nu} = 0. \quad (10)$$

For the sake of simplicity, in this paper, let us focus only upon the spatially flat case, where $k = 0$. It is well known that the metric which satisfies this condition is the Friedmann–Lemaître–Robertson–Walker (FLRW), conveniently written as

$$ds^2 = -dt^2 + a(t)^2 \left(dr^2 + r^2 d\theta^2 + r^2 \sin^2 \theta d\phi^2 \right), \quad (11)$$

where $a(t)$ is the scale factor that describes the expansion of space. For a connection with the same symmetries, there are different options to satisfy Equation (10), depending on the extra assumptions made about curvature, torsion and nonmetricity, as discussed below. The matter energy momentum tensor consistent with the cosmological symmetry is given in the same coordinates by

$$\mathcal{T}_{\mu\nu} = \begin{pmatrix} \rho(t) & 0 & 0 & 0 \\ 0 & a^2(t)p(t) & 0 & 0 \\ 0 & 0 & r^2 a^2(t)p(t) & 0 \\ 0 & 0 & 0 & r^2 a^2(t)p(t) \sin^2 \theta \end{pmatrix}, \quad (12)$$

where ρ is the energy density and p is the pressure of the matter.

3.2. General Relativity

In general relativity, one assumes the connection is torsion-free ($T^\lambda{}_{\mu\nu} = 0$) and metric-compatible ($Q_{\rho\mu\nu} = 0$), which leaves only the Levi-Civita part $\{\overset{\lambda}{\mu\nu}\}$ nonvanishing on the right-hand side of Equation (2). The gravitational field as described by spacetime geometry follows Einstein's field equations,

$$\overset{\text{LC}}{R}_{\mu\nu} - \frac{1}{2} g_{\mu\nu} \overset{\text{LC}}{R} = \kappa^2 \mathcal{T}_{\mu\nu}, \quad (13)$$

while the matter constituents obey the continuity equation

$$\overset{\text{LC}}{\nabla}_\mu \mathcal{T}^\mu{}_\nu = 0, \quad (14)$$

which in the case of a massive point particle, leads to

$$m \left(\frac{du^\mu}{d\tau} + \{\overset{\mu}{\rho\sigma}\} u^\rho u^\sigma \right) = 0. \quad (15)$$

Here, m is the mass, u^μ the four-velocity and τ is the proper time of the particle. The last equation is simultaneously the geodesic equation of the metric (giving the shortest distance), as well as the autoparallel curve of the Levi-Civita connection,

$$u^\nu \overset{\text{LC}}{\nabla}_\nu u^\mu = 0, \tag{16}$$

which says that the particle moves “straight” in the direction of the tangent vector u^ν of its trajectory. The connection coefficients $\{\mu_{\rho\sigma}\}$ in the second term of Equation (15) encode both the inertial effects (a fictional force arising when “straight” motion is described in curvilinear coordinates) and gravitational effects (external force accelerating the particle) together, a fundamental insight of Einstein called the equivalence principle.

In cosmology, it is straightforward to compute the Levi-Civita connection components (3) from metric (11)

$$\{\mu_{\rho\sigma}\} = \begin{bmatrix} \begin{bmatrix} 0 & 0 & 0 & 0 \\ 0 & \dot{a}\dot{a} & 0 & 0 \\ 0 & 0 & a\dot{a}r^2 & 0 \\ 0 & 0 & 0 & a\dot{a}r^2 \sin^2 \theta \end{bmatrix} & \begin{bmatrix} 0 & H & 0 & 0 \\ H & 0 & 0 & 0 \\ 0 & 0 & -r & 0 \\ 0 & 0 & 0 & -r \sin^2 \theta \end{bmatrix} \\ \begin{bmatrix} 0 & 0 & H & 0 \\ 0 & 0 & \frac{1}{r} & 0 \\ H & \frac{1}{r} & 0 & 0 \\ 0 & 0 & 0 & -\sin \theta \cos \theta \end{bmatrix} & \begin{bmatrix} 0 & 0 & 0 & H \\ 0 & 0 & 0 & \frac{1}{r} \\ 0 & 0 & 0 & \cot \theta \\ H & \frac{1}{r} & \cot \theta & 0 \end{bmatrix} \end{bmatrix}, \tag{17}$$

where the four matrices in columns are labelled by the first index μ , and the entries of the matrices are specified by the last two indices $\rho\sigma$. Here, the dot represents a derivative with respect to time t , and the Hubble function $H = \frac{\dot{a}}{a}$ measures the relative expansion rate of space. The connection coefficients (17) obey the cosmological symmetry by construction, and the respective Lie derivatives (10) vanish. From the connection, we can further calculate the curvature tensor (8) and its contractions. Substituting these, as well as the matter energy-momentum (12), into Einstein’s Equation (13) yields the Friedmann equations,

$$3H^2 = \kappa^2 \rho, \quad 2\dot{H} + 3H^2 = -\kappa^2 p, \tag{18}$$

and substitution into the continuity Equation (14) yields

$$\dot{\rho} + 3H(\rho + p) = 0. \tag{19}$$

The solutions of these equations for different types of matter combinations (relativistic/radiation, nonrelativistic/dust, cosmological constant, inflaton field, etc.) describe the evolution of the Universe at large scales. The massive particles moving in the Universe follow Equation (15) with the inertia and background expansion encoded in (17).

3.3. Teleparallel Equivalent of General Relativity

After accomplishing the remarkably successful geometrisation of the gravitational field in general relativity, Einstein endeavoured to find a unified geometric theory that would also include electromagnetism. In one of his attempts [30,31], he introduced a spacetime with teleparallelism, where the curvature (8) of the connection vanishes and vectors do not change their direction when parallel-transported along a closed loop. Such connections endowed with torsion (6) were first investigated by Weitzenböck a few years before [32]. Realizing that such a theory cannot accommodate electromagnetism properly, Einstein gave up the idea. However, the concept of teleparallel spacetimes was later invoked by Møller in the search for a description of the energy of gravitational fields [33,34], and then revived by Hayashi and Nakano to construct a possible gauge theory for the spacetime translation group [35], which eventually lead to the development of the teleparallel equivalent of general relativity [8,9] and its extensions [36].

In the teleparallel equivalent of general relativity, one assumes the connection $\overset{\text{TP}}{\Gamma}{}^\lambda{}_{\mu\nu}$ is “flat” in the sense of identically zero curvature ($\overset{\text{TP}}{R}{}^\sigma{}_{\rho\mu\nu} = 0$) and metric-compatible ($\overset{\text{TP}}{Q}{}_{\rho\mu\nu} = 0$). In the decomposition of the connection (2), this introduces some extra torsional components in the Levi-Civita part. It is important to realize that the Levi-Civita components depend on the metric and when considered among themselves can still be characterised by nontrivial curvature. The role of the extra torsional components in the connection is to “compensate” the Levi-Civita connection in making the overall curvature (8) vanish.

By introducing the torsion scalar

$$\overset{\text{TP}}{T} = \frac{1}{2} \overset{\text{TP}}{T}{}^\rho{}_{\mu\nu} \overset{\text{TP}}{S}{}_\rho{}^{\mu\nu} \tag{20}$$

where the torsion conjugate (or superpotential) is defined as

$$\overset{\text{TP}}{S}{}_\rho{}^{\mu\nu} = \overset{\text{TP}}{K}{}^{\mu\nu}{}_\rho - \delta_\rho^\mu \overset{\text{TP}}{T}{}^\sigma{}_{\nu}{}^{\sigma\nu} + \delta_\rho^\nu \overset{\text{TP}}{T}{}^\sigma{}_{\nu}{}^{\sigma\mu}, \tag{21}$$

the field equations of TEGR can be written as follows [37]

$$\overset{\text{LC}}{\nabla}{}_\rho \overset{\text{TP}}{S}{}_{(\mu\nu)}{}^\rho - \overset{\text{TP}}{t}{}_{\mu\nu} = \kappa^2 \mathcal{T}_{\mu\nu}. \tag{22}$$

An interesting aspect of this form is that the symmetric tensor

$$\overset{\text{TP}}{t}{}_{\mu\nu} = \frac{1}{2} \overset{\text{TP}}{S}{}_{(\mu}{}^{\rho\sigma} \overset{\text{TP}}{T}{}_{\nu)\rho\sigma} - \frac{1}{2} g_{\mu\nu} \overset{\text{TP}}{T} \tag{23}$$

appears in the equations in an analogous position as the energy momentum tensor of the matter. We might be tempted to interpret it as the energy momentum of the gravitational field¹, which acts as a self-source to the dynamics, like the nonlinear self-coupling term in the Yang–Mills equations. Although all geometric tensors that enter here are computed from the teleparallel connection, with a clever use of the geometric identities, it is possible to show that Equation (22) exactly matches Einstein’s field Equation (13). In other words, when all the terms in Equation (22) are expanded out in full, only the Levi-Civita part of the connection remains, while the torsional components of the connection cancel each other out. Hence, given a matter energy momentum, both GR and TEGR predict exactly the same evolution for the metric field. There is no equation to give the torsional part of the connection independent dynamics.

In the TEGR constructions, the matter sector is typically assumed to remain unaltered, i.e., maintaining couplings to the metric and Levi-Civita connection only. This guarantees that the continuity Equation (14) holds as before². Hence, the massive particles still follow the geodesics of the metric (15), but using the relation (2) we can rewrite it as

$$m \left(\frac{du^\mu}{d\tau} + \overset{\text{TP}}{\Gamma}{}^\mu{}_{\rho\sigma} u^\rho u^\sigma \right) = m \overset{\text{TP}}{K}{}^\mu{}_{\rho\sigma} u^\rho u^\sigma. \tag{24}$$

This form suggests an interesting interpretation. Namely, the right-hand side with contortion tensor looks like a force term (akin to the Lorentz force in electrodynamics), while the left-hand side says that in the absence of the force, a massive particle will move “straight” along an autoparallel of the teleparallel connection. Still, both GR and TEGR prescribe identical paths for the particle motion through spacetime. Thus, GR and TEGR are equivalent in the sense that they predict the same physical outcomes, but adding an extra connection allows one to present Equations (22) and (24) in a form where interpretation is more in line with the other well-established and understood theories of physics.

Let us take the Friedmann cosmology example. It can be confirmed that the following connection [29]

$${}^{\text{TP}}\Gamma^{\rho}_{\mu\nu} = \begin{bmatrix} \begin{bmatrix} 0 & 0 & 0 & 0 \\ 0 & 0 & 0 & 0 \\ 0 & 0 & 0 & 0 \\ 0 & 0 & 0 & 0 \end{bmatrix} & \begin{bmatrix} 0 & 0 & 0 & 0 \\ H & 0 & 0 & 0 \\ 0 & 0 & -r & 0 \\ 0 & 0 & 0 & -r \sin^2 \theta \end{bmatrix} \\ \begin{bmatrix} 0 & 0 & 0 & 0 \\ 0 & 0 & \frac{1}{r} & 0 \\ H & \frac{1}{r} & 0 & 0 \\ 0 & 0 & 0 & -\sin \theta \cos \theta \end{bmatrix} & \begin{bmatrix} 0 & 0 & 0 & 0 \\ 0 & 0 & 0 & \frac{1}{r} \\ 0 & 0 & 0 & \cot \theta \\ H & \frac{1}{r} & \cot \theta & 0 \end{bmatrix} \end{bmatrix} \quad (25)$$

is teleparallel, as the curvature (8) and nonmetricity (7) are zero and it obeys the cosmological symmetry, whereby the Lie derivatives with respect to the generators of spatial homogeneity and isotropy vanish, Equations (9) and (10). Substituting this connection, the metric (11) and matter (12) into Equation (22) reproduces the Friedmann Equation (17) in general relativity exactly, with

$${}^{\text{TP}}K_{\mu\nu} = \begin{bmatrix} 3H^2 & 0 & 0 & 0 \\ 0 & -\dot{a}^2 & 0 & 0 \\ 0 & 0 & -r^2\dot{a}^2 & 0 \\ 0 & 0 & 0 & -r^2 \sin^2(\theta)\dot{a}^2 \end{bmatrix}. \quad (26)$$

The last quantity vanishes for a constant scale factor a , as an expectedly empty space would not be a source of its own evolution.

For the particle motion, the “force” term on the right-hand side of Equation (24) is set by the contortion (4), and can easily be found by the subtraction of (17) from (25),

$${}^{\text{TP}}K^{\mu}_{\rho\sigma} = \begin{bmatrix} \begin{bmatrix} 0 & 0 & 0 & 0 \\ 0 & -a\dot{a} & 0 & 0 \\ 0 & 0 & -a\dot{a}r^2 & 0 \\ 0 & 0 & 0 & -a\dot{a}r^2 \sin^2 \theta \end{bmatrix} & \begin{bmatrix} 0 & -H & 0 & 0 \\ 0 & 0 & 0 & 0 \\ 0 & 0 & 0 & 0 \\ 0 & 0 & 0 & 0 \end{bmatrix} \\ \begin{bmatrix} 0 & 0 & -H & 0 \\ 0 & 0 & 0 & 0 \\ 0 & 0 & 0 & 0 \\ 0 & 0 & 0 & 0 \end{bmatrix} & \begin{bmatrix} 0 & 0 & 0 & -H \\ 0 & 0 & 0 & 0 \\ 0 & 0 & 0 & 0 \\ 0 & 0 & 0 & 0 \end{bmatrix} \end{bmatrix}. \quad (27)$$

It should not be a surprise that when there is no expansion ($\dot{a} = 0$) and the metric reduces to Minkowski, the contortion vanishes and the particle will feel no gravitational “force”, although there are still inertial effects present in the connection (25) on the left-hand side of (24) since we use spherical coordinates.

3.4. Symmetric Teleparallel Equivalent of General Relativity

From the discussion above, it is not hard to envision another option to present an alternative formulation of general relativity by employing nonmetricity instead of torsion, although the history of this idea dates not that far back [53]. In the symmetric teleparallel equivalent of general relativity [10,11,14], one assumes the connection $\overset{\text{STP}}{\Gamma}^{\lambda}_{\mu\nu}$ is “flat” ($\overset{\text{STP}}{R}^{\sigma}_{\rho\mu\nu} = 0$) and torsion-free ($\overset{\text{STP}}{T}^{\rho}_{\mu\nu} = 0$). Thus, in the decomposition of connection (2), we have extra nonmetricity-related components in the Levi-Civita part. Again, the Levi-Civita components considered among themselves can still be characterised by a nontrivial curvature, and the role of the extra nonmetricity components is to make the overall curvature (8) vanish.

By introducing the nonmetricity scalar

$$Q = \frac{1}{2} \overset{\text{STP}}{Q}_{\rho}{}^{\mu\nu} \overset{\text{STP}}{P}{}^{\rho}_{\mu\nu} \quad (28)$$

where the nonmetricity conjugate (or superpotential) is defined as³

$$P^{\rho}_{\mu\nu} = -\frac{1}{2}Q^{\rho}_{\mu\nu} + Q_{(\mu}{}^{\rho}{}_{\nu)} + \frac{1}{2}g_{\mu\nu}Q^{\rho\alpha}{}_{\alpha} - \frac{1}{2}\left(g_{\mu\nu}Q^{\rho\alpha}{}_{\alpha} + \delta^{\rho}{}_{(\mu}Q_{\nu)\alpha}{}^{\alpha}\right), \tag{29}$$

the field equations of STEGR can be written in the following form (adopted from [54])

$$\nabla^{\text{LC}}_{\rho} P^{\rho}_{\mu\nu} - t_{\mu\nu} = \kappa^2 \mathcal{T}_{\mu\nu} \tag{30}$$

Here, the symmetric tensor

$$t_{\mu\nu} = -L^{\rho}{}_{\alpha\rho} P^{\alpha}_{\mu\nu} + L^{\alpha}{}_{\mu\rho} P^{\rho}_{\alpha\nu} + L^{\alpha}{}_{\nu\rho} P^{\rho}_{\mu\alpha} - \frac{1}{2}P_{\rho\mu\nu} Q^{\rho\sigma}{}_{\sigma} - \frac{1}{2}P_{\nu\rho\sigma} Q^{\rho\sigma}{}_{\mu} + P_{\rho\sigma\mu} Q^{\rho\sigma}{}_{\nu} + \frac{1}{2}g_{\mu\nu} Q \tag{31}$$

again appears in the equations in an analogous position to the energy momentum tensor of the matter and we might be tempted to interpret it as a kind of energy momentum of the gravitational field. Although all geometric tensors in the field equations are computed from the teleparallel connection, with a clever use of the geometric identities, it is possible to show that Equation (31) matches Einstein’s field Equation (13) exactly. Indeed, when all the terms in Equation (22) are expanded out in full, only the Levi-Civita part of the connection remains, while the nonmetricity components of the connection cancel each other out. Hence, given a matter energy momentum, both GR and STEGR predict exactly the same evolution for the metric field. There is no equation to give the nonmetricity part of the connection independent dynamics.

Leaving the matter sector in STEGR unaltered from GR, i.e., maintaining couplings to the metric and Levi-Civita connection only⁴, guarantees that the continuity Equation (14) holds as before. Hence, the massive particles still follow the geodesics of metric (15), but using the relation (2), we can rewrite it as

$$m\left(\frac{du^{\mu}}{d\tau} + \overset{\text{STP}}{\Gamma}{}^{\mu}{}_{\rho\sigma} u^{\rho} u^{\sigma}\right) = m \overset{\text{STP}}{L}{}^{\mu}{}_{\rho\sigma} u^{\rho} u^{\sigma}. \tag{32}$$

Analogously to the torsional case, the right-hand side with the disformation tensor looks like a force term, while the left-hand side says that in the absence of the force, a massive particle will move “straight” along an autoparallel of the symmetric teleparallel connection. Yet, both GR and STEGR prescribe identical paths for the particle motion through spacetime. Therefore, GR and STEGR are equivalent in the sense that they predict the same physical outcomes, but adding an extra connection allows one to present Equations (31) and (32) in a form where interpretation is more in line with the other well-established and understood theories of physics.

The options for the symmetric teleparallel connection that obey cosmological symmetry (9) and (10) were determined in refs. [56,57]. It turns out that for spatially flat connections there are three sets of solutions. Perhaps the simplest of those is set 1 (in the notation of refs. [58,59])

$$\overset{\text{STP}}{\Gamma}{}^{\rho}_{\mu\nu} = \begin{bmatrix} \left[\begin{array}{cccc} \gamma(t) & 0 & 0 & 0 \\ 0 & 0 & 0 & 0 \\ 0 & 0 & 0 & 0 \\ 0 & 0 & 0 & 0 \end{array} \right] \left[\begin{array}{cccc} 0 & 0 & 0 & 0 \\ 0 & 0 & 0 & 0 \\ 0 & 0 & -r & 0 \\ 0 & 0 & 0 & -r \sin^2 \theta \end{array} \right] \\ \left[\begin{array}{cccc} 0 & 0 & 0 & 0 \\ 0 & 0 & \frac{1}{r} & 0 \\ 0 & \frac{1}{r} & 0 & 0 \\ 0 & 0 & 0 & -\sin \theta \cos \theta \end{array} \right] \left[\begin{array}{cccc} 0 & 0 & 0 & 0 \\ 0 & 0 & 0 & \frac{1}{r} \\ 0 & 0 & 0 & \cot \theta \\ 0 & \frac{1}{r} & \cot \theta & 0 \end{array} \right] \end{bmatrix} \tag{33}$$

where $\gamma(t)$ is a free function. Substituting this connection, metric (11) and matter (12) into Equation (31) reproduces the Friedmann Equation (17) in general relativity exactly, with

$${}^{\text{STP}}t_{\mu\nu} = \begin{bmatrix} 3\gamma H & 0 & 0 & 0 \\ 0 & -a^2(2H^2 + \gamma H) & 0 & 0 \\ 0 & 0 & -a^2r^2(2H^2 + \gamma H) & 0 \\ 0 & 0 & 0 & -a^2r^2 \sin^2(\theta)a^2(2H^2 + \gamma H) \end{bmatrix}. \tag{34}$$

Again, the last quantity vanishes for a constant scale factor a , which is consistent with the expectation that empty space does not act as a source of itself. Although the free function $\gamma(t)$ enters (34), it cancels out in the full field in Equation (31). This is not a surprise, as this function is not present in GR, and GR equations do not contain anything to determine it.

For the particle motion, the “force” term on the right-hand side of Equation (32) is set by the disformation and can be found by computing (5) from (33), yielding

$${}^{\text{STP}}L^{\mu}_{\rho\sigma} = \begin{bmatrix} \gamma & 0 & 0 & 0 \\ 0 & -Ha^2 & 0 & 0 \\ 0 & 0 & -r^2Ha^2 & 0 \\ 0 & 0 & 0 & -r^2Ha^2 \sin^2(\theta) \end{bmatrix} \begin{bmatrix} 0 & -H & 0 & 0 \\ -H & 0 & 0 & 0 \\ 0 & 0 & 0 & 0 \\ 0 & 0 & 0 & 0 \end{bmatrix} \\ \begin{bmatrix} 0 & 0 & -H & 0 \\ 0 & 0 & 0 & 0 \\ -H & 0 & 0 & 0 \\ 0 & 0 & 0 & 0 \end{bmatrix} \begin{bmatrix} 0 & 0 & 0 & -H \\ 0 & 0 & 0 & 0 \\ 0 & 0 & 0 & 0 \\ -H & 0 & 0 & 0 \end{bmatrix}. \tag{35}$$

Interestingly, when there is no expansion ($\dot{a} = 0$) and the metric reduces to Minkowski, the disformation will still depend on the arbitrary function γ . This does not affect the actual particle trajectory, though, as in the equations of particle motion (32), the γ terms drop out. We may take γ to vanish identically without any constraints from the equations. This just illustrates how adding the non-Riemannian part to make the overall connection vanish contains an aspect of arbitrariness, as the split between inertia and force is up to our liking at this stage.

The two other symmetric teleparallel connections that obey the cosmological symmetries are rather similar [56,57]. They both introduce an arbitrary function, which by assumption cannot be zero. The cosmological field equations and particle motion equations are quite analogous to the previous case, and do not introduce qualitatively new features for our purposes. It can just be remarked that the free function γ of set 1 does not appear in the cosmological equations of extended symmetric teleparallel theories either [56,57], but the functions present in the alternative sets 2 and 3 become dynamical and can easily trigger a finite-time singularity in the extended theories [59].

3.5. General Teleparallel Equivalent of General Relativity (GTEGR)

Besides only activating torsion, as in teleparallel gravity, or only activating nonmetricity, as in symmetric teleparallel gravity, one may also entertain the option of having both a torsion and nonmetricity different from zero, while the curvature is still restricted to vanish. In such a setting, it is possible to formulate the general teleparallel equivalent of general relativity which gives the same equations and predictions as GR [18]. For this theory, the connections with cosmological symmetries were determined in ref. [60], and considerations in relation to the notion of energy were given in ref. [61]. In view of the present paper, GTEGR does not add qualitatively new features, and we will not go deeper into the details here.

4. Discussion

In this paper, we argue that there are at least three conventional elements in the standard Λ CDM cosmology; in addition to (1) dark matter and (2) dark energy, there is also (3) the type of geometry. The conventionality of the first two entities is discussed by

Merritt [4]. They are introduced with the aim of evading consequences of observations that can falsify the standard Λ CDM cosmology. However, in principle, it is possible that dark matter particles can be detectable by some non-gravitational means, or the effects otherwise attributed to dark matter can be explained by a suitable (ultra-low acceleration) modification to the gravitational force law testable in some other experiments as well. Similarly, it is conceivable that the source of dark energy can be independently identified as some new classical field or a quantum field theory or quantum gravity effect. Thus, in principle, it is possible to break the ad hoc nature of dark matter and dark energy. The character of the third element seems to be different however.

The third convention emerges if we take into account that local properties of the standard cosmology can be given in different geometrical frameworks that are observationally equivalent. We can write the same equations in GR with a Levi-Civita connection that has curvature in TEGR with a teleparallel connection that has an identically zero curvature but nontrivial torsion; in STEGR with a symmetric teleparallel connection that is endowed with nonzero nonmetricity but vanishing curvature; or in GTEGR with a general teleparallel connection where the curvature is zero but both torsion and nonmetricity can be present. Despite invoking these different geometric structures, Einstein's field equations and particle motion equations reduce to the same immediate mathematical content in all formulations and predict the same physical outcomes for given initial conditions.

The situation is reminiscent of the geometric conventionality presented by Poincaré [6], who envisioned how an infinite Euclidean background can be transformed into a finite non-Euclidean background by introducing universal distorting forces. Poincaré concluded that the corresponding sets of geometric axioms are neither synthetic a priori nor experimental facts; they are conventions that allow us to choose the mathematical framework to be applied. The choice is not determined by experiments or observations, although it must be in line with their results and, last but not least, must avoid contradictions.

In the modern teleparallel version of geometric conventionalism, as we saw in Section 3, the split between the "source" and "kinetic" terms of the Einstein's field equations, or the "inertia" and "force" terms in the particle motion equations, is a convention, up to the choice of the formulation or different choices of connection classes within a given formulation. It may even be up to the choice of an arbitrary function in a particular class of connections within a given formulation. To be more precise, the metric structure in geometry can be related to a physical observable as giving a distance between spacetime points. It also defines the light cones that determine which points can be causally connected. Thus, the different formulations of GR do not diverge about the metric, otherwise the empirical equivalence would be broken. On the other hand, the different formulations prescribe different connections in setting up the underlying geometry. The basic role of the connection is to define which path is "straight", whereby any physicist immediately recalls Newton's first law. However, as soon as one departs from the absolute space of Newton and intermingles gravity with geometry, the "straightness" of particle motion becomes ambiguous. Even if for one connection some path (a collection of points) is "straight", i.e., autoparallel as defined by that connection, for another connection, the same path (the same collection of points) is not "straight" any more, while the deviation can be attributed to a corresponding "force" acting on the particle. Empirically, what is available for observation is the path, not its "straightness". The choice of the connection is a convention, in spite of how contrary to the usual GR intuition this statement is. If we can choose which type of geometry we use, then none of them can be considered as describing the "real" spacetime, at least from the point of view of local equations of motion.

At this point, one may object that the Levi-Civita connection is the unique connection obtainable from the metric and it is the minimal but sufficient choice to describe all phenomena within the purview of GR and its empirical equivalents. Hence, to keep the list of agents in the game as short as possible, by the principle of Occam's razor, we can drop the extra non-Riemannian parts of connection as they are superfluous, do not contribute any observable effects and are not even determined by the equations. While this view has

its merits, a counterargument can compare the choice of the connection to the choice of a gauge in electrodynamics. Although different gauge choices of the vector potential imply the same electric and magnetic field strengths and the same motion for a charged particle, in some gauges, the practical computations can become much more economical to perform. Similarly, it may happen that a good choice of the connection can considerably simplify the gravitational calculations. For example, in symmetric teleparallelism, there always exists a coordinate system where the connection vanishes identically in the whole spacetime, and thus the covariant derivatives reduce to plain partial derivatives, called a ‘coincident gauge’ [10].⁵ In practical terms, if picking a good extra connection would help in running the numerical simulations in gravity or assist in a consistent quantisation of gravity, the blade of Occam’s razor could be turned the other way.

Given that GR, TEGR, STEGR and GTEGR are empirically equivalent, it remains to ask whether they are also theoretically equivalent? The answer, of course, depends on the philosophical definition of the notion of theoretical equivalence. Instead of delving deeply into that discussion, let us instead mention a few aspects from a more physical point of view. Since the theories are still under active investigation and development, the following remarks only reflect the present state of understanding (of the authors).

First, the fundamental theories of physics obey the action principle, whereby a single mathematical expression encodes all information about the theory, as the equations, conserved quantities and other features can be derived from it. The actions of GR and those of TEGR, STEGR and GTEGR differ by their respective boundary terms [10,11,14]. This means that their field equations are fully equivalent in the usual spacetimes without boundaries, as in the case of Friedmann cosmology. That explains why Equations (13), (22) and (30) match. In more complicated situations of spacetimes with boundaries like the braneworld models, the presence of a boundary might require extra source terms in the action. However, the question of how the correspondence between the different formulations actually works out in that case has not received much attention yet. In addition, there is a broader issue of whether the equations of motion are all that are relevant in physics. While the boundary term in the action does not affect the field equations in the bulk, it can still play a role in something. For example, the correct account of the black hole entropy and thus the establishment of generalised thermodynamics wholly depends on the boundary term in the GR action [28]. The investigation into black hole thermodynamics in the teleparallel context has barely begun [45,46,63,64], and we do not know whether a consistent account can be given in all the formulations.

The second issue is the well-established problem of gravitational energy, where Noether’s theorem applied to GR does not yield a local quantity that would be both covariant and conserved [65]. At best, one can entertain global integral quantities for asymptotically flat spacetimes. Since the early days [33], the hope of finding a consistent definition of energy for the gravitational field has been one motivating factor in the investigations of teleparallel theories, and there are different proposals and arguments in the recent literature [38–51]. At the present moment, there is not yet a consensus on whether a universal definition of gravitational energy–momentum can be given, how it is given and whether it can be given in all or only in a specific formulation of the otherwise empirically equivalent family of formulations. Although different assignments of energy to spacetime configurations may not alter any of the observable predictions, it could be that a certain formulation of the theory is preferable in terms of elegance and consistency with the rest of physical theories. Or it could be that in the end, all formulations turn out to be equivalent also in this respect.

Third, the equivalence discussed so far concerns just the local properties of the theory, represented by the field equations and motion of test particles. The global properties of the corresponding spacetimes, including the effects of topology, have not yet been investigated much. It is a well-known fact in topology that not all spaces admit global parallelization. Even in the case of Friedmann cosmology, the metric (11) is compatible with different topologies by clever global indentifications, and such scenarios are not completely ruled

out by current observations [66]. Thus, it remains an open problem how the teleparallel constructions would fare in nontrivial topologies, and whether the equivalence would still stand.

5. Conclusions

We think that it is not surprising that our cosmological standard model contains so many parts that are fixed by conventions. Much more surprising is the fact that not all of our cosmological knowledge is a conventional narrative only.

Author Contributions: Investigation, validation, formal analysis, supervision, writing—review, editing, funding acquisition, project administration: L.J. and P.K.; conceptualization, methodology, writing—original draft preparation: P.K. All authors have read and agreed to the published version of the manuscript.

Funding: The work was supported by the Estonian Research Council grant PRG356 “Gauge Gravity”. The authors also acknowledge support from the European Regional Development Fund through the Center of Excellence TK133 “The Dark Side of the Universe”.

Data Availability Statement: Data are contained within the article.

Conflicts of Interest: The authors declare no conflict of interest.

Abbreviations

The following abbreviations are used in this manuscript:

FLRW	Friedmann–Lemaître–Robertson–Walker
GR	general relativity
GTEGR	general teleparallel equivalent of general relativity
STEGR	symmetric teleparallel equivalent of general relativity
TEGR	teleparallel equivalent of general relativity

Notes

- 1 The issue of gravitational energy-momentum in teleparallel gravity has seen quite some developments and arguments [38–51], but we do not intend to make a strong claim here.
- 2 Modification of the matter sector with added couplings to the non-Riemannian part of the connection typically introduces new terms in the continuity equation and particle motion equation [52], breaking the equivalence with GR.
- 3 Often in the literature the factor $\frac{1}{2}$ in (28) is moved into the definition (29).
- 4 For simple scalar, spinor and vector fields, we may actually replace the Levi-Civita connection with the symmetric teleparallel connection [55].
- 5 In these coordinates, the metric typically becomes more complicated though, which can considerably curb the benefits in calculational economy [62].

References

1. Perivolaropoulos, L.; Skara, F. Challenges for Λ CDM: An update. *New Astron. Rev.* **2022**, *95*, 101659. [CrossRef]
2. Heisenberg, L. A systematic approach to generalisations of General Relativity and their cosmological implications. *Phys. Rep.* **2019**, *796*, 1–113. [CrossRef]
3. Saridakis, E. N.; Lazkoz, R.; Salzano, V.; Vargas Moniz, P.; Capozziello, S.; Beltrán Jiménez, J.; De Laurentis, M.; Olmo, G. J. *Modified Gravity and Cosmology: An Update by the CANTATA Network*; Springer: Berlin/Heidelberg, Germany, 2021. [CrossRef]
4. Merritt, D. Cosmology and convention. *Stud. Hist. Philos. Mod. Phys.* **2017**, *57*, 41–52. [CrossRef]
5. Duhem, P. *La Théorie Physique: Son Objet et sa Structure*; M. Rivière: Paris, France, 1914.
6. Poincaré, H. *La Science et l’Hypothèse*; Flammarion: Paris, France, 1902.
7. Popper, K.R. *The Logic of Scientific Discovery*; Basic Books: New York, NY, USA, 1959.
8. Aldrovandi, R.; Pereira, J.G. *Teleparallel Gravity*; Springer: Dordrecht, The Netherlands, 2013; Volume 173. [CrossRef]
9. Krššák, M.; van den Hoogen, R.J.; Pereira, J.G.; Böhmer, C.G.; Coley, A.A. Teleparallel theories of gravity: Illuminating a fully invariant approach. *Class. Quant. Grav.* **2019**, *36*, 183001. [CrossRef]
10. Beltrán Jiménez, J.; Heisenberg, L.; Koivisto, T. Coincident General Relativity. *Phys. Rev. D* **2018**, *98*, 044048. [CrossRef]
11. Järvi, L.; Rünkla, M.; Saal, M.; Vilson, O. Nonmetricity formulation of general relativity and its scalar-tensor extension. *Phys. Rev. D* **2018**, *97*, 124025. [CrossRef]

12. Beltrán Jiménez, J.; Heisenberg, L.; Koivisto, T.S. The Geometrical Trinity of Gravity. *Universe* **2019**, *5*, 173. [CrossRef]
13. Capozziello, S.; De Falco, V.; Ferrara, C. Comparing equivalent gravities: Common features and differences. *Eur. Phys. J. C* **2022**, *82*, 865. [CrossRef]
14. Heisenberg, L. Review on $f(Q)$ Gravity. *arXiv* **2023**, arXiv:2309.15958.
15. Wolf, W.J.; Read, J. The Non-Relativistic Geometric Trinity of Gravity. *arXiv* **2023**, arXiv:2308.07100.
16. Wolf, W.J.; Sanchioni, M.; Read, J. Underdetermination in Classic and Modern Tests of General Relativity. *arXiv* **2023**, arXiv:2307.10074.
17. Capozziello, S.; De Falco, V.; Ferrara, C. The role of the boundary term in $f(Q, B)$ symmetric teleparallel gravity. *Eur. Phys. J. C* **2023**, *83*, 915. [CrossRef]
18. Beltrán Jiménez, J.; Heisenberg, L.; Iosifidis, D.; Jiménez-Cano, A.; Koivisto, T.S. General teleparallel quadratic gravity. *Phys. Lett. B* **2020**, *805*, 135422. [CrossRef]
19. Weatherall, J.O. Part 2: Theoretical equivalence in physics. *Philos. Compass* **2018**, *14*, e12591. [CrossRef]
20. Duerr, P.M. Theory (In-)Equivalence and conventionalism in $f(R)$ gravity. *Stud. Hist. Philos. Sci.* **2021**, *88*, 10–29. [CrossRef] [PubMed]
21. Coffey, K. Theoretical equivalence as interpretational equivalence. *Br. J. Philos. Sci.* **2014**, *65*, 821–844. [CrossRef]
22. Koberinski, A.; Falck, B.; Smeenk, C. Contemporary Philosophical Perspectives on the Cosmological Constant. *Universe* **2023**, *9*, 134. [CrossRef]
23. Quine, W.V.O. On empirically equivalent systems of the world. *Erkenntnis* **1975**, *9*, 313–328. [CrossRef]
24. Feynman, R.P. *Feynman Lectures on Gravitation*; Addison–Wesley Publishing Company: Boston, MA, USA, 1995.
25. Weinberg, S. *Gravitation and Cosmology: Principles and Applications of the General Theory of Relativity*; John Wiley and Sons, Inc.: Hoboken, NJ, USA, 1972.
26. Knox, E. Newton–Cartan theory and teleparallel gravity: The force of a formulation. *Stud. Hist. Philos. Mod. Phys.* **2011**, *42*, 264–275. [CrossRef]
27. Read, J.; Menon, T. The limitations of inertial frame spacetime functionalism. *Synthese* **2021**, *199* (Suppl. 2), S229–S251. [CrossRef]
28. Wolf, W.J.; Read, J. Respecting Boundaries: Theoretical equivalence and structure beyond dynamics. *Eur. J. Philos. Sci.* **2023**, *13*, 1–28. [CrossRef]
29. Hohmann, M.; Järv, L.; Krššák, M.; Pfeifer, C. Modified teleparallel theories of gravity in symmetric spacetimes. *Phys. Rev. D* **2019**, *100*, 084002. [CrossRef]
30. Einstein, A. Riemann-Geometrie mit Aufrechthaltung des Begriffes des Fernparallelismus. In *Sitzungsberichte der Preussischen Akademie der Wissenschaften, Physikalisch-Mathematische Klasse*; Berlin, Germany, 1928; pp. 217–221.
31. Einstein, A. Neue Möglichkeit für eine einheitliche Feldtheorie von Gravitation und Elektrizität. In *Sitzungsberichte der Preussische Akademie der Wissenschaften, Physikalisch-Mathematische Klasse*; Berlin, Germany, 1928; pp. 224–227.
32. Weitzenböck, R. *Invariantentheorie*; Noordhoff: Groningen, The Netherlands, 1928.
33. Møller, C. Conservation laws and absolute parallelism in general relativity. In *Volume 1: Det Kongelige Danske Videnskabernes Selskab, Matematisk-Fysiske Skrifter*; Munksgaard: Copenhagen, Denmark, 1961.
34. Pellegrini, C.; Plebański, J. Tetrad fields and gravitational fields. In *Volume 2: Det Kongelige Danske Videnskabernes Selskab, Matematisk-Fysiske Skrifter*; Munksgaard: Copenhagen, Denmark, 1963. [CrossRef]
35. Hayashi, K.; Nakano, T. Extended translation invariance and associated gauge fields. *Prog. Theor. Phys.* **1967**, *38*, 491–507. [CrossRef]
36. Bahamonde, S.; Dialektopoulos, K.F.; Escamilla-Rivera, C.; Farrugia, G.; Gakis, V.; Hendry, M.; Hohmann, M.; Levi Said, J.; Mifsud, J.; Di Valentino, E. Teleparallel gravity: From theory to cosmology. *Rept. Prog. Phys.* **2023**, *86*, 026901. [CrossRef] [PubMed]
37. Hohmann, M.; Järv, L.; Ualikhanova, U. Covariant formulation of scalar-torsion gravity. *Phys. Rev. D* **2018**, *97*, 104011. [CrossRef]
38. de Andrade, V.C.; Guillen, L.C.T.; Pereira, J.G. Gravitational energy momentum density in teleparallel gravity. *Phys. Rev. Lett.* **2000**, *84*, 4533–4536. [CrossRef] [PubMed]
39. Vargas, T. The Energy of the universe in teleparallel gravity. *Gen. Rel. Grav.* **2004**, *36*, 1255. [CrossRef]
40. Maluf, J.W.; da Rocha-Neto, J.F.; Toribio, T.M.L.; Castello-Branco, K.H. Energy and angular momentum of the gravitational field in the teleparallel geometry. *Phys. Rev. D* **2002**, *65*, 124001. [CrossRef]
41. Obukhov, Y.N.; Rubilar, G.F.; Pereira, J.G. Conserved currents in gravitational models with quasi-invariant Lagrangians: Application to teleparallel gravity. *Phys. Rev. D* **2006**, *74*, 104007. [CrossRef]
42. Ulhoa, S.C.; da Rocha Neto, J.F.; Maluf, J.W. The Gravitational Energy Problem for Cosmological Models in Teleparallel Gravity. *Int. J. Mod. Phys. D* **2010**, *19*, 1925–1935. [CrossRef]
43. Krššák, M.; Pereira, J.G. Spin Connection and Renormalization of Teleparallel Action. *Eur. Phys. J. C* **2015**, *75*, 519. [CrossRef]
44. Hohmann, M.; Järv, L.; Krššák, M.; Pfeifer, C. Teleparallel theories of gravity as analogue of nonlinear electrodynamics. *Phys. Rev. D* **2018**, *97*, 104042. [CrossRef]
45. Beltrán Jiménez, J.; Koivisto, T.S. Noether charges in the geometrical trinity of gravity. *Phys. Rev. D* **2022**, *105*, L021502. [CrossRef]
46. Gomes, D.A.; Beltrán Jiménez, J.; Koivisto, T.S. Energy and entropy in the geometrical trinity of gravity. *Phys. Rev. D* **2023**, *107*, 024044. [CrossRef]
47. Emtsova, E.D.; Petrov, A.N.; Toporensky, A.V. Conserved currents and superpotentials in teleparallel equivalent of GR. *Class. Quant. Grav.* **2020**, *37*, 095006. [CrossRef]

48. Emtsova, E.D.; Petrov, A.N.; Toporensky, A.V. Conserved quantities in STEGR and applications. *Eur. Phys. J. C* **2023**, *83*, 366. [CrossRef]
49. Formiga, J.B.; Gonçalves, V.R. Generalization of the ADM gravitational energy momentum. *Phys. Rev. D* **2022**, *106*, 044021. [CrossRef]
50. Maluf, J.W.; Carneiro, F.L.; Ulhoa, S.C.; da Rocha-Neto, J.F. Tetrad Fields, Reference Frames, and the Gravitational Energy-Momentum in the Teleparallel Equivalent of General Relativity. *arXiv* **2023**, arXiv:2306.03676.
51. Golovnev, A. A Pamphlet against The Energy. *arXiv* **2023**, arXiv:2306.12895.
52. Iosifidis, D.; Hehl, F.W. Motion of Test Particles in Spacetimes with Torsion and Nonmetricity. *arXiv* **2023**, arXiv:2310.15595.
53. Nester, J.M.; Yo, H.J. Symmetric teleparallel general relativity. *Chin. J. Phys.* **1999**, *37*, 113. [CrossRef]
54. Bahamonde, S.; Gigante Valcarcel, J.; Järv, L.; Lember, J. Black hole solutions in scalar-tensor symmetric teleparallel gravity. *J. Cosmol. Astropart. Phys.* **2022**, *8*, 082. [CrossRef]
55. Beltrán Jiménez, J.; Heisenberg, L.; Koivisto, T. The coupling of matter and spacetime geometry. *Class. Quant. Grav.* **2020**, *37*, 195013. [CrossRef]
56. Hohmann, M. General covariant symmetric teleparallel cosmology. *Phys. Rev. D* **2021**, *104*, 124077. [CrossRef]
57. D'Ambrosio, F.; Heisenberg, L.; Kuhn, S. Revisiting cosmologies in teleparallelism. *Class. Quant. Grav.* **2022**, *39*, 025013. [CrossRef]
58. Dimakis, N.; Paliathanasis, A.; Roumeliotis, M.; Christodoulakis, T. FLRW solutions in $f(Q)$ theory: The effect of using different connections. *Phys. Rev. D* **2022**, *106*, 043509. [CrossRef]
59. Jarv, L.; Pati, L. Stability of symmetric teleparallel scalar-tensor cosmologies with alternative connections. *arXiv* **2023**, arXiv:2309.04262.
60. Heisenberg, L.; Hohmann, M.; Kuhn, S. Homogeneous and isotropic cosmology in general teleparallel gravity. *Eur. Phys. J. C* **2023**, *83*, 315. [CrossRef]
61. Gomes, D.A.; Jiménez, J.B.; Koivisto, T.S. General Parallel Cosmology. *arXiv* **2023**, arXiv:2309.08554.
62. Bahamonde, S.; Järv, L. Coincident gauge for static spherical field configurations in symmetric teleparallel gravity. *Eur. Phys. J. C* **2022**, *82*, 963. [CrossRef]
63. Hammad, F.; Dijamco, D.; Torres-Rivas, A.; Bérubé, D. Noether charge and black hole entropy in teleparallel gravity. *Phys. Rev. D* **2019**, *100*, 124040. [CrossRef]
64. Fiorini, F.; González, P.A.; Vásquez, Y. Reference Frames and Black Hole Thermodynamics. *arXiv* **2023**, arXiv:2309.06293.
65. Duerr, P.M. Fantastic Beasts and where (not) to find them: Local gravitational energy and energy conservation in general relativity. *Stud. Hist. Phil. Sci. B* **2019**, *65*, 1–14. [CrossRef]
66. Luminet, J.P. The Status of Cosmic Topology after Planck Data. *Universe* **2016**, *2*, 1. [CrossRef]

Disclaimer/Publisher's Note: The statements, opinions and data contained in all publications are solely those of the individual author(s) and contributor(s) and not of MDPI and/or the editor(s). MDPI and/or the editor(s) disclaim responsibility for any injury to people or property resulting from any ideas, methods, instructions or products referred to in the content.

Improved Model of Primordial Black Hole Formation after Starobinsky Inflation

Sultan Saburov¹ and Sergei V. Ketov^{1,2,3,*} 

- ¹ Interdisciplinary Research Laboratory, Tomsk State University, Tomsk 634050, Russia; saburov@mail.tsu.ru
² Department of Physics, Tokyo Metropolitan University, 1-1 Minami-ohsawa, Hachioji 192-0397, Japan
³ Kavli Institute for the Physics and Mathematics of the Universe (WPI), The University of Tokyo Institutes for Advanced Study, Chiba 277-8583, Japan
* Correspondence: ketov@tmu.ac.jp

Abstract: A new (improved) model of inflation and primordial black hole (PBH) formation is proposed by combining the Starobinsky model of inflation, Appleby–Battye–Starobinsky (ABS) model of dark energy, and a quantum correction in the modified $F(R)$ gravity. The energy scale parameter in the ABS model is taken to be close to the inflationary scale, in order to describe double inflation instead of dark energy. The quantum correction is given by the term quartic in the spacetime scalar curvature R with a negative coefficient ($-\delta$) in the $F(R)$ function. It is demonstrated that very good agreement (within 1σ) with current measurements of the cosmic microwave background (CMB) radiation can be achieved by choosing the proper value of δ , thus solving the problem of low values of the tilt of CMB scalar perturbations in the earlier proposed model in arXiv:2205.00603. A large (by a factor of 10^7 against CMB) enhancement in the power spectrum of scalar perturbations is achieved by fine tuning the parameters of the model. It is found by numerical analysis that it can lead to formation of asteroid-size PBHs with masses up to 10^{20} g, which may form dark matter in the current universe.

Keywords: inflation; primordial black holes; dark matter



Citation: Saburov, S.; Ketov, S.V. Improved Model of Primordial Black Hole Formation after Starobinsky Inflation. *Universe* **2023**, *9*, 323. <https://doi.org/10.3390/universe9070323>

Academic Editors: Galina L. Klimchitskaya, Vladimir M. Mostepanenko and Sergey V. Sushkov

Received: 15 June 2023
Revised: 29 June 2023
Accepted: 5 July 2023
Published: 6 July 2023



Copyright: © 2023 by the authors. Licensee MDPI, Basel, Switzerland. This article is an open access article distributed under the terms and conditions of the Creative Commons Attribution (CC BY) license (<https://creativecommons.org/licenses/by/4.0/>).

1. Introduction

This year is the centennial anniversary of Friedmann’s prediction for expanding universe, which was based on a nonstationary solution to Einstein’s equations. In recent years, the expanding universe was extended by other important features, such as cosmological inflation, dark matter, and dark energy.

A paradigm of inflation in the early universe, proposed a long time ago [1,2] as a possible solution to internal problems in theoretical cosmology (flatness, horizon, initial conditions, and structure formation), is currently well supported by precision measurements of the cosmic microwave background (CMB) radiation by WMAP and Planck satellite missions combined with recent BICEP/Keck data [3–5]. The original (1980) Starobinsky model of inflation [6] gives a simple theoretical description of inflation by using only gravitational interactions, which is in very good agreement with the current CMB measurements. It is, therefore, natural to extend the Starobinsky model of inflation by including more features, such as production of primordial black holes (PBH). The PBH formation may explain the origin of black holes and dark matter in the current universe [7–12].

In modern terms, see, e.g., Refs. [13–15] for more details, the Starobinsky model is a special case among modified gravity theories with the action:

$$S = \frac{M_{\text{Pl}}^2}{2} \int d^4x \sqrt{-g} F(R) . \quad (1)$$

The Starobinsky F -function of spacetime scalar curvature R is given by:

$$F_S(R) = R + \frac{R^2}{6M^2}, \tag{2}$$

where $M_{\text{Pl}} = (8\pi G)^{-1/2} = 2.435 \times 10^{18}$ GeV is the reduced Planck mass and M is the only (mass) parameter. The known CMB amplitude determines $M \approx 1.3 \times 10^{-5} M_{\text{Pl}}$, so that the Starobinsky model has no free parameters.

An $F(R)$ -gravity model is well known to be equivalent to the quintessence (scalar-tensor) gravity model in terms of the inflaton scalar field ϕ with the scalar potential $V(R(\phi))$ in the parametric form, see, e.g., Refs. [16,17] for a derivation:

$$V(R) = M_{\text{Pl}}^2 \frac{F'R - F}{2(F')^2}, \quad \phi(R) = \sqrt{\frac{3}{2}} M_{\text{Pl}} \ln F', \tag{3}$$

where the primes denote the derivatives with respect to the given variable (R). It is usually impossible to analytically derive the inverse function $R(\phi)$ from a given function $\phi(R)$, with the notable exception being the Starobinsky case (2), where one obtains a simple and well-known answer:

$$V_S(\phi) = \frac{3}{4} M_{\text{Pl}}^2 M^2 \left[1 - \exp\left(-\sqrt{\frac{2}{3}} \phi / M_{\text{Pl}}\right) \right]^2. \tag{4}$$

To form PBH out of a gravitational collapse of large (curvature) perturbations in the early universe, one needs a large enhancement of the power spectrum of scalar perturbations by six or seven orders of magnitude against the CMB spectrum. In the context of single-field models of inflation, it can be achieved in the double inflation scenario via engineering a near-inflection point in the inflaton scalar potential at lower (than inflation) scales [10,18]. The potential (4) does not have an inflection point and, hence, does not lead to PBH production. However, one can modify the Starobinsky $F(R)$ -gravity function (2) by extra terms that lead to an inflection point. This should be done in agreement with CMB observables, leading to constraints on eligible F -functions. Moreover, there are other conditions, such as absence of ghosts and singularities, and the correct Newtonian limit. Once all the necessary conditions are satisfied, one has to achieve the required enhancement of the power spectrum and generate PBH with the masses beyond the Hawking radiation limit of 10^{15} g because, otherwise, all those PBH would evaporate before the present times.

These problems were partially solved in Ref. [19] by adding to the $F(R)$ -gravity function (2) the additional terms known in the literature as the Appleby–Battye–Starobinsky (ABS) model of dark energy [20], and described by the F -function:

$$F_{\text{ABS}}(R) = (1 - g)R + gE_{\text{AB}} \ln \left[\frac{\cosh\left(\frac{R}{E_{\text{AB}}} - b\right)}{\cosh(b)} \right], \tag{5}$$

where the Appleby–Battye parameter E_{AB} has been introduced as:

$$E_{\text{AB}} = \frac{R_0}{2g \ln(1 + e^{2b})} \tag{6}$$

with the new dimensional scale R_0 and the dimensionless positive parameters g and b . The function (5) was carefully chosen in Ref. [20] in order to meet the no-ghost (stability) conditions in modified $F(R)$ gravity, which are given by:

$$F'(R) > 0 \quad \text{and} \quad F''(R) > 0, \tag{7}$$

it avoids singularities, obeys the Newtonian limit, and mimics a positive cosmological constant representing the dark energy for $R \gg R_0$ with proper values of the parameters g and b defining the shape of the scalar potential. To describe the present dark energy in the universe, the parameter R_0 representing the vacuum value of the scalar curvature should be very small, $\sqrt{R_0} \sim 10^{-33}$ eV and, hence, the AB-parameter should be small too.

The shape of the F -function (5), thus, leads to a meta-stable de Sitter vacuum after inflation and, hence, a near-inflection point in the potential. In Ref. [19], the dark energy value of $\sqrt{R_0}$ was replaced by a much higher value of the order M below the inflationary scale $H_{\text{inf.}} \sim 10^{14}$ GeV.¹ The new model with the F -function:

$$F_{\text{modified}}(R) = F_{\text{ABS}}(R) + \frac{R^2}{6M^2} \tag{8}$$

leads to the desired enhancement of the power spectrum of scalar perturbations and the formation of PBH with the asteroid-size masses of an order of 10^{19} g, which may form the whole dark matter in the present universe. In order to obtain these results, the parameters g and b were fine tuned, but agreement with the observed CMB tilt n_s of scalar perturbations was not good enough (outside 1σ but within 3σ lower) in Ref. [19].

In this communication, we propose the improved (new) model of Starobinsky inflation and PBH formation, having very good agreement (within 1σ) to CMB measurements. The new model is defined in Section 2 by combining phenomenological and theoretical considerations. Inflation is studied in Section 3. The power spectrum is derived in Section 4 together with the PBH masses. Section 5 contains our Conclusion.

2. The New Model

Our improved modified gravity model is (phenomenologically) defined by the F -function:

$$F(R) = (1 - g_1)R + gE_{AB} \ln \left[\frac{\cosh\left(\frac{R}{E_{AB}} - b\right)}{\cosh(b)} \right] + \frac{R^2}{6M^2} - \delta \frac{R^4}{48M^6} , \tag{9}$$

where we have changed the coefficient at the first term with another parameter $g_1 \neq g$ and have added the new term quartic in R with the new parameter δ . The AB parameter E_{AB} is still defined by Equation (6), where $R_0 = \beta M^2$ with yet another parameter β . All the parameters (g_1, g, b, β, δ) are dimensionless by definition.

The significance of each term in Equation (9) can be explained as follows.

The second term in Equation (9) becomes approximately linear in R both for small and large values of R/E_{AB} , and thus, correlates with the first term linear in R . Hence, in the low-curvature regime for small values of R/E_{AB} , consistency with gravity measurements inside the Solar system requires the Einstein–Hilbert effective action, which implies the following relation:

$$g_1 = -g \tanh b . \tag{10}$$

Starobinsky inflation is essentially governed by the third term quadratic in R in Equation (9), which leads to inflaton slow-roll (SR) in the high-curvature regime for the values of R/M^2 between 220 and 10 [17]. The scalar potential (4) of the Starobinsky model has an infinite plateau, which allows arbitrary duration of inflation, measured by a number N_e of e-folds. However, the Starobinsky inflation is unstable against quantum gravity corrections of the higher order in the scalar curvature. As was demonstrated in Refs. [21–23], the leading superstring-inspired quantum correction should be quartic in R , while it eliminates the infinite plateau in the Starobinsky potential and, hence, restricts the maximal number of e-folds. In order to be consistent with CMB measurements, the value of the δ -coefficient should be small enough, for instance, $|\delta| < 3.9 \times 10^{-6}$ according to Ref. [21].

It was assumed in Ref. [21] that the coefficient in front of the R^4 term is positive, which led to the inflaton scalar potential going down and hilltop inflation. In this paper, this coefficient is taken to be negative ($-\delta < 0$), which leads to the potential going up before inflation, see the next Section. The quartic term with $\delta > 0$ in Equation (9) is also responsible for raising the CMB values of the scalar tilt n_s in the improved model (9) against those in Ref. [19], as is demonstrated below. A similar effect was noticed in the modified E-type inflationary models of alpha-attractors and PBH formation, proposed in Ref. [24].

PBH formation may happen at the energy scales below the inflationary scale, which are governed by the parameter $\sqrt{R_0}$ of the order M . Hence, the parameter β in Equation (9) should be of the order one. The remaining parameters g and b are also of the order one, while their values should be tuned in order to generate a large peak $\sim 10^{-2}$ in the power spectrum of scalar perturbations. This can only be done numerically by scanning the parameter space, as in Refs. [19,24].

We found that in the model (9), the parameters (β, g, b) must be fine tuned to very specific values, namely:

$$\beta \approx 3.00, \quad g \approx 2.25 \quad \text{and} \quad b \approx 2.89, \tag{11}$$

because, otherwise, a peak in the power spectrum is either absent, too small, or too high.

It is easy to verify that the first and second derivatives of the F -function (9) are positive:

$$F'(R) = 1 + g \tanh(b) + g \tanh\left(\frac{R}{E_{AB}} - b\right) + \frac{R}{3M^2} - \frac{\delta R^3}{12M^6} > 0 \tag{12}$$

and

$$F''(R) = \frac{g}{E_{AB}} \operatorname{sech}^2\left(\frac{R}{E_{AB}} - b\right) + \frac{1}{3M^2} - \frac{\delta R^2}{4M^6} > 0, \tag{13}$$

for the given values of the parameters and the relevant values of $R < 240M^2$.

3. Inflaton Potential and Slow-Roll

According to Equations (3) and (9), the scalar potential $V(\phi)$ of the inflaton field ϕ in the parametric form (with the parameter R) is given by:

$$\begin{aligned} \frac{V(R)}{M_{\text{Pl}}^4} &= \frac{1}{2} e^{-2\sqrt{\frac{2}{3}}\phi/M_{\text{Pl}}} \times \\ &\times \left\{ gR \tanh\left(\frac{R}{E_{AB}} - b\right) - gE_{AB} \ln\left[\frac{\cosh\left(\frac{R}{E_{AB}} - b\right)}{\cosh(b)}\right] + \frac{R^2}{6M^2} - \frac{\delta R^4}{16M^6} \right\}, \end{aligned} \tag{14}$$

where

$$\exp\left(\sqrt{\frac{2}{3}}\frac{\phi}{M_{\text{Pl}}}\right) = 1 + g \tanh(b) + g \tanh\left(\frac{R}{E_{AB}} - b\right) + \frac{R}{3M^2} - \frac{\delta R^3}{12M^6}. \tag{15}$$

The function $\phi(R)$ in Equation (15) cannot be inverted in a useful analytic form, so we employ numerical calculations with Mathematica in what follows. The profiles of the inflaton potential $V(\phi)$ for the selected values of R_0 and δ are given in Figure 1.

The plot on the left-hand side of Figure 1 demonstrates that the potential has two plateaus at different scales; it is going up for $\delta > 0$ before inflation, while the value of the parameter δ determines the location where the potential goes up at the beginning of SR inflation. The height of the higher (Starobinsky) plateau is determined by M , the height of the lower plateau is controlled by R_0 , the length of the lower plateau is controlled by g , and the flatness of the lower plateau is controlled by b . The plot on the right-hand side of

Figure 1 shows a shallow meta-stable de Sitter minimum (dip), a near-inflection point, and a small bump (local maximum).

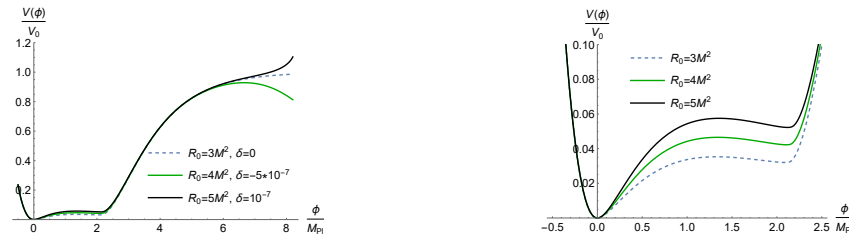


Figure 1. The inflaton potential for selected values of R_0 and δ at fixed $g = 2.25$ and $b = 2.89$ with $V_0 = \frac{3}{4} M_{\text{Pl}}^2 M^2$ (on the left). The potential for low values of ϕ / M_{Pl} are shown on the right.

The inflaton potential $V(\phi)$ for selected values of g at fixed $R_0 = 4M^2$ and $b = 2.89$ is displayed in Figure 2. This figure shows that duration of the second inflation (length of the lower plateau) is sensitive to the value of the parameter g . The longest lower plateau corresponds to $g \approx 3.0$.

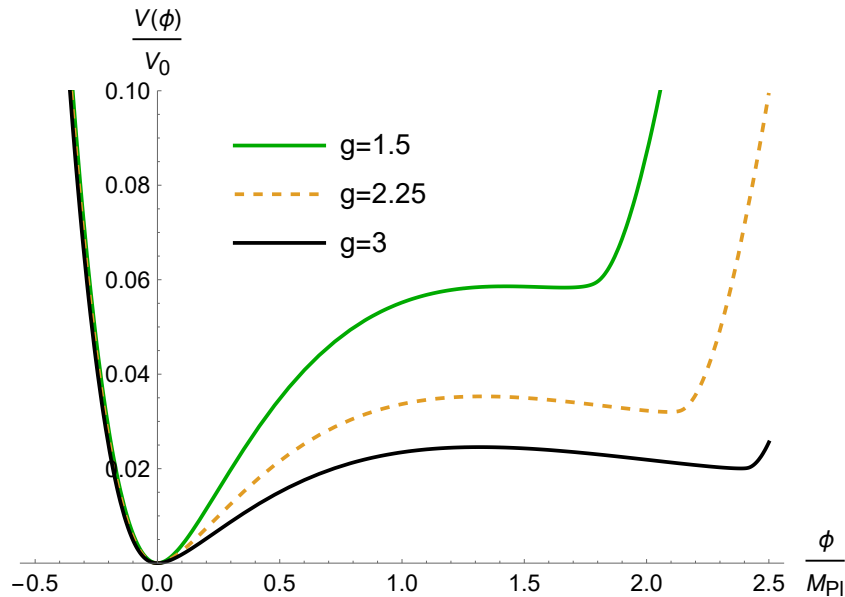


Figure 2. The inflaton potential for selected values of g at fixed $R_0 = 4M^2$ and $b = 2.89$.

The SR conditions are given by smallness of the standard SR parameters, $\epsilon_{\text{sr}} \ll 1$ and $|\eta_{\text{sr}}| \ll 1$, where:

$$\epsilon_{\text{sr}}(\phi) = \frac{M_{\text{Pl}}^2}{2} \left(\frac{V'(\phi)}{V(\phi)} \right)^2 \quad \text{and} \quad \eta_{\text{sr}}(\phi) = M_{\text{Pl}}^2 \frac{V''(\phi)}{V(\phi)}. \tag{16}$$

A duration of inflation is defined by the number N of e-folds:

$$N = \int_{t_{\text{in}}}^{t_{\text{end}}} H(t) dt \approx \frac{1}{M_{\text{Pl}}^2} \int_{\phi_{\text{end}}}^{\phi_{\text{in}}} \frac{V(\phi)}{V'(\phi)} d\phi, \tag{17}$$

where $H(t)$ is the Hubble function. The CMB observable (tilt) n_s of scalar perturbations and the tensor-to-scalar ratio r are related to the values of the SR parameters at the horizon exit with the standard pivot scale $k_* = 0.05 \text{ Mpc}^{-1}$, which (in our model) is close to the scale at the beginning of SR inflation by $M_{\text{Pl}} \delta t \approx 2$ or $\delta N \approx 1$ or $\delta \phi / M_{\text{Pl}} \sim 10^{-2}$. Hence, ϕ_{in} can be identified with ϕ_{exit} at the horizon exit in a derivation of the CMB tilts, leading to:

$$n_s = 1 + 2\eta_{\text{sr}}(\phi_{\text{in}}) - 6\epsilon_{\text{sr}}(\phi_{\text{in}}) \quad \text{and} \quad r = 16\epsilon_{\text{sr}}(\phi_{\text{in}}). \tag{18}$$

The running SR parameters for selected values of R_0 and δ are displayed in Figure 3.

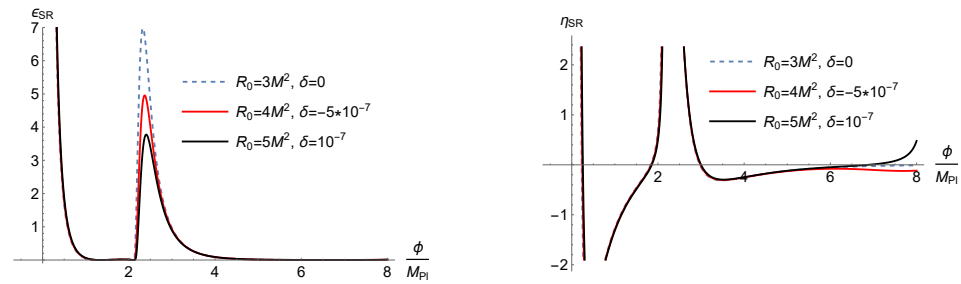


Figure 3. The SR parameter $\epsilon_{sr}(\phi)$ (on the left) and the SR parameter $\eta_{sr}(\phi)$ (on the right) for selected values of R_0 and δ at fixed $g = 2.25$ and $b = 2.89$. The end of Starobinsky inflation is reached at $\phi_{end} \approx 2.98M_{Pl}$ when $\epsilon_{sr}(\phi_{end}) \approx 1$.

It follows from Figure 3 that the peak in $\epsilon_{sr}(\phi)$ is sensitive to the value of R_0 , while the tails of $\eta_{sr}(\phi)$ are sensitive to the value of δ . Therefore, the value of δ affects the value of n_s , and then the value of r becomes weakly dependent upon δ , in agreement with Ref. [21].

The standard equations of motion of inflaton field $\phi(t)$ read:

$$\ddot{\phi} + 3H\dot{\phi} + V'(\phi) = 0, \quad 3H^2 = \frac{1}{M_{Pl}^2} \left[\frac{1}{2}\dot{\phi}^2 + V(\phi) \right], \quad (19)$$

where the dots denote the derivatives with respect to time t . These equations can be numerically solved with given initial conditions ϕ_{in} and $\dot{\phi}_{in}$. Due to the attractor type of Starobinsky inflation the dependence upon initial conditions is weak [25]. A solution with the initial conditions $\phi_{in} = 7.01M_{Pl}$ and $\dot{\phi}_{in} = 0$ leading to $\phi_{exit}/M_{Pl} = 6.98$ is given in Figure 4, where the Hubble function has two plateaus.

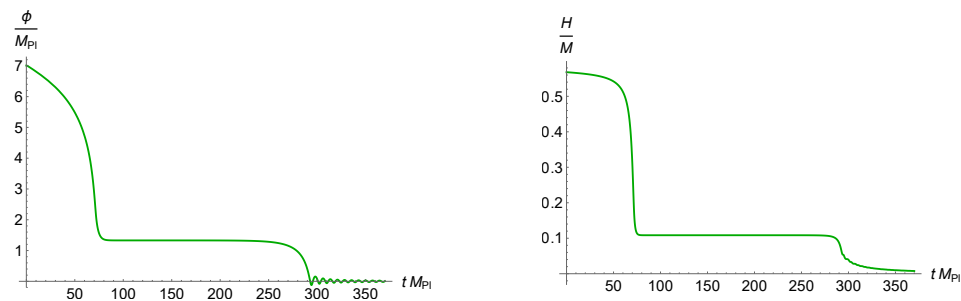


Figure 4. The evolution of inflaton field $\phi(t)$ and Hubble function $H(t)$ with the initial conditions $\phi_{in} = 7.01 M_{Pl}$ and $\dot{\phi}_{in} = 0$, and the parameters $\delta = 2.7 \cdot 10^{-8}$ and $R_0 = 3.0 M^2$.

Inflaton slowly rolls along both plateaus; between them, there is a period of ultra-slow-roll (USR) where dynamics are different [26,27]. Namely, the acceleration term should be kept, but the potential term can be ignored in the first equation of motion (19). Because of that, it is more illuminating to use the Hubble flow parameters outside the CMB region, which are defined by:

$$\epsilon_H = -\frac{\dot{H}}{H^2}, \quad \eta_H = \epsilon_H - \frac{\dot{\epsilon}_H}{2\epsilon_H H}. \quad (20)$$

The evolution is given in Figure 5. In the USR regime, the parameter ϵ_H becomes very small. The parameter η_H drops below -6 , while the corresponding hole (dip) defines the duration of the USR regime.

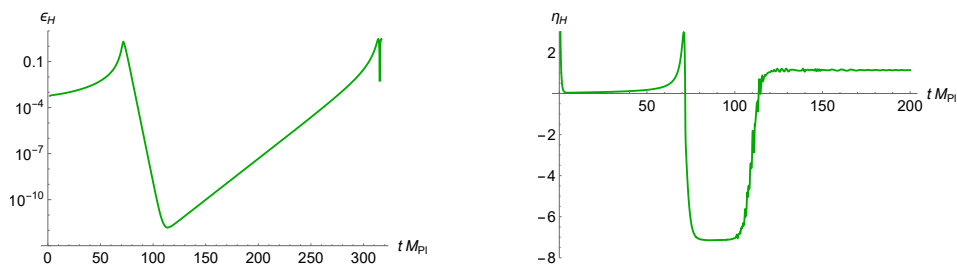


Figure 5. The evolution of the Hubble flow parameters $\epsilon_H(t)$ and $\eta_H(t)$ with the initial conditions $\phi_{in} = 7.01 M_{Pl}$ and $\dot{\phi}_{in} = 0$, and the parameters $\delta = 2.7 \cdot 10^{-8}$ and $R_0 = 3.0 M^2$.

4. Power Spectrum of Scalar Perturbations and PBH Masses

The power spectrum $P_\zeta(k)$ of scalar (curvature) perturbations, as a function of scale k , is usually derived as a solution to the Mukhanov–Sasaki (MS) Equation [28,29], which is often possible only numerically. However, we found that the following, well-known simple analytic formula [12,18,30]:

$$P_\zeta(t) = \frac{H^2}{8M_{Pl}^2 \pi^2 \epsilon_H} \tag{21}$$

gives a good approximation [19,24]. Our new result is given by Figure 6, which shows a large enhancement (peak) in the power spectrum by a factor of 10^7 against the CMB level (on the left-hand side from the peak).

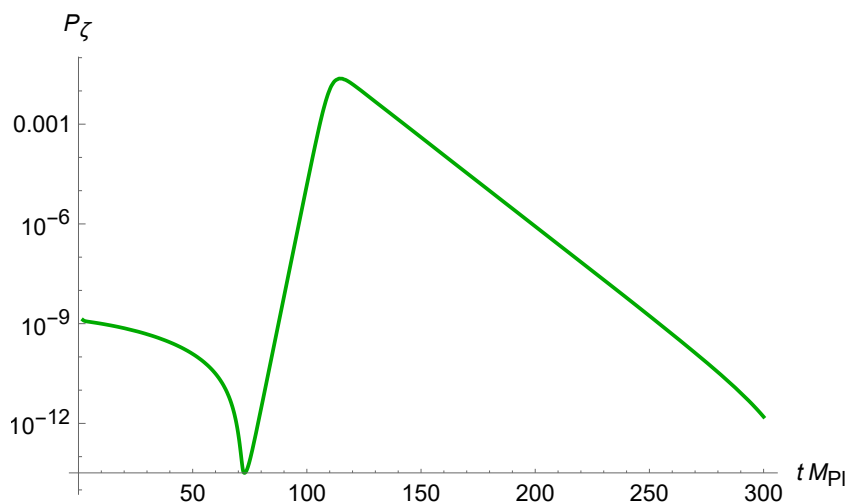


Figure 6. The primordial power spectrum $P_\zeta(t)$ of scalar (curvature) perturbations, derived from Equation (21).

The PBH masses can be estimated from the peak in the power spectrum as follows [31]:

$$M_{PBH} \simeq \frac{M_{Pl}^2}{H(t_{peak})} \exp \left[2(N_{total} - N_{peak}) + \int_{t_{peak}}^{t_{total}} \epsilon_H(t) H(t) dt \right], \tag{22}$$

where N_{peak} and t_{peak} stand for the peak event, while N_{total} and t_{total} denote the end of the whole inflation comprising three stages (SR/USR/SR).

According to Equation (22), the PBH masses are exponentially sensitive to the number of e-folds around the inflection point, $\Delta N = (N_{total} - N_{peak})$, while the integral in the exponential describes the subleading correction that is of the order one.

Our findings are summarized in Table 1 where the values of the key observables n_s , r , and M_{PBH} in our model are collected with the fine-tuned parameters $b = 2.89$ and $g = 2.25$. The height of the peak is sensitive to R_0 , whose value $R_0/M^2 = 3.001$ was chosen to obtain a height equal to 10^{-2} .

Table 1. CMB observables, PBH masses, and duration of inflation in our model.

ϕ_{in}/M_{Pl}	δ	n_s	r	M_{PBH}, g	N_{peak}	N_{total}	ΔN
6.36	2.55×10^{-7}	0.964959	0.0359	5.0×10^{19}	26	47	21
6.70	8.74×10^{-8}	0.964905	0.0182	2.0×10^{19}	34	54	20
7.01	2.70×10^{-8}	0.964944	0.0095	1.0×10^{20}	43	65	22
7.07	2.05×10^{-8}	0.964917	0.0083	2.6×10^{18}	45	64	19
7.12	1.60×10^{-8}	0.964925	0.0074	1.0×10^{17}	47	65	18
7.15	1.36×10^{-8}	0.964908	0.0070	5.0×10^{16}	49	66	17
7.20	1.02×10^{-8}	0.964961	0.0062	1.6×10^{15}	51	64	13

The tensor-to-scalar ratio r is inside the current observational bound, $r < 0.032$, except the first line in the table (given for comparison only). The tilt n_s of scalar perturbations agrees within 1σ with the current CMB measurements [3–5]:

$$n_s = 0.9649 \pm 0.0042 . \tag{23}$$

To obtain PBH masses beyond the Hawking (black hole) evaporation limit of $10^{15} g$, so that these PBH can survive in the present universe and form dark matter, the duration ΔN should be between 17 and 22 e-folds. It also follows from the table that the total duration of inflation should be between 54 and 66 e-folds.

Increasing the parameter δ allows us to compensate the decreasing scalar tilt n_s . When trying to increase the PBH masses by reducing the total duration of inflation, we find that the value of the tensor-to-scalar ratio r increases and reaches the maximal observationally allowed bound. Increasing ΔN even higher is also not possible, because it leads to the peak height beyond observational constraints. Therefore, it is not possible to increase the PBH masses beyond the asteroid-size with $10^{20} g$ or, equivalently, beyond $10^{-13} M_{Sun}$ in our model.

5. Conclusions

The main new results of this paper are summarised in the abstract. The modified gravity framework is entirely based on gravitational interactions, which implies the gravitational origin of both inflation and PBH formation in our approach. The good agreement (within 1σ) with CMB observations is achieved by fine tuning the parameters of the improved model. The PBH masses found are in the mass window that allows the whole dark matter composed of PBH of the asteroid size [11,12]. The stochastic gravitational waves induced by PBH production in the Starobinsky-like gravity were investigated in Ref. [32].

Fine tuning of the parameters in our model is necessary to obtain a significant enhancement of the power spectrum of scalar perturbations leading to the PBH with masses beyond the Hawking evaporation limit and, hence, the possible PBH dark matter, cf. Ref. [33].

A large peak in the primordial power spectrum may lead to large quantum corrections, which may rule out the near-inflection mechanism of PBH production in all single-field models of inflation [34–36]. However, validity of the mechanism based on a near-inflection point was recently defended in Refs. [37–41]. Modified gravity offers a different perspective on the issue of quantum corrections when assuming the gravitational origin of inflation (as in the Starobinsky model) and PBH production in the context of $F(R)$ gravity theories, as in our paper. Both inflation and PBH formation can be destroyed by adding to the F -function terms with the higher powers of R describing quantum gravity corrections, with the R^4 term being their representative. To avoid that, the coefficients in those terms should be small enough in order to keep validity of the gravitational effective action described by Equation (9). Naturally, there should also be a fundamental mechanism in quantum gravity that keeps these coefficients small; however, this issue is beyond the scope of this paper.

Author Contributions: All authors have contributed equally. All authors have read and agreed to the published version of the manuscript.

Funding: S.S. and S.V.K. were supported by Tomsk State University. S.V.K. was also supported by Tokyo Metropolitan University, the Japanese Society for Promotion of Science under the grant No. 22K03624, and the World Premier International Research Center Initiative (MEXT, Japan).

Data Availability Statement: No new data was created.

Acknowledgments: The authors are grateful to Antonio Iovino Junior, Theodoros Papanikolaou and Jacopo Fumagalli for correspondence.

Conflicts of Interest: The authors declare no conflict of interest.

Note

¹ Accordingly, we changed the notation for the AB-parameter denoted by ϵ_{AB} in Ref. [20] to E_{AB} .

References

- Guth, A.H. The Inflationary Universe: A Possible Solution to the Horizon and Flatness Problems. *Phys. Rev. D* **1981**, *23*, 347–356. [CrossRef]
- Linde, A.D. A New Inflationary Universe Scenario: A Possible Solution of the Horizon, Flatness, Homogeneity, Isotropy and Primordial Monopole Problems. *Phys. Lett. B* **1982**, *108*, 389–393. [CrossRef]
- Akrami, Y. et al. [Planck Collaboration]. Planck 2018 results. X. Constraints on inflation. *Astron. Astrophys.* **2020**, *641*, A10. [CrossRef]
- Ade, P.A.R. et al. [BICEP, Keck Collaboration]. Improved Constraints on Primordial Gravitational Waves using Planck, WMAP, and BICEP/Keck Observations through the 2018 Observing Season. *Phys. Rev. Lett.* **2021**, *127*, 151301. [CrossRef]
- Tristram, M.; Banday, A.J.; Górski, K.M.; Keskitalo, R.; Lawrence, C.R.; Andersen, K.J.; Wehus, I.K. Improved limits on the tensor-to-scalar ratio using BICEP and Planck data. *Phys. Rev. D* **2022**, *105*, 83524. [CrossRef]
- Starobinsky, A.A. A new type of isotropic cosmological models without singularity. *Phys. Lett. B* **1980**, *91*, 99–102. [CrossRef]
- Novikov, I.; Zeldovic, Y. Cosmology. *Ann. Rev. Astron. Astrophys.* **1967**, *5*, 627–649. [CrossRef]
- Hawking, S. Gravitationally collapsed objects of very low mass. *Mon. Not. R. Astron. Soc.* **1971**, *152*, 75. [CrossRef]
- Barrow, J.D.; Copeland, E.J.; Liddle, A.R. The Cosmology of black hole relics. *Phys. Rev. D* **1992**, *46*, 645–657. [CrossRef] [PubMed]
- Ivanov, P.; Naselsky, P.; Novikov, I. Inflation and primordial black holes as dark matter. *Phys. Rev. D* **1994**, *50*, 7173–7178. [CrossRef]
- Carr, B.; Kohri, K.; Sendouda, Y.; Yokoyama, J. Constraints on primordial black holes. *Rept. Prog. Phys.* **2021**, *84*, 116902. [CrossRef]
- Escrivà, A.; Kuhnel, F.; Tada, Y. Primordial Black Holes. *arXiv* **2022**, arXiv:2211.05767
- Ketov, S.V.; Starobinsky, A.A. Inflation and non-minimal scalar-curvature coupling in gravity and supergravity. *J. Cosmol. Astropart. Phys.* **2012**, *8*, 22. [CrossRef]
- Ketov, S.V. Multi-Field versus Single-Field in the Supergravity Models of Inflation and Primordial Black Holes. *Universe* **2021**, *7*, 115. [CrossRef]
- Ketov, S. On the large-field equivalence between Starobinsky and Higgs inflation in gravity and supergravity. In Proceedings of the 7th Symposium on Prospects in the Physics of Discrete Sources, Bergen, Norway, 29 November–3 December 2021; p. 14. [CrossRef]
- Maeda, K.-I. Towards the Einstein–Hilbert Action via Conformal Transformation. *Phys. Rev. D* **1989**, *39*, 3159. [CrossRef]
- Ivanov, V.R.; Ketov, S.V.; Pozdeeva, E.O.; Vernov, S.Y. Analytic extensions of Starobinsky model of inflation. *J. Cosmol. Astropart. Phys.* **2022**, *3*, 58. [CrossRef]
- Garcia-Bellido, J.; Morales, E.R. Primordial black holes from single field models of inflation. *Phys. Dark Univ.* **2017**, *18*, 47–54. [CrossRef]
- Frolovsky, D.; Ketov, S.V.; Saburov, S. Formation of primordial black holes after Starobinsky inflation. *Mod. Phys. Lett. A* **2022**, *37*, 2250135. [CrossRef]
- Appleby, S.A.; Battye, R.A.; Starobinsky, A.A. Curing singularities in cosmological evolution of F(R) gravity. *J. Cosmol. Astropart. Phys.* **2010**, *6*, 5. [CrossRef]
- Ketov, S.V.; Pozdeeva, E.O.; Vernov, S.Y. On the superstring-inspired quantum correction to the Starobinsky model of inflation. *J. Cosmol. Astropart. Phys.* **2022**, *12*, 32. [CrossRef]
- Ivanov, V.; Ketov, S.; Pozdeeva, E.; Vernov, S. On Extensions of the Starobinsky Model of Inflation. *Phys. Sci. Forum* **2023**, *7*, 6. [CrossRef]
- Pozdeeva, E.; Ketov, S.; Vernov, S. String-Inspired Correction to R^2 Inflation. *Phys. Sci. Forum* **2023**, *7*, 2.
- Frolovsky, D.; Ketov, S.V. Inflationary E-models revisited. *arXiv* **2023**, arXiv:2304.12558.
- Aoki, S.; Ishikawa, R.; Ketov, S.V. Pole inflation and primordial black holes formation in Starobinsky-like supergravity. *Class. Quant. Grav.* **2023**, *40*, 65002. [CrossRef]

26. Germani, C.; Prokopec, T. On primordial black holes from an inflection point. *Phys. Dark Univ.* **2017**, *18*, 6–10. [CrossRef]
27. Dimopoulos, K. Ultra slow-roll inflation demystified. *Phys. Lett. B* **2017**, *775*, 262–265. . [CrossRef]
28. Mukhanov, V.F. Gravitational Instability of the Universe Filled with a Scalar Field. *JETP Lett.* **1985**, *41*, 493–496.
29. Sasaki, M. Large Scale Quantum Fluctuations in the Inflationary Universe. *Prog. Theor. Phys.* **1986**, *76*, 1036. [CrossRef]
30. Karam, A.; Koivunen, N.; Tomberg, E.; Vaskonen, V.; Veermäe, H. Anatomy of single-field inflationary models for primordial black holes. *J. Cosmol. Astropart. Phys.* **2023**, *3*, 13. [CrossRef]
31. Pi, S.; Zhang, Y.-L.; Huang, Q.-G.; Sasaki, M. Scalon from R^2 -gravity as a heavy field. *J. Cosmol. Astropart. Phys.* **2018**, *5*, 42. [CrossRef]
32. Papanikolaou, T.; Tzerefos, C.; Basilakos, S.; Saridakis, E.N. Scalar induced gravitational waves from primordial black hole Poisson fluctuations in $f(R)$ gravity. *J. Cosmol. Astropart. Phys.* **2022**, *10*, 13. [CrossRef]
33. Cole, P.S.; Gow, A.D.; Byrnes, C.T.; Patil, S.P. Primordial black holes from single-field inflation: A fine-tuning audit. *arXiv* **2023**, arXiv:2304.01997.
34. Kristiano, J.; Yokoyama, J. Ruling Out Primordial Black Hole Formation From Single-Field Inflation. *arXiv* **2022**, arXiv:2211.03395
35. Kristiano, J.; Yokoyama, J. Response to criticism on “Ruling Out Primordial Black Hole Formation From Single-Field Inflation”: A note on bispectrum and one-loop correction in single-field inflation with primordial black hole formation. *arXiv* **2023**, arXiv:2303.00341.
36. Choudhury, S.; Panda, S.; Sami, M. Quantum loop effects on the power spectrum and constraints on primordial black holes. *arXiv* **2023**, arXiv:2303.06066.
37. Riotto, A. The Primordial Black Hole Formation from Single-Field Inflation is Not Ruled Out. *arXiv* **2023**, arXiv:2301.00599.
38. Riotto, A. The Primordial Black Hole Formation from Single-Field Inflation is Still Not Ruled Out. *arXiv* **2023**, arXiv:2303.01727.
39. Firouzjahi, H.; Riotto, A. Primordial Black Holes and Loops in Single-Field Inflation. *arXiv* **2023**, arXiv:2304.07801.
40. Franciolini, G.; Iovino, A., Jr.; Taoso, M.; Urbano, A. One loop to rule them all: Perturbativity in the presence of ultra slow-roll dynamics. *arXiv* **2023**, arXiv:2305.03491.
41. Fumagalli, J. Absence of one-loop effects on large scales from small scales in non-slow-roll dynamics. *arXiv* **2023**, arXiv:2305.19263.

Disclaimer/Publisher’s Note: The statements, opinions and data contained in all publications are solely those of the individual author(s) and contributor(s) and not of MDPI and/or the editor(s). MDPI and/or the editor(s) disclaim responsibility for any injury to people or property resulting from any ideas, methods, instructions or products referred to in the content.

On the Possibility of a Static Universe

Júlio C. Fabris^{1,2,3,*}, Felipe T. Falciano^{3,4}, Luiz F. Guimarães¹ and Nelson Pinto-Neto^{3,4}

¹ Núcleo Cosmo-Ufes & Departamento de Física, Universidade Federal do Espírito Santo, Av. Fernando Ferrari, 514, Goiabeiras, Vitória 29060-900, ES, Brazil; luiz.f.guimaraes@ufes.br

² Moscow Engineering Physics Institute, National Research Nuclear University MEPhI, Kashirskoe Shosse 31, 115409 Moscow, Russia

³ PPGCosmo, CCE—Federal University of Espírito Santo, Vitória 29075-910, ES, Brazil; ftovar@cbpf.br (F.T.F.); nelsonpn@cbpf.br (N.P.-N.)

⁴ CBPF—Brazilian Center for Research in Physics, Xavier Sigaud st. 150, Rio de Janeiro 22290-180, RJ, Brazil

* Correspondence: julio.fabris@cosmo-ufes.org

Abstract: After a century of cosmological observations, we have a solid standard model of cosmology. However, from a theoretical viewpoint, it is a compelling question if the cosmological data inevitably require an expanding universe independently of the theoretical framework. The possibility of obtaining a viable cosmological model with a constant scale-factor is discussed in the context of the Brans–Dicke class of scalar–tensor theories. It is shown that a flat spatial section requires the presence of a stiff matter fluid. However, some kinematical properties of the standard cosmological model can be reproduced. A realistic scenario may require a more complex class of scalar–tensor theories.

Keywords: cosmology; expanding universe; static universe; scalar-tensor theories



Citation: Fabris, J.C.; Falciano, F.T.; Guimarães, L.F.; Pinto-Neto, N. On the Possibility of a Static Universe. *Universe* **2024**, *10*, 92. <https://doi.org/10.3390/universe10020092>

Academic Editors: Galina L. Klimchitskaya, Vladimir M. Mostepanenko and Sergey V. Sushkov

Received: 5 January 2024

Revised: 5 February 2024

Accepted: 6 February 2024

Published: 16 February 2024



Copyright: © 2024 by the authors. Licensee MDPI, Basel, Switzerland. This article is an open access article distributed under the terms and conditions of the Creative Commons Attribution (CC BY) license (<https://creativecommons.org/licenses/by/4.0/>).

1. Introduction

The publication of the article of Alexander Friedmann in 1922 proposing the possibility of a dynamical universe [1] was one of the most important revolutions in our view of the cosmos. For the first time, to our knowledge, in the history of science, the universe was considered as an evolving system. Until Friedmann, the known universe was described essentially as a static system. Even, the first cosmological model constructed from the recently proposed new theory of gravity, General Relativity, was static and inevitably unstable due to the attractive character of the gravitational interaction [2,3]. In spite of the unstable nature of any static cosmological system, the Friedmann proposal of a dynamical universe initially received some opposition. It must be remembered that the concept of galaxies distributed in the universe emerged after a long debate and, only after the Friedmann article, that the measuring of the spectra of galaxies was obtained showing the systematic redshift of the spectral lines, an indication of cosmic expansion. Unfortunately, Friedmann did not live enough to watch the triumph of his speculations about a dynamical universe with the formulation of the law for the recessions of the galaxies made, mainly, by Hubble and Lemaître.

Is there any reason to consider the possibility of a static universe? The answer most probably is no, for two main reasons. First, to explain the redshift of the spectral lines of distant objects is not simple without a dynamical cosmos. The hypothesis of the tired light [4,5], for example, has difficulties in incorporating a hot phase and the consequent primordial nucleosynthesis and the spectrum of the Cosmic Microwave Background Radiation (CMB), besides structure formation. Second, due to the attractive character of gravity, any static universe would be unstable. This is a feature difficult to circumvent and it is hard to conceive a model within General Relativity that can change this picture.

Notwithstanding, the previous remarks refer to a *completely* static universe. It is possible to conceive of a universe with a constant scale factor, but with some other possible dynamical quantity [6–10]. This is the case for scalar–tensor theories where gravity is

coupled to a scalar field: there are specific configurations for which the scale factor is constant but the scalar field is dynamical. Since in many scalar–tensor theories the scalar field is connected with the gravitational coupling, a time-dependent scalar field may imply a cosmological dynamics in spite of a constant scale factor. There are simple examples where a stable configuration can be obtained with a constant scale factor and a dynamical gravitational coupling, but they are very particular. This will be discussed in next section. It is far from obvious how this particular configuration can be generalized in order to have a realistic cosmological scenario, incorporating the different phases of the evolution of the universe.

A cosmological scenario without expansion containing at least one static phase has been discussed by Wetterich, leading to a viable model [11,12]. The Wetterich model also contains contracting phases. The effects typically identified as being due to the expansion of the universe (redshift for example) are transferred to a time-dependent mass of the elementary particles [13–15]. In this model, the cosmic initial singularity can be avoided. The model is formulated by using a scalar field non-minimally coupled with the geometry and with the matter sector. A realistic scenario for all the phases of the universe can be achieved.

The possibility of a cosmological model with a constant scale factor in all cosmological phases has been qualitatively evoked in Ref. [16]. The static model should be constructed in the minimal coupled frame, connected with the non-minimal coupled frame through a conformal transformation. Note that the present approach is substantially different from that used in refs. [11,12], which considered a non-minimal coupled frame between a scalar field and geometry, besides a non-trivial coupling with the scalar field in the matter sector. Evidently, the present approach, formulated in the minimal coupled frame, may be seen as with less freedom than refs. [11,12]. Nevertheless, it allows a connection to some traditional theoretical frameworks, like the Jordan–Wagoner–Brans–Dicke theory, as the resulting theory presented in this paper contains a scalar field minimally coupled to gravity, but non-trivially coupled to the matter sector. Furthermore, the coupling parameter ω of the kinetic term of the scalar field is not constant. Our approach also differs from Wetterich’s previous work [13,14] inasmuch as he works with the original Brans–Dicke (BD) theory [17], where ω is a constant, and also includes a potential.

In the present text this possibility is investigated in more detail. It is shown that, at least in the context of BD theory with a dynamical BD parameter ω , as suggested in ref. [16], it is possible to obtain at most a kinematical consistent background description of the cosmic evolution. However, it appears important differences concerning how to obtain equivalent kinematical descriptions between the static model developed here and the dynamical Friedmann models. In the Friedmann models, the behavior of the scale factor is essentially dictated by the equation of state of the matter component. In the corresponding static universe with a dynamical gravitational coupling, a given description of the cosmic evolution is determined essentially by an appropriate choice of the non-trivial coupling function of the scalar field kinetic term, denoted by $\omega(\phi)$. In both cases, expanding or static universes, a similar cosmic red-shift relation can be obtained by choosing appropriately $\omega(\phi)$. In spite of this kinematical equivalence, important phenomena present in the cosmic history demanding a perturbative analysis, such as the CMB and structure formation, very probably can not be incorporated in a static scenario, even if a more detailed analysis is required. In this sense, the analysis to be made here can be seen as a kind of no-go theorem for a universe with a constant scale factor (but possibly with a dynamical gravitational coupling) in all its phases. Of course, it is not excluded that different classes of extensions of the GR theory may change the conclusions presented here.

In the next section we review the Einstein static universe and its instability and the particular cases of the BD theory with some possible static, stable configurations. From now on we use the term “static universe” to denote a universe with constant scale factor even if the gravitational coupling is varying. In Section 3, the Wagoner–Brans–Dicke–Jordan scalar-tensor theory is discussed both in the Jordan and Einstein frames. In Section 4, it

is shown how the variation of the mass of elementary particles can lead to a shift in the spectral lines of the hydrogen atom. In Section 5, it is shown how a static universe in the Einstein frame can lead to a scenario where the standard cosmological model is reproduced in the Jordan frame from the kinetic point of view. In Section 6, we conclude with some final remarks.

2. Stability of Static Models in GR and BD Theories

The static model in the GR and BD theories are briefly revised in what follows. The GR equations in presence of a cosmological constant Λ are

$$R_{\mu\nu} - \frac{1}{2}g_{\mu\nu}R = 8\pi GT_{\mu\nu} + g_{\mu\nu}\Lambda, \tag{1}$$

$$T^{\mu\nu}{}_{;\mu} = 0. \tag{2}$$

For a static metric, with a spatial curvature k (which can be positive, negative or zero), a pressureless fluid, a cosmological constant and fixing the constant scale factor equal to unity, the equations reduce to,

$$3k = 8\pi G\rho + \Lambda, \tag{3}$$

$$k = \Lambda, \tag{4}$$

$$\dot{\rho} = 0. \tag{5}$$

For $k = 0$, the universe turns out to be completely empty, while for k negative (a pseudo-sphere), the energy density becomes negative. Only for positive k do we have a consistent scenario with

$$4\pi G\rho = \Lambda > 0. \tag{6}$$

However, this solution is unstable. The perturbative equations in the synchronous coordinate condition $h_{\mu 0} = 0$ for a given fluid with density ρ and pressure p are given by [18],

$$\ddot{h} + 2H\dot{h} = 8\pi G\rho\delta, \tag{7}$$

$$\delta + (1 + \alpha)\left(\theta - \frac{\dot{h}}{2}\right) = 0, \tag{8}$$

$$(1 + \alpha)\left[\delta\theta + (2 - 3\alpha)H\theta\right] = \frac{v_s^2}{a^2}\delta, \tag{9}$$

These equations are valid even in presence of a cosmological constant. In these expressions, we have introduced the following definitions:

$$H = \frac{\dot{a}}{a}, \quad h = \frac{h_{kk}}{a^2}, \quad \delta = \frac{\delta\rho}{\rho}, \tag{10}$$

$$\theta = \partial_k\delta v^k, \quad \alpha = \frac{p}{\rho}, \quad v_s^2 = \frac{\partial p}{\partial\rho}. \tag{11}$$

H is the Hubble function, h_{kk} is the trace of metric fluctuations, δ is the density contrast, θ is related with the velocity perturbation, α is the equation of state parameter and v_s^2 is the sound speed. For a static universe with pressureless fluid ($\alpha = v_s^2 = 0$), the perturbed equations reduce to

$$\ddot{\delta} - 4\pi G\delta = 0, \quad \dot{\theta} = 0. \tag{12}$$

Consequently, the matter perturbation, expressed by the density contrast δ , grows exponentially, characterizing the instability due to the attractive nature of the gravitational interaction.

The perturbative analysis of the Brans-Dicke cosmological models has been carried out in ref. [19]. The inflationary case will be considered just as a simple example. The background solutions for an equation of state $p = -\rho$ are

$$a(t) \propto t^{\omega+1/2}, \tag{13}$$

$$\phi(t) \propto t^2. \tag{14}$$

The universe is static if $\omega = -1/2$. For this case, the perturbations behave as

$$\frac{\delta\phi}{\phi} \equiv \lambda = \frac{1}{t} \int \left\{ c_1 J_{3/2}(nt) + c_2 J_{-3/2}(nt) \right\}, \tag{15}$$

n denoting the wavenumber of the perturbations. The solution displays a growing mode and a decreasing mode. Asymptotically, the growing mode behaves as,

$$\lambda \propto t^2. \tag{16}$$

The growing mode is not exponential as in GR case. It presents a mild instability that is necessary, after all, to induce the formation of structures observed in the universe.

The same properties are verified for a matter dominated universe in a Brans–Dicke cosmology but with $\omega = -1$.

3. Field Equations in the Jordan and Einstein Frames

The example discussed in the previous section shows that it is possible to have a static universe in scalar-tensor theories without exponential instabilities. However, it is not clear how to describe the different expansion phases of the standard model in the static frame. Our proposal is to consider a dynamical parameter $\omega(\phi)$. Following the qualitative discussion presented in ref. [16], our starting point is the Bergmann–Wagoner–Brans–Dicke theory whose Lagrangian in the original Jordan frame is [17,20]

$$\mathcal{L} = \sqrt{-g} \left\{ \phi R - \omega(\phi) \frac{\phi_{;\rho} \phi^{;\rho}}{\phi} \right\} + \mathcal{L}_m(g_{\mu\nu}, \Psi), \tag{17}$$

with the matter Lagrangian given by $\mathcal{L}_m(g_{\mu\nu}, \Psi)$, Ψ representing the matter fields. The gravitational coupling is dynamical and related to the inverse of the scalar field ϕ .

The field equations are the following:

$$R_{\mu\nu} - \frac{1}{2} g_{\mu\nu} R = \frac{8\pi}{\phi} T_{\mu\nu} + \frac{\omega(\phi)}{\phi^2} \left(\phi_{;\mu} \phi_{;\nu} - \frac{1}{2} g_{\mu\nu} \phi_{;\rho} \phi^{;\rho} \right) + \frac{1}{\phi} \left(\phi_{;\mu;\nu} - g_{\mu\nu} \square\phi \right), \tag{18}$$

$$\square\phi = \frac{8\pi T}{3 + 2\omega(\phi)} - \frac{\omega_\phi}{3 + 2\omega(\phi)} \phi_{;\rho} \phi^{;\rho}, \tag{19}$$

$$T^{\mu\nu}_{;\mu} = 0. \tag{20}$$

Now, we perform a conformal transformation, with $g_{\mu\nu} = \phi^{-1} \tilde{g}_{\mu\nu}$, as indicated in the Appendix A. The new equations are:

$$\tilde{R}_{\mu\nu} - \frac{1}{2} \tilde{g}_{\mu\nu} \tilde{R} = 8\pi G \tilde{T}_{\mu\nu} + \frac{(\omega(\phi) + 3/2)}{\phi^2} \left(\phi_{;\mu} \phi_{;\nu} - \frac{1}{2} \tilde{g}_{\mu\nu} \phi_{;\rho} \phi^{;\rho} \right), \tag{21}$$

$$\tilde{\square}\phi = \frac{8\pi G \phi \tilde{T}}{3 + 2\omega(\phi)} - \left(\frac{\phi \omega_\phi}{3 + 2\omega(\phi)} - 1 \right) \frac{\phi_{;\rho} \phi^{;\rho}}{\phi}, \tag{22}$$

$$\tilde{T}^{\mu\nu}_{;\mu} = -\frac{\tilde{g}^{\nu\mu} \phi_{;\mu} \tilde{T}}{2\phi}. \tag{23}$$

In writing these equations, we have made the redefinition,

$$G\tilde{\rho} = \frac{\rho}{\phi^2}, \quad G\tilde{p} = \frac{p}{\phi^2}, \tag{24}$$

G being the present value of the cosmological coupling.

4. The Redshift Relation

In the static universe, the mass of the particles must vary with time in order to obtain a change in the spectral lines, as observed. The mechanism to generate the observed redshift will now be described.

In the Einstein frame, the energy conservation law for any perfect fluid satisfying $\tilde{p} = \alpha\tilde{\rho}$ in a homogeneous and isotropic spacetime reads,

$$\tilde{\rho}' + 3\tilde{H}(1 + \alpha)\tilde{\rho} = -\frac{(1 - 3\alpha)}{2} \frac{\phi'}{\phi} \tilde{\rho}, \tag{25}$$

where the primes mean derivative with respect to τ , and $\tilde{H} = b'/b$ is the Einstein Hubble function, which is considered to be zero. Integrating this equation for the case of a fluid composed of massive non-relativistic particles ($\alpha = 0$), we obtain

$$\tilde{\rho} = \tilde{\rho}_0 \left(\frac{\phi_0}{\phi}\right)^{1/2} = n\tilde{m}, \tag{26}$$

where n is the particle number density, which is a constant in a static universe, and $\tilde{\rho}_0$ is a constant. Hence, the relation between the constant mass m in the expanding universe and the varying mass \tilde{m} in the static universe is given by,

$$\tilde{m} \propto m\phi^{-1/2}. \tag{27}$$

Assuming that ϕ is positive and it decreases in time, namely $\infty > \phi > 0$, the masses increase with time, meaning that the wavelength of the emitted radiation will decrease with time. In other words, the electronic transition occurred in the past will have a wavelength greater than observed today in the laboratory. We remark that a decreasing ϕ implies a growing gravitational coupling and a decreasing Planck's mass. Also, the Planck length grows with time. Our approach is purely classical but it suggests that the quantum gravity regime may be achieved at much smaller energy scales as time goes on and the gravitational interaction becomes stronger.

The relation (27) is equivalent to the invariance of the test particle's Lagrangian under the conformal transformation

$$l = - \int mds = - \int m\phi^{-1/2}d\tilde{s} = - \int \tilde{m}d\tilde{s}. \tag{28}$$

The spectral lines of the hydrogen atom in the static universe are given by

$$\frac{1}{\lambda} = \frac{\Delta E}{hc} = \frac{\tilde{m}Z^2e^4}{4\pi c\hbar^3} \left(\frac{1}{n_f^2} - \frac{1}{n_i^2}\right), \tag{29}$$

with n_i and n_f designating the initial and final electronic principal quantum numbers. Hence, the wavelength of the emitted photon varies as

$$\lambda \propto \frac{1}{\tilde{m}} \propto \phi^{1/2}. \tag{30}$$

As a consequence, the photons emitted in the past have a higher wavelength compared with the emissions in the laboratory today.

The discussion above is an example of how the Jordan and Einstein frames may describe the same phenomena in a complete different way. For the discussion on the equivalence of both frames, see ref. [21] and references therein.

5. A Static Universe: General Relations

We will try now to construct a static universe in the Einstein frame. The difficulty lies in that the conservation law in the Jordan frame implies that each matter component depends only on the scale factor, making hard to obtain a transition from a cosmic phase to another. This can be achieved in the Einstein frame due to the second term in (23) and the presence of the arbitrary function $\omega(\phi)$.

The metric in the minimal coupled frame is given by,

$$d\tilde{s}^2 = d\tau^2 - \frac{b^2}{1 + k\frac{r^2}{4}}(dx^2 + dy^2 + dz^2), \tag{31}$$

with $r^2 = x^2 + y^2 + z^2$. We shall assume a barotropic equation of state $\tilde{p} = \alpha\tilde{\rho}$ with α constant. The Equations (21)–(23) become:

$$3\tilde{H}^2 + 3\frac{k}{b} = 8\pi G\tilde{\rho} + \left(\frac{3 + 2\omega}{4}\right)\left(\frac{\phi'}{\phi}\right)^2, \tag{32}$$

$$2\tilde{H}' + 3\tilde{H}^2 + \frac{k}{b} = -8\pi G\tilde{p} - \left(\frac{3 + 2\omega}{4}\right)\left(\frac{\phi'}{\phi}\right)^2, \tag{33}$$

$$\frac{\phi''}{\phi} + 3\tilde{H}\frac{\phi'}{\phi} = \frac{8\pi G}{3 + 2\omega}(1 - 3\alpha)\tilde{\rho} - \left(\frac{\phi\omega_\phi}{3 + 2\omega(\phi)} - 1\right)\left(\frac{\phi'}{\phi}\right)^2, \tag{34}$$

$$\tilde{\rho}' + 3\tilde{H}(1 + \alpha)\tilde{\rho} = -\frac{(1 - 3\alpha)}{2}\frac{\phi'}{\phi}\tilde{\rho}. \tag{35}$$

The primes mean derivative with respect to τ , and $\tilde{H} = b'/b$. A universe without expansion in this frame means $\tilde{H} = 0$, and without loss of generality we fix $b = 1$. The previous equations reduce to

$$3k = 8\pi G\tilde{\rho} + \left(\frac{3 + 2\omega}{4}\right)\left(\frac{\phi'}{\phi}\right)^2, \tag{36}$$

$$k = -8\pi G\alpha\tilde{\rho} - \left(\frac{3 + 2\omega}{4}\right)\left(\frac{\phi'}{\phi}\right)^2, \tag{37}$$

$$\frac{\phi''}{\phi} = \frac{8\pi G}{3 + 2\omega}(1 - 3\alpha)\tilde{\rho} - \left(\frac{\phi\omega_\phi}{3 + 2\omega(\phi)} - 1\right)\left(\frac{\phi'}{\phi}\right)^2, \tag{38}$$

$$\tilde{\rho}' = -\frac{(1 - 3\alpha)}{2}\frac{\phi'}{\phi}\tilde{\rho}. \tag{39}$$

The last equation can be easily integrated as

$$\tilde{\rho} = \tilde{\rho}_0\phi^{-\frac{(1-3\alpha)}{2}}. \tag{40}$$

Adding (36) and (37), we obtain

$$4k = 8\pi G(1 - \alpha)\tilde{\rho}. \tag{41}$$

Subtracting (36) and $3 \times$ (37),

$$0 = 8\pi G(1 + 3\alpha)\tilde{\rho} + (3 + 2\omega)\left(\frac{\phi'}{\phi}\right)^2 \tag{42}$$

Three conclusions can be obtained from these relations:

$$\alpha = 1 \rightarrow k = 0; \tag{43}$$

$$\alpha \neq 1, \frac{1}{3} \rightarrow \tilde{\rho} = \text{constant} \rightarrow \phi = \text{constant}, \quad k > 0 : \tag{44}$$

$$\alpha = \frac{1}{3} \rightarrow \tilde{\rho} = \text{constant} \rightarrow \phi = \text{constant or dynamical}, \quad k > 0. \tag{45}$$

The Einstein static model can be obtained from the previous relation by fixing ϕ constant, and a two fluid model, one a matter component ($\alpha = 0$) and a cosmological constant ($\alpha = -1$), leading to

$$k = 4\pi G\tilde{\rho}_m, \tag{46}$$

$$\tilde{\rho}_\Lambda = \frac{\tilde{\rho}_m}{2}. \tag{47}$$

6. An Example of a Static Universe

Let us consider specifically the case $\alpha = 1$, leading to $k = 0$, and evaluate the distance-redshift relation in this situation.

With the result for the matter density (40), and remembering that with $\alpha = 1$ and $k = 0$, Equation (36) becomes identical to Equation (37), while Equation (38) is just the derivative of those equations. Hence, there is just one equation to be integrated,

$$8\pi G\tilde{\rho} + \left(\frac{3+2\omega}{4}\right) \left(\frac{\phi'}{\phi}\right)^2 = 0. \tag{48}$$

Let us write $w(\phi) =: -3/2 - f(\phi)$. Then, as for $\alpha = 1$ one obtains $\tilde{\rho}/\tilde{\rho}_0 = \phi/\phi_0$, Equation (48) can be written as

$$\frac{f^{1/2}(\phi)}{\phi^{3/2}} d\phi = \sqrt{C_1} c d\tau, \tag{49}$$

where $C_1 = 16\pi G\tilde{\rho}_0/(\phi_0 c^2)$, remembering that the 0 subscript denotes quantities evaluated today, and c is the speed of light. With the integration from proper time τ_1 when a source emitted light towards an observer that receives it at τ_0 , we obtain

$$I(\phi_0) - I(\phi_1) = \sqrt{C_1} d, \tag{50}$$

where d is the distance between the source and the observer, which in a flat static universe is just $d = c(\tau_0 - \tau_1)$, and $I(\phi)$ is the function resulting from the integral in ϕ .

Using Equation (50) and writing $\phi_1 = (1+z)^2\phi_0$ we obtain the exact distance-redshift relation,

$$d = \frac{I(\phi_0) - I(\phi_0(1+z)^2)}{\sqrt{C_1}}, \tag{51}$$

For small z we obtain

$$d = \frac{cf^{1/2}(\phi_0)}{2\sqrt{G\tilde{\rho}_0}} z + \dots, \tag{52}$$

where the constant in front of z (without c) plays the role of the inverse of the Hubble constant in this scenario.

As an example, let us take a power law functional form for f , yielding,

$$\omega(\phi) = -\frac{3}{2} - \kappa\phi^n. \tag{53}$$

The parameter κ can be fixed equal to unity by absorbing it in the expression for ϕ . Equation (48) can be easily integrated, leading to

$$\phi = \phi_0(\pm\tau)^{\frac{2}{n-1}}. \tag{54}$$

In order to have $\infty > \phi > 0$ during time evolution, when the exponent is negative the plus sign must be chosen, implying $0 \leq \tau < \infty$, and vice-versa.

In the case of a spatially flat expanding universe dominated by stiff matter and described by standard GR, we have that $1 + z \propto a^{-1}(t) \propto t^{-1/3}$, where t is the proper time. In case of static universes in the Einstein frame of a generalized Brans–Dicke theory as described above, one has $1 + z \propto \phi^{1/2}(\tau) \propto \tau^{1/(n-1)}$ with respect to the proper time in the Einstein frame. Hence, in order to have the same proper time dependence, one must have $n = -2$.

Some observational tests of the unperturbed universe depend essentially on the behavior of the scale factor. It is possible to choose the functional form of $\omega(\phi)$ in order to mimic the scale factor of the standard cosmological model in its different phases by translating the results in the static Einstein frame to the Jordan frame where the scale factor is a function of time. First we remember that, with $b = 1$,

$$\begin{aligned} a &= \phi^{-1/2}, \\ dt &= \pm\phi^{-1/2}d\tau. \end{aligned} \tag{55}$$

Hence, using Equation (54), the scale factor in the Jordan frame is given, in terms of the cosmic time in the same frame, as

$$a = a_0(t)^{\frac{1}{2-n}}, \tag{57}$$

with $0 \leq t < \infty$ for $n < 2$. The convenient choice of n may lead to the same kinematical behavior of the standard cosmological model: $n = 0$ for the radiative phase, $n = 1/2$ for the matter dominated phase and $1 < n \leq \infty$ for the dark energy phase ($n = 2$ corresponds to a de Sitter phase and $n > 2$ to a phantom dark energy phase). In this way, the main phases of the expanding universe can be mapped in the corresponding static models by choosing conveniently the function $\omega(\phi)$.

In principle, a more general choice for $\omega(\phi)$ may lead to smooth transitions between these phases. For example,

$$\omega(\phi) = -\frac{3}{2} - \frac{\kappa_1\phi^2}{\sqrt{\kappa_2 + \kappa_3\phi^3 + \kappa_4\phi^4}}, \tag{58}$$

interpolates smoothly the radiative phase ($\phi \rightarrow \infty$) and a de Sitter phase ($\phi \rightarrow 0$) passing in between by a matter dominated phase. The parameters κ_i are constants. Since $\infty > \phi > 0$, all three main phases of the standard cosmological model would be generated by this functional form, with a smooth transition between them. The necessary duration of each phase may be achieved by choosing conveniently the values of the parameters κ_i . However, the explicit dependence of ϕ on τ can not be obtained in terms of elementary functions, requiring a numerical integration. Below we present a numerical calculation for the evolution of $\phi(\tau)$ in two scenarios: one with a continuous transition following (58), with $\kappa_2 = 0$ and $\kappa_1 = \kappa_3 = \kappa_4 = 1$, and the other with a piecewise transition at $\phi = 1$ from $\kappa_2 = \kappa_3 = 0$ and $\kappa_4 = 1$ (radiation) to $\kappa_2 = \kappa_4 = 0$ and $\kappa_3 = 1$ (matter), see Figure 1. In both cases, $\kappa_1 = 1$. We note that time runs from left to right (from larger to smaller values of τ).

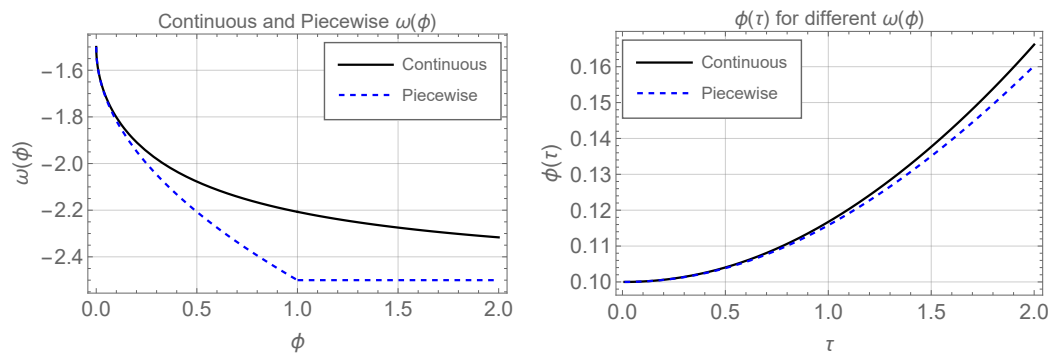


Figure 1. (Left) Comparison between $\omega(\phi)$ for the continuous case, (58), where $\kappa_1 = \kappa_3 = \kappa_4 = 1$ and $\kappa_2 = 0$, and the case where there is a sharp transition from $\kappa_2 = \kappa_3 = 0$ and $\kappa_1 = \kappa_4 = 1$ (radiation) to $\kappa_2 = \kappa_4 = 0$ and $\kappa_1 = \kappa_3 = 1$ (matter). (Right) Numerical evolution of the scalar field for the two aforementioned cases.

Among the possible limitations of the scenario sketched above, there is one that is particularly relevant; namely, the relation with the standard cosmological model established in the Jordan frame is purely kinematical. Even if we can satisfy some observational tests connected with Hubble–Lemaître law, a detailed perturbative study must be carried out in order to verify if, for example, the structure formation and CMB anisotropies are reproduced, at least in their general lines. This will be object of a separate study.

7. Final Remarks

The possibility to have a static universe compatible with the observational data has been discussed in this text. By static universe, it is understood here as a universe with a constant scale factor but with possible other dynamical fields, like a scalar field related to the gravitational coupling. The Brans–Dicke theory, with a variable ω , was used as an example. In this case, it has been shown that a spatially flat static universe is possible only if the content of the universe is given by a stiff matter fluid. A two-fluid model is also possible, including radiation, but only if there is positive spatial curvature. This can be verified by generalizing Equation (41) including radiation and stiff matter.

In spite of this deceiving limitation, it is possible that some more complex scalar–tensor theories may allow us to surmount the limitations of the static model discussed here. Appealing to other classes of Horndeski theories [22,23] may circumvent the restrictions given specially by relations (41) and (42). In this case, it is maybe possible to mimic different phases of the universe in the behavior of the dynamical scale factor by choosing a convenient function $\omega(\phi)$. This property may lead to a kinematical equivalence between the static universe and the standard mode at the background level. Otherwise, the static universe can be connected only to a given phase in the cosmic history, as in the models discussed in refs. [11,12], which contain, beside a static phase, contracting universes in other phases. However, it seems hard to maintain this equivalence at the perturbative level. This issue must be addressed in a separate analysis.

It is important to remember that the Brans–Dicke theory with a stiff matter fluid has many peculiarities as discussed in ref. [24]. It must be stressed that we have exploited here a conformal transformation in order to rewrite the theory formulated in the Jordan frame in the Einstein frame. The use of disformal transformations may bring other possibilities as discussed in ref. [25], where a particular attention has been given to the case of a stiff matter fluid. The use of the unimodular constraint can also lead to a well-posed scenario [26].

Author Contributions: Conceptualization, J.C.F., F.T.F., N.P.-N. and L.F.G.; Formal analysis, J.C.F., F.T.F., N.P.-N. and L.F.G.; Writing—original draft, J.C.F., F.T.F., N.P.-N. and L.F.G.; Writing—review & editing, J.C.F., F.T.F., N.P.-N. and L.F.G. All authors have read and agreed to the published version of the manuscript.

Funding: This research was funded by the National Scientific and Technological Research Council (CNPq, Brazil), the State Scientific and Innovation Funding Agency of Espírito Santo (FAPES, Brazil), and the Brazilian Federal Agency for Support and Evaluation of Graduate Education (CAPES, Brazil). NPN acknowledges the support of CNPq of Brazil under grant PQ-IB 310121/2021-3.

Data Availability Statement: Data are contained within the article.

Conflicts of Interest: The authors declare no conflicts of interest.

Appendix A. Conformal Transformation

Under the conformal transformation

$$g_{\mu\nu} = \phi^{-1} \tilde{g}_{\mu\nu}, \quad g^{\mu\nu} = \phi \tilde{g}^{\mu\nu}, \tag{A1}$$

the connection transforms as

$$\Gamma_{\mu\nu}^{\rho} = \tilde{\Gamma}_{\mu\nu}^{\rho} - \frac{1}{2} \left(\delta_{\mu}^{\rho} \frac{\partial_{\nu} \phi}{\phi} + \delta_{\nu}^{\rho} \frac{\partial_{\mu} \phi}{\phi} - \tilde{g}_{\mu\nu} \tilde{g}^{\rho\sigma} \frac{\partial_{\sigma} \phi}{\phi} \right). \tag{A2}$$

The Ricci tensor and the Ricci scalar takes the form

$$R_{\mu\nu} = \tilde{R}_{\mu\nu} + \frac{\phi_{;\mu;\nu}}{\phi} - \frac{1}{2} \frac{\phi_{;\mu} \phi_{;\nu}}{\phi^2} + \frac{1}{2} \tilde{g}_{\mu\nu} \left(\frac{\tilde{\square} \phi}{\phi} - 2 \frac{\phi_{;\rho} \phi^{;\rho}}{\phi^2} \right), \tag{A3}$$

$$R = \phi \left\{ \tilde{R} + 3 \frac{\tilde{\square} \phi}{\phi} - \frac{9}{2} \frac{\phi_{;\rho} \phi^{;\rho}}{\phi} \right\}, \tag{A4}$$

The energy momentum–tensor becomes

$$T^{\mu\nu} = (\rho + p) u^{\mu} u^{\nu} - p g^{\mu\nu} = \phi \left\{ (\rho + p) \tilde{u}^{\mu} \tilde{u}^{\nu} - p \tilde{g}^{\mu\nu} \right\} \tag{A5}$$

$$= \phi^3 \left\{ (\tilde{\rho} + \tilde{p}) \tilde{u}^{\mu} \tilde{u}^{\nu} - \tilde{p} \tilde{g}^{\mu\nu} \right\}, \tag{A6}$$

with

$$\tilde{\rho} = \rho \phi^{-2}, \quad \tilde{p} = p \phi^{-2}. \tag{A7}$$



References

1. Friedmann, A. Über die Krümmung des Raumes. *Z. Phys.* **1922**, *10*, 377. [CrossRef]
2. Einstein, A. Sitzungsberichte Berl. Akad. 1917, 142.
3. de Sitter, W. Einstein’s theory of gravitation and its astronomical consequences. *Mon. Not. R. Astronom. Soc.* **1916**, *76*, 699. [CrossRef]
4. Zwicky, F. On the redshift of spectral lines through interstellar space. *Proc. Natl. Acad. Sci. USA* **1929**, *15*, 773–779. [CrossRef]
5. Pecker, J.C.; Vigier, J.P. A Possible Tired-Light Mechanism. In Proceedings of the 124th Symposium of the International Astronomical Union, Beijing, China, 25–30 August 1986; pp. 507–511.
6. del Campo, S.; Herrera, R.; Labrana, P. On the Stability of Jordan-Brans-Dicke Static Universe. *J. Cosmol. Astropart. Phys.* **2009**, *2009*, 006. [CrossRef]
7. Atazadeh, K. Stability of the Einstein static universe in Einstein-Cartan theory. *J. Cosmol. Astropart. Phys.* **2014**, *2014*, 020. [CrossRef]
8. Huang, H.; Wu, P.; Yu, H. Stability of the Einstein static universe in the Jordan-Brans-Dicke theory. *Phys. Rev. D* **2014**, *89*, 103521. [CrossRef]
9. Darabi, F.; Atazadeh, K.; Heydarzade, Y. Einstein static universe in the Rastall theory of gravity. *Eur. Phys. J. Plus* **2018**, *133*, 249. [CrossRef]
10. Barrow, J.D.; Ellis, G.F.R.; Maartens, R.; Tsagas, C.G. On the stability of the Einstein static universe. *Class. Quant. Grav.* **2003**, *20*, L155–L164. [CrossRef]
11. Wetterich, C. Universe without expansion. *Phys. Dark Universe* **2013**, *2*, 184–187. [CrossRef]
12. Wetterich, C. Eternal universe. *Phys. Rev. D* **2014**, *90*, 043520. [CrossRef]
13. Wetterich, C. Cosmologies with variable Newton’s ‘constant’. *Nucl. Phys. B* **1988**, *302*, 645–667. [CrossRef]
14. Wetterich, C. Cosmology and the fate of dilatation symmetry. *Nucl. Phys. B* **1988**, *302*, 668–696. [CrossRef]

15. Wetterich, C.; Yamada, M. Variable Planck mass from the gauge invariant flow equation. *Phys. Rev. D* **2019**, *100*, 066017. [CrossRef]
16. Fabris, J.C. Some Remarks on Alternative (or Modified) Theories of Gravity. *arXiv* **2023**, arXiv:2311.14446.
17. Brans, C.H.; Dicke, R.H. Mach's principle and a relativistic theory of gravitation. *Phys. Rev.* **1961**, *124*, 925. [CrossRef]
18. Weinberg, S. *Gravitation and Cosmology*; Wiley: New York, NY, USA, 1972.
19. Baptista, J.P.; Fabris, J.C.; Gonçalves, S.V.B. Density perturbations in the Brans-Dicke theory. *Astrophys. Space Sci.* **1997**, *246*, 315–331. [CrossRef]
20. Barrow, J.D. Scalar-tensor cosmologies. *Phys. Rev. D* **1993**, *47*, 5329. [CrossRef]
21. Faraoni, V.; Gunzig, E. Einstein frame or Jordan frame? *Int. J. Theor. Phys.* **1999**, *38*, 217. [CrossRef]
22. Horndeski, G.W. Second-order scalar-tensor field equations in a four-dimensional space. *Int. J. Theor. Phys.* **1974**, *10*, 363. [CrossRef]
23. Kobayashi, T. Horndeski theory and beyond: A review. *Rep. Prog. Phys.* **2019**, *82*, 086901. [CrossRef]
24. Brando, G.; Fabris, J.C.; Falciano, F.T.; Galkina, O. Stiff matter solution in Brans-Dicke theory and the general relativity limit. *Int. J. Mod. Phys. D* **2019**, *28*, 1950156. [CrossRef]
25. Faraoni, V.; Zeyn, C. Disforming scalar–tensor cosmology. *arXiv* **2023**, arXiv:2401.00091.
26. Jain, P. A flat spacetime model of the universe. *Mod. Phys. Lett. A* **2012**, *27*, 1250201. [CrossRef]

Disclaimer/Publisher's Note: The statements, opinions and data contained in all publications are solely those of the individual author(s) and contributor(s) and not of MDPI and/or the editor(s). MDPI and/or the editor(s) disclaim responsibility for any injury to people or property resulting from any ideas, methods, instructions or products referred to in the content.

FLRW Transit Cosmological Model in $f(R, T)$ Gravity

Vijay Singh ^{1,†} , Siwaphiwe Jokweni ^{2,†} and Aroonkumar Beesham ^{2,3,4,*,†} 

¹ Department of Mathematics, Kirori Mal College, University of Delhi, Delhi 110007, India; gtrcosmo@gmail.com

² Department of Mathematical Sciences, University of Zululand, P Bag X1001, KwaDlangezwa 3886, South Africa; jokwenis@unizulu.ac.za

³ Faculty of Natural Sciences, Mangosuthu University of Technology, Jacobs 4026, South Africa

⁴ National Institute for Theoretical and Computational Sciences (NITheCS), Stellenbosch 7611, South Africa

* Correspondence: abeesham@yahoo.com

† These authors contributed equally to this work.

Abstract: A Friedmann–Lemaître–Robertson–Walker space–time model with all curvatures $k = 0, \pm 1$ is explored in $f(R, T)$ gravity, where R is the Ricci scalar, and T is the trace of the energy–momentum tensor. The solutions are obtained via the parametrization of the scale factor that leads to a model transiting from a decelerated universe to an accelerating one. The physical features of the model are discussed and analyzed in detail. The study shows that $f(R, T)$ gravity can be a good alternative to the hypothetical candidates of dark energy to describe the present accelerating expansion of the universe.

Keywords: $f(R, T)$ gravity; dark energy; scale factor



Citation: Singh, V.; Jokweni, S.; Beesham, A. FLRW Transit Cosmological Model in $f(R, T)$ Gravity. *Universe* **2024**, *10*, 272. <https://doi.org/10.3390/universe10070272>

Academic Editors: Galina L. Klimchitskaya, Vladimir M. Mostepanenko, Sergey V. Sushkov and Jean-Pierre Gazeau

Received: 27 February 2024

Revised: 30 May 2024

Accepted: 18 June 2024

Published: 24 June 2024



Copyright: © 2024 by the authors. Licensee MDPI, Basel, Switzerland. This article is an open access article distributed under the terms and conditions of the Creative Commons Attribution (CC BY) license (<https://creativecommons.org/licenses/by/4.0/>).

1. Introduction

Observational data such as Planck [1], baryon acoustic oscillations (BAO) [2], the Wilkinson microwave anisotropy probe (WMAP) [3], large-scale structures (LSS) [4], cosmic microwave background radiation (CMBR) [5], and Type-Ia supernova (SNe-Ia) [6–8], have become a vital pillar in comprehending modern cosmology. These observations suggest that the universe has undergone a pillar of accelerated expansion twice, viz., early inflation [9–11] and late-time acceleration. The inflationary phase has resolved the flatness and horizon problems [9] as well as the entropy problem partially. Acceleration at late-times is supposed to be caused by an unknown component known as dark energy (DE) that occupies approximately two-thirds of the total energy budget of the universe [12,13]. The most widely acknowledged Λ CDM (cold dark matter) model based on Einstein’s theory of general relativity (GR) explains the late-time acceleration phenomenon via a cosmological constant (CC), Λ [14,15], which is characterized by an equation of state (EoS) parameter $\omega = -1$.

Though the standard model explains various physical phenomena, such as the formation and evolution of the large-scale structure in the early universe and the abundance of matter and energy [16,17], etc., it experiences setbacks such as coincidence and fine-tuning problems [18,19]. Due to these setbacks, researchers have proposed some dynamic candidates for DE. These include quintessence [20], phantom energy [21,22], tachyons [23], Chaplygin gas [24], and k-essence [25]. However, due to the lack of evidence of the existence of any of these forms of DE, a class of researchers are not in favor of accommodating these hypothetical candidates of DE. Instead of such a theoretical form of energy, they prefer to seek some other alternatives to explain acceleration at late times. One way is to modify the action of GR. The modified theories naturally unify early-time inflation and late-time acceleration [26,27]. The most popular modified theories include $f(R)$ theories [28,29], scalar Gauss–Bonnet gravity $f(G)$ [30], generalized Gauss–Bonnet $f(R, G)$ [31], $f(T)$ theory [32], $f(Q)$ theory [33], and $f(Q, T)$ gravity [34].

Among modified gravity theories, initially, the focus was put only on altering the geometrical part of the EH action. Later, explicit coupling of an arbitrary function of the Ricci scalar R and the matter lagrangian \mathcal{L}_m was introduced, and a maximal extension of the EH action was proposed [35]. These theories came to be known as the $f(R, \mathcal{L}_m)$ gravity theories [36]. In 2011, Harko et al. [37], through non-minimal general coupling between geometry and matter, introduced $f(R, T)$ gravity, where T is the trace of the stress–energy tensor. Exotic imperfect fluids or quantum effects provide the rationale for selecting T as a Lagrangian argument. The authors argued that the variation of the stress–energy tensor with respect to the metric is represented by a source term. Consequently, the matter content, as well as the geometrical part, contribute to cosmic acceleration. Furthermore, neither ghosts nor Laplacian instabilities exist in this theory [38]. Additionally, the theory has passed observational tests on intra- and extra-galactic scales. This extraordinary behavior and observational validity set this theory apart from other theories of gravity by producing notable signatures and effects. Therefore, $f(R, T)$ gravity has gained a lot of interest and rose to the top of the list of potential solutions in many contexts on galactic and intra-galactic scales.

Jamil et al. [39] reconstructed some $f(R, T)$ gravity models and showed that the dust fluid reproduces Λ CDM, phantom-non-phantom era and phantom cosmology. Azizi [40] studied wormhole solutions in the framework of $f(R, T)$ gravity. Alvarenga et al. [41] studied the evolution of scalar cosmological perturbations in the metric formalism. Sharif et al. [42] studied the energy conditions for the FLRW universe with perfect fluid. Pasqua et al. [43] reconstructed modified holographic Ricci dark energy. Alves et al. [44] explored gravitational waves in this theory. Momeni et al. [45] presented a study of the generalized second law of thermodynamics in the scope of $f(R, T)$ gravity. Das et al. [46] generated a set of solutions describing the interior of a compact star which admits conformal motion. Using a perfect fluid as the only matter content, Shabani and Ziaie [47] studied classical bouncing solutions in a flat FLRW background. Deb et al. [48] explored the physical features of anisotropic strange stars beyond the standard maximum mass limit in $f(R, T)$ gravity. Elizalde and Khurshudyan [49] discussed the formation of specific static wormhole models. Ordines and Carlson [50] investigated changes in the earth’s atmospheric models coming from the $f(R, T)$ modified theory of gravity (for more details, see [51,52] and the references therein).

On the other hand, it is also well known that prior to the current accelerating expansion, the universe had undergone a decelerated phase in the past. However, constructing viable scaling models that allow the universe to transition from a decelerating to an accelerating phase is still a challenging task. An alternative is to seek the solutions of the field equations under an assumption which would be consistent with the observed kinematics of the universe. This phenomenon has piqued the interest of many researchers. Some theorists working in this area have attempted to study it by constructing cosmological models using geometrical parameters, such as the parametrization of the deceleration parameter, Hubble parameter, or scale factor, which can provide the transition from past deceleration to present acceleration [53–56]. Most of these models have been studied in homogeneous and isotropic backgrounds [57–65], but some studies have also been considered in homogeneous but anisotropic backgrounds [66–72].

Knowing the EoS of DE is one of the biggest challenges in theoretical physics [73–77] as well as in observational cosmology today [78,79]. The observations seem to favor an evolving EoS for DE [80,81]. Considering all curvatures $k = -1, 0, +1$, the present study deals with a transit FLRW model in $f(R, T)$ gravity. We consider a scale factor as proposed in Ref. [82]. We investigate the nature of matter and its sources, which exhibit cosmological evolution as suggested by the theoretical background and supported by the various observations. In particular, we seek to answer whether $f(R, T)$ gravity could be a possible alternative to various hypothetical forms of DE.

The work is organized as follows. The model and field equations followed by their solutions are presented in Section 2. The geometrical behavior of the deceleration parameter is also presented in the same section, and the constraints for a physically realistic scenario

are obtained therein. Thereafter, the nature of matter is examined. As compared to GR, in the $f(R, T)$ theory of gravity, due to coupling, some additional terms arise in the energy–momentum tensor. These extra terms may be considered as coupled matter or energy, which may behave as either perfect fluid or DE. The nature of this coupled matter is examined in Section 3. The behaviour of effective matter is studied in Section 4. The results are summarized in Section 5.

2. The Model in $f(R, T)$ Gravity

The spatially homogeneous and isotropic FLRW space–time metric is given as follows:

$$ds^2 = dt^2 - a^2(t) \left[\frac{dr^2}{1 - kr^2} + r^2(d\theta^2 + \sin^2 \theta d\phi^2) \right], \tag{1}$$

where $0 \leq \theta \leq \pi$, $0 \leq \phi \leq 2\pi$, a is the scale factor, and k represents the geometrical curvature of the universe, i.e., $k = 0$ implies a flat universe, $k = +1$ is a closed universe, and $k = -1$ is an open universe. We consider the energy–momentum tensor of the matter as follows:

$$T_{ij} = (\rho_m + p_m)u_i u_j - p g_{ij}, \tag{2}$$

where ρ_m is the energy density and p_m is the thermodynamic pressure of the matter. In comoving coordinates, $u^i = \delta_0^i$, where u^i is the four-velocity of the fluid that satisfies the condition $u_i u^i = 1$.

Harko et al. [37] considered some functional forms of $f(R, T)$ gravity models. The authors mentioned that in the $f(R, T)$ theory of gravity, the field equations are governed by the choice of the source of matter. Therefore, by choosing suitable matter fields, a different cosmological model is obtained by choosing a different functional form for f . In their paper, those authors took the simplest case, i.e., $f(R, T) = 2f(T) + R$, showing the equivalence with a cosmological model with an effective cosmological constant, which varies with Hubble parameter, i.e., $\Lambda \propto H^2$. It was also shown that gravitational coupling is no longer constant, but is now a function of time, viz., $G_{eff} = f'(T) \pm G$, where a prime represents a derivative with respect to the argument. Thus, the term $2f(T)$ in the gravitational action modifies the gravitational interaction between matter and curvature. Although there is not any fundamental basis for considering a linear combination of R and T , the authors showed that the choice of $f(T) = \lambda T$ for the dust matter leads to the power-law expansion of the universe, $a \propto t^\alpha$, where α depends on the coupling parameter λ .

The choice $f(R, T) = R + 2\lambda T$ also corresponds to GR with an additional matter content on the right side of the field equations. This allows for a wider variety of behaviour, which reduces to GR when $\lambda = 0$. The right side of the field equations are similar (but not the same) to general relativity, containing a fluid with viscosity or heat conduction. Hence, the entropy problem could be solved using the $f(R, T)$ theory. Several problems, such as the fine-tuning problem, coincidence problem, and cosmological constant problem can be solved by the dynamic Λ in theory, and it can still satisfy observations [83]. The variable Λ parameter occurring in the theory may be written as a function of T where T is the trace of T_{ij} , and is sometimes called “ $\Lambda(T)$ gravity”. Hence, this means that a variable Λ can be derived naturally from $f(R, T)$ gravity via a Lagrangian formulation. However, the choice $f(R, T) = R + 2\lambda T$ has not always been met with a positive reception by the scientific community in a few papers [84,85]. Such criticism has been addressed in Ref. [86] recently. Very recently, Jaekel et al. [87], on some observational grounds, proposed that $f(R, T) = R + \lambda T$ and $f(R, T) = R + e^T$ models should be ruled out. However, their analysis is biased. Staying on the conservative side, those authors considered the age of the universe as more than 14.16 Gyrs. Also, there are some other constraints that were followed in their study. These models are, at the very least, still viable at lower redshift limits, as shown in Ref. [88]. We shall return further to the comments in Ref. Jaekel et al. [87] later in the conclusion.

Moreover, it was shown earlier [89] that when reconstructing $f(R, T) = R + 2f(T)$, an exponential solution implies that $f(R, T) = R + \lambda T$. A similar result is true for power-law

solutions, but in this case, $f(R, T) = R + \lambda T^\alpha$, where α is a constant. It is well known that the conservation equation does not necessarily hold in $f(R, T)$ gravity—see Appendix A. Moreover, a scalar field with flat potential was studied earlier in the $f(R, T) = R + 2f(T)$ theory of gravity [90], looking for conditions for energy conservation. Surprisingly, it was found that the expression $f(R, T) = R + 2f(T)$ had the same form as before, viz., $f(R, T) = R + 2\lambda T$. Hence, this linear form of $f(R, T)$ has a significant physical and mathematical basis. Whilst being simple, this form allows one to investigate salient points of this theory. Hence, this simple form is popular with most researchers in the field. In the present study, we also consider this form.

The field equations in $f(R, T) = R + 2f(T)$ gravity with the system of units $8\pi G = 1 = c$, are obtained as follows:

$$R_{ij} - \frac{1}{2}Rg_{ij} = T_{ij} + 2(T_{ij} + pg_{ij})f'(T) + f(T)g_{ij}, \tag{3}$$

where a prime represents the derivative with respect to T . The above equation for $f(T) = \lambda T$, i.e., $f(R, T) = R + 2\lambda T$, where $T = \rho - 3p$, simplifies as follows:

$$R_{ij} - \frac{1}{2}Rg_{ij} = (1 + 2\lambda)T_{ij} + \lambda(\rho - p)g_{ij}. \tag{4}$$

For the (1) metric and the energy–momentum tensor (2), the above equation yields the following:

$$3H^2 + 3\frac{k}{a^2} = \rho_m + \lambda(3\rho_m - p_m), \tag{5}$$

$$2\dot{H} + 3H^2 + \frac{k}{a^2} = -p_m - \lambda(3p_m - \rho_m). \tag{6}$$

It is vital to note that in the $f(R, T)$ theory of gravity, both p_m and ρ_m do not reflect the effective pressure and energy density as in GR. Indeed, the coupling between matter and $f(R, T)$ gravity adds some additional terms visible on the RHS of the field equations. Additional contributions can be collected in terms of geometrical effective pressure and energy density. This can be associated with the dark sector. If the modified gravity sector is responsible for the late time accelerated phase, then the additional terms can be interpreted as DE. This is the convention that we adopt in this work. We term the additional terms with λ as “coupled matter” or “coupled energy”. Therefore, to distinguish the “main” matter from the “coupled” matter or energy, we write $\rho_f = \lambda(3\rho_m - p_m)$ and $p_f = \lambda(3p_m - \rho_m)$, which represents the coupled matter or energy.

Now, Einstein’s equations with the cosmological constant Λ on the right-hand side of the field equations are as follows:

$$R_{ij} - \frac{1}{2}Rg_{ij} = T_{ij} + \Lambda g_{ij}.$$

Comparing this with (4), we notice that a variable Λ in $f(R, T)$ gravity may be defined as follows:

$$\Lambda = \Lambda(T) = -(2p_m + T)\lambda = (\rho_m - p_m)\lambda.$$

Hence, we see that variable Λ arises naturally in $f(R, T)$ gravity. Thus, additional matter–geometry coupling terms work as a variable cosmological parameter. This can assist in solving the fine-tuning problem, coincidence problem, and cosmological constant problem. In addition, observations can also be satisfied [83].

Ideally, the solutions of (5) and (6) are supposed to be obtained by solving the conservation equation. However, as far as $f(R, T)$ gravity, as mentioned earlier, is concerned, the usual conservation equation in GR is not satisfied [37]. However, only in a few cases does the chosen $f(R, T)$ function lead to a conservation equation holding true. In Ref. [90], two of the present authors studied such a case. For a complete discussion on this, we would

like to refer to a recent study [91]. Secondly, if one tries to compute the analogue of the conservation equation in $f(R, T)$ gravity, this leads to very complicated expressions, and even more so if one inserts this into the Friedmann Equation (5). This is extremely difficult to solve; hence, most researchers resort to assuming some form of scale factor, Hubble parameter, deceleration parameter, equation of state parameter, etc.

The transition from a decelerated phase to an accelerated phase must be present in any realistic model. However, due to our lack of knowledge of dark energy, constructing viable scaling models that allow the universe to transition from a decelerating phase to an accelerating phase is still a challenging task. An alternative is to seek solutions of field equations under an assumption which would be consistent with the observed kinematics of the universe. This phenomenon has piqued the interest of many researchers. Some theorists working in this area have attempted to study it by constructing cosmological models using geometrical parameters, such as the parametrization of the deceleration parameter, Hubble parameter, or scale factor, which can provide the transition from past deceleration to present acceleration, and be consistent with observations. Many researchers have considered similar geometrical evolutions (for an extensive list, see Refs. given in [92]). Some authors [68,93–95] have studied another form of the hybrid scale factor, which also describes the transition from the decelerated to accelerated expansion of the universe. Apart from these works, there are a plethora of similar works.

We see that Equations (5) and (6) consist of three unknowns, i.e., ρ_m , p_m , and H . Hence, to determine a solution, one extra assumption is required. We have considered the simple parametrization of the scale factor as recently studied by Mishra and Dua [82]:

$$a(t) = \exp(\alpha t + \beta)^p, \tag{7}$$

where $\alpha > 0$, $\beta > 0$, and $0 < p < 1$ are arbitrary constants.

Now, let us discuss the scale factor considered here further. The approach to seek solutions of the field equations under an assumption which would be consistent with the observed kinematics of the universe is known as cosmography, which has been extensively studied in the literature. In Ref. [90], two of the present authors cited many such works conducted earlier. While following this reverse approach, the authors obtained similar scale factors.

As far as the parameters are concerned in solution (7), we have tried to consider the most general form. Later, while investigating, we realized that some of the parameters are just scaling and shifting parameters. Therefore, we dropped them out. If we would have analyzed without those parameters, it would be a very specific study, and one could argue why such a particular study must be considered. In any case, there are many papers in the literature where such parameters are included.

The Hubble parameter, $H = \dot{a}/a$ yields the following:

$$H(t) = \frac{\alpha p}{(\alpha t + \beta)^{1-p}}. \tag{8}$$

Using $a = a_0/(1+z)$, where a_0 is the present value of a , and z is the redshift, one obtains the $t - z$ relationship [82]:

$$\alpha t + \beta = [A - \log(1+z)]^{\frac{1}{p}},$$

where $A = (\alpha t_0 + \beta)^p$, t_0 is the present time. Using the above $t - z$ relationship, the Hubble parameter is obtained in terms of redshift z as follows:

$$H(z) = \alpha p [A - \log(1+z)]^{1-\frac{1}{p}}. \tag{9}$$

Similarly, the deceleration parameter, $q = -a\ddot{a}/\dot{a}^2$, in terms of the redshift, is as follows:

$$q(z) = -1 + \left(\frac{1}{p} - 1\right) [A - \log(1+z)]^{-1}, \tag{10}$$

where $A = (1/p - 1)/(1 + q_0)$, and q_0 is the present value of the deceleration parameter.

Recently, using the 51 points $H(z)$ data set [96] and the 1048 points Pantheon SNe-Ia data set [97] with $H_0 = 67.77 \text{ km s}^{-1} \text{ Mpc}^{-1}$ [98], Mishra and Dua [82] obtained observational constraints on q_0 and p , and reported the best-fitted values $q_0 \approx -0.40$ and $p = 0.47$ with the $H(z)$ data set and $q_0 \approx -0.54$ and $p = 0.66$ with the Pantheon data set.

Figure 1 plots the deceleration parameter q versus redshift z for the best-fitted values mentioned above. We observe that the universe transits from deceleration ($q > 0$) to acceleration ($q < 0$) at a redshift of $z = 0.8$ for the $H(z)$ data and $z = 1.2$ for the Pantheon data.

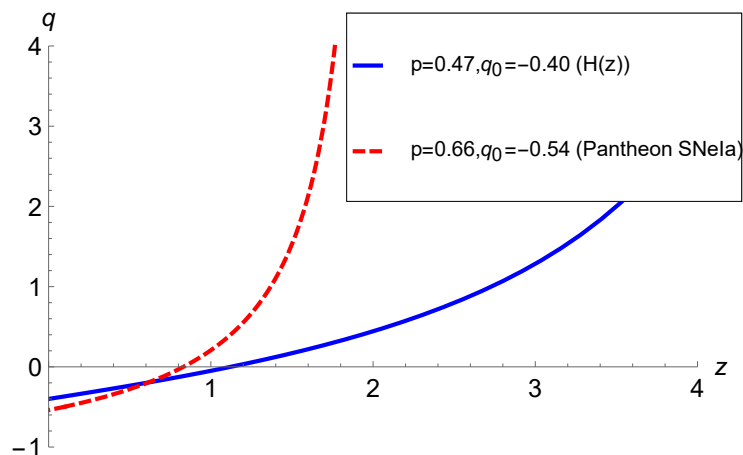


Figure 1. Deceleration parameter q in terms of redshift z with the best-fitted values of p and q_0 .

We note the following. Firstly, the deceleration parameter for the adopted form of the scale factor describes a transition from a deceleration in the past to acceleration in the future. Secondly, the values of p and the current deceleration parameter q_0 occur in our equation for the deceleration parameter $q(z)$. To plot our deceleration parameter, as in Figure 1, we use the values of q_0 and p obtained from observations, as mentioned above. The calculated values of the transition redshift z_t work out to be 0.8 and 1.2. Whilst this is somewhat higher than the value for the Λ CDM model, it is within the error bounds [99]. Thirdly, the usually quoted values of q_t are based on the Λ CDM model, and values for alternative theories or models could be somewhat different whilst the model has the required salient features.

The main objectives of our study are as follows:

- Investigating the nature of matter in the presence of which the model can yield the desired evolution of the universe.
- Examining the role of $f(R, T)$ gravity.
- Comparing and distinguishing outcomes from those of Einstein’s gravity.

Using (7) and (8) in (5) and (6), we obtain the energy density and pressure of matter as follows:

$$\rho_m = \frac{e^{-2(\beta+\alpha t)^p} \left[k(8\lambda + 3) + \alpha^2 p e^{2(\beta+\alpha t)^p} (\beta + \alpha t)^{p-2} (2\lambda - 2\lambda p + 3p(2\lambda + 1)(\beta + \alpha t)^p) \right]}{(2\lambda + 1)(4\lambda + 1)}, \tag{11}$$

$$p_m = - \frac{k e^{-2(\beta+\alpha t)^p} + \alpha^2 p (\beta + \alpha t)^{p-2} [2(3\lambda + 1)(p - 1) + 3p(2\lambda + 1)(\beta + \alpha t)^p]}{(1 + 4\lambda)(1 + 2\lambda)}. \tag{12}$$

The vital requirement is now to corroborate that the assumption we chose to find a solution results in a realistic cosmological model, e.g., $\rho \geq 0$. We note that $\rho_m \geq 0$ requires $\lambda \geq 0$ in all the three models $k = 0, \pm 1$.

Let us examine the behavior of actual matter. The EoS parameter of actual matter $\omega_m = p_m/\rho_m$ provides the following:

$$\omega_m = -\frac{k(\beta + \alpha t)^2 + \alpha^2 p e^{2(\beta + \alpha t)^p} (\beta + \alpha t)^p (2(3\lambda + 1)(p - 1) + 3p(2\lambda + 1)(\beta + \alpha t)^p)}{k(8\lambda + 3)(\beta + \alpha t)^2 + \alpha^2 p e^{2(\beta + \alpha t)^p} (\beta + \alpha t)^p (2\lambda - 2\lambda p + 3p(2\lambda + 1)(\beta + \alpha t)^p)}. \tag{13}$$

Since α is a scaling parameter and β is just a shifting parameter, the only crucial parameter in this study is p . Therefore, we set $\alpha = 1$ and $\beta = 0$ to study the behavior of the EoS parameter for the best-fitted values $p = 0.47$ ($H(z)$ data) and $p = 0.66$ (Pantheon data). Figures 2 and 3 depict the behavior of matter with the $H(z)$ and Pantheon data, respectively.

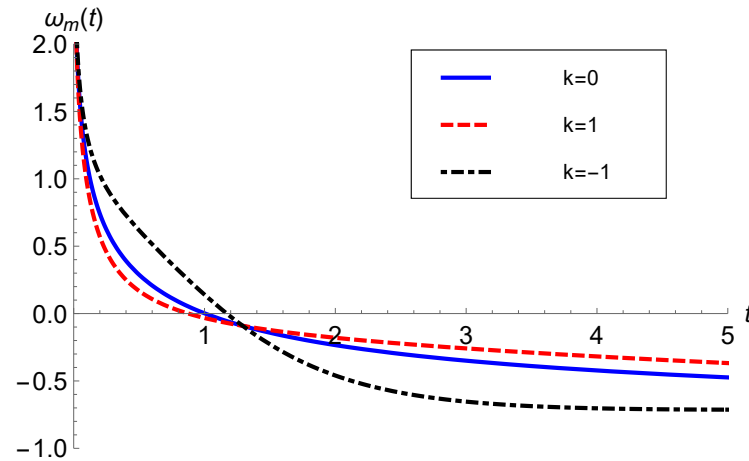


Figure 2. $\omega_m(t)$ versus t with $p = 0.47$ ($H(z)$ data) and $\lambda = 1$.

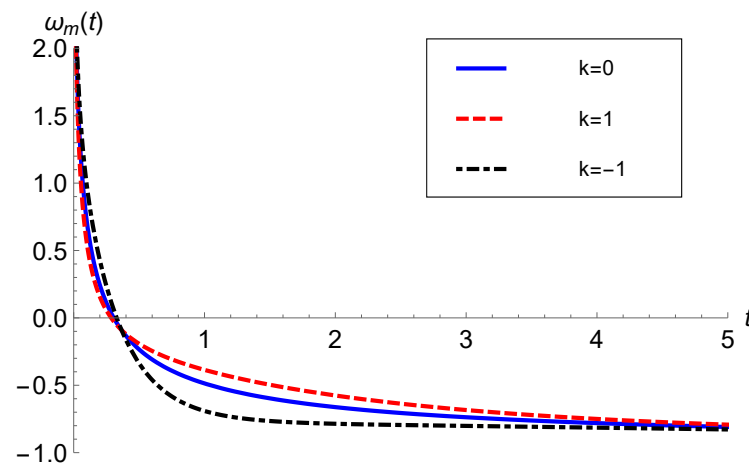


Figure 3. $\omega_m(t)$ versus t with $p = 0.66$ (Pantheon data) and $\lambda = 1$.

Analytically, we find that for all three spatial curvature models, $\omega_m = \frac{1}{\lambda} + 3$ at $t = 0$, and $\omega_m \rightarrow -1$ as $t \rightarrow \infty$. Therefore, ω_m starts with a finite value $\omega_m \geq 3$ with the evolution and approaches the cosmological constant at late times. Hence, the matter exhibits a unified description of all kinds of matter, including stiff matter ($\omega_m \geq 1$), radiation ($\omega_m = 1/3$), dust ($\omega_m = 0$), quintessence ($-1 < \omega_m \leq -1/3$), and a cosmological constant ($\omega_m = -1$), in the same order as is required for unified cosmological evolution.

3. The Behavior of Coupled Matter

The energy density and pressure of coupled matter are obtained as follows:

$$\rho_f = \frac{2\lambda \left[k(12\lambda + 5)e^{-2(\beta+\alpha t)^p} + \alpha^2 p(\beta + \alpha t)^{p-2} \{ 6p(2\lambda + 1)(\beta + \alpha t)^p + p - 1 \} \right]}{(1 + 4\lambda)(1 + 2\lambda)}, \tag{14}$$

$$p_f = \frac{2\lambda \left[\alpha^2 p(\beta + \alpha t)^{p-2} \{ 8\lambda + p(-8\lambda - 6(2\lambda + 1)(\beta + \alpha t)^p - 3) + 3 \} - k(4\lambda + 3)e^{-2(\beta+\alpha t)^p} \right]}{(1 + 4\lambda)(1 + 2\lambda)}. \tag{15}$$

In all three spatial curvature models, we note that the energy density of coupled matter is negative at very early stages of evolution, and turns out to be positive after a particular length of time. Since ρ_f becomes zero at the transition time, it is noteworthy to use the EoS parameter to study the behavior of coupled matter as $\omega_f = p_f/\rho_f$ would diverge at that instant of time. Alternatively, we study the implications of the energy conditions, which are stated as follows:

- Null energy conditions (NEC): $\rho + p \geq 0$;
- Weak energy conditions (WEC): $\rho \geq 0, \rho + p \geq 0$;
- Strong energy conditions (SEC): $\rho + 3p \geq 0$;
- Dominant energy conditions (DEC): $\rho \geq |p|$.

Figure 4 shows the behavior of energy density for a flat model, which shows that the WEC is violated at very early times. We observe the same behavior in closed and open models. Although the energy density of a field in classical physics is strictly positive, the energy density in quantum field theory can be negative due to quantum coherence effects [100]. The Casimir effect [101,102] and squeezed states of light [103] are two familiar examples which have been studied experimentally. As a result, all the known pointwise energy conditions in GR, such as the WEC and NEC, are allowed to be violated. Even for a scalar field in flat Minkowski spacetime, it can be proven that the existence of quantum states with negative energy density is inevitable [100]. The violation of the WEC of coupled matter can be advocated by any of such mechanisms.

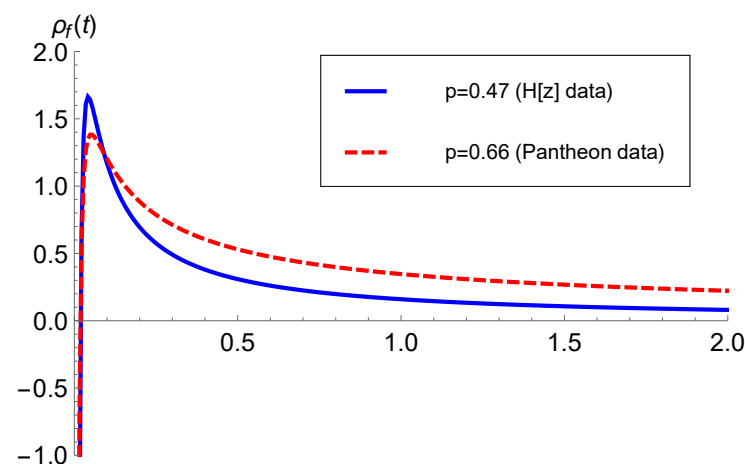


Figure 4. ρ_f versus t for flat model with $p = 0.47$ ($H(z)$ data), $p = 0.66$ (Pantheon data) and $\lambda = 1$.

The expression for $\rho_f + p_f$ is obtained as follows:

$$\rho_f + p_f = \frac{4\lambda \left[ke^{-2(\beta+\alpha t)^p} + \alpha^2 p(1 - p)(\beta + \alpha t)^{p-2} \right]}{2\lambda + 1}. \tag{16}$$

Since $\lambda > 0$ and $0 < p < 1$, the above expression implies $\rho_f + p_f \geq 0$ for flat and closed models. For $k = -1$, Figure 5 plots $p_f + \rho_f \geq 0$, implying the NEC also holds good for the open model.

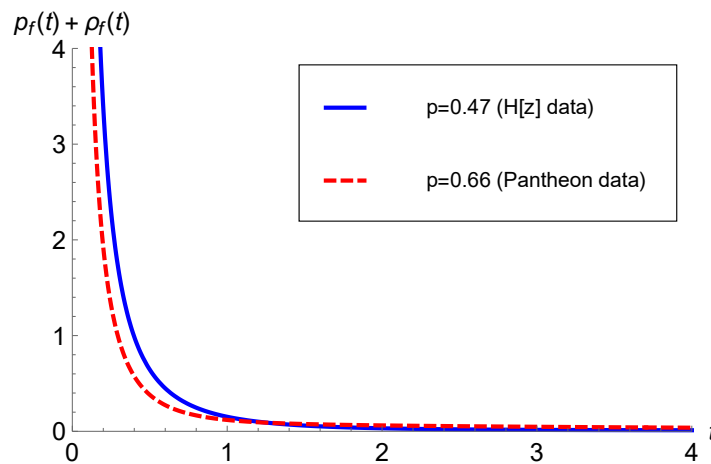


Figure 5. $\rho_f + p_f$ versus t for $k = -1$ with $\lambda = 1$.

Further, following is the expression of $\rho_f - p_f$,

$$\rho_f - p_f = \frac{8\lambda \left[2ke^{-2(\beta+\alpha t)^p} + \alpha^2 p \{ 3p(\beta + \alpha t)^p + p - 1 \} (\beta + \alpha t)^{p-2} \right]}{4\lambda + 1}. \tag{17}$$

Figures 6 and 7 plot $\rho_f - p_f$ with $H(z)$ and Pantheon data, respectively. Due to the domination of the $p - 1$ term at very early times, $\rho_f - p_f$ starts from a negative value, later it becomes positive, and, after attaining a maximum value, it starts decreasing and finally approaches zero at late times. Hence, the DEC is satisfied, except during the very early stages of evolution. This shows that coupled matter behaves as a phantom type of DE during the very early stage of evolution. Mechanically, phantom matter can originate from scalar fields with a global minimum in their effective potential [104], from higher-order curvature terms in higher-order theories of gravity [105–109], from bulk viscous stress due to particle production [110], in Brans–Dicke and non-minimally coupled scalar field theories [111], in strange effective quantum field theory [112,113], and by some other means (for details, see [114]). Most of these disparate prescriptions require the weakly coupled scalar field to be displaced from its equilibrium state. However, in the present study, we do not need any such hypothetical form of DE; rather, it is the natural outcome of matter–geometry coupling of $f(R, T)$ gravity.

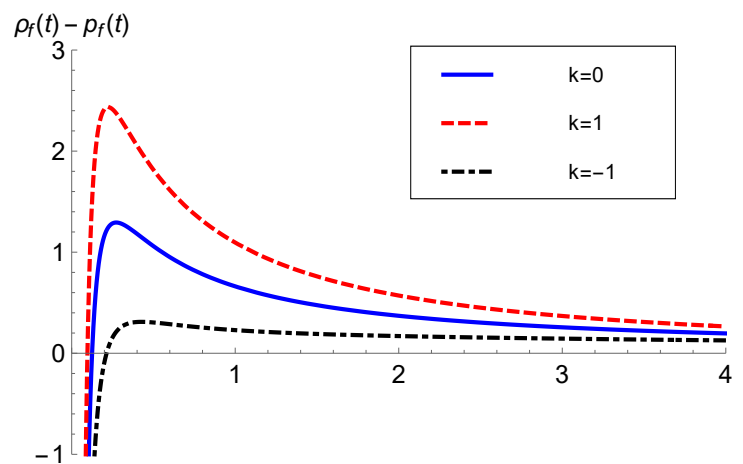


Figure 6. $\rho_f - p_f$ versus t with $p = 0.47$ ($H(z)$ data), and $\lambda = 1$.

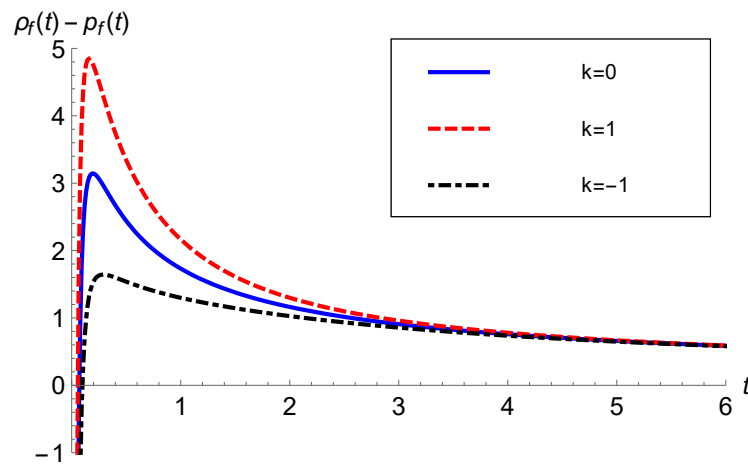


Figure 7. $\rho_f - p_f$ versus t with $p = 0.66$ (Pantheon data) and $\lambda = 1$.

Lastly, we have the follows:

$$\rho_f + 3p_f = \frac{8\lambda \left[\alpha^2 p (\beta + \alpha t)^{p-2} \{ -2(3\lambda + 1)(p - 1) - 3(2\lambda + 1)p(\beta + \alpha t)^p \} - k e^{-2(\beta + \alpha t)^p} \right]}{8\lambda^2 + 6\lambda + 1}. \tag{18}$$

Figures 8 and 9 depict the behavior of $\rho_f + 3p_f$ with $H(z)$ data and Pantheon data, respectively. In both models, $\rho_f + 3p_f$ becomes negative at late times. Hence, the SEC was violated during late-time evolution in all three models. This shows that coupled matter contributes as a quintessence type of DE and accelerates the expansion of the universe at late times. Again, it is interesting to note that no physical quintessence kind of matter is required to drive the late-time acceleration. Rather, the matter–geometry coupling of $f(R, T)$ gravity plays the role of DE in this model.

Thus, we observed that the main matter behaves as a phantom kind of DE, whereas the coupled matter acts as a quintessence kind of DE. However, since the model’s evolution in this study is controlled by effective matter, this makes it more crucial for the study of the behavior of effective matter together with individual matter sources.

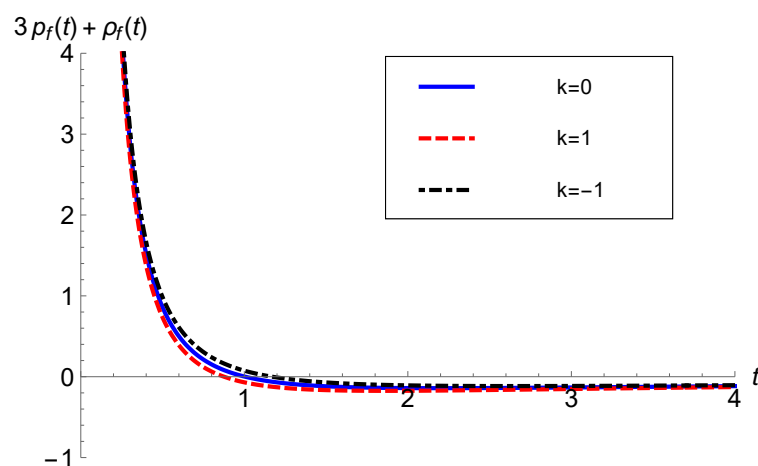


Figure 8. $\rho_f + 3p_f$ versus t with $p = 0.47$ ($H(z)$ data) and $\lambda = 1$.

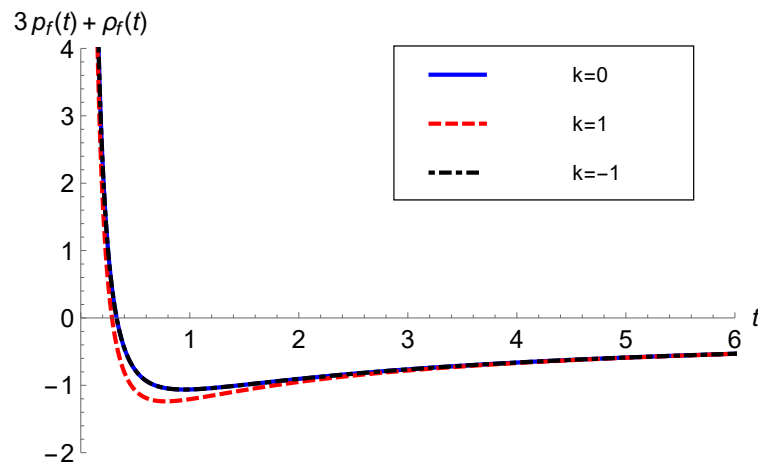


Figure 9. $\rho_f + 3p_f$ versus t with $p = 0.66$ (Pantheon data) and $\lambda = 1$.

4. The Behavior of Effective Matter

The energy density and pressure of effective matter can be obtained from $\rho_{eff} = \rho_m + \rho_f$ and $p_{eff} = p_m + p_f$, which also can be read from Equations (11) and (12) with $\lambda = 0$. Similarly, the EoS of effective matter can be read from Equation (13) with $\lambda = 0$, which implies that effective matter behaves similarly to GR. We note that effective matter obeys the WEC for all three curvature models. The behavior of effective matter with $H(z)$ and Pantheon data is illustrated in Figures 10 and 11, respectively.

The behavior of effective matter follows the same pattern as the matter discussed in Section 2. This can be observed by comparing Figures 2 and 3 with Figures 10 and 11. Therefore, the interpretation made for actual matter applies to the effective one, too. We note that the overall behavior of the effective matter follows the behavioral characteristics of the scalar field. Kinetic energy dominates the scalar potential early on in the evolution of the model. Thus, the scalar field behaves similarly to stiff matter. During inflation, this leads to extremely fast expansion driven by negative pressure. Just as a cosmological constant exerts stress at late times, the scalar field does as well as the potential term dominates the kinetic term during this era. It is important to note that the energy density is different to that during inflation. However, the effective matter in this study does not accommodate early inflation, but it effectively comprises the behavior of the hybrid scale factor considered in this study to transition from a decelerated era to the present accelerating era.

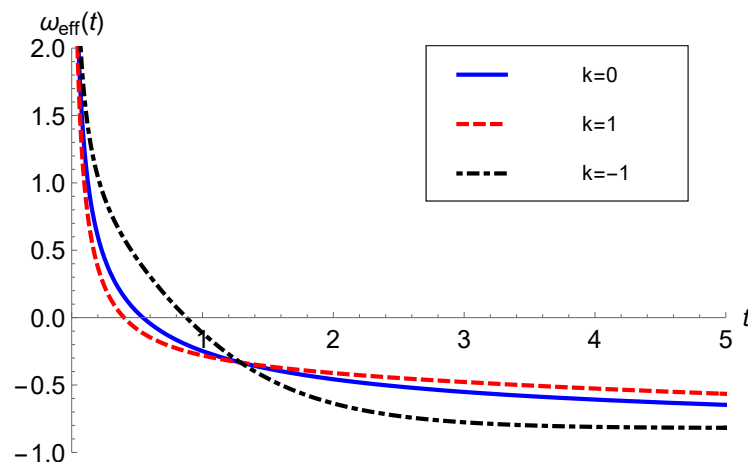


Figure 10. $\omega_{eff}(t)$ versus t with $p = 0.47$ ($H(z)$ data).

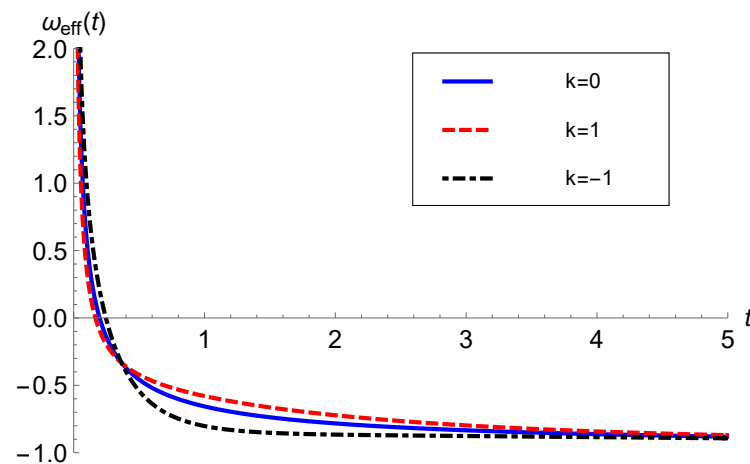


Figure 11. $\omega_{eff}(t)$ versus t with $p = 0.66$ (Pantheon data).

5. Conclusions

In this paper, we studied an FLRW space–time model filled with a perfect fluid in the framework of $f(R, T)$ gravity, where $f(R, T) = R + 2f(T)$ for all spatially curved models. In order to find solutions, we chose parametrization of the scale factor, $a(t) = a_0 e^{(at+\beta)^p}$, where $\alpha, \beta > 0$ and $0 < p < 1$, which yields a deceleration parameter consistent with early deceleration to a late-time acceleration phase for the parameters that best fit the data, viz. $p = 0.47$ ($H(z)$ data) and $p = 0.66$ (Pantheon data) [82]. The transition takes place at a redshift of $z = 0.8$ for the $H(z)$ data and $z = 1.2$ for the Pantheon data.

Figures 2 and 3 depict the behavior of matter for the $H(z)$ and Pantheon data, respectively. The kinematical dynamics of the model are independent of the theory and were studied earlier by Mishra and Dua [82] in the Brans–Dicke theory. To eschew repetition, the kinematical study is not presented in this paper. We found that a physically realistic cosmological model is possible only for $\lambda \geq 0$. We investigated the role of $f(R, T)$ gravity.

As compared to GR, in $f(R, T)$ gravity, due to coupling, if we look at the field equations on the right-hand side, there are extra terms. These extra terms may be termed coupled matter, which may behave either as perfect fluid or DE. First and foremost, we ascertain that all three spatial curvature models ($k = 0, \pm 1$) demand a positive coupling constant ($\lambda \geq 0$) to have a physically realistic scenario, i.e., to obey the WEC. Further, we identified the nature of the main matter and coupled matter to exhibit the transition from early deceleration to late time accelerated expansion. The main attributes of the models are the individual behaviors of primary matter and coupled matter, which are summarized below:

- The primary matter exhibits the characteristics of all kinds of matter, viz., stiff matter ($\omega_m \geq 1$), radiation ($\omega_m = 1/3$), dust ($\omega_m = 0$), quintessence ($-1 < \omega_m \leq -1/3$), and a cosmological constant ($\omega_m = -1$), in the same order as is required to depict the cosmic history, including the transition from a decelerating to an accelerating universe.
- The coupled matter satisfies the NEC throughout the evolution of the universe. However, it violates the WEC and the NEC during very early stages of evolution. It also violates the SEC at late times, which shows that the coupled matter contributes to quintessence DE.

Since effective matter governs how the universe evolves, in this investigation, it was crucial to study the behavior of effective matter separately from individual matter sources. Effective matter follows an evolving EoS, as shown in Figures 10 and 11. Effective matter exhibits a dual nature, i.e., a perfect fluid at early times and exotic matter at late times, which is consistent with observations. If geometric parameters govern the kinematic behavior in the $f(R, T)$ theory of gravity, then the way of behaving of the effective matter is not altered. Hence, as compared to GR, effective matter behaves similarly. It is also noteworthy to caption that all three spatial curvature models (flat, closed, and open) are indistinguishable as far as either the individual matter contents or effective matter are concerned.

It is noteworthy to mention here that Malik et al. [115] considered a more general form of the scale factor to study the bouncing cosmological scenario. The crucial element in facilitating a successful bounce is the violation of the NEC around the bouncing point, which the authors found in their study. However, our model does not violate the NEC at any stage of evolution. Moreover, the hybrid scale factor explored in the present study is completely different from that considered by Malik et al. and does not encounter a bounce at any stage. One can easily verify that the scale factor studied here is not a particular case of the one considered in [115]. However, there might be a possibility that the present model is one cycle of a bounce.

Further, we comment on Ref. [87]. Their conclusion is that $f(R, T)$ gravity is not able to provide a full cosmological scenario and should be ruled out as a modified gravity alternative to the DE phenomena. This is strongly based on the assumption that the universe is old enough to accommodate the existence of galactic globular clusters with ages of at least 14.16 Gyrs. This can be seen in their statement, “stay on the conservative side, let us consider that the universe should be older than 14.16 Gyrs”. In addition, the authors, in Equation (24), mentioned the age of the universe as $13.5^{+0.16}_{-0.14}$. However, they considered only the positive error (upper bound) in their work.

In justification of the above comment, we would like to acknowledge another study [88], where the authors challenged some of the available $f(R, T)$ models by arguing that, although the low- z evolution of $f(R, T)$ models can be reasonably supported by the available data, there is considerable discrepancy in high- z ($z > 1$) dynamics in comparison with standard Λ CDM cosmology. Thus, the proposal of ruling out $f(R, T) = R + \lambda T$ in Ref. [87] may be valid for the higher redshift zone. The $f(R, T)$ gravity model studied here is still viable for lower redshift, i.e., for late times.

We mentioned earlier that if one tries to substitute the analogue of the conservation equation into the Friedmann Equation (5), solving the resulting equation is difficult. However, in Ref. [87], the authors conducted a broad study of models with $f(R, T) = R + \lambda T^n$, where n is a constant. Their conclusion of Section III was that “ $f(R, T)$ cosmologies have a viable parameter space to describe the late-time cosmological observables”. Our model has $n = 1$ in their notation, so it also falls into the category of having “a viable parameter space to describe the late-time cosmological observables”. Secondly, those authors discussed the effects of radiation. This approach is highly problematic for at least two reasons: (1) $f(R, T)$ theory is not valid for pure radiation with $T = 0$, and (2) as the authors themselves acknowledge, radiation plays a negligible role in the late universe. However, the authors still wrote evolution equations, including terms with f_T , but without making any comments on how they computed the derivatives of f for $T = 0$. Even if they initially considered a $T \neq 0$ model, after substituting $T = 0$ in the field equations, an incorrect (from the point of view of the $f(R, T)$ theory) model was obtained. Since the $f(R, T)$ theory is not valid for $T = 0$, any pathological behavior shown for this case is not relevant for the understanding of the theory. Therefore, their study confirms through cosmological observations the validity of the correctly formulated and applied $f(R, T)$ theory [116].

As a final remark, the model explains late-time acceleration without including any form of hypothetical exotic matter, indicating that $f(R, T) = R + 2\lambda T$ gravity can be a good alternative to DE. In the absence of any fundamental physical phenomenon, the matter–geometry coupling terms simply can be interpreted as a variable cosmological parameter, which not only explains the current accelerating expansion but can also resolve problems such as the fine-tuning problem and the coincidence problem, whilst being consistent with cosmological observations [83].

Author Contributions: Conceptualization, S.J., V.S. and A.B.; methodology, V.S., S.J. and A.B.; software, V.S. and S.J.; validation, V.S. and A.B.; formal analysis, V.S.; data curation, V.S.; writing—original draft preparation, S.J.; writing—review and editing, V.S. and A.B.; visualization, V.S. and S.J.; supervision, V.S. and A.B.; project administration, A.B.; funding acquisition, S.J. and A.B. All authors have read and agreed to the published version of the manuscript.

Funding: This work was based on the research supported in part by the National Research Foundation of South Africa (Grant Numbers: 118511).

Data Availability Statement: The original contributions presented in the study are included in the article, further inquiries can be directed to the corresponding author.

Acknowledgments: The authors are grateful to the reviewers for their critical comments, which led to the improvement of the manuscript. A.B. acknowledges private correspondence with Tiberio Harko regarding some aspects of $f(R, T)$ gravity.

Conflicts of Interest: The authors declare no conflicts of interest. The funders had no role in the design of the study; in the collection, analyses, or interpretation of data; in the writing of the manuscript; or in the decision to publish the results.

Appendix A

In this appendix, we confirm that our model is non-conservative. Setting $\nu = 0$, in Equation (10) of Ref. [117], the covariant derivative of the field equations in $f(R, T)$ gravity lead to the following:

$$\dot{\rho} + 3H(\rho + p) = -\frac{\dot{\rho}}{\rho(1 + f_T)} [pf_T + (\rho - 3p)\{(\rho + p)f_{TT} + f_T\}], \quad (\text{A1})$$

where we considered $\kappa = 1$.

For $f(R, T) = R + 2\lambda T$, the above equation reduces to the following:

$$\dot{\rho} + 3H(\rho + p) = -\frac{\lambda\dot{\rho}(\rho - p)}{\rho(1 + 2\lambda)}. \quad (\text{A2})$$

Since ρ , p , and H are known in our model, one may verify that the above equation is violated for our study, which supports the fact that the conservation equation does not hold in $f(R, T)$ gravity, in general.

References

1. Aghanim, N.; Akrami, Y.; Ashdown, M.; Aumont, J.; Baccigalupi, C.; Ballardini, M.; Banday, A.J.; Barreiro, R.B.; Bartolo, N.; Basak, S.; et al. Planck 2018 results. VI. Cosmological parameters. *Astron. Astrophys.* **2018**, *641*, A6.
2. Anderson, L.; Aubourg, E.; Bailey, S.; Beutler, F.; Bhardwaj, V.; Blanton, M.; Bolton, A.S.; Brinkmann, J.; Brownstein, J.R.; Burden, A.; et al. The clustering of galaxies in the SDSS-III Baryon Oscillation Spectroscopic Survey: Baryon Acoustic Oscillations in the data release 9 spectroscopic galaxy sample. *Mon. Not. Roy. Astron. Soc.* **2013**, *427*, 3435. [CrossRef]
3. Bennett, C.L.; Larson, D.; Weiland, J.L.; Jarosik, N.; Hinshaw, G.; Odegard, N.; Smith, K.M.; Hill, R.S.; Gold, B.; Halpern, M.; et al. Nine-Year Wilkinson Microwave Anisotropy Probe (WMAP) Observations: Final maps and results (WMAP Collaboration). *Astrophys. J. Suppl.* **2013**, *208*, 20. [CrossRef]
4. Spergel, D.N.; Verde, L.; Peiris, H.V.; Komatsu, E.; Nolta, M.R.; Bennett, C.L.; Halpern, M.; Hinshaw, G.; Jarosik, N.; Kogut, A.; et al. First year Wilkinson Microwave Anisotropy Probe (WMAP) observations: Determination of cosmological parameters. *Astrophys. J. Suppl.* **2003**, *148*, 175–194. [CrossRef]
5. Netterfield, C.B.; Ade, P.A.; Bock, J.J.; Bond, J.R.; Borrill, J.; Boscaleri, A.; Coble, K.; Contaldi, C.R.; Crill, B.P.; de Bernardis, P.; et al. A measurement by BOOMERANG of multiple peaks in the angular power spectrum of the cosmic microwave background. *Astrophys. J.* **2002**, *571*, 604. [CrossRef]
6. Riess, A.G.; Filippenko, A.V.; Challis, P.; Clocchiatti, A.; Diercks, A.; Garnavich, P.M.; Gilliland, R.L.; Hogan, C.J.; Jha, S.; Kirshner, R.P.; et al. Observational evidence from supernovae for an accelerating universe and a cosmological constant. *Astrophys. J.* **1998**, *116*, 1009. [CrossRef]
7. Perlmutter, S.; Aldering, G.; Goldhaber, G.; Knop, R.A.; Nugent, P.; Castro, P.G.; Deustua, S.; Fabbro, S.; Goobar, A.; Groom, D.E.; et al. Measurements of Ω and Λ from 42 high-redshift supernovae. *Astrophys. J.* **1999**, *517*, 565. [CrossRef]
8. Schmidt, B.P.; Suntzeff, N.B.; Phillips, M.M.; Schommer, R.A.; Clocchiatti, A.; Kirshner, R.P.; Garnavich, P.; Challis, P.; Leibundgut, B.R.U.N.O.; Spyromilio, J.; et al. The high- z supernova search: Measuring cosmic deceleration and global curvature of the universe using type Ia supernovae. *Astrophys. J.* **1998**, *507*, 46. [CrossRef]
9. Guth, A.H. Inflationary universe: A possible solution to the horizon and flatness problems. *Phys. Rev.* **1981**, *23*, 347. [CrossRef]
10. Albrecht, A.; Steinhardt, P.J. Cosmology for grand unified theories with radiatively induced symmetry breaking. *Phys. Rev. Lett.* **1982**, *48*, 1220–1223. [CrossRef]
11. Linde, A. A new inflationary universe scenario: A possible solution of the horizon, flatness, homogeneity, isotropy and primordial monopole problems. *Phys. Lett. B* **1982**, *108*, 389–393. [CrossRef]

12. Frieman, J.A.; Turner, M.S.; Huterer, D. Dark Energy and the accelerating universe. *Ann. Rev. Astron. Astrophys.* **2008**, *46*, 385. [CrossRef]
13. Copeland, E.J.; Sami, M.; Tsujikawa, S. Dynamics of dark energy. *Int. J. Mod. Phys. D* **2006**, *15*, 1753–1936. [CrossRef]
14. Komatsu, E.; Dunkley, J.; Nolta, M.R.; Bennett, C.L.; Gold, B.; Hinshaw, G.; Jarosik, N.; Larson, D.; Limon, M.; Page, L.E.A.; et al. Five-year Wilkinson microwave anisotropy probe (WMAP) observations: Cosmological interpretation. *Astrophys. J. Suppl.* **2009**, *180*, 330–376. [CrossRef]
15. Sahni, V.; Starobinsky, A.A. The case for a positive cosmological Lambda-term. *Int. J. Mod. Phys. D* **2000**, *9*, 373–444. [CrossRef]
16. Popolo, A.D. Non-baryonic dark matter in cosmology. *AIP Conf. Proc.* **2013**, *1548*, 2–63.
17. Popolo, A.D.; Delliou, M.L.; Lee, X. Correlations in the matter distribution in CLASH galaxy clusters. *Phys. Dark Universe* **2019**, *26*, 100342. [CrossRef]
18. Weinberg, S. The cosmological constant problem. *Rev. Mod. Phys.* **1989**, *61*, 1. [CrossRef]
19. Astashenok, A.V.; Popolo, A.D. Cosmological measure with volume averaging and the vacuum energy problem. *Class. Quantum Grav.* **2012**, *29*, 085014. [CrossRef]
20. Martin, J. Quintessence: A mini-review. *Mod. Phys. Lett. A* **2008**, *23*, 1252–1265. [CrossRef]
21. Caldwell, R.R.; Kamionkowski, M.; Weinberg, N.N. Phantom energy: Dark energy with $\omega < -1$ causes a cosmic doomsday. *Phys. Rev. Lett.* **2003**, *91*, 071301. [PubMed]
22. Tonry, J.L.; Schmidt, B.P.; Barris, B.; Candia, P.; Challis, P.; Clocchiatti, A.; Coil, A.L.; Filippenko, A.V.; Garnavich, P.; Hogan, C.; et al. Cosmological results from high- z supernovae. *Astrophys. J.* **2003**, *594*, 1. [CrossRef]
23. Padmanabhan, T.; Choudhury, T.R. Can the clustered dark matter and the smooth dark energy arise from the same scalar field? *Phys. Rev. D* **2002**, *66*, 081301. [CrossRef]
24. Bento, M.C.; Bertolami, O.; Sen, A.A. Generalized Chaplygin gas, accelerated expansion, and dark-energy-matter unification. *Phys. Rev. D* **2002**, *66*, 043507. [CrossRef]
25. Takeshi, C.; Okabe, T.; Yamaguchi, M. Kinetically driven quintessence. *Phys. Rev. D* **2000**, *62*, 023511.
26. Nojiri, S.I.; Odintsov, S.D. Unifying inflation with Λ CDM epoch in modified $f(R)$ gravity consistent with Solar System tests. *Phys. Lett. B* **2007**, *657*, 238–245. [CrossRef]
27. Nojiri, S.I.; Odintsov, S.D. Unified cosmic history in modified gravity: From $f(R)$ theory to Lorentz non-invariant models. *Phys. Rep.* **2011**, *505*, 59–144. [CrossRef]
28. Sotiriou, T.P.; Faraoni, V. $f(R)$ theories of gravity. *Rev. Mod. Phys.* **2010**, *82*, 451. [CrossRef]
29. Felice, A.D.; Tsujikawa, S. $f(R)$ theories. *Living Rev. Relativ.* **2010**, *13*, 3. [CrossRef]
30. Nojiri, S.I.; Odintsov, S.D. Modified Gauss–Bonnet theory as gravitational alternative for dark energy. *Phys. Lett. B* **2005**, *631*, 1–6. [CrossRef]
31. Cognola, G.; Elizalde, E.; Nojiri, S.I.; Odintsov, S.D.; Zerbini, S. String-inspired Gauss–Bonnet gravity reconstructed from the universe expansion history and yielding the transition from matter dominance to dark energy. *Phys. Rev. D* **2007**, *75*, 086002. [CrossRef]
32. Mandal, S.; Sahoo, P.K. A complete cosmological scenario in teleparallel gravity. *Eur. Phys. J. Plus* **2020**, *135*, 706. [CrossRef]
33. Järvi, L.; Rünkla, M.; Saal, M.; Vilson, O. Nonmetricity formulation of general relativity and its scalar-tensor extension. *Phys. Rev. D* **2018**, *97*, 124025. [CrossRef]
34. Xu, Y.; Harko, T.; Shahidi, S.; Liang, S.D. Weyl type $f(Q, T)$ gravity, and its cosmological implications. *Eur. Phys. J. C* **2020**, *80*, 449. [CrossRef]
35. Bertolami, O.; Lobo, F.S.N.; Paramos, J. Nonminimal coupling of perfect fluids to curvature. *Phys. Rev. D* **2008**, *78*, 064036. [CrossRef]
36. Harko, T.; Lobo, F.S.N. $f(R, L_m)$ gravity. *Eur. Phys. J. C* **2010**, *70*, 373–379. [CrossRef]
37. Harko, T.; Lobo, F.S.; Nojiri, S.I.; Odintsov, S.D. $f(R, T)$ gravity. *Phys. Rev. D* **2011**, *84*, 024020. [CrossRef]
38. Tretyakov, P.V. Cosmology in modified $f(R, T)$ -gravity. *Eur. Phys. J. C* **2018**, *78*, 896. [CrossRef]
39. Jamil, M.; Momeni, D.; Raza, M.; Myrzakulov, R. Reconstruction of some cosmological models in $f(R, T)$ cosmology. *Eur. Phys. J. C* **2012**, *72*, 1999. [CrossRef]
40. Azizi, T. Wormhole geometries in $f(R, T)$ Gravity. *Int. J. Theor. Phys.* **2013**, *52*, 3486. [CrossRef]
41. Alvarenga, F.G.; de la Cruz-Dombriz, A.; Houndjo, M.J.S.; Rodrigues, M.E.; Sáez-Gómez, D. Dynamics of scalar perturbations in $f(R, T)$ gravity. *Phys. Rev. D* **2013**, *87*, 103526. [CrossRef]
42. Sharif, M.; Rani, S.; Myrzakulov, R. Analysis of $F(R, T)$ gravity models through energy conditions. *Eur. Phys. J. Plus* **2013**, *128*, 123. [CrossRef]
43. Pasqua, A.; Chattopadhyay, S.; Khomenkoc, I. A reconstruction of modified holographic Ricci dark energy in $f(R, T)$ gravity. *Can. J. Phys.* **2013**, *91*, 632. [CrossRef]
44. Alves, M.E.S.; Moraes, P.H.R.S.; de Araujo, J.C.N.; Malheiro, M. Gravitational waves in $f(R, T)$ and $f(R, T^\phi)$ theories of gravity. *Phys. Rev. D* **2016**, *94*, 024032. [CrossRef]
45. Momeni, D.; Moraes, P.H.R.S.; Myrzakulov, R. Generalized second law of thermodynamics in $f(R, T)$ theory of gravity. *Astrophys. Space Sci.* **2016**, *361*, 228. [CrossRef]
46. Das, A.; Rahaman, F.; Guha, B.K.; Ray, S. Compact stars in $f(R, T)$ gravity. *Eur. Phys. J. C* **2016**, *76*, 654. [CrossRef]
47. Shabani, H.; Ziaie, A.H. Bouncing cosmological solutions from $f(R, T)$ gravity. *Eur. Phys. J. C* **2018**, *78*, 397. [CrossRef]

48. Deb, D.; Ketov, S.V.; Maurya, S.K.; Khlopov, M.; Moraes, P.H.R.S.; Ray, S. Exploring physical features of anisotropic strange stars beyond standard maximum mass limit in gravity. *Mon. Not. Astron. Soc.* **2019**, *485*, 5652. [CrossRef]
49. Elizalde, E.; Khurshudyan, M. On wormhole formation in $f(R, T)$ gravity: Varying Chaplygin gas and barotropic fluid. *Phys. Rev. D* **2018**, *98*, 123525. [CrossRef]
50. Ordines, T.M.; Carlson, E.D. Limits on $f(R, T)$ gravity from Earth's atmosphere. *Phys. Rev. D* **2019**, *99*, 104052. [CrossRef]
51. Singh, V.; Beesham, A. Plane symmetric model in $f(R, T)$ gravity. *Eur. Phys. J. Plus* **2020**, *135*, 319. [CrossRef]
52. Singh, V.; Beesham, A. LRS Bianchi I model with constant expansion rate in $f(R, T)$. *Astrophys. Space Sci.* **2020**, *13*, 125. [CrossRef]
53. Banerjee, N.; Das, S. Acceleration of the universe with a simple trigonometric potential. *Gen. Relativ. Gravit.* **2005**, *37*, 1695–1703. [CrossRef]
54. Akarsu, A.; Dereli, T. Cosmological models with linearly varying deceleration parameter. *Int. J. Theor. Phys.* **2012**, *51*, 612–621. [CrossRef]
55. Mishra, B.; Tripathy, S.K.; Tarai, S. Cosmological models with a hybrid scale factor in an extended gravity theory. *Mod. Phys. Lett. A* **2018**, *33*, 1850052. [CrossRef]
56. Pradhan, A.; Goswami, G.; Beesham, A. The reconstruction of constant jerk parameter with $f(R, T)$ gravity. *J. High Energy Astrophys.* **2023**, *38*, 12–21. [CrossRef]
57. Chawla, C.; Mishra, R.K.; Pradhan, A. String cosmological models from early deceleration to current acceleration phase with varying G and Λ . *Eur. Phys. J. Plus* **2012**, *127*, 137. [CrossRef]
58. Mishra, R.K.; Chand, A. Cosmological models in alternative theory of gravity with bilinear deceleration parameter. *Astrophys. Space Sci.* **2016**, *361*, 259. [CrossRef]
59. Mishra, R.K.; Dua, H.; Chand, A. Bianchi-III cosmological model with BVDP in modified $f(R, T)$ theory. *Astrophys. Space Sci.* **2018**, *363*, 112. [CrossRef]
60. Mishra, R.K.; Dua, H. Phase transition of cosmological model with statistical techniques. *Astrophys. Space Sci.* **2020**, *365*, 131. [CrossRef]
61. Tiwari, R.K.; Sofuoglu, D. Quadratically varying deceleration parameter in $f(R, T)$ gravity. *Int. J. Geom. Methods Mod. Phys.* **2020**, *17*, 2030003. [CrossRef]
62. Katore, S.D.; Gore, S.V. Λ CDM cosmological models with quintessence in $f(R)$ theory of gravitation. *J. Astrophys. Astron.* **2020**, *41*, 12. [CrossRef]
63. Ahmed, N.; Fekry, M.; Shaker, A.A. Transition from decelerating to accelerating universe with quadratic equation of state in $f(R, T)$ gravity. *NRIAG J. Astron. Geophys.* **2019**, *8*, 198–203. [CrossRef]
64. Tiwari, R.K.; Sofuoglu, D.; Beesham, A. FRW universe in $f(R, T)$ gravity. *Int. J. Geom. Methods Mod. Phys.* **2021**, *18*, 2150104. [CrossRef]
65. Pradhan, A.; Garg, P.; Dixit, A. FRW cosmological models with cosmological constant in $f(R, T)$ theory of gravity. *Can. J. Phys.* **2021**, *999*, 741–753. [CrossRef]
66. Pradhan, A.; Saha, B.; Rikhvitsky, V. Bianchi type-I transit cosmological models with time dependent gravitational and cosmological constants: Reexamined. *Indian J. Phys.* **2015**, *89*, 503–513. [CrossRef]
67. Yadav, A.K. Cosmological constant dominated transit universe from the early deceleration phase to the current acceleration phase in Bianchi-V spacetime. *Chin. Phys. Lett.* **2012**, *29*, 079801. [CrossRef]
68. Tripathy, S.K.; Mishra, B.; Khlopov, M.; Ray, S. Cosmological models with a hybrid scale factor. *Int. J. Mod. Phys.* **2021**, *30*, 2140005. [CrossRef]
69. Tarai, S.; Ray, P.P.; Mishra, B.; Tripathy, S.K. Effect of bulk viscosity in cosmic acceleration. *Int. J. Geom. Methods Mod. Phys.* **2022**, *19*, 2250060. [CrossRef]
70. Mishra, B.; Tripathy, S.K.; Tarai, S. Accelerating models with a hybrid scale factor in extended gravity. *J. Astrophys. Astron.* **2021**, *42*, 2. [CrossRef]
71. Tiwari, R.K.; Beesham, A.; Mishra, S.; Dubey, V. Anisotropic Cosmological Model in a Modified Theory of Gravitation. *Universe* **2021**, *7*, 226. [CrossRef]
72. Jokweni, S.; Singh, V.; Beesham, A. LRS Bianchi-I Transit Cosmological Models in $f(R, T)$ Gravity. *Phys. Sci. Forum* **2023**, *7*, 34. [CrossRef]
73. Linder, E.V. Exploring the expansion history of the universe. *Phys. Rev. Lett.* **2003**, *90*, 091301. [CrossRef]
74. Ray, S.; Mukhopadhyay, U.; Duttachowdhury, S.B. Dark energy models with a time-dependent gravitational constant. *Int. J. Mod. Phys. D* **2007**, *16*, 1791. [CrossRef]
75. Mukhopadhyay, U.; Ray, S.; Duttachowdhury, S.B. Λ -CDM universe: A phenomenological approach with many possibilities. *Int. J. Mod. Phys. D* **2008**, *17*, 301. [CrossRef]
76. Linder, E.V. The dynamics of quintessence, the quintessence of dynamics. *Gen. Rel. Grav.* **2008**, *40*, 329–356. [CrossRef]
77. Ray, S.; Rahaman, F.; Mukhopadhyay, U.; Sarkar, R. Variable equation of state for generalized dark energy model. *Int. J. Theor. Phys.* **2011**, *50*, 2687–2696. [CrossRef]
78. Knop, R.A.; Aldering, G.; Amanullah, R.; Astier, P.; Blanc, G.; Burns, M.S.; Conley, A.; Deustua, S.E.; Doi, M.; Ellis, R.S.; et al. New constraints on Ω_M , Ω_Λ , and Ω from an independent set of 11 high-redshift supernovae observed with the Hubble Space Telescope. *Astrophys. J.* **2003**, *598*, 102. [CrossRef]



79. Tegmark, M.; Blanton, M.R.; Strauss, M.A.; Hoyle, F.; Schlegel, D.; Scoccimarro, R.; Vogeley, M.S.; Weinberg, D.H.; Zehavi, I.; Berlind, A.; et al. The three-dimensional power spectrum of galaxies from the sloan digital sky survey. *Astrophys. J.* **2004**, *606*, 702. [CrossRef]
80. Huterer, D.; Turner, M.S. Probing dark energy: Methods and strategies. *Phys. Rev. D* **2001**, *64*, 123527. [CrossRef]
81. Huterer, D.; Cooray, A. Uncorrelated estimates of dark energy evolution. *Phys. Rev. D* **2005**, *71*, 023506. [CrossRef]
82. Mishra, R.K.; Dua, H. Evolution of FLRW universe in Brans-Dicke gravity theory. *Astrophys. Space Sci.* **2021**, *366*, 6. [CrossRef]
83. Basilakos, S. Solving the main cosmological puzzles with a generalized time varying vacuum energy. *Astron. Astrophys.* **2009**, *508*, 575. [CrossRef]
84. Saha, B. Interacting Scalar and Electromagnetic Fields in $f(R, T)$ Theory of Gravity. *Int. J. Theor. Phys.* **2015**, *54*, 3776. [CrossRef]
85. Fisher, S.B.; Carlson, E.D. Reexamining $f(R, T)$ gravity. *Phys. Rev. D* **2019**, *100*, 064059. [CrossRef]
86. Harko, T.; Moraes, P.H. Comment on Reexamining $f(R, T)$ gravity. *Phys. Rev. D* **2020**, *101*, 108501. [CrossRef]
87. Jaekel, A.P.; da Silva, J.P.; Velten, H. Revisiting $f(R, T)$ cosmologies. *Phys. Dark Univ.* **2024**, *43*, 101401. [CrossRef]
88. Velten, H.; Carames, T.R.P. Cosmological inviability of $f(R, T)$ gravity. *Phys. Rev. D* **2017**, *95*, 123536. [CrossRef]
89. Singh, C.P.; Singh, V. Reconstruction of modified $f(R, T)$ gravity with perfect fluid cosmological models. *Gen. Relativ. Grav.* **2014**, *46*, 1696. [CrossRef]
90. Singh, V.; Beesham, A. The $f(R, T^\phi)$ gravity models with conservation of energy–momentum tensor. *Eur. Phys. J. C* **2018**, *78*, 564. [CrossRef]
91. Bertini, N.R.; Velten, H. Fully conservative $f(R, T)$ gravity and Solar System constraints. *Phys. Rev. D* **2023**, *107*, 124005. [CrossRef]
92. Singh, V.; Beesham, A. A time-varying deceleration parameter for unified description of cosmological evolution. *Int. J. Geom. Meth. Mod. Phys.* **2018**, *15*, 1850145. [CrossRef]
93. Narawade, S.A.; Koussour, M.; Mishra, B. Observational Constraints on Hybrid Scale Factor in $f(Q, T)$ Gravity with Anisotropic Space-Time. *Annalen Der Physik* **2023**, *535*, 2300161. [CrossRef]
94. Singh, S.S.; Anjana Devi, L. Interacting anisotropic dark energy with hybrid expansion in $f(R, T)$ gravity. *New Astr.* **2022**, *90*, 101656. [CrossRef]
95. Aydiner, E. Late time transition of Universe and the hybrid scale factor. *Eur. Phys. J. C* **2022**, *82*, 39. [CrossRef]
96. Magana, J.; Amante, M.H.; Garcia-Aspeitia, M.A.; Motta, V. The Cardassian expansion revisited: Constraints from updated Hubble parameter measurements and type Ia supernova data. *Mon. Not. R. Astron. Soc.* **2018**, *476*, 1036–1049. [CrossRef]
97. Scolnic, D.M.; Jones, D.O.; Rest, A.; Pan, Y.C.; Chornock, R.; Foley, R.J.; Huber, M.E.; Kessler, R.; Narayan, G.; Riess, A.G.; et al. The complete light-curve sample of spectroscopically confirmed SNe Ia from Pan-STARRS1 and cosmological constraints from the combined pantheon sample. *Astrophys. J.* **2018**, *859*, 101. [CrossRef]
98. Macaulay, E.; Nichol, R.C.; Bacon, D.; Brout, D.; Davis, T.M.; Zhang, B.; Bassett, B.A.; Scolnic, D.; A. Möller, A.; D’Andrea, C.B.; et al. First cosmological results using Type Ia supernovae from the Dark Energy Survey: Measurement of the Hubble constant. *Mon. Not. R. Astron. Soc.* **2019**, *486*, 2184–2196. [CrossRef]
99. Kumar, D.; Jain, D.; Mahajan, S.; Mukherjee, A.; Rana, A. Constraints on the transition redshift using Hubble phase space portrait. *Int. J. Mod. Phys. D* **2023**, *32*, 2350039. [CrossRef]
100. Epstein, H.; Glaser, V.; Jaffe, A. Nonpositivity of the energy density in quantized field theories. *Nuovo Cimento* **1965**, *36*, 1016. [CrossRef]
101. Lamoreaux, S.K. Demonstration of the Casimir Force in the 0.6 to 6 μm Range. *Phys. Rev. Lett.* **1997**, *78*, 5. [CrossRef]
102. Mohideen, U.; Roy, A. Precision measurement of the Casimir force from 0.1 to 0.9 μm . *Phys. Rev. Lett.* **1998**, *81*, 4549. [CrossRef]
103. Wu, L.A.; Kimble, H.J.; Hall, J.L.; Wu, H. Generation of squeezed states by parametric down conversion. *Phys. Rev. Lett.* **1986**, *57*, 2520. [CrossRef] [PubMed]
104. Linde, A.D. Phase transitions in gauge theories and cosmology. *Rep. Prog. Phys.* **1985**, *42*, 389. [CrossRef]
105. Barrow, J.D.; Ottewil, A. The stability of general relativistic cosmological theory. *J. Phys. A Math. Gen.* **1983**, *16*, 2757. [CrossRef]
106. Hawking, S.W.; Luttrell, J.C. Higher derivatives in quantum cosmology: (I). The isotropic case. *Nucl. Phys. B* **1984**, *247*, 250. [CrossRef]
107. Whitt, B. Fourth-order gravity as general relativity plus matter. *Phys. Lett. B* **1984**, *145*, 176. [CrossRef]
108. Mijic, M.B.; Morris, M.B.; Suen, W.W. The R^2 cosmology: Inflation without a phase transition. *Phys. Rev. D* **1986**, *34*, 2934. [CrossRef] [PubMed]
109. Pollock, M.D. On the initial conditions for super-exponential inflation. *Phys. Lett. B* **1988**, *215*, 635. [CrossRef]
110. Barrow, J.D. String-driven inflationary and deflationary cosmological models. *Nucl. Phys. B* **1988**, *310*, 743. [CrossRef]
111. Torres, D.F. Quintessence, superquintessence, and observable quantities in Brans-Dicke and nonminimally coupled theories. *Phys. Rev. D* **2002**, *66*, 043522. [CrossRef]
112. Nojiri, S.; Odintsov, S.D. Quantum de Sitter cosmology and phantom matter. *Phys. Lett. B* **2003**, *562*, 147. [CrossRef]
113. Nojiri, S.; Odintsov, S.D. Effective equation of state and energy conditions in phantom/tachyon inflationary cosmology perturbed by quantum effects. *Phys. Lett. B* **2003**, *571*, 1. [CrossRef]
114. Piao, Y.S.; Zhang, Y.Z. Phantom inflation and primordial perturbation spectrum. *Phys. Rev. D* **2004**, *70*, 063513. [CrossRef]
115. Malik, A.; Naz, T.; Rauf, A.; Shamir, M.F.; Yousaf, Z. $f(R, T)$ Gravity Bouncing Universe with Cosmological Parameters. *Eur. Phys. J. Plus* **2024**, *139*, 276. [CrossRef]

116. Harko, T. (Babes-Bolyai University, 1 Kogalniceanu Street, Cluj, Romania). Private communication, 2024.
117. Baffou, E.H.; Kpadonou, A.V.; Rodrigues, M.E.; Houndjo, M.J.S.; Tossa, J. Cosmological viable $f(R, T)$ dark energy model: Dynamics and stability. *Astrophys. Space Sci.* **2015**, *356*, 173–180. [CrossRef]

Disclaimer/Publisher's Note: The statements, opinions and data contained in all publications are solely those of the individual author(s) and contributor(s) and not of MDPI and/or the editor(s). MDPI and/or the editor(s) disclaim responsibility for any injury to people or property resulting from any ideas, methods, instructions or products referred to in the content.

Article

An Isotropic Cosmological Model with Aetherically Active Axionic Dark Matter

Alexander Balakin ^{*,†}  and Amir Shakirzyanov [†] 

Department of General Relativity and Gravitation, Institute of Physics, Kazan Federal University, Kremlevskaya Str. 16a, Kazan 420008, Russia; shamirf@mail.ru

* Correspondence: alexander.balakin@kpfu.ru

† These authors contributed equally to this work.

Abstract: Within the framework of the extended Einstein–aether–axion theory, we studied the model of a two-level aetheric control over the evolution of a spatially isotropic homogeneous Universe filled with axionic dark matter. Two guiding functions are introduced, which depend on the expansion scalar of the aether flow being equal to the tripled Hubble function. The guiding function of the first type enters the aetheric effective metric, which modifies the kinetic term of the axionic system; the guiding function of the second type predetermines the structure of the potential axion field. We obtained new exact solutions to the total set of master equations in the model (with and without cosmological constant), and studied four analytically solvable submodels in detail, for which both guiding functions are reconstructed and illustrations of their behavior are presented.

Keywords: alternative theories of gravity; Einstein–aether theory; axion



Citation: Balakin, A.; Shakirzyanov, A. An Isotropic Cosmological Model with Aetherically Active Axionic Dark Matter. *Universe* **2024**, *10*, 74. <https://doi.org/10.3390/universe10020074>

Academic Editors: Galina L. Klimchitskaya, Vladimir M. Mostepanenko, Sergey V. Sushkov, Lorenzo Iorio and Antonino Del Popolo

Received: 4 December 2023

Revised: 3 January 2024

Accepted: 1 February 2024

Published: 4 February 2024



Copyright: © 2024 by the authors. Licensee MDPI, Basel, Switzerland. This article is an open access article distributed under the terms and conditions of the Creative Commons Attribution (CC BY) license (<https://creativecommons.org/licenses/by/4.0/>).

1. Introduction

A century ago Alexander Friedmann formulated the prediction that our Universe expands, and this event predetermined all further developments in cosmology and space sciences. While remaining within this general concept, modern cosmology focuses on describing the details of this expansion; in particular, the rate of expansion at different epochs. New sensational results obtained from observations made in the last decade have become the basis for restructuring our ideas about the history of the early Universe. The discovery of gravitational radiation was the first important event, which made theorists think about the validity of previous ideas. Indeed, in 2015, the first observation of gravitational waves from the black hole merger [1] presented researchers with a dilemma. In this event the masses of the colliding black holes were predicted to be of 36 and 29 $M_{(\text{Sun})}$, while mass values in the range 2.5–10 $M_{(\text{Sun})}$, predicted by the theory of stellar collapse, seemed to be reasonable. Then, the gravitational wave event indicated, as GW trigger S190521g (GW 190521) [2] has shown, that the black holes with the masses 85 and 66 $M_{(\text{Sun})}$ collided; the general consensus is that the mass of at least one of these black holes lies in a mass range that excludes its birth from being due to the collapse of a star. The discovery of black hole with so-called intermediate mass of 91.000 $M_{(\text{Sun})}$ [3], the existence of which can not be explained by the existing theories, completed the formulation of the dilemma: either it is necessary to abandon this interpretation, or admit that there is a new unknown mechanism for the formation of black holes. Fortunately, the second trend has triumphed and now theorists are actively involved in adequately extending the models for the birth of black holes. Another amazing theory is connected to observations from the newest James Webb Space Telescope (JWST). New observational data suggest the discovery of an extremely magnified monster star, estimations of the masses of warm dark matter particles and of the axion dark matter particles [4] and the abundance of carbon-containing molecules [5]. But the most important event, from our point of view, is the discovery of enormous distant galaxies that should not exist if one follows the standard model of the early Universe

evolution. To be brief, the galaxies found in the JWST images [6] appeared to be shockingly big, and the stars in them too old, and these findings are in conflict with existing models. In other words, rapid development is predicted in the theory of the evolution of the early Universe over the next few years, and modifications to the current cosmological models are highly welcome.

At the moment, the most adequate picture of the Universe contains an early era of inflation, epochs of the domination of radiation and matter, and a late era of accelerated expansion. The theorists dream is to unify the entire history of the Universe within the framework of one cosmological model (see, e.g., [7–13]). The main obstacle to solving this problem is the difficulty in finding a unified equation of state for cosmic substrates that determines the rate of evolution of the Universe in the corresponding epoch. One of the attempts made was the search for the time-dependent parameters of the equation of state, and the introduction of a cosmological term depending on time. However, such attempts were considered unsuccessful because cosmological time is not an invariant, and therefore such equations of state are associated with the loss of covariance in the theory. A similar problem arises, when one tries to define the equation of state in terms of the redshift value Z , or equivalently, via the scale factor $a(t)$.

We follow another type of logic. We admit that the parameters of the equation of state depend on the set of scalars, which are formed on the basis of fundamental fields inherent to the cosmological model under consideration. To be more precise, we take the unit timelike vector field U^j associated with the four-vector velocity of the dynamic aether [14–17] and consider the invariants obtained in the course of the decomposition of its covariant derivative $\nabla_k U^j$. In other words, we use four differential invariants (the expansion scalar of the aether flow, $\Theta = \nabla_k U^k$, the squares of the four-vector acceleration, and of the shear and vorticity tensors, a^2 , σ^2 , ω^2 , respectively), as the arguments of the parameters included in the equations of state. This means that we follow the paradigm of aetheric control over the evolution of physical systems (see, e.g., [18–22]). We must emphasize that, depending on the spacetime symmetry of the model, a part of the listed arguments can disappear. For instance, for the static spherically symmetrical model, we find that $\Theta = 0$, $\sigma^2 = 0$, $\omega^2 = 0$, and we construct the guiding functions using a^2 only. For the Gödel spacetime, the only ω^2 is non-vanishing. For the spacetime with planar gravitational waves we have to work with two non-vanishing scalars: Θ and σ^2 . Spatially isotropic homogeneous cosmological models are unique in this sense, since for them, only the scalar Θ is non-vanishing, and this scalar coincides with the tripled Hubble function $\Theta = 3H(t)$. In this context, the function $H(t)$ can be chosen as an appropriate argument of the guiding parameters of such cosmological models, unifying the paradigm of aetheric control over the evolution of physical systems on the one hand, and the physical interpretation of the theory predictions on the other hand. Since the function H has the dimensionality of inverse time (we consider the units with $c = 1$), this quantity is often used to determine a specific time scale in a corresponding cosmological epoch.

In this paper we work within the Einstein–aether–axion model on the Friedmann–Lemaître–Robertson–Walker spacetime platform, and consider the interaction of the gravitational field, the pseudoscalar (axion) field ϕ , and the unit timelike vector field U^j . Two guiding functions depending on the scalar Θ are introduced into the Lagrangian. The guiding function of the first type, $\mathcal{A}(\Theta)$, enters the so-called aetheric effective metric $G^{mn} = g^{mn} + \mathcal{A}U^m U^n$ (see [23] for history, mathematical details, and motives); it modifies the kinetic term associated with the axion field, and thus it controls the evolution of the kinetic energy of the axionic dark matter in the Universe (see, e.g., [24–29], which present the history of axions, and [30–34], where various aspects of the problem of axions in cosmology are discussed). The guiding function of the second type, $\Phi_*(\Theta)$, enters the potential of the axion field, $V(\phi, \Phi_*)$, thus performing control over the evolution of the potential energy of the axionic dark matter. The set of master equations for the model is solved in quadratures and partially in the analytic form; the corresponding functions $\mathcal{A}(\Theta)$ and $\Phi_*(\Theta)$ are reconstructed.

The paper is organized as follows. Section 2 contains a description of the mathematical formalism. In Section 3 we analyze the key equations of the spatially isotropic homogeneous cosmological model and discuss the obtained solutions. Section 4 contains a discussion and conclusions.

2. The Formalism of the Extended Einstein–Aether–Axion Theory

2.1. The Extended Action Functional and Auxiliary Quantities

The extended Einstein–aether–axion theory is formulated on the basis of the following action functional:

$$-S_{(\text{total})} = \int d^4x \sqrt{-g} \left\{ \frac{1}{2\kappa} \left[R + 2\Lambda + \lambda(g_{mn}U^mU^n - 1) + \mathcal{K}^{ab}_{mn} \nabla_a U^m \nabla_b U^n \right] + \frac{1}{2} \Psi_0^2 [V(\phi, \Phi_*) - G^{mn} \nabla_m \phi \nabla_n \phi] \right\}. \tag{1}$$

In this formula, the standard elements of this theory appear, such as the determinant of the spacetime metric g , the Ricci scalar R , the cosmological constant Λ , the Einstein constant κ , the Lagrange multiplier λ , the unit timelike vector field U^i , associated with the velocity four-vector of the aether flow, and the covariant derivative ∇_k with the connection consistent with spacetime metric g_{mn} , i.e., $\nabla_k g_{mn} = 0$. Kinetic terms for the vector and axion fields contain the effective aetheric metric

$$\mathcal{K}^{ab}_{mn} = C_1 G^{ab} G_{mn} + C_2 \delta_m^a \delta_n^b + C_3 \delta_n^a \delta_m^b + C_4 U^a U^b G_{mn}, \tag{2}$$

$$G^{mn} = g^{mn} + \mathcal{A} U^m U^n, \tag{3}$$

where the scalar $\mathcal{A}(\theta)$ is the guiding function of the first type, and C_1, C_2, C_3, C_4 are the Jacobson coupling constants [14]. The potential of the axion field $V(\phi, \Phi_*)$ is considered to have the periodic form

$$V(\phi, \Phi_*) = \frac{m_A^2 \Phi_*^2}{2\pi^2} \left[1 - \cos \left(\frac{2\pi\phi}{\Phi_*} \right) \right], \tag{4}$$

where $\Phi_*(\Theta)$ is the guiding function of the second type, and the parameter Ψ_0 relates to the coupling constant of the axion–photon interaction $g_{A\gamma\gamma}$, $\frac{1}{\Psi_0} = g_{A\gamma\gamma}$. The potential (4) inherits the discrete symmetry $\frac{2\pi\phi}{\Phi_*} \rightarrow \frac{2\pi\phi}{\Phi_*} + 2\pi n$. This periodic potential has its minima at $\phi = n\Phi_*$. Near the minima, when $\phi \rightarrow n\Phi_* + \psi$ and $|\frac{2\pi\psi}{\Phi_*}|$ is small, the potential takes the standard form $V \rightarrow m_A^2 \psi^2$, where m_A is the axion rest mass. When $\phi = n\Phi_*$ (n is an integer), we deal with the axionic analog of the equilibrium state [19], since $V|_{\phi=n\Phi_*} = 0$, and $\left(\frac{\partial V}{\partial \phi}\right)|_{\phi=n\Phi_*} = 0$.

The following decompositions are associated with the unit four-vector U^j :

$$\nabla_k = U_k D + \overset{\perp}{\nabla}_k, \quad D = U^s \nabla_s, \quad \overset{\perp}{\nabla}_k = \Delta_k^j \nabla_j, \quad \Delta_k^j = \delta_k^j - U^j U_k. \tag{5}$$

Here D is the convective derivative, and Δ_k^j is the projector. The covariant derivative $\nabla_k U_j$ can be decomposed as

$$\nabla_k U_j = U_k D U_j + \sigma_{kj} + \omega_{kj} + \frac{1}{3} \Delta_{kj} \Theta, \tag{6}$$

where the four-vector acceleration $D U_j \equiv a_j$, the symmetric traceless shear tensor σ_{kj} , the skew–symmetric vorticity tensor ω_{kj} , and the expansion scalar Θ are presented by the well-known formulas

$$DU_j = U^s \nabla_s U_j, \quad \sigma_{kj} = \frac{1}{2} \left(\nabla_k U_j + \nabla_j U_k \right) - \frac{1}{3} \Delta_{kj} \Theta, \quad \omega_{kj} = \frac{1}{2} \left(\nabla_k U_j - \nabla_j U_k \right), \quad \Theta = \nabla_k U^k. \quad (7)$$

This decomposition (6) allows us to introduce one linear and three quadratic scalars

$$\Theta = \nabla_k U^k, \quad a^2 = DU_k DU^k, \quad \sigma^2 = \sigma_{mn} \sigma^{mn}, \quad \omega^2 = \omega_{mn} \omega^{mn}, \quad (8)$$

and thus the kinetic term of the vector field can be rewritten in the form

$$\mathcal{K}_{mn}^{ab} (\nabla_a U^m) (\nabla_b U^n) = [C_1(1+\mathcal{A}) + C_4] a^2 + (C_1 + C_3) \sigma^2 + (C_1 - C_3) \omega^2 + \frac{1}{3} (C_1 + 3C_2 + C_3) \Theta^2. \quad (9)$$

Taking into account the constraints obtained after the detection of the event GRB170817 [35], we have to put $C_1 + C_3 = 0$ into (9).

2.2. Master Equations of the Model

2.2.1. Master Equations for the Unit Vector Field

Variations of the extended action functional (1) with respect to the Lagrange multiplier λ gives the normalization condition

$$g_{mn} U^m U^n = 1. \quad (10)$$

Variation with respect to the four-vector U^i gives the aetheric balance equations

$$\nabla_a \mathcal{J}^{aj} = \lambda U^j - \mathcal{A} \kappa \Psi_0^2 D\phi \nabla^j \phi - \nabla^j \left(\Omega_1 \frac{d\Phi_*}{d\Theta} + \Omega_2 \frac{d\mathcal{A}}{d\Theta} \right), \quad (11)$$

where the following definitions are used:

$$\mathcal{J}^{aj} = \mathcal{K}^{abjn} \nabla_b U_n = C_1 (\nabla^a U^j - \nabla^j U^a) + C_2 g^{aj} \Theta + (C_4 + C_1 \mathcal{A}) U^a DU^j, \quad (12)$$

$$\Omega_1 = \frac{\kappa \Psi_0^2 m_A^2}{2\pi^2} \left\{ \Phi_* \left[1 - \cos \left(\frac{2\pi\phi}{\Phi_*} \right) \right] - \pi\phi \sin \left(\frac{2\pi\phi}{\Phi_*} \right) \right\}, \quad (13)$$

$$\Omega_2 = -\frac{1}{2} \kappa \Psi_0^2 (D\phi)^2. \quad (14)$$

Convolution of (11) with U_j gives us the Lagrange multiplier λ :

$$\lambda = U_j \nabla_a \mathcal{J}^{aj} + \mathcal{A} \kappa \Psi_0^2 (D\phi)^2 + D \left(\Omega_1 \frac{d\Phi_*}{d\Theta} + \Omega_2 \frac{d\mathcal{A}}{d\Theta} \right). \quad (15)$$

2.2.2. Master Equation for the Axion Field

Variation in the extended action functional (1) with respect to the axion field yields means that

$$\nabla_m [(g^{mn} + \mathcal{A} U^m U^n) \nabla_n \phi] + \frac{m_A^2 \Phi_*}{2\pi} \sin \left(\frac{2\pi\phi}{\Phi_*} \right) = 0, \quad (16)$$

or equivalently,

$$(1+\mathcal{A}) D^2 \phi + [(1+\mathcal{A}) \Theta + D\mathcal{A}] D\phi - DU^m \nabla_m \phi + \nabla_m \nabla^m \phi + \frac{m_A^2 \Phi_*}{2\pi} \sin \left(\frac{2\pi\phi}{\Phi_*} \right) = 0. \quad (17)$$

Below, we use the ansatz that, when the axion field is in the equilibrium state, which corresponds to the basic minimum $\phi = \Phi_*$, we obtain the master equation for the guiding function of the second type $\Phi_*(\Theta)$, i.e.,

$$\nabla_m [(g^{mn} + \mathcal{A} U^m U^n) \nabla_n \Phi_*] = 0. \quad (18)$$

2.2.3. Master Equations for the Gravitational Field

Variation in the extended action functional (1) with respect to the metric gives the gravity field equation

$$R_{ik} - \frac{1}{2}Rg_{ik} - \Lambda g_{ik} = T_{ik}^{(U)} + \kappa T_{ik}^{(A)} + T_{ik}^{(INT)}. \tag{19}$$

The extended stress-energy tensor of the aether $T_{ik}^{(U)}$ contains the following elements:

$$T_{ik}^{(U)} = \frac{1}{2}g_{ik} \mathcal{K}_{mn}^{ab} \nabla_a U^m \nabla_b U^n + \nabla^m \left[U_{(i} \mathcal{J}_{k)m} - \mathcal{J}_{m(i} U_{k)} - \mathcal{J}_{(ik)} U_m \right] + U_i U_k U_j \nabla_a \mathcal{J}^{aj} + C_1 [(\nabla_m U_i)(\nabla^m U_k) - (\nabla_i U_m)(\nabla_k U^m)] + (C_4 + C_1 \mathcal{A})(DU_i DU_k - U_i U_k DU_m DU^m). \tag{20}$$

As usual, the parentheses symbolize the symmetrization of indices. The extended stress-energy tensor of the axion field is of the form:

$$T_{ik}^{(A)} = \Psi_0^2 \left[(1 + \mathcal{A}) \dot{\phi}^2 \left(U_i U_k - \frac{1}{2} g_{ik} \right) + \frac{1}{2} g_{ik} V \right]. \tag{21}$$

The part of the total stress-energy tensor associated with the interaction terms contains the derivatives of the guiding functions \mathcal{A} and Φ_* with respect to their argument Θ :

$$T_{ik}^{(INT)} = -g_{ik} \Theta \left(\Omega_1 \frac{d\Phi_*}{d\Theta} + \Omega_2 \frac{d\mathcal{A}}{d\Theta} \right) - \Delta_{ik} \left[D \left(\Omega_1 \frac{d\Phi_*}{d\Theta} + \Omega_2 \frac{d\mathcal{A}}{d\Theta} \right) \right]. \tag{22}$$

The Bianchi identity

$$\nabla^k \left[T_{ik}^{(U)} + \kappa T_{ik}^{(A)} + T_{ik}^{(INT)} \right] = 0 \tag{23}$$

automatically holds for the solutions to the master equations for the vector and pseudoscalar fields.

3. Application to the Spatially Isotropic Homogeneous Cosmological Model

3.1. The Spacetime Platform, Reduced Master Equations, and Their Solutions

3.1.1. Geometric Aspects

Below, we work with the Friedmann–Lemaître–Robinson–Walker type spacetime, using the metric

$$ds^2 = dt^2 - a^2(t) (dx^2 + dy^2 + dz^2). \tag{24}$$

The four-vector velocity of the aether flow is known to be in the form $U^j = \delta_0^j$, and the corresponding covariant derivative of the vector field has the following decomposition

$$\nabla_k U_i = \frac{1}{2} \dot{g}_{ik} = \frac{\dot{a}}{a} \Delta_{ik} = H \Delta_{ik} = \frac{1}{3} \Theta \Delta_{ik}. \tag{25}$$

Clearly, in this case, $DU_j = 0$, $\sigma_{mn} = 0$, $\omega_{mn} = 0$, $\Theta = 3H = 3\frac{\dot{a}}{a}$, and, standardly, the dot denote the derivative with respect to the cosmological time t .

3.1.2. Solution to the Equations for the Vector Field

Keeping in mind that $DU_j=0$, $\sigma_{mn}=0$, $\omega_{mn}=0$, we find that the extended Jacobson’s tensor (12) converts into

$$J^{aj} = C_2 \Theta g^{aj}, \tag{26}$$

and the equations for the unit vector field (11) take the form

$$C_2 \nabla_j \Theta = \lambda U_j - \kappa \Psi_0^2 \mathcal{A} U_j \dot{\phi}^2 - \nabla_j \left(\Omega_1 \frac{d\Phi_*}{d\Theta} + \Omega_2 \frac{d\mathcal{A}}{d\Theta} \right). \tag{27}$$

Equation (27) contains only one non-trivial equation, which gives the solution for the Lagrange multiplier λ :

$$\lambda = C_2\dot{\Theta} + \kappa\Psi_0^2\mathcal{A}\dot{\phi}^2 + \frac{d}{dt}\left(\Omega_1\frac{d\Phi_*}{d\Theta} + \Omega_2\frac{d\mathcal{A}}{d\Theta}\right). \tag{28}$$

Thus, the aetheric subset of the total system of master equations is solved.

3.1.3. First Integral of the Reduced Equation for the Axion Field

We suppose that the axion field ϕ is frozen at the first minimum of the axion potential, i.e., $\phi = \Phi_*(t)$. Then we put $\phi = \Phi_*$ into (17) and obtain the key equation for $\Phi_*(t)$

$$(1+\mathcal{A})\ddot{\Phi}_* + \left[3(1+\mathcal{A})\frac{\dot{a}}{a} + \dot{\mathcal{A}}\right]\dot{\Phi}_* = 0, \tag{29}$$

which admits the first integral with

$$\dot{\Phi}_*(t) = \frac{\text{const}}{a^3(t)[1+\mathcal{A}(t)]} = \dot{\Phi}_*(t_0) \left[\frac{a(t_0)}{a(t)}\right]^3 \frac{[1+\mathcal{A}(t_0)]}{[1+\mathcal{A}(t)]}. \tag{30}$$

The parameter t_0 describes the initial time moment; $\mathcal{A}(t_0)$ is the initial value of the guiding function of the first type; and $\dot{\Phi}_*(t_0)$ indicates the initial value of the first derivative of the guiding function of the second type.

3.1.4. Key Equations for the Gravity Field

When $\phi = \Phi_*$, the function Ω_1 takes zero value, and the reduced extended equations of the gravitational field can be converted into one key equation

$$\frac{1}{3}\Theta^2\left(1 + \frac{3}{2}C_2\right) - \Lambda = \frac{1}{2}\kappa\Psi_0^2\dot{\Phi}_*^2\left[1 + \mathcal{A} + \Theta\frac{d\mathcal{A}}{d\Theta}\right]. \tag{31}$$

Since $\dot{\Phi}_*$ has already been found and is of the form (30), we obtain the equation, which connects the scalar Θ with the reduced scale factor $x = \frac{a(t)}{a(t_0)}$ as follows:

$$\frac{1}{3}\Theta^2\left(1 + \frac{3}{2}C_2\right) - \Lambda = \frac{1}{2x^6}\kappa\Psi_0^2\dot{\Phi}_*^2(t_0)[1+\mathcal{A}(t_0)]^2\left[\frac{1}{1+\mathcal{A}} - \Theta\frac{d}{d\Theta}\left(\frac{1}{1+\mathcal{A}}\right)\right]. \tag{32}$$

Then, we assume that $C_2 > -\frac{2}{3}$, $\Lambda > 0$, and introduce the auxiliary parameters

$$H_\infty = \sqrt{\frac{\Lambda}{3\left(1 + \frac{3}{2}C_2\right)}}, \quad h^2 = \frac{\kappa\Psi_0^2\dot{\Phi}_*^2(t_0)[1+\mathcal{A}(t_0)]^2}{6\left(1 + \frac{3}{2}C_2\right)}. \tag{33}$$

Now we are ready to analyze the main equation of the model for the function $H(x)$

$$x^6\left[H^2 - H_\infty^2\right] = h^2\left[\frac{1}{1+\mathcal{A}} - H\frac{d}{dH}\left(\frac{1}{1+\mathcal{A}}\right)\right]. \tag{34}$$

3.2. Modeling of the Guiding Function of the First Type

When we discuss the structure of the guiding function of the first type we use two assumptions. First, we assume that $\mathcal{A} = 0$, if $\Theta = 0$. Second, we assume that the right-hand side of the Equation (34) is a regular function of its argument H , and thus we can use the decomposition

$$\left[\frac{1}{1+\mathcal{A}} - H\frac{d}{dH}\left(\frac{1}{1+\mathcal{A}}\right)\right] = 1 - \gamma_1H - \gamma_2H^2 - 2\gamma_3H^3 - 3\gamma_4H^4 - \dots \tag{35}$$

This decomposition allows us to reconstruct the function $\frac{1}{1+\mathcal{A}}$, which has the form

$$\frac{1}{1+\mathcal{A}} = 1 + \gamma_1 H \left[1 + \log \frac{H}{H_*} \right] + \gamma_2 H^2 + \gamma_3 H^3 + \gamma_4 H^4 + \dots \tag{36}$$

Here, H_* is some constant of integration. The key to our consideration is the analysis of the asymptotic regime ($x \rightarrow \infty$) of the equation

$$x^6 [H^2 - H_\infty^2] = h^2 [1 - \gamma_1 H - \gamma_2 H^2 - 2\gamma_3 H^3 - 3\gamma_4 H^4 - \dots]. \tag{37}$$

If we restrict ourselves with the term H^m in the right-hand side of (37), we see that, first, $H^{m-2} \propto x^6$, second, $H \propto x^{\frac{6}{m-2}}$, and third, $a(t) \propto t^{-\frac{m-2}{6}}$. In other words, if $m > 2$, the Universe collapses asymptotically, and this detail is in contradiction with the main idea of perpetual expansion. Of course, this point is disputable, but we follow this idea. Now we deal with the quadratic equation with respect to H

$$x^6 [H^2 - H_\infty^2] = h^2 [1 - \gamma_1 H - \gamma_2 H^2], \tag{38}$$

and its positive solution is

$$H(x) = \sqrt{\frac{\gamma_1^2 h^4}{4(x^6 + \gamma_2 h^2)^2} + \frac{H_\infty^2 x^6 + h^2}{x^6 + \gamma_2 h^2}} - \frac{\gamma_1 h^2}{2(x^6 + \gamma_2 h^2)}. \tag{39}$$

With the function $H(x)$, one can reconstruct the scale factor as the function of time if we use the formal quadrature

$$t - t_0 = \int_1^{a(t)} \frac{dx}{xH(x)}. \tag{40}$$

Clearly, there are two asymptotic regimes.

(1) When $\Lambda \neq 0$, $H \rightarrow H_\infty$ and thus $a(t) \propto e^{H_\infty t}$.

(2) When $\Lambda = 0$, $H \propto \frac{1}{x^3}$ and thus $a(t) \propto t^{\frac{1}{3}}$.

In order to have further progress in calculations, we consider four analytically solvable submodels.

3.2.1. First Analytically Solvable Submodel

Let us consider the model with $\gamma_1 = -\frac{1}{H_\infty}$ and $\gamma_2 = 0$. In this case the function $\mathcal{A}(H)$ satisfies the relationship

$$\frac{1}{1+\mathcal{A}} = 1 - \frac{H}{H_\infty} \left[1 + \log \frac{H}{H_*} \right]. \tag{41}$$

In order to simplify the analysis, we assume that $H_* = H_\infty$ and obtain the following expression for the guiding function of the first type

$$\mathcal{A} = \frac{\frac{H}{H_\infty} \left(1 + \log \frac{H}{H_\infty} \right)}{1 - \frac{H}{H_\infty} \left(1 + \log \frac{H}{H_\infty} \right)}. \tag{42}$$

Formally speaking, this function takes the infinite value, when the denominator is equal to zero. But this situation only appears at infinity $a = \infty$, when $H = H_\infty$. Now we deal with the key equation

$$H^2 - H_\infty^2 = \frac{h^2}{H_\infty x^6} (H_\infty + H), \tag{43}$$

we omit the negative root $H = -H_\infty$, and see that the positive solution is

$$H(x) = H_\infty + \frac{h^2}{H_\infty x^6}. \tag{44}$$

We should mention that this model is self-consistent when first, $H(t_0) > H_\infty$, and second, $h^2 = H_\infty[H(t_0) - H_\infty]$. According to the definition in (33) the last requirement links the values $\mathcal{A}(t_0)$, $\dot{\Phi}(t_0)$, and $H(t_0)$.

The scale factor $a(t)$ and the Hubble function $H(t)$ can now be presented in the form

$$a(t) = a(t_0) \left[\left(1 + \frac{h^2}{H_\infty^2} \right) e^{6H_\infty(t-t_0)} - \frac{h^2}{H_\infty^2} \right]^{\frac{1}{6}}, \tag{45}$$

$$H(t) = \frac{H_\infty}{\left\{ 1 - \left[1 - \frac{H_\infty}{H(t_0)} \right] e^{-6H_\infty(t-t_0)} \right\}}. \tag{46}$$

The acceleration parameter $-q(t)$ can be given by the formula

$$-q(t) = \frac{\ddot{a}}{aH^2} = 1 - \left(\frac{6h^2}{h^2 + H_\infty^2} \right) e^{-6H_\infty(t-t_0)} \tag{47}$$

is the monotonic function of time, and it asymptotically tends towards one at $t \rightarrow \infty$.

Finally, we intend to reconstruct the guiding function of the second type $\Phi_*(H)$. The simplest way is the following. First, using the replacements $t \rightarrow x = \frac{a(t)}{a(t_0)}$ and $\frac{d}{dt} \rightarrow xH(x) \frac{d}{dx}$, we rewrite the relationship (30) as follows

$$\Phi'_*(x) = -\frac{\dot{\Phi}_*(t_0)[1 + \mathcal{A}(t_0)]}{H_\infty x^4} \left[-\frac{H_\infty}{H} + 1 + \log \left(\frac{H}{H_\infty} \right) \right]. \tag{48}$$

Second, using (44), we integrate (48) and obtain

$$\Phi_*(x) = \Phi_*(t_0) + \frac{\dot{\Phi}_*(t_0)[1 + \mathcal{A}(t_0)]}{3H_\infty} \mathfrak{R}_1(x), \tag{49}$$

$$\begin{aligned} \mathfrak{R}_1(x) \equiv & \left(1 - \frac{1}{x^3} \right) + \frac{1}{x^3} \log \left(1 + \frac{h^2}{H_\infty^2 x^6} \right) - \log \left(1 + \frac{h^2}{H_\infty^2} \right) + \\ & + \frac{H_\infty}{|h|} \left(\arctan \frac{|h|}{H_\infty x^3} - \arctan \frac{|h|}{H_\infty} \right). \end{aligned} \tag{50}$$

Third, using the replacement $\frac{1}{x^6} = \frac{H_\infty}{h^2}(H - H_\infty)$, we recover the function $\Phi_*(H)$ based on the solution (49). The asymptotic value of the reconstructed guiding function is

$$\Phi_*(\infty) = \Phi_*(t_0) + \frac{\dot{\Phi}_*(t_0)[1 + \mathcal{A}(t_0)]}{3H_\infty} \mathfrak{R}_1(\infty), \tag{51}$$

$$\mathfrak{R}_1(\infty) = 1 - \log \left(1 + \frac{h^2}{H_\infty^2} \right) - \frac{H_\infty}{|h|} \arctan \frac{|h|}{H_\infty}.$$

Figure 1 illustrates the details of the function $\mathfrak{R}_1(x)$.

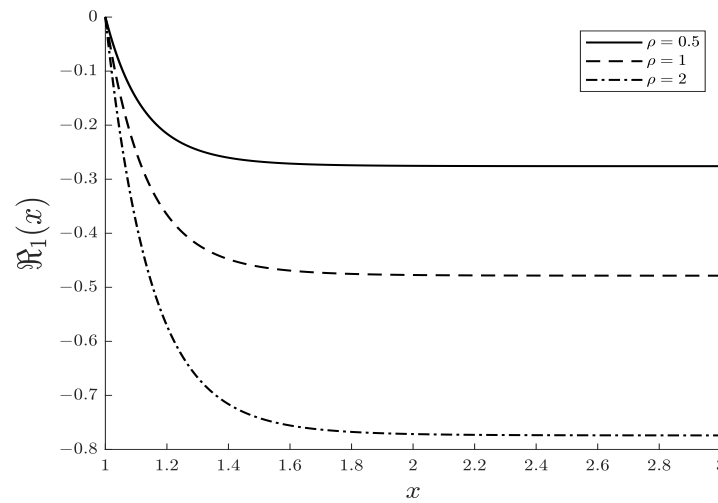


Figure 1. Illustration of the behavior of the function $\mathfrak{R}_1(x)$ (50), which enters the guiding function of the second type Φ_* , for three values of the parameter $\rho = \frac{|h|}{H_\infty}$. All the curves start with the value $\mathfrak{R}(1) = 0$ and tend monotonically towards their asymptotic values $\mathfrak{R}_1(\infty)$ (51).

3.2.2. Second Analytically Solvable Submodel

The second submodel relates to the case when $\Lambda \neq 0$, $\gamma_1 = 0$, and $\gamma_2 = \frac{\alpha^2}{H_\infty^2} > 0$. With these assumptions, the guiding function of the first type

$$\mathcal{A}(H) = -\frac{\gamma_2 H^2}{1 + \gamma_2 H^2} = -\frac{\alpha^2 H^2}{H_\infty^2 + \alpha^2 H^2} \tag{52}$$

is the regular function of the Hubble function H . From the key equation for the gravity field (38) we obtain

$$H(x) = H_\infty \sqrt{\frac{x^6 + \frac{h^2}{H_\infty^2}}{x^6 + \frac{\alpha^2 h^2}{H_\infty^2}}}. \tag{53}$$

The parameter α^2 is connected to the initial value of the Hubble function as follows:

$$H(t_0) \equiv H(x = 1) = H_\infty \sqrt{\frac{1 + \frac{h^2}{H_\infty^2}}{1 + \frac{\alpha^2 h^2}{H_\infty^2}}}. \tag{54}$$

Clearly, we have to distinguish the cases $\alpha^2 = 1$ and $\alpha^2 \neq 1$.

(1) When $\alpha^2 = 1$, we obtain that the Hubble function converts into the constant $H(x) = H(1) = H_\infty$, and we deal with the de Sitter type behavior of the Universe, for which $a(t) = a(t_0)e^{H_\infty(t-t_0)}$. The guiding function of the first type also is constant, as $\mathcal{A} = -\frac{1}{2}$, and the guiding function of the second type behaves as

$$\Phi_*(t) = \Phi_*(t_0) - \frac{\dot{\Phi}_*^2(t_0)a^3(t_0)}{3H_\infty} e^{-3H_\infty(t-t_0)}. \tag{55}$$

(2) When $\alpha^2 \neq 1$, the direct integration of (40) yields

$$e^{6H_\infty(t-t_*)} = \left| \frac{(z - \alpha)^\alpha (z + 1)}{(z + \alpha)^\alpha (z - 1)} \right|, \tag{56}$$

where we used the positive root $\alpha = +\sqrt{\alpha^2}$. The auxiliary function $z(t)$ and two new parameters, z_* and t_* , are:

$$z = \sqrt{\frac{H_\infty^2 \left[\frac{a(t)}{a(t_0)}\right]^6 + \alpha^2 h^2}{H_\infty^2 \left[\frac{a(t)}{a(t_0)}\right]^6 + h^2}}, \quad z_* = \sqrt{\frac{H_\infty^2 + \alpha^2 h^2}{H_\infty^2 + h^2}}, \tag{57}$$

$$t_* = t_0 - \frac{1}{6H_\infty} \log \left[\frac{(z_* + 1)(z_* - \alpha)^\alpha}{(z_* - 1)(z_* + \alpha)^\alpha} \right]. \tag{58}$$

According to (57), $z \rightarrow 1$ when $a \rightarrow \infty$; the corresponding asymptotic behavior is characterized by the de Sitter-type law

$$a(t, \alpha) \rightarrow a(t_0) \left(\frac{h}{2H_\infty} \right)^{\frac{1}{3}} \left| \frac{1 + \alpha}{1 - \alpha} \right|^{\frac{\alpha-1}{6}} e^{H_\infty(t-t_*)}. \tag{59}$$

The formulas (56)–(58) give us the implicit representation. The function $a(t)$ has no extrema; we have illustrated the behavior of the scale factor in the early epoch in Figure 2.

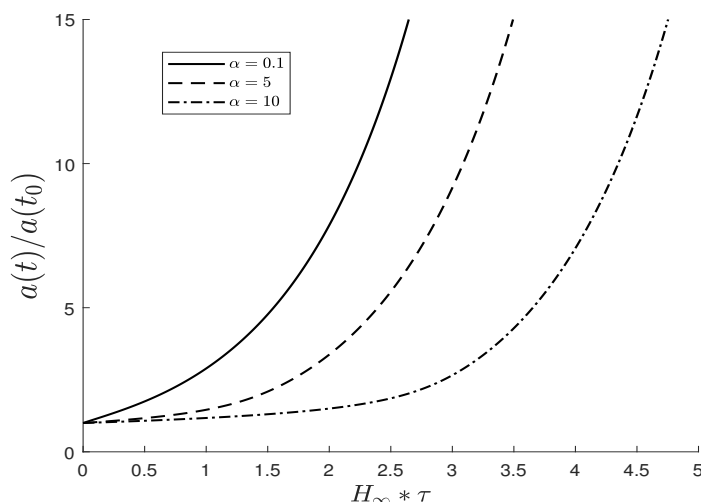


Figure 2. Illustration of the behavior of the reduced scale factor $\frac{a(t)}{a(t_0)}$ in the early epoch; this function is presented in the implicit form by (56). Here $\tau = t - t_0$.

The guiding function of the second type can be represented in terms of elliptic functions. For instance, if $0 < \alpha < 1$, the term

$$\Phi_*(x) = \Phi_*(t_0) - \frac{\dot{\Phi}_*(t_0)[1 + \mathcal{A}(t_0)]}{3H_\infty} \mathfrak{R}_2(x) \tag{60}$$

contains the special function $\mathfrak{R}_2(x)$, which is equal to

$$\begin{aligned} \mathfrak{R}_2(x) &= \int_1^{x^{\frac{1}{3}}} dz \left[\sqrt{\frac{1 + \alpha^2 \frac{h^2}{H_\infty^2} z^2}{1 + \frac{h^2}{H_\infty^2} z^2}} + \alpha^2 \sqrt{\frac{1 + \frac{h^2}{H_\infty^2} z^2}{1 + \alpha^2 \frac{h^2}{H_\infty^2} z^2}} \right] = \\ &= \frac{H_\infty}{h} \left\{ (1 + \alpha^2)[F(\varphi, k) - F(\varphi_*, k)] - 2[E(\varphi, k) - E(\varphi_*, k)] \right\} + \\ &\quad + \frac{2}{x^{\frac{1}{3}}} \sqrt{\frac{H_\infty^2 x^6 + \alpha^2 h^2}{H_\infty^2 x^6 + h^2}} - 2 \sqrt{\frac{H_\infty^2 + \alpha^2 h^2}{H_\infty^2 + h^2}}, \end{aligned} \tag{61}$$

where the elliptic functions of the first and second types, respectively,

$$F(\varphi, k) \equiv \int_0^\varphi \frac{d\psi}{\sqrt{1 - k^2 \sin^2 \psi}}, \quad E(\varphi, k) \equiv \int_0^\varphi d\psi \sqrt{1 - k^2 \sin^2 \psi} \tag{62}$$

are characterized by the arguments

$$\varphi = \arctan\left(\frac{h}{H_\infty x^3}\right), \quad \varphi_* = \arctan\left(\frac{h}{H_\infty}\right), \quad k = \sqrt{1 - \alpha^2}. \tag{63}$$

The asymptotic value of the guiding function of the second type is

$$\Phi_*(x) = \Phi_*(t_0) + \frac{\dot{\Phi}_*(t_0)[1 + \mathcal{A}(t_0)]}{3H_\infty} \left\{ \frac{H_\infty}{h} [(1 + \alpha^2)F(\varphi_*, k) - 2E(\varphi_*, k)] + 2\sqrt{\frac{H_\infty^2 + \alpha^2 h^2}{H_\infty^2 + h^2}} \right\}. \tag{64}$$

3.2.3. Third Analytically Solvable Submodel

Now we assume that the cosmological constant is equal to zero, $\Lambda = 0$, i.e., $H_\infty = 0$. Also, we assume that $\gamma_1 = 0$ and $\gamma_2 = \frac{v^6}{h^2} > 0$. Again, we find that $\mathcal{A}(H)$ is regular

$$\mathcal{A}(H) = -\frac{v^6 H^2}{h^2 + v^6 H^2}, \tag{65}$$

and the Hubble function is in the form

$$H(x) = \frac{|h|}{\sqrt{x^6 + v^6}}. \tag{66}$$

Then, we obtain the reduced scale factor $x(t)$ in the implicit form

$$\frac{3|h|}{v^3}(t - t_{**}) = \sqrt{1 + \frac{x^6}{v^6}} - \log \left[\sqrt{1 + \frac{v^6}{x^6}} + \frac{v^3}{x^3} \right], \tag{67}$$

where we introduce, for simplicity, the formal parameter t_{**}

$$t_{**} = t_0 - \frac{1}{3|h|} \sqrt{1 + v^6} - \frac{v^3}{3|h|} \log(\sqrt{1 + v^6} - v^3). \tag{68}$$

Finally, we obtain the guiding function of the second type as the function of the reduced scale factor

$$\Phi_*(x) = \Phi_*(t_0) + \frac{1}{3|h|} \dot{\Phi}_*(t_0)[1 + \mathcal{A}(t_0)] \mathfrak{R}_3(x). \tag{69}$$

$$\mathfrak{R}_3(x) \equiv \log \left[\frac{(x^3 + \sqrt{v^6 + x^6})}{(1 + \sqrt{1 + v^6})} \right] - 2\sqrt{1 + \frac{v^6}{x^6}} + 2\sqrt{1 + v^6}.$$

In the asymptotic limit $x \rightarrow \infty$, the function $\Phi_*(H)$ has the form

$$\Phi_*(H) = \Phi_*(t_0) - \frac{1}{3|h|} \dot{\Phi}_*(t_0)[1 + \mathcal{A}(t_0)] \log\left(\frac{v^3 H}{2|h|}\right). \tag{70}$$

Figure 3 illustrates the behavior of the function $\mathfrak{R}_3(x)$.

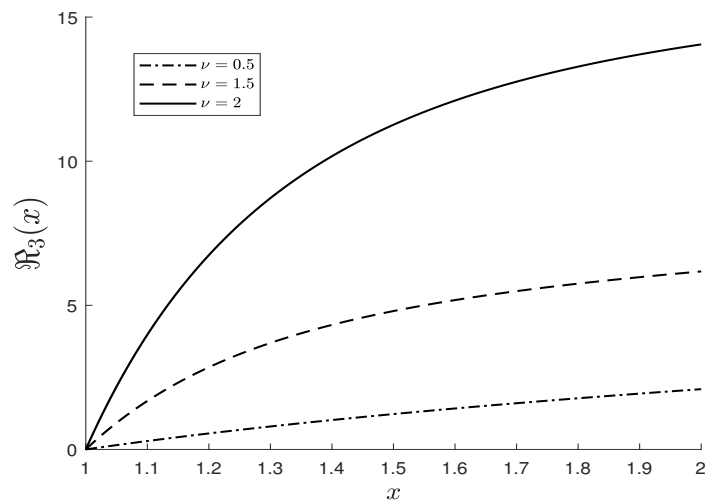


Figure 3. Illustration of the behavior of the function $\mathfrak{R}_3(x)$ for three values of the parameter ν .

3.2.4. Special Case

The final interesting submodel relates to the case $\mathcal{A} = -1$, for which the aetheric effective metric converts into the projector $G^{mn} \rightarrow \Delta^{mn} = g^{mn} - U^m U^n$. For a guiding function like the first type, the axion field Equation (17) admits the solution depending on time if, and only if, $\phi = n\Phi_*$, and thus $V = 0$. The equation for the gravity field (31) gives the de Sitter-type solution $H = H_\infty$, and the Equation (29) turns into the identity $0 = 0$. In other words, the second type of guiding function happens to be arbitrarily constant $\Phi_*(t) = \Phi_*(H_\infty)$.

4. Discussion and Conclusions

In the presented work we studied new exact solutions to the master equations for the extended version of the Einstein–aether–axion theory. The main idea of the theory’s extension is based on the introduction of two guiding functions $\mathcal{A}(\Theta)$ and $\Phi_*(\Theta)$, which depend on the expansion scalar of the aether flow, $\Theta = \nabla_k U^k$. This choice is dictated by the fact that, within the Friedmann–Lemaître–Robinson–Walker model, there is only one non-vanishing invariant reconstructed using the covariant derivative $\nabla_k U^j$ of the aether four-vector velocity U^j . The bonus of this approach is that, in the FLRW model, $\Theta = 3H$, and thus the aetheric control over the axion system evolution happens to be described in terms of the Hubble function $H(t)$, which is intrinsic for this model and has a clear physical meaning. As for why we used namely two guiding functions, we kept in mind that, generally, the axion system is characterized by two state functions: kinetic and potential energy. The modification of the kinetic term in the Lagrangian of the extended theory is performed using the effective aetheric metric $G^{mn} = g^{mn} + \mathcal{A}U^m U^n$ (see (1)), where the scalar $\mathcal{A}(\Theta)$ has been indicated as the first type of guiding function. The modification of the axion field potential is carried out by the introduction of the guiding function of the second type $\Phi_*(\Theta)$, which predetermines the location and depth of the potential minima (see (4)).

The next question is how one can find $\mathcal{A}(\Theta)$ and $\Phi_*(\Theta)$. We have proposed the following idea. If the axion field is frozen in the first minimum of the potential, i.e., is in the first equilibrium state $\phi = \Phi_*$, we see that the corresponding equation for the axion field (see (18) and (29)) can be indicated as the master equation for the guiding function of the second type. Fortunately, the Equation (29) admits the first integral (30), which can be put into the equations for the gravity field, thus providing the key Equation (31) to be self-closed equation for the scalar function $\Theta(x)$, or equivalently, for the Hubble function $H(x)$. When H is found, the guiding function of the second type Φ_* can be reconstructed by the direct integration (see the results (49), (60), (61) and (69)).

Regarding the search for the guiding function of the first type $\mathcal{A}(\Theta)$, we follow the idea that, first, the right-hand side of the key equation of the gravity field (34) has to be a regular function, second, the model has to describe the perpetual Universe expansion without Big Rip and Big Crunch. From these two requirements, we restore the function $\mathcal{A}(H)$ up to three arbitrary parameters γ_1 , γ_2 and H_* using the formula

$$\frac{1}{1+\mathcal{A}} = 1 + \gamma_1 H \left[1 + \log \frac{H}{H_*} \right] + \gamma_2 H^2.$$

The Hubble function $H(x)$ is the solution to the quadratic equation and its positive root has the form (39) for arbitrary parameters γ_1 , γ_2 and H_* ; only the scale factor, as the function of cosmological time $a(t)$, can be presented in quadratures. In order to obtain the results presented in the analytical and special functions, we considered four particular submodels, selecting the listed parameters in a specific way. And our research objectives were achieved.

The last point of discussion is connected with an application of the extended model for the interpretation of observational data, in particular, for the estimation of the axion mass. In this context, we would like to draw attention to the equation of the axion field evolution (17). When the value of the axion field is close to one of the potential minima, i.e., $\phi \rightarrow n\Phi_* + \psi$ with $\left| \frac{2\pi\psi}{\Phi_*} \right| \ll 1$, we deal with the linear differential equation, in which the quantity $M(\Theta) = \frac{m_\Lambda}{\sqrt{1+\mathcal{A}}}$ plays the role of an effective axion mass depending on the scalar of expansion of the aether flow Θ . Preliminary analysis shows that, for some choices of the guiding function $\mathcal{A}(\Theta)$, this equation admits unstable solutions, which are associated with the axionization of the early Universe in analogy with the results obtained in [20]. The growth of the number of axions in the early Universe leads to the formation of the axionic dark matter detected in our epoch; thus, the parameters of the presented extended model could be linked with the mass density of the relic axions. Clearly, this part of work should be more detailed; however, it is beyond the scope of this article and is planned to form the content of the next publication.

Author Contributions: Conceptualization, A.B.; methodology, A.B.; software, A.S.; validation, A.S.; formal analysis, A.S.; investigation, A.B.; resources, A.S.; data curation, A.S.; writing—original draft preparation, A.B.; writing—review and editing, A.B.; visualization, A.S.; supervision, A.B. All authors have read and agreed to the published version of the manuscript.

Funding: This research was funded by Russian Science Foundation (Grant No 21-12-00130).

Data Availability Statement: Data are contained within the article.

Acknowledgments: The work was invited by the Editors of the Special Issue “The Friedmann Cosmology: A Century Later”: G.L. Klimchitskaya, V.M. Mostepanenko and S.V. Sushkov.

Conflicts of Interest: The authors declare no conflicts of interest.

References

1. Abbott, B.P. et al. [LIGO Scientific Collaboration and Virgo Collaboration]. Observation of Gravitational Waves from a Binary Black Hole Merger. *Phys. Rev. Lett.* **2016**, *116*, 061102. [CrossRef]
2. Abbott, R.; Abbott, T.D.; Abraham, S.; Acernese, F.; Ackley, K.; Adams, C.; Adhikari, R.X.; Adya, V.B.; Affeldt, C.; Agathos, M.; et al. GW190521: A Binary Black Hole Merger with a Total Mass of 150 M(Sun). *Phys. Rev. Lett.* **2020**, *125*, 101102. [CrossRef]
3. Pechetti, R.; Seth, A.; Kamann, S.; Caldwell, N.; Strader, J.; den Brok, M.; Luetzgendorf, N.; Neumayer, N.; Voggel, K. Detection of a 100,000 M(Sun) black hole in M31’s Most Massive Globular Cluster: A Tidally Stripped Nucleus. *Astrophys. J.* **2022**, *924*, 48. [CrossRef]
4. Diego, J.M.; Sun, B.; Yan, H.; Furtak, L.J.; Zackrisson, E.; Dai, L.; Kelly, P.; Nonino, M.; Adams, N.; Meena, A.K.; et al. JWST’s PEARLS: Mothra, a new kaiju star at $z=2.091$ extremely magnified by MACS0416, and implications for dark matter models. *Astron. Astrophys.* **2023**, *679*, A31. [CrossRef]
5. Spilker, J.S.; Phadke, K.A.; Aravena, M.; Archipley, M.; Bayliss, M.B.; Birkin, J.E.; Béthermin, M.; Burgoyne, J.; Cathey, J.; Chapman, S.C.; et al. Spatial variations in aromatic hydrocarbon emission in a dust-rich galaxy. *Nature* **2023**, *618*, 708–711. [CrossRef]
6. James Webb Telescope Discoveries Tracker. Available online: <https://www.jameswebbdiscovery.com/> (accessed on 2 February 2024).

7. Calderon, R.; L’Huillier, B.; Polarski, D.; Shafieloo, A.; Starobinsky, A.A. Joint reconstructions of growth and expansion histories from stage-IV surveys with minimal assumptions: Dark Energy beyond? *Phys. Rev. D* **2022**, *106*, 083513. [CrossRef]
8. Calderon, R.; L’Huillier, B.; Polarski, D.; Shafieloo, A.; Starobinsky, A.A. Joint reconstructions of growth and expansion histories from stage-IV surveys with minimal assumptions. II. Modified gravity and massive neutrinos. *Phys. Rev. D* **2023**, *108*, 023504. [CrossRef]
9. Capozziello, S.; Nojiri, S.; Odintsov, S.D. Unified phantom cosmology: Inflation, dark energy and dark matter under the same standard. *Phys. Lett. B* **2006**, *632*, 597–604. [CrossRef]
10. Sotiriou, T.P. Unification of inflation and cosmic acceleration in the Palatini formalism. *Phys. Rev. D* **2006**, *73*, 063515. [CrossRef]
11. Nojiri, S.; Odintsov, S.D.; Oikonomou, V.K. Unifying inflation with early and late-time dark energy in $F(R)$ gravity. *Phys. Dark Universe* **2020**, *29*, 100602. [CrossRef]
12. Odintsov, S.D.; Oikonomou, V.K. Unification of inflation with dark energy in $f(R)$ Gravity and axion dark matter. *Phys. Rev. D* **2019**, *99*, 104070. [CrossRef]
13. Oikonomou, V.K. Unifying of inflation with early and late dark energy epochs in axion $F(R)$ gravity. *Phys. Rev. D* **2021**, *103*, 044036. [CrossRef]
14. Jacobson, T.; Mattingly, D. Gravity with a dynamical preferred frame. *Phys. Rev. D* **2001**, *64*, 024028. [CrossRef]
15. Jacobson, T. Einstein-aether gravity: A status report. *PoSQG-Ph* **2007**, *020*, 020.
16. Jacobson, T.; Mattingly, D. Einstein-aether waves. *Phys. Rev. D* **2004**, *70*, 024003. [CrossRef]
17. Heinicke, C.; Baekler, P.; Hehl, F.W. Einstein-aether theory, violation of Lorentz invariance, and metric-affine gravity. *Phys. Rev. D* **2005**, *72*, 025012. [CrossRef]
18. Balakin, A.B.; Shakirzyanov, A.F. Axionic extension of the Einstein-aether theory: How does dynamic aether regulate the state of axionic dark matter? *Phys. Dark Universe* **2019**, *24*, 100283. [CrossRef]
19. Balakin, A.B.; Shakirzyanov, A.F. Is the axionic Dark Matter an equilibrium System? *Universe* **2020**, *6*, 192. [CrossRef]
20. Balakin, A.B.; Ilin, A.S.; Shakirzyanov, A.F. Interaction of the Cosmic Dark Fluid with Dynamic Aether: Parametric Mechanism of Axion Generation in the Early Universe. *Symmetry* **2023**, *15*, 1824. [CrossRef]
21. Balakin, A.B.; Efremova, A.O. Interaction of the axionic dark matter, dynamic aether, spinor and gravity fields as an origin of oscillations of the fermion effective mass. *Eur. Phys. J. C* **2021**, *81*, 674. [CrossRef]
22. Balakin, A.B.; Efremova, A.O. Dynamic aether as a trigger for spontaneous spinorization in early Universe. *Universe* **2023**, *9*, 481. [CrossRef]
23. Balakin, A.B.; Shakirzyanov, A.F. The extended Einstein-Maxwell-aether-axion theory: Effective metric as an instrument of the aetheric control over the axion dynamics. *Gravit. Cosmol.* **2024**, *30*, 57–67.
24. Peccei, R.D.; Quinn, H.R. CP conservation in the presence of instantons. *Phys. Rev. Lett.* **1977**, *38*, 1440–1443. [CrossRef]
25. Weinberg, S. A new light boson? *Phys. Rev. Lett.* **1978**, *40*, 223–226. [CrossRef]
26. Wilczek, F. Problem of strong P and T invariance in the presence of instantons. *Phys. Rev. Lett.* **1978**, *40*, 279–282. [CrossRef]
27. Ni, W.-T. Equivalence principles and electromagnetism. *Phys. Rev. Lett.* **1977**, *38*, 301–304. [CrossRef]
28. Sikivie, P. Experimental tests of the “invisible” axion. *Phys. Rev. Lett.* **1983**, *51*, 1415–1417. [CrossRef]
29. Wilczek, F. Two applications of axion electrodynamics. *Phys. Rev. Lett.* **1987**, *58*, 1799–1802. [CrossRef]
30. Bertone, G.; Hooper, D.; Silk, J. Particle Dark Matter: Evidence, Candidates and Constraints. *Phys. Rep.* **2005**, *405*, 279–390. [CrossRef]
31. Duffy, L.D.; van Bibber, K. Axions as dark matter particles. *New J. Phys.* **2009**, *11*, 105008. [CrossRef]
32. Khlopov, M. *Fundamentals of Cosmic Particle Physics*; CISP-Springer: Cambridge, UK, 2012.
33. Del Popolo, A. Nonbaryonic dark matter in cosmology. *Int. J. Mod. Phys. D* **2014**, *23*, 1430005. [CrossRef]
34. Marsh, D.J.E. Axion cosmology. *Phys. Rep.* **2016**, *643*, 1–79. [CrossRef]
35. Abbott, B.P. et al. [LIGO Scientific Collaboration, Virgo Collaboration, Fermi Gamma-Ray Burst Monitor, INTEGRAL]. Gravitational Waves and Gamma-rays from a Binary Neutron Star Merger: GW170817 and GRB 170817A. *Astrophys. J. Lett.* **2017**, *848*, L13. [CrossRef]

Disclaimer/Publisher’s Note: The statements, opinions and data contained in all publications are solely those of the individual author(s) and contributor(s) and not of MDPI and/or the editor(s). MDPI and/or the editor(s) disclaim responsibility for any injury to people or property resulting from any ideas, methods, instructions or products referred to in the content.

Article

Primordial Black Holes from Spatially Varying Cosmological Constant Induced by Field Fluctuations in Extra Dimensions

Arkady A. Popov¹, Sergey G. Rubin^{1,2,*} and Alexander S. Sakharov^{3,4}

¹ Geometry Department, N.I. Lobachevsky Institute of Mathematics and Mechanics, Kazan Federal University, Kremlyovskaya ulitsa 18, Kazan 420008, Russia; geom2017@mail.ru

² Physics of Elementary Particles Department, National Research Nuclear University MEPhI (Moscow Engineering Physics Institute), Kashirskoe shosse 31, Moscow 115409, Russia

³ Physics and Astronomy Department, Manhattan College, 4513 Manhattan College Parkway, Riverdale, NY 10471, USA; alexandre.sakharov@cern.ch

⁴ Experimental Physics Department, CERN, CH-1211 Geneva 23, Switzerland

* Correspondence: sgrubin@mephi.ru

Abstract: The origin and evolution of supermassive black holes (SMBHs) in our universe have sparked controversy. In this study, we explore the hypothesis that some of these black holes may have seeded from the direct collapse of dark energy domains with density significantly higher than the surrounding regions. The mechanism of the origin of such domains relies on the inflationary evolution of a scalar field acting in D dimensions, which is associated with the cosmological constant in our four-dimensional spacetime manifold. Inner space quantum fluctuations of the field during inflation are responsible for the spatial variations of the dark energy density in our space. This finding holds particular significance, especially considering recent evidence from pulsar timing array observations, which supports the existence of a stochastic gravitational wave background consisting of SMBH mergers.

Keywords: primordial black hole; supermassive black hole; cosmological constant; dark energy; extra dimensions; inflation



Citation: Popov, A.A.; Rubin, S.G.; Sakharov, A.S. Primordial Black Holes from Spatially Varying Cosmological Constant Induced by Field Fluctuations in Extra Dimensions. *Universe* **2024**, *10*, 166. <https://doi.org/10.3390/universe10040166>

Academic Editors: Galina L. Klimchitskaya and Vladimir M. Mostepanenko

Received: 26 December 2023

Revised: 25 March 2024

Accepted: 27 March 2024

Published: 31 March 2024



Copyright: © 2024 by the authors. Licensee MDPI, Basel, Switzerland. This article is an open access article distributed under the terms and conditions of the Creative Commons Attribution (CC BY) license (<https://creativecommons.org/licenses/by/4.0/>).

1. Introduction

Primordial black holes (PBHs) have been extensively studied over the decades [1–10] and offer a scenario with the potential to leave distinct imprints on cosmic history. Depending on the ratio of their abundance relative to the overall dark matter (DM), $f_{\text{PBH}} = \Omega_{\text{PBH}}/\Omega_{\text{DM}}$, the range of possible PBH masses M_{PBH} spans a wide spectrum, including PBHs of small masses [9] which have undergone scrutiny through various observations (for comprehensive reviews, refer to [8,10]). Additionally, since PBHs formed during the early stages of the Universe, they have the capacity to develop bound binaries via multiple mechanisms [8,11,12]. As these binaries become close, they emit gravitational waves (GWs) continuously until a final dramatic burst occurs at the point of their ultimate merger. Notably, for black holes of stellar mass, such mergers have already been detected by ground-based interferometers [13,14]. Moreover, it is plausible that several of these observed mergers might be attributed to the coalescence of PBHs [15–20].

PBHs with masses exceeding $10^2 M_{\odot}$ hold particular significance due to their impact on the growth of massive objects during the evolution of the early Universe. Notably, it is well-established that galactic nuclei host supermassive black holes (SMBHs) with masses surpassing $10^6 M_{\odot}$ [21–23]. It has been theorized that PBHs could be their progenitors, achieving such masses through processes like merging, accretion [24–29], or the direct collapse of primordial fluctuations [30,31]. In the latter scenario, SPBHs are constrained to constitute less than $O(0.1\%)$ of dark matter (DM). As they have been present since the dawn of the matter-dominated era, they can serve as cosmic seeds, enhancing galaxy

formation [32,33]. Furthermore, different observations have provided evidence for the existence of intermediate-mass black holes (IMBHs) with masses ranging from $10^4 M_{\odot}$ to $10^6 M_{\odot}$ [34]. Additionally, a subdominant fraction of dark matter may consist of immensely massive PBHs, exceeding $10^{12} M_{\odot}$ [35], capable of traversing the intergalactic medium.

SMBHs may be responsible for the generation of early galaxies reported by JWST [36]. They can bind in binary systems which leads to late time merging and radiation of gravitational waves in the nHz frequency range that are detectable by pulsar timing array (PTA) experiments [37–43]. The results from the PTA observations have been extensively analyzed and interpreted in numerous studies, including recent ones such as [44–113] and earlier analyses such as [114–126], which are related to the previously published NANOGrav signal evidence [127]. These interpretations and effects may independently explain the PTA gravitational wave signal. They can also be considered in combination with the modeling of gravitational waves originating from supermassive black hole binaries (SMBHBs).

In this paper, we propose and validate a mechanism for the formation of PBHs based on the generation of specially varying cosmological constants, which may be generic for theories with compact extra dimensions. Considering extra dimensions allows us to examine fluctuations of fields within the internal space during inflation in addition to fluctuations of ordinary scalar fields. However, the fate of these field fluctuations differs significantly from those associated with conventional four-dimensional scalar fields. While conventional field fluctuations transform their energy density into radiation during the FRW stage through decay into other particle-like species, the energy density associated with scalar fields within the internal space remains unchanged, effectively stored within the scalar field itself, manifesting as a cosmological constant. Fluctuations of the scalar field within the internal space manifest as spatial variations of the local Λ term. Domains containing an extraordinarily high cosmological constant may collapse into PBHs. After the end of inflation, the horizon expands and the particle energy density decreases, approaching its present-day value. Simultaneously, the energy density associated with the Λ term, being dependent on the Hubble parameter, also decreases over time, converging to its present-day value, which equals the dark energy density. There must exist a moment in time when both the energy density of matter and the energy density associated with the Λ term are equal. Evidently, since the value of Λ varies across space coordinates, this equality primarily arises within the densest regions, implying the existence of a density contrast close to unity in domains with high values of Λ . Once such a domain becomes encompassed by the cosmological horizon, it may evolve into a PBH. We assert that PBHs formed through the proposed mechanism are cosmologically feasible candidates for seeding SMBHs and explaining the observed IMBHs.

The flexible metrics characterizing extra dimensions constitute a continuous set of static classical solutions derived from the generalized Einstein igat [128,129], and they share fixed Lagrangian parameters. This approach, distinct from the brane world model, renders the extra dimensions invisible due to their small size. However, unlike Kaluza–Klein geometries, these dimensions exhibit inhomogeneity. The concept of such geometries was initially introduced in [130] with further discussion in [131]. Subsequent research, as presented in [132], applied a top-down approach to elucidate observed physical laws. It demonstrated that incorporating quantum corrections to initial parameters established at high energies eases the renormalization procedure.

Investigating the evolution of extra field distributions leading to a static state is a crucial endeavor. This aspect has been explored in previous works such as [133]. The outcomes reveal that the resultant metric and field distribution are contingent upon both model parameters and initial conditions. Notably, the extra-dimensional stationary field distributions evolve in tandem with the energy density across distinct volumes below the horizon, which are replicated during inflation. This particular aspect forms the focal point of our investigation.

Furthermore, our current investigation is grounded in nonlinear $f(R)$ gravity, as extensively discussed in reviews such as [134,135]. This framework holds significant

potential for diverse cosmological implications, with one notably remarkable consequence being the emergence of dark matter [136]. Several viable $f(R)$ models in 4D space aligning with observational constraints have been proposed in works such as [128,129,137–139].

This paper is structured as follows: In Section 2, we provide a concise overview of the mathematical setup employed in the extra-dimensional framework under consideration. Section 3 is dedicated to exploring the distinct behaviors of fluctuations in our space compared to those in extra dimensions. Section 4 is focused on deriving the conditions essential for the formation of PBHs and estimating their mass spectrum. The conclusions of our study are summarized in Section 5.

2. Static Field Distribution in Internal Space

The primary objective of this section is to revisit the foundational concepts of extra-dimensional frameworks that give rise to a continuum set of static metric distributions. This issue has been elaborated in our previous papers [133], and we refer the reader to them for details.

Consider $f(R)$ gravity with a minimally coupled scalar field ζ in a $D = 4 + n$ -dimensional manifold $M_D = M_4 \times M_n$:

$$S = \frac{m_D^{D-2}}{2} \int_{M_D} d^D X \sqrt{|g_D|} \left(f(R) + \partial^M \zeta \partial_M \zeta - 2V(\zeta) \right), \tag{1}$$

where $g_D \equiv \text{Det}g_{MN}$; $M, N = \overline{1, D}$; $X^A = (x^\mu, y^a)$; the coordinate set $x^\mu, \mu = 1, 2, 3, 4$ describes the four-dimensional space M_4 , and the set $y^a, a = 5, 6, \dots, n$ describes the n -dimensional manifold M_n , which is assumed to be a closed manifold without boundary; $f(R)$ is a function of the D -dimensional Ricci scalar R ; and m_D is the D -dimensional Planck mass. Below, we will work in the units $m_D = 1$. Note that the main results of this work hold even for the simplest form of the potential V .

$$V(\zeta) = \frac{1}{2} m^2 \zeta^2. \tag{2}$$

The metric is postulated to have the form

$$ds^2 = e^{2\gamma(u)} \left[dt^2 - e^{2Ht} (dv^2 + v^2 d\Omega_2^2) \right] - du^2 - r(u)^2 d\Omega_{n-1}^2. \tag{3}$$

Such a metric ansatz has been extensively studied within the realm of linear gravity [140–143], particularly in addressing the hierarchy problem [133,144–146]. Our approach is based on the concept of compact extra dimensions. A preliminary investigation suggests that their scale could be as small as 10^{-28} cm or even smaller. This implies that the extra dimensions remain invisible to our instruments, and our rulers and clocks do not measure intervals of space and time at a specific value of u . Instead, all metric functions, such as the function $e^{\gamma(u)}$, should be averaged over the extra space. The way to achieve this is discussed in [133] and briefly presented below.

The equations of motion, see [128,129], represented by

$$-\frac{1}{2} \delta_M^N f(R) + \left(R_M^N + \nabla_M \nabla^N - \delta_M^N \square \right) f_R = -T_M^N, \tag{4}$$

$$f_R = df/dR, \quad T_M^N = (\partial_M \zeta)(\partial^N \zeta) - \frac{1}{2} (\partial_C \zeta)(\partial^C \zeta) \delta_M^N + V(\zeta) \delta_M^N,$$

possess a continuum set of solutions just as the differential equations do. We choose those solutions that exhibit homogeneity in the spatial coordinates x and inhomogeneity in the internal coordinates y . We consider only those solutions that refer to the compact extra space. This means that the metric function $r(u)$ must have two zeros. This condition is fulfilled at the coordinates u_{min} and u_{max} , i.e., $r(u_{min}) = r(u_{max}) = 0$, which is the result of

numerical calculations. These coordinate values depend on additional conditions which are different in different space domains.

The parameterization of these solutions is determined by additional conditions, such as $r'(y = 0)$, $r(y = 0)$, $\gamma(y = 0)$, $\gamma'(y = 0)$, $\zeta(y = 0)$, and $\zeta'(y = 0)$, which are essential for solving the second-order differential equations.

After integration over the extra-dimensional coordinates, the action (1) reduces to the effective action [130]

$$S = \frac{m_p^2}{2} \int_{m_p} d^4x \sqrt{|g_4|} (a_{eff} R_4^2 + R_4 + c_{eff}). \tag{5}$$

The term c_{eff} represents the cosmological constant Λ :

$$\Lambda = -\frac{1}{2} c_{eff}, \tag{6}$$

assuming the scalar function ζ is homogeneous in a 3-dimensional space under horizon. This value varies in different space regions due to the fluctuations at the inflationary stage. We are interested in those space domains where the effective parameter Λ is considerably large as compared to values in the surrounding space. Here, g_4 is the determinant of the 4D metric:

$$ds_4^2 = g_{4,\mu\nu} dx^\mu dx^\nu = dt^2 - e^{2Ht} \delta_{ij} dx^i dx^j. \tag{7}$$

The effective parameters are expressed as follows

$$\begin{aligned} m_p^2 &= \mathcal{V}_{n-1} \int_{u_{min}}^{u_{max}} f_R(R_n) e^{2\gamma} r^{n-1} du, \\ a_{eff} &= \frac{\mathcal{V}_{n-1}}{2m_p^2} \int_{u_{min}}^{u_{max}} f_{RR}(R_n) e^{4\gamma} r^{n-1} du, \\ c_{eff}[\zeta] &= \frac{\mathcal{V}_{n-1}}{m_p^2} \int_{u_{min}}^{u_{max}} (f(R_n) - \zeta(u)^2 - m^2 \zeta(u)^2) e^{4\gamma} r^{n-1} du, \end{aligned} \tag{8}$$

where $\mathcal{V}_{n-1} = \int d^{n-1}x \sqrt{|g_{n-1}|} = \frac{2\pi^{n/2}}{\Gamma(n/2)}$ is the volume of $n - 1$ -dim sphere.

The right-hand side of Equation (8) is expressed in units where $m_D = 1$. This relation allows us to articulate the D-dimensional Planck mass in terms of the four-dimensional Planck mass m_p . In this context, we assume that the functions $\gamma(u)$, $r(u)$, $\zeta(u)$, $R(u)$ constitute a specific solution to the system (4), with details available in [130] for a specific value of the Hubble parameter H . Figure 1 illustrates some examples of static distributions. This approximation remains valid during the inflationary period and at the present time, particularly when the Hubble parameter remains nearly constant.

Our comprehension of the specific value of the energy density, denoted as $\rho_\Lambda = \Lambda m_p^2 / (8\pi) = -c_{eff} m_p^2 / (16\pi)$, is quite limited. Observational constraints provide an upper limit of approximately $10^{-123} m_p^2$ at the present time. Understanding this density during inflation is even more uncertain, with the sanity bound being $\rho_\Lambda (H \simeq 10^{-6} m_p) \ll H^2 \simeq 10^{-12} m_p^2$, implying its negligible impact on the inflation rate. Post-inflation, considering the variation in the Hubble parameter becomes crucial, and establishing a connection between ρ_Λ and this parameter remains elusive. Multiple factors contribute to the complexity of this issue, including quantum corrections, the influence of other fields, and the effects of averaging after the horizon crossing. Furthermore, obtaining an accurate solution to the dynamic equations during the reheating stage appears challenging. The subsequent section is dedicated to a detailed discussion of these aspects.

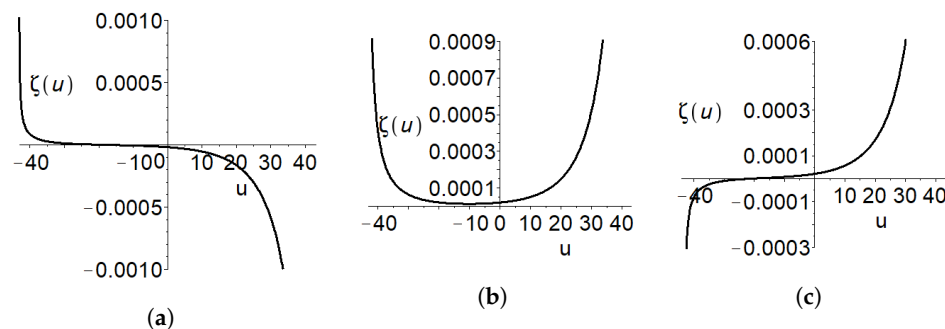


Figure 1. Solution of (4) for the following parameters $n = 3$, $f(R) = 300R^2 + R + 0.002$, $H = 0$, $V(\zeta) = 0.01 \zeta^2/2$ and boundary conditions $r(0) = 50$, $\gamma(0) = 0$, $r'(0) = \gamma'(0) = R'(0) = 0$, $u_{max} = u_{min} \simeq 43.178$, **(a)** $R(0) \simeq 0.00396$, $\zeta(0) = -2 \times 10^{-5}$, $\zeta'(0) = 6 \times 10^{-8}$, **(b)** $R(0) \simeq 0.00395$, $\zeta(0) = 2 \times 10^{-5}$, $\zeta'(0) = 1.5 \times 10^{-6}$, **(c)** $R(0) \simeq 0.00396$, $\zeta(0) = -2 \times 10^{-6}$, $\zeta'(0) = 2 \times 10^{-6}$. The parameter u is expressed in D-dimensional Planck units.

Clearly, both the extra dimensions and the scalar field experience fluctuations in the D-dimensional space. Quantum fluctuations during inflation are expected to induce significant deviations from their initial values (distributions), especially during the later stages of inflation when scales much smaller than those relevant for CMB observations exit the inflating Hubble patches. Specifically, fluctuations in the parameter c_{eff} during inflation can lead to spatial variations in the cosmological constant. The cosmological effects of these variations are the primary focus of investigation in the subsequent sections of the paper. These fluctuations may be substantial, giving rise to domains where the density of dark energy is significantly higher compared to the surrounding regions. Such domains could persist for an extended duration, provided gravity exerts a strong influence.

3. Inflationary Field Dynamics in Extra Space

The evolution of the Universe is significantly influenced by field fluctuations during inflation. Following the completion of inflation, the rapid decrease of the Hubble parameter induces vigorous damped fluctuations of the field, ultimately converging asymptotically to one of the minima of its potential. These inhomogeneities, influenced by gravitational effects, give rise to a large-scale structure after the conclusion of the radiation-dominated stage.

We consider the presence of extra spatial dimensions, allowing for fluctuations in fields within this inner space. The destiny of these field fluctuations differs fundamentally from those inherent to the usual, four-dimensional scalar fields described above. This distinction arises from the fact that stationary distributions of fields constitute a set of measured continuum, as established in the early study [130].

Similar to the situation with usual fields, during the FRW epoch, the asymptotic distribution of the fields in the inner space undergoes variations in causally disconnected regions due to random fluctuations during inflation. However, a significant distinction arises: while the energy density of usual fields is transformed into radiation at the FRW stage through the decay of the fields into other particle-like species, the energy density associated with the scalar fields in the inner space remains in its initial form, being stored in the scalar field. Therefore, the evolution of the energy density of the fields in the inner space is still governed by the Hubble parameter, resulting in a slower decrease compared to the energy density stored in particle-like species generated from the decay of typical scalar fields, which could exist during the inflationary epoch. To distinguish between these two kinds of energy densities, we use the notation ρ for the energy stored in the ordinary fields fluctuating in the observable three-dimensional space, which is eventually converted into particle-like species, and ρ_Λ for the energy remaining stored in the scalar field exhibiting inhomogeneities in the inner space. By choosing the model parameters such that $\rho \gg \rho_\Lambda$, we ensure that the impact of the field distribution in the inner space on the expansion rate, as well as on the rate of horizon growth, can be safely neglected.

After the end of inflation, the horizon expands and the particle energy density ρ decreases, approaching its present-day value $\rho(t_0)$. Simultaneously, ρ_Λ , being dependent on the Hubble parameter, also decreases over time, converging to the present-day value $\rho_\Lambda(t_0)$, which equals the dark energy density. Since $\rho_\Lambda(t_0) > \rho(t_0)$, there must exist a moment in time, denoted by t_* , when both densities are equal, $\rho(t_*) = \rho_\Lambda(t_*)$. Evidently, since the value $\rho_\Lambda(t_*)$ varies across space coordinates, this equality primarily arises within the densest regions, implying a density contrast $\delta\rho/\rho \simeq 1$.

4. Formation of PBHs Induced by Inhomogeneous Cosmological Constants

As indicated in the preceding section, our setup involves the total energy density, which comprises the 4D energy density ρ , represented either by a scalar field or particle-like species created after the conversion of this field into radiation at the reheating stage, and ρ_Λ , associated with the energy density emerging from the scalar field distribution in the inner space. During the inflationary stage and for some period afterward, the Universe was dominated by the 4D energy density, such that $\rho \gg \rho_\Lambda$, while at the present time, $\rho \lesssim \rho_{\Lambda_{\text{obs}}}$, where the current observable value of the dark energy density is given by $\rho_{\Lambda_{\text{obs}}} \sim 10^{-123} m_{\text{Pl}}^4$. Therefore, at some moment t_* during the evolution of the Universe, both types of energy density become equal, resulting in

$$\rho(t_*) = \rho_\Lambda(t_*) . \tag{9}$$

If the equality condition (9) occurs within a causally connected domain, it implies that the density contrast, expressed in this particular case as

$$\frac{\delta\rho}{\rho}(t_*) \approx \frac{\rho_\Lambda(t_*)}{\rho(t_*) + \rho_{\Lambda_{\text{obs}}}(t_*)} , \tag{10}$$

exceeds unity.

Let us consider a scenario in which fluctuations of scalar fields in the internal space during inflation lead to the formation of a domain with size $R(t_{\text{end}})$, determined at the end of inflationary epoch t_{end} , filled with a cosmological constant Λ_1 that exceeds its observable average value Λ_{obs} . After the inflationary period, during the FRW epoch, the domain of size $R(t_{\text{end}})$ undergoes simple conformal stretching due to the expansion of the Universe

$$R(t) = \frac{a(t)}{a(t_{\text{end}})} R(t_{\text{end}}) , \tag{11}$$

where $a(t)$ is the scale factor. It is evident that at a time $t_1 \gtrsim t_*$, ensuring $\frac{\delta\rho}{\rho(t_*)} > 1$, the domain reaches a radius of $R(t_1)$ as described by Equation (11), acquiring the mass M_1 . Subsequently, it becomes encompassed by a Hubble radius $H^{-1}(t_1) = H_1$, thereby becoming detached from the cosmological expansion and initiating collapse. Within about a Hubble time, it will convert into a black hole (BH) of mass $M_{\text{PBH}} = \zeta M_1$. Below, we assume that almost the entirety of the energy contained in the domain is deposited into the BH, so that $\zeta \simeq 1$.

Since the interior of such a domain can exert repulsive gravity due to its substantial energy dominance within the encompassing Hubble horizon, it may maintain a negative pressure, particularly if the density contrast $\frac{\delta\rho}{\rho(t_1)}$ exceeds a threshold of around 10. In such a scenario, the domain enters the Hubble radius at $t_1 \gg t_*$ and starts expanding faster than the background, eventually reaching the inflationary vacuum and potentially developing a wormhole to a baby universe. Such a wormhole would appear as a BH in the FRW Universe. In this paper, we focus on the regime with the most plausible collapse rather than expansion, where $t_1 \approx t_*$, and thus, the size of the domain filled with Λ_1 is close to the Hubble radius at the moment when local dominance of the cosmological term occurs, i.e., when the condition $\frac{\delta\rho}{\rho(t_*)} \approx 1$ is reached.

If the cosmological constant Λ_1 substantially exceeds its universe-averaged value Λ_{obs} , then the component $\rho_{\Lambda_{\text{obs}}}(t_*)$ can be neglected in (10). Therefore, the conditions for reaching a density contrast (10) exceeding unity can be described as

$$\rho_{\Lambda_1} \equiv \frac{\Lambda_1}{8\pi G} \gtrsim \rho(t_1) \equiv \frac{3H_1^2}{8\pi G}, \tag{12}$$

where G stands for the Newtonian constant, H_1 denotes the Hubble rate at t_1 , and the Λ term is measured in units of the Planck mass square.

Thus, an overdense object with a size given by

$$l_1 = H_1^{-1} = \sqrt{\frac{3}{\Lambda_1}} \tag{13}$$

is formed, with its mass as measured by a distant observer being expressed as

$$M_1 \simeq \frac{4\pi\rho\Lambda_1}{3H_1^3} = \frac{2\sqrt{3}}{\sqrt{\Lambda_1}G}. \tag{14}$$

This mass is determined by the localized value of the cosmological constant Λ_1 within a specific domain, which surpasses its universe-average value outside the domain. The validity of Equation (14) in the case of an overdense domain emerging due to fluctuations in extra dimensions is rigorously proven in Appendix A. Thus, it appears that the Schwarzschild radius of the above object, given by

$$R_S = 2GM_1 = 4\sqrt{\frac{3}{\Lambda_1}}, \tag{15}$$

exceeds the size of the Λ_1 overdense domain given by Equation (13). Hence, assuming that the spherical shape of the domain is not significantly disturbed, it will be converted into a BH. To account for the population of unevaporated black holes, it is instructive to express the mass of such Λ -term-induced PBHs (Λ PBHs) in units of solar masses:

$$M_{\Lambda\text{PBH}} = \frac{3.4 \times 10^{-38}}{\sqrt{\Lambda/m_{\text{Pl}}^2}} M_{\odot}. \tag{16}$$

If we consider that the growth of supermassive black holes (SMBHs) observed today originated from seed black holes, then this process must have commenced in the early Universe, approximately 3 million years after the Big Bang, with seeds heavier than $10^2 M_{\odot}$. Additionally, there is evidence of the existence of intermediate-mass black holes (IMBHs) with masses ranging from $10^2 M_{\odot}$ up to about $10^6 M_{\odot}$. Thus, attributing the seeding objects with masses from $10^2 M_{\odot}$ to $10^6 M_{\odot}$ to Λ PBHs implies that they appeared as a result of the collapse of domains containing Λ -terms spanning the range

$$\Lambda_1 \simeq 10^{-78} m_{\text{Pl}}^2 \div 10^{-86} m_{\text{Pl}}^2. \tag{17}$$

In the subsequent analysis, we examine the comparability of the spectrum of the population of Λ PBHs with the constraints on the abundance of PBHs within the considered mass range.

A domain of radius $R \approx H_{\text{inf}}^{-1}$, filled with $\Lambda \neq \Lambda_{\text{obs}}$, that emerges at the time moment t_{Λ} , during inflation with a total duration t_{inf} , when the Universe is yet to inflate over $\Delta N_{\Lambda} = H_{\text{inf}}(t_{\text{inf}} - t_{\Lambda}) = N_{\text{inf}} - N_{\Lambda}$ e-folds, undergoes stretching during expansion as

$$R(\Delta N_{\Lambda}) \approx H_{\text{inf}}^{-1} e^{\Delta N_{\Lambda}}. \tag{18}$$

The number of domains created in a comoving volume dV within an e-fold interval dN_Λ is determined by

$$dN = \Gamma_\Lambda H_{\text{inf}}^3 e^{3N_\Lambda} dV dN_\Lambda, \tag{19}$$

where Γ_Λ represents the formation rate of domains with Λ per Hubble time-space volume H_{inf}^{-4} . By expressing N_Λ from (18), we can derive the number distribution of domains with respect to their physical radius R as

$$d\mathcal{N} = \Gamma_\Lambda \frac{e^{3N_\Lambda} dV}{R^4} dR. \tag{20}$$

Therefore, the number density in the physical inflationary volume $dV_{\text{inf}} = e^{3N_\Lambda} dV$ is

$$\frac{dn}{dR} = \frac{d\mathcal{N}}{dR dV_{\text{inf}}} = \frac{\Gamma_\Lambda}{R^4}. \tag{21}$$

In the context of the setup discussed in this section, where domains of high-density contrast and obeying the condition (12) are considered, the distribution (21) covers a range of scales from $R_{\text{min}} \simeq H_{\text{inf}}^{-1}$ to $R_{\text{max}} \equiv R(\Delta N_{\Lambda_1}) \approx H_{\text{inf}}^{-1} e^{(N_{\text{inf}} - N_{\Lambda_1})}$, where N_{Λ_1} represents the number of e-folds when the probability of the appearance of at least one domain with Λ_1 becomes significant. This probability becomes notable over the course of the progression of inflation, which lasts for a sufficient number of N_{inf} e-folds necessary to address the horizon and flatness problems.

It is worth noting that if inflation were to occur above the TeV scale, the comoving Hubble scale at the end of inflation would be less than one astronomical unit. Consequently, a causally connected patch could encompass our entire observable Universe today, which has a size of about 30 Gpc, if there were more than 40 e-folds of inflation. Similarly, if inflation occurred at the GUT scale ($\simeq 10^{16}$ GeV), then it would require more than 60 e-folds. The upper bound on the value of the Hubble scale during slow-roll inflation provided by Planck [147] is

$$H_{\text{inf}} = 6 \times 10^{13} \text{ GeV}. \tag{22}$$

The mass distribution of black holes formed during the collapse of domains with values of Λ deviating from Λ_{obs} is determined by the size distribution (21), scaled with respect to the expansion of the Universe (11). This distribution can be expressed as

$$dn = \Gamma_\Lambda \frac{dR}{t_{\text{eq}}^{3/2} R^{5/2}}, \tag{23}$$

at the equality time $t_{\text{eq}} = 51\text{kyr}$. A convenient characteristic of this distribution, which facilitates comparison of the PBH yield with constraints on their abundance in different mass ranges (see, for instance, Figure 18 in [10]), is the mass density of PBHs per logarithmic mass interval, expressed in units of the total density of the Universe:

$$\frac{d\Omega_{\text{PBH}}}{d \ln M_{\text{PBH}}} = \frac{1}{\rho_{\text{eq}}} \frac{dn}{d \ln M_{\text{PBH}}} M_{\text{PBH}}, \tag{24}$$

where $\rho_{\text{eq}} = m_{\text{Pl}}^2 / (6\pi t_{\text{eq}}^2)$ represents the matter density at the time of equality. Using (23), we can obtain

$$\frac{dn}{d \ln M_{\text{PBH}}} = \frac{(4\pi)^{1/2} \Gamma_\Lambda}{3\sqrt{3} t_{\text{eq}}^{3/2}} \rho_\Lambda^{1/2} M_{\text{PBH}}^{-1/2}, \tag{25}$$

where ρ_Λ is the energy density contained in the domain filled with Λ term which reads as

$$\rho_\Lambda = \frac{\Lambda m_{\text{Pl}}^2}{8\pi}. \tag{26}$$

where we recall that Λ is expressed in units of m_{Pl}^2 . Thus, (24) can be expanded as

$$\frac{d\Omega_{\text{PBH}}}{d \ln M_{\text{PBH}}} = \sqrt{6\pi}\Gamma_{\Lambda} \left(\frac{\Lambda}{m_{\text{Pl}}^2}\right)^{1/2} t_{\text{eq}}^{1/2} M_{\text{PBH}}^{1/2} \approx 2.5 \times 10^{66} \Gamma_{\Lambda} \left(\frac{\Lambda}{m_{\text{Pl}}^2}\right)^{1/2} \left(\frac{M_{\text{PBH}}}{M_{\odot}}\right)^{1/2}. \quad (27)$$

For those values of Λ within the domains of inhomogeneities, as indicated in (17), the rate Γ_{Λ} can be approximated as (a detailed derivation is provided in Appendix B):

$$\Gamma_{\Lambda} \simeq Q\Lambda, \quad (28)$$

where

$$Q = \frac{8\pi^2}{3} \frac{m_p^2}{H_{\text{inf}}^4}. \quad (29)$$

Substituting this into expression (27) and using relations (16), (28) and (29), we finally obtain

$$\frac{d\Omega_{\text{PBH}}}{d \ln M_{\text{PBH}}} \approx 2.6 \times 10^{-26} \left(\frac{H_{\text{inf}}}{m_{\text{Pl}}}\right)^{-4} \left(\frac{M_{\text{PBH}}}{M_{\odot}}\right)^{-1}. \quad (30)$$

Comparing distribution (30) with the model

$$\Omega_{\text{PBH}} \sim 10^9 \beta \left(\frac{M_{\text{PBH}}}{M_{\odot}}\right)^{-1/2} \quad (31)$$

used in [10] to quote the constraints on the density fraction β deposited in PBHs at the moment of their formation, we arrive at the following condition

$$\frac{H_{\text{inf}}}{m_{\text{Pl}}} \simeq 6 \times 10^{-9} \beta^{-1/4} \left(\frac{M_{\text{PBH}}}{M_{\odot}}\right)^{-1/8}. \quad (32)$$

Condition (32) is useful for assessing the consistency of Λ PBH formation with cosmological constraints on the abundance of PBHs across different mass ranges. By analyzing the combined constraints on β for a monochromatic mass function, as presented in Figure 18 of [10], we can verify the consistency of considering Λ PBHs as candidates for seeding SMBHs and IMBHs, taking into account the CMB constraints on the inflation scale. For the seeding masses $M_{\Lambda\text{PBH}} \approx 10^2 M_{\odot}$, the abundance is constrained to the level of $\beta \approx 10^{-14}$ [10], which is saturated at the inflation energy scale $H_{\text{inf}} \simeq 10^{-5} m_{\text{Pl}}$. At this level of precision, this can be considered as the saturation point, ensuring that it does not exceed the CMB Planck limit (22). Similar estimates of the inflation scale can be obtained for IMBHs in the mass range $10^2 M_{\odot} \leq M_{\Lambda\text{PBH}} \leq 5 \times 10^5 M_{\odot}$, where $\beta \approx 10^{-15}$ [10]. For IMBH with masses $M_{\Lambda\text{PBH}} \approx 10^6 M_{\odot}$, the energy scale $H_{\text{inf}} \simeq 10^{-7} m_{\text{Pl}}$ saturates the constraint $\beta \approx 10^{-7}$ [10]. Similarly, the constraint $\beta \approx 3 \times 10^{-7}$ [10] imposed for the mass scale $M_{\Lambda\text{PBH}} \approx 10^{10} M_{\odot}$, which is typically relevant for currently observed biggest SMBHs, is saturated at the inflation scale $H_{\text{inf}} \simeq 10^{-7} m_{\text{Pl}}$. Therefore, it can be concluded that Λ PBHs are cosmologically consistent for serving as seeds for SMBHs as well as explaining the observed IMBHs.

Additionally, Λ PBHs with masses as low as $M_{\Lambda\text{PBH}} \approx 10^{-2} M_{\odot}$ remain compatible with the constraint $\beta \simeq 10^{-11}$ [10] imposed by the upper CMB inflation scale limit (22). This scenario corresponds to $\Lambda_1 \simeq 10^{-76} m_{\text{Pl}}^2$, where the formation mechanism of Λ PBHs would generate about 10 times the mass of the Jupiter PBHs. Such PBHs could potentially account for a component of DM.

5. Concluding Remarks

It is theorized that the large-scale structure of the Universe was shaped by quantum fluctuations of scalar fields and/or metrics during inflation. These fluctuations, scaled exponentially with conserved amplitude, gave rise to primordial inhomogeneities, cul-

minating in the formation of the cosmic web that represents the Universe’s structure. In theories involving extra dimensions, fluctuations of fields within these dimensions can also be considered. However, the fate of these field fluctuations differs significantly from those associated with conventional four-dimensional scalar fields.

While conventional field fluctuations transform their energy density into radiation during the FRW stage through decay into other particle-like species, the energy density associated with scalar fields within the internal space remains unchanged, effectively stored within the scalar field itself, manifesting as a cosmological constant. Fluctuations of the scalar field within the internal space manifest as spatial variations of the local Λ term. Domains containing an extraordinarily high cosmological constant may collapse into PBHs.

Upon investigating the mass distribution of such Λ PBHs, we find that it may satisfy existing cosmological constraints on the abundance of PBHs without conflicting with the upper bound on the inflation energy scale inferred from CMB measurements, within the mass range from $10^{-2} M_{\odot}$ up to $10^{10} M_{\odot}$. Of particular interest is the possibility of associating Λ PBHs with masses of $10^2 M_{\odot}$ with seeds or supermassive black holes (SMBHs) and associating those with masses spanning the range from $10^2 M_{\odot}$ to $10^6 M_{\odot}$ with intermediate-mass black holes (IMBHs). The lightest Λ PBHs of masses $10^{-2} M_{\odot}$ can potentially contribute to the dark matter budget of the Universe.

The inevitable clustering of PBHs formed by the connected mechanism, driven by inflationary dynamics, leads to the formation of a Swiss cheese-like special structure of domains filled with high values of the Λ term. This clustering may impact the characteristics of the observable spectrum of gravitational waves in the nanohertz frequency band, which are believed to be a signal from SMBHBs [148].

Author Contributions: Conceptualization, S.G.R., A.S.S. and A.A.P.; methodology, S.G.R., A.S.S., and A.A.P.; validation, S.G.R., A.S.S. and A.A.P.; formal analysis, S.G.R., A.S.S. and A.A.P. All authors have read and agreed to the published version of the manuscript.

Funding: The work of S.G.R. was funded by the Ministry of Science and Higher Education of the Russian Federation, Project “New Phenomena in Particle Physics and the Early Universe” FSWU-2023-0073, and the Kazan Federal University Strategic Academic Leadership Program. The work of A.A.P. was funded by the development program of the Volga Region Mathematical Center (agreement No. 075-02-2023-944).

Data Availability Statement: No new data were created or analyzed in this study. Data sharing is not applicable to this article.

Conflicts of Interest: The authors declare no conflicts of interest.

Appendix A. Justification of Formula (14) for Mass Measurement by a Distant Observer

Here, we explore the conditions under which Equation (14) can be reliably used. We consider a three-dimensional space of volume $\Lambda_1 > \Lambda_0$. Our objective is to estimate the mass of such a region as observed by a distant observer. For our estimation, we make several assumptions: the field distribution varies slowly, allowing us to neglect its time dependence; we operate far below the inflationary scale, implying that the term aR^2 is negligible; the domain with the higher energy density has approximately spherical geometry; and the amount of ordinary matter is negligible.

We set the four-dimensional effective action Equation (5) as

$$S_4 = \frac{m_p^2}{2} \int dt d\theta d\varphi \sqrt{|g_4|} [aR^2 + R - 2\Lambda(v)] \tag{A1}$$

and assume that the D dimensional metric depends on the radial coordinate v , leading to the interval in the form

$$ds^2 = A(v)dt^2 - \frac{1}{B(v)}dv^2 - v^2 d\Omega_2^2, \tag{A2}$$

which evolves the action (A1) into the following expression

$$S_4 = \frac{m_p^2}{2} \int dt dv d\theta d\varphi \sqrt{|g_4|} [R - 2\Lambda(v)], \tag{A3}$$

where the term aR^2 is neglected. Now, the situation is essentially simplified, allowing for the analytical evaluation of the mass using the nontrivial equations of the theory

$$\frac{B'}{v} + \frac{B}{v^2} - \frac{1}{v^2} + \Lambda = 0, \tag{A4}$$

$$\frac{B}{v} \frac{A'}{A} + \frac{B}{v^2} - \frac{1}{v^2} + \Lambda = 0, \tag{A5}$$

$$\frac{B}{2} \frac{A''}{A} - \frac{B}{4} \frac{A'^2}{A^2} + \frac{B'}{4} \frac{A'}{A} + \frac{B}{2v} \frac{A'}{A} + \frac{B'}{2v} + \Lambda = 0. \tag{A6}$$

Subtracting the first two equations yields

$$B(v) = A(v), \tag{A7}$$

so that Equations (A4) and (A5) are reduced to a single equation

$$\frac{A'}{v} + \frac{A}{v^2} - \frac{1}{v^2} + \Lambda = 0, \tag{A8}$$

with the solution

$$A(v) = \frac{1}{v} \int_0^v (1 - \Lambda(v)v^2) dv - \frac{2C_1}{v}. \tag{A9}$$

We assume that the value of Λ remains constant within the sphere of radius l_* , denoted as $\Lambda(l_*) = \Lambda_1$. Therefore, inside the sphere, (A9) is converted into the expression

$$A(v)|_{v \leq l_*} = 1 - \frac{\Lambda_1 l_*^2}{3} - \frac{2C_1}{l_*}. \tag{A10}$$

Since, in our setup, there is no point-like mass producing the singularity in the center, $C_1 = 0$, and hence, we obtain the well-known de Sitter metric. For a distant observer in the Minkowski space we assume $\Lambda(v) = 0$ everywhere outside the sphere of radius l_* so that one can derive

$$A(v)|_{v > l_*} = A(v)|_{v \leq l_*} + \frac{1}{v} \int_{l_*}^v dv = 1 - \frac{\Lambda_1 l_*^2}{3v}. \tag{A11}$$

Thus, the mass of the domain filled with Λ_1 reads $2M_\infty = \Lambda_1 l_*^3 m_p^2 / 3$ and finally can be expressed as

$$M_\infty = \frac{4\pi\rho_\Lambda l_*^3}{3} \tag{A12}$$

providing the definition $\Lambda_1 = 8\pi\rho_\Lambda / m_p^2$. Note that taking into account (A7), (A10) and (A11), Equation (A6) becomes an identity.

Appendix B. Probability of Domain Formation with Specific Energy Density during Inflation

To estimate the volume fraction $dP(\Lambda)$ filled with a specific value of the energy density $\rho_\Lambda = \Lambda m_p^2 / 8\pi$, we need to relate the field fluctuations in the extra dimensions during the inflationary stage to the parameter Λ . Following the approach outlined in [149], we consider the extra metric as the background one, allowing the parameter c_{eff} to vary together with the scalar field ζ . The scalar field fluctuates intensively during inflation.

Therefore, our first approximation is to assume a pure de Sitter metric, such that the function $\zeta(x, y)$ is governed by the equation

$$\zeta'' + \left(4\gamma' + (n - 1)\frac{r'}{r}\right)\zeta' - V_\zeta = 0. \tag{A13}$$

This equation, one of Equation set (4), has an asymptote of $\zeta_1(u)$ in a chosen 3D volume under the horizon. The surrounding 3D space is characterized by another static configuration $\zeta_0(u) \neq \zeta_1(u)$.

The parameter value $c_{\text{eff}}[\zeta_0]$ expressed by the last equation in Equation (8), is assumed to be small in order to avoid disrupting the dynamics of the inflationary stage. Additionally, it is assumed to tend to a post-inflationary value of $10^{-123}m_P^2$. Therefore, the quantity

$$c_{\text{eff}}[\zeta_1] \neq 0, \tag{A14}$$

is responsible for the excess energy density.

The scalar field action (1) can be reduced to the standard form

$$S_{\text{scalar}} = \frac{1}{2} \int d^4x \sqrt{g_4} \int d^n y \sqrt{g_n} [(\partial\phi)^2 - m^2\phi^2] \tag{A15}$$

by using the substitution

$$\phi = m^{\frac{D-2}{2}} \zeta. \tag{A16}$$

Exact calculation of the probability for a specific fluctuation $\zeta_1(u)$ is quite difficult. For estimation purposes, we can use an approximation in the spirit of the Kaluza–Klein approach, where the scalar field is represented in the form

$$\phi_1(x, y) = \phi_0(y) + \delta\phi(x, y), \quad \delta\phi(x, y) = \sum_a \phi^{(a)}(x) Y_a(y), \tag{A17}$$

with the standard normalization

$$1 = \int d^n y \sqrt{g_n} Y_a(y)^2, \tag{A18}$$

where $\phi_0(y)$ is an initial static classical part of the scalar field for which $c_{\text{eff}} = 0$, and the difference $\delta\phi(x, y)$ is decomposed into a series of orthogonal normalized functions Y_a . Here, for convenience, we use the dimensionalities $[\zeta] = 1, [\phi] = m^{1+n/2}, [Y_a] = m^{n/2} \rightarrow [\phi^{(a)}] = m$ and neglect the internal n -dimensional metric variation.

Substituting (A17) into (A15), we obtain the action in the form

$$S = \sum_a \frac{1}{2} \int d^4x \sqrt{g_4} [\partial_\mu \phi^{(a)} \partial^\mu \phi^{(a)} - \mu_a^2 \phi^{(a)2}] + S[\zeta_0], \quad \mu_a^2 = m^2 + \lambda_a, \tag{A19}$$

at the inflationary stage, where the term $S[\zeta_0]$ tends to zero at the present time by definition. The discrete set of eigenvalues $\lambda_a, a = 0, \pm 1, \pm 2 \dots$ depends on the specific form of the extra space metric. Assuming that $\phi^{(a)}$ represents long-wave fluctuations that freeze at the inflationary stage, i.e., $\phi^{(a)} = \text{const}$, we obtain the relation between the Lambda term and the scalar field fluctuation under the horizon stems from the equalities

$$-2\Lambda \equiv c_{\text{eff}}[\zeta(u)] = -\frac{\sum_a \mu_a^2 \phi^{(a)2}}{m_P^2}, \tag{A20}$$

as follows from (5) and (A19).

The excitation amplitudes $\phi^{(a)}$ act as independent free fields with an initial amplitude equal to $\phi_0(u)$ [149]. The probability of finding a set of functions $\phi^{(a)}$

$$dP(\{\phi_a\}) \simeq \left[\prod_a d\phi^{(a)} \cdot \sqrt{q_a/\pi} \right] \exp \left[-\sum_a q_a \phi^{(a)2} \right], \quad q_a = \frac{4\pi^2}{3} \frac{\mu_a^2}{H^4}. \quad (\text{A21})$$

According to (A20),

$$\sum_a q_a \phi^{(a)2} = \frac{4\pi^2}{3} H^{-4} \sum_a \mu_a^2 \phi^{(a)2} = \frac{8\pi^2}{3} \frac{m_p^2}{H^4} \Lambda \quad (\text{A22})$$

The final expression for the probability is

$$dP(\Lambda) \simeq d\Lambda \cdot Q \exp[-Q\Lambda], \quad Q = \frac{8\pi^2}{3} \frac{m_p^2}{H^4}, \quad (\text{A23})$$

where the pre-exponent follows from the normalization. The number of domains with specific Λ is related to the probability as

$$dn = e^{3N} dP(\Lambda). \quad (\text{A24})$$

References

- Zel'dovich, Y.B.; Novikov, I.D. The Hypothesis of Cores Retarded during Expansion and the Hot Cosmological Model. *Sov. Astron. J.* **1967**, *10*, 602–603.
- Hawking, S. Gravitationally collapsed objects of very low mass. *Mon. Not. R. Astron. Soc.* **1971**, *152*, 75. [CrossRef]
- Carr, B.J.; Hawking, S.W. Black holes in the early Universe. *Mon. Not. Roy. Astron. Soc.* **1974**, *168*, 399–416. [CrossRef]
- Khlopov, M.Y.; Polnarev, A.G. Primordial Black Holes As A Cosmological Test Of Grand Unification. *Phys. Lett. B* **1980**, *97*, 383–387. [CrossRef]
- Polnarev, A.G.; Khlopov, M.I. Cosmology, primary black holes and supermassive particles. *Uspekhi Fizicheskikh Nauk* **1985**, *145*, 369–401. [CrossRef]
- Khlopov, M.Y. Primordial black holes. *Res. Astron. Astrophys.* **2010**, *10*, 495–528. [CrossRef]
- Belotsky, K.M.; Dokuchaev, V.I.; Eroshenko, Y.N.; Esipova, E.A.; Khlopov, M.Y.; Khromykh, L.A.; Kirillov, A.A.; Nikulin, V.V.; Rubin, S.G.; Svadkovsky, I.V. Clusters of Primordial Black Holes. *Eur. Phys. J. C* **2019**, *79*, 246. [CrossRef]
- Sasaki, M.; Suyama, T.; Tanaka, T.; Yokoyama, S. Primordial black holes—perspectives in gravitational wave astronomy. *Class. Quantum Gravity* **2018**, *35*, 063001. [CrossRef]
- Gundhi, A.; Ketov, S.V.; Steinwachs, C.F. Primordial black hole dark matter in dilaton-extended two-field Starobinsky inflation. *Phys. Rev. D* **2021**, *103*, 083518. [CrossRef]
- Carr, B.; Kohri, K.; Sendouda, Y.; Yokoyama, J. Constraints on primordial black holes. *Rept. Prog. Phys.* **2021**, *84*, 116902. [CrossRef]
- Raidal, M.; Vaskonen, V.; Veermäe, H. Gravitational Waves from Primordial Black Hole Mergers. *J. Cosmol. Astropart. Phys.* **2017**, *09*, 037. [CrossRef]
- Raidal, M.; Spethmann, C.; Vaskonen, V.; Veermäe, H. Formation and Evolution of Primordial Black Hole Binaries in the Early Universe. *J. Cosmol. Astropart. Phys.* **2019**, *02*, 018. [CrossRef]
- Abbott, B.P. et al. [LIGO Scientific Collaboration and Virgo Collaboration] Binary Black Hole Mergers in the first Advanced LIGO Observing Run. *Phys. Rev. X* **2016**, *6*, 041015. Erratum in *Phys. Rev. X* **2018**, *8*, 039903. [CrossRef]
- Abbott, R. et al. [LIGO Scientific Collaboration and Virgo Collaboration]. GWTC-2: Compact Binary Coalescences Observed by LIGO and Virgo During the First Half of the Third Observing Run. *Phys. Rev. X* **2021**, *11*, 021053. [CrossRef]
- Sasaki, M.; Suyama, T.; Tanaka, T.; Yokoyama, S. Primordial Black Hole Scenario for the Gravitational-Wave Event GW150914. *Phys. Rev. Lett.* **2016**, *117*, 061101. Erratum in *Phys. Rev. Lett.* **2018**, *121*, 059901. [CrossRef] [PubMed]
- Hall, A.; Gow, A.D.; Byrnes, C.T. Bayesian analysis of LIGO-Virgo mergers: Primordial vs. astrophysical black hole populations. *Phys. Rev. D* **2020**, *102*, 123524. [CrossRef]
- Jedamzik, K. Primordial Black Hole Dark Matter and the LIGO/Virgo observations. *J. Cosmol. Astropart. Phys.* **2020**, *9*, 022. [CrossRef]
- De Luca, V.; Franciolini, G.; Pani, P.; Riotto, A. Primordial Black Holes Confront LIGO/Virgo data: Current situation. *J. Cosmol. Astropart. Phys.* **2020**, *6*, 044. [CrossRef]
- Franciolini, G.; Baibhav, V.; De Luca, V.; Ng, K.K.Y.; Wong, K.W.K.; Berti, E.; Pani, P.; Riotto, A.; Vitale, S. Searching for a subpopulation of primordial black holes in LIGO-Virgo gravitational-wave data. *Phys. Rev. D* **2022**, *105*, 083526. [CrossRef]

20. Romero-Rodriguez, A.; Martinez, M.; Pujolàs, O.; Sakellariadou, M.; Vaskonen, V. Search for a Scalar Induced Stochastic Gravitational Wave Background in the Third LIGO-Virgo Observing Run. *Phys. Rev. Lett.* **2022**, *128*, 051301. [CrossRef] [PubMed]
21. Ferrarese, L.; Ford, H. Supermassive black holes in galactic nuclei: Past, present and future research. *Space Sci. Rev.* **2005**, *116*, 523–624. [CrossRef]
22. Gültekin, K.; Richstone, D.O.; Gebhardt, K.; Lauer, T.R.; Tremaine, S.; Aller, M.C.; Bender, R.; Dressler, A.; Faber, S.M.; Filippenko, A.V.; et al. The M-sigma and M-L Relations in Galactic Bulges and Determinations of their Intrinsic Scatter. *Astrophys. J.* **2009**, *698*, 198–221. [CrossRef]
23. Kormendy, J.; Ho, L.C. Coevolution (Or Not) of Supermassive Black Holes and Host Galaxies. *Ann. Rev. Astron. Astrophys.* **2013**, *51*, 511–653. [CrossRef]
24. Ali-Haïmoud, Y.; Kamionkowski, M. Cosmic microwave background limits on accreting primordial black holes. *Phys. Rev. D* **2017**, *95*, 043534. [CrossRef]
25. Bean, R.; Magueijo, J. Could supermassive black holes be quintessential primordial black holes? *Phys. Rev. D* **2002**, *66*, 063505. [CrossRef]
26. Kawasaki, M.; Kusenko, A.; Yanagida, T.T. Primordial seeds of supermassive black holes. *Phys. Lett. B* **2012**, *711*, 1–5. [CrossRef]
27. Clesse, S.; García-Bellido, J. The clustering of massive Primordial Black Holes as Dark Matter: measuring their mass distribution with Advanced LIGO. *Phys. Dark Univ.* **2017**, *15*, 142–147. [CrossRef]
28. Clesse, S.; García-Bellido, J. Seven Hints for Primordial Black Hole Dark Matter. *Phys. Dark Univ.* **2018**, *22*, 137–146. [CrossRef]
29. Serpico, P.D.; Poulin, V.; Inman, D.; Kohri, K. Cosmic microwave background bounds on primordial black holes including dark matter halo accretion. *Phys. Rev. Res.* **2020**, *2*, 023204. [CrossRef]
30. Nakama, T.; Suyama, T.; Yokoyama, J. Supermassive black holes formed by direct collapse of inflationary perturbations. *Phys. Rev. D* **2016**, *94*, 103522. [CrossRef]
31. Nakama, T.; Carr, B.; Silk, J. Limits on primordial black holes from μ distortions in cosmic microwave background. *Phys. Rev. D* **2018**, *97*, 043525. [CrossRef]
32. Carr, B.; Silk, J. Primordial Black Holes as Generators of Cosmic Structures. *Mon. Not. Roy. Astron. Soc.* **2018**, *478*, 3756–3775. [CrossRef]
33. Inman, D.; Ali-Haïmoud, Y. Early structure formation in primordial black hole cosmologies. *Phys. Rev. D* **2019**, *100*, 083528. [CrossRef]
34. Greene, J.E.; Strader, J.; Ho, L.C. Intermediate-Mass Black Holes. *Ann. Rev. Astron. Astrophys.* **2020**, *58*, 257–312. [CrossRef]
35. Carr, B.; Kuhnel, F.; Visinelli, L. Constraints on Stupendously Large Black Holes. *Mon. Not. Roy. Astron. Soc.* **2021**, *501*, 2029–2043. [CrossRef]
36. Liu, B.; Bromm, V. Accelerating Early Massive Galaxy Formation with Primordial Black Holes. *Astrophys. J. Lett.* **2022**, *937*, L30, [CrossRef]
37. Goncharov, B.; Shannon, R.M.; Reardon, D.J.; Hobbs, G.; Zic, A.; Bailes, M.; Curyło, M.; Dai, S.; Kerr, M.; Lower, M.E.; et al. On the Evidence for a Common—Spectrum Process in the Search for the Nanohertz Gravitational—Wave Background with the Parkes Pulsar Timing Array. *Astrophys. J. Lett.* **2021**, *917*, L19. [CrossRef]
38. Chen, S.; Caballero, R.N.; Guo, Y.J.; Chalumeau, A.; Liu, K.; Shaifullah, G.; Lee, K.J.; Babak, S.; Desvignes, G.; Parthasarathy, A.; et al. Common-red-signal analysis with 24-yr high-precision timing of the European Pulsar Timing Array: inferences in the stochastic gravitational-wave background search. *Mon. Not. Roy. Astron. Soc.* **2021**, *508*, 4970–4993. [CrossRef]
39. Antoniadis, J.; Arumugam, P.; Arumugam, S.; Babak, S.; Bagchi, M.; Nielsen, A.S.B.; Bassa, C.G.; Bathula, A.; Berthereau, A.; Bonetti, M.; et al. The second data release from the European Pulsar Timing Array—III. Search for gravitational wave signals. *Astron. Astrophys.* **2023**, *678*, A50. [CrossRef]
40. Reardon, D.J.; Zic, A.; Shannon, R.M.; Hobbs, G.B.; Bailes, M.; Di Marco, V.; AKapur, g.; Rogers, A.F.; Thrane, E.; Askew, J.; et al. Search for an Isotropic Gravitational-wave Background with the Parkes Pulsar Timing Array. *Astrophys. J. Lett.* **2023**, *951*, L6. [CrossRef]
41. Xu, H.; Chen, S.; Guo, Y.; Jiang, J.; Wang, B.; Xu, J.; Xue, Z.; Caballero, R.N.; Yuan, J.; Xu, Y.; et al. Searching for the Nano-Hertz Stochastic Gravitational Wave Background with the Chinese Pulsar Timing Array Data Release I. *Res. Astron. Astrophys.* **2023**, *23*, 075024. [CrossRef]
42. Agazie, G.; Anumarlapudi, A.; Archibald, A.M.; Baker, P.T.; Bécsy, B.; Blecha, L.; Bonilla, A.; Brazier, A.; Brook, P.R.; Burke-Spolaor, S.; et al. The NANOGrav 15 yr Data Set: Constraints on Supermassive Black Hole Binaries from the Gravitational-wave Background. *Astrophys. J. Lett.* **2023**, *952*, L37. [CrossRef]
43. Agazie, G.; Anumarlapudi, A.; Archibald, A.M.; Arzoumanian, Z.; Baker, P.T.; Bécsy, B.; Blecha, L.; Brazier, A.; Brook, P.R.; Burke-Spolaor, S.; et al. The NANOGrav 15 yr Data Set: Evidence for a Gravitational-wave Background. *Astrophys. J. Lett.* **2023**, *951*, L8. [CrossRef]
44. Valli, R.; Tiede, C.; Vigna-Gómez, A.; Cuadra, J.; Siwek, M.; Ma, J.Z.; D’Orazio, D.J.; Zrake, J.; de Mink, S.E. Long-term Evolution of Binary Orbits Induced by Circumbinary Disks. *arXiv* **2024**. [CrossRef]
45. Alonso-Álvarez, G.; Cline, J.M.; Dewar, C. Self-interacting dark matter solves the final parsec problem of supermassive black hole mergers. *arXiv* **2024**. [CrossRef]
46. Buchmuller, W. Metastable strings and grand unification. *arXiv* **2024**. [CrossRef]

47. Winkler, M.W.; Freese, K. Origin of the Stochastic Gravitational Wave Background: First-Order Phase Transition vs. Black Hole Mergers. *arXiv* **2024**. [CrossRef]
48. Conaci, A.; Delle Rose, L.; Dev, P.S.B.; Ghoshal, A. Slaying Axion-Like Particles via Gravitational Waves and Primordial Black Holes from Supercooled Phase Transition. *arXiv* **2024**. [CrossRef]
49. Choudhury, S.; Karde, A.; Panda, S.; Sami, M. Realisation of the ultra-slow roll phase in Galileon inflation and PBH overproduction. *arXiv* **2024**. [CrossRef]
50. Padmanabhan, H.; Loeb, A. Constraints on Supermassive Black Hole Binaries from JWST and NANOGrav. *arXiv* **2024**. [CrossRef]
51. Hu, L.; Cai, R.G.; Wang, S.J. Distinctive GWBs from eccentric inspiraling SMBH binaries with a DM spike. *arXiv* **2023**. [CrossRef]
52. Lacy, M.; Engholm, A.; Farrah, D.; Ejercito, K. Constraints on Cosmological Coupling from the Accretion History of Supermassive Black Holes. *Astrophys. J. Lett.* **2024**, *961*, L33. [CrossRef]
53. Eichhorn, A.; Fernandes, P.G.S.; Held, A.; Silva, H.O. Breaking black-hole uniqueness at supermassive scales. *arXiv* **2023**. [CrossRef]
54. Zhang, F. Final parsec evolution in the presence of intermediate mass black holes. *arXiv* **2023**. [CrossRef]
55. Sato-Polito, G.; Zaldarriaga, M.; Quataert, E. Where are NANOGrav's big black holes? *arXiv* **2023**. [CrossRef]
56. Liu, B.; Bromm, V. Impact of primordial black holes on the formation of the first stars and galaxies. *arXiv* **2023**. [CrossRef]
57. Ellis, J.; Fairbairn, M.; Urrutia, J.; Vaskonen, V. Probing supermassive black hole seed scenarios with gravitational wave measurements. *arXiv* **2023**. [CrossRef]
58. Huang, H.L.; Jiang, J.Q.; Piao, Y.S. Merger rate of supermassive primordial black hole binaries. *arXiv* **2023**. [CrossRef]
59. Bromley, B.C.; Sandick, P.; Shams Es Haghi, B. Supermassive Black Hole Binaries in Ultralight Dark Matter. *arXiv* **2023**. [CrossRef]
60. Davis, M.C.; Grace, K.E.; Trump, J.R.; Runnoe, J.C.; Henkel, A.; Blecha, L.; Brandt, W.N.; Casey-Clyde, J.A.; Charisi, M.; Witt, C. Reliable Identification of Binary Supermassive Black Holes from Rubin Observatory Time-Domain Monitoring. *arXiv* **2023**. [CrossRef]
61. Harris, C.; Gültekin, K. Connecting Core Galaxy Properties to the Massive Black Hole Binary Population. *arXiv* **2023**. [CrossRef]
62. Koo, H.; Bak, D.; Park, I.; Hong, S.E.; Lee, J.W. Final parsec problem of black hole mergers and ultralight dark matter. *arXiv* **2023**. [CrossRef]
63. Ramazanov, S. Spectrum of gravitational waves from long-lasting primordial sources. *arXiv* **2023**. [CrossRef]
64. D'Orazio, D.J.; Charisi, M. Observational Signatures of Supermassive Black Hole Binaries. *arXiv* **2023**. [CrossRef]
65. Kasai, K.; Kawasaki, M.; Kitajima, N.; Murai, K.; Neda, S.; Takahashi, F. Primordial Origin of Supermassive Black Holes from Axion Bubbles. *arXiv* **2023**. [CrossRef]
66. Stamou, I.; Clesse, S. Primordial Black Holes without fine-tuning from a light stochastic spectator field. *arXiv* **2023**. [CrossRef]
67. Dolgov, A.D. Tension between HST/JWST and Λ CDM Cosmology, PBH, and Antimatter in the Galaxy. In Proceedings of the 14th Frascati workshop on Multifrequency Behaviour of High Energy Cosmic Sources, Palermo, Italy, 12–17 June 2023.
68. Huang, F.; Bi, Y.C.; Cao, Z.; Huang, Q.G. Impacts of Gravitational-Wave Background from Supermassive Black Hole Binaries on the Detection of Compact Binaries by LISA. *arXiv* **2023**. [CrossRef]
69. Evans, A.E.; Blecha, L.; Bhowmick, A.K. Building Semi-Analytic Black Hole Seeding Models Using IllustrisTNG Host Galaxies. *arXiv* **2023**. [CrossRef]
70. Gardiner, E.C.; Kelley, L.Z.; Lemke, A.M.; Mitridate, A. Beyond the Background: Gravitational Wave Anisotropy and Continuous Waves from Supermassive Black Hole Binaries. *arXiv* **2023**. [CrossRef]
71. Serra, F. Black Holes through the Lenses of Effective Field Theory. Ph.D. Thesis, Scuola Normale Superiore, Pisa, Italy, 2023. [CrossRef]
72. Cyr, B.; Kite, T.; Chluba, J.; Hill, J.C.; Jeong, D.; Acharya, S.K.; Bolliet, B.; Patil, S.P. Disentangling the primordial nature of stochastic gravitational wave backgrounds with CMB spectral distortions. *arXiv* **2023**. [CrossRef]
73. Agazie, G. et al. [The International Pulsar Timing Array Collaboration]. Comparing recent PTA results on the nanohertz stochastic gravitational wave background. *arXiv* **2023**. [CrossRef]
74. Flores, M.M.; Kusenko, A.; Pearce, L.; Perez-Gonzalez, Y.F.; White, G. Testing high scale supersymmetry via second order gravitational waves. *Phys. Rev. D* **2023**, *108*, 123002. [CrossRef]
75. Kawasaki, M.; Murai, K. Enhancement of gravitational waves at Q-ball decay including non-linear density perturbations. *J. Cosmol. Astropart. Phys.* **2024**, *1*, 050. [CrossRef]
76. Ellis, J.; Fairbairn, M.; Franciolini, G.; Hütsi, G.; Iovino, A.; Lewicki, M.; Raidal, M.; Urrutia, J.; Vaskonen, V.; Veermäe, H. What is the source of the PTA GW signal? *Phys. Rev. D* **2024**, *109*, 023522. [CrossRef]
77. Bhaumik, N.; Jain, R.K.; Lewicki, M. Ultralow mass primordial black holes in the early Universe can explain the pulsar timing array signal. *Phys. Rev. D* **2023**, *108*, 123532. [CrossRef]
78. Babichev, E.; Gorbunov, D.; Ramazanov, S.; Samanta, R.; Vikman, A. NANOGrav spectral index $\gamma=3$ from melting domain walls. *Phys. Rev. D* **2023**, *108*, 123529. [CrossRef]
79. Buchmuller, W.; Domcke, V.; Schmitz, K. Metastable cosmic strings. *J. Cosmol. Astropart. Phys.* **2023**, *11*, 020. [CrossRef]
80. Gouttenoire, Y. First-Order Phase Transition Interpretation of Pulsar Timing Array Signal Is Consistent with Solar-Mass Black Holes. *Phys. Rev. Lett.* **2023**, *131*, 171404. [CrossRef] [PubMed]
81. Wu, Y.M.; Chen, Z.C.; Huang, Q.G. Cosmological Interpretation for the Stochastic Signal in Pulsar Timing Arrays. *arXiv* **2023**. [CrossRef]

82. Zhang, C.; Dai, N.; Gao, Q.; Gong, Y.; Jiang, T.; Lu, X. Detecting new fundamental fields with pulsar timing arrays. *Phys. Rev. D* **2023**, *108*, 104069. [CrossRef]
83. Gouttenoire, Y.; Trifinopoulos, S.; Valogiannis, G.; Vanvlasselaer, M. Scrutinizing the Primordial Black Holes Interpretation of PTA Gravitational Waves and JWST Early Galaxies. *arXiv* **2023**. [CrossRef]
84. Bi, Y.C.; Wu, Y.M.; Chen, Z.C.; Huang, Q.G. Implications for the supermassive black hole binaries from the NANOGrav 15-year data set. *Sci. China Phys. Mech. Astron.* **2023**, *66*, 120402. [CrossRef]
85. Broadhurst, T.; Chen, C.; Liu, T.; Zheng, K.F. Binary Supermassive Black Holes Orbiting Dark Matter Solitons: From the Dual AGN in UGC4211 to NanoHertz Gravitational Waves. *arXiv* **2023**. [CrossRef]
86. Huang, H.L.; Cai, Y.; Jiang, J.Q.; Zhang, J.; Piao, Y.S. Supermassive primordial black holes in multiverse: for nano-Hertz gravitational wave and high-redshift JWST galaxies. *arXiv* **2023**. [CrossRef]
87. Ellis, J.; Lewicki, M.; Lin, C.; Vaskonen, V. Cosmic superstrings revisited in light of NANOGrav 15-year data. *Phys. Rev. D* **2023**, *108*, 103511. [CrossRef]
88. Ellis, J.; Fairbairn, M.; Hütsi, G.; Raidal, J.; Urrutia, J.; Vaskonen, V.; Veermäe, H. Gravitational waves from supermassive black hole binaries in light of the NANOGrav 15-year data. *Phys. Rev. D* **2024**, *109*, L021302. [CrossRef]
89. Addazi, A.; Cai, Y.F.; Marciano, A.; Visinelli, L. Have pulsar timing array methods detected a cosmological phase transition? *Phys. Rev. D* **2024**, *109*, 015028. [CrossRef]
90. Furusawa, K.; Tashiro, H.; Yokoyama, S.; Ichiki, K. Probing the Mass Relation between Supermassive Black Holes and Dark Matter Halos at High Redshifts by Gravitational Wave Experiments. *Astrophys. J.* **2023**, *959*, 117. [CrossRef]
91. Chen, Z.C.; Li, J.; Liu, L.; Yi, Z. Probing the speed of scalar-induced gravitational waves with pulsar timing arrays. *arXiv* **2024**. [CrossRef]
92. Li, H.J.; Zhou, Y.F. Gravitational waves from axion domain walls in double level crossings. *arXiv* **2024**. [CrossRef]
93. Liu, J. Distinguishing the nanohertz gravitational-wave sources by the observations of compact dark matter subhalos. *Phys. Rev. D* **2023**, *108*, 123544. [CrossRef]
94. Chen, Z.C.; Li, S.L.; Wu, P.; Yu, H. NANOGrav hints for first-order confinement-deconfinement phase transition in different QCD-matter scenarios. *arXiv* **2023**. [CrossRef]
95. Kitajima, N.; Lee, J.; Takahashi, F.; Yin, W. Stability of domain walls with inflationary fluctuations under potential bias, and gravitational wave signatures. *arXiv* **2023**. [CrossRef]
96. Bagui, E. et al. [LISA Cosmology Working Group]. Primordial black holes and their gravitational-wave signatures. *arXiv* **2023**. [CrossRef]
97. Liu, L.; Wu, Y.; Chen, Z.C. Simultaneously probing the sound speed and equation of state of the early Universe with pulsar timing arrays. *arXiv* **2023**. [CrossRef]
98. Chung, D.J.H.; Tadepalli, S.C. Power spectrum in the chaotic regime of axionic blue isocurvature perturbations. *Phys. Rev. D* **2024**, *109*, 023539. [CrossRef]
99. King, S.F.; Roshan, R.; Wang, X.; White, G.; Yamazaki, M. Quantum gravity effects on dark matter and gravitational waves. *Phys. Rev. D* **2024**, *109*, 024057. [CrossRef]
100. Zhu, M.; Ye, G.; Cai, Y. Pulsar timing array observations as possible hints for nonsingular cosmology. *Eur. Phys. J. C* **2023**, *83*, 816. [CrossRef]
101. Liu, L.; Chen, Z.C.; Huang, Q.G. Probing the equation of state of the early Universe with pulsar timing arrays. *J. Cosmol. Astropart. Phys.* **2023**, *11*, 071. [CrossRef]
102. Ahmadvand, M.; Bian, L.; Shakeri, S. Heavy QCD axion model in light of pulsar timing arrays. *Phys. Rev. D* **2023**, *108*, 115020. [CrossRef]
103. Zhang, Z.; Cai, C.; Su, Y.H.; Wang, S.; Yu, Z.H.; Zhang, H.H. Nano-Hertz gravitational waves from collapsing domain walls associated with freeze-in dark matter in light of pulsar timing array observations. *Phys. Rev. D* **2023**, *108*, 095037. [CrossRef]
104. Cannizzaro, E.; Franciolini, G.; Pani, P. Novel tests of gravity using nano-Hertz stochastic gravitational-wave background signals. *arXiv* **2023**. [CrossRef]
105. Jin, J.H.; Chen, Z.C.; Yi, Z.; You, Z.Q.; Liu, L.; Wu, Y. Confronting sound speed resonance with pulsar timing arrays. *J. Cosmol. Astropart. Phys.* **2023**, *09*, 016. [CrossRef]
106. Servant, G.; Simakachorn, P. Constraining postinflationary axions with pulsar timing arrays. *Phys. Rev. D* **2023**, *108*, 123516. [CrossRef]
107. Li, S.P.; Xie, K.P. Collider test of nano-Hertz gravitational waves from pulsar timing arrays. *Phys. Rev. D* **2023**, *108*, 055018. [CrossRef]
108. Gouttenoire, Y.; Vitagliano, E. Domain wall interpretation of the PTA signal confronting black hole overproduction. *arXiv* **2023**. [CrossRef]
109. Blasi, S.; Mariotti, A.; Rase, A.; Sevrin, A. Axionic domain walls at Pulsar Timing Arrays: QCD bias and particle friction. *J. High Energy Phys.* **2023**, *11*, 169. [CrossRef]
110. Vagnozzi, S. Inflationary interpretation of the stochastic gravitational wave background signal detected by pulsar timing array experiments. *J. High Energy Astrophys.* **2023**, *39*, 81–98. [CrossRef]
111. Franciolini, G.; Iovino, Junior, A.; Vaskonen, V.; Veermäe, H. Recent Gravitational Wave Observation by Pulsar Timing Arrays and Primordial Black Holes: The Importance of Non-Gaussianities. *Phys. Rev. Lett.* **2023**, *131*, 201401. [CrossRef]

112. Athron, P.; Fowlie, A.; Lu, C.T.; Morris, L.; Wu, L.; Wu, Y.; Xu, Z. Can supercooled phase transitions explain the gravitational wave background observed by pulsar timing arrays? *arXiv* **2023**. [CrossRef]
113. Zeng, Z.M.; Liu, J.; Guo, Z.K. Enhanced curvature perturbations from spherical domain walls nucleated during inflation. *Phys. Rev. D* **2023**, *108*, 063005. [CrossRef]
114. Gonzalez, D.; Kitajima, N.; Takahashi, F.; Yin, W. Stability of domain wall network with initial inflationary fluctuations and its implications for cosmic birefringence. *Phys. Lett. B* **2023**, *843*, 137990. [CrossRef]
115. Blasi, S.; Mariotti, A.; Rase, A.; Sevrin, A.; Turbang, K. Friction on ALP domain walls and gravitational waves. *J. Cosmol. Astropart. Phys.* **2023**, *4*, 008. [CrossRef]
116. Chattopadhyay, P.; Chaudhuri, A.; Khlopov, M.Y. Dark Matter from Evaporating PBH dominated in the Early Universe. *arXiv* **2022**. [CrossRef]
117. Wu, Y.; Xie, K.P.; Zhou, Y.L. Classification of Abelian domain walls. *Phys. Rev. D* **2022**, *106*, 075019. [CrossRef]
118. Ferreira, R.Z.; Notari, A.; Pujolas, O.; Rompineve, F. Gravitational waves from domain walls in Pulsar Timing Array datasets. *J. Cosmol. Astropart. Phys.* **2023**, *2*, 001. [CrossRef]
119. Wu, Y.; Xie, K.P.; Zhou, Y.L. Collapsing domain walls beyond Z2. *Phys. Rev. D* **2022**, *105*, 095013. [CrossRef]
120. Ashoorioon, A.; Rezazadeh, K.; Rostami, A. NANOGrav signal from the end of inflation and the LIGO mass and heavier primordial black holes. *Phys. Lett. B* **2022**, *835*, 137542. [CrossRef]
121. Sun, S.; Yang, X.Y.; Zhang, Y.L. Pulsar timing residual induced by wideband ultralight dark matter with spin 0,1,2. *Phys. Rev. D* **2022**, *106*, 066006. [CrossRef]
122. Babichev, E.; Gorbunov, D.; Ramazanov, S.; Vikman, A. Gravitational shine of dark domain walls. *J. Cosmol. Astropart. Phys.* **2022**, *4*, 028. [CrossRef]
123. Benetti, M.; Graef, L.L.; Vagnozzi, S. Primordial gravitational waves from NANOGrav: A broken power-law approach. *Phys. Rev. D* **2022**, *105*, 043520. [CrossRef]
124. Kirillov, A.A.; Rubin, S.G. On Mass Spectra of Primordial Black Holes. *Front. Astron. Space Sci.* **2021**, *8*, 777661. [CrossRef]
125. Brandenburg, A.; Clarke, E.; He, Y.; Kahnashvili, T. Can we observe the QCD phase transition-generated gravitational waves through pulsar timing arrays? *Phys. Rev. D* **2021**, *104*, 043513. [CrossRef]
126. Sakharov, A.S.; Eroshenko, Y.N.; Rubin, S.G. Looking at the NANOGrav signal through the anthropic window of axionlike particles. *Phys. Rev. D* **2021**, *104*, 043005. [CrossRef]
127. Arzoumanian, Z. et al. [The NANOGrav Collaboration]. The NANOGrav 12.5 yr Data Set: Search for an Isotropic Stochastic Gravitational-wave Background. *Astrophys. J. Lett.* **2020**, *905*, L34. [CrossRef]
128. Nojiri, S.; Odintsov, S.D.; Tretyakov, P.V. Dark energy from modified F(R)-scalar-Gauss Bonnet gravity. *Phys. Lett. B* **2007**, *651*, 224–231. [CrossRef]
129. Nojiri, S.; Odintsov, S.D.; Oikonomou, V.K. Modified Gravity Theories on a Nutshell: Inflation, Bounce and Late-time Evolution. *Phys. Rept.* **2017**, *692*, 1–104. [CrossRef]
130. Rubin, S.G. Scalar field localization on deformed extra space. *Eur. Phys. J.* **2015**, *C75*, 333. [CrossRef]
131. Bronnikov, K.A.; Budaev, R.I.; Grobov, A.V.; Dmitriev, A.E.; Rubin, S.G. Inhomogeneous compact extra dimensions. *J. Cosmol. Astropart. Phys.* **2017**, *10*, 001. [CrossRef]
132. Rubin, S.G. Inhomogeneous extra space as a tool for the top-down approach. *Adv. High Energy Phys.* **2018**, *2018*, 2767410. [CrossRef]
133. Bronnikov, K.A.; Popov, A.A.; Rubin, S.G. Multi-scale hierarchy from multidimensional gravity. *Phys. Dark Univ.* **2023**, *42*, 101378. [CrossRef]
134. Nojiri, S.; Odintsov, S.D. Introduction to modified gravity and gravitational alternative for dark energy. *eConf* **2006**, C0602061, 06. [CrossRef]
135. Sotiriou, T.P.; Faraoni, V. f(R) Theories Of Gravity. *Rev. Mod. Phys.* **2010**, *82*, 451–497. [CrossRef]
136. Arbuzova, E.; Dolgov, A.; Singh, R. R^2 -Cosmology and New Windows for Superheavy Dark Matter. *Symmetry* **2021**, *13*, 877. [CrossRef]
137. De Felice, A.; Tsujikawa, S. f(R) theories. *Living Rev. Rel.* **2010**, *13*, 3. [CrossRef]
138. Bamba, K.; Makarenko, A.N.; Myagky, A.N.; Nojiri, S.; Odintsov, S.D. Bounce cosmology from F(R) gravity and F(R) bigravity. *J. Cosmol. Astropart. Phys.* **2014**, *1*, 8. [CrossRef]
139. Sokolowski, L.M. Metric gravity theories and cosmology:II. Stability of a ground state in f(R) theories. *Class. Quant. Grav.* **2007**, *24*, 3713–3734. [CrossRef]
140. Olasagasti, I.; Vilenkin, A. Gravity of higher-dimensional global defects. *Phys. Rev. D* **2000**, *62*, 044014. [CrossRef]
141. Cho, I.; Vilenkin, A. Gravity of superheavy higher-dimensional global defects. *Phys. Rev. D* **2003**, *68*, 025013. [CrossRef]
142. Shimonon, S.; Chiba, T. Numerical solutions of inflating higher dimensional global defects. *Phys. Rev. D* **2005**, *71*, 084002. [CrossRef]
143. Ringeval, C.; Peter, P.; Uzan, J.P. Stability of six-dimensional hyperstring braneworlds. *Phys. Rev. D* **2005**, *71*, 104018. [CrossRef]
144. Gregory, R. Nonsingular Global String Compactifications. *Phys. Rev. Lett.* **2000**, *84*, 2564–2567. [CrossRef] [PubMed]
145. Gherghetta, T.; Shaposhnikov, M. Localizing Gravity on a Stringlike Defect in Six Dimensions. *Phys. Rev. Lett.* **2000**, *85*, 240–243. [CrossRef] [PubMed]

146. Bronnikov, K.; Meierovich, B. Global strings in extra dimensions: A full map of solutions, matter trapping and the hierarchy problem. *J. Exp. Theor. Phys.* **2008**, *106*, 247–264. [CrossRef]
147. Akrami, Y. et al. [Planck Collaboration]. Planck 2018 results. X. Constraints on inflation. *Astron. Astrophys.* **2020**, *641*, A10. [CrossRef]
148. Depta, P.F.; Schmidt-Hoberg, K.; Schwaller, P.; Tasillo, C. Do pulsar timing arrays observe merging primordial black holes? *arXiv* **2023**. [CrossRef]
149. Rubin, S.G.; Fabris, J.C. Distortion of extra dimensions in the inflationary Multiverse. *arXiv* **2021**. [CrossRef]

Disclaimer/Publisher’s Note: The statements, opinions and data contained in all publications are solely those of the individual author(s) and contributor(s) and not of MDPI and/or the editor(s). MDPI and/or the editor(s) disclaim responsibility for any injury to people or property resulting from any ideas, methods, instructions or products referred to in the content.

Neutrino at Different Epochs of the Friedmann Universe

Alexandre V. Ivanchik *, Oleg A. Kurichin and Vlad Yu. Yurchenko

Ioffe Institute, Polytekhnicheskaya 26, Saint-Petersburg 194021, Russia; o.chinkuir@gmail.com (O.A.K.); yurchvlad@gmail.com (V.Y.Y.)

* Correspondence: iav@astro.ioffe.ru

Abstract: At least two relics of the Big Bang have survived: the cosmological microwave background (CMB) and the cosmological neutrino background (C ν B). Being the second most abundant particle in the universe, the neutrino has a significant impact on its evolution from the Big Bang to the present day. Neutrinos affect the following cosmological processes: the expansion rate of the universe, its chemical and isotopic composition, the CMB anisotropy and the formation of the large-scale structure of the universe. Another relic neutrino background is theoretically predicted, it consists of non-equilibrium antineutrinos of Primordial Nucleosynthesis arising as a result of the decay of neutrons and tritium nuclei. Such antineutrinos are an indicator of the baryon asymmetry of the universe. In addition to experimentally detectable active neutrinos, the existence of sterile neutrinos is theoretically predicted to generate neutrino masses and explain their oscillations. Sterile neutrinos can also solve such cosmological problems as the baryonic asymmetry of the universe and the nature of dark matter. The recent results of several independent experiments point to the possibility of the existence of a light sterile neutrino. However, the existence of such a neutrino is inconsistent with the predictions of the Standard Cosmological Model. The inclusion of a non-zero lepton asymmetry of the universe and/or increasing the energy density of active neutrinos can eliminate these contradictions and reconcile the possible existence of sterile neutrinos with Primordial Nucleosynthesis, the CMB anisotropy, and also reduce the H $_0$ -tension. In this brief review, we discuss the influence of the physical properties of active and sterile neutrinos on the evolution of the universe from the Big Bang to the present day.

Keywords: cosmology; neutrino; sterile neutrino; lepton asymmetry; baryon asymmetry; primordial nucleosynthesis; CMB; H $_0$ -tension



Citation: Ivanchik, A.V.; Kurichin, O.A.; Yurchenko, V.Y. Neutrino at Different Epochs of the Friedmann Universe. *Universe* **2024**, *10*, 169. <https://doi.org/10.3390/universe10040169>

Academic Editors: Galina L. Klimchitskaya, Vladimir M. Mostepanenko and Sergey V. Sushkov

Received: 10 February 2024

Revised: 25 March 2024

Accepted: 29 March 2024

Published: 2 April 2024



Copyright: © 2024 by the authors. Licensee MDPI, Basel, Switzerland. This article is an open access article distributed under the terms and conditions of the Creative Commons Attribution (CC BY) license (<https://creativecommons.org/licenses/by/4.0/>).

1. Introduction

Modern conceptions of the structure of matter are based on the so-called Standard Model of elementary particle physics and fundamental interactions (see e.g., [1]), the confirmation of which was successfully completed with the discovery of the Higgs boson. However, despite the great predictive power of the Standard Model and its numerous experimental confirmations, there are a number of problems that cannot be solved within its framework. A significant portion of these problems are related to observational cosmology. These include the problem of the baryon asymmetry of the universe [2,3], the unknown nature of dark matter [4,5] and dark energy [6,7]. Separately, there is the phenomenon of neutrino oscillations [8,9]: the process of spontaneous transformation of one flavor of neutrino into another, due to the presence of a non-zero neutrino mass. This last circumstance may be the most obvious indication of the need to go beyond the Standard Model.

Modern ideas about the evolution of the universe are based on another standard model: the Λ CDM cosmological model [10,11]. At the same time, the model is adapted from time to time as observational data accumulates and theoretical ideas about the structure of the world develop. Both of these models are closely interconnected today. For example, elementary particles of the SM (and their properties) played a significant, and sometimes decisive role at different stages of the evolution of the universe (see Figure 1).

Having started from a singular state and passed through the inflation stage, in the first moments of the Big Bang our universe entered the radiation-dominated stage of its evolution. Most of the time during this stage, it was neutrinos and photons that determined the dynamics of the expansion of the universe (see Figure 1). This affected the process of Primordial Nucleosynthesis which took place in the first minutes after the Big Bang, during which, in addition to the already existing relic neutrinos ($C\nu B$), nonequilibrium antineutrinos appeared from the decays of neutrons and tritium nuclei [12,13]. The discovery of these neutrinos would open a “window” into the first minutes of the hot universe, and would also allow us to test the existence of the baryon asymmetry of the universe on the largest scales.

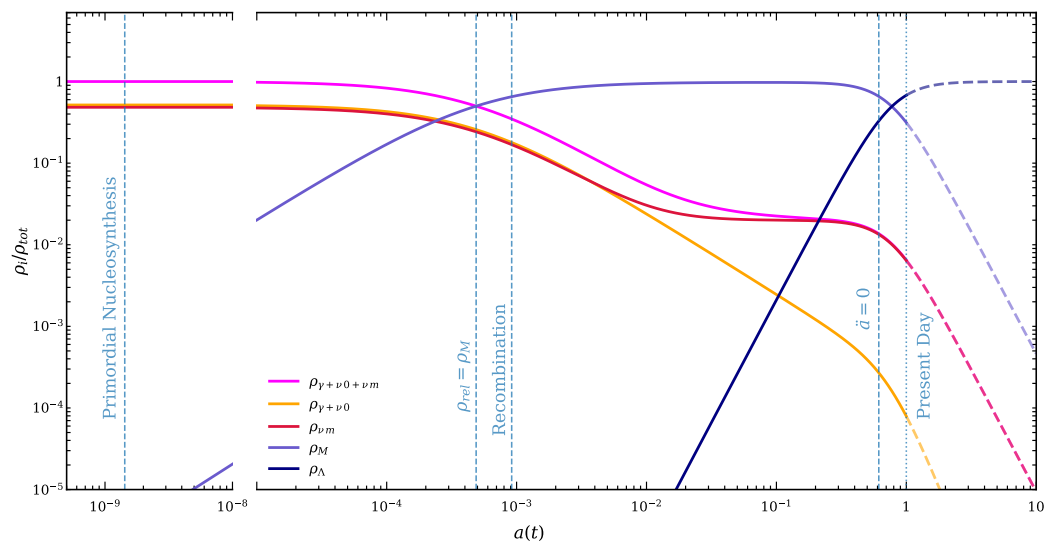


Figure 1. The contributions to the total energy density of the universe from different components as a function of the scale factor $a(t)$. The components include photons (ρ_γ), non-relativistic matter (ρ_M), which consists of cold dark and baryonic matter, $\rho_M = \rho_{\text{CDM}} + \rho_b$, neutrinos (ρ_ν) and dark energy (ρ_Λ). The values of the cosmological parameters were taken from the Planck results [14]. Vertical dashed lines mark key cosmological milestones: Primordial Nucleosynthesis, radiation-matter equality ($\rho_{\text{rel}} = \rho_M$), Primordial Recombination, and the moment of transition from the decelerating to accelerating expansion of the universe ($\ddot{a}(t) = 0$). For calculations, we utilised the neutrino energy density in the following way: two neutrino flavors are precisely massless ($\rho_{\nu 0}$, yellow curve), and ($\rho_{\nu m}$, red curve), one neutrino flavor has mass $m_\nu = 0.06$ eV (the same as utilized in the Planck analysis [14]). The massless neutrinos behave completely like radiation during the whole course of the evolution of the universe, while the massive one behaves like radiation in the early universe and like non-relativistic matter at later stages.

The next process in which we can see the influence of neutrinos is the process of Primordial Recombination, which took place about 380 thousand years after the Big Bang. At the end of this process, the CMB anisotropy is formed, the observation and analysis of which allows us to obtain high precision estimates of key cosmological parameters [14].

Later, having become non-relativistic, the neutrino increases the contribution to the energy density of the universe of the non-relativistic components, which previously consisted of cold dark matter (Ω_{CDM}) and baryonic matter (Ω_b), and the character of the equation of state changes from relativistic to non-relativistic, so the neutrino component, in a special way, influences the formation of the large-scale structure of the universe.

Possible extensions of the Standard Model of elementary particles suggest the existence of sterile neutrinos. Apparently, the first to introduce the concept of “sterile neutrinos” was Bruno Pontecorvo in 1967 [15]. Their introduction potentially makes it possible to solve not only the problems of generating the masses of the active neutrinos and their oscillations, but also such cosmological problems as the baryon asymmetry of the universe (BAU) and

the nature of dark matter (see, e.g., [16,17]). At the same time, the physical properties of both active and possible sterile neutrinos significantly affect the values of the determined cosmological parameters [18].

The recent results of a number of independent experiments [19,20] indicate the possibility of the existence of a light sterile neutrino ($m_{\nu s} \sim 1\text{--}3$ eV). The presence of such a neutrino is in poor agreement with the predictions of the Standard Cosmological Model, but these contradictions can be removed, for example, by introducing a non-zero lepton asymmetry of the universe, $\xi_\nu \sim 10^{-2}$, and/or increasing the energy density of active neutrinos. These changes make it possible to reconcile the possible existence of a light sterile neutrino with Primordial Nucleosynthesis, the CMB anisotropy, and also reduce the H_0 -tension¹.

It should be noted that the results of experiments on the detection of light sterile neutrinos are not always consistent with each other. For example, in a recent STEREO collaboration paper [23] the authors reject the hypothesis of the existence of a sterile neutrino on this mass scale. Therefore, the question of the existence of a light sterile neutrino cannot be regarded as finally settled.

Detailed discussions on the influence of neutrino properties on cosmological evolution can be found in large reviews (see, e.g., [24,25]). In our brief review, we emphasise the aspects related to the modern data on active and possible light sterile neutrinos and their influence on various cosmological processes.

Nowadays, there is little doubt about the existence of cosmological neutrinos. The most promising method for their detection is the use of the inverse beta decay of tritium, proposed by S. Weinberg in 1962 [26]. Unfortunately, due to the drastic smallness of the their interaction cross sections at low energies, it has not been possible to register them directly so far. If in the future this can be done, we will directly obtain information about the first seconds, minutes and hours of the early universe.

2. The Enigmatic Neutrino

Each of the particles of the Standard Model (see Figure 2) deserves a separate story, but perhaps the most enigmatic particle is still the neutrino, because the explanation of its amazing properties may require going beyond the Standard Model and will have an impact on another Standard Model: the Λ CDM cosmological model.

Neutrinos do not have an electrical charge; they are born and participate only in weak interactions. There are three generations (flavors) of neutrinos, ν_e, ν_μ, ν_τ , corresponding to the three generations of charged leptons, electron e , muon μ and tau lepton τ (Figure 2). In the Standard Model, neutrinos are precisely massless particles, but the phenomenon of neutrino oscillations—the process of spontaneous transformation of neutrinos of one flavor into another—is a direct indication that neutrinos have mass. The explanation of this phenomenon requires an extension of the Standard Model of elementary particles. Although the observed oscillations of neutrinos unambiguously indicate the existence of their mass, it is still not possible to measure it by direct methods, and only lower and upper limits on the sum of the neutrino masses have been experimentally obtained [1]:

$$0.06 \text{ eV} \lesssim \sum m_\nu \lesssim 0.12 \text{ eV} \tag{1}$$

The lower limit on the sum of the masses is calculated on the basis of experimental data on the neutrino squared mass differences $\Delta m_{ij}^2 = m_i^2 - m_j^2$, obtained from a number of independent experiments [1]. The upper limit is estimated by analysing the cosmological data [14]. However, the unique properties of neutrinos do not end there; in addition, the following can be pointed out:

- Neutrinos are the second most abundant particles in the universe (after photons). The density of relic photons in the present era is $n_\gamma = 412 \text{ cm}^{-3}$, whereas the density of relic neutrinos (taking into account three flavors of neutrinos and antineutrinos) is $n_\nu = 336 \text{ cm}^{-3}$.

- It is the lightest known particle with non-zero mass; the neutrino is more than a million times lighter than the electron (see Equation (1)).
- They explicitly break the symmetry of right and left; neutrinos are solely left-handed, antineutrinos are solely right-handed.
- Neutrinos are one of the components of dark matter. Their contribution to the total energy density of dark matter may be up to 1% in the present cosmological epoch.
- Neutrinos have one of the smallest cross sections for interaction with matter ($\sigma \sim 10^{-44} \text{ cm}^2$ at MeV energies) which determines their enormous penetrating ability, allowing us to see the interiors of stars. In the future, they may allow us to study the first seconds, minutes, and hours of the birth of our universe; the early universe is opaque to electromagnetic radiation.

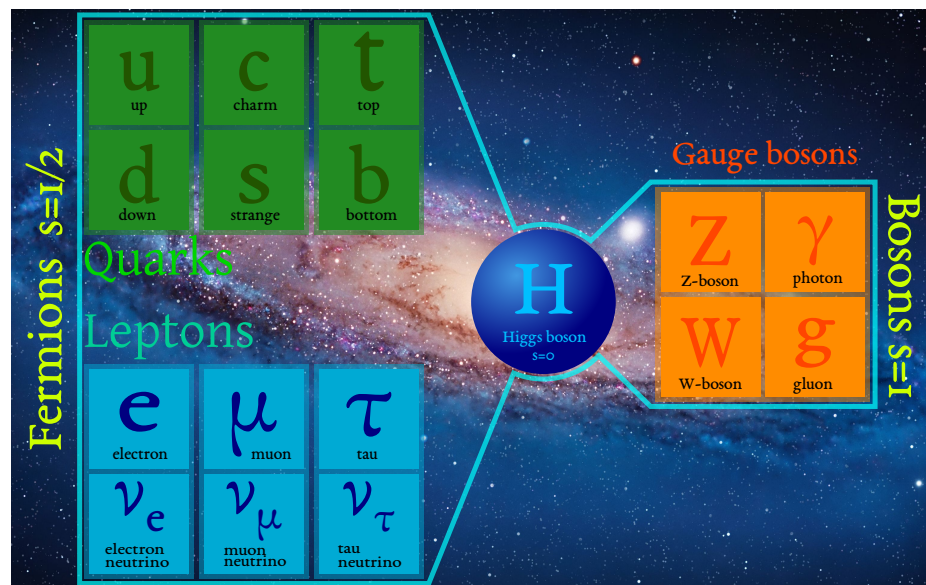


Figure 2. The Standard Model of elementary particle physics is the quark-lepton structure of matter. It consists of three generations of fermions. Each generation includes two quarks and two leptons (charged and neutral), which interact with each other via gauge bosons. In this scheme of the quark-lepton structure of matter, phenomena such as the existence of neutrino masses and their oscillations, and the nature of dark matter and dark energy find no explanation.

3. Grand Unified Neutrino Spectrum

The first known detection of antineutrinos from nuclear reactors occurred in 1956, about which Fredericks Reines and Clyde Cowan sent a radiogram to Wolfgang Pauli from New York to Zurich. Subsequently, solar neutrinos, atmospheric neutrinos resulting from the interaction of cosmic rays with atmospheric matter (mostly nitrogen and oxygen nuclei), and, finally, ultra-high energy neutrinos ($E_\nu \gtrsim 10^{14} \text{ eV}$), which might originate from active galactic nuclei, were recorded.

The energy range over which neutrinos are now observed is indeed enormous: from MeV (10^6 eV) to PeV (10^{15} eV) energies (for example, IceCube has detected a few neutrinos with energies above 10^{15} eV [27]), but it can be extended by even more than ten orders of magnitude due to the theoretically predicted low-energy cosmological neutrinos² ($10^{-4} \lesssim E_\nu \lesssim 10 \text{ eV}$) and ultrahigh-energy cosmogenic neutrinos ($E_\nu \gtrsim 10^{16} \text{ eV}$), the latter arise from the interaction of cosmic rays with the CMB photons, interstellar and intergalactic matter (see, e.g., [28]).

Figure 3 shows the so-called “Grand Unified Neutrino Spectrum”³, it presents the theoretical and observational spectra of neutrinos of various natures (data used for plotting this spectrum can be found in the paper [13]). It can be seen that the most numerous neutrinos are cosmological ones, which were born in the first moments after the Big Bang. For example, the flux of solar neutrinos at the Earth’s surface is 64 billion particles per

square centimetre per second ($6.4 \times 10^{10} \text{ cm}^{-2} \text{ s}^{-1}$), while the flux of the CνB neutrinos is at least three trillion particles $\text{cm}^{-2} \text{ s}^{-1}$ ($\gtrsim 3 \times 10^{12} \text{ cm}^{-2} \text{ s}^{-1}$).

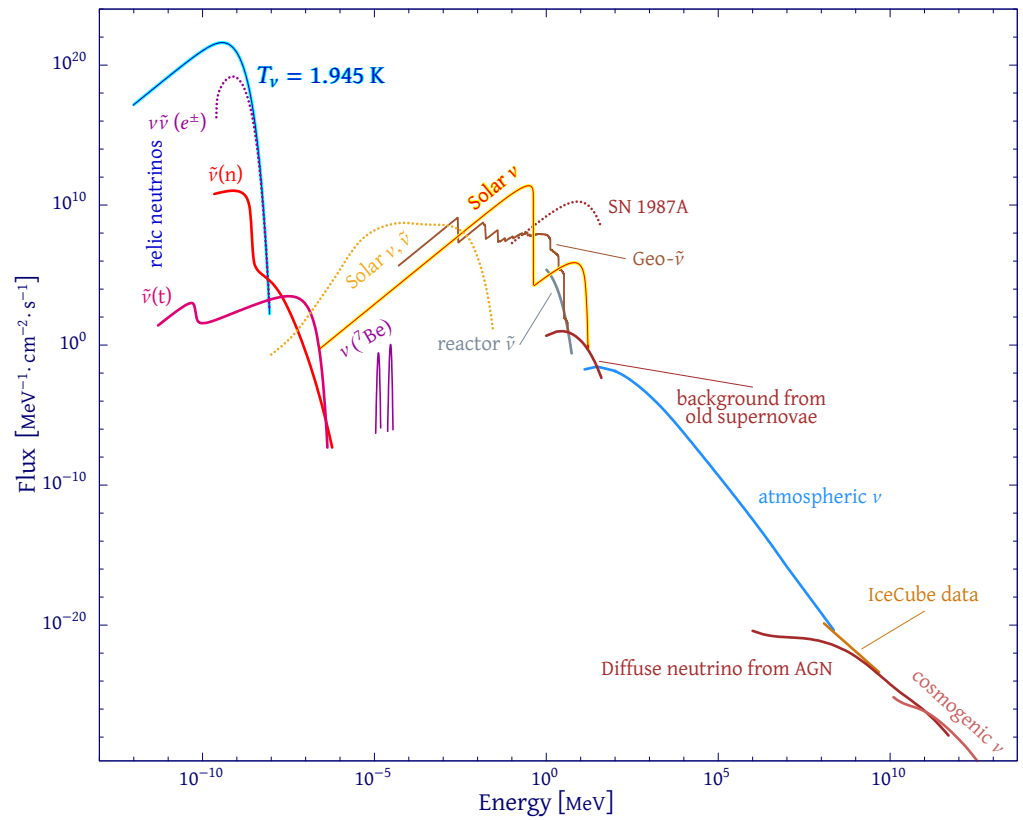


Figure 3. Observed and theoretically calculated spectra of neutrinos and antineutrinos generated by various natural phenomena (local and cosmological). For a detailed discussion of all components of the overall spectrum, see [29].

The cosmological neutrinos, like the CMB photons, have a thermal equilibrium spectrum (shown in Figure 4) which for neutrinos is given by the Fermi–Dirac distribution:

$$n_\nu dp = \frac{1}{(2\pi\hbar)^3} \frac{4\pi p^2 dp}{\exp(pc/kT) + 1}. \tag{2}$$

In this paper we will focus on cosmological neutrinos and their impact on various stages of the evolution of the universe.

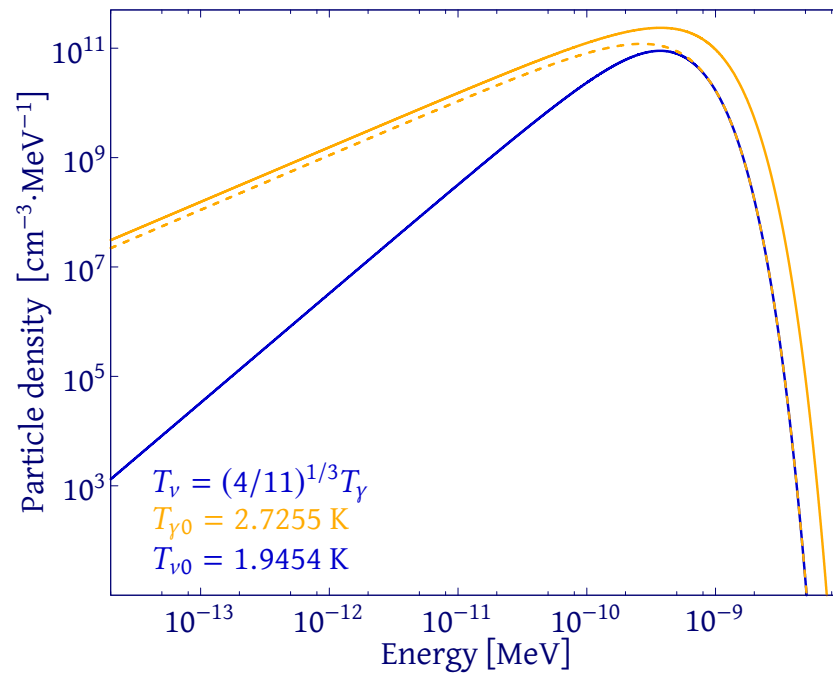


Figure 4. The present-day Planckian spectrum of the CMB photons with temperature $T_{\gamma 0} = 2.7255$ K and the Fermi–Dirac spectrum of the CνB neutrinos with temperature $T_{\nu 0} = 1.9454$ K, which are related as follows $T_{\nu} = (4/11)^{1/3} T_{\gamma}$ (see e.g., [10]). The photon spectrum is hotter due to electron–positron annihilation that occurred within the first hundred seconds after the Big Bang. The dotted curve shows what the photon spectrum would be with the temperature of the neutrino ($T_{\gamma 0} = T_{\nu 0} = 1.9454$ K).

4. Cosmological Manifestations of Neutrinos

4.1. Radiation-Dominated Epoch, Primordial Nucleosynthesis

In the first moments of the Big Bang, the universe enters the radiation-dominated stage of its evolution, which lasts about 50 thousand years. At this time, neutrinos, along with photons, play a crucial role in the dynamics of the expansion of the universe. Primordial Nucleosynthesis, which took place in the first minutes after the Big Bang, is the earliest moment in the history of the universe that we can probe. As a result of this process, the first lightest nuclei and their isotopes (D, He, Li) appeared, forming the primordial chemical composition of the baryonic matter of the universe. Astronomical observations of the relative abundance of these elements and their comparison with theoretical predictions allow us to estimate one of the key cosmological parameters: the baryon/photon ratio, $\eta = n_b/n_{\gamma}$. This quantity is related to the baryon density in the universe $\rho_b(\Omega_b)$, as $\eta = 2.74 \times 10^{-8} \Omega_b h^2$ (see e.g., [30]). Here $\Omega_b \equiv \rho_b/\rho_c$ is the relative baryon density, $\rho_c = 3H_0^2/8\pi G_N$ is the present critical density, H_0 is the present value of the Hubble parameter, G_N is the Newton constant, and h , the present value of the Hubble parameter measured in units of $100 \text{ km s}^{-1} \text{ Mpc}^{-1}$.

The most precise estimates of the primordial abundances up to date are as follows:

- Abundance of the primordial ^4He (Y_p) is estimated via the analysis of the spectroscopic samples of dwarf metal-poor galaxies. The analysis yields the estimate $Y_p = 0.247 \pm 0.002$ [31,32].
- Abundance of the primordial D is estimated via the analysis of the quasar spectra containing absorption lines of damped Lyman-alpha (DLA) systems associated with metal-poor intergalactic medium, whose chemical composition is close to the primordial one. The analysis yields $\text{D}/\text{H} = (2.533 \pm 0.024) \times 10^{-5}$ (see [33] and references therein). There are circumstances that make it difficult to obtain estimates (and their uncertainties) for the abundance of primordial deuterium; a discussion of this problem is presented in [34].

- Abundance of the primordial ${}^7\text{Li}$ is estimated via the spectral analysis of metal-poor old stars in the halo of our galaxy. The analysis yields the estimate ${}^7\text{Li}/\text{H} = (1.6 \pm 0.3) \times 10^{-10}$ [35,36].

Figure 5 shows the calculated abundances of primordial ${}^4\text{He}$, D , ${}^7\text{Li}$ as a function of the abundance of baryons in the universe (dark blue lines) and the observed values of the primordial abundances, marked via coloured rectangles.

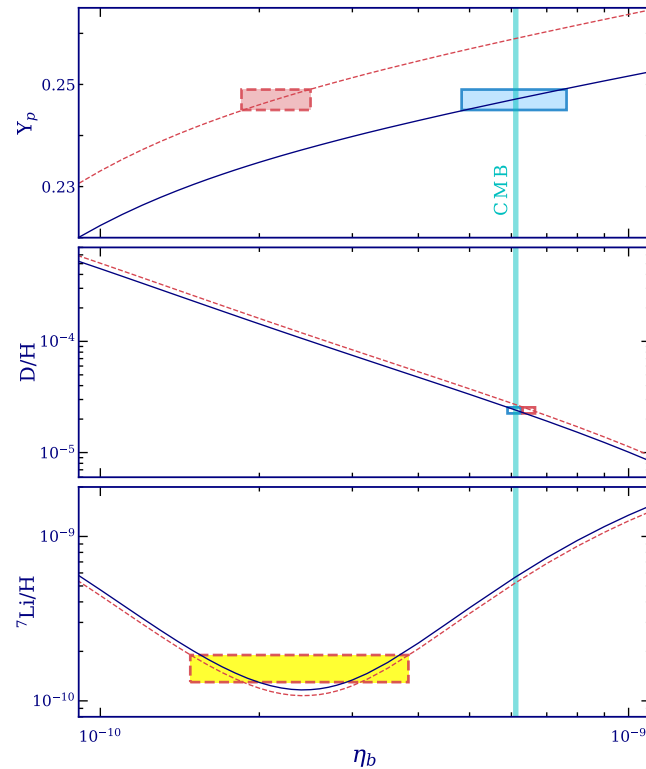


Figure 5. Dependence of the primordial abundances ${}^4\text{He}$ (Y_p), D , ${}^7\text{Li}$ on the baryon–photon ratio η . The dark blue solid lines correspond to the calculated values in the framework of the standard theory of Primordial Nucleosynthesis with three types of active neutrinos ($\Delta N_{\text{eff}} = 0$). Coloured rectangles indicate observed values of primordial abundances. The vertical turquoise line corresponds to the value of η estimated as a result of analysis of the CMB anisotropy measured by the Planck satellite [14]. It can be seen that for ${}^4\text{He}$ and D the observational data is consistent with the prediction from the CMB anisotropy, while the observed abundance of ${}^7\text{Li}$ is significantly lower than the predicted value, which is referred as the “Lithium problem”. Red dotted lines and red rectangles correspond to the theory of Primordial Nucleosynthesis in the presence of an additional type of neutrino ($\Delta N_{\text{eff}} = 1$).

Primordial Nucleosynthesis was historically the first way to estimate the total baryon density of the universe, other methods allowed astrophysicists to estimate the number of baryons only in particular astrophysical objects (stars, interstellar and intergalactic gas, galaxy clusters). However, later another independent way to estimate the total baryon density of the universe appeared. It is the analysis of the CMB anisotropy formed during the process of Primordial Recombination, which occurred 380 thousand years after the Big Bang. The primordial abundance estimates based on this method are also shown in Figure 5 with the vertical light blue line. It can be seen that for ${}^4\text{He}$ and D the observational data are consistent with the prediction from the CMB anisotropy [14], while the observed value ${}^7\text{Li}/\text{H} = (1.6 \pm 0.3) \times 10^{-10}$ [35,36] is significantly lower than the predicted value ${}^7\text{Li}/\text{H} = (4.7 \pm 0.7) \times 10^{-10}$ [37]. The latter is referred to as the “Lithium problem”, which still has no explanation.

Independent estimates of the $\eta = n_b/n_\gamma$ based on Primordial Nucleosynthesis and the CMB anisotropy refer to different cosmological epochs. Therefore they make it possible not

only to test the Λ CDM model for self-consistency, but also, in the case of a detected discrepancy, can serve as a tool to search for “physics beyond”, which represents a generalisation and extension of the Standard Models of cosmology and particle physics.

4.2. Antineutrinos of Primordial Nucleosynthesis

In addition to the relic neutrinos from the Big Bang, antineutrinos of Primordial Nucleosynthesis have recently been theoretically predicted [12,13].

The initial building material for all nuclei synthesised in Primordial Nucleosynthesis are protons and neutrons. The neutrons, in addition to participation in nuclear transformations during collisions with other nuclei, are also subject to spontaneous β^- -decay ($n \rightarrow p + e^- + \bar{\nu}_e$). The lifetime of a neutron relative to this process is $\tau_n \simeq 880.2$ s [38]. The electron and antineutrino created in the decay carry away almost all the available decay energy $Q_n \simeq 782.3$ keV [39]. Most decays of neutrons occur after neutrino decoupling (which took place approximately 0.1 s after the Big Bang at temperature $T \sim 2$ MeV), so the antineutrinos produced in these decays are no longer thermalized. Thus, neutron decays during the course of Primordial Nucleosynthesis are a source of non-thermal antineutrinos which will uniformly and isotropically fill the universe at the end of Primordial Nucleosynthesis.

Among the nuclei with noticeable mass fractions that are created in Primordial Nucleosynthesis, there is a nucleus that, like the neutron, is unstable with respect to β^- decay. This is the tritium nucleus (T). The lifetime of this nucleus is $\tau_T \simeq 17.66$ years [40], the decay energy is $Q_T \simeq 18.59$ keV [39].

The calculated spectra of antineutrinos from decays of neutrons and tritons in the early universe are presented in Figure 6. The figure shows the spectra of neutrinos and antineutrinos from all sources generating the largest fluxes in the chosen energy range. It can be seen that the antineutrino fluxes of Primordial Nucleosynthesis in the energy range (10^{-2} – 10^{-1}) eV exceed the fluxes from all other sources of neutrinos and antineutrinos. If these nonequilibrium antineutrinos were discovered, we would be able to directly probe the universe in its first minutes and hours after the Big Bang. At the moment, only the CMB studies provide such an opportunity, but this corresponds to a much later cosmological epoch (~ 400 thousand years after the Big Bang).

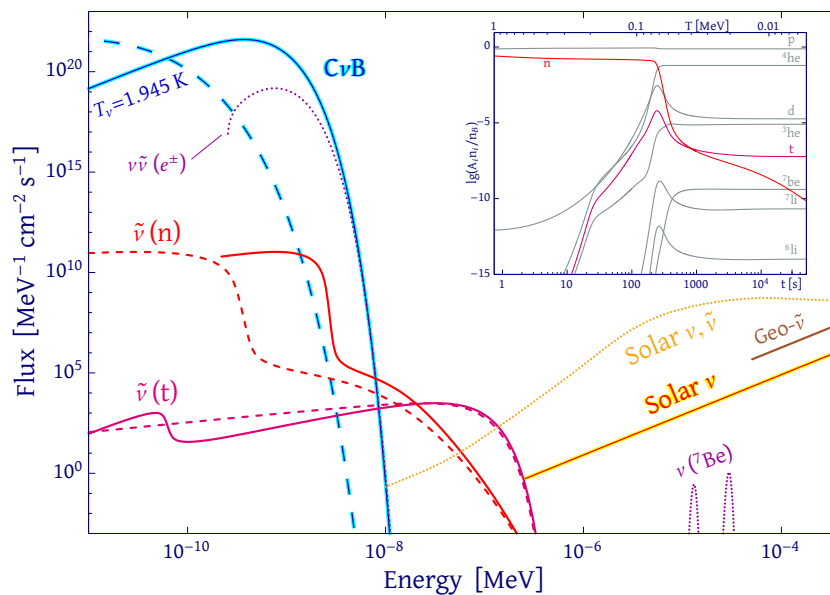


Figure 6. Spectra of antineutrinos from β^- -decays of neutrons (n) and tritium nuclei (t) (red and red curves). Solid curves show spectra calculated for massless antineutrinos. The dashed curves show the spectra calculated for antineutrinos with mass $m_{\nu} = 0.01$ eV. Note that there is an energy range where the antineutrino fluxes of Primordial Nucleosynthesis exceed the neutrino fluxes of the Big Bang (blue curve) and solar neutrinos (yellow solid and dotted curves). The figure is based on our works [12,13].

4.3. Antineutrinos of Primordial Nucleosynthesis as the Probe of Baryon Asymmetry of the Universe

Direct observational evidence that allows us to conclude that matter predominates in the observable part of the universe and antimatter is absent include the absence of significant annihilation radiation: in the solar system, in our galaxy, and in galaxy clusters, as well as the composition of cosmic rays. The potential observation of relic antineutrinos would allow us to see the most distant, causally unconnected regions to date. The discovery of relic antineutrinos of Primordial Nucleosynthesis could provide evidence of either the baryon asymmetry of most of the visible universe or detect regions with a predominance of antimatter, since the existence of such regions would lead to the generation of relic neutrinos from the decays of antineutrons and antitritium.

5. Sterile Neutrinos as an Extension of the Standard Model of Particle Physics and the Λ CDM Cosmological Model

One option for expanding the Standard Model of particle physics is to introduce sterile neutrinos, which do not participate in any Standard Model interactions. The introduction of such particles provides a solution to several problems at once: (i) they make it possible to generate masses of active types of neutrinos (electron, muon and tau neutrinos), (ii) they are suitable for the role of dark matter, (iii) they can become a source for the generation of the baryon asymmetry of the universe (see e.g., [16,17]). At the same time, the mass range of sterile neutrinos is not determined; they can be light, on the order of several eV, and very heavy, up to 10^{15} GeV. Their role in relation to cosmology is determined by their mass [41], as follows:

1. Superheavy sterile neutrinos with masses of $\sim 10^2$ – 10^{15} GeV. Such neutrinos are capable of generating baryon asymmetry in the early universe through the mechanism described in [42]. Moreover, their lifetime is so short that they will decay even before the Primordial Nucleosynthesis and thermodynamics will “erase” all traces of their existence. Today, only the fact of the presence of baryon asymmetry in the universe could indicate such a possibility (not excluding others).
2. Heavy sterile neutrinos with masses of ~ 1 keV– 10^2 GeV. Such neutrinos have lifetimes comparable to or longer than the current age of the universe, and are therefore good candidates for cold dark matter particles. In addition, at high temperatures (~ 100 GeV), they can lead to the generation of lepton asymmetry due to oscillations with active neutrinos [43].
3. Light sterile neutrinos with masses of ~ 1 eV– 1 keV could have a significant impact on cosmology, which will be discussed in more detail below.

Hints of the possible existence of sterile neutrinos appeared more than ten years ago in various independent experiments (see e.g., [18]), the latest of which talk about the possible existence of light ($m_{\nu,s} \sim 1$ – 3 eV) sterile neutrinos [19,20]. Such sterile neutrinos may have mixing angles comparable to those of active species. Today, the status of these experiments is quite controversial, since the results obtained do not always agree with each other, and sometimes they are said to be completely inconsistent. For example, in a recent work [23] it is stated that the hypothesis about the existence of a light sterile neutrino could be rejected. However, there is still a region of parameters of oscillations of a light sterile neutrino, which formally does not contradict either the results of the STEREO experiment [23], or the results of the Neutrino-4 experiment [19]. Therefore the question of the existence of a light sterile neutrino cannot be considered finally decided. In addition, sterile neutrinos of electron-volt masses do not fit well into the standard Λ CDM cosmological model. Firstly, the introduction of such neutrinos leads to a discrepancy between the theoretical predictions of Primordial Nucleosynthesis and observational data (see Figure 5 and [37,41]). Secondly, such neutrinos remain relativistic at the epoch of formation of the CMB anisotropy, and, consequently, change the size of the sound horizon, which also leads to a discrepancy between the observational data and the theoretical model (this will be discussed below). Thirdly, such sterile neutrinos are so-called “hot-warm

dark matter" (see, e.g., [11]), and can interfere with cosmological structure formation on small scales, and later become a non-relativistic contribution to it (see e.g., [44]). Fourthly, constraints on the mixing parameters and mass splitting for electronvolt sterile neutrinos, obtained on the basis of cosmological data from Primordial Nucleosynthesis, the CMB anisotropy and baryonic acoustic oscillations (BAO), given in [45], show that in order for the hypothesis of existence of such particles to be consistent with the Λ CDM model, mixing parameters should be sufficiently small ($|U_{\alpha 4}|^2 \sim 10^{-4} - 10^{-2}$). This contradicts the experimental results obtained in [19]: $|U_{\alpha 4}|^2 \gtrsim 10^{-1}$. Thus, there is a strong tension between the existence of such sterile neutrinos and the standard Λ CDM model. However, there is a way out of this situation, and below we provide a discussion of possible options for expanding the Λ CDM model, which allow us to reconcile cosmological observational data with the hypothesis of the existence of a light sterile neutrino.

Light Sterile Neutrinos at the Radiation-Dominated Stage and During the Era of Primordial Nucleosynthesis

The existence of a light sterile neutrino will lead to a change in the energy density at the radiation-dominated stage, which is conveniently parameterized using the so-called effective number of neutrino species N_{eff} , which, in turn, is determined by the relation:

$$\frac{\rho_\nu}{\rho_\gamma} = \frac{7}{8} N_{\text{eff}} \left(\frac{T_\nu}{T_\gamma} \right)^4 = \frac{7}{8} N_{\text{eff}} \left(\frac{4}{11} \right)^{4/3} \tag{3}$$

where ρ_ν and ρ_γ are the energy densities of neutrinos and photons, and the last factor is the fourth power of the ratio of neutrino and photon temperatures, $T_\nu/T_\gamma = (4/11)^{1/3}$ [10]. The contribution to the energy density from three active types of neutrino $N_{\text{eff}} \equiv N_{\text{eff}}^0 = 3.046$ [46,47]. By introducing the value ΔN_{eff} , which determines the addition to N_{eff} in the case of the presence of a light sterile neutrino, and taking into account that the temperature of sterile and active neutrinos coincides, we can write the total energy density

$$\rho_R = \rho_\gamma \left(1 + \frac{7}{8} (N_{\text{eff}} + \Delta N_{\text{eff}}) \left(\frac{4}{11} \right)^{4/3} \right) \tag{4}$$

whence follows:

$$\Delta N_{\text{eff}} = \left(\frac{7}{8} \left(\frac{4}{11} \right)^{4/3} \right)^{-1} \frac{\rho_\nu^{(s)}}{\rho_\gamma} = \left[\frac{7}{8} \frac{\pi^2}{15} T_\nu^4 \right]^{-1} \frac{1}{\pi^2} \int p^3 f_s(p) dp \tag{5}$$

where $\rho_\nu^{(s)}$ is the energy density of sterile neutrinos, $f_s(p)$ is their distribution function, T_ν is the temperature of active neutrinos. The form of the distribution function of sterile neutrinos depends on the method of their generation. If sterile neutrinos are produced in some thermal processes, then they would have a Fermi–Dirac distribution function, like active neutrinos. This will lead to $\Delta N_{\text{eff}} = 1$. If the generation of sterile neutrinos is non-thermal (e.g., via the Dodelson–Widrow mechanism [48]), the distribution function may be different. However, calculations carried out in the studies [41,49] using current data on neutrino mixing parameters showed that light sterile neutrinos with a mass of the order of several eVs become completely thermalized by the neutrino decoupling time due to oscillations with the active species. Thus, light sterile neutrinos remain in the expanding universe as an additional relativistic degree of freedom with $\Delta N_{\text{eff}} = 1$.

However, it should be noted that the oscillation parameters of light sterile neutrinos obtained in experiments have quite large uncertainties and thus the reliability of these results requires further confirmation. For example, explicit PMNS matrix for classical 3-flavor and extended 3 + 1-flavor mixing presented in [50] (Section 11) exhibits orders of magnitude larger uncertainties in the matrix elements for 3 + 1 mixing. In the case of significantly smaller mixing angles, the thermalization of sterile neutrinos will be incom-

plete and, therefore, the number of relativistic degrees of freedom will be in the interval $0 \leq \Delta N_{\text{eff}} < 1$ (this case is considered in [18]).

In the case of complete thermalization, $\Delta N_{\text{eff}} = 1$, which significantly changes the expansion rate of the universe and, accordingly, the predictions of Primordial Nucleosynthesis. From Figure 5 (top panel) it is clear that the presence of a light sterile neutrino, which increases the effective number of neutrino species to four, leads to a significant change in the theoretical prediction of the abundance of ^4He , incompatible with observational data on deuterium and the CMB anisotropy. Nowadays, this is the strictest constraint on the possible existence of a light sterile neutrino.

A solution to this problem can be found in the case of the existence of non-zero lepton (neutrino) asymmetry $L_\nu = (n_\nu - n_{\bar{\nu}})/(n_\nu + n_{\bar{\nu}})$. Here $n_{\nu,\bar{\nu}}$ is the number density of neutrinos and antineutrinos and is defined with the following equation:

$$n_{\nu,\bar{\nu}} = \int \frac{4\pi p^2}{(2\pi\hbar)^3} \frac{dp}{\exp\left(\frac{E \mp \mu}{kT}\right) + 1} \tag{6}$$

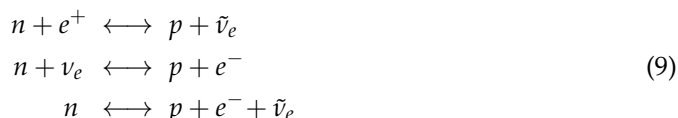
Direct substitution of number densities shows that the lepton asymmetry L_ν can be expressed in terms of the dimensionless parameter $\xi = \mu/kT$, where μ is the chemical potential of the neutrino, as follows:

$$L_\nu = -\frac{1}{\Gamma(3) (Li_3(-e^\xi) + Li_3(-e^{-\xi}))} \left(\frac{\pi^2}{3} \xi + \frac{\xi^3}{3} \right) \tag{7}$$

where $Li_3(x)$ is the polylogarithm function and $\Gamma(x)$ is the gamma function. For small values of ξ this gives:

$$L_\nu \approx \frac{\pi^2}{9\xi(3)} \xi \left(1 + \frac{\xi^2}{\pi^2} \right) \approx 0.91 \times \xi \tag{8}$$

For temperatures above 2 MeV weak interaction reactions proceeded intensively, including those that determined the neutron–proton ratio:



As long as the rate of weak interactions exceeds the expansion rate of the universe, it enables the neutron–proton ratio to track its equilibrium value:

$$\left(\frac{n}{p}\right)_{eq} = \exp\left(-\frac{\Delta m}{kT}\right) \tag{10}$$

where n and p are number densities of neutron and protons, $\Delta m = m_n - m_p = 1.293$ MeV.

For temperatures below 2 MeV the rate of weak interactions becomes less than the rate of expansion of the universe, which leads to the removal of the neutron–proton mixture from thermodynamic equilibrium with the primordial plasma (so-called “neutron freeze-out” [37]). Up to the start of Primordial Nucleosynthesis the neutron–proton ratio decreases slowly due to the β -decay of free neutrons. The evolution of neutron density can be described via the equation [10]:

$$\frac{dX_n}{dt} = -\lambda(n \rightarrow p)X_n + \lambda(p \rightarrow n)(1 - X_n) \tag{11}$$

where $X_n = n/(n + p)$. In the equation, the λ are the rates of the corresponding reactions, which depend on the lepton asymmetry (explicit formulae can be found in [51]). The presence of non-zero lepton asymmetry leads to an increase in the rate $\lambda(n \rightarrow p)$ and a decrease in the rate $\lambda(p \rightarrow n)$. These reactions in conjunction lead to an overall decrease

of the neutron–proton ratio, which in turns leads to decreased production of ^4He during Primordial Nucleosynthesis. In the case of non-zero lepton asymmetry the neutron–proton ratio shifts from its equilibrium value (10) [52]:

$$\frac{n}{p} = \exp\left(-\frac{\Delta m + \mu}{kT}\right) = \left(\frac{n}{p}\right)_{eq} \times \exp(-\zeta) \tag{12}$$

It is worth noting, however, that the presence of non-zero lepton asymmetry itself leads to an increase in the total energy density of ultrarelativistic particles, and, consequently, the expansion rate of the universe. The increase of the expansion rate in turn leads to higher abundance of primordial ^4He . Direct calculation shows that this effect is quite small compared to the previously discussed one [52], and thus the higher ^4He yield associated with the increased expansion rate is offset by the lower neutron–proton ratio at the start of Primordial Nucleosynthesis.

Of all the primordial elements, ^4He is the most sensitive element to the neutron–proton ratio [30]. This is due to the fact that all the neutrons that existed at the start of Primordial Nucleosynthesis will either decay to protons, or form primordial nuclei (mainly ^4He ones). Thus the total abundance of primordial helium can be approximated as

$$Y_p \approx \frac{2n/p}{1+n/p} \tag{13}$$

where n/p is neutron–proton ratio at start of Primordial Nucleosynthesis, which is evaluated using Equation (11). In the case of non-zero lepton asymmetry this equation transforms to

$$Y_p \approx \frac{2(n/p)_{eq} \times e^{-\zeta}}{1+(n/p)_{eq} \times e^{-\zeta}} \tag{14}$$

For small values of ζ this equation simplifies:

$$Y_p \approx Y_p^{eq} \left[1 - \zeta \left(1 - \frac{Y_p^{eq}}{2} \right) \right] \tag{15}$$

where Y_p^{eq} is the value of Y_p with zero lepton asymmetry and is a function of η and the effective number of neutrino species N_{eff} . Thus, the presence of the lepton asymmetry leads to a decreased abundance of primordial ^4He .

Using the described methodology for taking non-zero lepton asymmetry into account, we calculated the abundance of primordial ^4He as a function of baryon–photon ratio η , N_{eff} and ζ . The results are presented on the left panel of the Figure 7. In the calculation we considered three cases: standard Primordial Nucleosynthesis with $\Delta N_{eff} = 0$ and $\zeta = 0$ (dark blue curve), Primordial Nucleosynthesis with $\Delta N_{eff} = 1$ and $\zeta = 0$ (red curve), and Primordial Nucleosynthesis $\Delta N_{eff} = 0$ and $\zeta \neq 0$ (yellow curve). Fitting the theoretical calculation to the observed abundance of primordial helium from [32], we found that the increase of the Y_p associated with the presence of a fully-thermalized light sterile neutrino can be completely compensated by the non-zero lepton asymmetry with the value $\zeta = 0.052 \pm 0.001$.

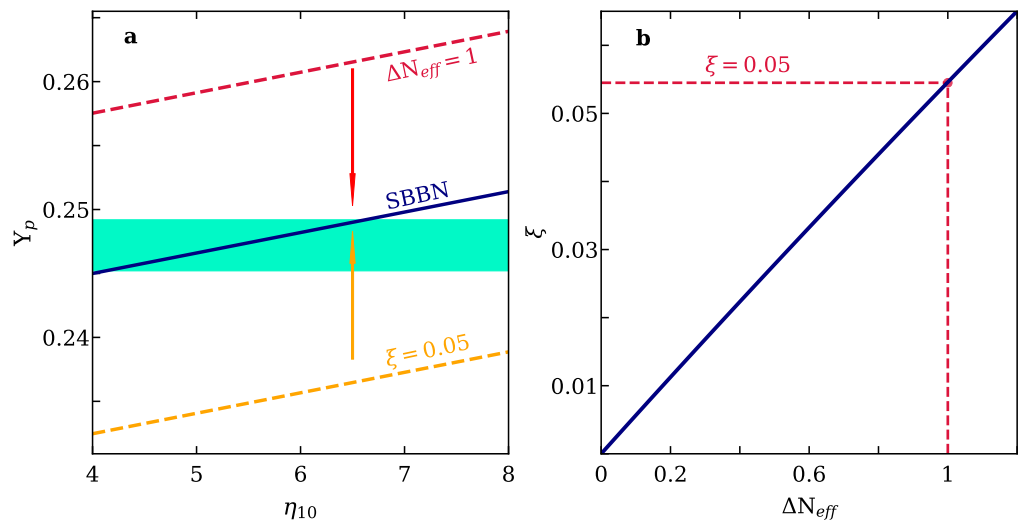


Figure 7. (a) The calculated dependencies of Y_p on the baryon-to-photon ratio η_{10} ($\eta_{10} = \eta \times 10^{10}$). The red dashed curve shows the dependence $Y_p(\eta_{10})$ in the presence of one light sterile neutrino (compare with Figure 5). The yellow dashed curve shows the dependence $Y_p(\eta_{10})$ in the presence of lepton asymmetry $\xi_e = 0.05$. The dark blue curve shows the dependence $Y_p(\eta_{10})$ in the standard case. The cyan stripe indicates the observed abundance of ^4He taken from [31]. (b) The panel shows the value of lepton asymmetry ξ , which allows one to completely compensate for the influence of the additional relativistic degree of freedom associated with a light sterile neutrino.

6. The Influence of Neutrinos on the Formation of the CMB Anisotropy

After the radiation-dominated era (~ 50 thousand years after the Big Bang), comes the era of dominance of non-relativistic matter: cold dark and baryonic matter. Then, after approximately 7 billion years, the universe transits from the decelerating to accelerating expansion, while the neutrino affects the dynamics of the expansion of the universe at each stage of the evolution. The expansion rate of the universe, characterised by the Hubble parameter, is defined via the following equation:

$$H(a) \equiv \frac{1}{a} \frac{da}{dt} = H_0 \sqrt{\Omega_\Lambda + \Omega_{\text{cdm}} a^{-3} + \Omega_b a^{-3} + \Omega_\gamma a^{-4} + \sum_\nu \Omega_\nu f_\nu(a)} \quad (16)$$

where H_0 is the current value of the Hubble parameter, $\Omega_{\text{CDM}}, \Omega_b, \Omega_\gamma, \Omega_\nu$ and Ω_Λ are the fractions of energy densities of cold dark matter, baryons, photons, neutrinos and dark energy in the universe at the moment, and the functions $f_\nu(a)$ determine the dependence of the neutrino contribution on the scale factor of the universe, i.e., in the corresponding cosmological era.

Figure 8, taken from our paper [18], presents the effective number of neutrino species, taking into account the possible existence of a light sterile neutrino. It can be seen that in the early stages of the evolution of the universe, all neutrinos are relativistic and therefore make a significant contribution to the energy density and the expansion rate of the universe, which in turn determines the size of the sound horizon at the time of Primordial Recombination. Sterile neutrinos with a mass of 2.7 eV [19] become non-relativistic before the recombination and even earlier at the radiation-dominated stage, therefore it can be classified as “warm” dark matter. Sterile neutrinos with a mass of 1 eV [20] become non-relativistic during the transition from the radiation-dominated to the matter-dominated stage, therefore it is “hot-warm” dark matter. Active neutrinos with masses less than 0.1 eV become non-relativistic after the recombination, therefore they compose “hot” dark matter. All these factors influence the formation of the CMB anisotropy, the study of which makes it possible to obtain estimates of cosmological parameters with unprecedented accuracy.

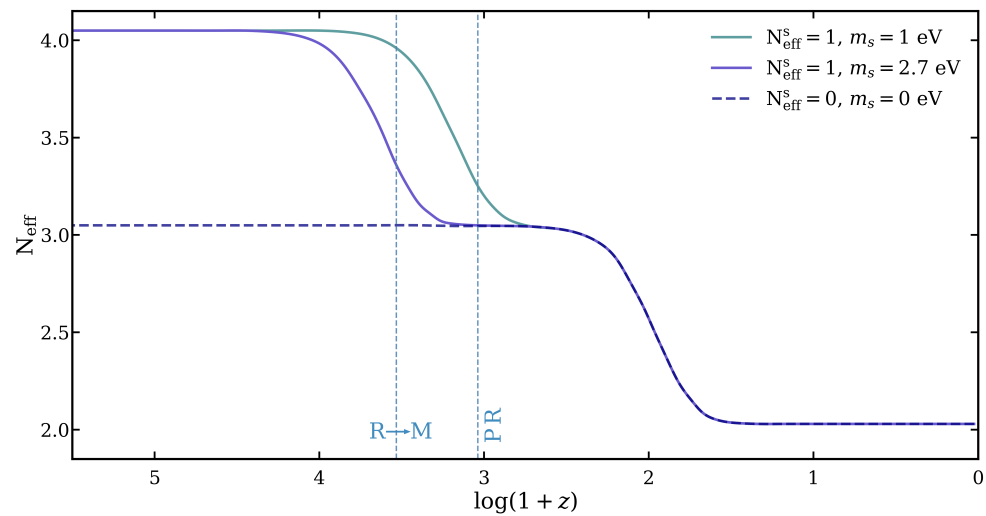


Figure 8. The effective number of relativistic neutrino species taking into account the possible existence of a light sterile neutrino as a function of cosmological redshift z . Vertical dashed lines represent the moment of transition from the radiation to the matter dominated stage (R→M) and the moment of Primordial Recombination (P.R). It can be seen that in the early stages of the evolution of the universe, all neutrinos are relativistic. Sterile neutrinos with a mass of 2.7 eV [19] become non-relativistic before the recombination and even earlier at the radiation-dominated stage, therefore it can be classified as “warm” dark matter. Sterile neutrinos with a mass of 1 eV [20] become non-relativistic during the transition from the radiation-dominated to the matter-dominated stage, therefore it is “hot-warm” dark matter. Active neutrinos with masses less than 0.1 eV become non-relativistic after the recombination, therefore they compose “hot” dark matter.

An analysis of the CMB anisotropy (Planck Collaboration, [14]) within the standard spatially-flat 6-parameter Λ CDM cosmology allows us to estimate key cosmological parameters: Ω_b , Ω_{CDM} , θ_* , n_s , A_s , τ , which represent the present-day values of the baryon and cold dark matter densities, the angular size of the sound horizon, the scalar spectral index, the amplitude of scalar perturbations, and the optical depth of the reionized plasma, respectively. In turn, using the obtained values of these six parameters it is possible to determine a number of other cosmological quantities (for instance, the Hubble constant H_0 , the age of the universe t_0 , the dark energy density Ω_Λ).

The possible existence of sterile neutrinos or/and changes in the physical parameters of active neutrinos (for instance, $T_\nu \neq T_{\nu 0}$ or $L_\nu \neq 0$) can be included into an analysis of the CMB anisotropy as additional free parameters. It will lead to a noticeable redistribution of estimates of other cosmological parameters while the model remains consistent with the observational data on the CMB anisotropy [18]. This effect is shown in Figure 9 and in Table 1. To assess this effect, the CMB anisotropy data was analysed in the following cases: standard Λ CDM model, a Λ CDM model with an additional light sterile neutrino, and a Λ CDM model with non-standard active neutrino temperature [18]. For the analysis of the CMB anisotropy the neutrinos were treated in the same way as described in the Planck Collaboration paper [14]: the analysis assumes a normal neutrino mass ordering and active flavors with masses $m_1 = m_2 = 0$ and $m_3 = 0.06$ eV. Additionally, in the case of a 3 + 1 neutrino mixing scenario, a light sterile neutrino with a mass 2.7 eV [19], or with a mass of 1 eV [20] was included. The upper panel of Figure 9 demonstrates the effect of a straightforward addition of sterile neutrinos or a non-standard temperature of active neutrinos into a model in which other cosmological parameters are fixed at standard values. It is easy to see that changing the Λ CDM model in this way leads to a very strong discrepancy between the fit and observational data. It should be noted that similar analyses of the CMB anisotropy have been carried out previously (see e.g., [45,53–55]). In these studies, the authors derived constraints on the parameters of sterile neutrinos based on the CMB anisotropy and other cosmological data. This was achieved either by fixing values of

the fitted parameters or by imposing certain priors on them. Thus the resulting constraints on the sterile neutrinos and the effective number of relativistic degrees of freedom turned out to be relatively small. Lower panels of Figure 9 demonstrate fits of the CMB anisotropy data in the following cases: (b) the standard Λ CDM model, (c) Λ CDM with the inclusion of a light sterile neutrino, and (d) Λ CDM with the modified value of active neutrino temperature. In all three cases, all of the fitted parameters, including six standard ones and additional parameter associated with the corresponding effect, were set free. It can be seen that all three fits are in a good consistency with the observational data on the CMB anisotropy. This consistency is achieved via redistribution of all estimates of the model parameters (see Table 1).

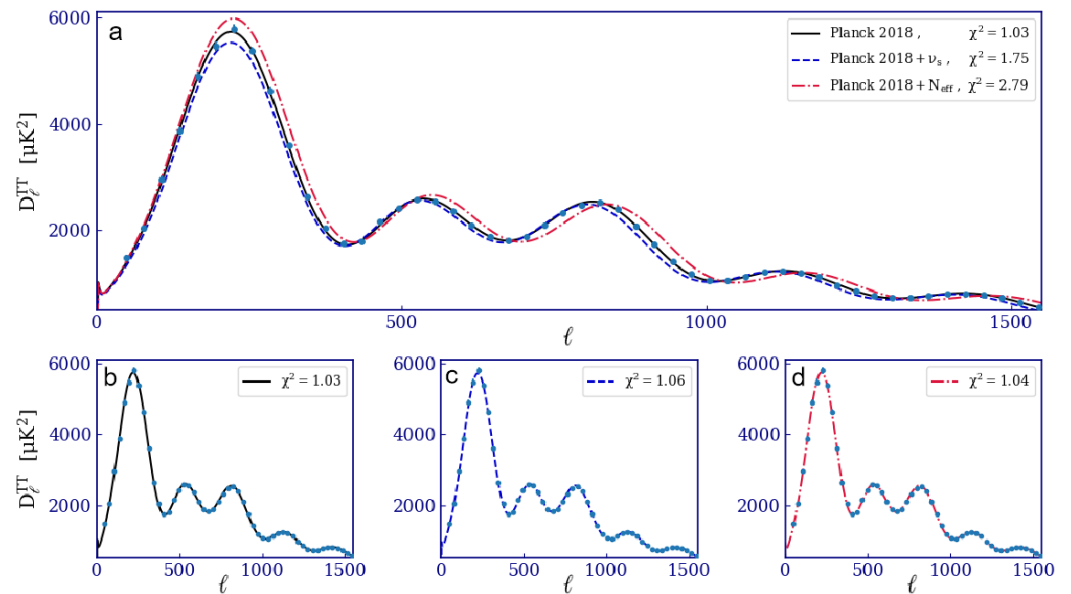


Figure 9. Observational data on the CMB anisotropy (blue dots) and the results of its fitting with theoretical models. The goodness-of-fit can be assessed using the reduced χ^2 value, which is one of the output values of the Planck Collaboration code [14]. (a) The best-fits to the observational data are for models with all standard cosmological parameters having their values fixed. The solid black curve represents the standard Λ CDM model, the dashed blue curve represents the standard Λ CDM model with the addition of a light sterile neutrino (for a total of four neutrino flavors), the dashed red curve represents the standard Λ CDM model with the additional relativistic degree of freedom, but with three neutrino flavors. (b) The black curve represents the best-fit curve for the standard Λ CDM model (the same as on panel (a)). (c) The dashed blue curve represents the best-fit for the Λ CDM model with the addition of a light sterile neutrino, and all key cosmological parameters set free. (d) The dashed red curve represents the best-fit for the Λ CDM model with the additional relativistic degree of freedom, and all cosmological key parameters set free. Thus, the hypothesis of the existence of light sterile neutrinos does not contradict the observed CMB anisotropy.

The resulting estimates of the key cosmological parameters are presented in Table 1. It should be noted, that both of the non-standard cases can be parameterised in terms of the effective number of neutrino species N_{eff} . While in the third and in the fourth columns N_{eff} have similar values (4 and 3.9 correspondingly), the physical reasons behind the values are completely different. In the third column N_{eff} equals 4 due to a physical presence of additional particle; a completely thermalised light sterile neutrino. In the fourth column N_{eff} equals 3.9 due to the higher temperature of the three active flavors $T_\nu = 2.07$ K (see Equation (3)). This fact leads to different cosmological consequences. The inclusion of a light sterile neutrino not only noticeably changes the estimates of the cosmological parameters, but also significantly worsens the Hubble tension. On the other hand, the consideration of a non-standard temperature of active neutrinos leads only to a slight redistribution of the cosmological parameters (compare the fourth and the

second columns). Moreover, the increase of the temperature of active neutrinos leads to agreement between the CMB estimate of $H_0 = 72.81 \pm 0.62 \text{ km s}^{-1} \text{ Mpc}^{-1}$ [18] and the “late” estimate of the $H_0 = 73.04 \pm 1.04 \text{ km s}^{-1} \text{ Mpc}^{-1}$ [21] (i.e., to the solution of the Hubble tension). In the analyses presented in [18] it was found that to fully agree between the two estimates, the neutrino temperature needs to be $T_\nu = 2.07 \text{ K}$, which is slightly higher than the standard value of $T_{\nu 0} = 1.94 \text{ K}$ [10]. There are different mechanisms for active neutrino heating, for example it can be due to a decay of keV-mass sterile neutrinos during the whole course of the evolution of the universe [18], a decay of MeV-mass sterile neutrinos before Primordial Nucleosynthesis [56], or other special mechanisms.

Thus, the introduction of an eV-mass sterile neutrino into the ΛCDM model is consistent with the CMB anisotropy, but at the same time it enhances the Hubble tension. This problem, in turn, may be solved by a heating of the active neutrinos, which in a minimal way can be provided by the decays of heavy sterile neutrinos that compose dark matter.

Table 1. Dependence of estimates of the cosmological parameters on the effective number of neutrino species N_{eff} and the present-day neutrino temperature T_{CvB}^0 . The second column contains estimates obtained for the standard ΛCDM model in the Planck Collaboration analyses [14]. The third column contains estimates obtained for the ΛCDM model with three active and one light sterile neutrino mixing. The last column contains estimates obtained for the case of the ΛCDM model with only three active neutrinos with non-standard temperature. The parameters are evaluated for a light sterile neutrino with mass $m_\nu = 2.7 \text{ eV}$. The estimates of Ω_i are given in percentages (as $100\% \times \Omega_i$) and H_0 is given in units $\text{km s}^{-1} \text{ Mpc}^{-1}$. The values of Ω_{CDM} and Ω_Λ are defined as follows: $\Omega_{\text{m}} = \Omega_{\text{CDM}} + \Omega_{\text{b}} + \Omega_{\nu}$, $\Omega_\Lambda = 1 - \Omega_{\text{m}}$.

Parameter	Planck 2018	$T_{\text{CvB}}^0 = 1.94 \text{ K}$ $N_{\text{eff}} = 4$	$T_{\text{CvB}}^0 = 2.07 \text{ K}$ $N_{\text{eff}} = 3.9$
Ω_{CDM}	26.45 ± 0.50	32.36 ± 0.57	24.92 ± 0.49
Ω_{b}	4.93 ± 0.09	5.88 ± 0.11	4.33 ± 0.08
Ω_{ν}	0.14	7.58	0.15
Ω_{m}	31.53 ± 0.73	45.8 ± 1.1	29.41 ± 0.87
Ω_Λ	68.47 ± 0.73	54.2 ± 1.1	70.58 ± 0.87
H_0	67.36 ± 0.54 ¹	62.20 ± 0.53	72.81 ± 0.62

¹ The “Late” H_0 measurement (independent of the ΛCDM model) carried out by SH0ES collaboration gives $H_0 = 73.04 \pm 1.04 \text{ km s}^{-1} \text{ Mpc}^{-1}$ [21]. A significant discrepancy between “late” and CMB measurements of H_0 is referred to as H_0 -tension.

7. The Influence of Neutrinos on Subsequent Stages of the Evolution of the Universe

The influence of neutrinos in the late stages of the evolution of the universe is to participate in the formation of the large-scale structure of the universe and is determined by which class of dark matter the neutrino belongs to. Active neutrinos with masses in the range $0.06 \text{ eV} \lesssim \sum m_\nu \lesssim 0.12 \text{ eV}$ remain relativistic at the matter-dominated stage even after the primordial recombination (see Figure 8). Moreover, the light neutrino component (for instance, for the normal neutrino mass hierarchy $m_1 < m_2 \ll m_3$, when $m_1 < m_2 \ll 0.06 \text{ eV}$) remains relativistic up to the present day. Such neutrinos are a component of “hot” dark matter and their effect is the damping of structure formation on small scales. Heavy sterile neutrinos with masses of the order of keV or more can compose warm and cold dark matter. These cases of light active neutrinos and heavy sterile neutrinos, in terms of their influence on the formation of the large-scale structure of the universe, have been analyzed in detail many times and can be considered as the standard cases (see e.g., [44] and references therein). At first view, the case of a light sterile neutrino ($m_{\nu s} \sim 1\text{--}3 \text{ eV}$) could be referred to the first case of active neutrinos from the point of view of the formation of the large-scale structure, but the reconciliation of the existence of such a neutrino with the CMB anisotropy leads to a significant redistribution of the values of the key cosmological parameters (see Section 6), which in turn should be taken into account when modeling the large-scale structure of the universe.

8. Conclusions

Neutrino astronomy has opened up new opportunities for us to study the universe in the diversity of its manifestations. Cosmological relic neutrinos, born in the very first moments of the Big Bang, participate in all stages of the evolution of the universe, making a significant contribution to the dynamics of its expansion, in contrast to photons, whose energy density dominates only in the early stages, or from dark matter and dark energy, whose contribution becomes significant only in later epochs.

The possible existence of a light sterile neutrino ($m_{\nu_s} \sim 1\text{--}3$ eV) is in poor agreement with the predictions of the Standard Cosmological Model. It contradicts the predictions of both the Primordial Nucleosynthesis and the CMB anisotropy data. However, these contradictions can be removed by an extension of the Standard Cosmological Model, for example, by introducing a non-zero lepton asymmetry of the universe $\zeta_\nu \sim 10^{-2}$ or additional relativistic degrees of freedom. Additionally, the CMB anisotropy data can be reconciled with the possible existence of a light sterile neutrino by changing the values of the key cosmological parameters. We show that it leads to a significant redistribution of the constituent components of matter $\Omega_i = \rho_i / \rho_c$ (within 10%). This fact must be taken into account in the later stages of the evolution of the universe, namely when modelling the formation of the large-scale structure of the universe.

The spectrum of the antineutrinos of Primordial Nucleosynthesis contains additional information about the course of non-equilibrium processes in the early universe, in the first minutes and hours after the Big Bang. Additionally, its detection would allow us to test the baryonic asymmetry of the universe on the largest scales, since the existence of antimatter-dominated regions would lead to the generation of relic neutrinos from the decays of antineutrons and antitritium.

If in the future it will be possible to detect cosmological neutrinos, due to their very high penetrating power, we will directly obtain information about the first seconds, minutes and hours of the evolution of the universe after the Big Bang.

Author Contributions: A.V.I. provided main idea, conceptualisation, provided general supervision and project management, and performed overall validation and control. V.Y.Y. and O.A.K. carried out formal analysis, provided software for the calculations required for the paper, and worked on visualization of the results. All authors contributed equally to the initial draft of the paper. The review and forthcoming editing were performed by A.V.I. and O.A.K. All authors have read and agreed to the published version of the manuscript.

Funding: This research was funded by RSF grant number 23-12-00166.

Conflicts of Interest: The authors declare no conflicts of interest.

Notes

- ¹ The H_0 -tension is the most statistically significant deviation in modern cosmology ($\sim 5\sigma$ CL), which is the discrepancy between the estimates of the Hubble parameter obtained on cosmological data [14] and “late” model-independent measurements of H_0 in the local universe [21]. A detailed discussion of possible solutions can be found in the review [22].
- ² In reality, cosmological neutrinos are a mixture of neutrinos and antineutrinos, however, in the scientific literature, where this does not lead to confusion, neutrinos and antineutrinos are commonly referenced as neutrinos.
- ³ The title is taken from [29].

References

1. Particle Data Group. Review of Particle Physics. *Prog. Theor. Exp. Phys.* **2022**, *2022*, 083C01. [CrossRef]
2. Sakharov, A. Violation of CP Invariance, C Asymmetry, and Baryon Asymmetry of the universe. *JETP Lett.* **1967**, *5*, 32–35.
3. Riotto, A.; Trodden, M. Recent Progress in Baryogenesis. *Annu. Rev. Nucl. Part. Sci.* **1999**, *49*, 35–75. [CrossRef]
4. Bertone, G.; Hooper, D.; Silk, J. Particle dark matter: Evidence, candidates and constraints. *Phys. Rep.* **2005**, *405*, 279–390. [CrossRef]
5. Feng, J. Dark Matter Candidates from Particle Physics and Methods of Detection. *Annu. Rev. Astron. Astrophys.* **2010**, *48*, 495–545. [CrossRef]
6. Copeland, E.; Sami, M.; Tsujikawa, S. Dynamics of Dark Energy. *Int. J. Mod. Phys. D* **2006**, *15*, 1753–1935. [CrossRef]

7. Frieman, J.; Turner, M.; Huterer, D. Dark Energy and the Accelerating universe. *Annu. Rev. Astron. Astrophys.* **2008**, *46*, 385–432. [CrossRef]
8. Bilenky, S.; Petcov, S. Massive neutrinos and neutrino oscillations. *Rev. Mod. Phys.* **1987**, *59*, 671–754. [CrossRef]
9. De Salas, P.; Forero, D.; Gariazzo, S.; Martínez-Miravé, P.; Mena, O.; Ternes, C.; Tórtola, M.; Valle, J. 2020 global reassessment of the neutrino oscillation picture. *J. High Energy Phys.* **2021**, *2*, 71. [CrossRef]
10. Weinberg, S. *Cosmology*; Oxford University Press: Oxford, UK, 2008; p. 611.
11. Gorbunov, D.; Rubakov, V. *Introduction to the Theory of the Early universe: Hot Big Bang Theory*; World Scientific Publishing Co. Pte., Ltd.: Singapore, 2011; p. 488
12. Ivanchik, A.V.; Yurchenko, V.Y. Relic neutrinos: Antineutrinos of primordial nucleosynthesis. *Phys. Rev. D* **2018**, *98*, 081301. [CrossRef]
13. Yurchenko, V.Y.; Ivanchik, A.V. Spectral features of non-equilibrium antineutrinos of primordial nucleosynthesis. *Astropart. Phys.* **2021**, *127*, 102537. [CrossRef]
14. Aghanim, N.; Akrami, Y.; Ashdown, M.; Aumont, J.; Baccigalupi, C.; Ballardini, M.; Banday, A.; Barreiro, R.; Bartolo, N.; Basak, S.; et al. [Planck Collaboration] Planck 2018 results. VI. Cosmological parameters. *Astron. Astrophys.* **2020**, *641*, A6.
15. Pontecorvo, B. Neutrino Experiments and the Problem of Conservation of Leptonic Charge. *Sov. Phys. JETP* **1967**, *26*, 984–988.
16. Asaka, T.; Shaposhnikov, M. The ν MSM, dark matter and baryon asymmetry of the universe. *Phys. Lett. B* **2005**, *620*, 17–26. [CrossRef]
17. Boyarsky, A.; Ruchayskiy, O.; Shaposhnikov, M. The Role of Sterile Neutrinos in Cosmology and Astrophysics. *Ann. Rev. Nucl. Part. Sci.* **2009**, *59*, 191–214. [CrossRef]
18. Chernikov, P.; Ivanchik, A. The influence of the effective number of active and sterile neutrinos on the determination of the values of cosmological parameters. *Astron. Lett.* **2022**, *48*, 689–701. [CrossRef]
19. Serebrov, A.; Samoilo, R.; Ivochkin, V.; Fomin, A.; Zinoviev, V.; Neustroev, P.; Golovtsov, V.; Volkov, S.; Chernyj, A.; Zhrebtsov, O.; et al. Search for sterile neutrinos with the Neutrino-4 experiment and measurement results. *Phys. Rev. D* **2021**, *104*, 032003. [CrossRef]
20. Barinov, V.; Cleveland, B.; Danshin, S.; Ejiri, H.; Elliott, S.; Frekers, D.; Gavrín, V.; Gorbachev, V.; Gorbunov, D.; Haxton, W.; et al. Results from the Baksan Experiment on Sterile Transitions (BEST). *Phys. Rev. Lett.* **2022**, *128*, 232501. [CrossRef] [PubMed]
21. Riess, A.; Yuan, W.; Macri, L.; Scolnic, D.; Brout, D.; Casertano, S.; Jones, D.; Murakami, Y.; Anand, G.; Breuval, L.; et al. A Comprehensive Measurement of the Local Value of the Hubble Constant with 1 km/s/Mpc Uncertainty from the Hubble Space Telescope and the SH0ES Team. *Astrophys. J. Lett.* **2022**, *934*, L7. [CrossRef]
22. Di Valentino, E.; Mena, O.; Pan, S.; Visinelli, L.; Yang, W.; Melchiorri, A.; Mota, D.; Riess, A.; Silk, J. In the realm of the Hubble tension—A review of solutions. *Clas. Quant. Grav.* **2021**, *38*, 153001. [CrossRef]
23. Almazán, H.; Bernard, L.; Blanchet, A.; Bonhomme, A.; Buck, C.; Chalil, A.; Del Amo Sanchez, P.; El Atmani, I.; Labit, L.; Lamblin, J.; et al. [The STEREO Collaboration] STEREO neutrino spectrum of ^{235}U fission rejects sterile neutrino hypothesis. *Nature* **2023**, *613*, 257–261.
24. Dolgov, A. Neutrinos in cosmology. *Phys. Rep.* **2002**, *370*, 333–535. [CrossRef]
25. Lesgourgues, J.; Pastor, S. Massive neutrinos and cosmology. *Phys. Rep.* **2006**, *429*, 307–379. [CrossRef]
26. Weinberg, S. Universal Neutrino Degeneracy. *Phys. Rev.* **1962**, *128*, 1457. [CrossRef]
27. IceCube Collaboration. Evidence for High-Energy Extraterrestrial Neutrinos at the IceCube Detector. *Science* **2013**, *342*, 1242856. [CrossRef] [PubMed]
28. Ackermann, M.; Bustamante, M.; Lu, L.; Otte, N.; Reno, M.; Wissel, S.; Ackermann, M.; Agarwalla, S.; Alvarez-Muñiz, J.; Alves Batista, R.; et al. High-energy and ultra-high-energy neutrinos: A Snowmass white paper. *J. High Energy Astrophys.* **2022**, *36*, 55–110. [CrossRef]
29. Vitagliano, E.; Tamborra, I.; Raffelt, G. Grand unified neutrino spectrum at Earth: Sources and spectral components. *Rev. Mod. Phys.* **2020**, *48*, 045006. [CrossRef]
30. Steigman, G. Primordial Nucleosynthesis in the Precision Cosmology Era. *Annu. Rev. Nucl. Part. Sci.* **2007**, *57*, 463–491. [CrossRef]
31. Kurichin, O.; Kislitsyn, P.; Ivanchik, A. Determination of H II Region Metallicity in the Context of Estimating the Primordial Helium Abundance. *Astron. Lett.* **2021**, *47*, 674–685. [CrossRef]
32. Kurichin, O.; Kislitsyn, P.; Klimenko, V.; Balashev, S.; Ivanchik, A. A new determination of the primordial helium abundance using the analyses of H II region spectra from SDSS. *Mon. Not. R. Astron. Soc.* **2021**, *502*, 3045–3056. [CrossRef]
33. Kislitsyn, P.; Balashev, S.; Murphy, M.; Ledoux, C.; Noterdaeme, P.; Ivanchik, A. A New Precise Determination of the Primordial Abundance of Deuterium: Measurement in the metal-poor sub-DLA system at $z = 3.42$ towards quasar J1332+0052. *Mon. Not. R. Astron. Soc.* **2024**, *528*, 4068–4081. [CrossRef]
34. Balashev, S.; Zavarygin, E.; Ivanchik, A.; Telikova, K.; Varshalovich, D. The primordial deuterium abundance: SubDLA system at $z_{\text{abs}} = 2.437$ towards the QSO J1444+2919. *Mon. Not. R. Astron. Soc.* **2016**, *458*, 2188–2198. [CrossRef]
35. Ryan, S.; Beers, T.; Olive, K.; Fields, B.; Norris, J. Primordial Lithium and Big Bang Nucleosynthesis. *Astrophys. J.* **2000**, *530*, L57–L60. [CrossRef] [PubMed]
36. Sbordone, L.; Bonifacio, P.; Caffau, E.; Ludwig, H.; Behara, N.; González Hernández, J.; Steffen, M.; Cayrel, R.; Freytag, B.; van't Veer, C.; et al. The metal-poor end of the Spite plateau. *Astron. Astrophys.* **2010**, *522*, A26. [CrossRef]
37. Fields, B.; Olive, K.; Yeh, T.; Young, C. Big-Bang Nucleosynthesis after Planck. *J. Cosmol. Astropart. Phys.* **2020**, *3*, 10. [CrossRef]

38. Serebrov, A.P.; Kolomensky, E.A.; Fomin, A.K.; Krasnoshchekova, I.A.; Vassiljev, A.V.; Prudnikov, D.M.; Shoka, I.V.; Chechkin, A.V.; Chaikovskiy, M.E.; Varlamov, V.E.; et al. Neutron lifetime measurements with a large gravitational trap for ultracold neutrons. *Phys. Rev. C* **2018**, *97*, 055503. [CrossRef]
39. Wang, M.; Audi, G.; Kondev, F.; Huang, W.; Naimi, S.; Xu, X. The AME2016 atomic mass evaluation (II). Tables, graphs and references. *Chin. Phys. C* **2017**, *41*, 030003. [CrossRef]
40. Akulov, Y.; Mamyrin, B. Half-life and $fT_{1/2}$ value for the bare triton. *Phys. Lett. B* **2005**, *610*, 45–49. [CrossRef]
41. Gorbunov, D. Sterile neutrinos and their role in particle physics and cosmology. *Phys. Uspekhi* **2014**, *57*, 503–511. [CrossRef]
42. Fukugita, M.; Yanagida, T. Baryogenesis without grand unification. *Phys. Lett. B* **1986**, *174*, 45–47. [CrossRef]
43. Akhmedov, E.; Rubakov, V.; Smirnov, A. Baryogenesis via Neutrino Oscillations. *Phys. Rev. Lett.* **1998**, *81*, 1359–1362. [CrossRef]
44. Abazajian, K. Sterile neutrinos in cosmology. *Phys. Rep.* **2017**, *711*, 1–28. [CrossRef]
45. Hagstotz, S.; de Salas, P.; Gariazzo, S.; Pastor, S.; Gerbino, M.; Lattanzi, M.; Vagnozzi, S.; Freese, K. Bounds on light sterile neutrino mass and mixing from cosmology and laboratory searches. *Phys. Rev. D* **2020**, *104*, 123524. [CrossRef]
46. Froustey, J.; Pitrou, C.; Volpe, M. Neutrino decoupling including flavour oscillations and Primordial Nucleosynthesis. *J. Cosmol. Astropart. Phys.* **2020**, *2020*, 15. [CrossRef]
47. Bennett, J.; Buldgen, G.; de Salas, P.; Drewes, M.; Gariazzo, S.; Pastor, S.; Wong, Y. Towards a precision calculation of the effective number of neutrinos N_{eff} in the Standard Model. Part II. Neutrino decoupling in the presence of flavour oscillations and finite-temperature QED. *J. Cosmol. Astropart. Phys.* **2021**, *2021*, 73. [CrossRef]
48. Dodelson, S.; Widrow, L. Sterile neutrinos as dark matter. *Phys. Rev. Lett.* **1994**, *72*, 17. [CrossRef] [PubMed]
49. Serebrov, A.; Samoilov, R.; Chaikovskii, M.; Zhrebtsov, O. The result of the Neutrino-4 experiment, sterile neutrinos and dark matter, the fourth neutrino and the Hubble constant. *arXiv* **2023**, arXiv:2302.09958.
50. Serebrov, A.; Samoilov, R.; Chaikovskii, M. Analysis of the result of the Neutrino-4 experiment in conjunction with other experiments on the search for sterile neutrinos within the framework of the 3 + 1 neutrino model. *arXiv* **2023**, arXiv:2112.14856.
51. Wagoner, R.; Fowler, W.; Hoyle, F. On the Synthesis of Elements at Very High Temperatures. *Astrophys. J.* **1967**, *148*, 3. [CrossRef]
52. Simha, V.; Steigman, G. Constraining the universal lepton asymmetry. *J. Cosmol. Astropart. Phys.* **2008**, *2008*, 11. [CrossRef]
53. Knee, A.; Contreras, D.; Scott, D. Cosmological constraints on sterile neutrino oscillations from Planck. *J. Cosmol. Astropart. Phys.* **2019**, *2019*, 39. [CrossRef]
54. Adams, M.; Bezrukov, F.; Elvin-Poole, J.; Evans, J.; Guzowski, P.; Fearraigh, B.; Söldner-Rembold, S. Direct comparison of sterile neutrino constraints from cosmological data, ν_e disappearance data and $\nu_\mu \rightarrow \nu_e$ appearance data in a 3 + 1 model. *Eur. Phys. J. C* **2020**, *80*, 758. [CrossRef]
55. Pan, S.; Seto, O.; Takahashi, T.; Toda, Y. Constraints on sterile neutrinos and the cosmological tensions. *arXiv* **2023**, arXiv:2312.15435.
56. Gelmini, G.; Kusenko, A.; Takhistov, V. Possible hints of sterile neutrinos in recent measurements of the Hubble parameter. *J. Cosmol. Astropart. Phys.* **2021**, *2021*, 2. [CrossRef]

Disclaimer/Publisher’s Note: The statements, opinions and data contained in all publications are solely those of the individual author(s) and contributor(s) and not of MDPI and/or the editor(s). MDPI and/or the editor(s) disclaim responsibility for any injury to people or property resulting from any ideas, methods, instructions or products referred to in the content.

Article

A Critical Discussion on the H_0 Tension [†]

Salvatore Capozziello ^{1,2,3,*}, Giuseppe Sarracino ⁴ and Giulia De Somma ^{2,4,5}

¹ Dipartimento di Fisica “E. Pancini”, Università degli Studi di Napoli “Federico II”, Complesso Universitario Monte S. Angelo, Via Cinthia 9 Edificio G, 80126 Napoli, Italy

² Istituto Nazionale di Fisica Nucleare (INFN), Sezione di Napoli, Complesso Universitario Monte S. Angelo, Via Cinthia 9 Edificio G, 80126 Napoli, Italy; giulia.desomma@inaf.it

³ Scuola Superiore Meridionale, Largo San Marcellino 10, 80138 Napoli, Italy

⁴ INAF-Osservatorio Astronomico di Capodimonte, Via Moiariello 16, 80131 Napoli, Italy; giuseppe.sarracino@inaf.it

⁵ INAF-Osservatorio Astronomico d’Abruzzo, Via Maggini sn, 64100 Teramo, Italy

* Correspondence: capozziello@na.infn.it

[†] This manuscript is dedicated to the memory of Alexey A. Starobinsky, who recently passed away. He was a distinguished scientist who greatly contributed to the developments of modern cosmology and theories of gravity with his deep insights and outstanding results.

Abstract: A critical discussion on the H_0 Hubble constant tension is presented by considering both early and late-type observations. From recent precise measurements, discrepancies emerge when comparing results for some cosmological quantities obtained at different redshifts. We highlight the most relevant measurements of H_0 and propose potential ideas to solve its tension. These solutions concern the exploration of new physics beyond the Λ CDM model or the evaluation of H_0 by other methods. In particular, we focus on the role of the look-back time.

Keywords: observational cosmology; Hubble tension; look-back time



Citation: Capozziello, S.; Sarracino, G.; De Somma, G. A Critical Discussion on the H_0 Tension. *Universe* **2024**, *10*, 140. <https://doi.org/10.3390/universe10030140>

Academic Editors: Galina L. Klimchitskaya, Vladimir M. Mostepanenko and Sergey V. Sushkov

Received: 27 January 2024

Revised: 8 March 2024

Accepted: 10 March 2024

Published: 13 March 2024



Copyright: © 2024 by the authors. Licensee MDPI, Basel, Switzerland. This article is an open access article distributed under the terms and conditions of the Creative Commons Attribution (CC BY) license (<https://creativecommons.org/licenses/by/4.0/>).

1. Introduction

The Λ Cold Dark Matter (Λ CDM) model is considered the cosmological standard, capable of describing the observed Universe by fixing only six free parameters [1]. These are the dark matter density, the baryon density, the observed angular size of the sound horizon at recombination, the scalar spectral index, the curvature fluctuation amplitude, and the reionization optical depth.

Applying general assumptions on these parameters, it is possible to derive the other cosmological quantities, including the Hubble constant H_0 and the other cosmographic parameters [2]. The result is a self-consistent picture of our Universe in good agreement with observations.

This relatively simple model is able to describe a large part of the history of the Universe with good precision, from the end of the so-called inflationary era [3,4] to the current epoch. According to the Λ CDM, our Universe is composed by three major constituents: a cosmological constant Λ , associated with the so-called dark energy, accounting for approximately 68% of the total density, a cold (non-relativistic) dark matter component, which should account for 27% of the cosmic pie [1,5–17], and lastly, the remaining 5%, composed by baryonic matter, stars, galaxies, and all the luminous structures. The accuracy of this model is remarkable when compared with cosmological observations, such as the accelerated expansion of the Universe [7] deduced from the observed light curves of Supernovae Type Ia (SNe Ia). Cosmic acceleration can be addressed by the presence of a cosmological constant or, in general, by some unknown form of dark energy, acting as a negative pressure in the cosmological equations.

On the other hand, dark matter was initially introduced to account for the virial theorem applied to clusters of galaxies [18]. Subsequent observations revealed that it is

also a fundamental component needed to explain the rotation curves of galaxies, which, otherwise, would not be well fitted by Newtonian dynamics [19,20] if only galactic baryonic components are taken into account.

Despite its overwhelming successes, the Λ CDM model presents some critical issues that captured the attention of scientific community. The most relevant challenges are the nature of dark energy and dark matter, as well as the ongoing tension of the Hubble constant derived by different measurements at different scales. After decades of precise measurements and tests [17,21–23], no direct or indirect evidence of exotic particles constituting cosmic dark fluids has been found. Consequently, according to the Λ CDM model, we have no final answer, at the fundamental level, on the constituents of the observed Universe for approximately 95%.

A further issue is related to the H_0 tension, that is the discrepancy between the late-type measurements of H_0 [24], usually linked to the cosmological ladder [25,26], and the early-type ones, associated with measurements of the Cosmic Microwave Background Radiation (CMBR). The most recent results from two prominent collaborations, SH0ES and Planck, report values of H_0 as 73.04 ± 1.04 km/(s Mpc) at a 68% confidence level (CL) for the former [24] and 67.4 ± 0.5 km/(s Mpc) at 68% CL for the latter [1]. As it stands, there is a 5σ tension between these two measurements [24], which, in principle, should provide the same result. Furthermore, this tension extends beyond these two collaborations and involves several late and early-type observations [25].

To address these issues, different approaches have been considered like extensions of General Relativity (GR), on which the Λ CDM model is based. For instance, a particular extension, known as $f(R)$ gravity [27–32]), has been considered in cosmological applications [33–37] to address different issues related to the Λ CDM model, like the late-time dark energy [14,27], and the early inflationary behavior [4]. The philosophy of these approaches is that, instead of searching for new exotic ingredients, the gravitational sector should be improved according to the scales. In this perspective, the H_0 tension could also be fixed improving geometry [29,38–40].

Other alternatives imply Extended Theories of Electromagnetism or the improvement of the Standard Model of Particles [41–43]. Furthermore, the H_0 tension could be also related to some fundamental quantum concepts, like the Compton Length and the Heisenberg Uncertainty Principle, applied to the cosmological setting [44,45].

Finally, under the standard of “new physics” a large amount of investigations have been pursued both in early and late Universe [46–74].

A recent research line explores the possibility of a “variable H_0 constant”, i.e., the idea that the measured value of the Hubble constant might depend on the redshift (i.e., the scale) at which it is measured [75–89]. In this context, the H_0 constant can be evaluated by the look-back time [90]. The approach consists in determining H_0 at any redshift z starting from the look-back time of the related sources.

In this paper, a critical discussion on H_0 tension will be presented. The outline is the following. Section 2 provides a brief summary of the Λ CDM model. Section 3 is devoted to the most prominent measurements related to H_0 . In Section 4, we discuss the look-back time approach to the H_0 tension starting from the results in [90]. Section 5, a redshift-dependent H_0 is considered. We explore, in particular, its consequences on cosmological distances. In Section 6, we discuss the results and draw conclusions.

2. A Summary of the Λ CDM Model

The Λ CDM model is a straightforward byproduct of GR. Assuming the Cosmological Principle, the Universe is homogeneous and isotropic beyond a certain scale, which is, more or less, over ~ 120 Mpc. This assumption is supported by several observations considering large sets of data [25,91–93]. The Cosmological Principle is implemented by the Friedman-Lemaître-Robertson-Walker (FLRW) metric [94]:

$$ds^2 = c^2 dt^2 - a^2(t) \left[\frac{dr^2}{1 - kr^2} + r^2 \Omega^2 \right], \quad (1)$$

where Ω represents the angular component of the metric, $a(t)$ is the scale factor, and k is the spatial curvature constant. It can be equal to $-1, 0, 1$ depending on the curvature of the cosmological spatial submanifold. According to Equation (1), the Einstein field equations can be recast as:

$$\left(\frac{\dot{a}}{a}\right)^2 + \frac{kc^2}{a^2} = \frac{8\pi G\rho}{3} + \frac{\Lambda c^2}{3}, \tag{2}$$

$$\frac{\ddot{a}}{a} = -\frac{4\pi G}{3}\left(\rho + \frac{3p}{c^2}\right) + \frac{\Lambda c^2}{3}, \tag{3}$$

which are the Friedman equations leading the cosmological expansion [95]. These equations are complemented by the continuity equation and the equation of state defined as:

$$\dot{\rho} + 3\frac{\dot{a}}{a}\left(\rho + \frac{p}{c^2}\right) = 0 \tag{4}$$

$$p = w\rho c^2. \tag{5}$$

Here, G is the gravitational constant, p is the pressure, ρ the density, w is the cosmological equation of state parameter, equal to -1 for the Λ CDM model, and Λ is the cosmological constant. These are the equations on which dynamics of Λ CDM model is based. The scale factor can be written as a function of the redshift as follows [2]:

$$a(t) = \frac{a_0}{(1+z)}, \tag{6}$$

where $a_0 = 1$ is the scale factor normalized at our epoch. This allows us to write the cosmological distances as a function of the redshift [96]. It is possible to rewrite Equation (2) in terms of the cosmological densities as follows [97]

$$\frac{H^2(z)}{H_0^2} = \Omega_r(1+z)^4 + \Omega_M(1+z)^3 + \Omega_k(1+z)^2 + \Omega_\Lambda, \tag{7}$$

where $H(z) = \dot{a}/a$ is the Hubble Parameter, H_0 is the Hubble Constant, i.e., the Hubble parameter derived for $z = 0$, thus for the Universe at our epoch, Ω_r is the radiation energy density parameter, Ω_M is the matter density parameter, where both dark and luminous matter are taken into account, Ω_k is the “density” associated to the curvature, being equal to zero for a flat Universe, and Ω_Λ is the density associated with the cosmological constant. All these quantities, apart from $H(z)$, are derived at present epoch. From this equation, we can define

$$E(z) = \frac{H(z)}{H_0} = \sqrt{\Omega_r(1+z)^4 + \Omega_M(1+z)^3 + \Omega_k(1+z)^2 + \Omega_\Lambda}. \tag{8}$$

This equation allows us to express cosmological distances as a function of $E(z)$. It is worth noticing that $E(z)$ depends only on the redshift and the densities of the today Universe, while it does not depend directly on H_0 . The luminosity distance $d_L(z)$, derived from the intrinsic luminosity and the photon flux received by a given cosmological source, is:

$$d_L(z) = (1+z)d_M(z), \tag{9}$$

where $d_M(z)$ is the transverse comoving distance. It is

$$d_M(z) = \frac{c}{H_0} \int_0^z \frac{dz'}{E(z')}, \tag{10}$$

for a flat Universe with $\Omega_K = 0$.

For an open Universe with $\Omega_K > 0$, it is

$$d_M(z) = \frac{c}{H_0\sqrt{\Omega_K}} \sinh\left(\frac{H_0\sqrt{\Omega_K}}{c} \int_0^z \frac{dz'}{E(z')}\right). \tag{11}$$

For a closed Universe with $\Omega_K < 0$, it is

$$d_M(z) = \frac{c}{H_0\sqrt{|\Omega_K|}} \sin\left(\frac{H_0\sqrt{|\Omega_K|}}{c} \int_0^z \frac{dz'}{E(z')}\right). \tag{12}$$

The luminosity distance is essential in observational cosmology because it can be associated with the “standard candles”. These are astrophysical objects whose intrinsic luminosity can be derived from some intrinsic physical mechanism. Such a mechanism is generally correlated with quantities that are independent of the source distance, and so can be used to measure $d_L(z)$ intrinsically. Standard candles are a key component of the cosmic distance ladder and play a crucial role in determining H_0 .

Another important tool for the estimation of cosmic distance ladder is the angular diameter distance, defined as

$$d_A(z) = \frac{d_M(z)}{(1+z)}. \tag{13}$$

It is important because it is linked to the “standard rulers” (i.e., astrophysical objects whose geometrical features can be deduced from their intrinsic physics). We will describe a particular probe employing this definition. Finally, another very important distance definition is linked to the look-back time, which is the time the photon takes to reach us from a certain redshift. It is defined as:

$$T_{lt}(z) = \frac{1}{H_0} \int_0^z \frac{dz'}{(1+z')E(z')}. \tag{14}$$

It is strictly connected to the light-travel distance, i.e., the path traveled by the photon to reach us from an astrophysical source in the expanding Universe. It is

$$d_{lt}(z) = cT_{lt}(z). \tag{15}$$

The last two equations are the starting point for the analysis presented in [90], and the novel discussions presented in this work. We have to note here that, in all the cosmological distance definitions, H_0 plays the role of a normalization constant, as it is not directly involved in the integral functions, which, in turn, depend only on the different cosmological components and the redshift.

3. The H_0 Measurements and the Tension

Over the past decades, several methods and astrophysical sources have been employed to measure H_0 with high precision allowing us to obtain, remarkably, very small uncertainties on the measurements [17,25]. This new era of precision cosmology is also the main reason for the H_0 tension, which is at the center of attention of the scientific community. As previously mentioned, we observe a significant 5σ tension between the latest SH0ES and Planck collaborations’ results [1,24], but, as we will see, these derivations are actually representative of two entire sets of measurements: the former of the early-type and model-dependent observations, while the latter of the direct late-type and model-independent ones.

3.1. Late and Early-Type Measurements

Regarding the late-type measurements, many observations, including those by the SH0ES collaboration, are based on the cosmic distance ladder method. In this approach, each step builds upon the previous one through calibration methods, especially in redshift regions where multiple probes are available. This method enables us to reach relatively

deep redshift ranges while preserving the precision provided by low-redshift probes, renowned for their accuracy.

The cosmic distance ladder consists of three primary steps [24,98]. The first involves precise geometric distance measurements, allowing us to directly calculate the distances of nearby objects. This step is reliable because it depends on a straightforward geometrical method and does not require extensive knowledge of the astrophysical probe used for distance measurement. There are three possible anchors for this first rung: Milky Way Cepheid parallaxes, detached-eclipsing binary measurements in the Large Magellanic Cloud [99], and the water-maser host NGC 4258 [100,101]. These three anchors provide approximately 1%, 1.2%, and 1.5% precision in the calibration of H_0 , respectively. In recent years, a strong improvement in the Cepheid parallax measurements has been provided by the European Space Agency (ESA) Gaia mission [102–105]. Gaia, designed for astrometry, photometry, and spectroscopy, has created the most accurate 3D map of the Milky Way. The latest release, covering the first 34 months of observations, has provided the largest dataset of Cepheids ever (around 3000 Milky Way Cepheids) allowing us to measure the parallaxes and consequently the distances of Cepheids with unprecedented accuracy [106].

The second step involves primary distance indicators, often Classical Cepheids, which exhibit an intrinsic relationship between their luminosities and periods, the so-called Period-luminosity relation (PL) [107–109]. Although this step is valuable, it may be influenced by potential systematic effects such as the metallicity dependence of the coefficients of the PL relation, which need to be addressed [110–113].

The third step includes probes like SNe Ia, which use primary distance indicators as anchors in regions where both are detected. SNe Ia, with their higher luminosities, can explore relatively high-redshift regions.

Let us discuss in more detail how the SNe Ia are employed as standard candles, given that they are one of the most important components of the cosmological ladder approach [114]. The most updated SNe Ia dataset is the Pantheon+ sample [115], which was used for the latest H_0 measurements [24,116] and serves as a natural successor to the earlier Pantheon set. [117]. The Pantheon+ sample is composed of 1701 lightcurves taken from 1550 different SNe Ia, covering a redshift range from $z = 0.01$ up to $z = 2.26$.

In general, the physics behind these astrophysical objects is well-understood. SNe Ia are the byproduct of the explosions of white dwarfs in binary systems exceeding the Chandrasekhar limit due to mass transfer from their companion star. Since this limit is a fundamental constraint for the stability of all white dwarfs, all SNe Ia light curves share similar features. Specifically, the prevailing model, consistent with the majority of SNe Ia observations, is the single-degenerate Chandrasekhar mass explosion [118]. In this model, the white dwarf accretes mass from its less evolved companion star, typically a red giant, which has a significantly lower density, especially in its outer regions. SNe Ia light curves are well-fitted by the deflagration model shown in [119]. They are primarily powered by the β -decay of the radioactive isotope ^{56}Ni produced during the explosion [120].

Observationally, this model predicts that SNe Ia light curves typically exhibit an absolute magnitude around $M \simeq -19$ [121]. However, both super-luminous [122] and sub-luminous [123] SNe Ia have been observed, suggesting the involvement of more complex mechanisms, such as the delayed detonation scenario for super-luminous SNe Ia [124]. Even so, a phenomenological relation has been observed between the peak magnitude of the light curve and the luminosity decline rate in each SN Ia [125], which makes them a proper standardizable candle. Their use as a cosmological probe is based on the following equation

$$\mu_{th,SNeIa} = m - M = 5 \log(d_L) + 25, \quad (16)$$

where m is the apparent magnitude of the astrophysical object, M is its absolute magnitude, and the luminosity distance is expressed in Mpc. This quantity is confronted with the detected distance modulus μ_{obs} of the SNe Ia, from which a best-fit of the desired cosmological parameter (as well as of the absolute magnitude M) can be performed by employing the following χ -squared function

$$\chi_{SNeIa}^2 = (\mu_{th} - \mu_{obs})^T \times C_{SNeIa}^{-1} \times (\mu_{th} - \mu_{obs}), \quad (17)$$

where C_{SNeIa}^{-1} is the inverse of the covariance matrix [81].

It is worth noticing that the absolute magnitude of SNe Ia is treated as a general parameter. This introduces a degeneracy with H_0 , which can be resolved either by fixing M to a certain value or through calibration processes involving primary distance indicators like Classical Cepheids in the cosmological ladder approach [115].

Furthermore, alternative probes can be employed in the cosmological ladder approach. For instance, the tip of the red giant branch (TRGB) [126], in place of the Classical Cepheids [127], or type II SNe [128], the Tully-Fisher relation for galaxies [129], and surface brightness fluctuations [130], as substitutes for SNe Ia in the corresponding cosmological step. The surface brightness fluctuations have also been used as primary distance indicators [131]).

Regarding the results obtained from these methods, a general consensus has emerged around the values derived by the SH0ES collaboration. Indeed, their data have been reanalyzed using different statistical methods, without a significant modification of the final results [25,132–137]. Some investigations have also included Cepheids from outside our Galaxy, to address potential biases in measurements linked to specific Cepheid populations [101].

An alternative calibration of the SNe Ia, using the TRGB methodology, has produced results that differ from those provided by the SH0ES Collaboration. For example, studies by [127,138,139] derived a value of $H_0 = 69.6 \pm 1.9$ km/(s Mpc) at a 68% confidence level, which falls between the values from SH0ES and Planck collaborations. However, there are other studies involving the use of TRGB as calibrators for SNe Ia whose results are consistent with the other late-type observations [140–144]. This has led to ongoing discussions about TRGB-based observations [131,145], particularly regarding methodologies to account for potential systematic effects [138,141] and a possible empirical relation between different TRGB observations, similar to what has been derived for Classical Cepheids [145].

As mentioned earlier, the cosmological ladder can be used by considering also other probes, such as the surface brightness fluctuations of galaxies, as alternatives to the SNe Ia, or as an intermediate step between Cepheids and SNe Ia [146]. The results remain consistent with the other late-type measurements, even if there are higher errors in the determinations of H_0 from these sources [130,147]. A similar approach can also be employed for SNe type II [128,148], and the Tully-Fisher relation for galaxies [129,149,150], obtaining results which remain consistent with the SH0ES collaboration.

While the cosmological ladder is an intuitive method for determining H_0 independently from the cosmological model, it requires very precise knowledge of the astrophysical processes associated with each used probe, especially in the first steps of the ladder. This is because any potential unaccounted-for systematic effect in the first rung could propagate to subsequent ones, as they are calibrated on the preceding. Therefore, using alternating astrophysical objects for the same step becomes a crucial test, as the cross-test between different collaborations using the same probes, to identify and remove possible systematic issues.

The cosmological ladder framework is not the only possible methodology for estimating H_0 at late times. An example is the strong lensing time delay estimates, which are independent of cosmological models but do require assumptions about foreground and lens mass distributions [25]. Even with this independent alternative method, the results remain consistent with the other late-type approaches [151–154]. It is interesting to mention that, in [154], a decreasing trend in the measure of H_0 with the redshift has been noted, in agreement with the previously mentioned “variable H_0 constant” [75,81,90,155], which will be the focus of the following analysis.

As we can see, for the late-type measurements, different probes and different methods provide results that are generally in agreement (apart from some exceptions). We may conclude that the tension is very unlikely to be due to systematic or statistical problems in the data themselves, but rather due to a more intrinsic, physical issue. Indeed, different

averages of the late Universe estimates of H_0 are in a $4.5\text{--}6.3\sigma$ tension with values provided by the Planck Collaboration [25,156,157].

Let us now discuss measurements of H_0 based on assumptions and observations related to the early physics of the Universe. In addition to the latest values derived by the Planck Collaboration [1], there are other independent measurements, involving CMBR, all of which consistently yield lower values for H_0 if compared to late-type observations [158–160].

Early-time phenomenology can be traced even at low redshift values, with notable examples derived through various probes including the Baryon Acoustic Oscillations (BAO) [161–165], Big Bang Nucleosynthesis measurements of the primordial deuterium [166], and weak lensing measurements [16]. These probes yield H_0 estimates consistent with those of Planck Collaboration [165], and different data reanalyses support these results [73,74,167–173]. However, it is essential remembering that early-type measurements are model-dependent, and work within the Λ CDM scenario and the Standard Model. Without these assumptions, constraints on H_0 and other cosmological parameters are remarkably loosened [25,174]. Additionally, these measurements provide estimates for all the six free parameters underlying the Λ CDM model, which, in turn, are used to derive all the other cosmological parameters from the observation of the CMBR peaks.

Let us go into more detail about the BAO. They are also utilized independently for cosmological computations [165] because they consider another kind of cosmological distance, the angular-diameter one. BAO are widely used in literature to complement various analyses with other probes, see Refs. [42,175], and in standalone cosmological computations [165].

BAO are density fluctuations of the visible baryonic matter, caused by acoustic density waves in the early primordial plasma. As such, they are relics of phenomena occurred in early times and observed at lower redshift values such as in cluster formations and galaxy distributions. These phenomena are closely related to the acoustic peaks measured from the CMBR [161] which result from cosmological perturbations generating sound waves in the relativistic plasma of the early Universe [176].

In the past decade, BAO-related measurements have significantly improved in precision [165], which has proven to be mandatory for modern cosmological applications. This is because the acoustic features in matter correlations are relatively weak and occur at large scales [161,177].

Furthermore, these acoustic peaks are associated with different behavior of ordinary and dark matter when they are solicited by perturbations. Ordinary matter expands as a spherical wave, while dark matter remains in place [178]. After this event, both dark matter and baryon perturbation start the formation of large-scale structures. Given that, the central perturbation in the dark matter dominates over the baryonic shell, the acoustic feature is manifested as a single spike in the correlation function at approximately 150 Mpc between pairs of galaxies. This scale is typically close to the sound horizon [179].

It is important to note that, given their nature, behind each BAO-related measurement, there are tens of thousands of observations regarding large structures such as galaxies or clusters of galaxies. The largest spectroscopic survey to date is the Baryon Oscillation Spectroscopic Survey (BOSS [180]), one of the main objectives of the Sloan Digital Sky Survey (SDSS)-III Collaboration [181]. Indeed, this collaboration conducted spectroscopy on over 1.5 million galaxies, generating valuable BAO-related data points. This dataset was later complemented by the extended Baryon Oscillation Spectroscopic Survey (eBOSS [182]), which was the cosmological survey within the SDSS-IV [183].

As previously stated, BAO may be used as cosmological probes starting from the angular-diameter distance. However, unlike SNe Ia, BAO-related measurements can vary in their definitions. For instance, in the set composed of 16 BAO employed in [42,43,175], compiled from [162–165,184], some of the data offer information about the following quantity

$$d_V(z) = \left[d_M^2(z) \frac{cz}{H(z)} \right]^{\frac{1}{3}}, \quad (18)$$

where d_M is the transverse comoving distance defined in Equations (10)–(12) and $H(z)$ is defined in Equation (7). Also, other cosmological quantities inferred by BAO are the following parameter

$$A(z) = \frac{100d_V(z)\sqrt{\Omega_M h^2}}{cz}, \tag{19}$$

where $h = H_0/(100 \text{ km s}^{-1} \text{ Mpc}^{-1})$; the so-called Hubble distance

$$d_H(z) = \frac{c}{H(z)}, \tag{20}$$

and the comoving distance itself. It is important to emphasize that all these definitions are interconnected, but they are not identical. This is a relevant point when constructing the covariance matrix using these heterogeneous measurements.

Additionally, it is worth noting that the majority of the BAO measurements have been rescaled by a factor denoted as r_d , that is the distance between the end of inflation and the decoupling of baryons from photons after the recombination epoch. The value of this factor is approximately 150 Mpc and it is defined as [165].

$$r_d = \int_{z_d}^{\infty} \frac{c_s(z)}{H(z)} dz, \tag{21}$$

where $c_s(z)$ is the sound speed, while z_d is the redshift of the drag epoch, which in turn corresponds to the time when baryons decouple from the photons. This decoupling typically occurs at a redshift of $z \approx 1020$, a value influenced by the physics of the early Universe. This quantity can be approximated using a formula involving cosmological parameters [185], that is

$$r_d = \frac{55.154 \cdot e^{[-72.3(\Omega_\nu h^2 + 0.0006)^2]}}{(\Omega_M h^2)^{0.25351} (\Omega_b h^2)^{0.12807}} \text{ Mpc}, \tag{22}$$

where Ω_b is the baryonic density and Ω_ν is the neutrino density. It is important to notice that, although they are observed in lower redshift regions, their link to early-Universe physics implies that the cosmological computations derived from them are consistent with the Planck Collaboration results, including those related to H_0 [165].

3.2. Overcoming the Tension

The H_0 tension is one of the most compelling problems of modern cosmology, and, as such, both observational and theoretical approaches have been explored by the scientific community to address it. From the former point of view, a new independent window has opened by the observations of gravitational waves [186]. Indeed, these detections have already been used as ‘standard sirens’, to derive new estimates for H_0 [187–190].

At present, the precision of these measurements does not allow us to understand if they reduce the tension or if they are more in agreement with either the early or late-type measurements. However, given that we are still in the early stages of the gravitational waves era, a considerable improvement is expected from future observations, especially from the next generations of gravitational wave detectors. This holds great potential as a completely independent, non-electromagnetic method for measuring H_0 , providing a new window to solve the tension issue.

Other important measurable quantities for the cosmological studies are the look-back time and the related age of the Universe, which have been used to infer H_0 observationally, as it is the case of the ages of the observed astrophysical objects [155,191–195].

Furthermore, interesting observations of high redshift galaxies have been performed by the James Webb Space Telescope. The observed galaxies appear to have unexpectedly high stellar masses which may be in conflict with the age of the Universe as inferred by

Planck [196]. It remains unclear whether this potential discrepancy may be attributed to galaxy evolution models or if it has a cosmological origin.

Another possible independent method to infer H_0 is based on the $H(z)$ function and its evolution with the redshift, allowing us to extrapolate H_0 by requiring $z = 0$. This would be a completely model-independent procedure being able to derive this value, independently from other methodologies. A possible approach for this analysis is based on the so-called cosmic chronometers [26,197], i.e., the age evolution of galaxies, as well as on techniques like Gaussian Process regression [198,199], or cosmography via different polynomials [14,36,200]. These approaches have provided estimates of H_0 ranging from values consistent with Planck collaboration to values consistent with late-type estimates [25]. It is important to note that an extrapolation of H_0 at $z = 0$ from the $H(z)$ function could be in contrast with assuming a variable H_0 . We will discuss this point in the next section.

From an observational standpoint, another potential approach to address the H_0 tension involves the extension of cosmological ladder to higher redshift, in view to bridge the gap between early and late-type measurements. For this aim, one needs to observe astrophysical objects at high z acting as standard candles. An example is represented by the Gamma-Ray Bursts (GRBs), for which different correlations between their intrinsic physical parameters can be observed [201–205], allowing us to use them as distance indicators [71,72,175,206–211].

Other promising high-redshift indicators are Quasars [212]. For these objects, empirical correlations among physical parameters have been found, so, as in the case of GRBs, they could constitute a formidable and populated set of objects to test the Universe at high redshift [213–218].

From a more theoretical point of view, the idea that new physics could be behind the tension is fascinating the scientific community, especially if one considers that this is not the only issue that the Λ CDM model, and more in general GR itself, presents [17,29]. Other notable examples are the nature of dark energy and dark matter that seems to escape any probe at fundamental level. A popular approach to address these issues is to consider extensions of Λ CDM model and GR. As previously mentioned, $f(R)$ gravity [29] and other modified theories [17,39] have been applied for various cosmological and astrophysical tests [17,39,82,84,85,219,220].

These modifications include the possibility of treating the dark energy component as a variable fluid rather than a cosmological constant [221,222]. This constant can be represented by a scalar field ϕ rolling slowly down a flat component of a potential $V(\phi)$ and giving rise to the models known as quintessence [223]. In this sense, the Chevallier-Polanski-Linder (CPL) parameterization for the dark energy component [224,225] is one of the most widely studied modifications to the standard scenario.

Other possible approaches include models where interactions between dark energy and dark matter are taken into account [226,227]. The main issue of this framework is the degeneracy existing between different models, which try to address the same problems in completely different ways, thus not allowing us to achieve a natural and definitive extension of the Λ CDM model and GR [228–230].

New physics may also be linked to modifications of the underlying phenomenology at both the early and late stages of the Universe [25,88]. Examples for early epochs include:

1. Early Dark Energy, which behaves as a cosmological constant for $z \leq 3000$, and then decays as fast as the radiation density (or even faster) at late times [50,52,231] via a slow-roll phase transition. While promising, this approach presents problems from both observational and theoretical perspectives [232]. Therefore, a modification has been proposed, called New Early Dark Energy, where instead of a slow phase transition, we have an almost instantaneous one [233]. This idea is similar to the aforementioned quintessence for late times.
2. Extra relativistic degrees of freedom at the recombination, parameterized by the number of neutrino species, N_{eff} . According to our current understanding, for active

- massless neutrino families $N_{eff} \sim 3.044$ [234]. This number affects the inferred value of H_0 . Various models regarding further dark radiation have been proposed [235–238].
3. Modifying the recombination history, by shifting the sound horizon for BAO at recombination. This can be achieved by either varying the early-time expansion history or by modifying the redshift of recombination. Various methods have been proposed to accomplish this, including exotic scenarios in the early Universe [239–241].

The proposed new physics at late times modifies our interpretation of dark energy in various ways. Apart from what we have mentioned before, we recall the following:

1. Considering a cosmological bulk viscous fluid, characterized by a peculiar form of its pressure term, which is made up of two parts, where the first one is the usual component linked to the density via an equation of state, while the second is linked to the viscosity [242–245].
2. A chameleon field for dark energy, whose mass varies in accordance with the matter density of the considered environment, and whose variability would imply a measurement on H_0 dependent on the particular region in which has been performed [246–250].
3. Diffusion models, implying an interaction between dark energy and dark matter via a non-conserved energy tensor $T_{\mu\nu}$ [251–253], which seems to reduce the H_0 tension with different types of matter fields [254].
4. General dynamical behavior for dark energy, following a philosophy similar to the CPL parameterization. In this sense, one could define emergent dark energy, which has had no effects in the early stages of the Universe, as it completely emerges at late times [255–257].
5. A Running Vacuum model, linked to possibly Quantum Field Theory or String Theory, could be used to explain theoretically a possible phenomenological dependence of cosmological and gravitational constants with the cosmic time [258,259]. This kind of model can actually encompass different assumptions regarding the behavior of dark energy. It has also been successfully tested [260,261].
6. The presence of local inhomogeneities that could affect the late-time measurements of H_0 , which may be either due to possible observational issues like incomplete sky sampling, astrophysical problems like incorrect modelling of the local structures, or a more fundamental nature, like the departure of the FLRW assumption at very small scales [262–266].

Alternatives to extensions of GR have also been sought. These alternatives include considerations for potential extensions of the Maxwellian Electromagnetism [267] in a cosmological setting, introducing a second, optical component to the measured redshift of astrophysical sources in cosmological models without dark energy [41–43].

In order to represent a valid alternative to the Λ CDM model, evidence of this kind of effect has to be found. A possible approach is to investigate the upper limits on the photon mass [268–271], especially considering that some extensions propose massive photons [272,273].

Another investigated possibility is dealing with the H_0 tension as an evidence of a more fundamental limit on observations, linked to Quantum Mechanical concepts like the Compton Length and the Heisenberg Uncertainty Principle [44,45]. This approach seeks for addressing the tension without attributing it to unlikely experimental errors or unknown novel physics.

The previously mentioned alternatives offer promising solutions for addressing the H_0 tension and providing a satisfactory explanation for its existence. The main issue is to determine if one of these alternatives truly resolves the tension or if the solution lies within a completely different framework. To accomplish this issue, one not only needs to provide definitive evidence of peculiar effects beyond the Λ CDM model, but also to build up an appropriate extension of the standard framework containing not only novel ideas to solve the H_0 and other tensions but also retaining the outstanding success achieved by GR and Λ CDM model when they are compared with observations.

As said, a novel approach considers the possibility of an evolution of H_0 constant with redshift as a way to address the tension [75–88]. In this sense, the evolution of H_0 and the corresponding tension are considered as a sort of “diagnostics” of a symptom of the breaking-down of the Λ CDM model (or even of the FLRW metric, because it would suggest, according to this interpretation, that the parameterization $H(z) = H_0 E(z)$ is not working), marking the points in which observations are not consistent with the model [75–80].

In this context, a dependence of H_0 on the redshift has been observed in real SNe Ia data and interpreted through the $f(R)$ gravity formalism [81–85,88]. More specifically, in [81], a functional form

$$H_0^z = H_0 / (1 + z)^\alpha, \tag{23}$$

has been assumed and fitted with the Pantheon set of SNe Ia [117]. Results show that α is not consistent with 0 within 1σ , hinting at a smooth, slow, but continuous, decrease in H_0 value with the redshift. A variable H_0 could be due to a possible break-down, at some scale, of the Cosmological Principle on which the Λ CDM model is based (for general reviews, see [25,229,274], for discussions on diagnostics, see [77,155,264,275]).

It is worth emphasizing that H_0 measurements discussed in this section represent only a part of those obtained in recent years. For a more comprehensive overview, refer to Figure 1 taken from [25].

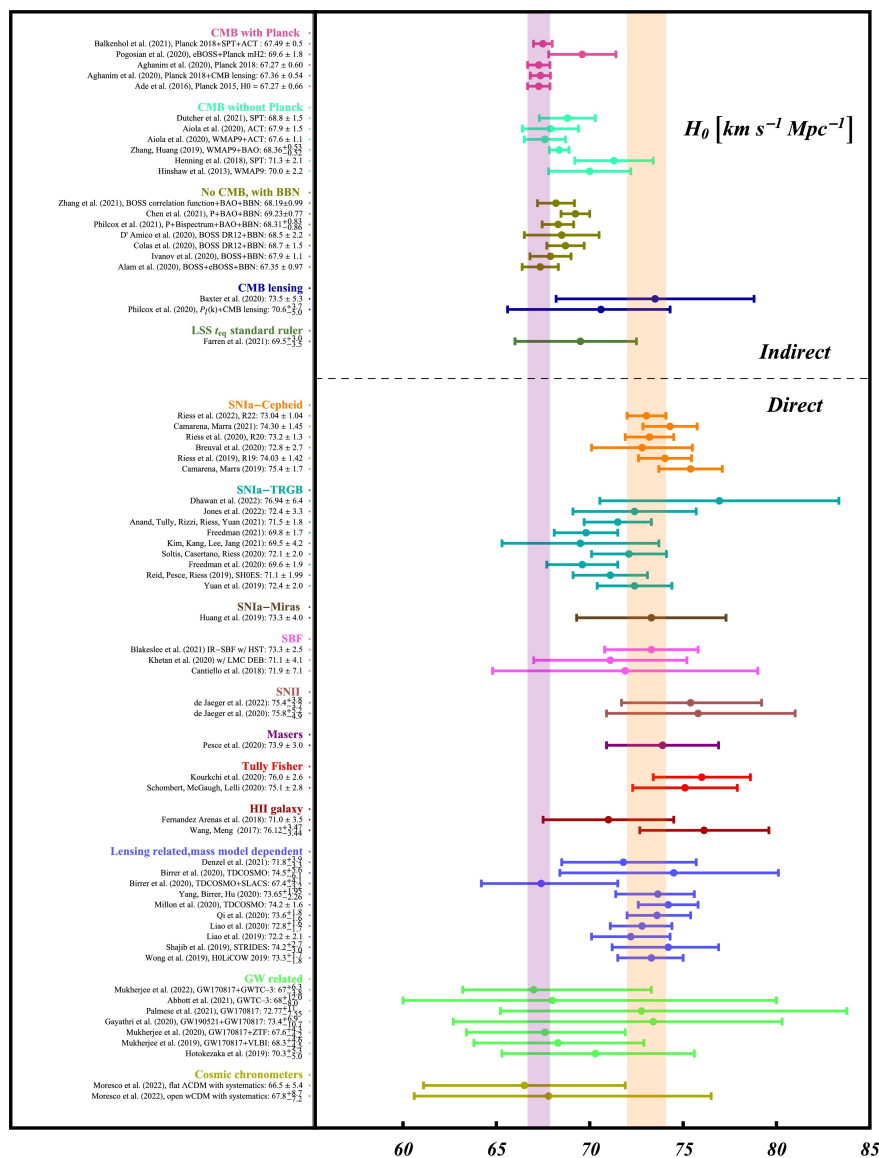


Figure 1. A summary of H_0 measurements performed both at early and late times. Credits to [25].

4. The H_0 Tension and the Look-Back Time

4.1. The $T(z)$ Parameterization

Let us now delve into the approach proposed in [90], where H_0 is derived from the look-back time defined in Equation (14). We will further discuss and improve this parameterization. Let us start from showing that, operatively, we can take into account a Taylor expansion of the scale factor as follows

$$a(t) = a_0 + \frac{d(a(t_0))}{dt} [T(z) - T_0] + \dots = a_0 + H_0 [T(z) - T_0] + \dots \tag{24}$$

We can assume that $a_0 = 1$ and approximate $H_0 = 1/T_0$, where T_0 is the age of the Universe today. This approximation is at 5% if compared with the Planck data. It is easy to obtain the integral

$$H_0^{(\infty)} = \frac{1}{T_0} \int_0^\infty \frac{dz'}{(1+z')E(z')} \tag{25}$$

This approximation is mandatory in view to justify our approach. Clearly, considering only the first-order term, we recover the parameterization

$$T(z) = \frac{T_0}{(1+z)} = a(t)T_0, \tag{26}$$

that allows us to label the universe age at various redshifts $T(z)$ starting from T_0 . The definition of look-back time can be recast as:

$$H_0 = \frac{1}{T_{lt}(z)} \int_0^z \frac{dz'}{(1+z')E(z')} \tag{27}$$

According to this equation, we can infer H_0 from $T_{lt}(z)$ at any z . This result is consistent with the age of the Universe, by considering the general definition

$$T_{lt}(z) = T_0 - T(z), \tag{28}$$

where T_0 and $T(z)$ are the Universe age, today and at a given redshift, respectively. Considering Equation (26), we can derive

$$H_0^{(z)} = \frac{(1+z)}{T_0 z} \int_0^z \frac{dz'}{(1+z')E(z')} \tag{29}$$

Equation (26) can be confronted with other parameterizations. The idea is linking different ages of the Universe with today's epoch, avoiding the integral time evolution, depending on $E(z)$, as in Equation (29). In other words, one can adopt a point-by-point labeling process. The most natural label that we may use is the scaling factor itself $a(t)$, which expresses how the size of the Universe changes with its expansion. In this perspective, $T(z)$ is a projection of T_0 at a given redshift. This is the main reason why we have operatively computed this labeling from Equation (24).

As noted in [90], for $z \rightarrow +\infty$, it is $\lim_{z \rightarrow +\infty} \frac{z+1}{z} = 1$, and thus it is easy to recover Equation (25) from our approach, which can also be interpreted as the definition of Universe age, denoted as T_0 . This means that the parameterization is in agreement with the age definition at high values of z . Additionally, in Ref. [90], it is demonstrated that this parameterization is remarkably consistent with different H_0 measurements, ranging from late and early epochs, where different probes are taken into account. More specifically, we report here results obtained by the Planck collaboration for the following quantities [1]:

$$T_0 = 13.797 \text{ Gyr}, \quad \Omega_r = 9.252 \times 10^{-5}, \quad \Omega_M = 0.3153, \quad \Omega_\Lambda = 0.6847. \tag{30}$$

which have been compared with the following H_0 observations at 68% CL:

- $H_0 = 73.04 \pm 1.04$ km/(s Mpc) from the SH0ES collaboration, inferred by the cosmic distance ladder method considering Classical Cepheids + SNe Ia up to $z = 0.15$ [24];
- $H_0 = 67.4 \pm 0.5$ km/(s Mpc) from the Planck collaboration, obtained by the CMBR observations at $z \sim 1100$ [1];
- $H_0 = 69.9 \pm 1.9$ km/(s Mpc), obtained by using the TRGB as an anchor for SNe Ia instead of the Classical Cepheids, at $z = 0.08$ [127];
- $H_0 = 75.8 \pm 5.0$ km/(s Mpc), derived from SNe Type II as the last step of the cosmological ladder, at $z = 0.45$ [128];
- $H_0 = 73.3 \pm 4.0$ km/(s Mpc), derived from the Mira Variables employed as anchors of SNe Ia, at $z \sim 0.15$ [276];
- $H_0 = 76.0 \pm 2.6$ km/(s Mpc), derived from the Tully-Fisher relation for spiral galaxies, at $z = 0.5$ [129];
- $H_0 = 73.3 \pm 2.5$ km/(s Mpc), derived from the surface brightness fluctuations for the galaxies, at $z = 0.33$ [130];
- $H_0 = 69.5 \pm 3.3$ km/(s Mpc), inferred from the Large Scale Structure t_{eq} standard ruler, and thus confronted to our computations at the redshift of equivalence $z_{eq} \sim 3300$ [277];
- $H_0 = 72.0 \pm 1.9$ km/(s Mpc), inferred from the masers + SNe Ia and compared at $z \sim 0.15$ [100];
- $H_0 = 73.3 \pm 1.8$ km/(s Mpc), derived from gravitational lensed quasars, confronted at $z = 0.745$ [153];
- $H_0 = 67.9 \pm 1.5$ km/(s Mpc), which is a measurement provided by the CMBR independently from the Planck collaboration, and as such corresponding at the reionization epoch $z \sim 1100$ [159];
- $H_0 = 69.6 \pm 2.1$ km/(s Mpc), linked to the 21 cm absorption line and corresponding at the beginning of the so-called Cosmic Dawn, i.e., when the first stars formed ($z \sim 17.2$), in combination with CMBR data and considering a Chaplygin gas model for the dark sector [278];
- $H_0 = 73.4 \pm 8.8$ km/(s Mpc), deduced by gravitational waves, at $z = 0.438$ [189].

We remind that the corresponding redshift for each measurement has been determined by considering either the upper limit of the redshift range of the sample used to infer H_0 or the redshift associated with the specific physical process.

Results reported in [90] are displayed in left panel of Figure 2. They will be used as reference for our tests. Here, we consider also the effects of 5% approximation in assuming $H_0 = 1/T_0$. Essentially, error bands at 5% can be taken into account. Results are shown in the right panel of Figure 2, where we see that the model is still consistent with the H_0 measurements. We have also performed a polynomial fit of the H_0 measurements, independent of the cosmological model. It is worth noticing that it is consistent with late and early measurements, while it results shifted with respect to the peak. This feature has to be expected due to the lack of direct H_0 in the intermediate redshift range.

It is important to discuss the value of T_0 used in the analysis. This quantity is linked to H_0 . More specifically, an anti-correlation exists between T_0 and H_0 has been reported in Ref. [279]. An independent way to test H_0 is to compare measurements with estimate ages of old objects such as stars and globular clusters.

In this sense, different measurements are consistent with T_0 derived from early-type observations [191,280–283]. This suggests that the H_0 value, inferred from late-type observations, would imply a Universe that is too young according to these measurements. Therefore, novel physics might be required to reconcile H_0 with the late-type derivations.

This is the first reason why we started from the values provided by the Planck Collaboration. The second one is that both T_0 and H_0 , according to Planck, are derived quantities which have been computed by the six aforementioned free parameters. Therefore, even if T_0 and H_0 are linked, we do not incur in a circularity problem [1].

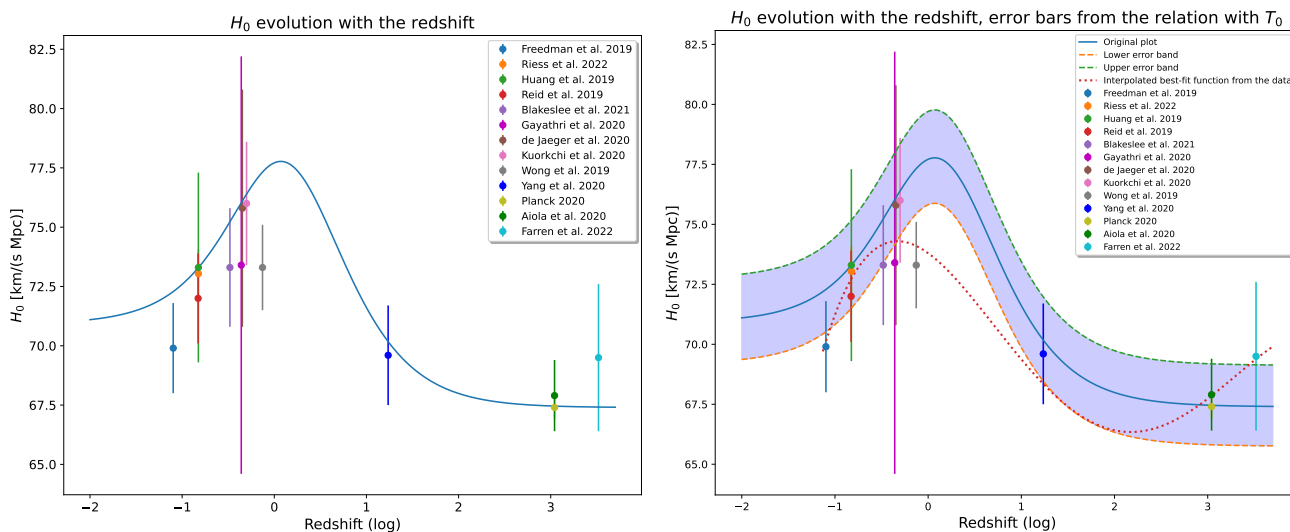


Figure 2. (Left panel) The values of H_0 derived from Equation (29) are plotted against the redshift and confronted with observational data [90]. For each measurement, the redshift value has been selected either at the upper limit of the redshift range of the sample or at the redshift corresponding to the specific physical phenomenon considered for the estimation (cosmic dawn, recombination, equivalence epoch, and so on). **(Right panel)** the same plots, but considering a 5% uncertainty on our model linked to the relation between T_0 and H_0 , and also a polynomial fit on the H_0 measurements. The x -axis is reported in a logarithmic scale. We recall that the measurements have been taken from [1,24,100,127–130,153,159,189,276–278]

Considering Equation (24), it is easy to see that the first order expansion works at low redshifts but it should decrease in efficiency at higher values of z . Notably, from Equation (25), we recover T_0 at higher redshifts. Furthermore, we may note that the evolution of $a(t)$, depending on the given cosmological eras dominated by different densities, is quite similar to a linear behavior, as shown in Figure 3. Here, we compare the evolution of $a(t)$, obtained by a 9th-degree polynomial fit, with a straight line. We may note that the two curves are remarkably similar for a large range of $T(z)$ values and easily converge to the above limit of H_0^z at high redshifts.

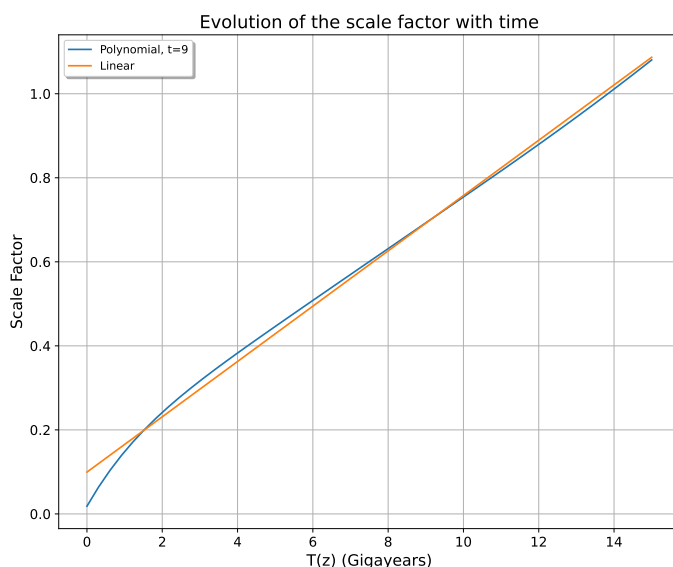


Figure 3. Evolution of the scale factor $a(t)$ with time. The blue curve represents the best fit using a 9th-degree polynomial to reproduce its numerical evolution as precisely as possible, while the orange curve is the fit with a straight line.

To further validate our claims, we can try different parameterizations, which may be derived from different assumptions on the dominating cosmological densities in the function $E(z)$. This means that we do not consider our labeling, but specific approximations of the cosmological models. By taking into account the definition on $T(z)$ in Equation (14), via the time-evolution integral, one can derive

$$T(z) = \frac{1}{H_0} \int_z^\infty \frac{dz'}{(1+z')E(z')} \tag{31}$$

In general, this integral has to be solved numerically, but it is possible to find simple analytical formulas linking it to T_0 for specific approximations of $E(z)$. Let us start from a matter-dominated Universe. In this case, it is $E(z) = \sqrt{\Omega_M(1+z)^3}$, from which $T(z)$ becomes

$$T(z) = \frac{1}{H_0} \int_z^\infty \frac{dz'}{(1+z')^{5/2}} \tag{32}$$

It can be solved analytically and one finds that the following parameterization is exactly valid [284]:

$$T(z) = \frac{T_0}{(1+z)^{3/2}} \tag{33}$$

If we introduce this new parameterization into our equations and compare the derived $H_0^{(z)}$ with the actual measurements, we obtain results shown in the left panel of Figure 4. It is worth noticing that this approach does not perform well in this case, as it produces a theoretical curve for H_0 that yields unreasonable results for low values of z , and it is not consistent with the late-type measurements, even for redshift regions where the Universe may be considered matter-dominated.

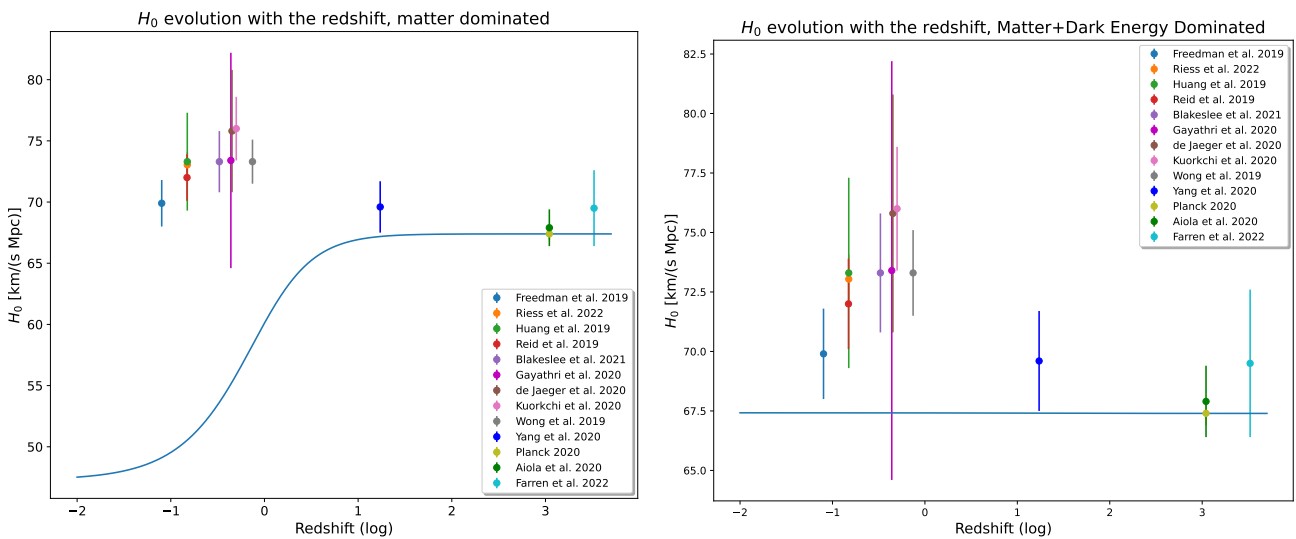


Figure 4. (Left panel) the value of H_0 derived considering $T(z) = \frac{T_0}{(1+z)^{3/2}}$ as a function of the redshift, confronted with observational data. (Right Panel) the same comparison, but with a parameterization consistent with the Universe dominated by matter and dark energy. The x -axis is in logarithmic scale. We recall that the measurements have been taken from [1,24,100,127–130,153,159,189,276–278]

If we, instead, consider a flat Universe with only dark energy and matter components (that is what we observe for the vast majority of the Universe lifetime, neglecting the radiation contribution), it is $E(z) = \sqrt{\Omega_M(1+z)^3 + \Omega_\Lambda}$. We find, starting from the equations derived in [285] for this particular case, that $T(z)$ can be expressed as

$$T(z) = \frac{2}{3H_0} \left(1 + \frac{\Omega_M}{\Omega_\Lambda}\right)^{1/2} \sinh^{-1} \left[\left(\frac{\Omega_\Lambda}{\Omega_M}\right)^{1/2} (1+z)^{-3/2} \right] \tag{34}$$

From this equation, T_0 can be easily recovered in the limit $z \rightarrow 0$. In other words, the relation between $T(z)$ and T_0 is as follows:

$$T(z) = \frac{\sinh^{-1} \left[\left(\frac{\Omega_\Lambda}{\Omega_M} \right)^{1/2} (1+z)^{-3/2} \right]}{\sinh^{-1} \left[\left(\frac{\Omega_\Lambda}{\Omega_M} \right)^{1/2} \right]} T_0. \tag{35}$$

By introducing the last equation in our approach, we obtain the results shown in the right panel of Figure 4. We observe that the derived estimate for H_0^z is independent of the redshift and aligns with the measurements provided by the Planck collaboration. However, it is not consistent with measurements of H_0 obtained at lower redshifts. It is worth noticing that this estimate depends on the ratio Ω_Λ/Ω_M , which, in our case, is fixed to the values provided by Planck, but can be modified for other inferred values of these quantities.

As additional case, we have considered a radiation-dominated Universe, where $E(z) = \sqrt{\Omega_r(1+z)^4}$ and

$$T(z) = \frac{T_0}{(1+z)^2}. \tag{36}$$

Furthermore, without any assumption, we can directly use the integral definitions of $T(z)$ and T_0 . The plots of these two cases are shown in Figure 5.

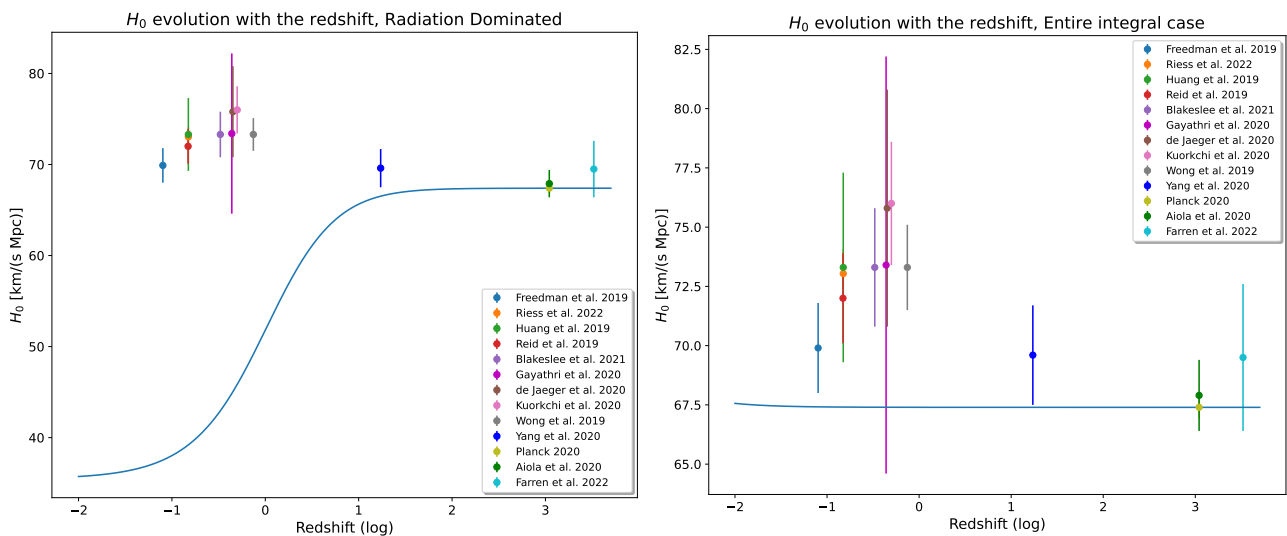


Figure 5. (Left panel) The value of H_0 derived from $T(z) = \frac{T_0}{(1+z)^2}$, plotted against the redshift and compared with observational data. **(Right panel)** The same comparison, but taking into account the integral definitions of T_0 and $T(z)$. The x-axis is in logarithmic scale. We recall that the measurements have been taken from [1,24,100,127–130,153,159,189,276–278]

The result obtained for the radiation-dominated Universe is reported in the left panel. Notably, we observe unreasonable values for H_0 even with respect to the matter-dominated case. On the right panel, we show the result obtained adopting the general integral for $T(z)$, that is Equation (31). Here, we obtain a constant value for H_0 around 67.4 km/(s Mpc), independent of the redshift. This is because, by adopting the integral, we fall into a circularity problem which gives the H_0 provided by the Planck Collaboration at all redshifts. This result is also remarkably consistent with the one obtained by Equation (35) for the Universe dominated by dark energy and matter.

Interestingly, we emphasize that the parameterization presented in Equation (26) is the only one consistent with both early and late-type measurements. In this framework, it can be exactly derived from an empty Universe with $E(z) = \sqrt{\Omega_k(1+z)^2}$. However, it is essential to note that such a Universe is in severe disagreement with cosmological

observations [1]. This discrepancy highlights the conceptual difference between our labeling approach and the derivation of $T(z)$ through the integral in Equation (31).

In summary, the parameterization shown in Equation (26) has been chosen as a labeling process connecting the age of the Universe at various epochs through a point-by-point approach. Mathematically, it can be derived from a reliable approximation of the scale factor as a function of time, working also for high-redshift. Among the different tests, it stands out as the only parameterization that aligns with the H_0 observations at both early and late epochs. It is worth stressing that, apart our labelling $T(z)$, the other tests have been performed considering other parameterizations. This does not exclude the possibility of choosing other relations between $T(z)$ and T_0 which involve more complex functions as $T(z) = T_0/(1 + P(z))$ where $P(z)$ can be some function of the redshift (e.g., a polynomial) as considered in cosmography [2]. From this more general approach, one could obtain realistic models capable of matching better the cosmic history.

4.2. A Variable H_0 from Late-Type Estimates

The look-back time parameterization of H_0 can be compared with late-type measurements for the cosmological parameters Ω_M and Ω_Λ . For this comparison, we will use results obtained by the cosmological ladder approach involving the SNe Ia of the Pantheon+ set [115,116]. In particular, we consider two different sets of results regarding Ω_M and Ω_Λ . In both cases, we use the value for T_0 provided by the Planck results, since an estimate for this quantity cannot be derived directly from the cosmological computations reported in Ref. [116]. For the first set, we start from the values obtained in [116] for a flat Λ CDM model where they imposed $\Omega_M + \Omega_\Lambda = 1$. They found

$$\Omega_M = 0.334 \pm 0.018, \quad \Omega_\Lambda = 0.666 \pm 0.018. \quad (37)$$

Considering the best-fit values of these quantities in our model, and comparing the results with the aforementioned H_0 measurements, we find the results displayed in the left panel of Figure 6. We note how, in general, the curve obtained by our model is consistent with the majority of the H_0 measurements. However, we notice an interesting tension with the measurement provided by the Planck collaboration, which is, instead, remarkably matched by the curve displayed in Figure 2.

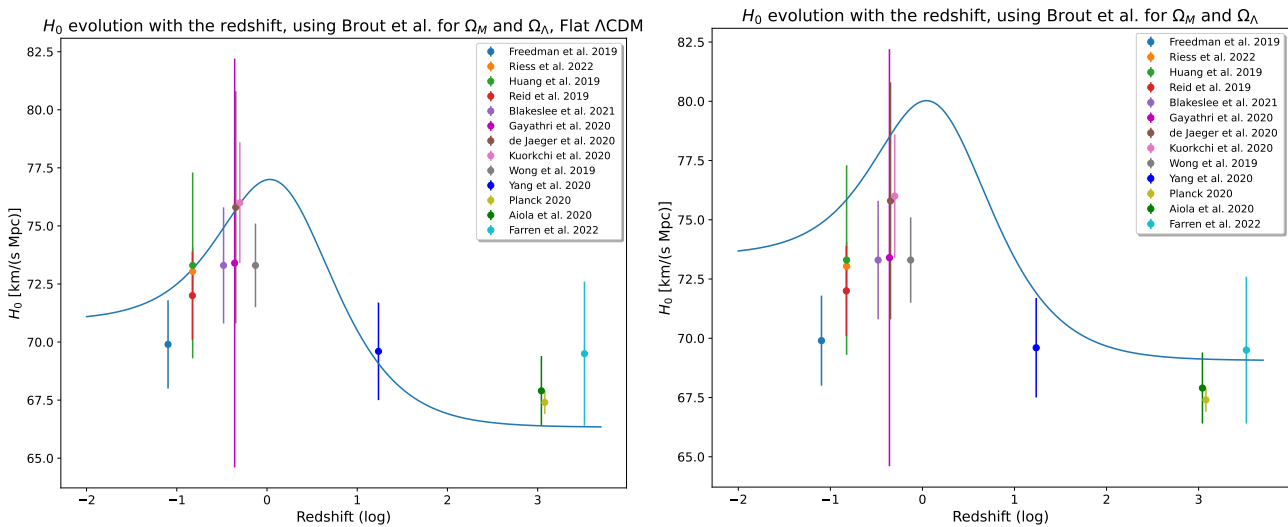


Figure 6. (Left panel) the value of H_0 derived from our methodology considering $T(z) = \frac{T_0}{(1+z)}$ plotted against the redshift and compared with observational data, starting from the Pantheon+ results for a flat Λ CDM model. (Right panel) the same comparison, but relaxing the flatness assumption. The x-axis is in logarithmic scale. We recall that the measurements have been taken from [1,24,100,127–130,153,159,189,276–278].

Indeed, we note how, at high redshift, the value for H_0 provided by this model decreases to 66.34 km/(s Mpc), which is more than 2σ in tension with the Planck measurement. An interesting observation is that this value is smaller than the measured one, contrary to what would be expected, given that late-type measurements usually translate with higher estimates for H_0 .

From this, we may conclude that the different values provided for Ω_M and Ω_Λ from early and late-type measurements have a significant impact on the comparison of our model with measurements.

This conclusion is further supported by the second case we have considered, in which we have taken into account the results for Ω_M and Ω_Λ obtained in [116] relaxing the flatness assumption for the Λ CDM, for which

$$\Omega_M = 0.306 \pm 0.057, \quad \Omega_\Lambda = 0.625 \pm 0.084, \quad (38)$$

while for the value of Ω_r , we rely on the value provided by Planck. Using our model for these starting values, we derive the right panel of Figure 6. We observe a shift towards higher values of H_0 with respect to the results obtained in the left panel of the same figure and note that the curve is inconsistent with many observations, particularly those concerning the late Universe. In this comparison, it is important to point out the large uncertainties on Ω_M and Ω_Λ values, which could play a significant role.

5. A Variable H_0 in Λ CDM Model

Let us discuss now the implications of our approach in the context of Λ CDM model. As previously mentioned, a variable H_0 can be interpreted as a possible hint for the breakdown of FLRW metric and the Λ CDM model [75,155]. Such a variation can be explained in the context of ETGs [29,81]. However, our analysis reveals that a variable H_0 can be entirely derived within the framework of Λ CDM model, starting from some fundamental concepts and from the parameterization in Equation (26), without making any a priori assumption on the evolution of H_0 . This finding does not contradict the role of H_0 in the Friedman equations because the variation of this constant is strictly connected to the redshift at which it has been measured.

A robust confirmation of such a hypothesis would be attainable by conducting independent measurements within the intermediate redshift range, where we observe the peak in our H_0 estimate as shown in Figure 2.

Notably, the Pantheon and Pantheon+ SNe Ia datasets [115,117], spanning up to $z = 2.26$, encompass a broad redshift range, albeit with a majority of SNe Ia situated in the low-redshift region. H_0 estimates already exist in this range, (e.g., [175,209,214]) but depend on calibration processes involving probes at lower redshifts. Consequently, promising new insights are anticipated from forthcoming investigations utilizing novel probes, such as quasars, gravitational wave standard sirens, galaxy clusters, Lyman- α lines, or GRBs (as reported in [186,210,211,215,286,287]).

In this context, the Euclid Mission [288,289] could play a pivotal role. While its main focus is investigating the nature of dark energy via a wide set of observations of galaxy clusters and weak lensing phenomena [290] by also testing possible modifications of GR [291,292], it also holds the potential to provide precise estimates of cosmological parameters like H_0 within the intermediate redshift range. Additionally, given the wide survey expected by Euclid, even though not primarily centered on transient phenomena such as SNe Ia, is likely to contribute significantly also to these types of observations [293].

Let us discuss now the implications of a variable H_0 on the cosmological observations. To achieve this, we have investigated, as an example, how luminosity and light-travel distances behave with the H_0^z function in Equation (27), and compared these distances with the results obtained by assuming the fixed values measured by the SH0ES and Planck collaborations. We selected the first distance because it is arguably the most relevant for cosmological measurements, and the second due to its connection with the look-back

time. It is worth noticing that similar considerations apply to other cosmological distances. The results are presented in Figure 7.

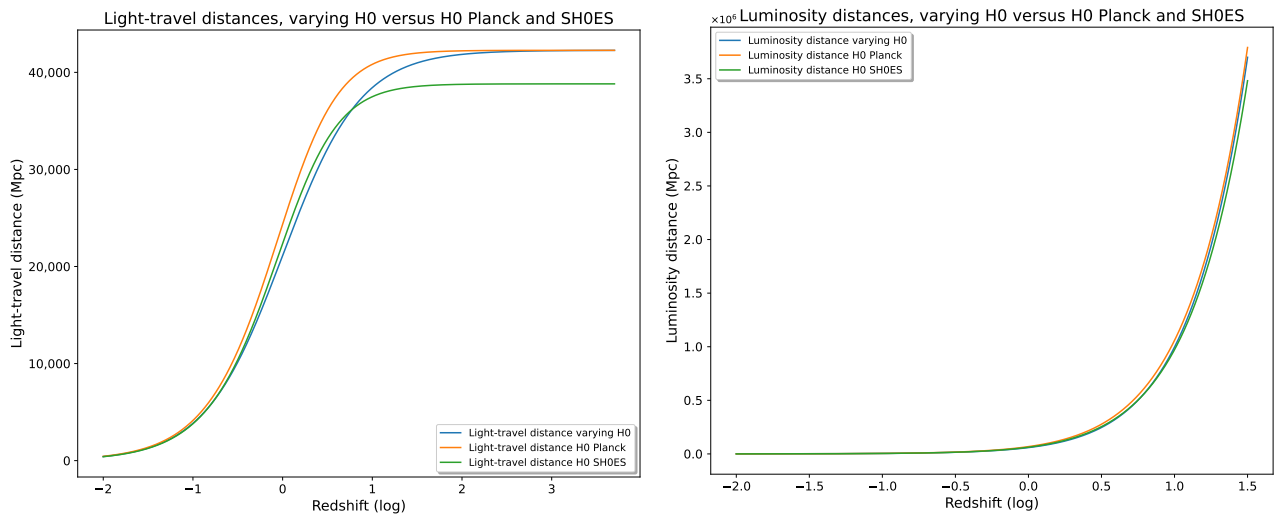


Figure 7. (Left panel) a comparison between the light-travel distance computed using the H_0^2 function (Equation (27)), with the distances derived by using the fixed values for H_0 provided by the SH0ES and Planck collaborations. (Right panel) the same comparison as in the left panel, but considering the luminosity distance. The x-axis is in logarithmic scale for both panels. Note that there are different scales on the x-axis in the two plots.

Both panels in this figure demonstrate how our approach naturally connects the two distances derived from fixed values of H_0 without significantly changing the overall behavior in the investigated redshift range. The effect is particularly evident in the left panel, where the light-travel distance is represented. We see how the distance computed by our approach is similar to the one derived from the SH0ES observations, converging towards the Planck results at higher redshifts. This can be attributed to the role of H_0 , which is a normalization constant, not linked to any astrophysical source. In conclusion, while a variable H_0 does impact the definitions of cosmological distances, it neither substantially changes the conclusions drawn from our method, especially at lower redshifts, nor it changes the value of the distances so that it could be in contrast with observations.

6. Discussion and Conclusions

In this work, we provided, without claiming for completeness, a summary of H_0 measurements in both early and late-type frameworks, highlighting the existence of a tension independent of the particular probe or methodology used. This independence emphasizes the decreasing probability that the tension stems from potential instrument-related biases or unaddressed systematic effects.

We explored how this tension has been tackled in the context of new physics, beyond the Λ CDM model. Various approaches have been proposed, yielding promising results. However, the main problem is the substantial degeneracy among the different proposed frameworks, which does not allow us, up to now, to define a unique and definitive extension of the Λ CDM model. From this point of view, it is crucial to understand that, whichever the extended framework may be, it has to be able to reproduce the Λ CDM results where the concordance among the vast majority of measurements is evident. This check is essential in view to recover self-consistent models in agreement with cosmic history.

A recent approach has brought significant attention to the possibility of a “running H_0 ” [75], both in the observations context and in the interpretation of a quantity that is traditionally regarded as “constant”.

In this framework, we reported the analysis performed in [90], which defines the Hubble constant via the look-back time. It is possible to provide a general formula consistent

with the measurements of this quantity both at early and late epochs just considering the related look-back time measurement of H_0 at any epoch. Here, we delve further into this direction starting from Equation (26) and discussing the consequences on the various cosmological distances.

Specifically, we highlight that the formula $T(z) = T_0/(1+z)$ arises naturally through a point-by-point labeling of the age of the Universe at different redshifts, without the need to account for the cosmological evolution already incorporated into the function $E(z)$.

To validate our assumption, we show how it can be mathematically derived from a reliable approximation of the scale factor $a(t)$, and how other parameterizations, which can be derived from specific assumptions on the densities at various epochs, do not effectively fit observational measurements of H_0 .

We have also considered different values of Ω_M and Ω_Λ , taken by late-type results from the SH0ES + Pantheon + sets, finding significant effects in our comparisons, particularly regarding the value for H_0 provided by the Planck collaboration, which is not recovered in these cases. This observation is interesting because it allows us to conclude that the different measurements of Ω_M and Ω_Λ , for late and early epochs, introduce a notable tension.

In particular, we derived the light-travel and luminosity distances as functions of our variable H_0 and compared the results with those obtained using the fixed values provided by early and late-time measurements. We found that, by our new definition, it is possible to obtain distances able to link the SH0ES and Planck distances, without significantly modifying their overall behavior. In our opinion, this is an important check because the absence of unreasonable results, starting from different distance definitions, confirms the reliability of the approach.

An issue that may arise pertains to the measurements of the aforementioned $H(z)$ function and the extrapolation to the H_0 value. In fact, one should be able to discern between variations related to the functional form of $H(z)$ and the variable nature of H_0 at different redshifts.

An important point that must be emphasized is that our results have been achieved entirely within the framework of the Λ CDM scenario, without requiring modifications or extensions. Theoretically, a variable H_0 can be interpreted as a breakdown of the FLRW metric. In our case, H_0 is an integration constant related to the size of the Universe at a given redshift. In other words, the value of H_0 could depend on the redshift at which it is measured, thus not undermining its role in the cosmological equations but removing the tension issue. It is worth noticing how a better fit with respect to the measurements can be obtained by starting from the early estimate of densities rather than the late ones. However, this does not exclude the necessity of extending GR and Λ CDM model, given other issues like the nature of dark energy and dark matter, and the lack of a self-consistent Quantum Gravity theory [29].

Observationally, H_0 tension is not the only tension in cosmology [25]. For example, there is the so-called $S_8 = \sigma_8\sqrt{\Omega_M/0.3}$ tension, where S_8 is a parameter indicating the strength with which matter is clustered in the Universe. On this parameter, a discrepancy at $2 - 3\sigma$ level [25] exists between the measurements inferred by the Planck data and low-redshift probes, such as the weak gravitational lens and clusters of galaxies [294,295]. It is essential to investigate whether similar considerations to those discussed above can also apply to S_8 or if it represents an independent signal of deviations from the cosmological Standard Model.

Furthermore, other measurements challenge the Λ CDM model, like some evidence of a possible non-zero curvature of the Universe [296], as well as anomalies in CMB observations, i.e., apparent correlations between the Solar System plane and certain aspects of CMB. This evidence seems to provide a preferred reference position which should not be possible if the Cosmological Principle is always valid [297–299].

In conclusion, our analysis suggests that new physics, in the form of extensions or modifications to Λ CDM model, may not be necessary to address the specific issue of H_0

tension, but it does not exclude its necessity for other fundamental issues. In a forthcoming study, we will discuss the other tensions under the standard of look-back time approach.

Author Contributions: Conceptualization, S.C. and G.S.; Methodology, G.S. and G.D.S.; Formal analysis, S.C. and G.D.S.; Investigation, G.D.S.; Data curation, G.S.; Writing—original draft, S.C. All authors have read and agreed to the published version of the manuscript.

Funding: This research received no external funding.

Data Availability Statement: Data are contained within the article.

Acknowledgments: This paper is based upon work from the COST Action CA21136, “Addressing observational tensions in cosmology with systematics and fundamental physics” (CosmoVerse) supported by COST (European Cooperation in Science and Technology). The authors acknowledge the support by Istituto Nazionale di Fisica Nucleare, Sez. di Napoli, Iniziativa Specifica QGSKY. The authors express their gratitude for valuable and constructive discussions to Giada Bargiacchi, Micol Benetti, Eoin Colgain, Maria Giovanna Dainotti, David Kraljic, Stefan Ruester, Shahin Sheikh-Jabbari, and Alessandro D.A.M. Spallicci. Finally, we want to thank the anonymous referees for their feedback and useful suggestions.

Conflicts of Interest: The authors declare no conflict of interest.

References

1. Aghanim, N.; Akrami, Y.; Ashdown, M.; Aumont, J.; Baccigalupi, C.; Ballardini, M.; Banday, A.J.; Barreiro, R.B.; Bartolo, N.; Basak, S.; et al. Planck 2018 results. *Astron. Astrophys.* **2020**, *641*, A6. [CrossRef]
2. Weinberg, S. *Gravitation and Cosmology: Principles and Applications of the General Theory of Relativity*; John Wiley and Sons: New York, NY, USA, 1972.
3. Guth, A.H. Inflationary universe: A possible solution to the horizon and flatness problems. *Phys. Lett. D* **1981**, *23*, 347–356. [CrossRef]
4. Starobinsky, A. Spectrum of relict gravitational radiation and the early state of the universe. *J. Exp. Theor. Phys. Lett.* **1979**, *30*, 682–685.
5. Particle Data Group; Zyla, P.; Barnett, R.M.; Beringer, J.; Dahl, O.; Dwyer, D.A.; Groom, D.E.; Lin, C.J.; Lugovsky, K.S.; Pianori, E.; et al. Review of particle physics. *Progr. Theor. Exp. Phys.* **2020**, *2020*, 083C01.
6. Particle Data Group; Workman, R.L.; Burkert, V.D.; Crede, V.; Klempt, E.; Thoma, U.; Tiator, L.; Agashe, K.; Aielli, G.; Allanach, B.C.; et al. Review of particle physics. *Prog. Theor. Exp. Phys.* **2022**, *2022*, 083C01. [CrossRef]
7. Riess, A.G.; Filippenko, A.V.; Challis, P.; Clocchiatti, A.; Diercks, A.; Garnavich, P.M.; Gilliland, R.L.; Hogan, C.J.; Jha, S.; Kirshner, R.P.; et al. Observational Evidence from Supernovae for an Accelerating Universe and a Cosmological Constant. *Astron. J.* **1998**, *116*, 1009–1038. [CrossRef]
8. Riess, A.G.; Strolger, L.G.; Casertano, S.; Ferguson, H.C.; Mobasher, B.; Gold, B.; Challis, P.J.; Filippenko, A.V.; Jha, S.; Li, W.; et al. New Hubble Space Telescope Discoveries of Type Ia Supernovae at $z \geq 1$: Narrowing Constraints on the Early Behavior of Dark Energy. *Astrophys. J.* **2007**, *659*, 98–121. [CrossRef]
9. Perlmutter, S.; Aldering, G.; Goldhaber, G.; Knop, R.A.; Nugent, P.; Castro, P.G.; Deustua, S.; Fabbro, S.; Goobar, A.; Groom, D.E.; et al. Measurements of Ω and Λ from 42 High-Redshift Supernovae. *Astrophys. J.* **1999**, *517*, 565–586. [CrossRef]
10. Bahcall, N.A.; Ostriker, J.P.; Perlmutter, S.; Steinhardt, P.J. The Cosmic Triangle: Revealing the State of the Universe. *Science* **1999**, *284*, 1481–1488. [CrossRef]
11. Spergel, D.N.; Verde, L.; Peiris, H.V.; Komatsu, E.; Nolta, M.R.; Bennett, C.L.; Halpern, M.; Hinshaw, G.; Jarosik, N.; Kogut, A.; et al. First-Year Wilkinson Microwave Anisotropy Probe (WMAP) Observations: Determination of Cosmological Parameters. *Astrophys. J. Suppl. Ser.* **2003**, *148*, 175–194. [CrossRef]
12. Schimd, C.; Tereno, I.; Uzan, J.P.; Mellier, Y.; van Waerbeke, L.; Semboloni, E.; Hoekstra, H.; Fu, L.; Riazuelo, A. Tracking quintessence by cosmic shear. *Astron. Astrophys.* **2006**, *463*, 405–421. [CrossRef]
13. McDonald, P.; Seljak, U.; Burles, S.; Schlegel, D.J.; Weinberg, D.H.; Cen, R.; Shih, D.; Schaye, J.; Schneider, D.P.; Bahcall, N.A.; et al. The Ly α Forest Power Spectrum from the Sloan Digital Sky Survey. *Astrophys. J. Suppl. Ser.* **2006**, *163*, 80–109. [CrossRef]
14. Bamba, K.; Capozziello, S.; Nojiri, S.; Odintsov, S.D. Dark energy cosmology: The equivalent description via different theoretical models and cosmography tests. *Astrophys. Space Sci.* **2012**, *342*, 155–228. [CrossRef]
15. Joyce, A.; Jain, B.; Khoury, J.; Trodden, M. Beyond the cosmological standard model. *Phys. Rep.* **2015**, *568*, 1–98. [CrossRef]
16. Abbott, T.M.C.; Allam, S.; Andersen, P.; Angus, C.; Asorey, J.; Avelino, A.; Avila, S.; Bassett, B.A.; Bechtol, K.; Bernstein, G.M.; et al. First Cosmology Results using Type Ia Supernovae from the Dark Energy Survey: Constraints on Cosmological Parameters. *Astrophys. J.* **2019**, *872*, L30. [CrossRef]
17. Salucci, P.; Esposito, G.; Lambiase, G.; Battista, E.; Benetti, M.; Bini, D.; Boco, L.; Sharma, G.; Bozza, V.; Buoninfante, L.; et al. Einstein, Planck and Vera Rubin: Relevant Encounters Between the Cosmological and the Quantum Worlds. *Front. Phys.* **2021**, *8*, 579. [CrossRef]

18. Zwicky, F. Die Rotverschiebung von extragalaktischen Nebeln. *Helv. Phys. Acta* **1933**, *6*, 110–127.
19. Babcock, H.W. The rotation of the Andromeda Nebula. *Lick Obs. Bull.* **1939**, *498*, 41–51. [CrossRef]
20. Rubin, V.C.; Ford, V.K. Rotation of the Andromeda Nebula from a Spectroscopic Survey of Emission Regions. *Astrophys. J.* **1970**, *159*, 379. [CrossRef]
21. Schnee, R.W. Introduction to dark matter experiments. In *Physics of the Large and the Small: TASI 2009*; Csaki, C., Dodelso, S., Eds.; World Scientific Publishing Co. Pte. Ltd.: Singapore, 2011; pp. 775–829. [CrossRef]
22. Mitsou, V.A. Overview of searches for dark matter at the LHC. *J. Phys. Conf. Ser.* **2015**, *651*, 012023. [CrossRef]
23. Aprile, E.; Aalbers, J.; Agostini, F.; Alfonsi, M.; Amaro, F.D.; Anthony, M.; Antunes, B.; Arneodo, F.; Balata, M.; Barrow, P.; et al. The XENON1T dark matter experiment. *Eur. Phys. J. C* **2017**, *77*, 881. [CrossRef]
24. Riess, A.G.; Yuan, W.; Macri, L.M.; Scolnic, D.; Brout, D.; Casertano, S.; Jones, D.O.; Murakami, Y.; Anand, G.S.; Breuval, L.; et al. A Comprehensive Measurement of the Local Value of the Hubble Constant with 1 km/s/Mpc Uncertainty from the Hubble Space Telescope and the SH0ES Team. *Astrophys. J. Lett.* **2022**, *934*, L7. [CrossRef]
25. Abdalla, E.; Abellán, G.F.; Aboubrahim, A.; Agnello, A.; Akarsu, Ö.; Akrami, Y.; Alestas, G.; Aloni, D.; Amendola, L.; Anchordoqui, L.A.; et al. Cosmology intertwined: A review of the particle physics, astrophysics, and cosmology associated with the cosmological tensions and anomalies. *J. High Energy Astrophys.* **2022**, *34*, 49–211. [CrossRef]
26. Moresco, M.; Amati, L.; Amendola, L.; Birrer, S.; Blakeslee, J.P.; Cantiello, M.; Cimatti, A.; Darling, J.; Valle, M.D.; Fishbach, M.; et al. Unveiling the Universe with emerging cosmological probes. *Living Rev. Relativ.* **2022**, *25*, 6. [CrossRef]
27. Capozziello, S. Curvature Quintessence. *Int. J. Mod. Phys. D* **2002**, *11*, 483–491. [CrossRef]
28. Nojiri, S.; Odintsov, S.D. Unified cosmic history in modified gravity: From $F(R)$ theory to Lorentz non-invariant models. *Phys. Rep.* **2011**, *505*, 59–144. [CrossRef]
29. Capozziello, S.; Laurentis, M.D. Extended Theories of Gravity. *Phys. Rep.* **2011**, *509*, 167–321. [CrossRef]
30. Capozziello, S.; Laurentis, M.D.; Odintsov, S.; Stabile, A. Hydrostatic equilibrium and stellar structure in $f(R)$ -gravity. *Phys. Rev. D* **2011**, *83*, 064004. [CrossRef]
31. Nojiri, S.; Odintsov, S.; Oikonomou, V. Modified gravity theories on a nutshell: Inflation, bounce and late-time evolution. *Phys. Rep.* **2017**, *692*, 1–104. [CrossRef]
32. Felice, A.D.; Tsujikawa, S. $f(R)$ Theories. *Living Rev. Relativ.* **2010**, *13*, 3. [CrossRef]
33. Hu, W.; Sawicki, I. Models of $f(R)$ Cosmic Acceleration that Evade Solar-System Tests. *Phys. Rev. D* **2007**, *76*, 064004. [CrossRef]
34. Capozziello, S.; Cardone, V.F.; Troisi, A. Reconciling dark energy models with $f(R)$ theories. *Phys. Rev. D* **2005**, *71*, 043503. [CrossRef]
35. Oikonomou, V. Effects of a pre-inflationary de Sitter bounce on the primordial gravitational waves in $f(R)$ gravity theories. *Nucl. Phys. B* **2022**, *984*, 115985. [CrossRef]
36. Capozziello, S.; D’Agostino, R.; Luongo, O. Extended Gravity Cosmography. *Int. J. Mod. Phys. D* **2019**, *28*, 1930016. [CrossRef]
37. Bajardi, F.; D’Agostino, R.; Benetti, M.; De Falco, V.; Capozziello, S. Early and late time cosmology: The $f(R)$ gravity perspective. *Eur. Phys. J. Plus* **2022**, *137*, 1239. [CrossRef]
38. Cai, Y.F.; Capozziello, S.; De Laurentis, M.; Saridakis, E.N. $f(T)$ teleparallel gravity and cosmology. *Rep. Prog. Phys.* **2016**, *79*, 106901. [CrossRef] [PubMed]
39. Benetti, M.; Capozziello, S.; Lambiase, G. Updating constraints on $f(T)$ teleparallel cosmology and the consistency with big bang nucleosynthesis. *Mon. Not. R. Astron. Soc.* **2021**, *500*, 1795–1805. [CrossRef]
40. Nojiri, S.; Odintsov, S.; Oikonomou, V. Integral $F(R)$ gravity and saddle point condition as a remedy for the H_0 -tension. *Nucl. Phys. B* **2022**, *980*, 115850. [CrossRef]
41. Spallicci, A.D.A.M.; Helayél-Neto, J.A.; López-Corredoira, M.; Capozziello, S. Cosmology and photon frequency shift induced by the Standard-Model Extension. *Eur. Phys. J. C* **2021**, *81*, 4. [CrossRef]
42. Spallicci, A.D.A.M.; Sarracino, G.; Capozziello, S. Investigating dark energy by electromagnetic frequency shifts. *Eur. Phys. J. Plus* **2022**, *137*, 253. [CrossRef]
43. Sarracino, G.; Spallicci, A.D.A.M.; Capozziello, S. Investigating dark energy by electromagnetic frequency shifts II: the Pantheon+ sample. *Eur. Phys. J. Plus* **2022**, *137*, 1386. [CrossRef]
44. Capozziello, S.; Benetti, M.; Spallicci, A.D.A.M. Addressing the cosmological H_0 tension by the Heisenberg uncertainty. *Found. Phys.* **2020**, *50*, 893. [CrossRef]
45. Spallicci, A.D.A.M.; Benetti, M.; Capozziello, S. Heisenberg principle at cosmological scales. *Found. Phys.* **2022**, *52*, 23. [CrossRef]
46. Bernal, J.L.; Verde, L.; Riess, A.G. The trouble with H_0 . *J. Cosmol. Astropart. Phys.* **2016**, *2016*, 019. [CrossRef]
47. Mörtzell, E.; Dhawan, S. Does the Hubble constant tension call for new physics? *J. Cosmol. Astropart. Phys.* **2018**, *2018*, 025. [CrossRef]
48. Vagnozzi, S.; Dhawan, S.; Gerbino, M.; Freese, K.; Goobar, A.; Mena, O. Constraints on the sum of the neutrino masses in dynamical dark energy models with $w(z) \leq -1$ are tighter than those obtained in Λ CDM. *Phys. Rev. D* **2018**, *98*, 083501. [CrossRef]
49. Yang, W.; Pan, S.; Valentino, E.D.; Nunes, R.C.; Vagnozzi, S.; Mota, D.F. Tale of stable interacting dark energy, observational signatures, and the H_0 tension. *J. Cosmol. Astropart. Phys.* **2018**, *2018*, 019. [CrossRef]
50. Poulin, V.; Smith, T.L.; Karwal, T.; Kamionkowski, M. Early Dark Energy can Resolve the Hubble Tension. *Phys. Rev. Lett.* **2019**, *122*, 221301. [CrossRef]

51. Kreisch, C.D.; Cyr-Racine, F.Y.; Doré, O. Neutrino puzzle: Anomalies, interactions, and cosmological tensions. *Phys. Rev. D* **2020**, *101*, 103520. [CrossRef]
52. Agrawal, P.; Cyr-Racine, F.Y.; Pinner, D.; Randall, L. Rock 'n' Roll Solutions to the Hubble Tension. *Phys. Dark Universe* **2023**, *42*, 101347. [CrossRef]
53. Valentino, E.D.; Ferreira, R.Z.; Visinelli, L.; Danielsson, U. Late time transitions in the quintessence field and the H_0 tension. *Phys. Dark Universe* **2019**, *26*, 100385. [CrossRef]
54. Pan, S.; Yang, W.; Valentino, E.D.; Saridakis, E.N.; Chakraborty, S. Interacting scenarios with dynamical dark energy: Observational constraints and alleviation of the H_0 tension. *Phys. Rev. D* **2019**, *100*, 103520. [CrossRef]
55. Vagnozzi, S. New physics in light of the H_0 tension: An alternative view. *Phys. Rev. D* **2020**, *102*, 023518. [CrossRef]
56. Visinelli, L.; Vagnozzi, S.; Danielsson, U. Revisiting a Negative Cosmological Constant from Low-Redshift Data. *Symmetry* **2019**, *11*, 1035. [CrossRef]
57. Knox, L.; Millea, M. Hubble constant hunter's guide. *Phys. Rev. D* **2020**, *101*, 043533. [CrossRef]
58. Valentino, E.D.; Melchiorri, A.; Mena, O.; Vagnozzi, S. Interacting dark energy in the early 2020s: A promising solution to the H_0 and cosmic shear tensions. *Phys. Dark Universe* **2020**, *30*, 100666. [CrossRef]
59. Valentino, E.D.; Melchiorri, A.; Mena, O.; Vagnozzi, S. Non-minimal dark sector physics and cosmological tensions. *Phys. Rev. D* **2020**, *101*, 063502. [CrossRef]
60. Valentino, E.D.; Mukherjee, A.; Sen, A.A. Dark Energy with Phantom Crossing and the H_0 Tension. *Entropy* **2021**, *23*, 404. [CrossRef]
61. Smith, T.L.; Poulin, V.; Bernal, J.L.; Boddy, K.K.; Kamionkowski, M.; Murgia, R. Early dark energy is not excluded by current large-scale structure data. *Phys. Rev. D* **2021**, *103*, 123542. [CrossRef]
62. Vagnozzi, S. Consistency tests of Λ CDM from the early integrated Sachs-Wolfe effect: Implications for early-time new physics and the Hubble tension. *Phys. Rev. D* **2021**, *104*, 063524. [CrossRef]
63. Nunes, R.C.; Valentino, E.D. Dark sector interaction and the supernova absolute magnitude tension. *Phys. Rev. D* **2021**, *104*, 063529. [CrossRef]
64. Cyr-Racine, F.Y.; Ge, F.; Knox, L. Symmetry of Cosmological Observables, a Mirror World Dark Sector, and the Hubble Constant. *Phys. Rev. Lett.* **2022**, *128*, 201301. [CrossRef]
65. Anchordoqui, L.A.; Valentino, E.D.; Pan, S.; Yang, W. Dissecting the H_0 and S_8 tensions with Planck + BAO + supernova type Ia in multi-parameter cosmologies. *J. High Energy Astrophys.* **2021**, *32*, 28–64. [CrossRef]
66. Poulin, V.; Smith, T.L.; Bartlett, A. Dark energy at early times and ACT data: A larger Hubble constant without late-time priors. *Phys. Rev. D* **2021**, *104*, 123550. [CrossRef]
67. Alestas, G.; Camarena, D.; Valentino, E.D.; Kazantzidis, L.; Marra, V.; Nesseris, S.; Perivolaropoulos, L. Late-transition versus smooth $H(z)$ deformation models for the resolution of the Hubble crisis. *Phys. Rev. D* **2022**, *105*, 063538. [CrossRef]
68. Smith, T.L.; Lucca, M.; Poulin, V.; Abellan, G.F.; Balkenhol, L.; Benabed, K.; Galli, S.; Murgia, R. Hints of early dark energy in Planck, SPT, and ACT data: New physics or systematics? *Phys. Rev. D* **2022**, *106*, 043526. [CrossRef]
69. Reeves, A.; Herold, L.; Vagnozzi, S.; Sherwin, B.D.; Ferreira, E.G.M. Restoring cosmological concordance with early dark energy and massive neutrinos? *Mon. Not. R. Astron. Soc.* **2023**, *520*, 3688–3695. [CrossRef]
70. Poulin, V.; Smith, T.L.; Karwal, T. The Ups and Downs of Early Dark Energy solutions to the Hubble tension: A review of models, hints and constraints circa 2023. *arXiv* **2023**, arXiv:2302.09032.
71. Demianski, M.; Piedipalumbo, E.; Sawant, D.; Amati, L. Cosmology with gamma-ray bursts I. The Hubble diagram through the calibrated $E_{p,i} - E_{iso}$ correlation. *Astron. Astrophys.* **2017**, *598*, A112. [CrossRef]
72. Lusso, E.; Piedipalumbo, E.; Risaliti, G.; Paolillo, M.; Bisogni, S.; Nardini, E.; Amati, L. Tension with the flat Λ CDM model from a high-redshift Hubble diagram of supernovae, quasars, and gamma-ray bursts. *Astron. Astrophys.* **2019**, *628*, L4. [CrossRef]
73. Ryan, J.; Chen, Y.; Ratra, B. Baryon acoustic oscillation, Hubble parameter, and angular size measurement constraints on the Hubble constant, dark energy dynamics, and spatial curvature. *Mon. Not. R. Astron. Soc.* **2019**, *488*, 3844–3856. [CrossRef]
74. Cao, S.; Ryan, J.; Ratra, B. Using Pantheon and DES supernova, baryon acoustic oscillation, and Hubble parameter data to constrain the Hubble constant, dark energy dynamics, and spatial curvature. *Mon. Not. R. Astron. Soc.* **2021**, *504*, 300–310. [CrossRef]
75. Krishnan, C.; Colgáin, E.Ó.; Sheikh-Jabbari, M.; Yang, T. Running Hubble tension and a H_0 diagnostic. *Phys. Rev. D* **2021**, *103*, 103509. [CrossRef]
76. Colgáin, E.Ó.; Sheikh-Jabbari, M.; Yang, T. Elucidating cosmological model dependence with H_0 . *Eur. Phys. J. C* **2021**, *81*, 892. [CrossRef]
77. Krishnan, C.; Mondol, R. H_0 as a Universal FLRW Diagnostic. *arXiv* **2022**, arXiv:2201.13384.
78. Colgáin, E.Ó.; Sheikh-Jabbari, M.; Solomon, R.; Bargiacchi, G.; Capozziello, S.; Dainotti, M.; Stojkovic, D. Revealing intrinsic flat Λ CDM biases with standardizable candles. *Phys. Rev. D* **2022**, *106*, L041301. [CrossRef]
79. Colgáin, E.Ó.; Sheikh-Jabbari, M.M.; Solomon, R.; Dainotti, M.G.; Stojkovic, D. Putting Flat Λ CDM In The (Redshift) Bin. *arXiv* **2022**, arXiv:2206.11447.
80. Colgáin, E.Ó.; Sheikh-Jabbari, M.M.; Solomon, R. High Redshift Λ CDM Cosmology: To Bin or not to Bin? *arXiv* **2022**, arXiv:2211.02129.

81. Dainotti, M.G.; Simone, B.D.; Schiavone, T.; Montani, G.; Rinaldi, E.; Lambiase, G. On the Hubble Constant Tension in the SNe Ia Pantheon Sample. *Astrophys. J.* **2021**, *912*, 150. [CrossRef]
82. Dainotti, M.G.; Simone, B.D.; Schiavone, T.; Montani, G.; Rinaldi, E.; Lambiase, G.; Bogdan, M.; Ugale, S. On the Evolution of the Hubble Constant with the SNe Ia Pantheon Sample and Baryon Acoustic Oscillations: A Feasibility Study for GRB-Cosmology in 2030. *Galaxies* **2022**, *10*, 24. [CrossRef]
83. Dainotti, M.; De Simone, B.; Montani, G.; Schiavone, T.; Lambiase, G. The Hubble constant tension: Current status and future perspectives through new cosmological probes. *arXiv* **2023**, arXiv:2301.10572.
84. Schiavone, T.; Montani, G.; Dainotti, M.G.; De Simone, B.; Rinaldi, E.; Lambiase, G. Running Hubble constant from the SNe Ia Pantheon sample? *arXiv* **2022**, arXiv:2205.07033.
85. Schiavone, T.; Montani, G.; Bombacigno, F. $f(R)$ gravity in the Jordan frame as a paradigm for the Hubble tension. *Mon. Not. R. Astron. Soc. Lett.* **2023**, *522*, L72–L77. [CrossRef]
86. Malekjani, M.; Conville, R.M.; Colgáin, E.Ó.; Pourojaghi, S.; Sheikh-Jabbari, M.M. Negative Dark Energy Density from High Redshift Pantheon+ Supernovae. *arXiv* **2023**, arXiv:2301.12725. <https://doi.org/10.48550/ARXIV.2301.12725>.
87. Gurzadyan, V.G.; Fimin, N.N.; Chechetkin, V.M. Cosmic voids and the kinetic analysis. *Astron. Astrophys.* **2022**, *666*, A149. [CrossRef]
88. Hu, J.P.; Wang, F.Y. Hubble Tension: The Evidence of New Physics. *Universe* **2023**, *9*, 94. [CrossRef]
89. Jia, X.A.; Hu, J.P.; Wang, F.Y. Evidence of a decreasing trend for the Hubble constant. *Astron. Astrophys.* **2023**, *674*, A45. [CrossRef]
90. Capozziello, S.; Sarracino, G.; Spallicci, A.D.A.M. Questioning the H_0 tension via the look-back time. *Phys. Dark Universe* **2023**, *40*, 101201. [CrossRef]
91. Mecke, K.R.; Buchert, T.; Wagner, H. Robust morphological measures for large-scale structure in the Universe. *Astron. Astrophys.* **1994**, *288*, 697–704. [CrossRef]
92. Yadav, J.K.; Bagla, J.S.; Khandai, N. Fractal dimension as a measure of the scale of homogeneity. *Mon. Not. R. Astron. Soc.* **2010**, *405*, 2009–2015. [CrossRef]
93. Wiegand, A.; Buchert, T.; Ostermann, M. Direct Minkowski Functional analysis of large redshift surveys: A new high-speed code tested on the luminous red galaxy Sloan Digital Sky Survey-DR7 catalogue. *Mon. Not. R. Astron. Soc.* **2014**, *443*, 241–259. [CrossRef]
94. Robertson, H.P. Kinematics and World-Structure. *Astrophys. J.* **1935**, *82*, 284. [CrossRef]
95. Friedmann, A. Über die Krümmung des Raumes. *Z. Fur Phys.* **1922**, *10*, 377–386. [CrossRef]
96. Hogg, D.W. Distance measures in cosmology. *arXiv* **1999**, arXiv:astro-ph/9905116.
97. Nemiroff, R.J.; Patla, B. Adventures in Friedmann cosmology: A detailed expansion of the cosmological Friedmann equations. *Am. J. Phys.* **2008**, *76*, 265–276. [CrossRef]
98. Riess, A.G.; Casertano, S.; Yuan, W.; Bowers, J.B.; Macri, L.; Zinn, J.C.; Scolnic, D. Cosmic Distances Calibrated to 1% Precision with Gaia EDR3 Parallaxes and Hubble Space Telescope Photometry of 75 Milky Way Cepheids Confirm Tension with Λ CDM. *Astrophys. J. Lett.* **2021**, *908*, L6. [CrossRef]
99. Pietrzyński, G.; Graczyk, D.; Gallenne, A.; Gieren, W.; Thompson, I.B.; Pilecki, B.; Karczmarek, P.; Górski, M.; Suchomska, K.; Taormina, M.; et al. A distance to the Large Magellanic Cloud that is precise to one per cent. *Nature* **2019**, *567*, 200–203. [CrossRef]
100. Reid, M.J.; Pesce, D.W.; Riess, A.G. An Improved Distance to NGC 4258 and Its Implications for the Hubble Constant. *Astrophys. J.* **2019**, *886*, L27. [CrossRef]
101. Riess, A.G.; Casertano, S.; Yuan, W.; Macri, L.M.; Scolnic, D. Large Magellanic Cloud Cepheid Standards Provide a 1% Foundation for the Determination of the Hubble Constant and Stronger Evidence for Physics beyond Λ CDM. *Astrophys. J.* **2019**, *876*, 85. [CrossRef]
102. Gaia Collaboration; Prusti, T.; de Bruijne, J.H.J.; Brown, A.G.A.; Vallenari, A.; Babusiaux, C.; Bailer-Jones, C.A.L.; Bastian, U.; Biermann, M.; Evans, D.W.; et al. The Gaia mission. *Astron. Astrophys.* **2016**, *595*, A1. [CrossRef]
103. Gaia Collaboration; Brown, A.G.A.; Vallenari, A.; Prusti, T.; de Bruijne, J.H.J.; Mignard, F.; Drimmel, R.; Babusiaux, C.; Bailer-Jones, C.A.L.; Bastian, U.; et al. Gaia Data Release 1. Summary of the astrometric, photometric, and survey properties. *Astron. Astrophys.* **2016**, *595*, A2. [CrossRef]
104. Gaia Collaboration; Brown, A.G.A.; Vallenari, A.; Prusti, T.; de Bruijne, J.H.J.; Babusiaux, C.; Bailer-Jones, C.A.L.; Biermann, M.; Evans, D.W.; Eyer, L.; et al. Gaia Data Release 2. Summary of the contents and survey properties. *Astron. Astrophys.* **2018**, *616*, A1. [CrossRef]
105. Brown, A.G.A.; Vallenari, A.; Prusti, T.; de Bruijne, J.H.J.; Babusiaux, C.; Biermann, M.; Creevey, O.L.; Evans, D.W.; Eyer, L.; Hutton, A.; et al. Gaia Early Data Release 3. *Astron. Astrophys.* **2021**, *650*, C3. [CrossRef]
106. Ripepi, V.; Clementini, G.; Molinaro, R.; Leccia, S.; Plachy, E.; Molnár, L.; Rimoldini, L.; Musella, I.; Marconi, M.; Garofalo, A.; et al. Gaia Data Release 3. Specific processing and validation of all sky RR Lyrae and Cepheid stars: The Cepheid sample. *Astron. Astrophys.* **2023**, *674*, A17. [CrossRef]
107. Marconi, M.; Molinaro, R.; Bono, G.; Pietrzyński, G.; Gieren, W.; Pilecki, B.; Stellingwerf, R.F.; Graczyk, D.; Smolec, R.; Konorski, P.; et al. The Eclipsing Binary Cepheid OGLE-LMC-CEP-0227 in the Large Magellanic Cloud: Pulsation modelling of light and radial velocity curves. *Astrophys. J.* **2013**, *768*, L6. [CrossRef]
108. Somma, G.D.; Marconi, M.; Molinaro, R.; Cignoni, M.; Musella, I.; Ripepi, V. An Extended Theoretical Scenario for Classical Cepheids. I. Modeling Galactic Cepheids in the Gaia Photometric System. *Astrophys. J. Suppl. Ser.* **2020**, *247*, 30. [CrossRef]

109. De Somma, G.; Marconi, M.; Molinaro, R.; Cignoni, M.; Musella, I.; Ripepi, V. Gaia Parallaxes Versus Updated Pulsation Model Predictions. In *Proceedings of the RR Lyrae/Cepheid 2019: Frontiers of Classical Pulsators*; Astronomical Society of the Pacific Conference Series; Kinemuchi, K., Lovekin, C., Neilson, H., Vivas, K., Eds.; Astronomical Society of the Pacific: San Francisco, CA, USA, 2021; Volume 529, p. 27.
110. Marconi, M.; Musella, I.; Fiorentino, G. Cepheid Pulsation Models at Varying Metallicity and $\Delta Y/\Delta Z$. *Astrophys. J.* **2005**, *632*, 590–610. [CrossRef]
111. Ripepi, V.; Catanzaro, G.; Molinaro, R.; Gatto, M.; De Somma, G.; Marconi, M.; Romaniello, M.; Leccia, S.; Musella, I.; Trentin, E.; et al. Cepheid metallicity in the Leavitt law (C-metal) survey—I. HARPS-N@TNG spectroscopy of 47 classical Cepheids and 1 BL Her variables. *Mon. Not. R. Astron. Soc.* **2021**, *508*, 4047–4071. [CrossRef]
112. De Somma, G.; Marconi, M.; Molinaro, R.; Ripepi, V.; Leccia, S.; Musella, I. An Updated Metal-dependent Theoretical Scenario for Classical Cepheids. *Astrophys. J. Suppl. Ser.* **2022**, *262*, 25. [CrossRef]
113. Breuval, L.; Riess, A.G.; Kervella, P.; Anderson, R.I.; Romaniello, M. An Improved Calibration of the Wavelength Dependence of Metallicity on the Cepheid Leavitt Law. *Astrophys. J.* **2022**, *939*, 89. [CrossRef]
114. Meng, X.; Gao, Y.; Han, Z. SNe Ia as a cosmological probe. *Int. J. Mod. Phys. D* **2015**, *24*, 1530029. [CrossRef]
115. Scolnic, D.; Brout, D.; Carr, A.; Riess, A.G.; Davis, T.M.; Dwomoh, A.; Jones, D.O.; Ali, N.; Charvu, P.; Chen, R.; et al. The Pantheon+ Analysis: The Full Data Set and Light-curve Release. *Astrophys. J.* **2022**, *938*, 113. [CrossRef]
116. Brout, D.; Scolnic, D.; Popovic, B.; Riess, A.G.; Carr, A.; Zuntz, J.; Kessler, R.; Davis, T.M.; Hinton, S.; Jones, D.; et al. The Pantheon+ Analysis: Cosmological Constraints. *Astrophys. J.* **2022**, *938*, 110. [CrossRef]
117. Scolnic, D.M.; Jones, D.O.; Rest, A.; Pan, Y.C.; Chornock, R.; Foley, R.J.; Huber, M.E.; Kessler, R.; Narayan, G.; Riess, A.G.; et al. The complete light-curve sample of spectroscopically confirmed SNe Ia from Pan-STARRS1 and cosmological constraints from the combined Pantheon sample. *Astrophys. J.* **2018**, *859*, 101. [CrossRef]
118. Hillebrandt, W.; Niemeyer, J.C. Type Ia Supernova Explosion Models. *Annu. Rev. Astron. Astrophys.* **2000**, *38*, 191–230. [CrossRef]
119. Nomoto, K.; Thielemann, F.K.; Yokoi, K. Accreting white dwarf models for type I supern. III. Carbon deflagration supernovae. *Astrophys. J.* **1984**, *286*, 644–658. [CrossRef]
120. Colgate, S.A.; McKee, C. Early Supernova Luminosity. *Astrophys. J.* **1969**, *157*, 623. [CrossRef]
121. Carroll, S.M. The Cosmological Constant. *Living Rev. Relativ.* **2001**, *4*, 1. [CrossRef]
122. Filippenko, A.V.; Richmond, M.W.; Matheson, T.; Shields, J.C.; Burbidge, E.M.; Cohen, R.D.; Dickinson, M.; Malkan, M.A.; Nelson, B.; Pietz, J.; et al. The Peculiar Type IA SN 1991T: Detonation of a White Dwarf? *Astrophys. J. Lett.* **1992**, *384*, L15. [CrossRef]
123. Filippenko, A.V.; Richmond, M.W.; Branch, D.; Gaskell, M.; Herbst, W.; Ford, C.H.; Treffers, R.R.; Matheson, T.; Ho, L.C.; Dey, A.; et al. The Subluminous, Spectroscopically Peculiar Type Ia Supernova 1991bg in the Elliptical Galaxy NGC 4374. *Astrophys. J.* **1992**, *104*, 1543. [CrossRef]
124. Khokhlov, A.M. Delayed detonation model for type IA supernovae. *Astron. Astrophys.* **1991**, *245*, 114–128.
125. Phillips, M.M. The Absolute Magnitudes of Type IA Supernovae. *Astrophys. J. Lett.* **1993**, *413*, L105. [CrossRef]
126. Salaris, M.; Cassisi, S. The “tip” of the red giant branch as a distance indicator: Results from evolutionary models. *Mon. Not. R. Astron. Soc.* **1997**, *289*, 406–414. [CrossRef]
127. Freedman, W.L.; Madore, B.F.; Hatt, D.; Hoyt, T.J.; Jang, I.S.; Beaton, R.L.; Burns, C.R.; Lee, M.G.; Monson, A.J.; Neeley, J.R.; et al. The Carnegie-Chicago Hubble Program. VIII. An Independent Determination of the Hubble Constant Based on the Tip of the Red Giant Branch. *Astrophys. J.* **2019**, *882*, 34. [CrossRef]
128. de Jaeger, T.; Stahl, B.E.; Zheng, W.; Filippenko, A.V.; Riess, A.G.; Galbany, L. A measurement of the Hubble constant from Type II supernovae. *Mon. Not. R. Astron. Soc.* **2020**, *496*, 3402–3411. [CrossRef]
129. Kourkchi, E.; Tully, R.B.; Anand, G.S.; Courtois, H.M.; Dupuy, A.; Neill, J.D.; Rizzi, L.; Seibert, M. Cosmicflows-4: The Calibration of Optical and Infrared Tully-Fisher Relations. *Astrophys. J.* **2020**, *896*, 3. [CrossRef]
130. Blakeslee, J.P.; Jensen, J.B.; Ma, C.P.; Milne, P.A.; Greene, J.E. The Hubble Constant from Infrared Surface Brightness Fluctuation Distances. *Astrophys. J.* **2021**, *911*, 65. [CrossRef]
131. Uddin, S.A.; Burns, C.R.; Phillips, M.M.; Suntzeff, N.B.; Freedman, W.L.; Brown, P.J.; Morrell, N.; Hamuy, M.; Krisciunas, K.; Wang, L.; et al. Carnegie Supernova Project-I and -II: Measurements of H_0 using Cepheid, TRGB, and SBF Distance Calibration to Type Ia Supernovae. *arXiv* **2023**, arXiv:2308.01875.
132. Cardona, W.; Kunz, M.; Pettorino, V. Determining H_0 with Bayesian hyper-parameters. *J. Cosmol. Astropart. Phys.* **2017**, *2017*, 056. [CrossRef]
133. Camarena, D.; Marra, V. Local determination of the Hubble constant and the deceleration parameter. *Phys. Rev. Res.* **2020**, *2*. [CrossRef]
134. Dhawan, S.; Jha, S.W.; Leibundgut, B. Measuring the Hubble constant with Type Ia supernovae as near-infrared standard candles. *Astron. Astrophys.* **2018**, *609*, A72. [CrossRef]
135. Burns, C.R.; Parent, E.; Phillips, M.M.; Stritzinger, M.; Krisciunas, K.; Suntzeff, N.B.; Hsiao, E.Y.; Contreras, C.; Anais, J.; Boldt, L.; et al. The Carnegie Supernova Project: Absolute Calibration and the Hubble Constant. *Astrophys. J.* **2018**, *869*, 56. [CrossRef]
136. Follin, B.; Knox, L. Insensitivity of the distance ladder Hubble constant determination to Cepheid calibration modelling choices. *Mon. Not. R. Astron. Soc.* **2018**, *477*, 4534–4542. [CrossRef]
137. Feeney, S.M.; Mortlock, D.J.; Dalmaso, N. Clarifying the Hubble constant tension with a Bayesian hierarchical model of the local distance ladder. *Mon. Not. R. Astron. Soc.* **2018**, *476*, 3861–3882. [CrossRef]

138. Freedman, W.L.; Madore, B.F.; Hoyt, T.; Jang, I.S.; Beaton, R.; Lee, M.G.; Monson, A.; Neeley, J.; Rich, J. Calibration of the Tip of the Red Giant Branch. *Astrophys. J.* **2020**, *891*, 57. [CrossRef]
139. Freedman, W.L. Measurements of the Hubble Constant: Tensions in Perspective. *Astrophys. J.* **2021**, *919*, 16. [CrossRef]
140. Jang, I.S.; Lee, M.G. The Tip of the Red Giant Branch Distances to Typa Ia Supernova Host Galaxies. V. NGC 3021, NGC 3370, and NGC 1309 and the Value of the Hubble Constant. *Astrophys. J.* **2017**, *836*, 74. [CrossRef]
141. Yuan, W.; Riess, A.G.; Macri, L.M.; Casertano, S.; Scolnic, D.M. Consistent Calibration of the Tip of the Red Giant Branch in the Large Magellanic Cloud on the Hubble Space Telescope Photometric System and a Redetermination of the Hubble Constant. *Astrophys. J.* **2019**, *886*, 61. [CrossRef]
142. Kim, Y.J.; Kang, J.; Lee, M.G.; Jang, I.S. Determination of the Local Hubble Constant from Virgo Infall Using TRGB Distances. *Astrophys. J.* **2020**, *905*, 104. [CrossRef]
143. Jones, D.O.; Mandel, K.S.; Kirshner, R.P.; Thorp, S.; Challis, P.M.; Avelino, A.; Brout, D.; Burns, C.; Foley, R.J.; Pan, Y.C.; et al. Cosmological Results from the RAISIN Survey: Using Type Ia Supernovae in the Near Infrared as a Novel Path to Measure the Dark Energy Equation of State. *Astrophys. J.* **2022**, *933*, 172. [CrossRef]
144. Dhawan, S.; Goobar, A.; Johansson, J.; Jang, I.S.; Rigault, M.; Harvey, L.; Maguire, K.; Freedman, W.L.; Madore, B.F.; Smith, M.; et al. A Uniform Type Ia Supernova Distance Ladder with the Zwicky Transient Facility: Absolute Calibration Based on the Tip of the Red Giant Branch Method. *Astrophys. J.* **2022**, *934*, 185. [CrossRef]
145. Scolnic, D.; Riess, A.G.; Wu, J.; Li, S.; Anand, G.S.; Beaton, R.; Casertano, S.; Anderson, R.; Dhawan, S.; Ke, X. CATS: The Hubble Constant from Standardized TRGB and Type Ia Supernova Measurements. *Astrophys. J. Lett.* **2023**, *954*, L31. [CrossRef]
146. Khetan, N.; Izzo, L.; Branchesi, M.; Wojtak, R.; Cantiello, M.; Murugesan, C.; Agnello, A.; Cappellaro, E.; Valle, M.D.; Gall, C.; et al. A new measurement of the Hubble constant using Type Ia supernovae calibrated with surface brightness fluctuations. *Astron. Astrophys.* **2021**, *647*, A72. [CrossRef]
147. Cantiello, M.; Jensen, J.B.; Blakeslee, J.P.; Berger, E.; Levan, A.J.; Tanvir, N.R.; Raimondo, G.; Brocato, E.; Alexander, K.D.; Blanchard, P.K.; et al. A Precise Distance to the Host Galaxy of the Binary Neutron Star Merger GW170817 Using Surface Brightness Fluctuations. *Astrophys. J.* **2018**, *854*, L31. [CrossRef]
148. de Jaeger, T.; Galbany, L.; Riess, A.G.; Stahl, B.E.; Shappee, B.J.; Filippenko, A.V.; Zheng, W. A 5% measurement of the Hubble-Lemaître constant from Type II supernovae. *Mon. Not. R. Astron. Soc.* **2022**, *514*, 4620–4628. [CrossRef]
149. Schombert, J.; McGaugh, S.; Lelli, F. Using the Baryonic Tully-Fisher Relation to Measure H_0 . *Astron. J.* **2020**, *160*, 71. [CrossRef]
150. Kourkchi, E.; Tully, R.B.; Courtois, H.M.; Dupuy, A.; Guinet, D. Cosmicflows-4: The baryonic Tully-Fisher relation providing ~ 10000 distances. *Mon. Not. R. Astron. Soc.* **2022**, *511*, 6160–6178. [CrossRef]
151. Bonvin, V.; Courbin, F.; Suyu, S.H.; Marshall, P.J.; Rusu, C.E.; Sluse, D.; Tewes, M.; Wong, K.C.; Collett, T.; Fassnacht, C.D.; et al. H0LiCOW V. New COSMOGRAIL time delays of HE 0435-1223: H_0 to 3.8% precision from strong lensing in a flat Λ CDM model. *Mon. Not. R. Astron. Soc.* **2016**, *465*, 4914–4930. [CrossRef]
152. Birrer, S.; Treu, T.; Rusu, C.E.; Bonvin, V.; Fassnacht, C.D.; Chan, J.H.H.; Agnello, A.; Shajib, A.J.; Chen, G.C.F.; Auger, M.; et al. H0LiCOW IX. Cosmographic analysis of the doubly imaged quasar SDSS 1206+332 and a new measurement of the Hubble constant. *Mon. Not. R. Astron. Soc.* **2019**, *484*, 4726–4753. [CrossRef]
153. Wong, K.C.; Suyu, S.H.; Chen, G.C.F.; Rusu, C.E.; Millon, M.; Sluse, D.; Bonvin, V.; Fassnacht, C.D.; Taubenberger, S.; Auger, M.W.; et al. H0LiCOW-XIII. A 2.4 per cent measurement of H_0 from lensed quasars: 5.3σ tension between early- and late-Universe probes. *Mon. Not. R. Astron. Soc.* **2019**, *498*, 1420–1439. [CrossRef]
154. Millon, M.; Galan, A.; Courbin, F.; Treu, T.; Suyu, S.H.; Ding, X.; Birrer, S.; Chen, G.C.F.; Shajib, A.J.; Sluse, D.; et al. TDCOSMO. *Astron. Astrophys.* **2020**, *639*, A101. [CrossRef]
155. Krishnan, C.; Mohayaee, R.; Colgáin, E.Ó.; Sheikh-Jabbari, M.M.; Yin, L. Does Hubble tension signal a breakdown in FLRW cosmology? *Class. Quantum Gravity* **2021**, *38*, 184001. [CrossRef]
156. Verde, L.; Treu, T.; Riess, A.G. Tensions between the early and late Universe. *Nat. Astron.* **2019**, *3*, 891–895. [CrossRef]
157. Di Valentino, E. A combined analysis of the H_0 late time direct measurements and the impact on the Dark Energy sector. *Mon. Not. R. Astron. Soc.* **2021**, *502*, 2065–2073. [CrossRef]
158. Hinshaw, G.; Larson, D.; Komatsu, E.; Spergel, D.N.; Bennett, C.L.; Dunkley, J.; Nolte, M.R.; Halpern, M.; Hill, R.S.; Odegard, N.; et al. Nine-Year Wilkinson Microwave Anisotropy Probe (WMAP) Observations: Cosmological Parameter Results. *Astrophys. J. Suppl. Ser.* **2013**, *208*, 19. [CrossRef]
159. Aiola, S.; Calabrese, E.; Maurin, L.; Naess, S.; Schmitt, B.L.; Abitbol, M.H.; Addison, G.E.; Ade, P.A.R.; Alonso, D.; Amiri, M.; et al. The Atacama Cosmology Telescope: DR4 maps and cosmological parameters. *J. Cosmol. Astropart. Phys.* **2020**, *2020*, 047. [CrossRef]
160. Dutcher, D.; Balkenhol, L.; Ade, P.; Ahmed, Z.; Anderes, E.; Anderson, A.; Archibley, M.; Avva, J.; Aylor, K.; Barry, P.; et al. Measurements of the E-Mode Polarization and Temperature-E-Mode Correlation of the CMB from SPT-3G 2018 Data. *Phys. Rev. D* **2021**, *104*, 022003. [CrossRef]
161. Eisenstein, D.J.; Zehavi, I.; Hogg, D.W.; Scoccimarro, R.; Blanton, M.R.; Nichol, R.C.; Scranton, R.; Seo, H.; Tegmark, M.; Zheng, Z.; et al. Detection of the Baryon Acoustic Peak in the Large-Scale Correlation Function of SDSS Luminous Red Galaxies. *Astrophys. J.* **2005**, *633*, 560–574. [CrossRef]

162. Beutler, F.; Blake, C.; Colless, M.; Jones, D.H.; Staveley-Smith, L.; Campbell, L.; Parker, Q.; Saunders, W.; Watson, F. The 6dF Galaxy Survey: Baryon acoustic oscillations and the local Hubble constant. *Mon. Not. R. Astron. Soc.* **2011**, *416*, 3017–3032. [CrossRef]
163. Blake, C.; Brough, S.; Colless, M.; Contreras, C.; Couch, W.; Croom, S.; Croton, D.; Davis, T.M.; Drinkwater, M.J.; Forster, K.; et al. The WiggleZ Dark Energy Survey: Joint measurements of the expansion and growth history at $z < 1$. *Mon. Not. R. Astron. Soc.* **2012**, *425*, 405–414. [CrossRef]
164. du Mas des Bourboux, H.; Rich, J.; Font-Ribera, A.; de Sainte Agathe, V.; Farr, J.; Etourneau, T.; Goff, J.M.L.; Cuceu, A.; Balland, C.; Bautista, J.E.; et al. The Completed SDSS-IV Extended Baryon Oscillation Spectroscopic Survey: Baryon Acoustic Oscillations with Ly α Forests. *Astrophys. J.* **2020**, *901*, 153. [CrossRef]
165. Alam, S.; Aubert, M.; Avila, S.; Balland, C.; Bautista, J.E.; Bershad, M.A.; Bizyaev, D.; Blanton, M.R.; Bovy, A.S.B.J.; Brinkmann, J.; et al. Completed SDSS-IV extended Baryon Oscillation Spectroscopic Survey: Cosmological implications from two decades of spectroscopic surveys at the Apache Point Observatory. *Phys. Rev. D* **2021**, *103*, 083553. [CrossRef]
166. Cooke, R.J.; Pettini, M.; Steidel, C.C. One Percent Determination of the Primordial Deuterium Abundance. *Astrophys. J.* **2018**, *855*, 102. [CrossRef]
167. Ivanov, M.M.; Simonović, M.; Zaldarriaga, M. Cosmological parameters from the BOSS galaxy power spectrum. *J. Cosmol. Astropart. Phys.* **2020**, *2020*, 042. [CrossRef]
168. d’Amico, G.; Gleyzes, J.; Kokron, N.; Markovic, K.; Senatore, L.; Zhang, P.; Beutler, F.; Gil-Marín, H. The cosmological analysis of the SDSS/BOSS data from the Effective Field Theory of Large-Scale Structure. *J. Cosmol. Astropart. Phys.* **2020**, *2020*, 005. [CrossRef]
169. Philcox, O.H.; Ivanov, M.M.; Simonović, M.; Zaldarriaga, M. Combining full-shape and BAO analyses of galaxy power spectra: A 1.6% CMB-independent constraint on H_0 . *J. Cosmol. Astropart. Phys.* **2020**, *2020*, 032. [CrossRef]
170. Ivanov, M.M. Cosmological constraints from the power spectrum of eBOSS emission line galaxies. *Phys. Rev. D* **2021**, *104*, 103514. [CrossRef]
171. Ivanov, M.M.; Philcox, O.H.; Simonović, M.; Zaldarriaga, M.; Nischimichi, T.; Takada, M. Cosmological constraints without nonlinear redshift-space distortions. *Phys. Rev. D* **2022**, *105*, 043531. [CrossRef]
172. Philcox, O.H.; Ivanov, M.M. The BOSS DR12 Full-Shape Cosmology: Λ CDM Constraints from the Large-Scale Galaxy Power Spectrum and Bispectrum Monopole. *Phys. Rev. D* **2022**, *105*, 043517. [CrossRef]
173. Chen, S.F.; Vlah, Z.; White, M. A new analysis of galaxy 2-point functions in the BOSS survey, including full-shape information and post-reconstruction BAO. *J. Cosmol. Astropart. Phys.* **2022**, *2022*, 008. [CrossRef]
174. Brieden, S.; Gil-Marín, H.; Verde, L. Model-independent versus model-dependent interpretation of the SDSS-III BOSS power spectrum: Bridging the divide. *Phys. Rev. D* **2021**, *104*, L121301. [CrossRef]
175. Dainotti, M.G.; Sarracino, G.; Capozziello, S. Gamma-ray bursts, supernovae Ia, and baryon acoustic oscillations: A binned cosmological analysis. *Publ. Astron. Soc. Jpn.* **2022**, *74*, 1095–1113. [CrossRef]
176. Bond, J.R.; Efstathiou, G. The statistics of cosmic background radiation fluctuations. *Mon. Not. R. Astron. Soc.* **1987**, *226*, 655–687. [CrossRef]
177. Eisenstein, D.J.; Hu, W. Baryonic Features in the Matter Transfer Function. *Astrophys. J.* **1998**, *496*, 605–614. [CrossRef]
178. Bashinsky, S.; Bertschinger, E. Position-Space Description of the Cosmic Microwave Background and Its Temperature Correlation Function. *Phys. Rev. Lett.* **2001**, *87*, 081301. [CrossRef] [PubMed]
179. Bassett, B.A.; Hlozek, R. Baryon Acoustic Oscillations. *arXiv* **2009**, arXiv:0910.5224.
180. Dawson, K.S.; Schlegel, D.J.; Ahn, C.P.; Anderson, S.F.; Aubourg, É.; Bailey, S.; Barkhouser, R.H.; Bautista, J.E.; Beifiori, A.; Berlind, A.A.; et al. The Baryon Oscillation Spectroscopic Survey of SDSS-III. *Astron. J.* **2013**, *145*, 10. [CrossRef]
181. Eisenstein, D.J.; Weinberg, D.H.; Agol, E.; Aihara, H.; Prieto, C.A.; Anderson, S.F.; Arns, J.A.; Aubourg, É.; Bailey, S.; Balbinot, E.; et al. SDSS-III: Massive Spectroscopic Surveys of the Distant Universe, the Milky Way Galaxy, and Extra-Solar Planetary Systems. *Astron. J.* **2011**, *142*, 72. [CrossRef]
182. Dawson, K.S.; Kneib, J.P.; Percival, W.J.; Alam, S.; Albareti, F.D.; Anderson, S.F.; Armengaud, E.; Aubourg, É.; Bailey, S.; Bautista, J.E.; et al. The SDSS-IV extended Baryon Oscillation Spectroscopic Survey: Overview and Early Data. *Astron. J.* **2016**, *151*, 44. [CrossRef]
183. Blanton, M.R.; Bershad, M.A.; Abolfathi, B.; Albareti, F.D.; Allende Prieto, C.; Almeida, A.; Alonso-García, J.; Anders, F.; Anderson, S.F.; Andrews, B.; et al. Sloan Digital Sky Survey IV: Mapping the Milky Way, Nearby Galaxies, and the Distant Universe. *Astrophys. J.* **2017**, *154*, 28. [CrossRef]
184. Ross, A.J.; Samushia, L.; Howlett, C.; Percival, W.J.; Burden, A.; Manera, M. The clustering of the SDSS DR7 main Galaxy sample—I. A 4 per cent distance measure at $z = 0.15$. *Mon. Not. R. Astron. Soc.* **2015**, *449*, 835–847. [CrossRef]
185. Aubourg, E.; Bailey, S.; Bautista, J.E.; Beutler, F.; Bhardwaj, V.; Bizyaev, D.; Blanton, M.; Blomqvist, M.; Bolton, A.S.; Bovy, J.; et al. Cosmological implications of baryon acoustic oscillation measurements. *Phys. Rev. D* **2015**, *92*, 123516. [CrossRef]
186. Abbott, B.P.; Abbott, R.; Abbott, T.; Acernese, F.; Ackley, K.; Adams, C.; Adams, T.; Addesso, P.; Adhikari, R.; Adya, V.; et al. GW170817: Observation of Gravitational Waves from a Binary Neutron Star Inspiral. *Phys. Rev. Lett.* **2017**, *119*, 161101. [CrossRef] [PubMed]

187. Guidorzi, C.; Margutti, R.; Brout, D.; Scolnic, D.; Fong, W.; Alexander, K.D.; Cowperthwaite, P.S.; Annis, J.; Berger, E.; Blanchard, P.K.; et al. Improved Constraints on H_0 from a Combined Analysis of Gravitational-wave and Electromagnetic Emission from GW170817. *Astrophys. J.* **2017**, *851*, L36. [CrossRef]
188. Soares-Santos, M.; Palmese, A.; Hartley, W.; Annis, J.; Garcia-Bellido, J.; Lahav, O.; Doctor, Z.; Fishbach, M.; Holz, D.E.; Lin, H.; et al. First Measurement of the Hubble Constant from a Dark Standard Siren using the Dark Energy Survey Galaxies and the LIGO/Virgo Binary-Black-hole Merger GW170814. *Astrophys. J.* **2019**, *876*, L7. [CrossRef]
189. Gayathri, V.; Healy, J.; Lange, J.; O'Brien, B.; Szczepanczyk, M.; Bartos, I.; Campanelli, M.; Klimentko, S.; Lousto, C.; O'Shaughnessy, R. Hubble Constant Measurement with GW190521 as an Eccentric Black Hole Merger. *arXiv* **2020**, arXiv:2009.14247.
190. Palmese, A.; Bom, C.R.; Mucesh, S.; Hartley, W.G. A Standard Siren Measurement of the Hubble Constant Using Gravitational-wave Events from the First Three LIGO/Virgo Observing Runs and the DESI Legacy Survey. *Astrophys. J.* **2023**, *943*, 56. [CrossRef]
191. Jimenez, R.; Cimatti, A.; Verde, L.; Moresco, M.; Wandelt, B. The local and distant Universe: Stellar ages and H_0 . *J. Cosmol. Astropart. Phys.* **2019**, *2019*, 043. [CrossRef]
192. Bernal, J.L.; Verde, L.; Jimenez, R.; Kamionkowski, M.; Valcin, D.; Wandelt, B.D. Trouble beyond H_0 and the new cosmic triangles. *Phys. Rev. D* **2021**, *103*, 103533. [CrossRef]
193. Boylan-Kolchin, M.; Weisz, D.R. Uncertain times: The redshift-time relation from cosmology and stars. *Mon. Not. R. Astron. Soc.* **2021**, *505*, 2764–2783. [CrossRef]
194. Vagnozzi, S.; Pacucci, F.; Loeb, A. Implications for the Hubble tension from the ages of the oldest astrophysical objects. *J. High Energy Astrophys.* **2022**, *36*, 27–35. [CrossRef]
195. Cimatti, A.; Moresco, M. Revisiting oldest stars as cosmological probes: New constraints on the Hubble constant. *arXiv* **2023**, arXiv:2302.07899.
196. Boylan-Kolchin, M. Stress testing Λ CDM with high-redshift galaxy candidates. *Nat. Astron.* **2023**, *7*, 731–735. [CrossRef]
197. Moresco, M.; Cimatti, A.; Jimenez, R.; Pozzetti, L.; Zamorani, G.; Bolzonella, M.; Dunlop, J.; Lamareille, F.; Mignoli, M.; Pearce, H.; et al. Improved constraints on the expansion rate of the Universe up to $z \sim 1.1$ from the spectroscopic evolution of cosmic chronometers. *J. Cosmol. Astropart. Phys.* **2012**, *2012*, 006. [CrossRef]
198. Holsclaw, T.; Alam, U.; Sansó, B.; Lee, H.; Heitmann, K.; Habib, S.; Higdon, D. Nonparametric reconstruction of the dark energy equation of state. *Phys. Rev. D* **2010**, *82*, 103502. [CrossRef]
199. Holsclaw, T.; Alam, U.; Sansó, B.; Lee, H.; Heitmann, K.; Habib, S.; Higdon, D. Nonparametric Dark Energy Reconstruction from Supernova Data. *Phys. Rev. Lett.* **2010**, *105*, 241302. [CrossRef]
200. Bargiacchi, G.; Risaliti, G.; Benetti, M.; Capozziello, S.; Lusso, E.; Saccardi, A.; Signorini, M. Cosmography by orthogonalized logarithmic polynomials. *Astron. Astrophys.* **2021**, *649*, A65. [CrossRef]
201. Amati, L.; Frontera, F.; Tavani, M.; in't Zand, J.J.M.; Antonelli, A.; Costa, E.; Feroci, M.; Guidorzi, C.; Heise, J.; Masetti, N.; et al. Intrinsic spectra and energetics of BeppoSAX Gamma-Ray Bursts with known redshifts. *Astron. Astrophys.* **2002**, *390*, 81–89. [CrossRef]
202. Ghirlanda, G.; Ghisellini, G.; Lazzati, D. The Collimation-corrected Gamma-Ray Burst Energies Correlate with the Peak Energy of Their νF_ν Spectrum. *Astrophys. J.* **2004**, *616*, 331–338. [CrossRef]
203. Dainotti, M.G.; Cardone, V.F.; Capozziello, S. A time-luminosity correlation for γ -ray bursts in the X-rays. *Mon. Not. R. Astron. Soc. Lett.* **2008**, *391*, L79–L83. [CrossRef]
204. Kumar, P.; Zhang, B. The physics of gamma-ray bursts and relativistic jets. *Phys. Rep.* **2015**, *561*, 1–109. [CrossRef]
205. Dainotti, M.G.; Lenart, A.L.; Sarracino, G.; Nagataki, S.; Capozziello, S.; Fraija, N. The X-ray Fundamental Plane of the Platinum Sample, the Kilonovae, and the SNe Ib/c Associated with GRBs. *Astrophys. J.* **2020**, *904*, 97. [CrossRef]
206. Cardone, V.F.; Capozziello, S.; Dainotti, M.G. An updated gamma-ray bursts Hubble diagram. *Mon. Not. R. Astron. Soc.* **2009**, *400*, 775–790. [CrossRef]
207. Cardone, V.F.; Dainotti, M.G.; Capozziello, S.; Willingale, R. Constraining cosmological parameters by gamma-ray burst X-ray afterglow light curves. *Mon. Not. R. Astron. Soc.* **2010**, *408*, 1181–1186. [CrossRef]
208. Amati, L.; D'Agostino, R.; Luongo, O.; Muccino, M.; Tantalò, M. Addressing the circularity problem in the Ep-Eiso correlation of gamma-ray bursts. *Mon. Not. R. Astron. Soc. Lett.* **2019**, *486*, L46–L51. [CrossRef]
209. Dainotti, M.G.; Lenart, A.L.; Chraya, A.; Sarracino, G.; Nagataki, S.; Fraija, N.; Capozziello, S.; Bogdan, M. The gamma-ray bursts fundamental plane correlation as a cosmological tool. *Mon. Not. R. Astron. Soc.* **2022**, *518*, 2201–2240. [CrossRef]
210. Bargiacchi, G.; Dainotti, M.G.; Nagataki, S.; Capozziello, S. Gamma-ray bursts, quasars, baryonic acoustic oscillations, and supernovae Ia: New statistical insights and cosmological constraints. *Mon. Not. R. Astron. Soc.* **2023**, *521*, 3909–3924. [CrossRef]
211. Dainotti, M.G.; Nielson, V.; Sarracino, G.; Rinaldi, E.; Nagataki, S.; Capozziello, S.; Gnedin, O.Y.; Bargiacchi, G. Optical and X-ray GRB Fundamental Planes as cosmological distance indicators. *Mon. Not. R. Astron. Soc.* **2022**, *514*, 1828–1856. [CrossRef]
212. Risaliti, G.; Lusso, E. A Hubble diagram for quasars. *Astrophys. J.* **2015**, *815*, 33. [CrossRef]
213. Risaliti, G.; Lusso, E. Cosmological Constraints from the Hubble Diagram of Quasars at High Redshifts. *Nat. Astron.* **2019**, *3*, 272–277. [CrossRef]
214. Bargiacchi, G.; Benetti, M.; Capozziello, S.; Lusso, E.; Risaliti, G.; Signorini, M. Quasar cosmology: Dark energy evolution and spatial curvature. *Mon. Not. R. Astron. Soc.* **2022**, *515*, 1795–1806. [CrossRef]

215. Lenart, A.L.; Bargiacchi, G.; Dainotti, M.G.; Nagataki, S.; Capozziello, S. A Bias-free Cosmological Analysis with Quasars Alleviating H_0 Tension. *Astrophys. J. Suppl. Ser.* **2023**, *264*, 46. [CrossRef]
216. Risaliti, G.; Lusso, E.; Nardini, E.; Bargiacchi, G.; Bisogni, S.; Sacchi, A.; Signorini, M.; Trefoloni, B. Quasars as high-redshift standard candles. *Astron. Nachrichten* **2023**, *344*, e230054. [CrossRef]
217. Signorini, M.; Risaliti, G.; Lusso, E.; Nardini, E.; Bargiacchi, G.; Sacchi, A.; Trefoloni, B. Quasars as standard candles. *Astron. Astrophys.* **2023**, *676*, A143. [CrossRef]
218. Dainotti, M.G.; Bargiacchi, G.; Lenart, A.L.; Nagataki, S.; Capozziello, S. Quasars: Standard Candles up to $z = 7.5$ with the Precision of Supernovae Ia. *Astrophys. J.* **2023**, *950*, 45. [CrossRef]
219. Psaltis, D. Probes and Tests of Strong-Field Gravity with Observations in the Electromagnetic Spectrum. *Living Rev. Relativ.* **2008**, *11*, 9. [CrossRef]
220. Feola, P.; Forteza, X.J.; Capozziello, S.; Cianci, R.; Vignolo, S. Mass-radius relation for neutron stars in $f(R) = R + \alpha R^2$ gravity: A comparison between purely metric and torsion formulations. *Phys. Rev. D* **2020**, *101*, 044037. [CrossRef]
221. Peebles, P.J.E.; Ratra, B. Cosmology with a Time-Variable Cosmological “Constant”. *Astrophys. J. Lett.* **1988**, *325*, L17. [CrossRef]
222. Ratra, B.; Peebles, P.J.E. Cosmological consequences of a rolling homogeneous scalar field. *Phys. Rev. D* **1988**, *37*, 3406–3427. [CrossRef]
223. Copeland, E.J.; Sami, M.; Tsujikawa, S. Dynamics Of Dark Energy. *Int. J. Mod. Phys. D* **2006**, *15*, 1753–1935. [CrossRef]
224. Chevallier, M.; Polarski, D. Accelerating Universes with Scaling Dark Matter. *Int. J. Mod. Phys. D* **2001**, *10*, 213–223. [CrossRef]
225. Linder, E.V. Exploring the Expansion History of the Universe. *Phys. Rev. Lett.* **2003**, *90*, 091301. [CrossRef]
226. Piedipalumbo, E.; Scudellaro, P.; Esposito, G.; Rubano, C. A matter-dominated cosmological model with variable G and Λ and its confrontation with observational data. *Gen. Relativ. Gravit.* **2012**, *44*, 2477–2501. [CrossRef]
227. Bonometto, S.; Mezzetti, M.; Mainini, R. Strongly coupled dark energy with warm dark matter vs. LCDM. *J. Cosmol. Astropart. Phys.* **2017**, *2017*, 011. [CrossRef]
228. Valentino, E.D.; Mena, O.; Pan, S.; Visinelli, L.; Yang, W.; Melchiorri, A.; Mota, D.F.; Riess, A.G.; Silk, J. In the realm of the Hubble tension—a review of solutions. *Class. Quantum Gravity* **2021**, *38*, 153001. [CrossRef]
229. Perivolaropoulos, L.; Skara, F. Challenges for Λ CDM: An update. *New Astron. Rev.* **2022**, *95*, 101659. [CrossRef]
230. Schöneberg, N.; Abellán, G.F.; Sánchez, A.P.; Witte, S.J.; Poulin, V.; Lesgourgues, J. The H_0 Olympics: A fair ranking of proposed models. *Phys. Rep.* **2022**, *984*, 1–55. [CrossRef]
231. Karwal, T.; Kamionkowski, M. Dark energy at early times, the Hubble parameter, and the string axiverse. *Phys. Rev. D* **2016**, *94*, 103523. [CrossRef]
232. Hill, J.C.; McDonough, E.; Toomey, M.W.; Alexander, S. Early dark energy does not restore cosmological concordance. *Phys. Rev. D* **2020**, *102*, 043507. [CrossRef]
233. Niedermann, F.; Sloth, M.S. New early dark energy is compatible with current LSS data. *Phys. Rev. D* **2021**, *103*, 103537. [CrossRef]
234. Mangano, G.; Miele, G.; Pastor, S.; Pinto, T.; Pisanti, O.; Serpico, P.D. Relic neutrino decoupling including flavour oscillations. *Nucl. Phys. B* **2005**, *729*, 221–234. [CrossRef]
235. Jacques, T.D.; Krauss, L.M.; Lunardini, C. Additional light sterile neutrinos and cosmology. *Phys. Rev. D* **2013**, *87*, 083515. [CrossRef]
236. Weinberg, S. Goldstone Bosons as Fractional Cosmic Neutrinos. *Phys. Rev. Lett.* **2013**, *110*, 241301. [CrossRef]
237. Allahverdi, R.; Cicoli, M.; Dutta, B.; Sinha, K. Correlation between dark matter and dark radiation in string compactifications. *J. Cosmol. Astropart. Phys.* **2014**, *2014*, 002. [CrossRef]
238. Valentino, E.D.; Giusarma, E.; Mena, O.; Melchiorri, A.; Silk, J. Cosmological limits on neutrino unknowns versus low redshift priors. *Phys. Rev. D* **2016**, *93*, 083527. [CrossRef]
239. Hart, L.; Chluba, J. New constraints on time-dependent variations of fundamental constants using Planck data. *Mon. Not. R. Astron. Soc.* **2017**, *474*, 1850–1861. [CrossRef]
240. Jedamzik, K.; Pogosian, L. Relieving the Hubble Tension with Primordial Magnetic Fields. *Phys. Rev. Lett.* **2020**, *125*, 181302. [CrossRef]
241. Bose, B.; Lombriser, L. Easing cosmic tensions with an open and hotter universe. *Phys. Rev. D* **2021**, *103*, L081304. [CrossRef]
242. Brevik, I.; Gorbunova, O. Dark energy and viscous cosmology. *Gen. Relativ. Gravit.* **2005**, *37*, 2039–2045. [CrossRef]
243. Wang, D.; Yan, Y.J.; Meng, X.H. A new pressure-parametrization unified dark fluid model. *Eur. Phys. J. C* **2017**, *77*, 263. [CrossRef]
244. Yang, W.; Pan, S.; Valentino, E.D.; Paliathanasis, A.; Lu, J. Challenging bulk viscous unified scenarios with cosmological observations. *Phys. Rev. D* **2019**, *100*, 103518. [CrossRef]
245. da Silva, W.J.C.; Silva, R. Growth of matter perturbations in the extended viscous dark energy models. *Eur. Phys. J. C* **2021**, *81*, 403. [CrossRef]
246. Khoury, J.; Weltman, A. Chameleon Fields: Awaiting Surprises for Tests of Gravity in Space. *Phys. Rev. Lett.* **2004**, *93*, 171104. [CrossRef] [PubMed]
247. Khoury, J.; Weltman, A. Chameleon cosmology. *Phys. Rev. D* **2004**, *69*, 044026. [CrossRef]
248. Vagnozzi, S.; Visinelli, L.; Brax, P.; Davis, A.C.; Sakstein, J. Direct detection of dark energy: The XENON1T excess and future prospects. *Phys. Rev. D* **2021**, *104*, 063023. [CrossRef]

249. Cai, R.G.; Guo, Z.K.; Li, L.; Wang, S.J.; Yu, W.W. Chameleon dark energy can resolve the Hubble tension. *Phys. Rev. D* **2021**, *103*, L121302. [CrossRef]
250. Benisty, D.; Davis, A.C. Dark energy interactions near the Galactic Center. *Phys. Rev. D* **2022**, *105*, 024052. [CrossRef]
251. Haba, Z.; Stachowski, A.; Szydlowski, M. Dynamics of the diffusive DM-DE interaction—Dynamical system approach. *J. Cosmol. Astropart. Phys.* **2016**, *2016*, 024. [CrossRef]
252. Koutsoumbas, G.; Ntreqis, K.; Papantonopoulos, E.; Saridakis, E.N. Unification of dark matter-dark energy in generalized Galileon theories. *J. Cosmol. Astropart. Phys.* **2018**, *2018*, 003. [CrossRef]
253. Calogero, S.; Velten, H. Cosmology with matter diffusion. *J. Cosmol. Astropart. Phys.* **2013**, *2013*, 025. [CrossRef]
254. Perez, A.; Sudarsky, D.; Wilson-Ewing, E. Resolving the H_0 tension with diffusion. *Gen. Relativ. Gravit.* **2021**, *53*, 7. [CrossRef]
255. Li, X.; Shafieloo, A. A Simple Phenomenological Emergent Dark Energy Model can Resolve the Hubble Tension. *Astrophys. J.* **2019**, *883*, L3. [CrossRef]
256. Pan, S.; Yang, W.; Valentino, E.D.; Shafieloo, A.; Chakraborty, S. Reconciling H_0 tension in a six parameter space? *J. Cosmol. Astropart. Phys.* **2020**, *2020*, 062. [CrossRef]
257. Rezaei, M.; Naderi, T.; Malekjani, M.; Mehrabi, A. A Bayesian comparison between Λ CDM and phenomenologically emergent dark energy models. *Eur. Phys. J. C* **2020**, *80*, 374. [CrossRef]
258. Solà, J. Cosmological constant and vacuum energy: Old and new ideas. *J. Phys. Conf. Ser.* **2013**, *453*, 012015. [CrossRef]
259. Solà, J.; Gómez-Valent, A. The $\bar{\Lambda}$ CDM cosmology: From inflation to dark energy through running Λ . *Int. J. Mod. Phys. D* **2015**, *24*, 1541003. [CrossRef]
260. Peracaula, J.S.; de Cruz Pérez, J.; Gómez-Valent, A. Possible signals of vacuum dynamics in the Universe. *Mon. Not. R. Astron. Soc.* **2018**, *478*, 4357–4373. [CrossRef]
261. Gómez-Valent, A.; Peracaula, J.S. Density perturbations for running vacuum: A successful approach to structure formation and to the σ_8 -tension. *Mon. Not. R. Astron. Soc.* **2018**, *478*, 126–145. [CrossRef]
262. Camarena, D.; Marra, V. Impact of the cosmic variance on H_0 on cosmological analyses. *Phys. Rev. D* **2018**, *98*, 023537. [CrossRef]
263. Bengaly, C.A.P.; Andrade, U.; Alcaniz, J.S. How does an incomplete sky coverage affect the Hubble Constant variance? *Eur. Phys. J. C* **2019**, *79*, 768. [CrossRef]
264. Krishnan, C.; Mohayaee, R.; Colgáin, E.O.; Sheikh-Jabbari, M.; Yin, L. Hints of FLRW breakdown from supernovae. *Phys. Rev. D* **2022**, *105*, 063514. [CrossRef]
265. Kalbouneh, B.; Marinoni, C.; Bel, J. Multipole expansion of the local expansion rate. *Phys. Rev. D* **2023**, *107*, 023507. [CrossRef]
266. Giani, L.; Howlett, C.; Said, K.; Davis, T.; Vagnozzi, S. An effective description of Laniakea: Impact on cosmology and the local determination of the Hubble constant. *J. Cosmol. Astropart. Phys.* **2024**, *2024*, 071. [CrossRef]
267. Helayël-Neto, J.A.; Spallicci, A.D.A.M. Frequency variation for *Vacuo* Photon Propag. Standard-Model Extension. *Eur. Phys. J. C* **2019**, *79*, 590. [CrossRef]
268. Bonetti, L.; dos Santos Filho, L.R.; Helayël-Neto, J.A.; Spallicci, A.D.A.M. Effective photon mass from Super and Lorentz symmetry breaking. *Phys. Lett. B* **2017**, *764*, 203. [CrossRef]
269. Bonetti, L.; dos Santos Filho, L.R.; Helayël-Neto, J.A.; Spallicci, A.D.A.M. Photon sector analysis of Super and Lorentz symmetry breaking: effective photon mass, bi-refringence and dissipation. *Eur. Phys. J. C* **2018**, *78*, 811. [CrossRef]
270. Goldhaber, A.S.; Nieto, M.M. Photon and graviton mass limits. *Rev. Mod. Phys.* **2010**, *82*, 939. [CrossRef]
271. Retinò, A.; Spallicci, A.D.A.M.; Vaivads, A. Solar wind test of the de Broglie-Proca massive photon with Cluster multi-spacecraft data. *Astropart. Phys.* **2016**, *82*, 49. [CrossRef]
272. de Broglie, L. *Nouvelles Recherches sur la Lumière*; Actualités Scientifiques et Industrielles; Hermann & Cie: Paris, France, 1936; Volume 411.
273. Proca, A. Sur les équations fondamentales des particules élémentaires. *C. R. Acad. Sci. Paris* **1936**, *202*, 1490.
274. Kumar Aluri, P.; Cea, P.; Chingangbam, P.; Chu, M.C.; Clowes, R.G.; Hutsemékers, D.; Kochappan, J.P.; Lopez, A.M.; Liu, L.; Martens, N.C.M.; et al. Is the observable Universe consistent with the cosmological principle? *Class. Quantum Gravity* **2023**, *40*, 094001. [CrossRef]
275. Krishnan, C.; Mondol, R.; Sheikh-Jabbari, M. Dipole cosmology: The Copernican paradigm beyond FLRW. *J. Cosmol. Astropart. Phys.* **2023**, *2023*, 020. [CrossRef]
276. Huang, C.D.; Riess, A.G.; Yuan, W.; Macri, L.M.; Zakamska, N.L.; Casertano, S.; Whitelock, P.A.; Hoffmann, S.L.; Filippenko, A.V.; Scolnic, D. Hubble Space Telescope Observations of Mira Variables in the SN Ia Host NGC 1559: An Alternative Candle to Measure the Hubble Constant. *Astrophys. J.* **2020**, *889*, 5. [CrossRef]
277. Farren, G.S.; Philcox, O.H.E.; Sherwin, B.D. Determining the Hubble constant without the sound horizon: Perspectives with future galaxy surveys. *Phys. Rev. D* **2022**, *105*, 063503. [CrossRef]
278. Yang, W.; Pan, S.; Vagnozzi, S.; Valentino, E.D.; Mota, D.F.; Capozziello, S. Dawn of the dark: Unified dark sectors and the EDGES Cosmic Dawn 21-cm signal. *J. Cosmol. Astropart. Phys.* **2019**, *2019*, 044. [CrossRef]
279. Bernardis, F.D.; Melchiorri, A.; Verde, L.; Jimenez, R. The cosmic neutrino background and the age of the Universe. *J. Cosmol. Astropart. Phys.* **2008**, *2008*, 020. [CrossRef]
280. Vandenberg, D.A.; Bolte, M.; Stetson, P.B. The Age of the Galactic Globular Cluster System. *Annu. Rev. Astron. Astrophys.* **1996**, *34*, 461–510. [CrossRef]
281. Soderblom, D.R. The Ages of Stars. *Annu. Rev. Astron. Astrophys.* **2010**, *48*, 581–629. [CrossRef]

282. Catelan, M. The ages of (the oldest) stars. *Proc. Int. Astron. Union* **2017**, *13*, 11–20. [CrossRef]
283. Valcin, D.; Bernal, J.L.; Jimenez, R.; Verde, L.; Wandelt, B.D. Inferring the age of the universe with globular clusters. *J. Cosmol. Astropart. Phys.* **2020**, *2020*, 002. [CrossRef]
284. Sazhin, M.V.; Sazhina, O.S.; Chadayammuri, U. The Scale Factor in the Universe with Dark Energy. *arXiv* **2011**, arXiv:astro-ph.CO/1109.2258.
285. Weinberg, E.J. Some problems with extended inflation. *Phys. Rev. D* **1989**, *40*, 3950–3959. [CrossRef]
286. Califano, M.; de Martino, I.; Vernieri, D.; Capozziello, S. Exploiting the Einstein Telescope to solve the Hubble tension. *Phys. Rev. D* **2023**, *107*, 123519. [CrossRef]
287. Califano, M.; de Martino, I.; Vernieri, D.; Capozziello, S. Constraining Λ CDM cosmological parameters with Einstein Telescope mock data. *Mon. Not. R. Astron. Soc.* **2022**, *518*, 3372–3385. [CrossRef]
288. Laureijs, R.; Amiaux, J.; Arduini, S.; Auguères, J.L.; Brinchmann, J.; Cole, R.; Cropper, M.; Dabin, C.; Duvet, L.; Ealet, A.; et al. Euclid Definition Study Report. *arXiv* **2011**, arXiv:astro-ph.CO/1110.3193.
289. Scaramella, R.; Amiaux, J.; Mellier, Y.; Burigana, C.; Carvalho, C.S.; Cuillandre, J.C.; Silva, A.D.; Derosa, A.; Dinis, J.; Maiorano, E.; et al. Euclid preparation. I. The Euclid Wide Survey. *Astron. Astrophys.* **2022**, *662*, A112. [CrossRef]
290. Blanchard, A.; Camera, S.; Carbone, C.; Cardone, V.F.; Casas, S.; Clesse, S.; Ilić, S.; Kilbinger, M.; Kitching, T.; Kunz, M.; et al. Euclid preparation. VII. Forecast validation for Euclid cosmological probes. *Astron. Astrophys.* **2020**, *642*, A191. [CrossRef]
291. Frusciante, N.; Pace, F.; Cardone, V.F.; Casas, S.; Tutusaus, I.; Ballardini, M.; Bellini, E.; Benevento, G.; Bose, B.; Valageas, P.; et al. Euclid: Constraining linearly scale-independent modifications of gravity with the spectroscopic and photometric primary probes. *arXiv* **2023**, arXiv:astro-ph.CO/2306.12368.
292. Casas, S.; Cardone, V.F.; Sapone, D.; Frusciante, N.; Pace, F.; Parimbelli, G.; Archidiacono, M.; Koyama, K.; Tutusaus, I.; Camera, S.; et al. Euclid: Constraints on $f(R)$ cosmologies from the spectroscopic and photometric primary probes. *arXiv* **2023**, arXiv:astro-ph.CO/2306.11053.
293. Bailey, A.C.; Vincenzi, M.; Scolnic, D.; Cuillandre, J.C.; Rhodes, J.; Hook, I.; Peterson, E.R.; Popovic, B. Type Ia supernova observations combining data from the Euclid mission and the Vera C. Rubin Observatory. *Mon. Not. R. Astron. Soc.* **2023**, *524*, 5432–5441. [CrossRef]
294. Joudaki, S.; Blake, C.; Heymans, C.; Choi, A.; Harnois-Deraps, J.; Hildebrandt, H.; Joachimi, B.; Johnson, A.; Mead, A.; Parkinson, D.; et al. CFHTLenS revisited: Assessing concordance with Planck including astrophysical systematics. *Mon. Not. R. Astron. Soc.* **2016**, *465*, 2033–2052. [CrossRef]
295. Abbott, T.; Aguena, M.; Alarcon, A.; Allam, S.; Alves, O.; Amon, A.; Andrade-Oliveira, F.; Annis, J.; Avila, S.; Bacon, D.; et al. Dark Energy Survey Year 3 results: Cosmological constraints from galaxy clustering and weak lensing. *Phys. Rev. D* **2022**, *105*, 023520. [CrossRef]
296. Di Valentino, E.; Melchiorri, A.; Silk, J. Planck evidence for a closed Universe and a possible crisis for cosmology. *Nat. Astron.* **2019**, *4*, 196–203. [CrossRef]
297. Challinor, A. CMB anisotropy science: A review. *Proc. Int. Astron. Union* **2012**, *8*, 42–52. [CrossRef]
298. Schwarz, D.J.; Copi, C.J.; Huterer, D.; Starkman, G.D. CMB anomalies after Planck. *Class. Quantum Gravity* **2016**, *33*, 184001. [CrossRef]
299. Akrami, Y.; Ashdown, M.; Aumont, J.; Baccigalupi, C.; Ballardini, M.; Banday, A.J.; Barreiro, R.B.; Bartolo, N.; Basak, S.; Benabed, K.; et al. Planck2018 results: VII. Isotropy and statistics of the CMB. *Astron. Astrophys.* **2020**, *641*, A7. [CrossRef]

Disclaimer/Publisher’s Note: The statements, opinions and data contained in all publications are solely those of the individual author(s) and contributor(s) and not of MDPI and/or the editor(s). MDPI and/or the editor(s) disclaim responsibility for any injury to people or property resulting from any ideas, methods, instructions or products referred to in the content.

Review

The Nature of Dark Energy and Constraints on Its Hypothetical Constituents from Force Measurements

Galina L. Klimchitskaya ^{1,2,*}  and Vladimir M. Mostepanenko ^{1,2,3} 

¹ Central Astronomical Observatory at Pulkovo of the Russian Academy of Sciences, 196140 Saint Petersburg, Russia; vmostepa@gmail.com

² Peter the Great Saint Petersburg Polytechnic University, 195251 Saint Petersburg, Russia

³ Kazan Federal University, 420008 Kazan, Russia

* Correspondence: g.klimchitskaya@gmail.com

Abstract: This review considers the theoretical approaches to the understanding of dark energy, which comprises approximately 68% of the energy of our Universe and explains the acceleration in its expansion. Following a discussion of the main approach based on Einstein's equations with the cosmological term, the explanations of dark energy using the concept of some kind of scalar field are elucidated. These include the concept of a quintessence and modifications of the general theory of relativity by means of the scalar–tensor gravity exploiting the chameleon, symmetron and environment-dependent dilaton fields and corresponding particles. After mentioning several laboratory experiments allowing us to constrain the hypothetical scalar fields modeling the dark energy, special attention is devoted to the possibility of constraining the parameters of chameleon, symmetron and environment-dependent dilaton fields from measuring the Casimir force. It is concluded that the parameters of each of these fields can be significantly strengthened in near future by using the next-generation setups in preparation suitable for measuring the Casimir force at larger separations.

Keywords: dark energy; cosmological constant; chameleon; symmetron; environment-dependent dilaton; Casimir force



Citation: Klimchitskaya, G.L.; Mostepanenko, V.M. The Nature of Dark Energy and Constraints on Its Hypothetical Constituents from Force Measurements. *Universe* **2024**, *10*, 119. <https://doi.org/10.3390/universe10030119>

Academic Editor: Gerald B. Cleaver

Received: 29 January 2024

Revised: 25 February 2024

Accepted: 28 February 2024

Published: 4 March 2024



Copyright: © 2024 by the authors. Licensee MDPI, Basel, Switzerland. This article is an open access article distributed under the terms and conditions of the Creative Commons Attribution (CC BY) license (<https://creativecommons.org/licenses/by/4.0/>).

1. Introduction

The concept of expanding Universe, which goes back to the Friedmann solutions of Einstein's equations published in 1922 [1] and 1924 [2], assumes that its expansion should decelerate with time due to the gravitational attraction of both visible and dark matter. It was a big surprise when, analyzing the redshift data of supernovae in binary systems, the two research teams independently found in 1998 that the Universe expansion is accelerating (see the pioneer Refs. [3,4] and reviews [5,6]).

If one wishes to explain the acceleration of the Universe expansion in the framework of the general theory of relativity, it is necessary to admit that there is an additional form of invisible matter with a positive energy density $\varepsilon > 0$, as it holds for both the usual and dark matter, but with a negative pressure, $P < 0$. Such a matter is characterized by the equation of state

$$P = -w\varepsilon, \quad (1)$$

where an acceleration in the expansion holds for $w > 1/3$. This kind of invisible matter violating the strong energy condition was called dark energy.

The advent of dark energy would not be so unusual if it constituted a small fraction of the total energy of the Universe. It turned out, however, that if one would like to preserve the standard cosmological scenario based on the general theory of relativity, the observational data demand that the dark energy constitutes about 68% of the Universe's energy [5,6]. When it is considered that the dark matter contributes approximately 27% of the Universe's energy, only 5% remains for the visible, baryonic, matter.

There are many theoretical approaches to the understanding of the nature of dark energy. These approaches can be grouped into four main divisions. The first of them describes dark energy by means of the cosmological constant Λ introduced into equations of the general theory of relativity by Einstein [7] for other purposes.

The second group of approaches to the description of dark energy considers it as some kind of classical time-varying scalar field called a quintessence. The cosmological applications of similar fields were considered in Refs. [8,9], whereas the term quintessence was introduced in Ref. [10].

The third group of approaches allows any change in the action and equations of the general theory of relativity by combining the metrical tensor with the classical scalar field within the formalism of scalar–tensor gravity in order to make the concept of dark energy unnecessary [11]. The chameleon field, symmetron field and the environment-dependent dilaton field were used in the literature for this purpose. Some of these approaches dispense with the need for either dark energy or dark matter (see, e.g., Ref. [12]). The modifications of the gravitational theory are also allowed in the unified models of dark matter and dark energy introducing the so-called dark fluid [13].

Note that the main ideas of the above three groups of approaches can be considered as based on the concepts of classical physics, although quantum physics was used in their further developments. As to the approaches of the fourth group aiming to understand the nature of dark energy, they consider it as composed of some hypothetical elementary particles with unusual physical properties that give rise to the negative pressure. The most popular particles of such kind are the chameleons, which possess a variable mass depending on the density of matter in the environment [14,15]. Another candidate for a dark energy particle is the symmetron whose interaction constant with the usual matter depends on the environmental density [16–18]. There are also other hypothetical particle candidates for the role of constituents of dark energy, e.g., the environment-dependent dilaton [19]. The classical fields with the variable masses and interaction constants were introduced in the third group of approaches mentioned above, whereas the unusual particles, such as chameleons, symmetrons, etc., are the result of their quantization.

In this review, we compare the approaches from the above four groups by the level of their credibility and discuss the main particle candidates for the role of dark energy constituents. Next, we pass to the constraints on the parameters of chameleon, symmetron and environment-dependent dilaton fields following from different laboratory experiments. The main attention is paid to the constraints that can be obtained from measuring the Casimir force arising between the closely spaced macroscopic bodies due to the zero-point and thermal fluctuations of the electromagnetic field.

There are also many alternative attempts to solve the dark energy issue, which are listed below for completeness. Thus, one can mention suggestions to consider modified gravity theories that introduce additional degrees of freedom in the gravitational and/or matter action [20,21]. It was also suggested to phenomenologically modify the Friedmann equation by additional terms that depend on the matter density in a nonlinear way [22–24]. Another option considered in the literature is to alter the mass–energy evolution equation with bulk viscosity terms [25–27].

Alternatively, some authors believe that dark energy may be only an apparent effect. They hypothesize that the supernovae data may be biased if the observer is located in a local underdense region (see, e.g., Ref. [28]) or suppose that the supernovae sources tend to be associated with overdensities (see, e.g., Ref. [29]). Finally, many papers focus on the role of matter inhomogeneities and anisotropies that may affect the cosmic expansion due to backreaction or statistical sampling effects (see, e.g., Refs. [30–34]).

The review is organized as follows. In Section 2, the theoretical approaches to understanding of the physical nature of dark energy based on classical physics are briefly considered and compared. Section 3 is devoted to a discussion of different particle candidates for the role of constituents of dark energy. The already obtained laboratory constraints on the parameters of chameleon, symmetron and environment-dependent dilaton fields,

as well as the prospective constraints obtainable from force measurements, including the Casimir force, are presented in Section 4. Section 5 contains the discussion and in Section 6 the reader will find our conclusions.

Below the relativistic units are used with $c = \hbar = 1$, where c is the speed of light and \hbar is the reduced Planck constant.

2. Approaches to Theoretical Description of Dark Energy Based on Classical Physics

As discussed in Section 1, there are three groups of such kind approaches to understanding of what the dark energy is and none of them is either excluded or finally confirmed.

We begin with probably the most common approach describing the accelerations in the Universe expansion on the basis of classical Einstein equations with the cosmological term

$$R_{ik} - \frac{1}{2}Rg_{ik} - \Lambda g_{ik} = 8\pi GT_{ik}, \tag{2}$$

where R_{ik} is the Ricci tensor, R is the scalar curvature of space-time, Λ is the cosmological constant, g_{ik} is the metrical tensor, G is the gravitational constant and T_{ik} is the stress–energy tensor of both visible and dark matter.

Equation (2) provides a very plausible explanation for the dark energy because in the homogenous isotropic 3-space of expanding Universe the metrical tensor is diagonal. Thus, raising the index k in Equation (2) and rearranging the cosmological term to the right-hand side of this equation, one obtains

$$R_i^k - \frac{1}{2}R\delta_i^k = 8\pi G \left(T_i^k + \frac{\Lambda}{8\pi G} \delta_i^k \right), \tag{3}$$

where δ_i^k is the Kronecker symbol. From this equation it is seen that the effective stress–energy tensor caused by the cosmological constant is

$$T_{(\Lambda)i}^k = \frac{\Lambda}{8\pi G} \delta_i^k. \tag{4}$$

Taking into account that in the homogeneous isotropic space for the stress–energy tensor of any kind of matter it holds [35]

$$T_0^0 = \varepsilon, \quad T_1^1 = T_2^2 = T_3^3 = -P, \tag{5}$$

where ε is the energy density and P is the pressure, one obtains from Equation (4) the energy density, pressure and equation of state of the dark energy resulting from the cosmological constant

$$\varepsilon_\Lambda = \frac{\Lambda}{8\pi G}, \quad P_\Lambda = -\frac{\Lambda}{8\pi G}, \quad P_\Lambda = -\varepsilon_\Lambda. \tag{6}$$

Thus, in this case, Equation (1) is satisfied with $w = w_\Lambda = 1$ in violation of the second inequality of the strong energy condition

$$\varepsilon + P \geq 0, \quad \varepsilon + 3P \geq 0 \tag{7}$$

valid for the usual and dark matter.

In spite of the fact that Equation (2) belongs to classical physics, it has long been understood [36] that the leading divergent term in the vacuum expectation values of the stress–energy tensor of quantized fields has the same geometric form as the cosmological term

$$\langle 0|T_{ik}|0\rangle = I_\infty g_{ik}, \tag{8}$$

where I_∞ is an infinitely large constant. This is valid in both the Minkowski space–time and in the curved background of expanding Universe [37,38] as can be seen, for instance, by the method of dimensional regularization [39].

From Equations (5) and (8), it follows that

$$\begin{aligned} \langle 0|T_0^0|0\rangle &= \varepsilon_{\text{vac}} = I_\infty, \\ \langle 0|T_1^1|0\rangle &= \langle 0|T_2^2|0\rangle = \langle 0|T_3^3|0\rangle = -P_{\text{vac}} = I_\infty, \end{aligned} \tag{9}$$

i.e., the equation of state of the quantum vacuum

$$P_{\text{vac}} = -\varepsilon_{\text{vac}} \tag{10}$$

is the same as due to the cosmological constant in Equation (6).

Thus, the vacuum stress–energy tensor of quantized fields could offer a plausible explanation for a generation of the cosmological constant. However, the great difficulty, called the vacuum catastrophe [40], arises from the infinitely large values of I_∞ , ε_{vac} and P_{vac} . Even if one makes a cutoff in the expression for I_∞ at the Planck momentum, the obtained energy density is of the order

$$\varepsilon_{\text{vac}} \sim 10^{111} \text{ J/m}^3. \tag{11}$$

At the same time, the observed acceleration in the Universe expansion demands the value of the cosmological constant in Equation (2)

$$\Lambda \approx 10^{-52} \text{ m}^{-2}. \tag{12}$$

This results in the corresponding value of the vacuum energy density

$$\varepsilon_\Lambda = \frac{\Lambda}{8\pi G} \sim 10^{-9} \text{ J/m}^3, \tag{13}$$

which is different by the factor of 10^{120} from the estimation of ε_{vac} in Equation (11) obtained from quantum field theory [6,41]. In Ref. [39], it was suggested to consider the value of Λ from Equation (12) as a renormalized value of the cosmological constant as opposed to the enormously large bare value

$$\Lambda_{\text{vac}} = 8\pi G\varepsilon_{\text{vac}} \sim 10^{68} \text{ m}^{-2}. \tag{14}$$

Some grounds for such an approach are given by the quantum field theory in curved space–time [37,38], but the rigorous justification could be reached only in the framework of quantum theory of gravitation which is not yet available.

In spite of this problem, the cosmological constant, whose value is determined experimentally like the values of all other fundamental constants, provides a pretty convincing explanation for the acceleration in the Universe expansion. In fact, Equation (2) including the cosmological term can be considered as entirely classical with no connection with the problem of quantum vacuum. As a result, the cosmological constant is commonly considered as one of the main elements of the standard cosmological model Lambda-CDM along with the cold dark matter formed by the nonrelativistic particles (axions, weakly interacting massive particles) and the usual barionic matter.

The second group of approaches to an explanation of the acceleration in the Universe expansion considers dark energy as a time-varying classical scalar field Φ called quintessence [8–10]. Unlike the dark energy described by the cosmological constant, where the quantity w in Equation (1) is constant, $w = 1$, for the quintessence w depends on the form of the field potential $V(\Phi)$ and may vary with time.

There are many models of the quintessence dark energy proposed in the literature (see, for instance, Refs. [42–49] and review [50]) using different forms of the potential

$V(\Phi)$ [10,43,44,50–56]. Typically the sum of the actions of the general theory of relativity and the quintessence field is chosen in the form

$$S = \int d^4x \sqrt{-g} \left[\frac{1}{16\pi G} R - \frac{1}{2} g^{ik} \frac{\partial \Phi}{\partial x^i} \frac{\partial \Phi}{\partial x^k} - V(\Phi) \right], \tag{15}$$

where g is the determinant of the metrical tensor and the interaction with the usual baryonic matter ψ is lacking. Because of this, the total action is the sum of S and the action of the baryonic matter $S_m[\psi]$.

In the space-time of expanding Universe the quantity w takes the form [50]

$$w \equiv w_\Phi = \frac{2V(\Phi) - \left(\frac{\partial \Phi}{\partial t}\right)^2}{2V(\Phi) + \left(\frac{\partial \Phi}{\partial t}\right)^2}. \tag{16}$$

It was shown that with the exponential potential [42,43,50]

$$V(\Phi) = V_q(\Phi) = V_0 e^{-\lambda \sqrt{8\pi G} \Phi}, \tag{17}$$

where $\lambda = \text{const}$, the equation of state of the quintessence dark energy approaches to Equation (1) with $w = w_q = 1 - \lambda^2/3$. As a result, the quintessence approach to the dark energy becomes capable to make approximately the same theoretical predictions for the accelerated expansion of the Universe as the standard model using the cosmological constant.

Note also that in some models of a quintessence the quantity w defined in Equation (1) satisfies the inequality $w > 1$. This means that the kinetic energy of a quintessence field is negative leading to a catastrophic acceleration of the Universe expansion without bounds. As a result, the distances between individual particles, even inside an atom, go to infinity. In the literature, this is called the Big Rip caused by the phantom energy [57]. There are also models of kinetic quintessence with a nonstandard form of negative kinetic energy but $0 < w < 1$ [58]. The fact is worth mentioning that the concept of a quintessence field is used for a solution of the so-called coincidence problem, i.e., why the energy densities of dark matter and dark energy are of the same order of magnitude in the present epoch of cosmic history [44] (see also Refs. [36,41]).

The third group of theoretical approaches essentially based on the classical physics admits modifications of the general theory of relativity in such a way that an introduction of the dark energy could be obviated. The most well-known modification of the general theory of relativity is the scalar–tensor theory, which assumes that the gravitational interaction is determined by the combined action of the metrical tensor and the scalar field Φ (see the pioneering paper [59], reviews [60,61] and the monograph [62]).

The typical action of the scalar–tensor theory is the sum of the action defined in Equation (15) and the action of usual matter, S_m , which is, however, coupled with the field Φ in this case

$$S_{\text{int}} = S_{\text{int}}[A^2(\Phi)g_{ik}, \psi], \tag{18}$$

where $A(\Phi)$ is some function describing the coupling to matter. Thus, in the Brans–Dicke theory [59]

$$A(\Phi) = A_{\text{BD}}(\Phi) = e^{-\frac{\sqrt{\pi G}}{C} \Phi}, \tag{19}$$

where $C = \text{const}$.

Due to Equation (18) the effective potential depends on the usual matter. For example, for the dust-like matter with an energy density $T_0^0 = \varepsilon$ and $P = 0$, one has [11]

$$V_{\text{eff}}(\Phi) = V(\Phi) + \varepsilon, \quad \square \Phi = \frac{\partial V_{\text{eff}}(\Phi)}{\partial \Phi}. \tag{20}$$

Both the potential $V(\Phi)$ and the function $A(\Phi)$ take different forms in various models proposed in the literature [20]. Thus, the chameleon field with a choice [14,15,63]

$$\begin{aligned} V(\Phi) = V_{\text{ch}}(\Phi) &= \frac{M^{4+n}}{\Phi^n}, & A(\Phi) = A_{\text{ch}}(\Phi) &\approx 1 + C\sqrt{8\pi G}\Phi, \\ V_{\text{eff}}(\Phi) = V_{\text{eff, ch}}(\Phi) &= V_{\text{ch}}(\Phi) + C\sqrt{8\pi G}\varepsilon\Phi, \end{aligned} \tag{21}$$

where M is a parameter with the dimension of mass, n is an integer number, C is a constant of the order of unity, is used in the models of dark energy. The effective mass of chameleon field is larger in the regions of larger density, $m_{\Phi}^2 \sim \varepsilon^{(n+2)/(n+1)}$.

Another choice used in the models of dark energy is the symmetron field for which [17,18]

$$\begin{aligned} V(\Phi) = V_{\text{s}}(\Phi) &= -\frac{m^2}{2}\Phi^2 + \frac{\lambda}{4}\Phi^4, & A(\Phi) = A_{\text{s}}(\Phi) &\approx 1 + \frac{\Phi^2}{2M^2}, \\ V_{\text{eff}}(\Phi) = V_{\text{eff, s}}(\Phi) &= V_{\text{s}}(\Phi) + \varepsilon A(\Phi), \end{aligned} \tag{22}$$

where λ is the dimensionless constant of self-interaction and m is one more parameter with the dimension of mass. The coupling strength of the symmetron field to the usual matter is of the order of Φ/M . It is perceptible in the regions of low density $\varepsilon/M^2 \ll m^2$ and goes to zero in the regions of sufficiently high density $\varepsilon/M^2 > m^2$ [64].

Another class of modifications of the general theory of relativity replaces the standard action of this theory linear in R with a nonlinear one [62,65]

$$S = \frac{1}{16\pi G} \int d^4x \sqrt{-g} f(R) + \int d^4x \sqrt{-g} \mathcal{L}_M, \tag{23}$$

where \mathcal{L}_M is the Lagrangian density of the usual matter, $f(R)$ can be presented as a series expansion

$$f(R) = \dots + \frac{\beta_{-2}}{R^2} + \frac{\beta_{-1}}{R} + f(0) + R + \beta_2 R^2 + \dots, \tag{24}$$

and $f(0) = 2\Lambda$ is expressed via the cosmological constant.

As shown in Ref. [65], the function of the form $f \sim 1/R^n$ with $n > 0$ in Equation (23) can explain the observed acceleration in the Universe expansion. It was shown, however, that the theories described by the action (23) are in fact the versions of the scalar–tensor theories of gravity considered above [66,67]. Thus, the dynamically equivalent action to (23) written in terms of an additional scalar field χ is

$$S = \frac{1}{16\pi G} \int d^4x \sqrt{-g} [f(\chi) + f'(\chi)(R - \chi)] + \int d^4x \sqrt{-g} \mathcal{L}_M. \tag{25}$$

Really, the variation of this action with respect to χ results in the equation of motion

$$f''(\chi)(R - \chi) = 0, \tag{26}$$

where $f'(\chi) = \partial f(\chi)/\partial \chi$. This means that $\chi = R$ if $f''(\chi) \neq 0$ and Equation (25) reduces to Equation (23).

Next, by introducing one more scalar field $\Phi = f'(\chi)$, one can transform the action (23) to the action of a Brans–Dicke theory with the potential [67]

$$V(\Phi) = \chi(\Phi)\Phi - f(\chi(\Phi)). \tag{27}$$

This means that any constraints obtained for a chameleon or symmetron fields from measuring the Casimir force (see Section 4) can be reformulated as the corresponding constraints on the function $f'(R)$ known as the scalaron field or, alternatively, as the

cosmological scalar field in theories of modified $f(R)$ gravity. The latter, however, is outside the scope of this review.

A comprehensive review of these and many others theories of modified gravity and their applications to cosmology is given in Ref. [20].

As is seen from the above, both the second and third groups of approaches to the theoretical description of an acceleration in the Universe expansion are heavily based on the consideration of some hypothetical scalar field whose form of potential, the function describing an interaction with matter and some parameters are not fixed uniquely. In this sense, the first approach exploiting the cosmological term in Einstein's equations seems preferable because it operates with only one parameter, the cosmological constant, which can be considered as a fundamental constant like the electric charge, speed of light, Planck constant etc. In the next section we discuss what could be added to this situation by the quantum theory, which brings an interpretation of the classical scalar fields used in the models considered above in terms of particles.

3. Particle Candidates for the Role of Constituents of Dark Energy

As discussed in previous section, the classical chameleon and symmetron fields were introduced in the context of modified gravity. This makes their immediate quantization problematic because the consistent quantum theory related to the standard part of gravitation described by the metrical tensor is not yet available. For this reason, the action of the form of Equation (15) or the sum of Equations (15) and (18) cannot be directly presented in the operator form.

It is possible, however, to consider the action of a scalar field Φ and its interaction with the matter fields separately of the gravitational action containing the scalar curvature. In so doing, the metrical tensor in the action (18), describing an interaction of the matter fields with Φ , is understood as the usual function in the spirit of quantum field theory in curved space-time [37,38].

Using this approach, the chameleon field can be quantized and the resulting particles are called the chameleons. Then it is possible to consider the interaction of chameleons with the curved gravitational background and with the elementary particles of the Standard Model. Thus, the quantum corrections to the chameleon potential were investigated in Ref. [68]. The effect of production of chameleons from vacuum in the early Universe was considered in the linear approximation in Ref. [69] by the method of Bogoliubov transformations. It was shown that in the radiation dominated Universe this effect makes a strong impact on the Universe evolution.

In addition to interaction with the baryon particles, chameleons can be coupled to photons via the additional term of the form $\Phi F_{ik} F^{ik}$, where F_{ik} is the tensor of the electromagnetic field. This term is in fact the linear approximation to the exact interaction which contains the chameleon field in the exponent [70]

$$S_{\text{int, ch}} = -\frac{1}{4} \int d^4x e^{\frac{\Phi}{M}} F_{ik} F^{ik}, \tag{28}$$

where M is a fictitious mass controlling the coupling strength of chameleons to photons. Due to the interaction (28), chameleons can be turned to photons and vice versa in an external magnetic field.

Similar situation also holds as to the quantization of the symmetron field. If one considers its action separately from the action of gravitation, the symmetron field can be quantized with the metrical tensor g_{ik} being a classical function. The resulting quanta are called symmetrons. As discussed in Section 2, the coupling of symmetron field to the usual baryonic matter vanishes if the local energy density is large enough and is restored in the regions with sufficiently low energy density.

On the classical level, the symmetron field does not interact with the electromagnetic field. However, in the framework of quantum field theory, it was shown that quantum

corrections generate the interaction Lagrangian density between symmetrons and photons of the form [64,71]

$$\mathcal{L}_s = \frac{\Phi^2}{M^2} A_s^{-4} g^{ik} g^{ln} F_{il} F_{kn}, \tag{29}$$

where M is some new energy scale and $A_s = A_s(\Phi)$ is defined in Equation (22). This is the so-called axion-like coupling.

One more particle with unusual physical properties, which can be considered as a hypothetical constituent of dark energy, is the environment-dependent dilaton. The dilaton scalar field and its associated particles arise in many theoretical approaches beyond the Standard Model, e.g., in the extra-dimensional theories with a varied volume of compactified space, in the scalar–tensor theories of gravity, in string theory etc. (see, e.g., Refs. [62,72–74]).

Below we consider the model of an environment-dependent dilaton field which is formulated in the context of scalar–tensor gravity. In fact this field combines the properties of the quintessence, chameleon and symmetron fields. Thus, similar to the chameleon and symmetron fields, it is described by the sum of actions defined in Equations (15) and (18). The function A describing the coupling of an environment-dependent dilaton to matter is of the same form as was discussed for symmetrons in Equation (22) [75,76]

$$A_d(\Phi) = 1 + \frac{A_0}{2M^2} (\Phi - \Phi_0)^2, \tag{30}$$

where Φ_0 is the current value of the dilaton field and A_0 is a constant.

As to the dilaton potential, it takes the exponential form [75,76] like for the quintessence field [see Equation (17)]

$$V_d(\Phi) = V_0 e^{-\lambda\sqrt{8\pi G}\Phi}, \tag{31}$$

as opposed to the power-type potentials (21) and (22) for the chameleon and symmetron fields, respectively.

In the regions of space with sufficiently high density of matter, it holds $\Phi \approx \Phi_0$ and the coupling of the dilaton field to matter becomes negligibly small, although in the regions with low density the coupling of the dilaton field to matter is of the order of gravitational strength. In this regard the environment-dependent dilaton behaves in the same way as the symmetron. Similar to chameleons, however, the effective mass of a dilaton increases with increasing density of the environment.

The quantization of the environment-dependent dilaton field can be performed under the same conditions as discussed above for the chameleon and symmetron fields. In addition to coupling with baryons, the dilaton particles can be coupled to photons. This coupling has the form of Equation (28), the same as for chameleons [77].

4. Constraints on the Particle Constituents of Dark Energy from Force Measurements

The hypothetical scalar fields (the chameleon, symmetron and environment-dependent dilaton) discussed in Sections 2 and 3 interact with the usual matter and can be constrained in the laboratory experiments in a number of ways. Thus, it was shown [78] that individual atoms inserted into large high-vacuum chamber do not screen the chameleon field and the force acting on them from this field can be measured by means of atom interferometry.

One more method for searching chameleon particles uses their interaction with the electromagnetic field. For observation of oscillations between the chameleon and photon states, the vacuum chamber was used where the magnetic field of 5 T was initiated [70]. As a result, in the plane (effective chameleon mass) \times (coupling to photon parameter), rather large region was excluded.

Strong limits on the parameters of chameleons were placed also by means of the gravity resonance spectroscopy used to measure the quantum states of ultracold neutrons confined near a mirror [79]. These limits are by the five orders of magnitude stronger than the previously known ones obtained from spectroscopic measurements [80].

The same methods can be used for searching and constraining the symmetrons and environment-dependent dilatons. For instance, in Refs. [81,82] it was shown that the parameters of symmetrons can be constrained by means of atom interferometry. As one more example, the possibility to constrain dilatons by measuring the dilaton–photon conversion in strong magnetic field was considered in Ref. [83] (see also the review [84] where several other possibilities are considered).

Constraints on the chameleon, symmetron and dilaton fields and respective particles can be obtained not only from the laboratory experiments mentioned above but from astrophysics and cosmology as well. One can mention constraints found from galaxy clusters' thermodynamic profiles, gravitational lensing and caustic techniques [85–88]. Specifically, the amplitude of the chameleon field and its coupling strength to matter were constrained by combining the gas and lensing measurements of the cluster [85]. The upper limits on the strength of chameleon force were placed by comparing X-ray and weak lensing profiles of the galaxy clusters [86]. It should be noted, however, that the constraints found from astrophysics and cosmology do not admit an immediate comparison with the laboratory constraints because the former unavoidably depend on some indefinite factors, whereas the latter are obtained in the fully controlled environments.

Below we concentrate our attention on constraining the parameters of chameleons, symmetrons and environment-dependent dilatons, which can be obtained from force measurements at short separations below a few micrometers. The point is that at such small distances between the material bodies the dominant force is not the gravitational one, but the Casimir force caused by the zero-point and thermal fluctuations of the electromagnetic field [89]. Precision measurements of the Casimir force have long been used for constraining the Yukawa-type corrections to Newton's law of gravitation and the interaction constant and mass of axions as the possible constituents of dark matter (see, e.g., Refs. [90–93] and reviews [94–96]).

The standard approach to obtaining constraints on some hypothetical force F_{hyp} from measuring the Casimir force is the following. According to the experimental data obtained over some separation interval, the theoretical expression for the Casimir force is confirmed within the total error ΔF , which includes the random and systematic experimental errors as well as possible theoretical uncertainties. The hypothetical force, e.g., from the Yukawa-type interaction or due to the axion exchange, is calculated in the experimental configuration as a function of separation and the parameters of this interaction. Since the hypothetical force was not observed, its magnitude is restricted by the inequality

$$|F_{\text{hyp}}(a)| < \Delta F(a), \quad (32)$$

where a is the value of separation. Then, by analyzing this inequality at different separations within the measurement interval, the strongest constraints on the parameters of hypothetical force are obtained [90–93,95].

This methodology can also be applied to the possible constituents of dark energy, such as chameleons, symmetrons and environment-dependent dilatons. The obtained results are considered in the following subsections.

4.1. Constraints on Chameleons from Measuring the Casimir Force

The possibility to constrain the chameleon parameters from measuring the Casimir force was proposed in Refs. [97,98] and further elaborated in Ref. [99]. Thus, in Ref. [99] the hypothetical force due to the presence of chameleons was calculated in the configurations of two parallel plates and a sphere above a plate. The latter configuration was used in all precise experiments on measuring the Casimir force [89].

As was noted in Section 2, different forms of the potential $V(\Phi)$ in Equation (15) have been proposed in the literature. The results of Ref. [99] are obtained with the most widely used potential of the form of Equation (21) and with the exponential potential

$$V_{\text{ch}}(\Phi) = \tilde{\Lambda}_0^4 e^{\frac{\tilde{\Lambda}_0^n}{\Phi^n}}. \tag{33}$$

The first term in the power expansion of Equation (33) corresponds to the vacuum energy density required for explanation of the accelerated expansion of the Universe and the second with $\tilde{\Lambda} = \tilde{\Lambda}_0 = M$ results in the potential (21).

Taking into account that the mass of the chameleon field strongly depends on the density of the environment, the macroscopic bodies are characterized by the so-called thin shells regarding this field [14,15]. Let the body have the density ρ_b and outside the body the density of matter is ρ_m . Then, deep inside the body,

$$\Phi \approx \Phi_b \equiv \Phi_{\text{min}}(\rho_b), \tag{34}$$

where the effective potential $V_{\text{eff}}(\Phi)$ reaches its minimum value at Φ_{min} . As to the region outside the body, there it holds

$$\Phi \approx \Phi_m \equiv \Phi_{\text{min}}(\rho_m). \tag{35}$$

According to Ref. [99], for the thin-shelled bodies almost all of the change from Φ_m to Φ_b happens in the thin shell near a surface of the body. It turned out that the hypothetical force due to the presence of chameleon field between the thin-shelled bodies is much weaker than for sufficiently thin bodies where the thin shell near the surface is not formed [97–99].

According to the analysis performed in Ref. [99], the test bodies used in measurements of the Casimir force (see Refs. [89,100] for a review) have the thin shells for the most realistic models of the chameleon field used in the literature. It was noted also [99] that if the thin shells in the test bodies are absent, all the constraints on Yukawa interaction obtained from measuring the Casimir force remain valid for the chameleon theories.

In Ref. [99], the chameleon force was calculated between two parallel plates and between a sphere and a plate with account of the effect of thin shells for the potentials of the form (21) and (33). As a result, rather wide regions were excluded in the plane (chameleon-to-matter coupling) \times (energy scale of chameleon potential) using the data of the most precise measurements of the Casimir force. For strengthening of the obtained constraints, it was suggested to perform measurements of the thermal Casimir force at larger separations and to use larger test bodies in order to avoid the effect of thin shells which decreases the magnitude of the chameleon force.

4.2. Constraints on a Symmetron Field from Measuring the Casimir Force

As discussed in Section 3, the coupling of the symmetron field to the barionic matter increases in the regions of low density and goes to zero with increasing density of matter. This field and the corresponding particles are described by the sum of actions (15) and (18), where the potential and the function $A(\Phi)$ describing the coupling to matter are given by Equation (22).

Constraints on the symmetron field following from measurements of the Casimir force can be obtained using the same methodology as described above in the case of a chameleon field. One should calculate the additional force caused by the symmetron field in the configuration of two plates or a sphere above a plate used in the Casimir experiments. If the theoretical expression for the Casimir force is confirmed by the measurement data in the limits of some error, then the magnitude of any additional force is restricted by this error.

In Ref. [101], the exact analytical solutions for the profiles of a symmetron field were found in the space near an infinite mirror occupying a semispace and between two such mirrors separated by a gap. The first of these solutions was applied for calculation of an additional frequency shift in the experiment measuring the reflection of ultracold neutrons

by a neutron mirror in the gravitational field of the Earth [102,103]. The second analytical solution concerning the case of two mirrors can be applied for calculation of the additional force induced by the symmetron field in the proposed CANNEX experiment on measuring the Casimir force between two parallel plates at separations up to 10 μm and more [104–106]. The principal scheme of the setup of this experiment, which is also discussed in Section 4.3, is shown in Figure 1 [104].

In the configuration of two parallel plates (like shown in Figure 1) and a sphere above a plate (up to now, the latter was used in the most precise measurements of the Casimir interaction) the additional force due to a symmetron field was calculated in Ref. [107]. For a sphere–plate geometry, these calculations were performed under the conditions $mR \ll 1$, $mR \sim 1$ and $mR \gg 1$, where m is the symmetron mass in the vacuum and R is the sphere radius, with account of the screening effects.

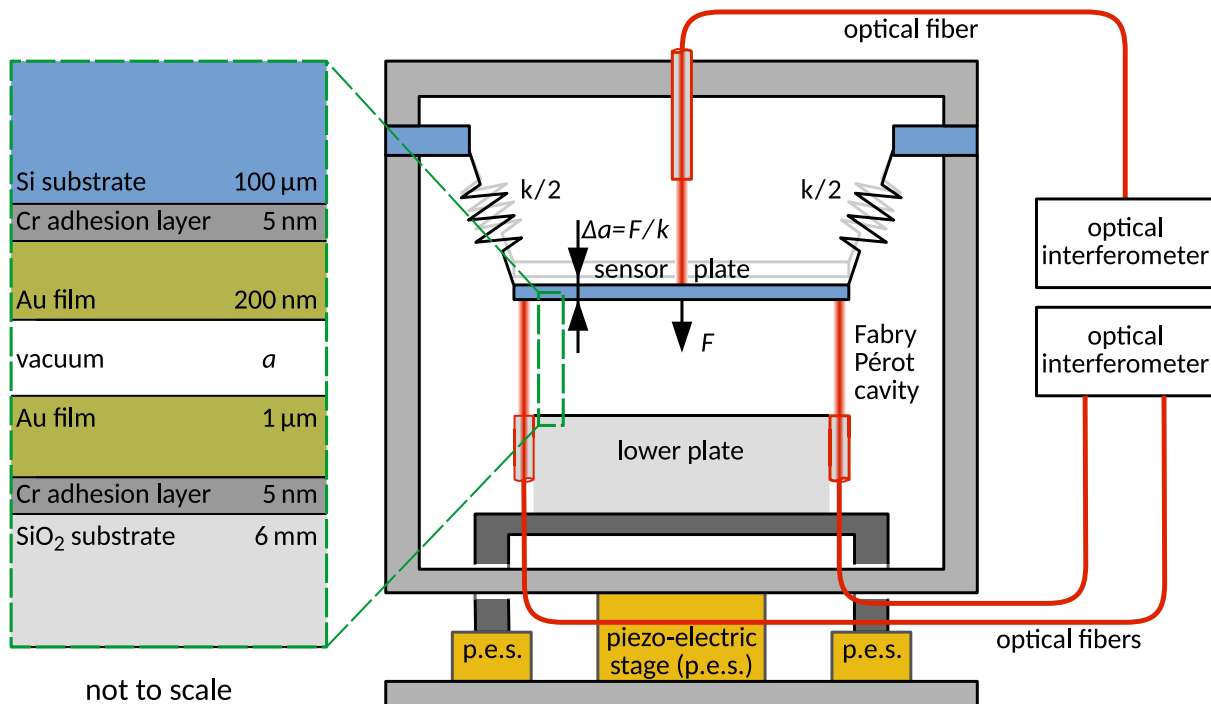


Figure 1. Schematic of the setup of CANNEX experiment for measuring the Casimir force between two parallel plates at large separations. The pressure between the fixed lower plate and the movable upper sensor plate separated by a distance a is measured by monitoring the extension Δa using the optical interferometer. The material structure of both the lower and upper plates is shown not to scale at the left of the figure.

In the case of two parallel plates of area S , it was found that at sufficiently small separations a between them satisfying the condition $am < \pi$ the additional symmetron force per plate area, i.e., the additional pressure, is given by [107]

$$P_s = \frac{F_s}{S} = -\frac{m^4}{4\lambda}. \tag{36}$$

At larger separations, the symmetron pressure goes to zero exponentially fast. These results are obtained for sufficiently dense plates with $\epsilon \gg m^2 M^2$, where M is the mass scale entering the effective potential in Equation (22). This condition allows us to put $\Phi \approx 0$ inside the plates.

When considering the sphere–plate configuration, it was also assumed that these bodies are sufficiently dense. Under this condition, for the spheres of large radii, $R \gg m^{-1}$, the following approximate expressions for the additional symmetron force were obtained [107]

$$\begin{aligned}
 F_s &= -\frac{m^4}{4\lambda} \pi R^2, & a < \frac{\pi}{m} - R, \\
 F_s &= -\frac{m^4}{4\lambda} \pi \left(\frac{\pi}{m} - a\right) \left(2R + a - \frac{\pi}{m}\right), & \frac{\pi}{m} - R < a < \frac{\pi}{m}, \\
 F_s &= 0, & a > \frac{\pi}{m},
 \end{aligned}
 \tag{37}$$

where a is the closest sphere–plate separation.

The approximate analytic calculation of F_s is also possible for the spheres of small radii $R \ll m^{-1}$ above a plate. The result is [107]

$$F_s = -\frac{4\pi m^3 R}{\sqrt{2}\lambda} \tanh\frac{m(a+R)}{\sqrt{2}} \operatorname{sech}^2\frac{m(a+R)}{\sqrt{2}}.
 \tag{38}$$

As is seen from Equation (38), in the limiting case $a \rightarrow 0$, i.e., when the sphere approaches the plate, the magnitude of the symmetron force decreases to

$$|F_s| = \frac{2\pi}{\lambda} m^2 (mR)^2,
 \tag{39}$$

where $mR \ll 1$ in this case.

In the region of intermediate values of the sphere radius $mR \sim 1$, the additional force due to the symmetron field was computed numerically [107].

For obtaining constraints on the parameters of a symmetron field, it was suggested [107] to use a setup similar to that of Ref. [108]. In the proposed setup, a sphere of $R = 150 \mu\text{m}$ radius is spaced at a distance $a = 15 \mu\text{m}$ from a rotating disk covered with rectangular trenches of $50 \mu\text{m}$ depth in high vacuum. As a result, the distance between the sphere bottom and the disk surface varies between $a_{\min} = 15 \mu\text{m}$ and $a_{\max} = 65 \mu\text{m}$. Taking into account that all the known forces at these separations are much smaller than the experimental error $\Delta F = 0.2 \text{ fN}$, the constraints on the symmetron force can be obtained from the inequality [107]

$$F_s(a_{\min}) - F_s(a_{\max}) = \pm \Delta F,
 \tag{40}$$

using the expressions for F presented above. The expected constraints which can be obtained in this way are discussed in Ref. [107].

4.3. Constraints on the Environment-Dependent Dilaton from Measuring the Casimir Force

The parameters of the environment-dependent dilaton can be constrained from the same experiments as the parameters of chameleon and symmetron. Thus, in Refs. [19,109] the dilaton parameters were constrained using the experimental data of Ref. [79] on measuring the quantum states of ultracold neutrons near a mirror. As discussed in Section 3, these data have already been used for constraining the parameters of a chameleon model.

In Ref. [19] it was also suggested to constrain the parameters of an environment-dependent dilaton from the CANNEX experiment (see Figure 1) on measuring the Casimir force between two parallel plates at large separations [104–106]. For this purpose, using the potential (31) and the coupling function (30), the exact solutions for a dilaton field were obtained in the configurations with one and two mirrors.

The additional dilaton pressure arising between two parallel plates with an effective area of 1 cm^2 was computed in Ref. [109] in application to the CANNEX experiment. In this experiment, it was assumed that the separation distance between the plates can be varied from 1.5 to $15 \mu\text{m}$. It was also suggested to vary the pressure around the plates by admitting Xe gas into the vacuum chamber. This option allows us to make the differential force measurements, which present many advantages in the case of an environment-dependent

force. As a result, the dilaton field between the plates and the corresponding additional pressure have been computed numerically under the condition

$$4\pi G A_0 \Phi^2 \ll 1. \quad (41)$$

This condition ensures that one can omit the coupling to matter of higher orders which is neglected in Equation (30).

Taking into account the planned sensitivity of the CANNEX experiment to force measurements equal to 0.1 nN/m^2 , the prospective constraints on the dilaton parameters λ and A_0 were obtained in Ref. [109] from an assumption that no extra forces in addition to the Casimir one were registered.

5. Discussion

In the foregoing, we have considered different models of dark energy, which makes up to approximately 68% of the total energy of the Universe. These models differ significantly in their physical meaning and theoretical background. In some sense, the model of dark energy using Einstein's equations with the cosmological term provides the most economic description of the dark energy which does not require any changes in the mathematical formalism of fundamental physical theories and introduction of additional physical substances with unusual properties. It follows that this model can be considered as preferable.

All the other types of models considered above, using the concepts of the quintessence, modified gravity and hypothetical particles with unusual physical properties, in any event are based on an introduction of some additional scalar field with one or other type of the interaction potential and the function describing its interaction with the baryonic matter. There are many models specifying these functions in the one way or another, and in each case much work should be done to reconcile the model properties with all the available data from different experiments and astrophysical observations.

It should be emphasized that the chameleon, symmetron and environment-dependent dilaton fields and corresponding particles are radically different from the particles and fields used in the Standard Model of elementary particle physics. The particles and fields introduced for the understanding of dark energy are not similar to those introduced, for instance, in different approaches to the theoretical description of dark matter. In fact, the hypothetical particle constituents of dark matter, such as axions or weakly interacting massive particles, can be understood as some extensions of the Standard Model. Axions, for instance, were introduced [110,111] for a resolution of the problem of strong CP violation in quantum chromodynamics with no relation to the concept of dark matter.

It might be well to point out that in the framework of quantum theory the explanation of dark energy in terms of the cosmological constant is burdened by the problem called the vacuum catastrophe (see Section 2) and the alternative explanations using a variety of scalar fields imply a departure from the well approved general theory of relativity in favor of the scalar-tensor theory. Because of this, one may expect that the final resolution of the problem of dark energy will be found only in the context of quantum theory of gravitation. Meantime any experimental constraints on the proposed models of dark energy are of much importance by guiding the most prospective ways for further progress in cosmology.

6. Conclusions

To conclude, none of the model approaches to understanding of the dark energy discussed above can be considered as fully satisfactory. This increases the role of experiment, which may not only confirm the theoretical predictions, but to place so strong constraints on the parameters of some model that it will become completely unusable. In this regard, the laboratory experiments are the most promising because all their parameters are under the strict control which is often not the case for astrophysical observations.

In the above, we mentioned several laboratory experiments aimed to constrain the parameters of chameleon, symmetron and environment-dependent dilaton fields, such as using the atom interferometry, the interaction of the hypothetical scalar fields with

the electromagnetic field and scattering of ultracold neutrons (see Section 4). The main attention, however, was devoted to the possibility of constraining the parameters of these scalar fields from precise measurements of the Casimir force.

As is shown in the literature reviewed in Section 4, the parameters of chameleon, symmetron and environment-dependent dilaton fields can be constrained from the experiments on measuring the Casimir force. The prospective constraints, which can be obtained in this way, are quite competitive, as compared to the other laboratory experiments. For obtaining these constraints, it will be necessary, however, to create the next generation of setups which will allow measuring the Casimir interaction at large separations up to 10 micrometers and even more.

This work is currently in progress. Its successful completion will allow us to not only place new more strong constraints on the models of dark energy, but also solve the remaining problems of the Casimir physics.

Author Contributions: Conceptualization, G.L.K. and V.M.M.; investigation, G.L.K. and V.M.M.; writing—original draft, V.M.M.; writing—review and editing, G.L.K. All authors have read and agreed to the published version of the manuscript.

Funding: This work was partially funded by the Ministry of Science and Higher Education of Russian Federation (“The World-Class Research Center: Advanced Digital Technologies”, contract No. 075-15-2022-311 dated 20 April 2022). The work of V.M.M. was also partially carried out in accordance with the Strategic Academic Leadership Program “Priority 2030” of the Kazan Federal University.

Institutional Review Board Statement: Not applicable.

Informed Consent Statement: Not applicable.

Data Availability Statement: No new data were created or analyzed in this study. Date sharing is not applicable to this article.

Conflicts of Interest: The authors declare no conflicts of interest.

References

1. Friedmann, A.A. Über die Krümmung des Raumes. *Z. Phys.* **1922**, *10*, 377–386. [CrossRef]
2. Friedmann, A.A. Über die Möglichkeit einer Welt mit konstanter negativer Krümmung des Raumes. *Z. Phys.* **1924**, *21*, 326–332. [CrossRef]
3. Riess, A.G.; Filippenko, A.V.; Challis, P.; Clocchiatti, A.; Diercks, A.; Garnavich, P.M.; Gilliland, R.L.; Hogan, C.J.; Jha, S.; Kirshner, R.P.; et al. Observational evidence from supernovae for an accelerating universe and a cosmological constant. *Astron. J.* **1998**, *116*, 1009–1038. [CrossRef]
4. Perlmutter, S.; Aldering, G.; Goldhaber, G.; Knop, R.A.; Nugent, P.; Castro, P.G.; Deustua, S.; Fabbro, S.; Goobar, A.; Groom, D.E.; et al. Measurements of Ω and Λ from 42 high-redshift supernovae. *Astrophys. J.* **1999**, *517*, 565–586. [CrossRef]
5. Peebles, P.J.E.; Ratra, B. The cosmological constant and dark energy. *Rev. Mod. Phys.* **2003**, *75*, 559–606. [CrossRef]
6. Frieman, J.A.; Turner, M.S.; Huterer, D. Dark energy and the accelerating universe. *Annu. Rev. Astron. Astrophys.* **2008**, *46*, 385–432. [CrossRef]
7. Einstein, A. Kosmologische Betrachtungen zur allgemeinen Relativitätstheorie. *Sitzungsber. K. Preuss. Akad. Wiss.* **1917**, *6*, 142–152.
8. Ratra, B.; Peebles, P.J.E. Cosmological consequences of a rolling homogeneous scalar field. *Phys. Rev. D* **1988**, *37*, 3406–3427. [CrossRef]
9. Wetterich, C. Cosmology and the fate of dilatation symmetry. *Nucl. Phys. B* **1988**, *302*, 668–696. [CrossRef]
10. Caldwell, R.R.; Dave, R.; Steinhardt, P.J. Cosmological Imprint of an Energy Component with General Equation of State. *Phys. Rev. Lett.* **1998**, *80*, 1582–1585. [CrossRef]
11. Joyce, A.; Lombriser, L.; Schmidt, F. Dark energy vs. modified gravity. *Ann. Rev. Nucl. Part. Sci.* **2016**, *66*, 95–122. [CrossRef]
12. Exirifard, Q. Phenomenological covariant approach to gravity. *Gen. Relat. Grav.* **2011**, *43*, 93–106. [CrossRef]
13. Arbey, A. Dark fluid: A complex scalar field to unify dark energy and dark matter. *Phys. Rev. D* **2006**, *74*, 043516. [CrossRef]
14. Khoury, J.; Weltman, A. Chameleon Fields: Awaiting Surprises for Tests of Gravity in Space. *Phys. Rev. Lett.* **2004**, *93*, 171104. [CrossRef] [PubMed]
15. Khoury, J.; Weltman, A. Chameleon cosmology. *Phys. Rev. D* **2004**, *69*, 044026. [CrossRef]
16. Olive, K.A.; Pospelov, M. Environmental dependence of masses and coupling constants. *Phys. Rev. D* **2008**, *77*, 043524. [CrossRef]
17. Hinterbichler, K.; Khoury, J. Screening Long-Range Forces through Local Symmetry Restoration. *Phys. Rev. Lett.* **2010**, *104*, 231301. [CrossRef]

18. Hinterbichler, K.; Khoury, J.; Levy, A.; Matas, A. Symmetron cosmology. *Phys. Rev. D* **2011**, *84*, 103521. [CrossRef]
19. Brax, P.; Fischer, H.; Käding, C.; Pitschmann, M. The environment dependent dilaton in the laboratory and the solar system. *Eur. Phys. J. C* **2022**, *82*, 934. [CrossRef]
20. Clifton, T.; Ferreira, P.G.; Padilla, A.; Skordis, C. Modified gravity and cosmology. *Phys. Rep.* **2012**, *513*, 1–189. [CrossRef]
21. Asimakis, P.; Basilakos, S.; Lymperis, A.; Petronikolou, M.; Saridakis, E.N. Modified gravity and cosmology with nonminimal direct or derivative coupling between matter and the Einstein tensor. *Phys. Rev. D* **2023**, *107*, 104006. [CrossRef]
22. Freese, K.; Lewis, M. Cardassian expansion: A model in which the universe is flat, matter dominated, and accelerating. *Phys. Lett. B* **2002**, *540*, 1–8. [CrossRef]
23. Xu, L. Revisiting Cardassian model and cosmic constraint. *Eur. Phys. J. C* **2012**, *72*, 2134. [CrossRef]
24. Magaña, J.; Amante, M.H.; Garcia-Aspeitia, M.A.; Motta, V. The Cardassian expansion revisited: Constraints from updated Hubble parameter measurements and type Ia supernova data. *Month. Not. Roy. Astr. Soc.* **2018**, *476*, 1036–1049. [CrossRef]
25. Lima, J.A.S.; Portugal, R.; Waga, I. Bulk-viscosity-driven asymmetric inflationary universe. *Phys. Rev. D* **1988**, *37*, 2755–2760. [CrossRef] [PubMed]
26. Breivik, I.; Elizalde, E.; Nojiri, S.; Odintsov, S.D. Viscous little rip cosmology. *Phys. Rev. D* **2011**, *84*, 103508. [CrossRef]
27. Herrera-Zamorano, L.; Hernández-Almada, A.; García-Aspeitia, M.A. Constraints and cosmography of CDM in presence of viscosity. *Eur. Phys. J. C* **2020**, *80*, 637. [CrossRef]
28. Célérier, M.-N. Do we really see a cosmological constant in the supernovae data? *Astron. Astrophys.* **2000**, *353*, 63–71.
29. Deledicque, V. Dark Energy Explained by a Bias in the Measurements. *Found. Phys.* **2022**, *52*, 57. [CrossRef]
30. Buchert, T.; Ehlers, J. Averaging inhomogeneous Newtonian cosmologies. *Astron. Astrophys.* **1997**, *320*, 1–7.
31. Wiltshire, D.L. Exact Solution to the Averaging Problem in Cosmology. *Phys. Rev. Lett.* **2007**, *99*, 251101. [CrossRef] [PubMed]
32. Kolb, E.W. Backreaction of inhomogeneities can mimic dark energy. *Class. Quant. Grav.* **2011**, *28*, 164009. [CrossRef]
33. Rácz, G.; Dobos, L.; Beck, R.; Szapudi, I.; Csabai, I. Concordance cosmology without dark energy. *Month. Not. Roy. Astr. Soc. Lett.* **2017**, *469*, L1–L5. [CrossRef]
34. Lapi, A.; Boco, L.; Cueli, M.M.; Haridasu, B.S.; Ronconi, T. Little ado about everything: η CDM, a cosmological model with fluctuation-driven acceleration at late times. *Astrophys. J.* **2023**, *959*, 83. [CrossRef]
35. Landau, E.M.; Lifshitz, E.M. *The Classical Theory of Fields*; Pergamon: Oxford, UK, 1971.
36. Zel'dovich, Y.B. The cosmological constant and the theory of elementary particles. *Uspekhi Fiz. Nauk* **1968**, *95*, 209–230; Translated: *Sov. Phys. Usp.* **1968**, *11*, 381–393. [CrossRef]
37. Birrell, N.D.; Davies, P.C.D. *Quantum Fields in Curved Space*; Cambridge University Press: Cambridge, UK, 1982.
38. Grib, A.A.; Mamayev, S.G.; Mostepanenko, V.M. *Vacuum Quantum Effects in Strong Fields*; Friedmann Laboratory Publishing: St. Petersburg, Russia, 1994.
39. Mostepanenko, V.M.; Klimchitskaya, G.L. Whether an enormously large energy density of the quantum vacuum is catastrophic. *Symmetry* **2019**, *11*, 314. [CrossRef]
40. Adler, R.J.; Casey, B.; Jacob, O.C. Vacuum catastrophe: An elementary exposition of the cosmological constant problem. *Am. J. Phys.* **1995**, *63*, 620–626. [CrossRef]
41. Weinberg, S. The cosmological constant problem. *Rev. Mod. Phys.* **1989**, *61*, 1–23. [CrossRef]
42. Ferreira, P.G.; Joyce, M. Cosmology with a primordial scaling field. *Phys. Rev. D* **1998**, *58*, 023503. [CrossRef]
43. Copeland, E.J.; Liddle, A.R.; Wands, D. Exponential potentials and cosmological scaling solutions. *Phys. Rev. D* **1998**, *57*, 4686–4690. [CrossRef]
44. Zlatev, I.; Wang, L.; Steinhardt, P.J. Quintessence, Cosmic Coincidence, and the Cosmological Constant. *Phys. Rev. Lett.* **1998**, *82*, 896–899. [CrossRef]
45. Choi, K. String or M theory axion as a quintessence. *Phys. Rev. D* **2000**, *62*, 043509. [CrossRef]
46. Scherrer, R.J.; Sen, A.A. Thawing quintessence with a nearly flat potential. *Phys. Rev. D* **2008**, *77*, 083515. [CrossRef]
47. Chiba, T. Slow-roll thawing quintessence. *Phys. Rev. D* **2009**, *79*, 083517. [CrossRef]
48. Panda, S.; Sumitomo, Y.; Trivedi, S.P. Axions as quintessence in string theory. *Phys. Rev. D* **2011**, *83*, 083506. [CrossRef]
49. Chiba, T.; De Felice, A.; Tsujikawa, S. Observational constraints on quintessence: Thawing, tracker, and scaling models. *Phys. Rev. D* **2013**, *87*, 083505. [CrossRef]
50. Tsujikawa, S. Quintessence: A review. *Class. Quant. Grav.* **2013**, *30*, 214003. [CrossRef]
51. Armendariz-Picon, C.; Mukhanov, V.; Steinhardt, P.J. Essentials of K-Essence. *Phys. Rev. D* **2001**, *63*, 103510. [CrossRef]
52. Kamenshchik, A.; Moschella, U.; Pasquier, V. An alternative to quintessence. *Phys. Lett. B* **2001**, *511*, 265–268. [CrossRef]
53. Corasaniti, P.S.; Copeland, E.J. Model independent approach to the dark energy equation of state. *Phys. Rev. D* **2003**, *67*, 063521. [CrossRef]
54. Dutta, S.; Scherrer, R.J. Hilltop quintessence. *Phys. Rev. D* **2008**, *78*, 123525. [CrossRef]
55. Chiba, T. Equation of state of tracker fields. *Phys. Rev. D* **2010**, *81*, 023515. [CrossRef]
56. Roy, N.; Bamba, K. Arbitrariness of potentials in interacting quintessence models. *Phys. Rev. D* **2019**, *99*, 123520. [CrossRef]
57. Caldwell, R.R.; Kamionkowski, M.; Weinberg, N.N. Phantom Energy: Dark Energy with $w < -1$ Causes a Cosmic Doomsday. *Phys. Rev. Lett.* **2003**, *91*, 071301.
58. Chiba, T.; Okabe, T.; Yamaguchi, M. Kinetically driven quintessence. *Phys. Rev. D* **2000**, *62*, 023511. [CrossRef]
59. Brans, C.; Dicke, R.H. Mach's principle and a relativistic theory of gravitation. *Phys. Rev.* **1961**, *124*, 925–935. [CrossRef]

60. Singh, T.; Singh, T. General class of scalar- tensor theories: A review. *Int. J. Mod. Phys. A* **1987**, *2*, 645–666. [CrossRef]
61. Quiros, I. Selected topics in scalar-tensor theories and beyond. *Int. J. Mod. Phys. D* **2019**, *28*, 1930012. [CrossRef]
62. Fujii, Y.; Maeda, K.-I. *The Scalar-Tensor Theory of Gravitation*; Cambridge University Press: Cambridge, UK, 2003.
63. Khoury, J. Chameleon field theories. *Class. Quant. Grav.* **2013**, *30*, 214004. [CrossRef]
64. Burrage, C.; Copeland, E.J.; Käding, C.; Millington, P. Symmetron scalar fields: Modified gravity, dark matter, or both? *Phys. Rev. D* **2019**, *99*, 043539. [CrossRef]
65. Carroll, S.M.; Duvvuri, V.; Trodden, M.; Turner, M.S. Is cosmic speed-up due to new gravitational physics? *Phys. Rev. D* **2004**, *70*, 043528. [CrossRef]
66. Chiba, T. 1/R gravity and scalar-tensor gravity. *Phys. Lett. B* **2003**, *575*, 1–3. [CrossRef]
67. Sotiriou, T.P.; Faraoni, V. $f(R)$ theories of gravity. *Rev. Mod. Phys.* **2010**, *82*, 451–498. [CrossRef]
68. Upadhye, A.; Hu, W.; Khoury, J. Quantum Stability of Chameleon Field Theories. *Phys. Rev. Lett.* **2012**, *109*, 041301. [CrossRef] [PubMed]
69. Erickcek, A.L.; Barnaby, N.; Burrage, C.; Huang, Z. Catastrophic Consequences of Kicking the Chameleon. *Phys. Rev. Lett.* **2013**, *110*, 171101. [CrossRef] [PubMed]
70. Chou, A.S.; Wester, W.; Baumbaugh, A.; Gustafson, H.R.; Irizarry-Valle, Y.; Mazur, P.O.; Steffen, J.H.; Tomlin, R.; Upadhye, A.; Weltman, A.; et al. Search for Chameleon Particles Using a Photon-Regeneration Technique. *Phys. Rev. Lett.* **2009**, *102*, 030402. [CrossRef] [PubMed]
71. Brax, P.; Burrage, C.; Davis, A.-C.; Seery, D.; Weltman, A. Anomalous coupling of scalars to gauge fields. *Phys. Lett. B* **2011**, *699*, 5–9. [CrossRef]
72. Damour, T.; Polyakov, A.M. The string dilaton and a least coupling principle. *Nucl. Phys. B* **1994**, *423*, 5–9. [CrossRef]
73. Berman, D.S.; Perry, M.J. M -theory and the string genus expansion. *Phys. Lett. B* **2006**, *635*, 131–135. [CrossRef]
74. Scott, T.C.; Zhang, X.; Mann, R.B.; Fee, G.J. Canonical reduction for dilatonic gravity in 3+1 dimensions. *Phys. Rev. D* **2016**, *93*, 084017. [CrossRef]
75. Joyce, A.; Jain, B.; Khoury, J.; Trodden, M. Beyond the cosmological standard model. *Phys. Rep.* **2015**, *568*, 1–98. [CrossRef]
76. Brax, P.; van de Bruck, C.; Davis, A.-C.; Li, B.; Shaw, D.J. Nonlinear structure formation with the environmentally dependent dilaton. *Phys. Rev. D* **2011**, *83*, 104026. [CrossRef]
77. Nojiri, S.; Odintsov, S.D. Conformal anomaly for dilaton coupled electromagnetic field. *Phys. Lett. B* **1998**, *426*, 29–35. [CrossRef]
78. Burrage, C.; Copeland, E.J.; Hinds, E.A. Probing dark energy with atom interferometry. *J. Cosmol. Astropart. Phys.* **2015**, *3*, 042. [CrossRef]
79. Jenke, T.; Cronenberg, G.; Burgdörfer, J.; Chizhova, L.A.; Geltenbort, P.; Ivanov, A.N.; Lauer, T.; Lins, T.; Rotter, S.; Saul, H.; et al. Gravity Resonance Spectroscopy Constrains Dark Energy and Dark Matter Scenarios. *Phys. Rev. Lett.* **2014**, *112*, 151105. [CrossRef] [PubMed]
80. Brax, P.; Pignol, G. Strongly Coupled Chameleons and the Neutronic Quantum Bouncer. *Phys. Rev. Lett.* **2011**, *107*, 111301. [CrossRef]
81. Burrage, C.; Kuribayashi-Coleman, A.; Stevenson, J.; Thrussell, B. Constraining symmetron fields with atom interferometry. *J. Cosmol. Astropart. Phys.* **2016**, *12*, 041. [CrossRef]
82. Chiow, S.-W.; Yu, N. Constraining symmetron dark energy using atom interferometry. *Phys. Rev. D* **2020**, *101*, 083501. [CrossRef]
83. Cho, Y.M.; Kim, J.H. Dilatonic dark matter and its experimental detection. *Phys. Rev. D* **2009**, *79*, 023504. [CrossRef]
84. Vardanyan, V.; Bartlett, D.J. Modeling and testing screening mechanisms in the laboratory and in space. *Universe* **2023**, *9*, 340 [CrossRef]
85. Terukina, A.; Lombriser, L.; Yamamoto, K.; Bacon, D.; Koyama, K.; Nichol, R.C. Testing chameleon gravity with the Coma cluster. *J. Cosm. Astropart. Phys.* **2014**, *2014*, 013. [CrossRef]
86. Wilcox, H.; Bacon, D.; Nichol, R.C.; Rooney, P.J.; Terukina, A.; Romer, A.K.; Koyama, K.; Zhao, G.B.; Hood, R.; Mann, R.G.; et al. The XMM Cluster Survey: Testing chameleon gravity using the profiles of clusters. *Month. Not. Roy. Astr. Soc.* **2015**, *452*, 1171–1183 [CrossRef]
87. Haridasu, B.S.; Karmakar, P.; De Petris, M.; Cardone, V.F.; Maoli, R. Testing generalized scalar-tensor theories of gravity with clusters of galaxies. *Phys. Rev. D* **2023**, *107*, 124059. [CrossRef]
88. Boumechta, Y.; Haridasu, B.S.; Pizzuti, L.; Butt, M.A.; Baccigalupi, C.; Lapi, A. Constraining chameleon screening using galaxy cluster dynamics. *Phys. Rev. D* **2023**, *108*, 044007. [CrossRef]
89. Bordag, M.; Klimchitskaya, G.L.; Mohideen, U.; Mostepanenko, V.M. *Advances in the Casimir Effect*; Oxford University Press: Oxford, UK, 2015.
90. Klimchitskaya, G.L.; Mostepanenko, V.M. Improved constraints on the coupling constants of axion-like particles to nucleons from recent Casimir-less experiment. *Eur. Phys. J. C* **2015**, *75*, 164. [CrossRef]
91. Klimchitskaya, G.L.; Mostepanenko, V.M. Constraints on axionlike particles and non-Newtonian gravity from measuring the difference of Casimir forces. *Phys. Rev. D* **2017**, *95*, 123013. [CrossRef]
92. Klimchitskaya, G.L. Recent breakthrough and outlook in constraining the non-Newtonian gravity and axion-like particles from Casimir physics. *Eur. Phys. J. C* **2017**, *77*, 315. [CrossRef]
93. Klimchitskaya, G.L.; Kuusk, P.; Mostepanenko, V.M. Constraints on non-Newtonian gravity and axionlike particles from measuring the Casimir force in nanometer separation range. *Phys. Rev. D* **2020**, *101*, 056013. [CrossRef]

94. Antoniadis, I.; Baessler, S.; Bücher, M.; Fedorov, V.V.; Hoedl, S.; Lambrecht, A.; Nesvizhevsky, V.V.; Pignol, G.; Protasov, K.V.; Reynaud, S.; et al. Short-range fundamental forces. *Compt. Rend.* **2011**, *12*, 755–778. [CrossRef]
95. Klimchitskaya, G.L. Constraints on theoretical predictions beyond the Standard Model from the Casimir effect and some other tabletop physics. *Universe* **2021**, *7*, 47. [CrossRef]
96. Klimchitskaya, G.L.; Mostepanenko, V.M. Testing gravity and predictions beyond the standard model at short distances: The Casimir effect. In *Modified and Quantum Gravity. From Theory to Experimental Searches on All Scales*; Pfeifer, C., Lämmerzahl, C., Eds.; Springer: Cham, Switzerland, 2023.
97. Mota, D.F.; Shaw, D.J. Strongly Coupled Chameleon Fields: New Horizons in Scalar Field Theory. *Phys. Rev. Lett.* **2006**, *97*, 151102. [CrossRef]
98. Mota, D.F.; Shaw, D.J. Evading equivalence principle violations, cosmological, and other experimental constraints in scalar field theories with a strong coupling to matter. *Phys. Rev. D* **2007**, *75*, 063501. [CrossRef]
99. Brax, P.; van de Bruck, C.; Davis, A.-C.; Mota, D.F.; Shaw, D. Detecting chameleons through Casimir force measurements. *Phys. Rev. D* **2007**, *76*, 124034. [CrossRef]
100. Klimchitskaya, G.L.; Mohideen, U.; Mostepanenko, V.M. The Casimir force between real materials: Experiment and theory. *Rev. Mod. Phys.* **2009**, *81*, 1827–1885. [CrossRef]
101. Brax, P.; Pitschmann, M. Exact solutions to nonlinear symmetron theory: One- and two-mirror systems. *Phys. Rev. D* **2018**, *97*, 064015. [CrossRef]
102. Abele, H.; Jenke, T.; Leeb, H.; Schmiedmayer, J. Ramsey’s method of separated oscillating fields and its application to gravitationally induced quantum phase shifts. *Phys. Rev. D* **2010**, *81*, 065019. [CrossRef]
103. Jenke, T.; Geltenbort, P.; Lemme, H.; Abele, H. Realization of a gravity-resonance-spectroscopy technique. *Nat. Phys.* **2011**, *7*, 468–472. [CrossRef]
104. Klimchitskaya, G.L.; Mostepanenko, V.M.; Sedmik, R.I.P.; Abele, H. Prospects for searching thermal effects, non-Newtonian gravity and axion-like particles: CANNEX test of the quantum vacuum. *Symmetry* **2019**, *11*, 407. [CrossRef]
105. Almasi, A.; Brax, P.; Iannuzzi, D.; Sedmik, R.I.P. Force sensor for chameleon and Casimir force experiments with parallel-plate configuration. *Phys. Rev. D* **2015**, *91*, 102002. [CrossRef]
106. Sedmik, R.I.P. Casimir and non-Newtonian force experiment (CANNEX): Review, status, and outlook. *Int. J. Mod. Phys. A* **2020**, *35*, 2040008. [CrossRef]
107. Elder, B.; Vardanyan, V.; Akrami, Y.; Brax, P.; Davis, A.-C.; Decca, R.S. Classical symmetron force in Casimir experiments. *Phys. Rev. D* **2020**, *101*, 064065. [CrossRef]
108. Chen, Y.J.; Tham, W.K.; Krause, D.E.; López, D.; Fischbach, E.; Decca, R.S. Stronger Limits on Hypothetical Yukawa Interactions in the 30–8000 Nm Range. *Phys. Rev. Lett.* **2016**, *116*, 221102. [CrossRef] [PubMed]
109. Fischer, H.; Käding, C.; Sedmik, R.I.P.; Abele, H.; Brax, P.; Pitschmann, M. Search for environment-dependent dilatons. *Phys. Dark Univ.* **2024**, *43*, 101419. [CrossRef]
110. Weinberg, S. A New Light Boson? *Phys. Rev. Lett.* **1978**, *40*, 223–226. [CrossRef]
111. Wilczek, F. Problem of Strong P and T Invariance in the Presence of Instantons. *Phys. Rev. Lett.* **1978**, *40*, 279–283. [CrossRef]

Disclaimer/Publisher’s Note: The statements, opinions and data contained in all publications are solely those of the individual author(s) and contributor(s) and not of MDPI and/or the editor(s). MDPI and/or the editor(s) disclaim responsibility for any injury to people or property resulting from any ideas, methods, instructions or products referred to in the content.

Article

Search for Wormhole Candidates: Accreting Wormholes with Monopole Magnetic Fields

Mikhail Piotrovich , Serguei Krasnikov , Stanislava Buliga  and Tinatin Natsvlshvili 

Central Astronomical Observatory at Pulkovo RAS, 196140 Saint-Petersburg, Russia; krasnikov.xxi@gmail.com (S.K.); aynim@yandex.ru (S.B.); tinatingao@mail.ru (T.N.)

* Correspondence: mpiotrovich@mail.ru

Abstract: The existence of even the simplest magnetized wormholes may lead to observable consequences. In the case where both the wormhole and the magnetic field around its mouths are static and spherically symmetric, and gas in the region near the wormhole falls radially into it, the former's spectrum contains bright cyclotron or synchrotron lines due to the interaction of charged plasma particles with the magnetic field. At the same time, due to spherical symmetry, the radiation is non-polarized. The emission of this just-described exotic type (non-thermal, but non-polarized) may be a wormhole signature. Also, in this scenario, the formation of an accretion disk is still quite possible at some distance from the wormhole, but a monopole magnetic field could complicate this process and lead to the emergence of asymmetrical and one-sided relativistic jets.

Keywords: wormholes; accretion; magnetic field



Citation: Piotrovich, M.; Krasnikov, S.; Buliga, S.; Natsvlshvili, T. Search for Wormhole Candidates: Accreting Wormholes with Monopole Magnetic Fields. *Universe* **2024**, *10*, 108. <https://doi.org/10.3390/universe10030108>

Academic Editors: Galina L. Klimchitskaya, Vladimir M. Mostepanenko and Sergey V. Sushkov

Received: 5 January 2024

Revised: 19 February 2024

Accepted: 23 February 2024

Published: 27 February 2024



Copyright: © 2024 by the authors. Licensee MDPI, Basel, Switzerland. This article is an open access article distributed under the terms and conditions of the Creative Commons Attribution (CC BY) license (<https://creativecommons.org/licenses/by/4.0/>).

1. Introduction

1.1. Wormholes

According to the “boring physics conjecture” [1], we live in \mathbb{R}^4 or, at best, in $\mathbb{R} \times \mathbb{S}^3$. On the other hand, Kardashev et al. [2] proposed the hypothesis that some galactic nuclei are, in fact, wormhole mouths (see also Bambi [3], Li and Bambi [4], Zhou et al. [5]). Evidently, the time is not ripe to discuss the topology of the Universe purely theoretically.

The study of wormholes is of serious interest since their properties and the very possibility of their existence can have a strong impact on our ideas about the cosmology of the Universe.

Wormholes (also known as “Einstein-Rosen bridges”) were first proposed by Einstein and Rosen [6] within the framework of general relativity. The Einstein–Rosen bridge solution describes an empty, spherically symmetric wormhole geometry that connects two asymptotically flat regions of spacetime. These hypothetical objects are essentially shortcuts through spacetime, connecting distant regions of the Universe or even different universes. This idea has generated great interest among scientists, inspiring many fascinating theories and proposals.

The solutions to the equations of general relativity allow for the existence of traversable and non-traversable (those that collapse too soon to be traversed) wormholes depending on the energy-matter content of spacetime. It should be noted that the theory of traversable wormholes, which could theoretically allow for fast interstellar travel, has a lot of constraints and challenges, including the requirement for negative energy density “exotic” matter that should stabilize the wormhole throat in order to prevent its collapse. Non-traversable wormholes also have important implications for theoretical physics and cosmology, allowing us to test the limits of general relativity and study the nature of spacetime under extreme conditions.

One of the serious problems in the study of wormholes is the preservation of causality. Traversable wormholes could allow time travel, which could lead to apparent paradoxes [7].

One such paradox is the classic “grandfather paradox”. Imagine a scenario where a man, equipped with the ability to travel through time, makes a fateful decision to eliminate his own grandfather during infancy. With resolve, he journeys into the past, sneaks up on the helpless infant, and takes a shot. What unfolds next? The situation seems to spiral into a paradox. On one hand, the baby is indeed killed. Yet, on the other hand, the act cannot come to pass, for if the grandfather perishes, the father of the time-traveler—and consequently the time-traveler himself—would never come into existence, leaving no one to carry out the fatal deed. Theoretical approaches have been proposed that allow spacetime to avoid paradoxes [8]. “The Chronology Protection Conjecture”, proposed by Stephen Hawking [9], suggests that in order to preserve causality, the laws of physics prevent the formation of closed time-like curves. The stability and consistency of wormholes within the framework of general relativity continue to be actively studied.

There are many authors who have tried to determine the unique observational features of wormholes [3–5,10–19], in particular, the features that distinguish wormholes from black holes. However, almost all of them have concluded that these features, even when they exist, are indeed difficult (and in some cases, simply impossible) to observe with modern astronomical equipment. In our work, we try to use objects and physical mechanisms that are well known in astrophysics, allowing us to obtain strong observational manifestations.

1.2. Accretion

Accretion is a very important phenomenon, occurring in various astrophysical objects such as normal stars and compact relativistic objects (including active galactic nuclei). The understanding of accretion processes is important for explaining the observed properties of these objects, such as their luminosity, spectral characteristics, and dynamics. In many astrophysical scenarios, magnetic fields play a significant role in shaping the flows of accreting matter. The interaction between magnetic fields and accreting matter adds additional complexity to the accretion process, leading to various phenomena such as the formation of magnetized accretion disks [20] and collimated jets [21,22] and the emergence of magnetic turbulence.

It is generally accepted that active galactic nuclei (AGNs) and quasars (QSOs) often possess a magnetized accretion disk [23,24]. There are many models of accretion disk structures. The most commonly used and well-known model is the standard Shakura–Sunyaev model [25]. In this model, the disk is held vertically by thermal pressure and turbulent viscosity is used to explain the transfer of angular momentum required by the accretion flow. Shakura–Sunyaev’s model is simple and convenient, but it has a number of problems. For example, this model does not predict X-ray emission in AGN spectra, and recent observations have shown that the size of the accretion disk is several times larger than that predicted by the Shakura–Sunyaev model (see, for example, Fausnaugh et al. [26]).

In addition, there are other models. We will list just a few of them. For example, Balbus and Hawley [27] showed that accretion disks have a robust mechanism for generating magnetohydrodynamic (MHD) turbulence due to magnetorotational instability. Miller and Stone [28] studied disks with initial Gaussian density profiles supported by thermal pressure. In the case of an initial axial magnetic field, Miller and Stone [28] observed that the saturated magnetic pressure dominates thermal pressure not only in the corona but also everywhere in the disk. Previously, Eardley and Lightman [29] and Field and Rogers [30] considered analytic models of thin accretion disks with angular momentum transfer due to magnetic stresses. Both these works included magnetic loops with sizes of the order of the disk thickness. Shalybkov and Rüdiger [31], Campbell [32], and Ogilvie and Livio [33] studied models of magnetized accretion disks with an externally imposed large-scale vertical magnetic field and anomalous magnetic field diffusion due to enhanced turbulent diffusion. In general, it can be said that studying accretion processes in the presence of magnetic fields is very important for advancing our understanding of astrophysical phenomena.

1.3. Magnetic Fields

Magnetic fields in the Universe are generated by various processes, such as dynamo action in stellar interiors, the amplification of primordial magnetic fields in the early Universe, and the compression and stretching of magnetic fields in accretion disks. Magnetic fields are typically classified based on their origin, strength, and topology. There are, for example, dipole, quadrupole, and toroidal fields. Monopole magnetic fields, which have isolated magnetic poles, are a hypothetical possibility that could have important consequences for astrophysics and fundamental physics if detected. The importance of the monopole field is that it directly connects the properties of experimentally observable fields with the topology of spacetime.

1.4. Wormholes with Monopole Magnetic Fields

Due to their unique properties, wormholes provide an interesting opportunity to use them as an object that can theoretically generate a monopole magnetic field. And, there are many works linking wormholes with a monopole field [34–42].

In the pioneering work of Misner and Wheeler [34], the concept of traversable wormholes was introduced, and it was also pointed out that they might have magnetic and scalar fields (“charge without charge”). After that, Bronnikov [35] and Ellis [36] considered a specific solution of Einstein’s equation where wormholes are supported by electromagnetic and scalar fields.

Agnese and Camera [37] demonstrated that a Kaluza–Klein theory in five dimensions, derived through a conformal gauge approach called the “total space”, can depict spacetimes that accommodate both magnetic monopoles and wormhole structures. This means that within this theoretical framework, it is possible to describe regions of space where magnetic charges exist alongside passages connecting different points in spacetime.

Prat-Camps et al. [38] used an interesting approach. While the idea of creating a wormhole in a laboratory may seem daunting, they used an unusual theoretical approach to construct a wormhole for electromagnetic waves using metamaterials. This would enable the transmission of electromagnetic waves through an invisible tunnel between two points in space. The researchers successfully built and demonstrated a magnetostatic wormhole. By utilizing magnetic metamaterials and metasurfaces, their wormhole was capable of transferring magnetic fields from one spatial point to another without detection. Experimental results illustrated that the magnetic field generated at one end of the wormhole appeared at the other end as an isolated monopole magnetic field. This created the illusion of a magnetic field traversing through a tunnel outside of conventional three-dimensional space.

Romero and Bellini [39] applied the Weitzböck-Induced Matter Theory (WIMT) to two specific metrics: the Gullstrand–Painlevé and Reissner–Nordström metrics. This method is a recent development that expands upon the Induced Matter Theory by utilizing Weitzböck’s geometry on a curved 5D manifold. The key insight exploited here is that the Riemann–Weitzenböck curvature tensor is consistently null. Through this approach, the study revealed the existence of currents, the interpretation of which suggests the potential presence of stable gravito-magnetic monopoles.

Romero and Bellini [40] utilized the Weitzenböck-Induced Matter Theory to analyze Schwarzschild wormholes within an extended 5D manifold, which included non-vacuum conditions. They investigated various ways of describing the wormholes, known as foliations, and examined the geodesic equations governing the motion of observers situated within a traversable wormhole. Additionally, the study explored how these observers could detect gravito-magnetic monopoles, which are essentially the gravitational analogs of magnetic monopoles, and contrasted them with gravito-electric sources typically observed in the outer region of Schwarzschild black holes. The researchers also calculated the densities of these monopoles and discussed their quantization according to the principles outlined by Dirac. Their analysis revealed a duality within the extended Einstein–Maxwell equations, linking electric and magnetic charges across spatial regions that are causally disconnected.

Romero and Bellini [41] focused on examining a traversable wormhole generated through a transformation applied to the 4D Dymnikova metric, which characterizes analytical black holes. The study employed a coordinate transformation method inspired by the Einstein–Rosen bridge to analyze a particular set of geodesics. These geodesics involved test particles carrying electric charges, which, due to the transformation, induced an effective magnetic monopole that could be observed by external observers situated outside the wormhole. Given that traditional Riemannian geometry does not account for the existence of magnetic monopoles, the study introduced torsional geometry as a potential explanation for the geometric induction of magnetic monopoles. The researchers derived an equation linking torsion and magnetic fields, along with a mathematical expression similar to Dirac’s equation that describes magnetic and electric charges. This formulation suggests that torsion could give rise to a fundamental length scale, enabling the generation of a magnetic field and introducing a discretization of spacetime.

Cañate [42] described the discovery of magnetically charged ultrastatic and spherically symmetric spacetime solutions within the framework of both linear and nonlinear electrodynamics, coupled with Einstein–scalar–Gauss–Bonnet (EsGB- $\mathcal{L}(\mathcal{F})$) gravity. These solutions are characterized by an electromagnetic Lagrangian density $\mathcal{L}(\mathcal{F})$, which solely depends on the electromagnetic invariant $\mathcal{F} = F_{\alpha\beta}F^{\alpha\beta}/4$. The paper highlighted a particular class of these solutions, where the electromagnetic invariant \mathcal{F} attains a strict global maximum value \mathcal{F}_0 across the entire solution domain, and the Lagrangian density $\mathcal{L}_0 = \mathcal{L}(\mathcal{F}_0) > 0$. It was shown that such solutions can be interpreted as ultrastatic wormhole spacetime geometries, with the radius of the wormhole throat determined by the scalar charge and the quantity \mathcal{L}_0 . Examples provided included Maxwell’s theory of electrodynamics (linear electrodynamics) with $\mathcal{L}_{\text{LED}} = \mathcal{F}$, which yields the magnetic dual of the purely electric Ellis–Bronnikov EsGB Maxwell wormhole. Additionally, nonlinear electrodynamics (NLED) models, such as Born–Infeld $\mathcal{L}_{\text{BI}} = -4\beta^2 + 4\beta^2\sqrt{1 + \mathcal{F}/(2\beta^2)}$ and Euler–Heisenberg in the weak-field limit $\mathcal{L}_{\text{EH}} = \mathcal{L}_{\text{LED}} + \gamma\mathcal{F}^2/2$, were discussed. Using these NLED models, two new magnetically charged ultrastatic traversable wormholes (EsGB Born–Infeld and EsGB Euler–Heisenberg wormholes) were presented as exact solutions within EsGB- $\mathcal{L}(\mathcal{F})$ gravity. These solutions do not require exotic matter, and it was demonstrated that they share the characteristic that, in the weak electromagnetic field region, the magnetically charged Ellis–Bronnikov EsGB Maxwell wormhole is recovered.

1.5. Polarization

Let us talk in more detail about the mechanisms for generating polarized radiation. Polarization, being sensitive to the anisotropy of the matter distribution, plays a crucial role in the study of optically unresolved central regions of AGNs, such as the accretion disk. An accretion disk is a typical example of a radiating region with a non-spherically symmetric electron density distribution. As a result of scattering by plasma electrons, the disk radiation becomes polarized. Polarimetric observations indicate that AGNs and QSOs have polarized emissions across a variety of wavelength ranges, from ultraviolet to radio waves, in continuous-wave and linear emissions [43–48]. These works discuss that the observed polarization has different mechanisms of origin: light scattering in accretion disks, which occurs on both free and bound electrons, and cyclotron and synchrotron radiation of charged particles. These mechanisms can work within different structures, such as plane and warped accretion disks, as well as toroidal clumpy rings surrounding the accretion disks and jets. Often, different models are proposed to explain the same source. There are many works devoted to the study of various aspects of the structure and radiation of AGNs and quasars. Of particular interest is the mechanism of the generation of relativistic jets. According to modern concepts, a large-scale magnetic field plays a key role in the launch of relativistic jets [21,22,49], and its toroidal component effectively collimates the jets [50,51]. The magnetic field manifests itself in linearly polarized synchrotron radiation and the Faraday rotation effect. In BL Lac objects (BL Lacs), the electric vector position

angle often coincides with the local direction of the jet [52–54], while quasars exhibit a distribution without a preferred direction [53].

1.6. Our Specific Approach

Previously, we considered the possible accretion of matter into a wormhole [55,56]. Specifically, we studied the case where accretion into a traversable wormhole occurs from both sides, each of which is located at the center of the active galactic nucleus. As a result, high-energy accretion flows collide inside the wormhole, which can lead to plasma heating to extremely high temperatures of up to 10^{14} K. Plasma with such parameters would exhibit a very specific spectrum, distinct from that of ordinary active galactic nuclei.

Now, we consider accretion in the presence of a magnetic field, assuming that the wormhole has a monopole magnetic field, which greatly distinguishes it from the much better-studied Kerr black hole.

In this paper, we argue that the existence of even the simplest magnetized wormholes may lead to observable consequences not yet discussed (to the best of our knowledge) in the literature. Indeed, consider the case where both the wormhole and the magnetic field around its mouth are static and spherically symmetric. Suppose that gas in the region near the wormhole falls radially into it. Then, the former’s spectrum contains bright cyclotron (or, in relativistic cases, synchrotron) lines due to the interaction of the charged plasma particles with the magnetic field. At the same time, due to spherical symmetry, the radiation is non-polarized. This is a rather unusual combination since in known astrophysical objects, cyclotron and synchrotron radiation is caused, as a rule, by a dipole-like magnetic field, which is not spherically symmetric. In addition, synchrotron radiation can be generated, for example, by relativistic jets, the geometry of which also leads to strong polarization.

Thus, we can speculate that the emission of the just-described exotic type (cyclotron or synchrotron, but non-polarized) may be a wormhole signature.

To convey the essence of this phenomenon we also show the possible trajectories of a charged particle near a wormhole using numerical simulations, under certain simplifying assumptions.

Very little is known about wormholes, including their birth and evolution. We try to compensate for this by applying the most general arguments to the simplest astrophysical monopole (the meaning of the word “simplest” is assumed to be intuitively clear). In particular, they must be static and spherically symmetric.

Although theoretically, the monopole object can be, for example, a magnetically charged Reissner–Nordström black hole with its horizons, singularities, and an infinite set of asymptotically flat ends, it is by no means simple. So, we do not consider such a case.

2. Our Model and Some Calculations

2.1. Toy Model and Basic Equations

The simplest compact radially magnetized object can be a wormhole based on the Reissner–Nordström spacetime (actually, as long as the magnetic field outside the object is a monopole, the structure of the former is irrelevant).

Pick three positive parameters: Q ; m , where $m > Q$; and r_0 , where the former two describe the magnetic charge and “mass” of the wormhole, respectively, and r_0 obeys the inequality

$$r_0 > r_{\text{Horizon}}, \quad r_{\text{Horizon}} \equiv m + \sqrt{m^2 - Q^2}$$

and characterizes “the size” of the wormhole. The auxiliary “half-wormhole”, W_1 , is defined as

$$W_1 : \quad ds^2 = -\nu(r) dt^2 + \nu(r)^{-1} dr^2 + r^2(d\theta^2 + \cos^2 \theta d\phi), \quad (1)$$

where

$$r > r_0, \quad t \in \mathbb{R}, \quad \nu \equiv 1 - \frac{2m}{r} + \frac{Q^2}{r^2}. \quad (2)$$

W_1 is *almost* the sought-after spacetime: it is static, spherically symmetric, and when endowed with the radial magnetic field

$$\mathbf{B} = \left(Q/r^2\right)\mathbf{e}_r \quad (3)$$

solves the Maxwell–Einstein equations. The only “drawback” of W_1 is that it has a single asymptotically flat end, so W_1 is an extendable—where one of its extensions is denoted as U_1 —funnel rather than a wormhole. To eliminate this drawback, we define the wormhole, W , as a pair of equal funnels, U_1 and U_2 , with their stems identified (the existence of a suitable isometry relating regions U_1 and U_2 is a non-trivial condition), as illustrated in Figure 1 in the work by Morris et al. [57].

2.2. Interaction of Accreting Matter with a Monopole Magnetic Field

A detailed description of the behavior of a plasma flow in the presence of a monopole magnetic field is an extremely difficult task and is beyond the scope of the current rather phenomenological study. And although in this work, we primarily consider spherical accretion, one can reasonably assume that a monopole field would impede the movement of plasma along Keplerian orbits near the wormhole and, in particular, complicate the formation of an accretion disk. However, the formation of an accretion disk is still quite possible at some distance from the wormhole, where the low magnetic field and low temperature (and, therefore, low degree of ionization) of the accreting matter would not allow the monopole field to strongly influence the matter. It should be noted that accretion disks near wormholes without their own magnetic fields have already been considered in the literature [11,56,58].

We can also purely phenomenologically study the formation of relativistic jets by the accretion disk at a wormhole with a monopole magnetic field. Since the disk wind would be suppressed by a monopole field, the formation of a jet is possible, most likely only through the Blandford–Znajek mechanism [21], in which the surrounding interstellar matter (not from the disk) is collimated due to the interaction of the disk’s poloidal magnetic field with the rotating black hole (in our case, the wormhole). Thus, if the wormhole rotates, jets can, in principle, form. Moreover, if the monopole field of a wormhole is much stronger than the dipole field of the accretion disk, the cyclotron radiation from them would be significantly stronger and at other frequencies compared to the black hole case. It is also possible that the jets themselves would be more powerful/faster, but this is not certain. If the strength of the wormhole’s monopole field is comparable to the disk’s dipole field, as a result of the superposition of fields at one of the poles of the dipole field, there would be a sharp decrease in the field’s strength. As a result, firstly, the cyclotron radiation from this side of the jet would be significantly weaker, and, secondly, the jet itself may be less powerful, less collimated, or even not formed at all (but this, again, is not certain; the mechanism of jet formation is quite complex and is still not fully understood). It should be noted that asymmetrical and one-sided jets have actually been observed near some active galactic nuclei [59–61], and this fact is rather difficult to explain using classical theories, whereas our wormhole model offers a simple explanation.

2.3. Numerical Simulation

Let us consider a simpler problem, namely the movement of one charged particle near a gravitating object with a monopole magnetic field in the simplified fictional space \mathbb{R}^3 (which is the Newtonian approximation of our metric W), where we use the Newton gravity approximation (here, the “mass” and the charge of the wormhole are described by the parameters m and Q , and it is a point-like object at the origin). In this case, the trajectory of the particle moving far enough from a gravitating object (so that relativistic effects can be neglected as a first approximation) can be obtained relatively easily (in our model, we use non-relativistic Maxwell equations). Let us consider, for example, a proton near a point-like object with the mass of the Sun M_\odot . In order to define the magnetic field strength, we set the value of the field B_{10} at a radius of $R = 10$ km. For simplicity, we neglect the loss of

proton energy due to cyclotron radiation since the trajectory is built on a time interval of only 0.01 s.

We have numerically calculated the proton trajectories for various values of parameters such as the magnetic field strength B_{10} , starting position R_{st} , and velocity V_{st} of a proton using a rather simple method. The force acting on the proton consists of the Lorentz force and the gravitational force $\vec{F} = \vec{F}_L + \vec{F}_g = q_p/c[\vec{V} \times \vec{B}] - GM_{\odot}m_p\vec{r}/r^3$, where q_p is the proton charge, c is the speed of light, \vec{V} is the proton speed, G is the gravitational constant, m_p is the proton mass, \vec{r} is the radius vector, $\vec{B} = \mu\vec{r}/r^3$ is the magnetic monopole field strength, and μ is the magnetic permeability, which, in our case, is $\mu = B_{10}R^2$.

In this calculation, for convenience, we measure the distance in centimeters, the mass in grams, and the time in 10^{-8} s. First, we set the starting position x_0, y_0, z_0 and starting velocity $\dot{x}_0, \dot{y}_0, \dot{z}_0$ in the Cartesian coordinate system. Then, at each iteration, the acceleration of the proton due to the Lorentz force and the Newtonian force of attraction are calculated as follows:

$$\begin{aligned} r &= (x^2 + y^2 + z^2)^{1/2}, \\ \ddot{x} &= ((y\dot{z} - \dot{y}z)(10^8 B_{10}) - xGM_{\odot})/r^3, \\ \ddot{y} &= ((z\dot{x} - \dot{z}x)(10^8 B_{10}) - yGM_{\odot})/r^3, \\ \ddot{z} &= ((x\dot{y} - \dot{x}y)(10^8 B_{10}) - zGM_{\odot})/r^3. \end{aligned} \tag{4}$$

After that, the change in speed due to acceleration and the change in coordinates due to speed are calculated as follows:

$$\begin{aligned} \dot{x} &\rightarrow \dot{x} + \ddot{x}dt, \\ \dot{y} &\rightarrow \dot{y} + \ddot{y}dt, \\ \dot{z} &\rightarrow \dot{z} + \ddot{z}dt, \\ x &\rightarrow x + \dot{x}dt, \\ y &\rightarrow y + \dot{y}dt, \\ z &\rightarrow z + \dot{z}dt, \end{aligned} \tag{5}$$

where in this case, the optimal value of time step dt turned out to be 0.001 in our units.

Thus, 10^9 iterations were performed for the proton flight time of 0.01 s. If the proton flew closer to the central object than 10 km, we considered that it would inevitably fall on the object and the calculation would be stopped. To avoid the accumulation of errors, we ensured that the total (kinetic plus potential) energy of the proton divided by the proton mass, $E_p/m_p = (\dot{x}^2 + \dot{y}^2 + \dot{z}^2)/2.0 - GM_{\odot}/\sqrt{(x^2 + y^2 + z^2)}$, did not change by more than 0.001.

Figure 1 shows some of these trajectories. We can see that even a relatively weak ($B_g \sim 1G$) monopole magnetic field prevents, as we conjectured earlier, the emergence of classical Keplerian orbits around the object. Instead, the proton begins to form spiral trajectories around radial magnetic field lines. The form of this spiral and the direction of the proton movement strongly depend on the parameters. In particular, at $\sim 67,000$ km/s, the proton's trajectory becomes closed (see the bottom picture in Figure 1). This is a kind of "first escape velocity" for this particular situation. However, it should be noted that if we take into account the loss of energy due to cyclotron radiation, such circular orbits would not be able to exist for long and would turn into spiral ones. Accordingly, at speeds lower than $\sim 67,000$ km/s, the proton moves toward the central object, and at speeds greater than $\sim 67,000$ km/s, it moves away from the central object. As the magnetic field strength increases, the radius of the helix quickly decreases, essentially leading to the almost radial motion of the proton.

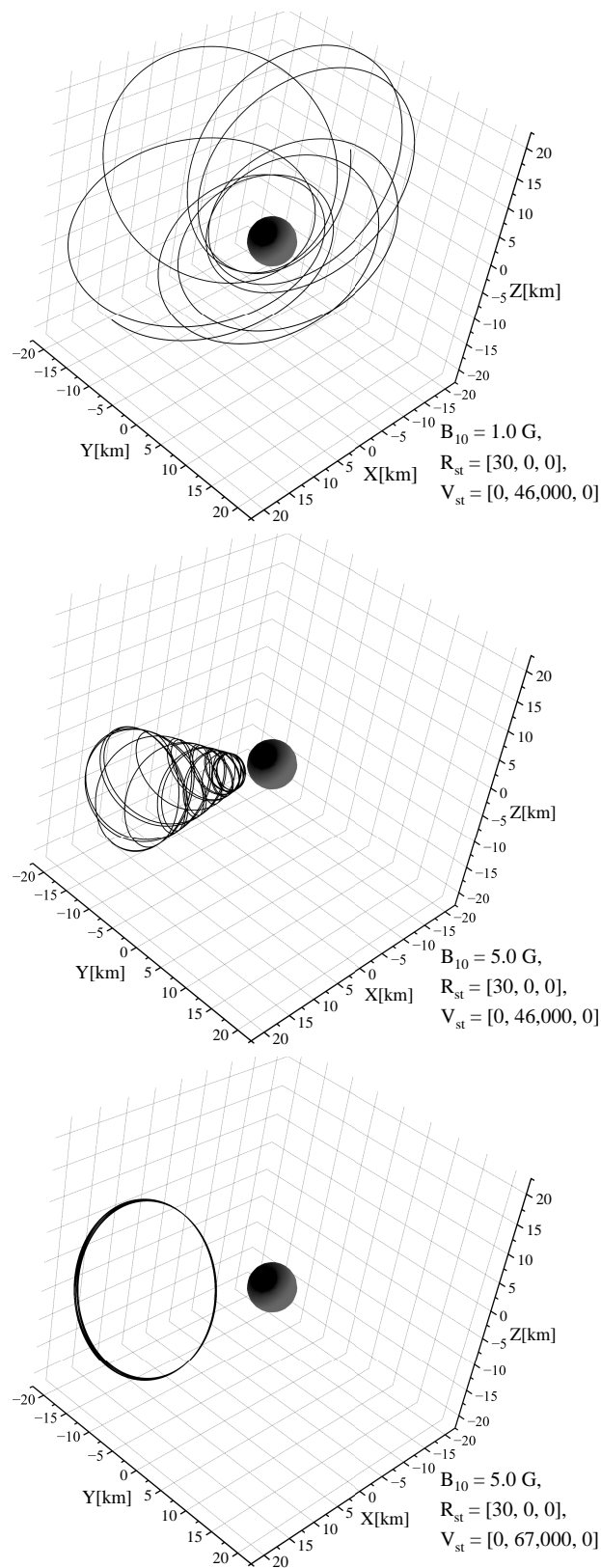


Figure 1. Trajectories (black line) of a proton near a point-like gravitating object (black sphere) in the fictional space with the mass of the Sun and a monopole magnetic field for different starting parameter values. B_{10} is the magnetic field strength at $R = 10$ km, and R_{st} and V_{st} are the starting position and speed of a particle in km and km/s, respectively.

3. Conclusions

The study of accretion into wormholes in the presence of a monopole magnetic field could have important consequences for fundamental physics and cosmology. Observations of accretion flow near wormholes could provide insights into the nature of dark matter, the origin of high-energy cosmic rays, and the nature and properties of compact objects in active galactic nuclei. Also, the study of wormholes and magnetic fields offers a unique opportunity to test the limits of general relativity and explore exotic spacetime geometries beyond the predictions of classical physics, offering a way to explore the interaction between gravity, magnetism, and spacetime geometry. Theoretical models, numerical simulations, and astronomical observations of hypothetical accreting wormholes can provide valuable information about the physical parameters, dynamics, and observable signatures of these interesting astrophysical objects.

In the current paper, we have shown that a wormhole with a monopole magnetic field can generate non-polarized cyclotron radiation, which is unusual for known astrophysical objects.

Possible candidates for such objects include both supermassive relativistic objects in the centers of galaxies and primordial wormholes of medium and small “mass” formed in the early Universe. In particular, the latter may appear as star-like objects with an unusual non-polarized non-thermal spectrum consisting of cyclotron or synchrotron emissions.

Calculations based on a toy model suggest that even a relatively weak (~ 1 G) monopole magnetic field prevents the emergence of classical Keplerian orbits around the object, which justifies our conjecture about the mainly radial character of accretion at a fairly close distance from the wormhole. However, the formation of an accretion disk is still quite possible at some distance from the wormhole.

Also, if we consider the case of the accretion disk, a monopole magnetic field could complicate its formation near the wormhole and lead to the emergence of asymmetrical and one-sided relativistic jets.

Future space missions and ground-based facilities will play important roles in advancing our understanding of magnetized accretion into relativistic objects and addressing open questions in modern astrophysics. Space observatories, such as the James Webb Space Telescope, the Nancy Grace Roman Space Telescope, and the European Space Agency’s Athena mission, will significantly improve sensitivity and wavelength coverage for studying magnetized accretion flows. Ground-based facilities such as the Atacama Large Millimeter/Submillimeter Array, the Square Kilometer Array, and the upcoming Giant Magellan Telescope and Extremely Large Telescope will allow astrophysicists to probe magnetized accretion with high angular resolution and sensitivity.

Author Contributions: Conceptualization, M.P. and S.K.; methodology, M.P. and S.K.; validation, M.P. and S.K.; formal analysis, M.P., S.K., S.B. and T.N.; investigation, S.B. and T.N.; resources, S.B. and T.N.; data curation, S.B. and T.N.; writing—original draft preparation, M.P., S.K. and S.B.; writing—review and editing, M.P. and S.K.; visualization, M.P.; supervision, M.P. and S.K.; project administration, M.P. All authors have read and agreed to the published version of the manuscript.

Funding: This research was supported by the state order of the Central Astronomical Observatory at Pulkovo as part of the planned research topic for “MAGION”—Physics and Evolution of Stars and Active Galactic Nuclei.

Data Availability Statement: Data are contained within the article.

Conflicts of Interest: The authors declare no conflicts of interest.

References

1. Visser, M. *Lorentzian Wormholes. From Einstein to Hawking*; American Institute of Physics: Woodbury, NY, USA, 1995.
2. Kardashev, N.S.; Novikov, I.D.; Shatskiy, A.A. Astrophysics of Wormholes. *Int. J. Mod. Phys. D* **2007**, *16*, 909–926. [CrossRef]
3. Bambi, C. Can the supermassive objects at the centers of galaxies be traversable wormholes? The first test of strong gravity for mm/sub-mm very long baseline interferometry facilities. *Phys. Rev. D* **2013**, *87*, 107501. [CrossRef]
4. Li, Z.; Bambi, C. Distinguishing black holes and wormholes with orbiting hot spots. *Phys. Rev. D* **2014**, *90*, 024071. [CrossRef]

5. Zhou, M.; Cardenas-Avendano, A.; Bambi, C.; Kleihaus, B.; Kunz, J. Search for astrophysical rotating Ellis wormholes with x-ray reflection spectroscopy. *Phys. Rev. D* **2016**, *94*, 024036. [CrossRef]
6. Einstein, A.; Rosen, N. The Particle Problem in the General Theory of Relativity. *Phys. Rev.* **1935**, *48*, 73–77. [CrossRef]
7. Einstein, A. *Albert Einstein: Philosopher-Scientist*; Cambridge University Press: Cambridge, UK, 1949.
8. Krasnikov, S. Time travel paradox. *Phys. Rev. D* **2002**, *65*, 064013. [CrossRef]
9. Hawking, S.W. Chronology protection conjecture. *Phys. Rev. D* **1992**, *46*, 603–611. [CrossRef] [PubMed]
10. Harko, T.; Kovács, Z.; Lobo, F.S.N. Electromagnetic signatures of thin accretion disks in wormhole geometries. *Phys. Rev. D* **2008**, *78*, 084005. [CrossRef]
11. Harko, T.; Kovács, Z.; Lobo, F.S.N. Thin accretion disks in stationary axisymmetric wormhole spacetimes. *Phys. Rev. D* **2009**, *79*, 064001. [CrossRef]
12. Tsukamoto, N.; Harada, T.; Yajima, K. Can we distinguish between black holes and wormholes by their Einstein-ring systems? *Phys. Rev. D* **2012**, *86*, 104062. [CrossRef]
13. Yoo, C.M.; Harada, T.; Tsukamoto, N. Wave effect in gravitational lensing by the Ellis wormhole. *Phys. Rev. D* **2013**, *87*, 084045. [CrossRef]
14. Bambi, C. Broad $K\alpha$ iron line from accretion disks around traversable wormholes. *Phys. Rev. D* **2013**, *87*, 084039. [CrossRef]
15. Dokuchaev, V.I.; Eroshenko, Y.N. Nonorientable wormholes as portals to the mirror world. *Phys. Rev. D* **2014**, *90*, 024056. [CrossRef]
16. Dai, D.C.; Stojkovic, D. Observing a wormhole. *Phys. Rev. D* **2019**, *100*, 083513. [CrossRef]
17. Paul, S.; Shaikh, R.; Banerjee, P.; Sarkar, T. Observational signatures of wormholes with thin accretion disks. *J. Cosmol. Astropart. Phys.* **2020**, *2020*, 055. [CrossRef]
18. Tripathi, A.; Zhou, B.; Abdikamalov, A.B.; Ayzenberg, D.; Bambi, C. Search for traversable wormholes in active galactic nuclei using X-ray data. *Phys. Rev. D* **2020**, *101*, 064030. [CrossRef]
19. Bambi, C.; Stojkovic, D. Astrophysical Wormholes. *Universe* **2021**, *7*, 136. [CrossRef]
20. Bardeen, J.M.; Wagoner, R.V. Relativistic Disks. I. Uniform Rotation. *Astrophys. J.* **1971**, *167*, 359. [CrossRef]
21. Blandford, R.D.; Znajek, R.L. Electromagnetic extraction of energy from Kerr black holes. *Mon. Not. R. Astron. Soc.* **1977**, *179*, 433–456. [CrossRef]
22. Blandford, R.D.; Payne, D.G. Hydromagnetic flows from accretion discs and the production of radio jets. *Mon. Not. R. Astron. Soc.* **1982**, *199*, 883–903. [CrossRef]
23. Blaes, O.M. Course 3: Physics Fundamentals of Luminous Accretion Disks around Black Holes. In *Accretion Discs, Jets and High Energy Phenomena in Astrophysics*; Beskin, V., Henri, G., Pelletier, G., Dalibard, J., Eds.; Springer: Berlin/Heidelberg, Germany, 2004; Volume 78, pp. 137–185.
24. Moran, J.M. The Black-Hole Accretion Disk in NGC 4258: One of Nature’s Most Beautiful Dynamical Systems. In *Proceedings of the Frontiers of Astrophysics: A Celebration of NRAO’s 50th Anniversary, Charlottesville, VA, USA, 18–21 June 2007*; Bridle, A.H., Condon, J.J., Hunt, G.C., Eds.; Astronomical Society of the Pacific Conference Series; Volume 395, p. 87.
25. Shakura, N.I.; Sunyaev, R.A. Black holes in binary systems. Observational appearance. *Astron. Astrophys.* **1973**, *24*, 337–355.
26. Fausnaugh, M.M.; Denney, K.D.; Barth, A.J.; Bentz, M.C.; Bottorff, M.C.; Carini, M.T.; Croxall, K.V.; De Rosa, G.; Goad, M.R.; Horne, K.; et al. Space Telescope and Optical Reverberation Mapping Project. III. Optical Continuum Emission and Broadband Time Delays in NGC 5548. *Astrophys. J.* **2016**, *821*, 56. [CrossRef]
27. Balbus, S.A.; Hawley, J.F. Instability, turbulence, and enhanced transport in accretion disks. *Rev. Mod. Phys.* **1998**, *70*, 1–53. [CrossRef]
28. Miller, K.A.; Stone, J.M. The Formation and Structure of a Strongly Magnetized Corona above a Weakly Magnetized Accretion Disk. *Astrophys. J.* **2000**, *534*, 398–419. [CrossRef]
29. Eardley, D.M.; Lightman, A.P. Magnetic viscosity in relativistic accretion disks. *Astrophys. J.* **1975**, *200*, 187–203. [CrossRef]
30. Field, G.B.; Rogers, R.D. Radiation from Magnetized Accretion Disks in Active Galactic Nuclei. *Astrophys. J.* **1993**, *403*, 94. [CrossRef]
31. Shalybkov, D.; Rüdiger, G. Magnetic field dragging and the vertical structure of thin accretion discs. *Mon. Not. R. Astron. Soc.* **2000**, *315*, 762–766. [CrossRef]
32. Campbell, C.G. An accretion disc model with a magnetic wind and turbulent viscosity. *Mon. Not. R. Astron. Soc.* **2000**, *317*, 501–527. [CrossRef]
33. Ogilvie, G.I.; Livio, M. Launching of Jets and the Vertical Structure of Accretion Disks. *Astrophys. J.* **2001**, *553*, 158–173. [CrossRef]
34. Misner, C.W.; Wheeler, J.A. Classical physics as geometry. *Ann. Phys.* **1957**, *2*, 525–603. [CrossRef]
35. Bronnikov, K.A. Scalar-tensor theory and scalar charge. *Acta Phys. Pol. B* **1973**, *4*, 251–266.
36. Ellis, H.G. Ether flow through a drainhole: A particle model in general relativity. *J. Math. Phys.* **1973**, *14*, 104–118. [CrossRef]
37. Agnese, A.G.; Camera, M.L. Kaluza-Klein Magnetic Monopoles and Wormholes. *Mod. Phys. Lett. A* **1996**, *11*, 181–185. [CrossRef]
38. Prat-Camps, J.; Navau, C.; Sanchez, A. A Magnetic Wormhole. *Sci. Rep.* **2015**, *5*, 12488. [CrossRef]
39. Romero, J.M.; Bellini, M. WIMT in Gullstrand-Painlevé and Reissner-Nordström metrics: Induced stable gravito-magnetic monopoles. *Eur. Phys. J. C* **2015**, *75*, 201. [CrossRef]
40. Romero, J.M.; Bellini, M. Gravito-magnetic monopoles in traversable wormholes from WIMT. *Phys. Dark Universe* **2017**, *15*, 47–52. [CrossRef]

41. Romero, J.M.; Bellini, M. Traversable wormhole magnetic monopoles from Dymnikova metric. *Eur. Phys. J. Plus* **2019**, *134*, 579. [CrossRef]
42. Cañate, P. Simple method to generate magnetically charged ultrastatic traversable wormholes without exotic matter in Einstein-scalar-Gauss-Bonnet gravity. *Phys. Rev. D* **2023**, *108*, 104048. [CrossRef]
43. Martin, P.G.; Thompson, I.B.; Maza, J.; Angel, J.R.P. The polarization of Seyfert galaxies. *Astrophys. J.* **1983**, *266*, 470–478. [CrossRef]
44. Impey, C.D.; Malkan, M.A.; Webb, W.; Petry, C.E. Ultraviolet Spectropolarimetry of High-Redshift Quasars with the Hubble Space Telescope. *Astrophys. J.* **1995**, *440*, 80. [CrossRef]
45. Wilkes, B.J.; Schmidt, G.D.; Smith, P.S.; Mathur, S.; McLeod, K.K. Optical Detection of the Hidden Nuclear Engine in NGC 4258. *Astrophys. J.* **1995**, *455*, L13. [CrossRef]
46. Barth, A.J.; Tran, H.D.; Brotherton, M.S.; Filippenko, A.V.; Ho, L.C.; van Breugel, W.; Antonucci, R.; Goodrich, R.W. Polarized Narrow-Line Emission from the Nucleus of NGC 4258. *Astron. J.* **1999**, *118*, 1609–1617. [CrossRef]
47. Smith, J.E.; Young, S.; Robinson, A.; Corbett, E.A.; Giannuzzo, M.E.; Axon, D.J.; Hough, J.H. A spectropolarimetric atlas of Seyfert 1 galaxies. *Mon. Not. R. Astron. Soc.* **2002**, *335*, 773–798. [CrossRef]
48. Modjaz, M.; Moran, J.M.; Kondratko, P.T.; Greenhill, L.J. Probing the Magnetic Field at Subparsec Radii in the Accretion Disk of NGC 4258. *Astrophys. J.* **2005**, *626*, 104–119. [CrossRef]
49. Lovelace, R.V.E.; Wang, J.C.L.; Sulkanen, M.E. Self-collimated Electromagnetic Jets from Magnetized Accretion Disks. *Astrophys. J.* **1987**, *315*, 504. [CrossRef]
50. Benford, G. Current-carrying beams in astrophysics: Models for double radio sources and jets. *Mon. Not. R. Astron. Soc.* **1978**, *183*, 29–48. [CrossRef]
51. Chan, K.L.; Henriksen, R.N. On the supersonic dynamics of magnetized jets of thermal gas in radio galaxies. *Astrophys. J.* **1980**, *241*, 534–551. [CrossRef]
52. Gabuzda, D.C.; Pushkarev, A.B.; Cawthorne, T.V. Analysis of $\lambda=6\text{cm}$ VLBI polarization observations of a complete sample of northern BL Lacertae objects. *Mon. Not. R. Astron. Soc.* **2000**, *319*, 1109–1124. [CrossRef]
53. Lister, M.L.; Homan, D.C. MOJAVE: Monitoring of Jets in Active Galactic Nuclei with VLBA Experiments. I. First-Epoch 15 GHz Linear Polarization Images. *Astron. J.* **2005**, *130*, 1389–1417. [CrossRef]
54. O’Sullivan, S.P.; Gabuzda, D.C. Magnetic field strength and spectral distribution of six parsec-scale active galactic nuclei jets. *Mon. Not. R. Astron. Soc.* **2009**, *400*, 26–42. [CrossRef]
55. Piotrovich, M.Y.; Krasnikov, S.V.; Buliga, S.D.; Natsvlshvili, T.M. Search for wormhole candidates in active galactic nuclei: radiation from colliding accreting flows. *Mon. Not. R. Astron. Soc.* **2020**, *498*, 3684–3686. [CrossRef]
56. Piotrovich, M.; Krasnikov, S.; Buliga, S.; Natsvlshvili, T. Possible Wormhole Candidates in Active Galactic Nuclei. *Universe* **2020**, *6*, 120. [CrossRef]
57. Morris, M.S.; Thorne, K.S.; Yurtsever, U. Wormholes, time machines, and the weak energy condition. *Phys. Rev. Lett.* **1988**, *61*, 1446–1449. [CrossRef] [PubMed]
58. Lobo, F.S.N. *Wormholes, Warp Drives and Energy Conditions*; Fundamental Theories of Physics; Springer: Cham, Switzerland, 2017; Volume 189. [CrossRef]
59. Bridle, A.H.; Perley, R.A. Extragalactic Radio Jets. *Annu. Rev. Astron. Astrophys.* **1984**, *22*, 319–358. [CrossRef]
60. Parma, P.; Fanti, C.; Fanti, R.; Morganti, R.; de Ruiter, H.R. VLA observations of low-luminosity radio galaxies. VI. Discussion of radio jets. *Astron. Astrophys.* **1987**, *181*, 244–264.
61. Cawthorne, T.V. Interpretation of parsec scale jets. In *Beams and Jets in Astrophysics*; Cambridge University Press: Cambridge, UK, 1991; Volume 19, p. 187.

Disclaimer/Publisher’s Note: The statements, opinions and data contained in all publications are solely those of the individual author(s) and contributor(s) and not of MDPI and/or the editor(s). MDPI and/or the editor(s) disclaim responsibility for any injury to people or property resulting from any ideas, methods, instructions or products referred to in the content.

Review

Prediction of the Expansion of the Universe Made by Alexander Friedmann and the Effect of Particle Creation in Cosmology

Vladimir M. Mostepanenko ^{1,2,3} 

¹ Central Astronomical Observatory at Pulkovo of the Russian Academy of Sciences, Saint Petersburg 196140, Russia; vmostepa@gmail.com

² Peter the Great Saint Petersburg Polytechnic University, Saint Petersburg 195251, Russia

³ Kazan Federal University, Kazan 420008, Russia

Abstract: This review devoted to the centenary of Alexander Friedmann's prediction of the Universe expansion presents the results obtained by him in 1922 and 1924 and an overview of their further developments. Special attention is paid to the role of mathematics, which enabled Friedmann to perform a radical departure from the conventional practice of considering our universe as a static system. The effect of particle creation in the expanding universe is discussed concurrently with the earlier investigated phenomenon of pair creation from a vacuum by an external electric field. The numbers of scalar and spinor particles created at different stages of the Universe's evolution are presented, and the possible role of the effect of the creation of particles in the formation of relativistic plasma and cold dark matter after the inflationary period is noted. It is stressed that by introducing the concept of the expanding universe, Friedmann made a contribution towards the understanding of the world around us that is compatible with those made by Ptolemy, Copernicus, and Newton in previous epochs.

Keywords: expanding universe; Friedmann cosmology; inflation; particle creation from vacuum



Citation: Mostepanenko, V.M. Prediction of the Expansion of the Universe Made by Alexander Friedmann and the Effect of Particle Creation in Cosmology. *Universe* **2024**, *10*, 84. <https://doi.org/10.3390/universe10020084>

Academic Editor: Panayiotis Stavrinou

Received: 22 January 2024

Revised: 5 February 2024

Accepted: 7 February 2024

Published: 9 February 2024



Copyright: © 2024 by the author. Licensee MDPI, Basel, Switzerland. This article is an open access article distributed under the terms and conditions of the Creative Commons Attribution (CC BY) license (<https://creativecommons.org/licenses/by/4.0/>).

1. Introduction

A hundred years ago, young mathematician Alexander Friedmann made an unexpected prediction that our universe expands with time. This prediction was in complete contradiction with all the previous scientific concepts of the Universe developed over the past millennia. One could mention the Ptolemy system, which was geocentric, and the Copernicus, Kepler, and Galilei system, which was heliocentric. Based on the laws of mechanics and gravitation discovered by him, Newton supposed [1] that our universe has an infinitely large volume, contains infinitely many stars and exists in time forever. As a theologian, Newton believed that the Universe was created by God. This means that not only all material bodies but also space and time are created in one creation act. The question of whether the existence of the Universe in time is finite or infinite must be solved by physics. All the mentioned pictures of the world are static in the sense that they do not change with time. And even Albert Einstein, after the creation of his general theory of relativity [2], especially modified its equations by introducing the cosmological constant in order to obtain the static model of the Universe [3] in agreement with the concepts of all previous epochs.

Like Einstein, Friedmann described the Universe as a whole on a basis of the general theory of relativity. In doing so, however, he restricted himself to the minimum number of additional assumptions. Specifically, following Newton and Einstein, he assumed that the 3-space of the Universe is homogeneous and isotropic, i.e., there are no preferential points and preferential directions. Otherwise, Friedmann acted as a mathematician by solving equations of the fundamental general theory of relativity and looking for the results obtained with no prejudice caused by some physical considerations like the desired

static character of any model of the Universe. This method of attack helped him to make an outstanding prediction that our universe expands with time, which was very soon confirmed by astronomical observations and became the cornerstone of modern cosmology.

In this brief review, we discuss the scientific results of Alexander Friedmann contained in his famous papers [4,5] by placing more emphasis on the outstanding role of mathematics in their obtainment. According to Friedmann's prediction, our universe started its evolution from a point (the so-called cosmological singularity), where it was characterized by the infinitely large values of the scalar curvature and energy density. A universe with a 3-space of negative or zero curvature, expands infinitely long, whereas a universe with a 3-space of positive curvature expands to some maximum size and then contracts down to a singular state.

Next, the outstanding phenomenon described by a unification of the general theory of relativity and quantum field theory is considered. This is the effect of particle–antiparticle pair creation from a vacuum, which occurs due to the Universe's expansion, as was understood for the first time by Erwin Schrödinger [6]. The effect of particle creation makes it possible to trace a mathematical analogy between the well-understood case of a non-stationary electric field and the expanding space–time of the Friedmann Universe. Main approaches to the definition of the concept of particles in the Friedmann cosmological models and the calculation results for a creation rate are presented. The role of the effect of particle creation at different stages of the Universe's evolution, including the epoch of inflation, is discussed.

This review is organized as follows. In Section 2, the Friedmann prediction of the Universe's expansion is considered with an emphasis on several facts from his biography and mathematical educational background. Section 3 is devoted to the effect of particle–antiparticle pair creation in the nonstationary electric field. Section 4 contains the primary information relative to the effect of particle creation in the Friedmann Universe. The crucial role of the effect of particle creation in the transition period between the inflationary and the radiation-dominated stages of the Universe's evolution is elucidated in Section 5. A discussion of the fundamental importance of Friedmann's prediction for modern cosmology is presented in Section 6, and we will finish with the conclusions in Section 7.

The system of units is one in which $c = \hbar = 1$ is used, where c is the speed of light and \hbar is the reduced Planck constant.

2. Role of Mathematics in Friedmann's Prediction of the Universe's Expansion

It was difficult to imagine that Alexander Friedmann, who was born on 6 June 1888 to an artistic family (his father was a ballet artist and composer and his mother was a pianist [7,8]) would become the outstanding mathematician and physicist who would radically change our picture of the world. However, his exceptional abilities in mathematics became apparent very early. In 1905, while still a schoolboy, Alexander Friedmann, together with his schoolmate Yakov Tamarkin, obtained new interesting results in the field of Bernoulli numbers. In the next year, it was David Hilbert who recommended their paper for publication in the prestigious mathematical journal *Mathematische Annalen* [9].

After his graduation from high school, Friedmann became a student of the Department of Mathematics at Saint Petersburg University, where he gained in-depth knowledge in different areas of mathematics and physics. His successes were always evaluated as "excellent". Because of this, after his graduation from the university in 1910, Friedmann remained at the same department in preparation for the position of Professor, under the supervision of the famous mathematician and academician Vladimir Steklov. During the next few years, he published many papers containing the solutions of several complicated problems of mathematical physics. Starting from 1913, Friedmann took an interest in the mathematical problems of dynamical meteorology, aerodynamics, and hydrodynamics, in which he obtained a lot of fundamental results which are well known to all experts in these fields and maintain their importance to the present day.

In 1920, Friedmann had close contacts with several professors of Petrograd (as St. Petersburg was called at that time) University who had just begun delivering lectures in the recently developed quantum physics and general theory of relativity. He took a great interest in the latter and embarked upon giving lectures on tensor calculus at the university as an introduction to the general theory of relativity. Friedmann was inspired by the idea that the Universe around us takes the form of Riemannian space–time, in which all bodies move freely along geodesic lines. This idea was radically different from Newton’s concept of the gravitational force which acts between all material bodies through an empty space.

In 1922, Friedmann applied the formalism of the general theory of relativity to the theoretical description of the Universe as a whole. As mentioned in Section 1, he restricted himself to the minimum physical assumptions by presuming that the 3-space of the Universe is homogeneous and isotropic. In this regard, Friedmann followed Einstein [3] and de Sitter [10].

Mathematically, the requirement of the homogeneity and isotropy of the 3-space is expressed in the following distance (interval) ds between two infinitesimally close space–time points $x^i = (t, \chi, \theta, \varphi)$ and $x^i + dx^i = (t + dt, \chi + d\chi, \theta + d\theta, \varphi + d\varphi)$:

$$ds^2 = g_{ik}dx^i dx^k \equiv dt^2 - a^2(t) \left[d\chi^2 + f^2(\chi)(d\theta^2 + \sin^2 \theta d\varphi^2) \right], \tag{1}$$

where t is the time variable, and the spatial coordinates $\chi, \theta,$ and φ are connected with the standard Cartesian coordinates (x^1, x^2, x^3) by the relations

$$x^1 = a(t)f(\chi) \sin \theta \cos \varphi, \quad x^2 = a(t)f(\chi) \sin \theta \sin \varphi, \quad x^3 = a(t)f(\chi) \cos \theta. \tag{2}$$

The quantity $a(t)$ in Equation (1) has the dimension of length. It represents the radius of the curvature of space. As to the function $f(\chi)$, it is defined as

$$f(\chi) = \begin{cases} \sin \chi, & \kappa = 1, \\ \sinh \chi, & \kappa = -1, \\ \chi, & \kappa = 0, \end{cases} \tag{3}$$

where κ is the sign of the curvature of the 3-space ($\kappa = 0$ corresponds to the flat 3-space). Depending on the value of $f(\chi)$ in Equation (3), the interval (1) relates to the closed space of the finite volume $V = 2\pi^2 a^3(t)$ and positive curvature, to the open space of an infinite volume and negative curvature, or to the quasi-Euclidean space of an infinite volume and zero curvature.

Working as a mathematician, Friedmann solved the following Einstein equations:

$$R_{ik} - \frac{1}{2}g_{ik}R - \Lambda g_{ik} = 8\pi G T_{ik}. \tag{4}$$

where R_{ik} is the Ricci tensor describing the curvature of space–time, $R = g^{ik}R_{ik}$ is the scalar curvature, Λ is the cosmological constant, G is the gravitational constant, T_{ik} is the stress–energy tensor of matter in the Universe, and g_{ik} is the metrical tensor, the components of which for $i, k = 0, 1, 2, 3$ are defined in Equation (1) for the case of a homogeneous and isotropic space. In this space, the stress–energy tensor is diagonal, and its components are the energy density, $T_0^0 = \varepsilon$, and pressure, $T_1^1 = T_2^2 = T_3^3 = -P$, of matter. It is important to note that R_{ik} and R can be calculated for any given g_{ik} . Note that the stress–energy tensor is also often called the energy–momentum tensor.

Substituting the metrical tensor g_{ik} defined in Equation (1) in Equation (4), one obtains two Friedmann equations for the unknown scale factor $a(t)$ and the energy density ε :

$$\begin{aligned} \frac{d^2 a}{dt^2} &= -\frac{4\pi G}{3} a(\varepsilon + 3P) + \frac{1}{3} a\Lambda, \\ \left(\frac{da}{dt}\right)^2 &= \frac{8\pi G}{3} a^2 \varepsilon - \kappa + \frac{1}{3} a^2 \Lambda. \end{aligned} \tag{5}$$

One should remember that the pressure P is connected with the energy density by the equation of state.

Note that, initially, Einstein introduced his Equation (4) with $\Lambda = 0$ [2]. The cosmological term Λg_{ik} was introduced by him later [3], specifically for obtaining the static model of the Universe.

Friedmann considered dust-like matter with the equation of state $P = 0$ (in our system of units, $\varepsilon = \rho$, where ρ is the density of matter). The closed universe ($\kappa = 1$) was considered by Friedmann in Ref. [4], published in 1922, and the open universe ($\kappa = -1$)—in Ref. [5], published in 1924.

For instance, if $\kappa = 1$ and $\Lambda = 0$, Equation (5) for dust-like matter is simplified to

$$\begin{aligned} \frac{d^2a}{dt^2} &= -\frac{4\pi G}{3}a\rho, \\ \left(\frac{da}{dt}\right)^2 &= \frac{8\pi G}{3}a^2\rho - 1. \end{aligned} \tag{6}$$

It is easy to check by the direct substitution that the solution of this system of equations can be represented in the following parametric form:

$$\begin{aligned} a &= \tilde{a}_0(1 - \cos \eta), & t &= \tilde{a}_0(\eta - \sin \eta), \\ \rho &= \frac{3}{4\pi G} \frac{1}{\tilde{a}_0^2} \frac{1}{(1 - \cos \eta)^3}, & 0 \leq \eta \leq 2\pi, \end{aligned} \tag{7}$$

where \tilde{a}_0 is the constant expressed via the total mass of matter in the closed universe M as $\tilde{a}_0 = 2GM/(3\pi)$.

If one considers $t, \eta \ll 1$, Equation (7) reduces to

$$a(t) \approx \left(\frac{9\tilde{a}_0}{2}\right)^{1/3} t^{2/3}, \quad \rho(t) \approx \frac{1}{6\pi G t^2}, \tag{8}$$

i.e., according to Friedmann, the evolution of the Universe starts from a point-like state $a(0) = 0$, where the density of matter $\rho = \infty$.

The Universe expands with time until the maximum size $a_{\max} = 2\tilde{a}_0$ is reached at $\eta = \pi, t = \pi\tilde{a}_0$ and then contracts to a point $a(2\pi\tilde{a}_0) = 0$. For $\kappa = -1$ or 0 , the expansion of the Universe also starts from a point (called the cosmological singularity), where the density of matter is infinitely large, but in this case the expansion goes on infinitely. Similar results were later obtained for the radiation-dominated Universe, where matter has the equation of state $P = \varepsilon/3$ (see Ref. [11] for details). This equation of state describes the hot Universe at the early stages of its evolution.

Thus, if $\Lambda = 0$, all the solutions of Equation (5) are nonstationary and describe the expanding (or contracting in the case $\kappa = 1$) Universe. According to Friedmann, the static cosmological solution of Einstein equations is possible only for the closed universe ($\kappa = 1$) with the cosmological constant $\Lambda \neq 0$ satisfying the following conditions:

$$\Lambda = 4\pi G(\varepsilon + 3P), \quad 4\pi G a^2(\varepsilon + P) = 1. \tag{9}$$

Under these conditions, Equation (5) reduces to

$$\frac{d^2a}{dt^2} = \frac{da}{dt} = 0, \tag{10}$$

which means that $a = \text{const}$. This is the static model of the Universe obtained by Einstein [3]. Friedmann did not discuss whether the Einstein model is stable relative to some disturbance which occurs at a definite time. This problem was investigated later after an experimental confirmation of the Universe's expansion (see Ref. [12] for a summary of the obtained

results). A more detailed consideration of the cosmological models with nonzero Λ can be found in Ref. [13].

We only mention the famous solution of Equation (5) obtained by de Sitter [10] for the empty universe with $\varepsilon = P = 0$ but with a nonzero cosmological constant Λ . In this case, Equation (5) takes the following form:

$$\frac{d^2a}{dt^2} = \frac{1}{3}a\Lambda, \quad \left(\frac{da}{dt}\right)^2 = -\kappa + \frac{1}{3}a^2\Lambda. \tag{11}$$

In the most simple, quasi-Euclidean case ($\kappa = 0$), the de Sitter solution of Equation (11) is

$$a(t) = \tilde{a}_0 \exp\left(\sqrt{\frac{\Lambda}{3}}t\right). \tag{12}$$

The closed ($\kappa = 1$) and open ($\kappa = -1$) de Sitter solutions of Equation (11) are, respectively,

$$a(t) = \sqrt{\frac{3}{\Lambda}} \cosh\left(\sqrt{\frac{\Lambda}{3}}t\right), \quad a(t) = \sqrt{\frac{3}{\Lambda}} \sinh\left(\sqrt{\frac{\Lambda}{3}}t\right). \tag{13}$$

The scale factors in Equations (12) and (13) are the exponentially increasing with time functions which leave the scalar curvature constant, $R = -4\Lambda$. The de Sitter solution found important applications in the theoretical description of the very early stages of the Universe’s evolution near the cosmological singularity (see Section 5).

Although Friedmann’s papers [4,5] were published in the leading journal of that time, his remarkable results did not gain widespread recognition for a long period of time. Just after the publication of Friedmann’s paper [4], Albert Einstein claimed [14] that the solutions found by Friedmann did not satisfy Equation (4) of the general theory of relativity. It was, however, Einstein who made a mistake in his note [14]. After receiving a letter explaining this from Friedmann, Einstein was obliged to recognize this fact in another published note [15].

From the experimental viewpoint, the expansion of the Universe predicted by Friedmann should manifest itself as the moving of all remote galaxies away from the Earth. This would lead to the redshift of the light emitted by them in accordance to the Doppler law. In fact, the redshift of the light from the Andromeda Nebula was registered by Slipher [16] as early as in 1913, i.e., before the Friedmann prediction.

In a systematic way, the experimental law connecting the redshift in the spectra of observable galaxies with the expansion of the Universe was found by Georges Lemaître in 1927 [17] and Edwin Hubble in 1929 [18] after they identified nebulas with remote galaxies [19]. Lemaître’s paper contains a rederivation of the main properties of the expanding universe from Einstein’s equations with no citation of the papers [4,5] by Friedmann, who passed away untimely of typhus on 16 September 1925 at the age of 37. Hubble’s paper [18] does not cite Alexander Friedmann’s papers either. Later on, the properties of homogeneous isotropic metrics were studied by H.P. Robertson [20] and A.G. Walker [21], whose papers also do not cite the Friedmann results.

In the meantime, after the elaboration of the theory of a hot universe by George Gamov [22], the prediction of the relic radiation [23] and its discovery by Arno Penzias and Robert Wilson [24], it became evident that the Friedmann solution describing the expanding Universe formed the foundation of modern cosmology and radically changed our picture of the world. Starting from the 1960s, Friedmann’s name as a pioneer of the theory of the Universe’s expansion became more and more popular. Friedmann’s background as a mathematician played a crucial role in his discovery, which was based on Einstein’s equations of the general theory of relativity alone with no unnecessary assumptions caused by either tradition or physical intuition. This is one more example of

what was characterized by E.P. Wigner as “The unreasonable effectiveness of mathematics in the natural sciences” [25].

Though being a mathematician, Friedmann considered his prediction of the Universe’s expansion very seriously and expected that it would receive experimental confirmation. In his book *“The World as Space and Time”*, written for the general reader and published in 1923 [26], Alexander Friedmann not only explained the main concepts of Einstein’s general theory of relativity, but also discussed his own model of the expanding Universe, which starts its evolution from a point. The front cover of this book is presented in Figure 1. According to Friedmann’s estimation contained in Ref. [26], the interval between the Universe’s creation and the present day is of about tens of billions of years. This estimation is in qualitative agreement with modern measurements, which result in 13.7 billion years for the Universe’s age. Thus, Friedmann predicted the most dramatic phenomenon of nature, which completely changed our picture of the world.



Figure 1. The front cover of the book [26]. Translation: Modern culture. A. Friedmann. The World as Space and Time. Academia, Petersburg, 1923.

3. Quantum Creation of Particle–Antiparticle Pairs in a Nonstationary Electric Field

As was mentioned in Section 1, the Universe’s expansion results in the effect of particle creation from the vacuum state of quantized fields. This is the quantum effect, which is described by the quantum field theory in curved space–time. It is most important at the very early stages of the Universe’s evolution near the cosmological singularity, where the Universe should be considered as a quantum object.

The quantum field theory and the general theory of relativity are very dissimilar theories. The former deals with the quantum fields defined on a flat Minkowski space–time, whereas the latter treats the gravitational field as a classical curved space–time. The quantum theory of gravitation is not yet available in spite of numerous attempts to develop it undertaken by many authors during half a century. It is possible, however, to consider the quantized matter fields defined not on a Minkowski background, but on a curved space–time of the expanding Universe. This theory has been well elaborated on since the beginning of the 1980s (see, for instance, the monographs [27–31]).

Some basic concepts of quantum field theory in curved space–time, including the concept of a particle, are, however, much more complicated and, unlike the standard quantum field theory, are not defined uniquely. Because of this, before considering the effect of particle creation in the Friedmann Universe, we discuss in this section the creation of particle–antiparticle pairs from a vacuum by the nonstationary space homogeneous electric field. Quantum electrodynamics allows us to describe this phenomenon in a rather transparent way [32–35]. At the same time, although, conceptually, the nonstationary electric

field and the expanding space–time of the Universe are quite different, mathematically, the description of the effect of particle creation in both cases turns out to be very similar. Thus, the formalism briefly presented in this section will provide rather useful guidance in the next section.

The spatially homogeneous nonstationary electric field directed along the $z = x^3$ axis can be described by the following vector potential:

$$A^k(x) = (0, 0, 0, A^3(t)), \tag{14}$$

which leads to the following field strength:

$$E(t) = \left(0, 0, -\frac{dA^3(t)}{dt}\right) = (0, 0, E_z(t)), \tag{15}$$

It is assumed that the field is switched off at $t \rightarrow \pm\infty$, i.e.,

$$\lim_{t \rightarrow \pm\infty} A^3(t) = A^3_{\pm} = const, \quad \lim_{t \rightarrow \pm\infty} E_z(t) = 0. \tag{16}$$

Let us consider first the complex scalar field of mass m interacting with the electric field (15). A complete orthonormal set of solutions to the Klein–Fock–Gordon equation is as follows:

$$\left[\left(\frac{\partial}{\partial x^k} + ieA_k \right) \left(\frac{\partial}{\partial x_k} + ieA^k \right) + m^2 \right] \varphi(x) = 0 \tag{17}$$

In the case of a vector potential, (14) takes the following form:

$$\varphi_{\mathbf{p}}^{\pm}(x) = \frac{1}{(2\pi)^{3/2} \sqrt{2\omega_{\pm}(\mathbf{p})}} e^{i\mathbf{p}\mathbf{x}} g^{\pm}(\mathbf{p}, t), \tag{18}$$

where $\mathbf{p} = (p_1, p_2, p_3)$ is the momentum, the functions g^{\pm} obey the following equation:

$$\frac{d^2 g^{\pm}(\mathbf{p}, t)}{dt^2} + \omega^2(\mathbf{p}, t) g^{\pm}(\mathbf{p}, t) = 0, \quad \omega^2(\mathbf{p}, t) = m^2 + p_{\perp}^2 + (p_3 - eA_2(t))^2 \tag{19}$$

and the following notations are used:

$$p_{\perp}^2 = p_1^2 + p_2^2, \quad \omega_{\pm}(\mathbf{p}) = \lim_{t \rightarrow -\infty} \omega(\mathbf{p}, t). \tag{20}$$

Equation (19) is the equation of oscillator with a variable frequency [34,35]. The positive- and negative-frequency solutions of this equation are defined by the following asymptotic behavior:

$$\lim_{t \rightarrow -\infty} g^{\pm}(\mathbf{p}, t) = e^{\pm i\omega_{\pm}(\mathbf{p})t}. \tag{21}$$

An operator of the complex scalar field is

$$\varphi(x) = \int d^3 p \left[\varphi_{\mathbf{p}}^{(-)}(x) a_{\mathbf{p}}^{(-)} + \varphi_{-\mathbf{p}}^{(+)}(x) a_{\mathbf{p}}^{(+)} \right], \tag{22}$$

where $a_{\mathbf{p}}^{(-)}$ is the annihilation operator for particles and $a_{\mathbf{p}}^{(+)}$ is the creation operator for antiparticles defined at $t \rightarrow -\infty$ when the scalar field is free. The vacuum state at $t \rightarrow -\infty$ is defined as

$$a_{\mathbf{p}}^{(-)} |0_{\text{in}}\rangle = a_{\mathbf{p}}^{(-)*} |0_{\text{in}}\rangle = 0, \tag{23}$$

where $a_{\mathbf{p}}^{(-)*}$ is the annihilation operator for antiparticles (the creation operator for particles is notated as $a_{\mathbf{p}}^{(+)*}$).

The Hamiltonian of the complex scalar field is defined by [36]

$$H^{(0)}(t) = \int d^3x T_{00}(x) = \int d^3x \left[2\partial_0\varphi^*(x)\partial_0\varphi(x) - \left(\frac{\partial}{\partial x^k} - ieA_k \right) \varphi^*(x) \left(\frac{\partial}{\partial x_k} + ieA^k \right) \varphi(x) + m^2\varphi^*(x)\varphi(x) \right]. \tag{24}$$

Substituting Equation (22) in Equation (24) and performing the integration with respect to x and to one of the momenta using (18), one obtains

$$H^{(0)}(t) = \int d^3p \omega(\mathbf{p}, t) \left[E(\mathbf{p}, t) \left(a_{\mathbf{p}}^{*(+)} a_{\mathbf{p}}^{(-)} + a_{-\mathbf{p}}^{*(-)} a_{-\mathbf{p}}^{(+)} \right) + F(\mathbf{p}, t) a_{\mathbf{p}}^{*(+)} a_{-\mathbf{p}}^{(+)} + F^*(\mathbf{p}, t) a_{-\mathbf{p}}^{*(-)} a_{\mathbf{p}}^{(-)} \right], \tag{25}$$

where

$$E(\mathbf{p}, t) = \frac{1}{2\omega_-(\mathbf{p})\omega(\mathbf{p}, t)} \left[\left| \frac{dg^{(+)}(\mathbf{p}, t)}{dt} \right|^2 + \omega^2(\mathbf{p}, t) |g^{(+)}(\mathbf{p}, t)|^2 \right],$$

$$F(\mathbf{p}, t) = \frac{1}{2\omega_-(\mathbf{p})\omega(\mathbf{p}, t)} \left[\left(\frac{dg^{(+)}(\mathbf{p}, t)}{dt} \right)^2 + \omega^2(\mathbf{p}, t) g^{(+)}(\mathbf{p}, t)^2 \right], \tag{26}$$

$$E^2(\mathbf{p}, t) - |F(\mathbf{p}, t)|^2 = 1.$$

Using Equation (21), Equation (27) leads to

$$\lim_{t \rightarrow -\infty} E(\mathbf{p}, t) = 1, \quad \lim_{t \rightarrow -\infty} F(\mathbf{p}, t) = 0. \tag{27}$$

As a result, at $t \rightarrow -\infty$ the Hamiltonian (24) takes the following diagonal form:

$$\lim_{t \rightarrow -\infty} H^{(0)}(t) = \int d^3p \omega_-(\mathbf{p}) \left(a_{\mathbf{p}}^{*(+)} a_{\mathbf{p}}^{(-)} + a_{-\mathbf{p}}^{*(-)} a_{-\mathbf{p}}^{(+)} \right), \tag{28}$$

as it should be for the Hamiltonian of free fields.

At any t , in the presence of a nonstationary electric field, the Hamiltonian (25) can be diagonalized by means of the canonical Bogoliubov transformations, which preserve the commutation relations for the creation–annihilation operators:

$$a_{\mathbf{p}}^{(-)} = \alpha_{\mathbf{p}}^*(t) b_{\mathbf{p}}^{(-)}(t) - \beta_{\mathbf{p}}(t) b_{-\mathbf{p}}^{(+)}(t),$$

$$a_{-\mathbf{p}}^{(+)} = \alpha_{-\mathbf{p}}^*(t) b_{\mathbf{p}}^{(-)}(t) - \beta_{-\mathbf{p}}(t) b_{-\mathbf{p}}^{(+)}(t), \tag{29}$$

where

$$|\alpha_{\mathbf{p}}(t)|^2 - |\beta_{\mathbf{p}}(t)|^2 = 1. \tag{30}$$

Note that an addition of the creation operators to the annihilation ones in Equation (29) due to the action of a nonstationary external field is equivalent to the fact that the negative-frequency solution of the wave equation defined at $t \rightarrow -\infty$ becomes the linear combination of the negative- and positive-frequency solutions defined at a later time t .

If the coefficients $\alpha_{\mathbf{p}}(t)$ and $\beta_{\mathbf{p}}(t)$ are given by

$$\frac{\beta_{\mathbf{p}}(t)}{\alpha_{\mathbf{p}}(t)} = \frac{E(\mathbf{p}, t) - 1}{F^*(\mathbf{p}, t)}, \quad |\beta_{\mathbf{p}}(t)|^2 = \frac{1}{2} [E(\mathbf{p}, t) - 1], \tag{31}$$

the Hamiltonian (25) takes a diagonal form at any t [34]:

$$H^{(0)}(t) = \int d^3p \omega(\mathbf{p}, t) \left[b_{\mathbf{p}}^{*(+)}(t) b_{\mathbf{p}}^{(-)}(t) + b_{-\mathbf{p}}^{*(-)}(t) b_{-\mathbf{p}}^{(+)}(t) \right]. \tag{32}$$

In doing so, the operators $b_{\mathbf{p}}^{*(+)}(t)$ and $b_{\mathbf{p}}^{(-)}(t)$ can be considered the creation and annihilation operators of quasiparticles defined at the moment t . The quasiparticle vacuum is defined by

$$b_{\mathbf{p}}^{(-)}(t) |0_t\rangle = b_{\mathbf{p}}^{*(-)}(t) |0_t\rangle = 0. \tag{33}$$

It is easily seen that

$$\lim_{t \rightarrow -\infty} \beta_{\mathbf{p}}(t) = 0, \quad \lim_{t \rightarrow -\infty} \alpha_{\mathbf{p}}(t) = 1, \tag{34}$$

so that the creation and annihilation operators of quasiparticles at $t \rightarrow -\infty$ coincide with the creation and annihilation operators $a_{\mathbf{p}}^{(\pm)}, a_{\mathbf{p}}^{*(\pm)}$ and the quasiparticle vacuum $|0_{-\infty}\rangle = |0_{\text{in}}\rangle$ defined in Equation (23).

Now, one can find the number of scalar quasiparticles with the momentum \mathbf{p} and antiparticles with the momentum $-\mathbf{p}$ created from the vacuum state $|0_{\text{in}}\rangle$:

$$N_{\mathbf{p}}^{(0)}(t) = \langle 0_{\text{in}} | b_{\mathbf{p}}^{*(+)}(t) b_{\mathbf{p}}^{(-)}(t) | 0_{\text{in}} \rangle = \langle 0_{\text{in}} | b_{-\mathbf{p}}^{(+)}(t) b_{-\mathbf{p}}^{*(-)}(t) | 0_{\text{in}} \rangle = |\beta_{\mathbf{p}}(t)|^2 \delta^3(\mathbf{p} = 0). \tag{35}$$

These quasiparticle pairs were created by the electric field during the time interval from $-\infty$ to t in the space of an infinitely large volume V . Taking into account that

$$\delta^3(\mathbf{p} = 0) = \frac{1}{(2\pi)^3} \int d^3x = \frac{V}{(2\pi)^3}, \tag{36}$$

for the total number of scalar quasiparticle pairs with any momentum created in the unit space volume, one obtains

$$n^{(0)}(t) = \frac{1}{V} \int d^3p N_{\mathbf{p}}^{(0)}(t) = \frac{1}{(2\pi)^3} \int d^3p |\beta_{\mathbf{p}}(t)|^2. \tag{37}$$

In the asymptotic limit $t \rightarrow \infty$, the electric field is switched off and in this "out" region the quasiparticles described by the operators $b_{\mathbf{p}}^{(\pm)}(\infty), b_{\mathbf{p}}^{*(\pm)}(\infty)$ become the real free particles. Thus, the total number of real boson pairs created by the electric field during the time of its existence is

$$n^{(0)} = \lim_{t \rightarrow \infty} n^{(0)}(t) = \frac{1}{(2\pi)^3} \int d^3p \left[\lim_{t \rightarrow \infty} |\beta_{\mathbf{p}}(t)|^2 \right]. \tag{38}$$

Similar results have been obtained for the fields and particles with nonzero spin. By omitting the technical details, here, we present only several facts concerning the case of spinor particles. Thus, after the separation of variables in the Dirac equation written for the spinor field interacting with the space homogeneous nonstationary electric field (14) and (15), it reduces to the oscillator equation with the following complex frequency [34,35]:

$$\frac{d^2 f^{(\pm)}(\mathbf{p}, t)}{dt^2} + \left[\omega^2(\mathbf{p}, t) + ie \frac{dA_3(t)}{dt} \right] f^{(\pm)}(\mathbf{p}, t) = 0, \tag{39}$$

where $\omega^2(\mathbf{p}, t)$ is presented in Equation (19) and the positive- and negative-frequency solutions are defined by the following asymptotic behaviors:

$$\lim_{t \rightarrow -\infty} f^{(\pm)}(\mathbf{p}, t) = \frac{1}{\sqrt{4\omega_-(\mathbf{p})[\omega_-(\mathbf{p}) + p^3 - eA_3^-]}} e^{\pm i\omega_-(\mathbf{p})t}. \tag{40}$$

The Hamiltonian of the spinor field interacting with the electric field (14) is given by

$$H^{(1/2)}(t) = \sum_{r=1,2} \int d^3p \omega(\mathbf{p}, t) \left[E(\mathbf{p}, t) \left(a_{\mathbf{p}r}^{*(+)} a_{\mathbf{p}r}^{(-)} - a_{-\mathbf{p}r}^{*(-)} a_{-\mathbf{p}r}^{(+)} \right) + F(\mathbf{p}, t) a_{\mathbf{p}r}^{*(+)} a_{-\mathbf{p}r}^{(+)} + F^*(\mathbf{p}, t) a_{-\mathbf{p}r}^{*(-)} a_{\mathbf{p}r}^{(-)} \right], \tag{41}$$

where the index $r = 1, 2$ corresponds to two possible spin projections on the axis x^3 and the coefficients E and F are defined as

$$E(\mathbf{p}, t) = \frac{4(m^2 + p_\perp^2)}{\omega(\mathbf{p}, t)} \text{Im} \left[f^{(+)*}(\mathbf{p}, t) \frac{df^{(+)}(\mathbf{p}, t)}{dt} \right] - \frac{p_3 - eA_3}{\omega(\mathbf{p}, t)},$$

$$E^2(\mathbf{p}, t) + |F(\mathbf{p}, t)|^2 = 1. \tag{42}$$

Similar to the case of a scalar field, the Hamiltonian (41) becomes diagonal in the asymptotic limit $t \rightarrow -\infty$:

$$H^{(1/2)}(t) = \sum_{r=1,2} \int d^3p \omega_-(\mathbf{p}) \left[a_{\mathbf{p}r}^{*(+)} a_{\mathbf{p}r}^{(-)} - a_{-\mathbf{p}r}^{*(-)} a_{-\mathbf{p}r}^{(+)} \right]. \tag{43}$$

At any t , the Hamiltonian (41) can be diagonalized by the canonical Bogoliubov transformation, preserving the anticommutation relations between the creation and annihilation operators of spinor particles:

$$a_{\mathbf{p}r}^{(-)} = \alpha_{\mathbf{p}}^*(t) b_{\mathbf{p}r}^{(-)}(t) - \beta_{\mathbf{p}}(t) b_{-\mathbf{p}r}^{(+)}(t),$$

$$a_{\mathbf{p}r}^{(+)} = \alpha_{\mathbf{p}}^*(t) b_{\mathbf{p}r}^{(+)}(t) - \beta_{-\mathbf{p}}(t) b_{-\mathbf{p}r}^{(-)}(t), \tag{44}$$

where

$$|\alpha_{\mathbf{p}}(t)|^2 + |\beta_{\mathbf{p}}(t)|^2 = 1. \tag{45}$$

If the coefficients of the Bogoliubov transformation (44) are equal to

$$\frac{\beta_{\mathbf{p}}(t)}{\alpha_{\mathbf{p}}(t)} = \frac{1 - E(\mathbf{p}, t)}{F^*(\mathbf{p}, t)}, \quad |\beta_{\mathbf{p}}(t)|^2 = \frac{1}{2} [1 - E(\mathbf{p}, t)], \tag{46}$$

the Hamiltonian (41) takes the diagonal form at any t in terms of the creation and annihilation operators of quasiparticles [34]:

$$H^{(1/2)}(t) = \sum_{r=1,2} \int d^3p \omega(\mathbf{p}, t) \left[b_{\mathbf{p}r}^{*(+)}(t) b_{\mathbf{p}r}^{(-)}(t) - b_{-\mathbf{p}r}^{*(-)}(t) b_{-\mathbf{p}r}^{(+)}(t) \right]. \tag{47}$$

Similar to Equation (33), the vacuum state of the quasiparticles is defined as

$$b_{\mathbf{p}r}^{(-)}(t) |0_t\rangle = b_{\mathbf{p}r}^{(+)}(t) |0_t\rangle = 0. \tag{48}$$

The number of spinor quasiparticles with momentum \mathbf{p} and spin projection r (and respective antiquasiparticles) created from the ground state $|0_{in}\rangle$ during the time interval from $-\infty$ to t is given by

$$N_{\mathbf{p}r}^{(1/2)}(t) = \langle 0_{in} | b_{\mathbf{p}r}^{*(+)}(t) b_{\mathbf{p}r}^{(-)}(t) | 0_{in} \rangle = \langle 0_{in} | b_{-\mathbf{p}r}^{(+)}(t) b_{-\mathbf{p}r}^{*(-)}(t) | 0_{in} \rangle = |\beta_{\mathbf{p}}(t)|^2 \delta^3(\mathbf{p} = 0). \tag{49}$$

This number does not depend on the spin state r .

The total number of fermion quasiparticle pairs created in the unit space volume during the time interval from $-\infty$ to t is obtained from Equation (49) with the help of Equation (36):

$$n^{(1/2)}(t) = \frac{1}{V} \sum_{r=1,2} \int d^3p N_{\mathbf{p}r}^{(1/2)}(t) = \frac{2}{(2\pi)^3} \int d^3p |\beta_{\mathbf{p}}(t)|^2. \tag{50}$$

Thus, the total number of real fermion pairs created in the unit volume by the electric field is

$$n^{(1/2)} = \frac{2}{(2\pi)^3} \int d^3p [\lim_{t \rightarrow \infty} |\beta_{\mathbf{p}}(t)|^2]. \tag{51}$$

The most simple exactly solvable example allowing an exact calculation of the numbers of created pairs (38) and (51) is the electric field of the following form [32,34]:

$$A^3 = -\frac{E_0}{k_0} \tanh(k_0 t), \quad E_z(t) = \frac{E_0}{\cosh^2(k_0 t)}. \tag{52}$$

This field is switched off in the asymptotic regimes $t \rightarrow \pm\infty$ (see Figure 2).

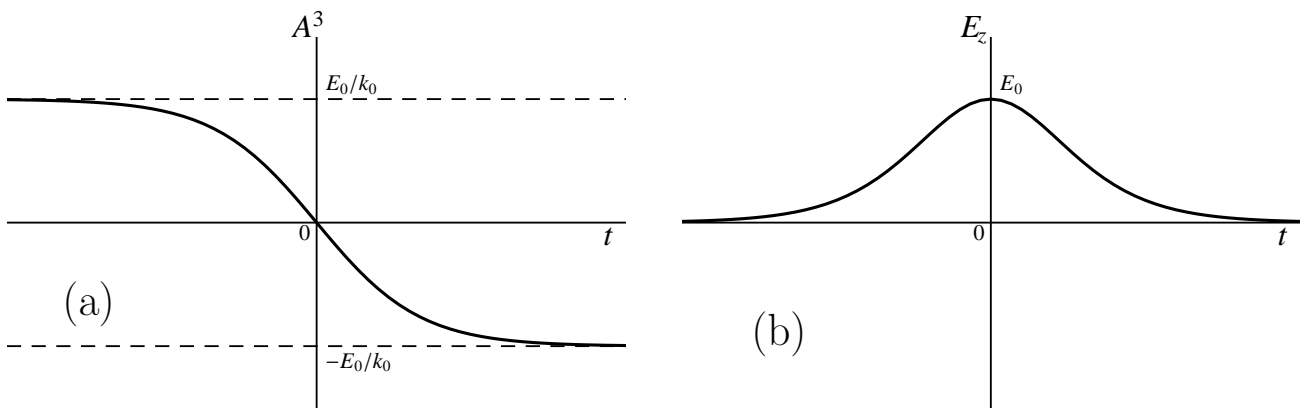


Figure 2. (a) The component of the vector potential and (b) the strength of the space homogeneous nonstationary electric field (52), which is switched off in the asymptotic regimes $t \rightarrow \pm\infty$, are shown as the functions of time.

In the limiting case $k_0 \rightarrow 0$, Equation (52) describes the space homogeneous constant electric field. Thus, Equations (38) and (51) allow for the rederivation of the famous Schwinger results for the pair creation from vacuum by a strong constant field derived by him [37,38] using another formalism.

For the inflationary cosmology (see Section 5, the effect of the exponential growth of the number of scalar particles created with some values of momentum by the periodic in time external field is of much importance. This effect was independently discovered in Ref. [39] for the sinusoidally depending on time A_3 and in Ref. [40] for the electric field of arbitrary form with a period T :

$$A_3(t + T) = A_3(t) \tag{53}$$

during the interval $[0, nT]$. Outside this interval, the electric field was assumed to be equal to zero, so that $A_{3-} = A_{3+} = const.$

It was shown that the number of pairs of scalar particles created by the periodic field with some momenta \mathbf{p} belonging to the instability zones of the oscillator equation during the time nT is the exponentially increasing function of the number of field periods n [40]:

$$n_{\mathbf{p}}^{(0)} = |\beta_{\mathbf{p}}(nT)|^2 = \frac{\sinh^2[nD(\mathbf{p})]}{\sinh^2 D(\mathbf{p})} \frac{1}{4\omega_+^2(\mathbf{p})} \left[\omega_+^2(\mathbf{p})g_1(\mathbf{p}, T) + \left. \frac{dg_2(\mathbf{p}, t)}{dt} \right|_{t=T} \right]^2. \tag{54}$$

Here, $g_1(\mathbf{p}, t)$ and $g_2(\mathbf{p}, t)$ are the solutions of the oscillator Equation (19) satisfying the following initial conditions:

$$\begin{cases} g_1(\mathbf{p}, 0) = 0, \\ \left. \frac{g_1(\mathbf{p}, t)}{dt} \right|_{t=0} = 1, \end{cases} \quad \begin{cases} g_2(\mathbf{p}, 0) = 1, \\ \left. \frac{g_2(\mathbf{p}, t)}{dt} \right|_{t=0} = 0, \end{cases} \tag{55}$$

and $\cosh D(\mathbf{p}) = g_2(\mathbf{p}, T)$, $\omega_+(\mathbf{p}) = \omega_-(\mathbf{p})$.

From Equation (54), it can be seen that the number of created pairs $n_{\mathbf{p}}^{(0)}$ increases with the number of field periods n as $\exp[2nD(\mathbf{p})]$.

The effect of particle creation from a vacuum by an electric field is not observed yet because it becomes sizable for the fields of the order of m^2/e , which are too large ($\sim 10^{16}$ V/cm for electrons). With the discovery of graphene, in which the fermion quasiparticles are massless or very light, the possibility of observing the creation of these quasiparticles in much weaker fields was proposed [41–46]. This is some kind of a condensed matter analogy to Schwinger’s particle creation from a vacuum in quantum electrodynamics.

The above brief discussion allows one to conclude that in quantum field theory and, specifically, in quantum electrodynamics, a description of the effect of particle creation from a vacuum by an external field is based on the S-matrix picture. The concept of real particles is defined in the "in" and "out" regions where the external electric field is switched off. It is common knowledge that in the absence of external fields the theory is invariant relative to the transformations from the Poincaré group, the Casimir operators of which classify particles by the values of their mass and spin [36]. Thus, in curved space–time, which does not become flat in the asymptotic regions, one could expect difficulties with the definition of the concept of particles. In the next section, it is shown that in the case of the expanding Universe, these difficulties can be solved in close analogy to the concept of quasiparticles in the presence of a nonstationary electric field.

4. The Effect of Particle Creation in the Friedmann Universe

As discussed in Section 2, the Friedmann models of the Universe are described by the interval (19). By solving the Einstein equations (4) for the metrical tensor g_{ik} defined in Equation (1), one obtains the scale factors of the closed, open, and quasi-Euclidean models. The matter fields (scalar and spinor, for instance) should be considered in the background of curved space–time defined in Equation (1).

The general covariant generalization of the Klein–Fock–Gordon equation (17) with the electric field $A_k = 0$ is given by

$$\left(\nabla_k \nabla^k + \zeta R + m^2 \right) \varphi(x) = 0, \tag{56}$$

where ∇_k is the covariant derivative and ζ is the so-called coupling coefficient. The most simple case $\zeta = 0$ is referred to as the minimal coupling. In the case $\zeta = 1/6$, considered in Refs. [47,48], Equation (56) becomes invariant under the conformal transformations when $m = 0$. This is called the conformal coupling.

As was first noticed by Schrödinger [6], the positive-frequency solution of Equation (56) with $\zeta = 0$ in the space–time with metric (1) defined at some moment t_0 becomes the linear combination of the negative- and positive-frequency solutions of the same equation defined at a later moment t . Schrödinger interpreted this fact as a creation of matter merely by the expansion of the Universe.

In more detail, the theory of particle creation in the expanding Universe was considered by Parker [49,50] (see also the review in [51]). This consideration was restricted to the quasi-Euclidean model with a flat 3-space ($\kappa = 0$). The space–time of this model, as well as of the other Friedmann models, is not asymptotically flat. Therefore, as discussed in the end of Section 3, the standard concept of particles used in quantum field theory is not applicable.

To solve this problem, Parker elaborated the concept of the so-called adiabatic particles. For this purpose, the solution of Equation (56) was searched in the form of WKB-like approximation including some unknown function, which was next determined from the demand that the number of created particles and of its derivatives of several first orders would take the minimum values. The creation rate of scalar particles defined in this way in the present epoch of the Universe’s evolution was calculated and found to be negligibly small. A similar approach was applied to the effect of creation of spinor particles in the expanding Universe with $\kappa = 0$ [52]. A simple model was proposed where the scalar particles described by the field equation with minimal coupling are created near the cosmological singularity with a black-body spectrum [53].

The separation of variables in Equation (56) for the quasi-Euclidean, closed and open models of the Universe [$\kappa = 0, \pm 1$ in Equations (1) and (3)] was made in the form

$$\varphi_J(x) = \frac{1}{a(\eta)} g_\lambda(\eta) \Phi_J(x), \tag{57}$$

where the dimensionless time variable η is connected with the proper synchronous time t by $dt = a(\eta)d\eta$, λ is the dimensionless momentum quantum number connected with the magnitude of the physical momentum by $p = \lambda/a(\eta)$, $J = (\lambda, l, m)$ is the collective index, and the explicit expressions for the functions φ_J in terms of the associated Legendre polynomials and spherical harmonics Y_{lm} in spaces with $\kappa = 0, \pm 1$ were found in Refs. [54–56].

The substitution of Equation (57) into Equations (1) and (17) results in the following equation for the functions g_λ :

$$\frac{d^2 g_\lambda(\eta)}{d\eta^2} + [\omega_\lambda^2(\eta) - q(\eta)] g_\lambda(\eta) = 0, \tag{58}$$

where

$$\omega_\lambda^2(\eta) = \lambda^2 + m^2 a^2(\eta), \quad q(\eta) = 6 \left(\frac{1}{6} - \xi \right) \left[\frac{1}{a(\eta)} \frac{d^2 a(\eta)}{d\eta^2} + \kappa \right]. \tag{59}$$

For $\kappa = 0, -1$ the dimensionless momentum λ varies from 0 to ∞ , and for $\kappa = 1$, it holds $\lambda = 1, 2, 3, \dots$

It is seen that Equation (58) describes the oscillator with a variable frequency like it was for a scalar field interacting with the nonstationary electric field [compare with Equation (19)]. In this case, the role of the electric field is played by the time-dependent scale factor of the Universe. Equation (58) takes the most simple form for the scalar field with conformal coupling ($\xi = 1/6$), which is physically the most natural generalization of the Klein–Fock–Gordon equation in curved space–time [47,48]. The point is that the massless particles are not characterized by the parameter with a dimension of length and, thus, the corresponding field equation must be invariant with respect to the conformal transformations. Because of this, we consider Equations (56) and (58) with $\xi = 1/6$. As a result, the function g_λ satisfies the following equation:

$$\frac{d^2 g_\lambda(\eta)}{d\eta^2} + \omega_\lambda^2(\eta) g_\lambda(\eta) = 0, \tag{60}$$

where

$$\omega_\lambda^2(\eta) = \lambda^2 + m^2 a^2(\eta). \tag{61}$$

An important difference in the scale factor of the expanding Universe $a(\eta)$ from the vector potential of an external field $A_3(t)$ is that $a(\eta)$ does not become constant at any η , which means that the space–time of the Universe does not become static. In this situation, the corpuscular interpretation of the field can be performed at some moment η_0 by imposing the initial conditions on the solutions of Equation (60):

$$g_\lambda(\eta_0) = \frac{1}{\sqrt{\omega_\lambda(\eta_0)}}, \quad \left. \frac{dg_\lambda(\eta)}{d\eta} \right|_{\eta=\eta_0} = i\omega_\lambda(\eta_0)g_\lambda(\eta_0) \tag{62}$$

and defining the positive- and negative-frequency solutions of Equation (56) as

$$\begin{aligned} \varphi_J^{(+)}(x) &= \frac{1}{\sqrt{2}a(\eta)} g_\lambda(\eta)\Phi_J^*(x), \\ \varphi_J^{(-)}(x) &= \frac{1}{\sqrt{2}a(\eta)} g_\lambda^*(\eta)\Phi_J(x). \end{aligned} \tag{63}$$

Similar to the case of the nonstationary electric field, the functions $\varphi_J^{(\pm)}$ lose the meaning of the negative- and positive-frequency solutions at a later moment $\eta > \eta_0$.

The field operator of the complex scalar field is defined similarly to Equation (22):

$$\varphi(x) = \int d\mu(J) \left[\varphi_J^{(-)}(x)a_J^{(-)} + \varphi_J^{(+)}(x)a_J^{(+)} \right], \tag{64}$$

where the measure on the set of quantum numbers is different for different values of κ :

$$\int d\mu(J) = \begin{cases} \int_0^\infty d\lambda \sum_{l=0}^\infty \sum_{m=-l}^l, & \kappa = -1, 0, \\ \sum_{\lambda=1}^\infty \sum_{l=0}^{\lambda-1} \sum_{m=-l}^l, & \kappa = 1. \end{cases} \tag{65}$$

Then, the vacuum state at the moment η_0 is defined as

$$a_J^{(-)}|0_{\eta_0}\rangle = \bar{a}_J^{(-)}|0_{\eta_0}\rangle = 0. \tag{66}$$

From the above, it becomes clear that it is not possible to introduce the universal concept of particles in the expanding space–time of the Friedmann Universe. It is possible, however, to define the quasiparticles depending on time like it was done in Section 3 for the case of a nonstationary electric field using the method of the diagonalization of the Hamiltonian of a quantized field. Such an approach was suggested in Refs. [57,58] as an alternative to the adiabatic particles introduced in Refs. [49–51].

It is important, however, that the stress–energy tensor and respective Hamiltonian of the quantized scalar field satisfying Equation (56) with $\zeta = 1/6$ should be obtained by the variation in the action not with respect to the field φ , but with respect to the metrical tensor g^{ik} . This is the so-called metrical stress–energy tensor [59]. As a result, the metrical Hamiltonian of the scalar field in the space–time of the expanding Universe takes the following form:

$$\begin{aligned} H^{(0)}(\eta) &= a^2(\eta) \int d^3x f^2(\chi) \sin\theta T_{00}^{\text{metr}}(x) \\ &= a^2(\eta) \int d^3x f^2(\chi) \sin\theta \left[2 \frac{\partial\varphi^*(x)}{\partial\eta} \frac{\partial\varphi(x)}{\partial\eta} - a^2(\eta) g^{ik} \frac{\partial\varphi^*(x)}{\partial x^i} \frac{\partial\varphi(x)}{\partial x^k} \right. \\ &\quad \left. + a^2(\eta) \left(m^2 + \frac{1}{6}R \right) \varphi^*(x)\varphi(x) - \frac{1}{3} \left(R_{00} + \nabla_0\nabla_0 - a^2(\eta)\nabla_k\nabla^k \right) \varphi^*(x)\varphi(x) \right]. \end{aligned} \tag{67}$$

After a substitution of Equation (64) in Equation (67), using the properties of functions (62), one obtains [60,61]

$$H^{(0)}(\eta) = \int d\mu(J)\omega_\lambda(\eta) \left[E_J(\eta) \left(a_J^{*(+)} a_J^{(-)} + a_J^{*(-)} a_J^{(+)} \right) + F_J(\eta) a_J^{*(+)} a_J^{(+)} + F_J^*(\eta) a_J^{*(-)} a_J^{(-)} \right], \tag{68}$$

where $\bar{J} = (\lambda, l, -m)$ and the coefficients E_J and F_J are expressed via the solutions of Equation (60) as

$$\begin{aligned} E_J(\eta) &= \frac{1}{2\omega_\lambda(\eta)} \left(\left| \frac{dg_\lambda(\eta)}{d\eta} \right|^2 + \omega_\lambda^2(\eta) |g_\lambda(\eta)|^2 \right), \\ F_J(\eta) &= \frac{(-1)^m}{2\omega_\lambda(\eta)} \left[\left(\frac{dg_\lambda(\eta)}{d\eta} \right)^2 + \omega_\lambda^2(\eta) g_\lambda^2(\eta) \right], \\ E_J^2(\eta) - |F_J(\eta)|^2 &= 1. \end{aligned} \tag{69}$$

From Equation (70), it is seen that $E_J(\eta)$ in fact depends on λ and does not depend on l and m , whereas $F_J(\eta)$ depends also on m . The quantity $E_J(\eta)$ represents the adiabatic invariant of the oscillator (60) and (61). From Equation (62), it follows that

$$E_J(\eta_0) = 1, \quad F_J(\eta_0) = 0, \tag{70}$$

i.e., the Hamiltonian (68) takes the diagonal form at the initial moment η_0 :

$$H^{(0)}(\eta_0) = \int d\mu(J)\omega_\lambda(\eta_0) \left(a_J^{*(+)} a_J^{(-)} + a_J^{*(-)} a_J^{(+)} \right) \tag{71}$$

in perfect analogy to Equation (28) obtained for the case of an electric field.

Similar to the case of a nonstationary electric field, at any moment, the Hamiltonian (68) can be diagonalized by the canonical Bogoliubov transformations:

$$\begin{aligned} a_J^{(-)} &= \alpha_J^*(\eta) b_J^{(-)}(\eta) - (-1)^m \beta_J(\eta) b_J^{(+)}(\eta), \\ a_J^{*(+)} &= \alpha_J^*(\eta) b_J^{(-)}(\eta) - (-1)^m \beta_J(\eta) b_J^{(+)}(\eta), \\ |\alpha_J(\eta)|^2 - |\beta_J(\eta)|^2 &= 1. \end{aligned} \tag{72}$$

For this purpose, the coefficients α_J and β_J should be chosen as

$$\frac{\beta_J(\eta)}{\alpha_J(\eta)} = (-1)^m \frac{E_J(\eta) - 1}{F_J^*(\eta)}, \quad |\beta_J(\eta)|^2 = \frac{1}{2} [E_J(\eta) - 1]. \tag{73}$$

Substituting Equation (73) with the coefficients (73) in Equation (68), one finds that the Hamiltonian of the scalar in the Friedmann Universe takes the following diagonal form:

$$H^{(0)}(\eta) = \int d\mu(J)\omega_\lambda(\eta) \left(b_J^{*(+)} b_J^{(-)} + b_J^{*(-)} b_J^{(+)} \right) \tag{74}$$

at any moment η .

The annihilation operators for quasiparticles and antiquasiparticles give the possibility to define the time-dependent vacuum state by the following equation:

$$b_J^{(-)}(\eta) |0_\eta\rangle = b_J^{*(-)}(\eta) |0_\eta\rangle = 0, \tag{75}$$

which is similar to Equation (33) in the case of a nonstationary electric field. It is evident that

$$b_j^{(\pm)}(\eta_0) = a_j^{(\pm)}, \quad b_j^{*(\pm)}(\eta_0) = a_j^{*(\pm)}. \tag{76}$$

Next, one can define the number of quasiparticle pairs created from the vacuum state $|0_{\eta_0}\rangle$ during the time interval from η_0 to η in the unit space volume:

$$\begin{aligned} n^{(0)}(\eta) &= \frac{1}{2\pi^2 a^3(\eta)} \int d\mu(\lambda) \langle 0_{\eta_0} | b_j^{*(+)}(\eta) b_j^{(-)}(\eta) | 0_{\eta_0} \rangle \\ &= \frac{1}{2\pi^2 a^3(\eta)} \int d\mu(\lambda) \langle 0_{\eta_0} | b_j^{(+)}(\eta) b_j^{*(-)}(\eta) | 0_{\eta_0} \rangle \\ &= \frac{1}{2\pi^2 a^3(\eta)} \int d\mu(\lambda) |\beta_j(\eta)|^2, \end{aligned} \tag{77}$$

where

$$\int d\mu(\lambda) = \begin{cases} \int_0^\infty \lambda^2 d\lambda, & \kappa = -1, 0, \\ \sum_{\lambda=1}^\infty \lambda^2, & \kappa = 1. \end{cases} \tag{78}$$

For the calculation of the number of created scalar particles, it is reasonable to put $\eta_0 = 0$ and impose on the scale factor $a(\eta)$ the requirement of smoothness at the initial moment $\eta_0 = 0$. This requirement does not contradict to the fact that at the point $\eta = 0$, there was the cosmological singularity where the invariants of the curvature tensor become infinitely large.

The typical scale factors used in the Friedmann cosmological models have the form $a(t) = a_0 t^q$; see, for instance, Equation (8), where $q = 2/3$ for dust-like matter $\varepsilon = \rho, P = 0$. In the vicinity of the cosmological singularity, matter is in the radiation-dominated state ($P = \varepsilon/3$). In this case, $q = 1/2$.

The calculations show that in the epoch $t \ll m^{-1}$ the number of quasiparticle pairs (78) created in the unit volume does not depend on the value of q [60,62]:

$$n^{(0)}(t) = \frac{m^3}{24\pi^2}. \tag{79}$$

An independence of the result (79) on time means that the decrease in the quasiparticle density due to the Universe’s expansion is compensated for by the creation of new quasiparticles.

In the epoch $t \gg m^{-1}$, for the radiation-dominated equation of state ($q = 1/2$), one obtains [62]

$$n^{(0)}(t) = 5.3 \times 10^{-4} m^3 (mt)^{-3/2}. \tag{80}$$

It was shown [62] that, for $t \gg m^{-1}$, the similar result

$$n^{(0)}(t) \sim m^3 (mt)^{-3q} \tag{81}$$

holds for any q satisfying the inequalities $0 < q < 2/3$.

The corresponding results have been obtained also for the energy density of created pairs (see Refs. [60,62] and the review [61]).

The creation of spinor particles in the space–time of the expanding Universe can be considered in perfect analogy with the scalar case, although the mathematical formalism becomes more involved. Thus, the general covariant generalization of the Dirac equation takes the form

$$\left(i\gamma^k(x) \vec{\nabla}_k - m \right) \psi(x) = 0, \tag{82}$$

where $\vec{\nabla}_k$ is the covariant derivative of a bispinor ψ in the Riemannian space-time and $\gamma^k(x)$ is the 4-vector relative to the general coordinate transformations, which is expressed via the standard Dirac γ -matrices and the tetrad $h_{(a)}^k$ as

$$\gamma^k(x) = h_{(a)}^k \gamma^a. \tag{83}$$

An important characteristic feature of Equation (82) is that in the limiting case $m \rightarrow 0$, it becomes invariant under the conformal transformations with no additional modifications.

The separation of the variables in Equation (82) for the space-time (1) was performed in Refs. [55,63]. This results in the oscillator equation for the time-dependent functions $f_{\lambda\pm}$:

$$\frac{d^2 f_{\lambda\pm}(\eta)}{d\eta^2} + \left[\omega_\lambda^2(\eta) \pm im \frac{da(\eta)}{d\eta} \right] f_{\lambda\pm}(\eta) = 0, \tag{84}$$

where ω_λ is defined in Equation (61). It is seen that although, physically, the space-time of the expanding Universe has little in common with the nonstationary electric field considered in Section 3, mathematically, Equation (84) is similar to Equation (39). In doing so, the mass of a spinor field in Equation (84) plays the same role as the electric charge in Equation (39), whereas the scale factor of the Universe a is akin to the vector potential A_3 .

The positive- and negative-frequency solutions of Equation (84) at the moment η_0 are defined by the following initial conditions [61]:

$$f_{\lambda\pm}^{(+)}(\eta_0) = \pm \left[\frac{\omega_\lambda(\eta_0) \mp ma(\eta_0)}{\omega_\lambda(\eta_0)} \right]^{1/2}, \quad f_{\lambda\pm}^{(-)}(\eta_0) = \left[\frac{\omega_\lambda(\eta_0) \pm ma(\eta_0)}{\omega_\lambda(\eta_0)} \right]^{1/2}. \tag{85}$$

It holds also that

$$\left. \frac{df_{\lambda\pm}^{(+)}(\eta)}{d\eta} \right|_{\eta=\eta_0} = i\omega_\lambda(\eta_0) f_{\lambda\pm}^{(+)}(\eta_0), \quad \left. \frac{df_{\lambda\pm}^{(-)}(\eta)}{d\eta} \right|_{\eta=\eta_0} = -i\omega_\lambda(\eta_0) f_{\lambda\pm}^{(-)}(\eta_0). \tag{86}$$

Now, the operator of the spinor field can be written in the form

$$\psi(x) = \int d\mu(J) \left[\psi_J^{(-)}(x) a_J^{(-)} + \psi_J^{(+)}(x) a_J^{(+)} \right], \tag{87}$$

where the collective index J includes four quantum numbers $J = (\lambda, j, l, M)$. In the case $\kappa = 0, -1$ it holds that $0 \leq \lambda < \infty, j = 1/2, 3/2, \dots$, for $\kappa = 1$ one has $\lambda = 3/2, 5/2, \dots, j = 1/2, 3/2, \dots, \lambda - 1$, and in both cases, $l = j \pm 1/2, -j \leq M \leq j$.

The vacuum state at the moment η_0 is defined by Equation (66). Substituting Equation (87) in the Hamiltonian of the spinor field

$$H^{(1/2)}(\eta) = \frac{i}{2} a^3(\eta) \int d^3x f^2(\chi) \sin\theta \psi^+(x) \overleftrightarrow{\partial}_\eta \psi(x), \tag{88}$$

one obtains it in the same form as in Equation (24), but with the coefficients E_J and F_J expressed via the solutions of Equation (84):

$$\begin{aligned} E_J(\eta) &= \frac{1}{\omega_\lambda(\eta)} \left[ma(\eta) \left(1 - |f_{\lambda+}^{(+)}|^2 \right) - \lambda \text{Re} \left(f_{\lambda-}^{(-)} f_{\lambda+}^{(+)} \right) \right], \\ F_J(\eta) &= \frac{1}{\omega_\lambda(\eta)} \left[ma(\eta) f_{\lambda+}^{(+)} f_{\lambda-}^{(+)} - \frac{\lambda}{2} \left(f_{\lambda+}^{(+)^2} - f_{\lambda-}^{(+)^2} \right) \right], \\ E_J^2(\eta) + |F_J(\eta)|^2 &= 1. \end{aligned} \tag{89}$$

These coefficients satisfy the initial conditions (70). As a consequence, at the moment η_0 , the Hamiltonian $H^{(1/2)}(\eta_0)$ takes the diagonal form. At any moment, the Hamiltonian of the spinor field can be diagonalized by the Bogoliubov transformations:

$$\begin{aligned} a_J^{(-)} &= \alpha_J^*(\eta) b_J^{(-)}(\eta) - \beta_J(\eta) b_J^{(+)}(\eta), \\ a_J^{(+)} &= \alpha_J^*(\eta) b_J^{(-)}(\eta) + \beta_J(\eta) b_J^{(+)}(\eta), \\ |\alpha_J(\eta)|^2 + |\beta_J(\eta)|^2 &= 1. \end{aligned} \tag{90}$$

which preserve the anticommutation relations for the creation and annihilation operators.

The Hamiltonian $H^{(1/2)}(\eta)$ takes the diagonal form (74) at any moment η if the Bogoliubov coefficients are defined as

$$\frac{\beta_J(\eta)}{\alpha_J(\eta)} = \frac{1 - E_J(\eta)}{F_J^*(\eta)}, \quad |\beta_J(\eta)|^2 = \frac{1}{2}[1 - E_J(\eta)]. \tag{91}$$

The number of spinor quasiparticle pairs created in the unit space volume is given by [63]

$$\begin{aligned} n^{(1/2)}(\eta) &= \frac{1}{\pi^2 a^3(\eta)} \int d\mu(\lambda) \langle 0_{\eta_0} | b_J^{(+)}(\eta) b_J^{(-)}(\eta) | 0_{\eta_0} \rangle \\ &= \frac{1}{\pi^2 a^3(\eta)} \int d\mu(\lambda) \langle 0_{\eta_0} | b_J^{(+)}(\eta) b_J^{(-)}(\eta) | 0_{\eta_0} \rangle \\ &= \frac{1}{\pi^2 a^3(\eta)} \int d\mu(\lambda) |\beta_J(\eta)|^2, \end{aligned} \tag{92}$$

where $J = (\lambda, j, j \pm 1/2, M)$, $\bar{J} = (\lambda, j, j \mp 1/2, -M)$ and

$$\int d\mu(\lambda) = \begin{cases} \int_0^\infty d\lambda \left(\lambda^2 - \frac{\kappa}{4}\right), & \kappa = -1, 0, \\ \sum_{\lambda=3/2}^\infty \left(\lambda^2 - \frac{1}{4}\right), & \kappa = 1. \end{cases} \tag{93}$$

It is notable that that the geometric nature of the spinor field reveals itself by the presence of κ in the measure of integration (93).

By using Equations (90), (91), and (93), one can calculate the number of spinor quasiparticles created at different epochs of the Universe’s evolution for the scale factors of power type $a(t) = a_0 t^q$. Thus, for $t \ll m^{-1}$, in the case $\kappa = 0$, it holds [64] that

$$n^{(1/2)}(t) = \frac{q^2}{3q - 1} \frac{m^2}{t}. \tag{94}$$

From the comparison of Equations (79) and (94), it is seen that $n^{(1/2)}/n^{(0)} \sim (mt)^{-1} \gg 1$. The additional terms which appear for $\kappa = \pm 1$ are much smaller than (94).

For the epoch $t \gg m^{-1}$, the density of the created spinor quasiparticles is expressed as [61]

$$n^{(1/2)}(t) = K^{(q)} m^3 (mt)^{-3q} + \frac{3q^2 m}{256\pi t^2}, \tag{95}$$

where for the radiation-dominated matter ($q = 1/2$), the coefficient is equal to $K^{(1/2)} = 3.9 \times 10^{-3}$.

As is seen from the above, in the nonstationary curved space–time, the concept of particle loses its unique meaning. The effect of particle creation takes place with any concept of a particle but, for instance, the number of created adiabatic particles may differ from the number of quasiparticles defined by the method of the diagonalization

of the Hamiltonian by means of the Bogoliubov transformations. The covariant quantity describing the quantum effects in the nonstationary space–time of cosmological models is the renormalized vacuum expectation value of the stress–energy tensor of quantized fields. This quantity includes the contributions of both the particle creation and vacuum polarization (see the monographs [27–31] for the obtained results).

5. The Role of Particle Creation in the Transition from Inflationary to Radiation-Dominated Epochs and Further Developments

As discussed in Sections 2 and 4, at the radiation-dominated stage of its evolution the Friedmann Universe is described by the power-type scale factor $a(t) = a_0 t^{1/2}$. This result is obtained by solving the classical Einstein equations, and it does not take into account the quantum effects. However, the extension of the radiation-dominated scale factor down to the Planck time $t_{pl} = G^{1/2} = 5.39 \times 10^{-44}$ s creates serious problems. One of them is the following. Calculations show that, at the Planck time, the size of the Universe was $a(t_{pl}) \sim 10^{-3}$ cm, i.e., it was by almost 30 orders of magnitude larger than the Planck length $l_{pl} = 1.62 \times 10^{-33}$ cm traveled by light during t_{pl} .

From this it follows that if the radiation scale factor were valid down to $t_0 = 0$, at $t = t_{pl}$ the Universe would comprise of about 10^{89} causally disconnected domains. No evidence, however, was found regarding differences in the temperature of relic radiation received from different directions in the sky. Thus, the initial expansion of the Universe happened much faster than it is predicted by the power-type law. This inconsistency was called the horizon problem.

As noted in the end of Section 4, the covariant description of the vacuum quantum effects in curved space–time is provided by the renormalized vacuum expectation value of the stress–energy tensor of quantized matter fields. In Refs. [65,66] published in the beginning of 1980, this quantity was considered a single source of curved space–time of the Universe. For this purpose, the self-consistent Einstein equations with no cosmological term,

$$R_{ik} - \frac{1}{2}Rg_{ik} = 8\pi G \langle 0|T_{ik}|0 \rangle_{\text{ren}} \tag{96}$$

have been solved and the de Sitter solutions were obtained. For instance, for a stress–energy tensor of massless scalar field in the closed Friedmann model, the solution of Equation (96) is

$$a(t) = \sqrt{\frac{G}{360\pi}} \cosh\left(t\sqrt{\frac{360\pi}{G}}\right), \tag{97}$$

i.e., for $t > t_{pl}$, the Universe’s expansion goes on exponentially fast. The comparison of Equation (97) with Equation (13) shows that the vacuum stress–energy tensor of the quantized scalar field plays the same role as the cosmological term in Einstein’s equations (4) with $T_{ik} = 0$. In Ref. [66], it was shown that under the impact of the creation of scalarons and their subsequent decay into standard particles the exponentially fast de Sitter expansion of the Universe passes into the power-type expansion of the radiation-dominated stage of its evolution.

In 1981, another approach to the understanding of the exponentially fast expansion of the Universe near the cosmological singularity was suggested, which was called inflation [67]. This approach introduces the minimally coupled classical scalar field $\phi = \phi(t)$ called the inflaton field with the following Lagrangian:

$$L(\phi) = \frac{1}{2} \left[\left(\frac{d\phi}{dt} \right)^2 - m^2 \phi^2 \right]. \tag{98}$$

The corresponding Klein–Fock–Gordon equation in the space–time with metric (1) is

$$\frac{d^2\phi}{dt^2} + \frac{3}{a} \frac{da}{dt} \frac{d\phi}{dt} + m^2 \phi = 0. \tag{99}$$

In the simplest case of the quasi-Euclidean model ($\kappa = 0$), the second equality in Equation (5) with $\Lambda = 0$ is

$$\frac{1}{a^2} \left(\frac{da}{dt} \right)^2 = \frac{8\pi G}{3} \varepsilon, \tag{100}$$

where the space–time is determined by the energy density of the inflaton field:

$$\varepsilon = \frac{1}{2} \left[\left(\frac{d\phi}{dt} \right)^2 + m^2 \phi^2 \right]. \tag{101}$$

According to Ref. [68], at the inflationary stage, the second term on the left-hand side of Equation (99) is much larger than the first one and the term $m^2 \phi^2$ in Equation (101) is much larger than $(d\phi/dt)^2$. As a result, the scale factor $a(t)$ found from Equations (100) and (101) takes the following quasi exponential form:

$$a(t) = \tilde{a}_0 \exp \left(2m \sqrt{\frac{\pi G}{3}} \phi t \right). \tag{102}$$

In subsequent years, many papers were published devoted to different versions of the inflationary cosmology (see, e.g., Refs. [69–72] and the monographs [73,74]).

The model of inflation has inspired a renewed interest in the effect of particle creation in the nonstationary external fields and in the space–time of the expanding Universe. The point is that at the end of the inflationary stage of the Universe’s evolution, the energy density becomes very low and the inflaton field oscillates near the minimum of its potential [in Equation (98), the simplest potential $V = m^2 \phi^2 / 2$ is chosen]. The standard elementary particles were created during this period, which was called the process of reheating after inflation [73,75].

The theory of the process of reheating is based on the effect of the exponential growth of the number of particle–antiparticle pairs created from vacuum by the time-periodic field with some momenta belonging to the instability zones of the Klein–Fock–Gordon equation (see Section 3). In this case, the role of a periodic electric field is played by the oscillating inflaton field [76,77]. The theory of reheating after inflation has been elaborated on by many authors (see, e.g., Refs. [78–87]). The main features of this theory are summarized in Ref. [68].

Over the last 25 years, the effect of particle creation in the expanding Universe continued to attract the considerable attention of experts in quantum field theory and cosmology. Here, we mention only several papers devoted to this subject. Thus, in Ref. [88], the effect of the creation of light particles called moduli during and after inflation was investigated not only numerically but also analytically. It was shown that the dominant contribution to the particle creation is given by the long-wavelength fluctuations of light scalar fields generated during inflation.

In Ref. [89], the complex WKB approximation technique was used to study the thermal particle creation in both the black holes and in the space–time of the expanding Universe. According to the results obtained, the temperature of the particle spectrum is determined by the slope of the scale factor of the cosmological model.

The effect of particle creation in the anisotropic expanding Universe (see the pioneer Ref. [90]) was further considered in Ref. [91] using the formalism of squeezed vacuum states for a minimally coupled scalar field. The semiclassical Einstein equations of the form of Equation (96), but in the anisotropic case, were discussed. Note that Ref. [90] presented the powerful regularization method for the vacuum stress–energy tensor and derived the dynamical equations for the nonstationary Bogoliubov coefficients, which were actively used in both anisotropic and isotropic spaces.

In Ref. [92], the above Equations (81) and (95) were used to describe the creation of superheavy scalar and spinor particles, the decay of which could explain the baryon number of the Universe and the nature of cold dark matter. Note that previously the

creation of superheavy particles as the constituents of dark matter in various models of inflation was analyzed in Ref. [93]. It was hypothesized that the decay products of the superheavy constituents of cold dark matter are observed as the cosmic rays of ultra-high energy [92].

The method of the diagonalization of the Hamiltonian of a quantized massless scalar field with minimal coupling was used in Ref. [94] to calculate the particle creation rate in the expanding Universe of the quasi-Euclidean type. It was assumed that the background matter is described by the equation of state of a perfect fluid, which may violate the strong energy condition $\varepsilon + P \geq 0, \varepsilon + 3P \geq 0$. According to the results obtained, the particle creation rate decreases with time if the strong energy condition is satisfied and increases otherwise.

The creation of dark matter particles, which interact only gravitationally, in the expanding Universe of the quasi-Euclidean type was investigated in Ref. [95]. In the suggested model, the real scalar field with an arbitrary coupling ξ , the quanta of which can be considered the candidates for dark matter particles, enters into the Lagrangian density along with the inflaton field, but does not interact with it. By calculating the particle creation rate from the adiabatic vacuum [28] during the transition period from inflation to reheating, it was shown that heavy scalar particles of this kind can be effectively produced if their mass is of the order of or less than the mass of an inflaton field.

The method of Hamiltonian diagonalization discussed in Sections 3 and 4 was also applied in Ref. [96] to describe the creation of superheavy particles conformally coupled to gravity in the model of quintessential inflation [97]. It was argued [96] that the subsequent decay of these particles leads to the formation of relativistic plasma and eventually results in the universally accepted picture of the hot universe.

Similar to the creation of particles in a nonstationary electric field, which has a condensed matter analogy with quasiparticles in graphene, there are the condensed matter analogies to the particle creation in cosmology. Recently, it was found [98] that the expanding Universe resembles the ultracold quantum fluid of light, where a spatial coordinate plays the role of time. According to the authors, they observed the acoustic peaks in the power spectrum, which is in quantitative agreement with theoretical predictions. The observed spectrum was compared with that of the cosmic microwave background power spectrum. Another possibility for the simulation of the process of particle creation in the expanding Universe in the laboratory by means of ultra-cold atoms in Raman optical lattices was considered in Ref. [99].

Some more recent publications devoted to the effect of particle creation in the expanding Universe are reflected on in the review [100].

6. Discussion

Herein, we have considered the prediction of the Universe's expansion made by Alexander Friedmann a century ago that holds the greatest importance and interest today. Particular attention has been given to the way in which this discovery was made. According to the adduced arguments, it is not an accident that such a breakthrough result was obtained by a mathematician. Several outstanding physicists, including the great Einstein, worked on the same subject, but they were tied by some additional considerations of a methodological character implying the static character of our Universe.

Quite to the contrary, Friedmann restricted himself only to the necessary minimum assumptions, such as the homogeneity and isotropy of space, and searched for the formal mathematical consequences following from the fundamental Einstein equations with no prejudice. In doing so, Friedmann discovered that typical cosmological solutions of Einstein equations describe the expanding Universe. This example shows that the mathematical formalisms of fundamental physical theories, such as the general theory of relativity, may, in some sense, be more clever than their creators and again raises the question raised by Wigner about the unreasonable effectiveness of mathematics in natural sciences [25].

The importance of Friedmann's prediction of the Universe's expansion is difficult to overestimate. After a comprehensive experimental confirmation, the concept of the expanding Universe laid the groundwork for the modern picture of the world. As substantiated in Ref. [101], this fact gives grounds to include the name of Friedmann along with the names of Ptolemy, Copernicus, and Newton, who created the scientific pictures of the Universe accepted in previous epochs.

The expansion of the Universe leads to many outstanding consequences and one of them, foreshadowed by Erwin Schrödinger, is the creation of particle–antiparticle pairs from the vacuum of quantized fields. According to a comparison performed in Sections 3 and 4, the effect of the creation of particles in the expanding Universe is mathematically analogous to that in the nonstationary electric field in spite of quite different physical situations in both cases.

The main results obtained in the literature on the creation of particles in the expanding Universe by the method of Hamiltonian diagonalization and other methods show that this effect played an important role at the very early stages of its evolution and, especially, during the transition period between the inflationary and radiation-dominated epochs. According to the results obtained, the effect of pair creation could also contribute to the formation of dark matter.

7. Conclusions

To conclude, in this brief review, devoted to the one hundredth anniversary of Alexander Friedmann's prediction of the Universe's expansion, we have considered several facts of his biography which were helpful for making this outstanding discovery. The results published by Friedmann in 1922 [4] and 1924 [5] were presented above with emphasis on the role of mathematics in their obtainment. Some historical facts, including the dispute with Albert Einstein, and further developments of the Friedmann cosmology, are elucidated.

The Universe's expansion leads to the quantum creation from a vacuum of particle–antiparticle pairs. This effect was discussed above in close connection with a more familiar effect of pair creation by the nonstationary electric field. The comparison studies of these two effects by the method of Hamiltonian diagonalization was performed and both the similarities and distinctions between them were analyzed. Several results for the numbers of scalar and spinor pairs created at different stages of the Universe's evolution are presented. Special attention was paid to the inflationary stage of the Universe's evolution and to the transition period to the epoch of the radiation-dominated Universe, where the effect of particle creation was of primary importance for the formation of relativistic plasma and cold dark matter.

By and large, the prediction of the Universe's expansion made by Alexander Friedmann laid the foundation for the development of modern cosmology during the last century and offered possibilities for the description of vacuum quantum effects in a nonstationary space–time by the formalism of quantum field theory in the presence of external fields.

Funding: This work was partially funded by the Ministry of Science and Higher Education of the Russian Federation (“The World-Class Research Center: Advanced Digital Technologies”, contract No. 075-15-2022-311 dated 20 April 2022). It was also partially carried out in accordance with the Strategic Academic Leadership Program “Priority 2030” of the Kazan Federal University.

Data Availability Statement: All references to the used data are contained in the text.

Acknowledgments: The author is grateful to G. L. Klimchitskaya for helpful discussions.

Conflicts of Interest: The author declares no conflicts of interest.

References

1. Newton, I. *The Mathematical Principles of Natural Philosophy*; Cambridge University Press: Cambridge, UK, 2021.
2. Einstein, A. Zur allgemeinen Relativitätstheorie. *Sitzungsber. Königlich Preuss. Akad. Wiss. (Berlin)* **1915**, *44*, 778–786; Translated: On the general theory of relativity. In *The Collected Papers of Albert Einstein. Volume 6: The Berlin Years: Writings, 1914–1917 (English Translation Supplement)*; Klein, M.J., Kox, A.J., Schulman, R., Eds.; Princeton University Press: Princeton, NJ, USA, 1997; pp. 98–106.
3. Einstein, A. Kosmologische Betrachtungen zur allgemeinen Relativitätstheorie. *Sitzungsber. Königlich Preuss. Akad. Wiss. (Berlin)* **1917**, *6*, 142–152; Translated: Cosmological considerations in the general theory of relativity. In *The Collected Papers of Albert Einstein. Volume 6: The Berlin Years: Writings, 1914–1917 (English Translation Supplement)*; Klein, M.J., Kox, A.J., Schulman, R., Eds.; Princeton University Press: Princeton, NJ, USA, 1997; pp. 421–432.
4. Friedmann, A.A. Über die Krümmung des Raumes. *Z. Phys.* **1922**, *10*, 377–386. [CrossRef]
5. Friedmann, A.A. Über die Möglichkeit einer Welt mit konstanter negativer Krümmung des Raumes. *Z. Phys.* **1924**, *21*, 326–332. [CrossRef]
6. Schrödinger, E. The proper vibrations of the expanding universe. *Physica* **1939**, *6*, 899–912. [CrossRef]
7. Frenkel', V.Y. Aleksandr Aleksandrovich Fridman (Friedmann): A biographical essay. *Uspekhi Fiz. Nauk* **1988**, *155*, 481–516; Translated: *Sov. Phys. Usp.* **1988**, *31*, 645–665. [CrossRef]
8. Tropp, E.A.; Frenkel, V.Y.; Chernin, A.D. *Alexander A. Friedmann: The Man Who Made the Universe Expand*; Cambridge University Press: Cambridge, UK, 2006.
9. Tamarkine, J.; Friedmann, A.A. Sur les congruences du second degré et les nombres de Bernoulli. *Math. Ann.* **1906**, *62*, 409–412. [CrossRef]
10. de Sitter, W. On Einstein's theory of gravitation and its astronomical consequences. First paper. *Mon. Not. R. Astron. Soc.* **1916**, *76*, 699–728. [CrossRef]
11. Landau, E.M.; Lifshitz, E.M. *The Classical Theory of Fields*; Pergamon: Oxford, UK, 1971.
12. Bonnor, W.B. The instability of the Einstein universe. *Mon. Not. R. Astron. Soc.* **1955**, *115*, 310–322. [CrossRef]
13. Zeldovich, Yu.B.; Novikov, I.D. *The Structure and Evolution of the Universe*; University of Chicago Press: Chicago, IL, USA, 1983.
14. Einstein, A. Bemerkung zu der Arbeit von A. Friedmann "Über die Krümmung des Raumes". *Z. Phys.* **1922**, *11*, 326; Translated: Comment on A. Friedman's paper: "On the curvature of space". In *The Collected Papers of Albert Einstein. Volume 13: The Berlin Years: & Correspondence, January 1922–March 1923 (English Translation Supplement)*; Kormos Buchwald, D.; Illy, J.; Rosenkranz, Z.; Sauer T., Eds.; Princeton University Press: Princeton, NJ, USA, 2013; pp. 271–272. [CrossRef]
15. Einstein, A. Notiz zu der Arbeit von A. Friedmann "Über die Krümmung des Raumes". *Z. Phys.* **1923**, *16*, 228; Translated: Note to the paper by A. Friedmann "On the curvature of space". In *The Collected Papers of Albert Einstein. Volume 14: The Berlin Years: & Correspondence, April 1923–May 1925 (English Translation Supplement)*; Kormos Buchwald, D.; Illy, J.; Rosenkranz, Z.; Sauer T., Eds.; Princeton University Press: Princeton, NJ, USA, 2015; p. 47. [CrossRef]
16. Slipher, V.M. The radial velocity of the Andromeda Nebula. *Lowell Observat. Bull.* **1913**, *2*, 56–57.
17. Lemaître, G. Un univers homogène de masse constante et de rayon croissant, rendant compte de la vitesse radiale des nébuleuses extra-galactiques. *Ann. Soc. Sci. Brux. A* **1927**, *47*, 49–59.
18. Hubble, E. A relation between distance and radial velocity among extra-galactic nebulae. *Proc. Nat. Acad. Sci. USA* **1929**, *15*, 168–173. [CrossRef]
19. Hubble, E.P. A spiral nebula as a stellar system, Messier 31. *Astrophys. J.* **1929**, *69*, 103–158. [CrossRef]
20. Robertson, H.P. Kinematics and world structure. *Astrophys. J.* **1935**, *82*, 284–301. [CrossRef]
21. Walker A.G. On Milne's theory of world-structure. *Proc. Lond. Math. Soc.* **1937**, *42*, 90–127. [CrossRef]
22. Gamow, G. Expanding universe and the origin of elements. *Phys. Rev.* **1946**, *70*, 572–573. [CrossRef]
23. Alpher, R.A.; Herman, R.C. Evolution of the Universe. *Nature* **1948**, *162*, 774–775. [CrossRef]
24. Penzias, A.A.; Wilson, R.W. A Measurement of Excess Antenna Temperature at 4080 Mc/s. *Astrophys. J. Lett.* **1965**, *142*, 419–421. [CrossRef]
25. Wigner, E.P. The unreasonable effectiveness of mathematics in the natural sciences. *Comm. Pure Appl. Math.* **1960**, *13*, 1–14. [CrossRef]
26. Friedmann, A.A. *Mir kak Prostranstvo i Vremya*; Academia: Petersburg, Russia, 1923; Translated *The World as Space and Time*; Minkowski Institute Press: Montreal, QC, Canada, 2014.
27. Grib, A.A.; Mamayev, S.G.; Mostepanenko, V.M. *Kvantovye Effekty v Intensivnykh Vneshnikh Polyakh*; Atomizdat: Moscow, Russia, 1980; Translated: *Vacuum Quantum Effects in Strong Fields*; Friedmann Laboratory Publishing: St. Petersburg, Russia, 1994.
28. Birrell, N.D.; Davies, P.C.D. *Quantum Fields in Curved Space*; Cambridge University Press: Cambridge, UK, 1982.
29. Fulling, S.A. *Aspects of Quantum Field Theory in Curved Space-Time*; Cambridge University Press: Cambridge, UK, 1989.
30. Mukhanov, V.; Winitzki, S. *Introduction to Quantum Effects in Gravity*; Cambridge University Press: Cambridge, UK, 2007.
31. Parker, L.; Toms, D. *Quantum Field Theory in Curved Spacetime: Quantized Fields and Gravity*; Cambridge University Press: Cambridge, UK, 2009.
32. Nikishov, A.I. Barrier scattering in field theory removal of Klein paradox. *Nucl. Phys. B* **1970**, *21*, 346–358. [CrossRef]
33. Brezin, E.; Itzykson, C. Pair production in vacuum by an alternating field. *Phys. Rev. D* **1970**, *2*, 1191–1198. [CrossRef]

34. Grib, V.M.; Mostepanenko, V.M.; Frolov, V.M. Particle creation from vacuum by a homogeneous electric field in the canonical formalism. *Teor. Matem. Fiz.* **1972**, *13*, 377–390; Translated: *Theor. Math. Phys.* **1972**, *13*, 1207–1217. [CrossRef]
35. Popov, V.S. Pair production in a variable and homogeneous electric field as an oscillator problem. *Zh. Eksp. Teor. Fiz.* **1972**, *62*, 1248–1262; Translated: *Sov. Phys. JETP* **1972**, *35*, 659–666.
36. Schweber, S.S. *Introduction to Relativistic Quantum Field Theory*; Dover Publications: New York, NY, USA, 2005.
37. Schwinger, J. On gauge invariance and vacuum polarization. *Phys. Rev.* **1951**, *82*, 664–679. [CrossRef]
38. Schwinger, J. The theory of quantized fields. V. *Phys. Rev.* **1954**, *93*, 615–626. [CrossRef]
39. Narozhnyi, N.B.; Nikishov, A.I. Pair production by a periodic electric field. *Zh. Eksp. Teor. Fiz.* **1973**, *65*, 862–874; Translated: *Sov. Phys. JETP* **1974**, *38*, 427–432.
40. Mostepanenko, V.M.; Frolov, V.M. Production of particles from vacuum by a uniform electric-field with periodic time-dependence. *Yad. Fiz.* **1974**, *19*, 885–896; Translated: *Sov. J. Nucl. Phys.* **1974**, *19*, 451–456.
41. Allor, D.; Cohen, T.D.; McGady, D.A. Schwinger mechanism and graphene. *Phys. Rev. D* **2008**, *78*, 096009. [CrossRef]
42. Beneventano, C.G.; Giacconi, P.; Santangelo, E.M.; Soldati, R. Planar QED at finite temperature and density: Hall conductivity, Berry’s phases and minimal conductivity of graphene. *J. Phys. A* **2009**, *42*, 275401. [CrossRef]
43. Klimchitskaya, G.L.; Mostepanenko, V.M. Creation of quasiparticles in graphene by a time-dependent electric field. *Phys. Rev. D* **2013**, *87*, 125011. [CrossRef]
44. Akal, I.; Egger, R.; Müller, C.; Villarba-Chávez, S. Low-dimensional approach to pair production in an oscillating electric field: Application to bandgap graphene layers. *Phys. Rev. D* **2016**, *93*, 116006. [CrossRef]
45. Akal, I.; Egger, R.; Müller, C.; Villarba-Chávez, S. Simulating dynamically assisted production of Dirac pairs in gapped graphene monolayers. *Phys. Rev. D* **2019**, *99*, 016025. [CrossRef]
46. Golub, A.; Egger, R.; Müller, C.; Villarba-Chávez, S. Dimensionality-Driven Photoproduction of Massive Dirac Pairs near Threshold in Gapped Graphene Monolayers. *Phys. Rev. Lett.* **2020**, *124*, 110403. [CrossRef]
47. Gürsey, F. Reformulation of general relativity in accordance with Mach’s principle. *Ann. Phys.* **1963**, *24*, 211–242. [CrossRef]
48. Penrose, R. Conformal treatment of infinity. In *Relativity, Groups, and Topology*; DeWitt, B.S., Ed.; Gordon and Breach: New York, NY, USA, 1964.
49. Parker, L. Particle Creation in Expanding Universes. *Phys. Rev. Lett.* **1968**, *21*, 562–564. [CrossRef]
50. Parker, L. Quantized fields and particle creation in expanding universes. I. *Phys. Rev.* **1969**, *183*, 1057–1068. [CrossRef]
51. Parker, L. Particle creation and particle number in an expanding universe. *J. Phys. A Math. Theor.* **2012**, *45*, 374023. [CrossRef]
52. Parker, L. Quantized fields and particle creation in expanding universes. II. *Phys. Rev. D* **1971**, *3*, 346–356. [CrossRef]
53. Parker, L. Thermal radiation produced by the expansion of the universe. *Nature* **1976**, *261*, 20–23. [CrossRef]
54. Grib, A.A.; Levitskii, B.A.; Mostepanenko, V.M. Particle creation from vacuum by a nonstationary gravitational field in the canonical formalism. *Teor. Matem. Fiz.* **1974**, *19*, 59–75; Translated: *Theor. Math. Phys.* **1974**, *19*, 349–361. [CrossRef]
55. Levitskii, B.A.; Mostepanenko, V.M.; Frolov, V.M. The properties of basis functions of expansions invariant relative to the group $O(4)$. *Dokl. USSR* **1975**, *220*, 61–64; Translated: *Sov. Phys. Dokl.* **1975**, *20*, 29–30.
56. Parker, L.; Fulling S.A. Adiabatic regularization of the energy-momentum tensor of a quantized field in homogeneous spaces. *Phys. Rev. D* **1974**, *9*, 341–354. [CrossRef]
57. Grib, A.A.; Mamayev, S.G. On field theory in Friedmann space. *Yad. Fiz.* **1969**, *10*, 1276–1281; Translated: *Sov. J. Nucl. Phys.* **1970**, *10*, 722–725.
58. Grib, A.A.; Mamayev, S.G. Creation of matter in Friedmann model of the Universe. *Yad. Fiz.* **1971**, *14*, 800–805; Translated: *Sov. J. Nucl. Phys.* **1972**, *14*, 450–452.
59. Chernikov, N.A.; Tagirov, E.A. Quantum theory of scalar field in de Sitter space-time. *Ann. Inst. H. Poincaré Phys. Théor.* **1968**, *9*, 109–141.
60. Grib, A.A.; Mamayev, S.G.; Mostepanenko, V.M. Particle creation from vacuum in homogeneous isotropic models of the Universe. *Gen. Relat. Gravit.* **1976**, *7*, 535–547. [CrossRef]
61. Grib, A.A.; Mamayev, S.G.; Mostepanenko, V.M. Vacuum stress-energy tensor and particle creation in isotropic cosmological models. *Fortschr. Der Phys.* **1980**, *28*, 173–199. [CrossRef]
62. Mamayev, S.G.; Mostepanenko, V.M.; Starobinskii, A.A. Particle creation from the vacuum near a homogeneous isotropic singularity. *Zh. Eksp. Teor. Fiz.* **1976**, *70*, 1577–1591; Translated: *Sov. Phys. JETP* **1976**, *43*, 823–830.
63. Mamayev, S.G.; Mostepanenko, V.M.; Frolov, V.M. Production of fermion pairs by a nonstationary gravitational field. *Yad. Fiz.* **1976**, *23*, 1118–1127; Translated: *Sov. J. Nucl. Phys.* **1976**, *23*, 592–597.
64. Mamayev, S.G.; Mostepanenko, V.M. Regularization of the fermion stress-energy tensor in isotropic models of the Universe. *Phys. Lett. A* **1978**, *67*, 165–168. [CrossRef]
65. Mamayev, S.G.; Mostepanenko V.M. Isotropic cosmological models determined by the vacuum quantum effects. *Zh. Eksp. Teor. Fiz.* **1980**, *78*, 20–27; Translated: *Sov. Phys. JETP* **1980**, *51*, 9–13.
66. Starobinsky, A.A. A new type of isotropic cosmological models without singularity. *Phys. Lett. A* **1980**, *91*, 99–102. [CrossRef]
67. Guth, A.H. Inflationary universe: A possible solution to the horizon and flatness problems. *Phys. Rev. D* **1981**, *23*, 347–356. [CrossRef]
68. Kofman, L.; Linde, A.D.; Starobinsky, A.A. Towards the theory of reheating after inflation. *Phys. Rev. D* **1997**, *56*, 3258–3295. [CrossRef]

69. Linde, A.D. A new inflationary universe scenario: A possible solution of the horizon, flatness, homogeneity, isotropy and primordial monopole problems. *Phys. Lett. B* **1982**, *108*, 389–393. [CrossRef]
70. Guth, A.H.; Weinberg, E.J. Could the universe have recovered from a slow first-order phase transition? *Nucl. Phys. B* **1983**, *212*, 321–364. [CrossRef]
71. Albrecht, A.; Steinhardt, P.J. Cosmology for Grand Unified Theories with Radiatively Induced Symmetry Breaking. *Phys. Rev. Lett.* **1982**, *48*, 1220–1223. [CrossRef]
72. Linde, A.D. Chaotic inflation. *Phys. Lett. B* **1983**, *129*, 177–181. [CrossRef]
73. Linde, A.D. *Particle Physics and Inflationary Cosmology*; Harwood: Chur, Switzerland, 1990.
74. Guth, A.H. *The Inflationary Universe: The Quest for a New Theory of Cosmic Origins*; Basic Books: New York, NY, USA, 1997.
75. Kofman, L.; Linde, A.; Starobinsky, A.A. Reheating after Inflation. *Phys. Rev. Lett.* **1994**, *73*, 3195–3198. [CrossRef]
76. Dolgov, A.D.; Kirilova, D.P. On particle creation by a time-dependent scalar field. *Yad. Fiz.* **1990**, *51*, 273–282; Translated: *Sov. J. Nucl. Phys.* **1990**, *51* 172–177.
77. Traschen, J.H.; Brandenberger, R.H. Particle production during out-of-equilibrium phase transitions. *Phys. Rev. D* **1990**, *42*, 2491–2504. [CrossRef] [PubMed]
78. Boyanovsky, D.; de Vega, H.J.; Holman, R.; Lee, D.-S.; Singh, A. Dissipation via particle production in scalar field theories. *Phys. Rev. D* **1995**, *51*, 4419–4444. [CrossRef] [PubMed]
79. Kaiser, D.I. Post-inflation reheating in an expanding universe. *Phys. Rev. D* **1996**, *53*, 1776–1783. [CrossRef] [PubMed]
80. Fujisaki, H.; Kumekawa, K.; Yamaguchi, M.; Yoshimura, M. Particle production and dissipative cosmic field. *Phys. Rev. D* **1996**, *53*, 6805–6812. [CrossRef] [PubMed]
81. Kasuya, S.; Kawasaki, M. Restriction to parametric resonant decay after inflation. *Phys. Lett. B* **1996**, *388*, 686–691. [CrossRef]
82. Son, D.T. Reheating and thermalization in a simple scalar model. *Phys. Rev. D* **1996**, *54*, 3745–3761. [CrossRef] [PubMed]
83. Riotto, A.; Tkachev, I.I. Non-equilibrium symmetry restoration beyond one loop. *Phys. Lett. B* **1996**, *385*, 57–62. [CrossRef]
84. Allahverdi, R.; Campbell, B.A. Cosmological reheating and self-interacting final state bosons. *Phys. Lett. B* **1997**, *395*, 169–177. [CrossRef]
85. Prokopec, T.; Roos, T.G. Lattice study of classical inflaton decay. *Phys. Rev. D* **1997**, *55*, 3768–3775. [CrossRef]
86. Khlebnikov, S.; Tkachev, I. Relic gravitational waves produced after preheating. *Phys. Rev. D* **1997**, *56*, 653–660. [CrossRef]
87. Moss, I.G.; Graham, C. Particle production and reheating of the inflationary universe. *Phys. Rev. D* **2008**, *78*, 123526. [CrossRef]
88. Felder, G.; Kofman, L.; Linde, A. Gravitational particle production and the moduli problem. *JHEP* **2000**, *2000*, 027. [CrossRef]
89. Biswas, S.; Shaw, A.; Misra, P. Particle production in expanding spacetime. *Gen. Relat. Gravit.* **2002**, *34*, 665–678. [CrossRef]
90. Zel'dovich, Y.B.; Starobinsky, A.A. Particle production and vacuum polarization in an anisotropic gravitational field. *Zh. Eksp. Teor. Fiz.* **1971**, *61*, 2161–2175; Translated: *Sov. Phys. JETP* **1972**, *34*, 1159–1166.
91. Suresh, P.K. Particle creation in anisotropically expanding Universe. *Int. J. Theor. Phys.* **2005**, *44*, 645–654. [CrossRef]
92. Grib, A.A.; Pavlov, Y.V. Dark matter in the early Universe and the creation of visible particles. *Gravit. Cosmol.* **2005**, *11*, 119–122.
93. Chung, D.J.H.; Crotty, P.; Kolb, E.W.; Riotto, A. Gravitational production of superheavy dark matter. *Phys. Rev. D* **2001**, *64*, 043503. [CrossRef]
94. Batista, A.B.; Fabris, J.C.; Houndjo, S.J.M. Particle production in an expanding universe dominated by dark energy fluid. *Gravit. Cosmol.* **2008**, *14*, 140–146. [CrossRef]
95. Ema, Y.; Nakayama, K.; Tanga, Y. Production of purely gravitational dark matter. *JHEP* **2018**, *2018*, 135. [CrossRef]
96. de Haro, J.; Pan, S.; Aresté Saló, L. Understanding gravitational particle production in quintessential inflation. *J. Cosmol. Astropart. Phys.* **2019**, *2019*, 056. [CrossRef]
97. Peebles, P.J.E.; Vilenkin, A. Quintessential inflation. *Phys. Rev. D* **1999**, *59*, 063505. [CrossRef]
98. Steinhauer, J.; Abuzarli, M.; Aladjidi, T.; Bienaimé, T.; Piekarski, C.; Liu, W.; Giacobino, E.; Bramati, A.; Glorieux, Q. Analogue cosmological particle creation in an ultracold quantum fluid of light. *Nat. Commun.* **2022**, *13*, 2890. [CrossRef]
99. Fulgado-Claudio, C.; Sánchez Velázquez, J.M.; Bermudez, A. Fermion production at the boundary of an expanding universe: A cold-atom gravitational analogue. *Quantum* **2023**, *7*, 1042. [CrossRef]
100. Ford, L.H. Cosmological particle production: A review. *Rep. Progr. Phys.* **2021**, *84*, 116901. [CrossRef]
101. Klimchitskaya, G.L.; Mostepanenko, V.M. Centenary of Alexander Friedmann's prediction of the Universe expansion and the quantum vacuum. *Physics* **2022**, *4*, 981–994. [CrossRef]

Disclaimer/Publisher's Note: The statements, opinions and data contained in all publications are solely those of the individual author(s) and contributor(s) and not of MDPI and/or the editor(s). MDPI and/or the editor(s) disclaim responsibility for any injury to people or property resulting from any ideas, methods, instructions or products referred to in the content.

Article

Conformally Invariant Gravity and Gravitating Mirages

Victor Berezin [†] and Inna Ivanova ^{*,†}

Institute for Nuclear Research of the Russian Academy of Sciences, 60th October Anniversary Prospect 7a, 117312 Moscow, Russia; berezin@inr.ac.ru

* Correspondence: pc_mouse@mail.ru

[†] These authors contributed equally to this work.

Abstract: The action of an ideal fluid in Euler variables with a variable number of particles is used for the phenomenological description of the processes of particle creation in strong external fields. It has been demonstrated that the conformal invariance of the creation law imposes quite strict restrictions on the possible types of sources. It is shown that combinations with the particle number density in the creation law can be interpreted as dark matter within the framework of this model.

Keywords: conformal invariance; perfect fluid; dark matter; cosmology

1. Introduction

Conformal invariance is a good candidate for the role of a fundamental symmetry, which, along with other symmetries, increases the likelihood of the Universe emerging from “nothing” [1]. Similar ideas are supported by many researchers such as Roger Penrose [2] and Gerard ‘t Hooft [3].

The conformally invariant gravitational Lagrangian contains terms that are quadratic in curvature. The results found by several independent research groups [4–9] show that such terms are linked to the conformal anomaly responsible for the particle creation. The conformal anomaly can be included in the action integral, where it consists of two parts: local and nonlocal. The local part is included in the gravitational Lagrangian as a set of counterterms and in the one-loop approximation is equal to the sum of the quadratic terms in the Riemann curvature tensor and its convolutions.

The study of particle production processes in the presence of strong external fields plays an important role both in cosmology and in black hole physics. It is especially difficult to calculate the back reaction for these problems, because it is necessary to take into account not only the influence on the metric from already produced particles, but also from vacuum polarization.

The exact solution of the quantum problem requires boundary conditions, and the latter can be imposed only after solving field equations with the energy–momentum tensor obtained by appropriate averaging from the quantum problem. In order to avoid these obstacles, we consider a phenomenological description of particle creation processes. It is a quantum process, but classical description is possible when the external fields are strong enough and the separation between just-created particles becomes of the order of their Compton length, and we can safely approximate them with some condensed matter. For example, F. Hoyle [10] used a classical creation field in order to introduce the idea of the continuous creation of matter. The thermodynamic approach to particle production at the expense of a gravitational field has been studied in [11]. Recently, J. Farnes [12] applied Hoyle’s creation tensor and the concept of negative mass to propose a single negative-mass fluid explanation of dark matter and dark energy.

In the phenomenological approach to particle creation, the nonlocal processes become, formally, the local ones. The same concerns also the trace anomalies, and, for example, in the article [13], it is shown that the non-local terms in the effective action become insignificant



Citation: Berezin, V.; Ivanova, I. Conformally Invariant Gravity and Gravitating Mirages. *Universe* **2024**, *10*, 147. <https://doi.org/10.3390/universe10030147>

Academic Editors: Sergey V. Sushkov, Galina L. Klimchitskaya, Vladimir M. Mostepanenko and Panayiotis Stavrinos

Received: 27 January 2024

Revised: 10 March 2024

Accepted: 15 March 2024

Published: 17 March 2024



Copyright: © 2024 by the authors. Licensee MDPI, Basel, Switzerland. This article is an open access article distributed under the terms and conditions of the Creative Commons Attribution (CC BY) license (<https://creativecommons.org/licenses/by/4.0/>).

under certain conditions. In this case, the use of anomaly-induced effective action can be considered as an example of a phenomenological description of particle production.

To describe the processes of particle creation in the presence of strong external fields, we use the action for an ideal fluid in Euler variables [14], in which the particle conservation law is replaced by the creation law [15]. This method makes it possible to study the process of particle creation phenomenologically at the classical level but while also taking into account the back reaction. In addition, it will be shown further that the use of the conformally invariant action of gravity in combination with the considered action of matter leads to a case in which we are actually dealing with a kind of Sakharov’s induced gravity [16].

When applying the model in consideration of cosmology, it can be assumed that it is most relevant for those phases of the evolution of the Universe when there was a rapid birth of particles. Take, for example, immediately after the supposed birth of the Universe, “nothing” [1], or at the end of inflation during the reheating [17]. Moreover, if the Universe was born anisotropic [18], then, as shown in the articles [21? ?], it was the birth of particles that led to its isotropization.

It is easy to verify that the law of particle creation is itself conformally invariant. If we assume that the source of particle creation is an external scalar field, then we obtain fairly strict restrictions on the possible types of sources. Specifically, they include conformally invariant combinations of geometric quantities, scalar fields, and particle number density. It turns out that it is the combinations with the particle number density that contribute to the hydrodynamic part of the energy-momentum tensor and act like dust and radiation. It is important to note that the above types of sources are not real matter but rather an echo of the quantum process of particle creation. In this regard, their interpretation as dark matter becomes possible.

2. Local Conformal Transformation

This paper considers Riemannian geometry, which is completely determined by specifying the metric $g_{\mu\nu}$. The affine connection $\Gamma_{\mu\nu}^\lambda(x)$ is specified using Christoffel symbols:

$$\Gamma_{\mu\nu}^\sigma = \Gamma_{\nu\mu}^\sigma \quad g_{\mu\nu;\sigma} = 0, \quad \Gamma_{\mu\nu}^\sigma = \frac{1}{2}g^{\sigma\lambda}(g_{\mu\lambda,\nu} + g_{\nu\lambda,\mu} - g_{\mu\nu,\lambda}), \quad (1)$$

It defines the parallel transport of vectors and tensors and their covariant derivatives

$$l_{;\lambda}^\mu = l_{,\lambda}^\mu + \Gamma_{\lambda\nu}^\mu l^\nu, \quad (2)$$

where “comma” denotes a partial derivative while “semicolon” denotes covariant derivative.

The Riemann tensor $R_{\nu\lambda\sigma}^\mu$ is defined as follows:

$$R_{\nu\lambda\sigma}^\mu = \frac{\partial\Gamma_{\nu\sigma}^\mu}{\partial x^\lambda} - \frac{\partial\Gamma_{\nu\lambda}^\mu}{\partial x^\sigma} + \Gamma_{\nu\lambda}^\mu \Gamma_{\nu\sigma}^\mu - \Gamma_{\nu\sigma}^\mu \Gamma_{\nu\lambda}^\mu, \quad (3)$$

Ricci tensor $R_{\mu\nu}$ is its convolution:

$$R_{\mu\nu} = R_{\mu\lambda\nu}^\lambda. \quad (4)$$

The curvature scalar is $R = g^{\mu\nu}R_{\mu\nu}$.

Next let us consider a local conformal transformation; by definition we have:

$$ds^2 = \Omega^2(x)d\hat{s}^2 = \Omega^2(x)\hat{g}_{\mu\nu}dx^\mu dx^\nu, \quad (5)$$

where $\Omega(x)$ is the conformal factor, and “hats” denotes the conformally transformed quantities.

It is worth noting that a local conformal transformation is fundamentally different from a coordinate change. Different coordinates correspond to different observers, but the geometry of space-time itself remains unchanged, in contrast to a local conformal transformation, which does not change the coordinates, but changes the geometry.

The metric and its determinant are transformed, evidently, in the following way:

$$g_{\mu\nu} = \Omega^2 \hat{g}_{\mu\nu}, \quad g^{\mu\nu} = \frac{1}{\Omega^2} \hat{g}^{\mu\nu}, \quad \sqrt{-g} = \Omega^4 \sqrt{-\hat{g}}. \tag{6}$$

An important geometric quantity that will be used below is the Weyl tensor $C_{\mu\nu\lambda\sigma}$, which is the traceless part of the Riemann tensor,

$$C_{\mu\nu\lambda\sigma} = R_{\mu\nu\lambda\sigma} - \frac{1}{2}R_{\mu\lambda}g_{\nu\sigma} + \frac{1}{2}R_{\mu\sigma}g_{\nu\lambda} - \frac{1}{2}R_{\nu\sigma}g_{\mu\lambda} + \frac{1}{2}R_{\nu\lambda}g_{\mu\sigma} + \frac{1}{6}R(g_{\mu\lambda}g_{\nu\sigma} - g_{\mu\sigma}g_{\nu\lambda}).$$

In the context of this work, its most important property is conformal invariance:

$$C^{\mu}_{\nu\lambda\sigma} = \hat{C}^{\mu}_{\nu\lambda\sigma}. \tag{7}$$

3. Phenomenological Description of Particle Creation

There are two types of dynamical variables in classical hydrodynamics: Lagrangian and Eulerian. The first ones are tied to the motion of individual particles, so the world line of each particle is subject to variation when applying the principle of least action. These coordinates are not suitable for describing the processes of creation or annihilation, and therefore, the Euler formalism is preferred, when dynamical variables are fields describing the average characteristics of the medium. This formalism was developed by J. R. Ray [14], who showed that the motion equation for an ideal fluid derived from this action coincides with the Euler equation. The advantage of this approach is that the continuity equation is explicitly incorporated into the action through the corresponding connection with the Lagrange multiplier.

Let us consider the action of an ideal fluid in Euler variables [14],

$$S_m = - \int \varepsilon(X, n) \sqrt{-g} d^4x + \int \lambda_0 (u_\mu u^\mu - 1) \sqrt{-g} d^4x + \int \lambda_1 (nu^\mu)_{;\mu} \sqrt{-g} d^4x + \int \lambda_2 X_{;\mu} u^\mu \sqrt{-g} d^4x. \tag{8}$$

The dynamical variables are the particle number density $n(x)$, the four-velocity $u^\mu(x)$, and the auxiliary dynamical variable $X(x)$ introduced in order to avoid the identically zero vorticity of particle flow. From the constraint with the Lagrangian multiplier λ_2 , it follows that $X(x)$ is constant along the trajectories, and therefore, the choice of this function defines the labeling of the trajectories.

The energy density ε provides us with the equation of state $p = p(\varepsilon)$, where

$$p = n \frac{\partial \varepsilon}{\partial n} - \varepsilon, \tag{9}$$

is the hydrodynamic pressure.

The corresponding constraints are obtained by varying the matter action with respect to the Lagrangian multipliers λ_0 , λ_1 , and λ_2 , the four velocity normalization $u^\mu u_\mu = 1$, the particle number conservation $(nu^\mu)_{;\mu} = 0$ and the enumeration of trajectories $X_{;\mu} u^\mu = 0$, respectively.

The energy momentum tensor is:

$$T^{\mu\nu} = (\varepsilon + p)u^\mu u^\nu - pg^{\mu\nu}. \tag{10}$$

As demonstrated in the article by [15], the process of particle creation can be described phenomenologically if the corresponding constraint in the action of an ideal fluid is modified:

$$(nu^\mu)_{;\mu} = \Phi(\text{inv}), \tag{11}$$

where function Φ depends on the invariants of the fields responsible for the creation process.

It is easy to show that the left-hand side of the creation law becomes conformally invariant when multiplied by the root of the modulus of the determinant of the metric:

$$n = \frac{\hat{n}}{\Omega^3}, \quad u^\mu = \frac{\hat{u}^\mu}{\Omega}, \quad \sqrt{-g} = \Omega^4 \sqrt{-\hat{g}}, \tag{12}$$

hence

$$\begin{aligned} (nu^\mu)_{;\mu} &= \frac{1}{\sqrt{-g}}(nu^\mu \sqrt{-g})_{;\mu} = \frac{1}{\sqrt{-g}} \left(\frac{\hat{n}}{\Omega^3} \frac{\hat{u}^\mu}{\Omega} \Omega^4 \sqrt{-\hat{g}} \right)_{;\mu} = \\ &= \frac{1}{\sqrt{-g}}(\hat{n}\hat{u}^\mu \sqrt{-\hat{g}})_{;\mu}, \end{aligned} \tag{13}$$

Then, it follows that, in turn, the quantity $\Phi\sqrt{-g}$ is also conformally invariant.

In the absence of classical external fields, the birth of particles is due to the vacuum polarization caused by gravity, so Φ is a function of geometric invariants. In Riemannian geometry in the four-dimensional case, the square of the Weyl tensor $C^2 = C_{\mu\nu\lambda\sigma} C^{\mu\nu\lambda\sigma}$ is the only possible choice if we restrict ourselves to invariants which are at most quadratic in the curvature tensor. The same result was obtained in [22] for particle creation by the vacuum fluctuations of the massless scalar field on the background of the homogeneous and slightly anisotropic cosmological spacetime. For our model, it is universal for any Riemannian geometry, irrespective of the form of the gravitational Lagrangian, and the back reaction is also taken into account. In this regard, it can be assumed that the creation law describes the relationship between the vacuum average values of the corresponding quantities.

If we consider a case in which some external scalar field φ is involved in the creation process, then additional possible contributions to the source function Φ appear:

$$\varphi \square \varphi - \frac{1}{6} \varphi^2 R + \Lambda \varphi^4, \tag{14}$$

It is easy to see that it is invariant under a conformal transformation when the scalar field changes as

$$\varphi = \frac{\hat{\varphi}}{\Omega}, \tag{15}$$

where \square denotes Laplace–Beltrami operator.

The particles in question are on shell quanta of the scalar field, so they can also produce “new” particles. The rate of particle creation in this case should depend on the density of the number of “old” particles, i.e., it is some function of n . Due to conformal invariance, the most natural choice is φn , and $n^{\frac{4}{3}}$. It is easy to verify that, when multiplied by $\sqrt{-g}$, they form conformal invariants. Theoretically, it is possible to use other degrees of φ and n , but this leads to the appearance of particles with the properties of exotic or phantom matter, so we will limit ourselves to the options presented above. Thus, our creation law takes the following form:

$$\Phi = \alpha C^2 + \beta \left(\varphi \square \varphi - \frac{1}{6} \varphi^2 R + \Lambda \varphi^4 \right) + \gamma_1 \varphi n + \gamma_2 n^{\frac{4}{3}}. \tag{16}$$

4. Induced Gravity

Let us consider the action of an ideal fluid modified in the manner indicated earlier:

$$\begin{aligned} S_m &= - \int \varepsilon(X, \varphi, n) \sqrt{-g} d^4x + \int \lambda_0 (u_\mu u^\mu - 1) \sqrt{-g} d^4x + \\ &+ \int \lambda_1 ((nu^\mu)_{;\mu} - \Phi) \sqrt{-g} d^4x + \int \lambda_2 X_{;\mu} u^\mu \sqrt{-g} d^4x, \end{aligned} \tag{17}$$

note that $\varepsilon = \varepsilon(X, \varphi, n)$.

Let us consider a situation in which the action of gravity is conformally invariant. This case is to a certain extent equivalent to induced gravity, in which there is nothing except the action of matter, since the Lagrangian multiplier λ_1 is defined up to a constant; therefore, even in the absence of a separate Lagrangian for gravity, we can distinguish terms proportional to C^2 and $\varphi^2 R$. For the first time, such models, in which there is no separate action for gravity, were studied by A.D. Sakharov [16]. He suggested that the gravitational field is not fundamental, but is the result of the averaged influence of the vacuum fluctuations of all other quantum fields; these ideas formed the basis of the theory of induced gravity. Thus, we assume:

$$S_m = S_{tot}. \tag{18}$$

Evidently,

$$\frac{\delta S_{tot}}{\delta \Omega} = \frac{\delta S_m}{\delta \Omega} = 0, \tag{19}$$

in the solutions. The only part of the action of matter that is not conformally invariant from the very beginning or does not vanish due to constraints is

$$\int \varepsilon(X, \varphi, n) \sqrt{-g} d^4x. \tag{20}$$

Since $n = \frac{\hat{n}}{\Omega^3}$, $\varphi = \frac{\hat{\varphi}}{\Omega}$, $\sqrt{-g} = \Omega^4 \sqrt{-\hat{g}}$, one gets:

$$\varphi \frac{\partial \varepsilon}{\partial \varphi} + 3n \frac{\partial \varepsilon}{\partial n} = 4 \varepsilon, \tag{21}$$

with the solution:

$$\varepsilon = F\left(\frac{n}{\varphi^3}\right) \varphi^4, \tag{22}$$

where F is an arbitrary function of one variable.

There are two important examples. For dust, that is, for $p = 0$, it follows from this equation that $\varepsilon = \mu_0 n \varphi$, where μ_0 is a constant. For radiation, $\varepsilon = 3p$, therefore, two options are possible: either $\varphi = 0$, or $\frac{\partial \varepsilon}{\partial \varphi} = 0$. That is, the energy density does not depend on the scalar field: $\varepsilon = \nu_0 n^{\frac{4}{3}}$. Note the resemblance with two "hydrodynamical" terms in the creation law.

5. Equations of Motion and Constraints

Let us derive the (modified) hydrodynamical equations of motion and constraints for the action in question:

$$S_m = - \int \varepsilon(X, \varphi, n) \sqrt{-g} d^4x + \int \lambda_0 (u_\mu u^\mu - 1) \sqrt{-g} d^4x + \int \lambda_2 X_{,\mu} u^\mu \sqrt{-g} d^4x + \int \lambda_1 \left((nu^\mu)_{;\mu} - \gamma_1 \varphi n - \gamma_2 n^{\frac{4}{3}} - \alpha C^2 - \beta \left(\varphi \square \varphi - \frac{1}{6} \varphi^2 R + \Lambda \varphi^4 \right) \right) \sqrt{-g} d^4x.$$

Dynamical variables are n , u^μ , φ , and X :

$$\delta \varphi : \quad \beta \left(\lambda_1 \square \varphi + \square(\lambda_1 \varphi) + 4\lambda_1 \Lambda \varphi^3 - \frac{1}{3} \lambda_1 \varphi R \right) + \gamma_1 n = - \frac{\partial \varepsilon}{\partial \varphi}, \tag{23}$$

$$\delta n : \quad - \frac{\partial \varepsilon}{\partial n} - \lambda_{1,\sigma} u^\sigma - \lambda_1 \gamma_1 \varphi - \frac{4}{3} \lambda_1 \gamma_2 n^{\frac{1}{3}} = 0, \tag{24}$$

$$\delta u^\mu : \quad \lambda_2 X_{,\mu} + 2\lambda_0 u_\mu - \lambda_{1,\mu} n = 0, \tag{25}$$

$$\delta X : -\frac{\partial \epsilon}{\partial X} - (\lambda_2 u^\sigma)_{;\sigma} = 0. \tag{26}$$

The corresponding constraints are:

$$\delta \lambda_0 : u_\sigma u^\sigma - 1 = 0, \tag{27}$$

$$\delta \lambda_1 : (n u^\sigma)_{;\sigma} = \Phi, \tag{28}$$

$$\delta \lambda_2 : X_{;\sigma} u^\sigma = 0. \tag{29}$$

From Equation (25) multiplied by u^μ and constraints we get:

$$2\lambda_0 = -n \frac{\partial \epsilon}{\partial n} - \lambda_1 \gamma_1 \varphi n - \frac{4}{3} \lambda_1 \gamma_2 n^{\frac{4}{3}}. \tag{30}$$

Let us calculate the hydrodynamical part of the energy–momentum tensor, that is, the energy–momentum tensor of the perfect fluid plus contribution from the γ_1 and γ_2 terms. From the general definition:

$$S_m = -\frac{1}{2} \int T^{\mu\nu} \delta g_{\mu\nu} \sqrt{-g} d^4x, \tag{31}$$

Taking into account Equation (30), we get:

$$\begin{aligned} T_{hydro}^{\mu\nu} &= \epsilon g^{\mu\nu} - 2\lambda_0 u^\mu u^\nu + g^{\mu\nu} \left(n \lambda_{1,\sigma} u^\sigma + \lambda_1 \gamma_1 \varphi n + \lambda_1 \gamma_2 n^{\frac{4}{3}} \right) = \\ &= \left(\epsilon + p + \lambda_1 \gamma_1 \varphi n + \frac{4}{3} \lambda_1 \gamma_2 n^{\frac{4}{3}} \right) u^\mu u^\nu - g^{\mu\nu} \left(p + \frac{1}{3} \lambda_1 \gamma_2 n^{\frac{4}{3}} \right). \end{aligned} \tag{32}$$

The remaining parts of the energy–momentum tensor are:

$$\begin{aligned} T^{\mu\nu}[\varphi] &= \lambda_1 \beta \Lambda \varphi^4 g^{\mu\nu} - \beta \partial_\sigma (\lambda_1 \varphi) \partial^\sigma \varphi g^{\mu\nu} + \beta \partial^\mu (\lambda_1 \varphi) \partial^\nu \varphi + \\ &+ \beta \partial^\nu (\lambda_1 \varphi) \partial^\mu \varphi + \frac{\beta}{3} \left\{ \lambda_1 \varphi^2 G^{\mu\nu} - \nabla^\mu \nabla^\nu (\lambda_1 \varphi^2) + g^{\mu\nu} \square (\lambda_1 \varphi^2) \right\}, \\ T^{\mu\nu}[C^2] &= -8\alpha \left(\nabla_\sigma \nabla_\eta + \frac{1}{2} R_{\sigma\eta} \right) (\lambda_1 C^{\mu\sigma\nu\eta}), \end{aligned} \tag{33}$$

where $G^{\mu\nu}$ is the Einstein tensor. Since we are dealing with induced gravity, then:

$$T^{\mu\nu} = T_{hydro}^{\mu\nu} + T^{\mu\nu}[\varphi] + T^{\mu\nu}[C^2] = 0. \tag{34}$$

It should be clarified that the trace of the energy–momentum tensor T is equal to zero, even for a non-zero gravitational part of the action, if it is conformally invariant. Let us show that the condition $T = 0$ reduces to Equation (21) obtained above:

$$\begin{aligned} T &= \epsilon - 3p + 4\beta \lambda_1 \Lambda \varphi^4 - \frac{\beta}{3} \lambda_1 \varphi^2 R + \beta \varphi \square (\lambda_1 \varphi) + \beta \lambda_1 \varphi \square \varphi + \lambda_1 \gamma_1 \varphi n = \\ &= \epsilon - 3p - \varphi \frac{\partial \epsilon}{\partial \varphi} = 4\epsilon - 3n \frac{\partial \epsilon}{\partial n} - \varphi \frac{\partial \epsilon}{\partial \varphi}, \end{aligned} \tag{35}$$

where in the second equality, the equation of motion obtained by variation in φ was used.

The terms from the creation law which contain the particle number density lead to the appearance of corresponding contributions to the hydrodynamic part of the energy–momentum tensor: the term with γ_1 is dust-like and the term with γ_2 is radiation-like. They are not real because the particle number density n refers to real created particles whose equation of state

can be arbitrary (anything). We can say that they are echoes of the process of creation itself. Thus, the most appropriate name for them is “gravitating mirages”.

Finding a general solution to the equations of motion is quite a difficult task, so we will limit ourselves to considering two special cases: $\varphi = 0$ and $\lambda_1 = const$.

In the first case, Equation (21) implies that our perfect fluid is radiation, then, according to (23), either n or γ_1 is zero. If $\gamma_1 = 0$, then it follows from (24) and (32) that:

$$\lambda_{1,\sigma} u^\sigma = -\frac{4}{3} n^{\frac{1}{3}} (v_0 + \lambda_1 \gamma_2), \tag{36}$$

$$T_{hydro}^{\mu\nu} = \frac{1}{3} n^{\frac{4}{3}} (v_0 + \lambda_1 \gamma_2) (4 u^\mu u^\nu - g^{\mu\nu}). \tag{37}$$

Using the gauge $n = n_0 = const$ and the comoving coordinate system, where $u^\sigma = \delta_0^\sigma$, we can find λ_1 considering that it depends only on the proper time t :

$$\lambda_1(t) = -\frac{v_0}{\gamma_2} + \left(\lambda_1(0) + \frac{v_0}{\gamma_2} \right) \exp\left\{ -\frac{4}{3} \gamma_2 n_0^{\frac{1}{3}} t \right\}. \tag{38}$$

Note that λ_1 tends to a constant $-\frac{v_0}{\gamma_2}$, while $t \rightarrow \infty$ if $\gamma_2 > 0$. In the second case from Equation (24), we get:

$$\frac{\partial \varepsilon}{\partial n} = -\lambda_1 \left(\gamma_1 \varphi + \gamma_2 n^{\frac{1}{3}} \right), \tag{39}$$

the solution is:

$$\varepsilon = -\lambda_1 \left(\gamma_1 n \varphi + \gamma_2 n^{\frac{4}{3}} \right) + f(\varphi). \tag{40}$$

Function $f(\varphi)$, then, can be found from the relation (22):

$$f(\varphi) = C \varphi^4, \tag{41}$$

where C is an arbitrary constant. The hydrodynamical part of the energy–momentum tensor is: $T_{hydro}^{\mu\nu} = C \varphi^4 g^{\mu\nu}$. This means that in this case, the term $f(\varphi)$ in ε is equivalent to the shift of the constant Λ . The equation of motion for φ reduces to the following:

$$2\lambda_1 \beta \left(\square \varphi - \frac{1}{6} R \varphi + 2\Lambda \varphi^3 \right) + 4C \varphi^3 = 0. \tag{42}$$

The conformal invariance of the equations of motion and the creation law makes it possible to simplify the problem by fixing the gauge. In the gauge $\varphi = \varphi_0 = const$ from the Equation (42) we get:

$$R = \frac{12\varphi_0^2}{\beta\lambda_1} (C + \lambda_1 \beta \Lambda) = const, \tag{43}$$

therefore the space-time in question is equivalent to the geometry with constant scalar curvature up to a conformal factor.

6. Cosmology

Let us consider cosmological solutions by which we understand the homogeneous and isotropic space-times described by the Robertson–Walker metric:

$$ds^2 = dt^2 - a^2(t) dl^2, \tag{44}$$

$$dl^2 = \gamma_{ij} dx^i dx^j = \frac{dr^2}{1 - kr^2} + r^2 (d\theta^2 + \sin^2 \theta d\varphi^2), \quad (k = 0, \pm 1),$$

with the scale factor $a(t)$. Due to the high level of the symmetry, we assume that all dynamic variables except the metric depend only on t and $u^\mu = \delta_0^\mu$, so the constraint for the λ_0 is automatically satisfied.

For this geometry, $C^\mu_{\nu\lambda\sigma} = 0$; therefore, $T^{\mu\nu}[C^2] = 0$. Since $T_1^1 = T_2^2 = T_3^3$, we can only use T^{00} and T . From the constraint for λ_2 , we get:

$$\dot{X} = 0 \Rightarrow X = const, \tag{45}$$

The dot denotes the derivative with respect to t .

The equations of motion for the metric (44) and the action of matter in question are:

$$T^{00} = \varepsilon + \beta \lambda_1 \left\{ \Lambda \varphi^4 + \dot{\varphi}^2 + \varphi^2 \frac{\dot{a}^2 + k}{a^2} + 2\varphi \dot{\varphi} \frac{\dot{a}}{a} \right\} + \beta \lambda_1 \varphi \left(\dot{\varphi} + \varphi \frac{\dot{a}}{a} \right) + \lambda_1 \left(\gamma_1 \varphi n + \gamma_2 n^{\frac{4}{3}} \right) = 0, \tag{46}$$

$$\varphi \ddot{\lambda}_1 + \dot{\lambda}_1 \left(3\varphi \frac{\dot{a}}{a} + 2\dot{\varphi} \right) + \lambda_1 \left(2\ddot{\varphi} + 6 \frac{\dot{a}}{a} \dot{\varphi} + 4\Lambda \varphi^3 - \frac{1}{3} \varphi R \right) + \lambda_1 \frac{\gamma_1}{\beta} n = -\frac{1}{\beta} \frac{\partial \varepsilon}{\partial \varphi}, \tag{47}$$

$$\Phi = \beta \varphi \left(\frac{1}{a^3} \frac{d}{dt} (a^3 \dot{\varphi}) - \frac{1}{6} \varphi R + \Lambda \varphi^3 \right) + \gamma_1 \varphi n + \gamma_2 n^{\frac{4}{3}} = \frac{1}{a^3} \frac{d}{dt} (a^3 n), \tag{48}$$

$$\frac{\partial \varepsilon}{\partial n} + \dot{\lambda}_1 + \lambda_1 \gamma_1 \varphi + \frac{4}{3} \lambda_1 \gamma_2 n^{\frac{1}{3}} = 0, \tag{49}$$

$$T = \varepsilon - 3p - \varphi \frac{\partial \varepsilon}{\partial \varphi} = 0, \tag{50}$$

where $R = -6 \frac{\ddot{a}\dot{a} + \dot{a}^2 + k}{a^2}$ is a scalar curvature.

The system of equations under consideration is degenerate, since the equation of motion on φ multiplied by $\dot{\varphi} + \varphi \frac{\dot{a}}{a}$ is obtained by differentiation with respect to t equation for T^{00} and using the rest. Thus, one of the equations can be eliminated, except for the case when $\dot{\varphi} + \varphi \frac{\dot{a}}{a} = 0$. An additional relation connecting the original equations is associated with the conservation of the energy–momentum tensor in quadratic gravity and, as a consequence, its special case—conformal gravity.

Let us consider the special case $\beta = 0$, in which the external scalar field is not dynamic, that is, the action does not contain derivatives φ . Moreover, from the equations, it follows that $\lambda_1 = const$, $\varepsilon = -\lambda_1 \left(\gamma_1 \varphi n + \gamma_2 n^{\frac{4}{3}} \right)$, and the functions $a(t)$ and $\varphi(t)$ are arbitrary. It should be noted that from the birth law in this case it follows that at $n = 0$, \dot{n} is also equal to zero; that is, in order for the birth of particles from the vacuum to begin, there must be a contribution from the term at β or geometry for which $C^2 \neq 0$.

As stated above, the conformal invariance of the action and, as a consequence, the equations of motion allow one to arbitrarily choose the gauge.

Let us suppose that we found somehow the specific solution for the set of dynamical variables $\{\hat{a}, \hat{n}, \hat{\varphi}\}$. Then, the general solution is $\{a, n, \varphi\}$, where $a = \hat{a}\Omega$, $\hat{n} = n\Omega^3$, $\hat{\varphi} = \varphi\Omega$ with arbitrary smooth function $\Omega(t)$. One can use such a freedom to choose the most appropriate gauge.

The free choice of gauge forces us to think about which of them is physical, that is, which is most consistent with the accumulated observational data. In the fourth section, we considered Equation (21), which follows from the conformal invariance of the action of gravity, for two special cases—dust and radiation. For dust, we found that the effective mass of particles, a factor of n , depends on the external scalar field, and in the general case is not constant. In this regard, we can assume that the gauge $\varphi = const$ is physical.

Below we will write the set of equations for two different gauges: $\varphi = \varphi_0 = const$ and $\hat{a} = 1$. The latter does not mean at all that the “real” Universe is static. It is chosen because in such a case the set of equations looks simplest. However, in our opinion, the gauge $\varphi = \varphi_0$ may be considered physical since the mass of the dust particles become constant.

Transition from the “comfortable” gauge $\hat{a} = 1$ to the physical gauge $\varphi = \varphi_0$ can be easily achieved in the following way. Since $a \varphi = \hat{a} \hat{\varphi}$, we have $a \varphi = \hat{\varphi}(\eta)$ and $a(\eta)^2 d\eta^2 = dt^2$, where η is the conformal time, and t is the cosmological time.

Let us consider the gauge $\varphi = \varphi_0$:

$$0 = T^{00} = \varepsilon + \beta \lambda_1 \left\{ \Lambda \varphi_0^4 + \varphi_0^2 \frac{\dot{a}^2 + k}{a^2} \right\} + \beta \dot{\lambda}_1 \varphi_0^2 \frac{\dot{a}}{a} + \lambda_1 \left(\gamma_1 \varphi_0 n + \gamma_2 n^{\frac{4}{3}} \right), \tag{51}$$

$$\varphi_0 \ddot{\lambda}_1 + 3 \dot{\lambda}_1 \varphi_0 \frac{\dot{a}}{a} + \lambda_1 \left(4 \Lambda \varphi_0^3 - \frac{1}{3} \varphi_0 R \right) + \lambda_1 \frac{\gamma_1}{\beta} n = - \frac{1}{\beta} \frac{\partial \varepsilon}{\partial \varphi}, \tag{52}$$

$$\beta \varphi_0 \left(- \frac{1}{6} \varphi_0 R + \Lambda \varphi_0^3 \right) + \gamma_1 \varphi_0 n + \gamma_2 n^{\frac{4}{3}} = \frac{1}{a^3} \frac{d}{dt} \left(a^3 n \right), \tag{53}$$

$$\frac{\partial \varepsilon}{\partial n} + \dot{\lambda}_1 + \lambda_1 \gamma_1 \varphi_0 + \frac{4}{3} \lambda_1 \gamma_2 n^{\frac{1}{3}} = 0, \tag{54}$$

$$4\varepsilon - 3n \frac{\partial \varepsilon}{\partial n} - \varphi_0 \frac{\partial \varepsilon}{\partial \varphi} = 0. \tag{55}$$

For $k = 0$, there is a particular solution with $n = n_0 = const$:

$$\frac{\dot{a}}{a} = \frac{3n_0}{\beta \varphi_0^2} - \gamma_1 \varphi_0 - \frac{4}{3} \gamma_2 n_0^{\frac{1}{3}}, \tag{56}$$

$$\begin{aligned} \beta \varphi_0^2 \left(\Lambda \varphi_0^2 + 2 \left(\frac{3n_0}{\beta \varphi_0^2} - \gamma_1 \varphi_0 - \frac{4}{3} \gamma_2 n_0^{\frac{1}{3}} \right)^2 \right) + \gamma_1 \varphi_0 n_0 + \gamma_2 n_0^{\frac{4}{3}} = \\ = 3n_0 \left(\frac{3n_0}{\beta \varphi_0^2} - \gamma_1 \varphi_0 - \frac{4}{3} \gamma_2 n_0^{\frac{1}{3}} \right), \end{aligned} \tag{57}$$

$$\varepsilon(n_0, \varphi_0) = \beta \varphi_0^2 \left(\frac{3n_0}{\beta \varphi_0^2} - \gamma_1 \varphi_0 - \frac{4}{3} \gamma_2 n_0^{\frac{1}{3}} \right) \frac{\partial \varepsilon}{\partial n} (n_0, \varphi_0). \tag{58}$$

Here we can draw an analogy with the solution with $k = 0$ obtained in the work of [23].

Transition to conformal time:

$$d\eta^2 = \frac{dt^2}{a(t)^2}, \quad ds^2 = a^2(\eta) \left\{ d\eta^2 - \frac{dr^2}{1 - kr^2} - r^2 d\Omega^2 \right\}, \tag{59}$$

This allows us to choose a gauge $a(\eta) = 1$ in which $\eta = t$. The equations of motion for this gauge are as follows:

$$T^{\eta\eta} = \beta \left(\varphi \dot{\lambda}_1 \dot{\varphi} + \lambda_1 \dot{\varphi}^2 + \lambda_1 \varphi^2 (k + \Lambda \varphi^2) \right) + \varepsilon + \lambda_1 \left(\gamma_1 \varphi n + \gamma_2 n^{\frac{4}{3}} \right) = 0, \tag{60}$$

$$\frac{1}{\beta} \frac{\partial \varepsilon}{\partial \varphi} + 2 \lambda_1 \dot{\varphi} + 2 \dot{\lambda}_1 \varphi + \varphi \ddot{\lambda}_1 + \lambda_1 \varphi (2k + 4 \Lambda \varphi^2) + \frac{\gamma_1}{\beta} \lambda_1 n = 0, \tag{61}$$

$$\frac{\partial \varepsilon}{\partial n} + \dot{\lambda}_1 + \lambda_1 \gamma_1 \varphi + \frac{4}{3} \lambda_1 \gamma_2 n^{\frac{1}{3}} = 0, \tag{62}$$

$$\dot{n} = \beta \left(\varphi \ddot{\varphi} + k \varphi^2 + \Lambda \varphi^4 \right) + \gamma_1 \varphi n + \gamma_2 n^{\frac{4}{3}}, \tag{63}$$

$$4\varepsilon - 3n \frac{\partial \varepsilon}{\partial n} - \varphi \frac{\partial \varepsilon}{\partial \varphi} = 0. \tag{64}$$

Let us consider the special case $\lambda_1 = const$:

$$\varepsilon = -\lambda_1 \left(\Phi - \beta \varphi \ddot{\varphi} + \beta \dot{\varphi}^2 \right), \tag{65}$$

$$\frac{\partial \varepsilon}{\partial n} = -\lambda_1 \frac{\partial \Phi_1}{\partial n}, \tag{66}$$

$$\dot{n} = \Phi, \tag{67}$$

$$4\varepsilon - 3n \frac{\partial \varepsilon}{\partial n} - \varphi \frac{\partial \varepsilon}{\partial \varphi} = 0. \tag{68}$$

Only four equations are used here because, as noted earlier, not all of the original equations are independent. From the condition $T = 0$ in this case it follows:

$$\varepsilon = -\lambda_1 \left(\gamma_1 \varphi n + \gamma_2 n^{\frac{4}{3}} \right) + C\varphi^4, \tag{69}$$

where C is some constant. Wherein field φ satisfies the equation:

$$\dot{\varphi}^2 = -k \varphi^2 - \left(\frac{C}{\beta \lambda_1} + \Lambda \right) \varphi^4. \tag{70}$$

For $k = 0$:

$$\varphi = \frac{\sigma}{\sqrt{-\left(\frac{C}{\beta \lambda_1} + \Lambda\right)}} \frac{1}{\eta + C_0}, \tag{71}$$

where $\sigma = \pm 1$ is a sign of $\dot{\varphi}$; for $k = \pm 1$ we have, respectively:

$$\sigma \operatorname{arctg} \left(\frac{1}{\sqrt{-\left(\frac{C}{\beta \lambda_1} + \Lambda\right) \varphi^2 - 1}} \right) = \eta + C_0, \quad k = 1, \tag{72}$$

$$\sigma \operatorname{arcth} \left(\frac{1}{\sqrt{-\left(\frac{C}{\beta \lambda_1} + \Lambda\right) \varphi^2 + 1}} \right) = \eta + C_0, \quad k = -1, \tag{73}$$

where C_0 is a constant depending on the initial conditions.

The scale factor $a(\eta)$ changes as follows under the conformal transformation $a = \Omega \hat{a}$; therefore, when going to the gauge $\hat{a} = 1$, $a = \Omega$. If initially $\varphi = \varphi_0 = const$, then $\hat{\varphi} = \varphi_0 \Omega = \varphi_0 a$; that is, the scalar field calculated in the gauge $\hat{a} = 1$, proportional to the scale factor in the gauge $\varphi = \varphi_0 = const$. In particular, the result obtained above for $\lambda_1 = const$ is consistent with that calculated earlier, since, when moving to the gauge $\varphi = \varphi_0 = const$, the scalar curvature remains constant:

$$R = -6 \frac{a'' + ak}{a^3} = 12 \left(\Lambda + \frac{C}{\beta \lambda_1} \right) \varphi_0^2, \tag{74}$$

where the prime denotes the derivative with respect to η and $a(\eta) = \frac{1}{\varphi_0} \hat{\varphi}(\eta)$ with function $\hat{\varphi}(\eta)$ defined by the Equations (71), (72) or (73) depending on k .

Let us consider the transition to the variable t from η for the case $k = 0$:

$$a = \frac{1}{\varphi_0} \frac{\sigma}{\sqrt{-\left(\frac{C}{\beta\lambda_1} + \Lambda\right)}} \frac{1}{\eta + C_0} \propto \exp\left\{\sigma \varphi_0 \sqrt{-\left(\frac{C}{\beta\lambda_1} + \Lambda\right)} t\right\}, \tag{75}$$

where we have chosen the minus sign in the relation: $dt = -a(\eta)d\eta$. Thus, if $\sigma\varphi_0 > 0$, we obtain exponential growth for the scale factor $a(t)$. Moreover, from Equation (70), it follows that the same is true for $k = \pm 1$ when $\hat{\varphi} \rightarrow \infty$, which is equivalent to $t \rightarrow \infty$. This is due to the fact that with $\lambda_1 = const$ in the gauge $\varphi = \varphi_0$ for the homogeneous and isotropic space-time with the metric (44), our model actually reduces to general relativity with the cosmological constant.

7. Discussion

The conformal invariance of the term in the action of matter, from which the particle creation law is obtained, leads to restrictions on the invariants of external fields responsible for the creation processes on which the function Φ depends. In the absence of classical external fields, when the only source of particle creation is gravity, the square of the Weyl tensor is the most basic option. Due to this fact, conformal invariance of the gravity action leads to a case in which the total action is equivalent to the matter action up to redefining Lagrange multiplier λ_1 .

When an external scalar field is introduced into the creation law, the following combination is chosen: $\varphi \square \varphi - \frac{1}{6} \varphi^2 R + \Lambda \varphi^4$, since it yields a nontrivial equation of motion and is conformally invariant when multiplied by $\sqrt{|g|}$.

In addition to the above, contributions to the creation law proportional to the particle number density are also possible. In cosmology, the γ_1 term can be interpreted as a dark matter. It is not real matter, but the “memory” of the process of the particle production. The conditions for its existence are $n \neq 0 (> 0)$. Thus, the real particles should already be produced. The dark matter will exist even after the particle creation stops. The γ_2 term becomes the hot universe, even without real photons and real temperature. Both of them are just images, but they are gravitating.

This interpretation is possible due to the fact that, in the hydrodynamic part of the energy–momentum tensor, the terms with γ_1 and γ_2 are not associated with any matter, but indicate the influence on gravity of the particle creation process itself, which can be used to explain the “missing” mass in the Universe. Moreover, their contribution is in many ways similar to the contribution from dust and radiation, which unites our model with the one presented in the article [12], where the matter creation also makes a contribution to the energy–momentum tensor similar to an ideal fluid.

As mentioned in the introduction, the phenomenological description of particle creation in cosmology is best suited to the early Universe. However, the solution obtained in our model for $\lambda_1 = const$ (75) shows that it is also applicable for the present phase of the evolution of the Universe.

In the absence of a scalar field, the matter under consideration within this model, when the action of gravity is conformally invariant, can only be radiation. For cosmological solutions, by which we mean homogeneous and isotropic geometry, without a scalar field the creation of particles cannot begin from the vacuum. On the other hand, if $n \neq 0$ or $\varphi \neq 0$, then, unlike the models discussed in the articles [21? ?], particle production is possible even in homogeneous and isotropic geometry, where the square of the Weyl tensor is zero.

From the conformal invariance of the gravity action for the model with an external scalar field it follows that, for dust, the energy density is proportional to the scalar field,

while for radiation, it does not depend on the scalar field. Therefore, the gauge $\varphi = \text{const}$ seems to be the most consistent with the observational data.

Author Contributions: The authors (V.B. and I.I.) contributed equally to this work. All authors have read and agreed to the published version of the manuscript.

Funding: This research received no external funding.

Data Availability Statement: No new data were created or analyzed in this study. Data sharing is not applicable to this article.

Conflicts of Interest: The authors declare no conflicts of interest.

References

- Vilenkin, A.V. Creation of Universes from Nothing. *Phys. Lett. B* **1982**, *117*, 25–28. [CrossRef]
- Penrose, R. On the Gravitization of Quantum Mechanics 1: Quantum State Reduction. *Found. Phys.* **2014**, *44*, 557–575. [CrossRef]
- Hooft, G. Singularities, horizons, firewalls, and local conformal symmetry. In *Proceedings of the 2nd Karl Schwarzschild Meeting on Gravitational Physics, Main, Germany, 20–24 July 2015*; Proceedings in Physics; Springer: Cham, Switzerland, 2018; Volume 208, pp. 1–12.
- Parker, L. Quantized Fields and Particle Creation in Expanding Universes. *Phys. Rev.* **1969**, *183*, 1057–1068. [CrossRef]
- Grib, A.A.; Mamaev S.G. On field theory in Friedmann space. *Sov. J. Nucl. Phys.* **1970**, *10*, 722–725.
- Zel'dovich, Y.B.; Pitaevsky, L.P. On the possibility of the creation of particles by a classical gravitational field. *Comm. Math. Phys.* **1971**, *23*, 185–188. [CrossRef]
- Hu, B.L.; Fulling, S.A.; Parker L. Quantized Scalar Fields in a Closed Anisotropic Universe. *Phys. Rev. D* **1973**, *8*, 2377–2385. [CrossRef]
- Hu, B.L.; Fulling, S.A.; Parker L. Conformal energy-momentum tensor in curved spacetime: Adiabatic regularization and renormalization. *Phys. Rev. D* **1974**, *10*, 3905.
- Fulling, S.A.; Parker, L. Renormalization in the theory of a quantized scalar field interacting with a robertson-walker spacetime. *Ann. Phys. D* **1974**, *87*, 176–204. [CrossRef]
- Hoyle, F. A Covariant Formulation of the Law of Creation of Matter. *Mon. Not. R. Astron. Soc.* **1960**, *120*, 256–262. [CrossRef]
- Prigogine, I.; Gehentau, J.; Gunzig, E.; Nardone, P. Thermodynamics of cosmological matter creation. *Proc. Natl. Acad. Sci. USA* **1988**, *85*, 7428–7432. [CrossRef]
- Farnes, J.S. A unifying theory of dark energy and dark matter: Negative masses and matter creation within a modified Λ CDM framework. *Astron. Astrophys.* **2018**, *620*, 1–20. [CrossRef]
- Netto, T.D.; Pelinson, A.M.; Shapiro, I.L.; Starobinsky A.A. From stable to unstable anomaly-induced inflation. *Eur. Phys. J. C* **2016**, *76*, 544–558. [CrossRef]
- Ray, J.R. Lagrangian Density for Perfect Fluids in General Relativity. *J. Math. Phys.* **1972**, *13*, 1451. [CrossRef]
- Berezin, V.A. Unusual Hydrodynamics. *Int. J. Mod. Phys. A* **1987**, *2*, 1591–1615. [CrossRef]
- Sakharov, A.D. Vacuum quantum fluctuations in curved space and the theory of gravitation. *Dokl. Akad. Nauk Ser. Fiz.* **1967**, *177*, 70–71.
- Kofman, L.; Linde, A.; Starobinsky, A. A. Reheating after Inflation. *Phys. Rev. Lett.* **1994**, *73*, 3195–3198. [CrossRef]
- Belinskii, V.A.; Khalatnikov, I.M.; Lifshitz, E.M. A general solution of the Einstein equations with a time singularity. *Adv. Phys.* **1982**, *31*, 639–667. [CrossRef]
- Zel'dovich, Y.B.; Starobinsky, A.A. Particle Production and Vacuum Polarization in an Anisotropic Gravitational Field. *Sov. Phys. JETP* **1972**, *34*, 1159.
- Zel'dovich, Y.B. Partifcle Production in Cosmology. *JETP Lett.* **1970**, *12*, 307.
- Lukash, V.N.; Starobinsky, A.A. The isotropization of the cosmological expansion owing to particle production. *Sov. Phys. JETP* **1974**, *39*, 742.
- Zel'dovich, Y.B.; Starobinskii, A.A. Rate of particle production in gravitational fields. *JETP Lett.* **1977**, *26*, 252–255.
- Hoyle, F.; Narlikar, J.V. Mach's principle and the creation of matter. *Proc. R. Soc. A* **1963**, *273*, 1–11.

Disclaimer/Publisher's Note: The statements, opinions and data contained in all publications are solely those of the individual author(s) and contributor(s) and not of MDPI and/or the editor(s). MDPI and/or the editor(s) disclaim responsibility for any injury to people or property resulting from any ideas, methods, instructions or products referred to in the content.

Article

Graviton to Photon Conversion in Curved Space-Time and External Magnetic Field

Alexander D. Dolgov^{1,2,*}, Lyubov A. Panasenko¹ and Vladimir A. Bochko¹

¹ Department of Physics, Novosibirsk State University, Pirogova 2, 630090 Novosibirsk, Russia; l.vetoshkina@nsu.ru (L.A.P.); v.bochko@nsu.ru (V.A.B.)

² Bogoliubov Laboratory of Theoretical Physics, Joint Institute for Nuclear Research, 141980 Dubna, Russia

* Correspondence: dolgov@nsu.ru

Abstract: The suppression of relic gravitational waves due to their conversion into electromagnetic radiation in a cosmological magnetic field is studied. The coupled system of equations describing gravitational and electromagnetic wave propagation in an arbitrary curved space-time and in external magnetic field is derived. The subsequent elimination of photons from the beam due to their interaction with the primary plasma is taken into account. The resulting system of equations is solved numerically in the Friedman–LeMaitre–Robertson–Walker metric for the upper limit of the intergalactic magnetic field strength of 1 nGs. We conclude that the gravitational wave conversion into photons in the intergalactic magnetic field cannot significantly change the amplitude of the relic gravitational wave and their frequency spectrum.

Keywords: gravitational waves; cosmological magnetic field; expanding universe; Heisenberg–Euler action; gravitational wave conversion; curved space-time; Friedman–LeMaitre–Robertson–Walker space-time



Citation: Dolgov, A.D.; Panasenko, L.A.; Bochko, V.A. Graviton to Photon Conversion in Curved Space-Time and External Magnetic Field. *Universe* **2024**, *10*, 7. <https://doi.org/10.3390/universe10010007>

Academic Editors: Galina L. Klimchitskaya, Vladimir M. Mostepanenko and Sergey V. Sushkov

Received: 5 November 2023

Revised: 22 December 2023

Accepted: 22 December 2023

Published: 25 December 2023



Copyright: © 2023 by the authors. Licensee MDPI, Basel, Switzerland. This article is an open access article distributed under the terms and conditions of the Creative Commons Attribution (CC BY) license (<https://creativecommons.org/licenses/by/4.0/>).

1. Introduction

The transformation between gravitons and photons in an external magnetic field was considered in a multitude of papers starting from 1961 [1–8]. The problem acquired particular importance in connection with the possible transformation of relic gravitational waves (GW) produced at the inflationary stage [9–12] into electromagnetic waves (EMW) in primordial magnetic fields. However, in all previous works see, e.g., [8,13] the calculations have always been conducted in Minkowski space-time, though the curvature effects in the very early universe could be quite essential.

In the present work, we go beyond the flat space-time restriction and consider graviton and photon propagation in an arbitrary curved background. The propagation of gravitational waves in curved space-time was almost always considered in the Friedman–LeMaitre–Robertson–Walker metric (FLRW), see, e.g., textbooks [14,15], except for some Bianchi type metrics and our recent paper [16], where an arbitrary background metric was allowed. Here, we derive the propagation equations for the coupled system of photons and gravitons in an arbitrary background. Next, we will turn to the Friedman–LeMaitre–Robertson–Walker (FLRW) space-time, which is a good approximation of the real universe. However, deviations from FLRW could be essential and lead to interesting observable effects.

For over a century, the Friedman equations have served as a basement for the conventional cosmological model. They well describe the early universe, that is homogeneous and isotropic to a very good approximation. They are operative also in the contemporary universe on very large scales. Friedman cosmology allows for description of cosmological dark matter and what is more surprising dark energy, though the physical nature of the latter is not yet established.

The propagation of gravitational waves in curved space-time was almost always considered in FLRW metric, except for some Bianchi type metrics and our recent paper [16], where an arbitrary background metric was allowed.

Here, we derive the coupled equations of motion for metric perturbations and electromagnetic waves over an arbitrary cosmological background in the external cosmic magnetic field. The metric perturbations and EMW are treated in the first order of the perturbation theory.

We introduce the full electromagnetic field \bar{A}_μ as the sum of an external classical component of the electromagnetic field A_μ and a small quantum fluctuation f_μ , which is considered as a perturbation,

$$\bar{A}_\mu = A_\mu + f_\mu. \tag{1}$$

The stress tensors of \bar{A}_μ, A_μ and f_μ are then introduced accordingly:

$$\bar{F}_{\mu,\nu} = \partial_\mu \bar{A}_\nu - \partial_\nu \bar{A}_\mu \tag{2}$$

$$F_{\mu\nu} = \partial_\mu A_\nu - \partial_\nu A_\mu, \tag{3}$$

$$f_{\mu\nu} = \partial_\mu f_\nu - \partial_\nu f_\mu. \tag{4}$$

The full metric tensor $\bar{g}_{\mu\nu}$ is expanded around the metric tensor of the background space-time $g_{\mu\nu}$ as

$$\bar{g}_{\mu\nu} = g_{\mu\nu} + h_{\mu\nu},$$

$$\bar{g}^{\mu\nu} = g^{\mu\nu} - h^{\mu\nu}$$

with $h_{\mu\nu}$ being a small perturbation of the metric.

The properties of the metric tensor $g_{\mu\nu}$ are specified by: the orthogonality condition $g_{\mu\nu}g^{\mu\lambda} = \delta_\nu^\lambda$, where δ_μ^λ is the Kronecker delta-symbol; rising and lowering of the indices of the tensors $h_{\mu\nu}$ and $f_{\mu\nu}$ by the background metric tensor $g^{\mu\nu}$. Note that the indices of the full and classical stress tensors of the electromagnetic fields are raised and lowered with the full metric tensor $\bar{g}_{\mu\nu}$.

The corrections to the metric determinant \bar{g} can be found from the first-order expansion of an arbitrary non-degenerate matrix \mathcal{M} :

$$\det[\mathcal{M} + \delta\mathcal{M}] = \det[\mathcal{M}] \left(1 + \text{Tr}[\mathcal{M}^{-1}\delta\mathcal{M}] \right). \tag{5}$$

So we obtain:

$$\det[\bar{g}_{\mu\nu}] = \det[g_{\mu\nu}h_{\mu\nu}] = \det[g_{\mu\nu}] (1 + g^{\mu\nu}h_{\mu\nu}). \tag{6}$$

It is assumed usually that tensor perturbations are traceless:

$$h \equiv g^{\mu\nu}h_{\mu\nu} = 0. \tag{7}$$

However, we see in what follows that the corrections to the Maxwell energy–momentum tensor are not traceless, see, e.g., Equations (69)–(115) and a nonzero trace of the gravitational field source leads to the nonzero h , so $\det[\bar{g}_{\mu\nu}] = \det[g_{\mu\nu}](1 + h)$.

The initially derived equations are supposed to be valid in an arbitrary space-time metric, but ultimately we assume that the background metric has the 3D-flat FLRW form:

$$ds^2 = dt^2 - a^2(t) \sum_{j=1,2,3} dx_j^2 \tag{8}$$

where $a(t)$ is the cosmological scale factor. The Hubble parameter is expressed through it in the usual way as $H = \dot{a}/a$. The curved metric reduces to the flat one when $a \rightarrow 1$.

The paper is organized as follows. We start in Section 2 with a brief reminder of the equation for metric perturbations over arbitrary space-time. In Section 3, we recall the

expansion of metric perturbations in terms of helicity eigenstates. After that, in Section 4 we show that the scalar and tensor modes can mix in the general case of inhomogeneous space. Further, in Section 5 we consider propagation of metric perturbation over FLRW space-time in an external magnetic field. In Section 6, the propagation of electromagnetic waves in a magnetic field is considered. In both sections, we start from the classical Maxwell and Hilbert–Einstein actions ignoring for a while the Heisenberg–Euler (HE) [17] corrections, the quantum trace anomaly and matter effects. They are taken into account step-by-step in the subsequent subsections. On the way, we discuss the definition of physical magnetic fields through the electromagnetic field tensor $F_{\mu\nu}$ in cosmological background (Section 5.3) and the impact of the HE-corrections to the electromagnetic wave propagation expressed through the physical magnetic field \mathbf{B} (Section 6.2). In Section 7, we analyze the full set, of differential equations (SDE) for $(g - \gamma)$ -coupled system, choose a reference frame, and simplify the system for the choice made. Next, in Section 8, we divide the task into two cases: $\mathbf{k} \parallel \mathbf{B}$ and $\mathbf{k} \perp \mathbf{B}$, and find out that the conversion effect is present only for the second case. In the last Section 9, we divide SDE into two independent subsystems and solve the first of them numerically. Lastly, we conclude the paper by summarizing the obtained results and formulating the prospects for future research.

2. Metric Perturbations in General Case

In [16], we obtained Equation (23) for the propagation of metric perturbations in arbitrary space-time. Let us write it for two lower indices:

$$D^2 h_{\mu\nu} - 2h^{\alpha\beta} R_{\alpha\mu\nu\beta} - (h_{\alpha\mu} R_\nu^\alpha + h_{\alpha\nu} R_\mu^\alpha) + h_{\mu\nu} R - g_{\mu\nu} \left(h^{\alpha\beta} R_{\alpha\beta} + \frac{1}{2} D^2 h \right) = -2(8\pi G) T_{\mu\nu}^{(1)}, \tag{9}$$

where G is the gravitational constant, $D^2 = D^\alpha D_\alpha$ and D_α is the covariant derivative, $R_{\alpha\mu\nu\beta}, R_{\mu\nu}, R$ are the Riemann tensor, Ricci tensor and scalar curvature, respectively.

The equation contains additional terms that disappear in the special cases of Minkowski and FLRW spaces. These extra terms could have significant effects on the GW and EMW propagation over background metric that differs from the FLRW one.

Let us note the agreement between Equations (9) and (2.33) from the work [18], published after our work [16]. The apparent difference with our result disappears in the Lorentz calibration

$$D_\mu h_\nu^\mu = \frac{1}{2} \partial_\nu h. \tag{10}$$

In this article, the authors obtained the same equation using a double variation of the action, while we obtained it by expanding the Einstein equation to first order in perturbation.

3. Helicity Decomposition and Choice of Gauge

Now it is worth recalling the formalism of the expansion of the perturbation $h_{\mu\nu}$ in terms of helicity states [19–23]. The generally accepted approach is that (along with the vectors C_i, G_i and the traceless tensor D_{ij}) four scalars A, B, E, F are introduced, through which the components of the metric perturbation are expressed:

$$h_{00} = -E, \tag{11}$$

$$h_{0i} = a \left(\frac{\partial F}{\partial x^i} + G_i \right), \tag{12}$$

$$h_{ij} = a^2 \left(A \delta_{ij} + \frac{\partial^2 B}{\partial x^i \partial x^j} + \frac{\partial C_i}{\partial x^j} + \frac{\partial C_j}{\partial x^i} + D_{ij} \right). \tag{13}$$

One can impose gauge conditions such that two scalars turn to zero. The so called synchronous gauge corresponds to the choice $E = 0$ and $F = 0$. Under this gauge there still remains some more freedom, that may allow to simplify algebra in a specific problem. The second well-known type of gauge is the Newtonian gauge, where $B = 0, F = 0,$

$E \equiv 2\Phi$, and $A \equiv -2\Psi$. The choice of this gauge better fits our task, so for the scalar sector we will use the Newtonian gauge.

In addition to the gauge in the scalar sector, the Lorentz gauge (10) is usually imposed on the entire tensor perturbation of metric. This calibration naturally arises in the case when the so-called harmonic Fock coordinates are used. It allows to obtain a simpler expression for the Ricci tensor and, as a consequence, to simplify the equation for the propagation of metric perturbations. Formerly in our paper [16], we have only used the Lorentz gauge.

4. Mixing of Metric Perturbation Modes

Note that from the expression for the trace of the Equation (9) it turns out that in the general case, for an arbitrary form of the Ricci tensor, there appears a mixing of scalar and tensor modes of metric perturbations. In general case it is impossible to separate the equations for these two sectors. Indeed, taking trace of Equation (9), we obtain the following expression

$$\partial^2 h + 4h^{\alpha\beta}R_{\alpha\beta} - hR = 16\pi GT_{\alpha}^{\alpha(1)}, \tag{14}$$

where $\partial^2 = \partial^\mu \partial_\mu$, and from which it is clearly seen that the second term in the left hand side includes both terms from the scalar and the tensor sectors.

In addition, it is important to pay attention to the trace from the source on the right-hand side of the equation. As will be shown below for the problem of graviton conversion into photons in an external magnetic field, the trace from the correction to the EMT contains a convolution of the background electromagnetic tensor and the tensor perturbation to the metric, $h_{\mu\nu}$, which also leads to mixing between scalar and tensor modes. This result is evident, because the expansion of metric perturbations in polarizations is valid for a problem with axial symmetry: in this problem there is only one specific direction—the direction of the wave vector \mathbf{k} of the metric perturbation. If space is for some reason unisotropic (as, for example, in the case of an external magnetic field or in the presence of an anisotropic stress tensor), this symmetry disappears.

5. Metric Perturbations in Magnetic Field

5.1. Equation in the FLRW Metric

Recall that in the FLRW metric

$$R_{00} = -3\frac{\ddot{a}}{a}, \tag{15}$$

$$R_{ij} = -g_{ij}\left(\frac{\ddot{a}}{a} + 2H^2\right). \tag{16}$$

$$R = -6\left(\frac{\ddot{a}}{a} + H^2\right). \tag{17}$$

We write the trace of the GW tensor in the following form:

$$h = g^{\mu\nu}h_{\mu\nu} = h_{00} - \frac{h_{xx} + h_{yy} + h_{zz}}{a^2} \equiv h_{00} + h_i^i, \tag{18}$$

where the notation $h_i^i = -(h_{xx} + h_{yy} + h_{zz})/a^2$ was introduced:

Let us write down the system of Equation (9) for the case of the FLRW metric. To do this, we will use the expressions (15)–(18). We get

$$D^2 h_{\mu\nu} - 2h^{\alpha\beta}R_{\alpha\mu\nu\beta} - g_{\mu\nu}\left[\frac{1}{2}\partial^2 h - 3\frac{\ddot{a}}{a}h_{00} - \left(\frac{\ddot{a}}{a} + 2H^2\right)h_i^i\right] - 6H^2 h_{00}\delta_{0\mu}\delta_{0\nu} - 2\left(\frac{2\ddot{a}}{a} + H^2\right)h_{\mu\nu}\left[1 - \delta_0^\mu\delta_0^\nu\right] = -16\pi GT_{\mu\nu}^{(1)}, \tag{19}$$

where the Latin indices are the spatial ones (vary from one to three).

For a medium where the perturbation propagates, we will consider a model of an ideal fluid. The total energy–momentum tensor in this case is determined through the full metric as follows

$$\bar{T}_{\mu\nu}^{medium} = -p\bar{g}_{\mu\nu} + (p + \rho)\bar{u}_\mu\bar{u}_\nu, \quad (20)$$

where ρ is the energy density, p is the pressure, u_μ is the four-speed. Then the right side of Equation (19) can be rewritten as

$$-16\pi GT_{\mu\nu}^{(1)} = -16\pi G \left(T_{\mu\nu}^{medium(1)} + T_{\mu\nu}^{EM(1)} \right) = 16\pi G p h_{\mu\nu} - 16\pi GT_{\mu\nu}^{EM(1)}, \quad (21)$$

where the first term in the last equality is obtained by expanding Equation (20) to the first order in perturbation at $u_j = 0$ (index j varies from one to three) and the second term is responsible for the perturbation of the EMT due to the presence of an external magnetic field.

The factor before the last term on the left side of the Equation (19) is exactly

$$-2 \left(2\frac{\ddot{a}}{a} + H^2 \right) = 16\pi G p. \quad (22)$$

Thus, Equation (19) can be simplified:

$$\begin{aligned} D^2 h_{\mu\nu} - 2h^{\alpha\beta} R_{\alpha\mu\nu\beta} - g_{\mu\nu} \left[\frac{1}{2} \partial^2 h - 3\frac{\ddot{a}}{a} h_{00} - \left(\frac{\ddot{a}}{a} + 2H^2 \right) h_i^i \right] - 6H^2 h_{00} \delta_{0\mu} \delta_{0\nu} \\ = -16\pi GT_{\mu\nu}^{EM(1)}, \end{aligned} \quad (23)$$

Now, for brevity, we omit the expressions for the components of the Riemann tensor and the Christoffel symbols in the covariant derivative and write the final equations for 00, 0j, and ij components separately:

$$\begin{aligned} \left[\partial_t^2 + 3H\partial_t - \frac{\Delta}{a^2} + 3 \left(\frac{\ddot{a}}{a} - 4H^2 \right) \right] h_{00} - \frac{1}{2} \partial^2 h + \left(4H^2 - \frac{\ddot{a}}{a} \right) h_i^i &= -16\pi GT_{00}^{EM(1)}, \\ 2H \left[\partial_j h_{00} + \frac{\partial_x h_{xj} + \partial_y h_{yj} + \partial_z h_{zj}}{a^2} \right] &= -16\pi GT_{0j}^{EM(1)}, \\ \left[\partial_t^2 + 3H\partial_t - \frac{\Delta}{a^2} \right] h_j^i + \delta_j^i \left[-\frac{\partial^2 h}{2} + \left(\frac{\ddot{a}}{a} + 2H^2 \right) h_{00} + \frac{\ddot{a}}{a} h_i^i \right] &= -16\pi GT_j^i{}^{EM(1)}, \end{aligned} \quad (24)$$

where notation (18) is used, and the last equation is written in terms of mixed components, since then it looks more consistent with the equation for the 00 component.

5.2. Corrections to the Energy–Momentum Tensor (EMT)

Corrections to the EMT are due to the presence of an external electromagnetic field. We will find them in accordance with the definition of EMT of matter:

$$\bar{T}_{\mu\nu} = \frac{2}{\sqrt{-\bar{g}}} \frac{\delta \bar{\mathcal{A}}_{mttr}}{\delta \bar{g}_{\mu\nu}}. \quad (25)$$

There are two contributions to the EMT perturbation: from the Maxwell action and from the Heisenberg–Euler action.

The gravity of the background magnetic field is negligible compared to the background of matter and we ignore its contribution to the EMT corrections.

5.2.1. Corrections to EMT Emerging from the Maxwell Action

The Maxwell action is written as follows:

$$\mathcal{A}_{Max} = -\frac{1}{4} \int d^4x \sqrt{-\bar{g}} \left(\bar{F}^2 + \bar{A}_\mu \bar{J}^\mu \right), \quad (26)$$

where $\bar{F}^2 = \bar{F}_{\mu\nu}\bar{F}^{\mu\nu} = \bar{g}^{\mu\alpha}\bar{g}^{\nu\beta}\bar{F}_{\mu\nu}\bar{F}_{\alpha\beta}$. Hence the energy-momentum tensor is

$$\bar{T}_{\mu\nu}^{(Max)} = \frac{1}{4}\bar{g}_{\mu\nu}\bar{F}^2 - \bar{F}_{\mu\alpha}\bar{F}_{\nu\beta}\bar{g}^{\alpha\beta}. \quad (27)$$

or for the mixed components:

$$\bar{T}_\nu^\mu{}^{(Max)} = \frac{1}{4}\delta_\nu^\mu\bar{F}^2 - \bar{F}_{\cdot\alpha}^\mu\bar{F}_{\nu}^{\cdot\alpha}. \quad (28)$$

Clearly this tensor is conserved and its trace is zero:

$$\bar{g}^{\mu\nu}\bar{T}_{\mu\nu}^{(Max)} \equiv \delta_\nu^\mu\bar{T}_\mu^\nu{}^{(Max)} = 0. \quad (29)$$

The vanishing of the EMT trace in Maxwell electrodynamics is a consequence of the conformal invariance of the Maxwell action (26). This is not so for higher order quantum corrections (trace anomaly), see Section 6.3.

The trace of the zero-order term with mixed components:

$$T_\nu^\mu{}^{(Max0)} = \frac{1}{4}\delta_\nu^\mu F^2 - F_{\cdot\alpha}^\mu F_{\nu}^{\cdot\alpha} \quad (30)$$

is also zero. Note that moving indices up or down in this equation is done by the background metric, e.g., $F_{\cdot\alpha}^\mu F_{\nu}^{\cdot\alpha} = g^{\mu\sigma}g^{\alpha\lambda}F_{\sigma\alpha}F_{\nu\lambda}$ and $F^2 = F_{\alpha\beta}F_{\sigma\lambda}g^{\alpha\sigma}g^{\beta\lambda}$.

The zero-order term is presumably small in comparison with the total cosmological energy-momentum tensor and can be neglected in what follows.

For the first order term with mixed components we obtain:

$$T_\nu^\mu{}^{(Max1)} = \frac{1}{2}\delta_\nu^\mu[(Ff) - (FFh)] + h^{\mu\sigma}F_{\sigma\alpha}F_{\nu}^{\cdot\alpha} + h^{\alpha\lambda}F_{\alpha}^\mu F_{\nu\lambda} - f_{\cdot\alpha}^\mu F_{\nu}^{\cdot\alpha} - F_{\cdot\alpha}^\mu f_{\nu}^{\cdot\alpha}, \quad (31)$$

where $(Ff) = F_{\alpha\beta}f^{\alpha\beta}$ and $(FFh) = F_{\alpha\beta}F_{\sigma}^{\beta}h^{\alpha\sigma}$. Evidently $T_\mu^\mu{}^{(Max1)} = 0$, as is expected.

5.2.2. Heisenberg–Euler (HE) Lagrangian

The second origin of EMT corrections is Heisenberg–Euler effective Lagrangian [17]. It describes quartic self-interaction of electromagnetic field and is induced by the loop of virtual electrons with four external electromagnetic legs. In the weak field limit, and low energies, much smaller than the electron mass, m_e , the corresponding action has the form:

$$\mathcal{A}_{HE}^{(0)} = \int d^4x \sqrt{-g} C_0 \left[(F_{\mu\nu}F^{\mu\nu})^2 + \frac{7}{4}(\tilde{F}^{\mu\nu}F_{\mu\nu})^2 \right]. \quad (32)$$

Here

$$C_0 = \alpha^2 / (90m_e^4) \quad (33)$$

and $\alpha = 1/137$ is the fine structure constant. At high temperatures C , α , and m_e change with T . At this stage, we omit the bar over $F_{\mu\nu}$ to simplify notations. The dual Maxwell tensor is defined as

$$\tilde{F}_{\alpha\beta} = \frac{\sqrt{-g}}{2}\epsilon_{\alpha\beta\mu\nu}F^{\mu\nu}, \quad \tilde{F}^{\alpha\beta} = \frac{1}{2\sqrt{-g}}\epsilon^{\alpha\beta\mu\nu}F_{\mu\nu}, \quad (34)$$

because the tensor quantity is $\sqrt{-g}\epsilon_{\alpha\beta\mu\nu}$ but not just $\epsilon_{\alpha\beta\mu\nu}$, see e.g., chapter 83 from textbook [24].

In what follows, we apply this action to photon propagation in an external magnetic field B and the weak field limit means $B \ll m_e^2$.

We need to generalize the Heisenberg–Euler action (32) to high energies/temperatures and curved FLRW space-time. To do so, let us start from the canonical action of photons and electrons written in terms of the conformal metric:

$$ds^2 = g_{\mu\nu}^{(c)} dx^\mu dx^\nu = a^2(\tau)(d\tau^2 - d\mathbf{r}^2) \equiv a^2(\tau)\eta_{\mu\nu} dx^\mu dx^\nu, \quad (35)$$

where $\eta_{\mu\nu} = \text{diag}[1, -1, -1, -1]$ is the Minkowski metric tensor, and $a(\tau)$ is the scale factor as a function of conformal time $\tau(t) = \int dt/a(t)$.

The action of photons and electrons written in terms of the inverse metric to $g_{\mu\nu}^{(c)}$, given by Equation (35), takes the form:

$$\mathcal{A}_{e\gamma} = \int d^4x a^4 \left[-\frac{g_c^{\mu\alpha} g_c^{\nu\beta}}{4} F_{\alpha\beta} F_{\mu\nu} + \bar{\psi} \left(i g_c^{\mu\nu} \Gamma_\mu \nabla_\nu - m_\psi \right) \psi + e g_c^{\mu\nu} A_\mu \bar{\psi} \Gamma_\nu \psi \right], \quad (36)$$

where Γ^μ is a generalization of the Dirac γ matrices for curved space-time. For FLRW metric they have the form $\Gamma_\mu = a\gamma_\mu$, where γ_μ are the usual Dirac matrices which anticommute as $[\gamma_\mu, \gamma_\nu] = \eta_{\mu\nu}$, $[\Gamma_\mu, \Gamma_\nu] = g_{\mu\nu}$; ∇_μ is the covariant derivative for spin-(1/2) field. For the FLRW metric, it has the form $\nabla_\mu = \partial_\mu + (3/2)\partial_\mu(\ln a)$.

Introducing conformally transformed spinor $\chi = \psi/a^{3/2}$, we arrive to the action:

$$\mathcal{A}_{e\gamma} = \int d^4x \left[-\frac{\eta^{\mu\alpha} \eta^{\nu\beta}}{4} F_{\alpha\beta} F_{\mu\nu} + \bar{\chi} \left(i \gamma^\mu \partial_\nu - am_\psi \right) \chi + ae \eta^{\mu\nu} A_\mu \bar{\chi} \gamma_\nu \chi \right]. \quad (37)$$

This is essentially the same action as it is in flat space-time with rescaled mass and charge: $m \rightarrow am$ and $e \rightarrow ae$, so formally $C_0 \sim e^4/m^4$ does not change, but since we plan to go to very high temperatures, even above the electroweak phase transition, where all bare masses of charged particles vanish, we have to substitute the high temperature value of the mass, to sum over all charged particles, and to take the high temperature value of the electromagnetic coupling α . So

$$C(T) = \sum_j \frac{\alpha^2(T) q_j^4}{90 m_j(T)^4}, \quad (38)$$

where q_j is the charge of the contributing to the loop particles in the electron charge units, e.g., for down or up quarks $q = -1/3$ or $2/3$.

The integrand in the expression for the action $\mathcal{A}_{\mathcal{HE}}$ is a scalar with respect to the general coordinate transformation, so we can use for it the same expression as (32) in arbitrary metric.

In the early universe, the Heisenberg–Euler action at high temperatures keeps the same form as (32) with substitution of $C(T)$ instead of C_0 :

$$\mathcal{A}_{HE} = \int d^4x \sqrt{-\bar{g}} C(T) \left[(\bar{F}^2)^2 + \frac{7}{4} (\bar{\tilde{F}}\bar{F})^2 \right], \quad (39)$$

where $F^2 = F_{\mu\nu} F^{\mu\nu}$, $\tilde{F}F = \tilde{F}_{\mu\nu} F^{\mu\nu}$, and we have returned bar over $F_{\mu\nu}$ and to the metric determinant in accordance with expansion (5).

The HE action given by Equation (39) leads to the following contribution to the energy-momentum tensor:

$$T_{\mu\nu}^{HE} = C(T) \left\{ -g_{\mu\nu} \left[(F_{\alpha\beta} F^{\alpha\beta})^2 - \frac{7}{4} (\tilde{F}^{\alpha\beta} F_{\alpha\beta})^2 \right] + 8(F_{\alpha\beta} F^{\alpha\beta}) F_{\mu\lambda} F_\nu^\lambda \right\}. \quad (40)$$

Here, the over-bars are eliminated to simplify notation but we keep in mind that this expression will be used with the non-expanded complete quantities, see Equation (5).

An explanatory comment may be in order here, namely, the second term containing the dual Maxwell tensor, $\tilde{F}_{\mu\nu}$, depends upon metric only through the factor $(\sqrt{-\bar{g}})^{-2}$, so with the account of the integration measure the action depends on metric as $(\sqrt{-\bar{g}})^{-1}$ instead on $(\sqrt{-\bar{g}})$. Hence, this gives the contribution to $T_{\mu\nu}$ from $(\tilde{F}F)^2$ proportional to $(+g_{\mu\nu})$ instead of the usual one proportional to $(-g_{\mu\nu})$.

One can see that the trace of tensor (40) is non-vanishing:

$$T_\mu^{\mu HE} = C(T) \left[4(F_{\alpha\beta} F^{\alpha\beta})^2 + 7(\tilde{F}^{\alpha\beta} F_{\alpha\beta})^2 \right] \neq 0. \quad (41)$$

It is instructive to check conservation of the energy–momentum tensor (40), though it surely must be true, since it was obtained by the variation of a scalar function over metric. Still, at least the verification of the conservation would indicate that the calculations are correct. Let us note that the conservation condition should be fulfilled only if $C = const.$ Evidently, the energy–momentum tensor (40) is non-conserved for a non-constant $C(T)$ because the dependence on temperature appears due to interaction and an exchange of energy with external system.

It would be more convenient to express the square of the dual electromagnetic tensor through F . It enters the action in the form, see Equation (34):

$$(\tilde{F}F)^2 = \tilde{F}^{\mu\nu} F_{\mu\nu} \tilde{F}_{\alpha\beta} F^{\alpha\beta} = \frac{1}{4} \epsilon^{\mu\nu\lambda\sigma} \epsilon_{\alpha\beta\tau\chi} F_{\lambda\sigma} F_{\mu\nu} F^{\tau\chi} F^{\alpha\beta}. \tag{42}$$

Expressing the product of epsilons through the Kronecker symbols and properly contracting the indices we obtain:

$$(\tilde{F}F)^2 = 2F^4 + 4F^{\alpha\beta} F_{\nu\alpha} F^{\mu\nu} F_{\mu\beta}, \tag{43}$$

where $F^4 \equiv (F^{\mu\nu} F_{\mu\nu})^2$. We can verify result (43) expressing the Maxwell tensor through electromagnetic fields \mathbf{B} and \mathbf{E} coming to the well-known relation $(\tilde{F}F)^2 = [-4(\mathbf{E} \cdot \mathbf{B})]^2$.

The first part of the action (39), proportional to F^4 , leads to the following contribution to the energy–momentum tensor

$$T_{\mu\nu}^{(1)} = C \left(-F^4 g_{\mu\nu} + 8F^2 F_{\mu\alpha} F_{\nu}{}^{\alpha} \right). \tag{44}$$

The same contribution, up to a numerical factor, comes from the first term in Equation (43). So to find the total EMT we need to find the variation of the second term of Equation (43). Eventually, the remaining part of the energy–momentum tensor is

$$T_{\mu\nu}^{(2)} = \frac{7C}{4} \left[\left(16F^2 F_{\mu\alpha} F_{\nu}{}^{\alpha} - 2F^4 g_{\mu\nu} \right) + \left(32F_{\mu}{}^{\lambda} F_{\lambda\alpha} F^{\alpha\beta} F_{\nu\beta} - 4F^{\alpha\beta} F_{\lambda\alpha} F^{\sigma\lambda} F_{\sigma\beta} g_{\mu\nu} \right) \right]. \tag{45}$$

Bringing together Equations (44) and (45) and raising one index we obtain for the total energy–momentum tensor, originating from the Heisenberg–Euler action, the following expression:

$$T_{\nu}^{\mu} = -\delta_{\nu}^{\mu} C \left[\frac{9}{2} F^4 + 7F^{\alpha\beta} F_{\lambda\alpha} F^{\sigma\lambda} F_{\sigma\beta} \right] + 36CF^2 F^{\mu\alpha} F_{\nu\alpha} + 56CF^{\mu\lambda} F_{\lambda\alpha} F^{\alpha\beta} F_{\nu\beta}. \tag{46}$$

Now, let us check the conservation of the obtained energy–momentum tensor (46) in the case of constant $C(T)$. We consider $T_{\mu\nu}^{(1)}$ and $T_{\mu\nu}^{(2)}$ separately.

$$T_{\nu;\mu}^{(1)\mu} = -4CF^2 F^{\alpha\beta} F_{\alpha\beta;\nu} + 8CF^2 F^{\mu\alpha} F_{\nu\alpha;\mu} + 8C(F^2 F^{\mu\alpha})_{;\mu} F_{\nu\alpha}, \tag{47}$$

where semicolons mean covariant derivatives in the background metric. The last term in this equation is zero according to the equation of motion corresponding to the Lagrangian $\mathcal{L} = F^4$.

The first two ones can be rewritten using the relation

$$F_{\alpha\beta;\sigma} + F_{\beta\sigma;\alpha} + F_{\sigma\alpha;\beta} = 0. \tag{48}$$

Renaming some dummy indices we come to

$$T_{\nu;\mu}^{(1)\mu} = 4CF^2 (F_{\alpha\mu;\nu} + 2F_{\nu\alpha;\mu}) F^{\mu\alpha} = 4CF^2 (F_{\nu\alpha;\mu} - F_{\mu\nu;\alpha}) F^{\mu\alpha} = 0. \tag{49}$$

Here, we proved EMT conservation law for those parts of the action which contain F^4 . It must be analogous for the EMT part originated from $F^{\alpha\beta} F_{\nu\alpha} F^{\mu\nu} F_{\mu\beta}$ (see Equation (43)).

$$\begin{aligned} & 4[-F^{\alpha\beta} F_{\lambda\alpha} F^{\sigma\lambda} F_{\sigma\beta} \delta_{\nu}^{\mu} + 8F^{\mu\lambda} F_{\lambda\alpha} F^{\alpha\beta} F_{\nu\beta}]_{;\mu} \\ & = 4[-4F^{\alpha\beta} F_{\lambda\alpha} F^{\mu\lambda} F_{\mu\beta;\nu} + 8F^{\mu\lambda} (F_{\lambda\alpha} F^{\alpha\beta} F_{\nu\beta})_{;\mu}], \end{aligned} \tag{50}$$

where we used the Maxwell equation $F^{\mu\nu}_{;\mu} = 0$. Considering the part inside square brackets and taking into account the equation of motion $F^{\mu\lambda}(F^{\alpha\beta}F_{\lambda\alpha})_{;\mu} = 0$, that follows from the part of the action:

$$\mathcal{A}_{HE}^{part} = 7C \int d^4x \sqrt{-g} F^{\alpha\beta} F_{\nu\alpha} F^{\mu\nu} F_{\mu\beta}, \tag{51}$$

(see Equations (39) and (43)), we arrive to

$$\begin{aligned} [-4F^{\alpha\beta}F_{\lambda\alpha}F^{\mu\lambda}F_{\mu\beta;\nu} + 8F^{\mu\lambda}(F_{\lambda\alpha}F^{\alpha\beta}F_{\nu\beta})_{;\mu}] &= 4F^{\mu\lambda}F^{\alpha\beta}F_{\lambda\alpha}(-F_{\mu\beta;\nu} + 2F_{\nu\beta;\mu}) \\ &= 4F^{\mu\lambda}F^{\alpha\beta}F_{\lambda\alpha}(-F_{\mu\beta;\nu} - F_{\beta\mu;\nu} - F_{\mu\nu;\beta} + F_{\nu\beta;\mu}) \\ &= 4F^{\mu\lambda}F^{\alpha\beta}F_{\lambda\alpha}(-F_{\mu\nu;\beta} + F_{\nu\beta;\mu}) = 0. \end{aligned} \tag{52}$$

For the transition to the third term of these equalities, we used Equation (48).

The conclusion for this section is that EMT originated from the Heisenberg–Euler action with $C = const$ is conserved

$$T_{\nu;\mu}^{(HE)\mu} = 0. \tag{53}$$

It is noteworthy that EMT (46) is not traceless. Indeed, it is equal to

$$T_{\mu}^{\mu} = C \left(18 F^4 + 28 F^{\mu\lambda} F_{\lambda\alpha} F^{\alpha\beta} F_{\mu\beta} \right). \tag{54}$$

5.2.3. Corrections to EMT Emerging from the HE Action

Now making the usual perturbation expansion (5), we find the following first-order correction to the energy–momentum tensor:

$$\begin{aligned} T_{\mu\nu}^{HE1} &= C(T) \left\{ -h_{\mu\nu} \left[(F_{\alpha\beta}F^{\alpha\beta})^2 - \frac{7}{4}(\tilde{F}^{\alpha\beta}F_{\alpha\beta})^2 \right] \right. \\ &- g_{\mu\nu} \left[4F^2 F_{\alpha\beta} f^{\alpha\beta} - 4F^2 F_{\alpha\beta} F_{\lambda\sigma} g^{\alpha\lambda} h^{\beta\sigma} - \frac{7}{2}(\tilde{F}F)\tilde{F}^{\alpha\beta} f_{\alpha\beta} \right. \\ &\quad + 8F^2(F_{\mu\lambda}f_{\nu}^{\lambda} + f_{\mu\lambda}F_{\nu}^{\lambda}) + 16F_{\mu\lambda}F_{\nu}^{\lambda}F^{\alpha\beta}f_{\alpha\beta} \\ &\quad \left. \left. - 8h^{\lambda\sigma}F_{\mu\lambda}F_{\nu\sigma}F^2 - 16F_{\mu\lambda}F_{\nu}^{\lambda}F_{\beta}^{\sigma}F_{\sigma\gamma}h^{\beta\gamma} \right] \right\}. \end{aligned} \tag{55}$$

This expression can be simplified, because in the absence of a background electric field $\tilde{F}F = 0$ and we get:

$$\begin{aligned} T_{\mu\nu}^{HE1} &= C(T) \left[-h_{\mu\nu}(F^2)^2 - 4F^2 g_{\mu\nu}(Ff - FFh) + 8F^2(f_{\nu\lambda}F_{\mu}^{\lambda} + f_{\mu\lambda}F_{\nu}^{\lambda}) \right. \\ &\quad \left. + 16F_{\mu\lambda}F_{\nu}^{\lambda}(Ff) - 8h^{\lambda\sigma}F_{\mu\lambda}F_{\nu\sigma}F^2 - 16F_{\mu\lambda}F_{\nu}^{\lambda}(FF)h \right]. \end{aligned} \tag{56}$$

The trace of this expression is nonvanishing:

$$T_{\alpha}^{\alpha HE1} = C(T) \left[16F^2(Ff) - 8F^2(hFF) - F^4h \right] \tag{57}$$

It is usually demanded in FLRW space-time that the source term $T_{\nu}^{(1)\mu}$ for gravitational wave Equation (24) must be traceless. To this end, one may separate the traceless part out of Equation (56) subtracting $g_{\mu\nu}T_{\alpha}^{\alpha HE1}/4$ out of it. However, this prescription would break the conservation of the source and, as is shown in Section 6 of paper [16], it would lead to a violation of the transversality conditions $D_{\mu}\psi_{\nu}^{\mu} = 0$. Indeed, in [16] we used the condition $\bar{D}_{\mu}\bar{T}_{\nu}^{\mu} = 0$ to prove a compatibility of the Einstein equations in the first perturbation order with gauge fixing conditions (89).

Note that the energy–momentum tensor (40) is non-conserved for a non-constant $C(T)$ because the dependence on the temperature appears due to interaction with external system. Thus, EMT is not formally conserved.

5.2.4. Summary

As a conclusion of this subsection, we write the result for the correction to the EMT from the Maxwell action and from the Heisenberg–Euler action, respectively:

$$T_{\mu\nu}^{Maxwell(1)} = \frac{1}{2}g_{\mu\nu}[Ff - FFh] + h_{\mu\sigma}F^{\sigma\alpha}F_{\nu\alpha} + h^{\alpha\sigma}F_{\mu\alpha}F_{\nu\sigma} - f_{\mu\alpha}F_{\nu}^{\cdot\alpha} - F_{\mu\alpha}f_{\nu}^{\cdot\alpha}, \tag{58}$$

$$T_{\mu\nu}^{HE(1)} = C(T) \left[-h_{\mu\nu}(F^2)^2 - 4F^2g_{\mu\nu}(Ff - FFh) + 8F^2(f_{\nu\lambda}F_{\mu}^{\cdot\lambda} + f_{\mu\lambda}F_{\nu}^{\cdot\lambda}) \right] + C(T) \left[16F_{\mu\lambda}F_{\nu}^{\cdot\lambda}(Ff) - 8h^{\lambda\sigma}F_{\mu\lambda}F_{\nu\sigma}F^2 - 16F_{\mu\lambda}F_{\nu}^{\cdot\lambda}(FFh) \right]. \tag{59}$$

where $Ff = F^{\alpha\beta}f_{\alpha\beta}$, $FFh = h_{\sigma}^{\alpha}F_{\alpha\beta}F^{\sigma\beta}$.

5.3. Maxwell Tensor and Cosmic Magnetic and Electric Fields

Equations (58) and (59) appear quite complicated. Further, we simplify these equations and express them in terms of physical magnetic fields. To understand the physical meaning of the different components of $F_{\mu\nu}$, $F^{\mu\nu}$, or F_{μ}^{ν} , let us start from the geodesic equation for a charged particle in external electric and magnetic field (see, e.g., book [24]. Equation (90.7)):

$$m \frac{Du^{\alpha}}{ds} = eF_{\cdot\beta}^{\alpha}u^{\beta}, \tag{60}$$

where $u^{\alpha} = dx^{\alpha}/ds$ is the particle four-velocity. From this equation, it is clear that physical electric field is the Maxwell tensor with mixed components, $E^j = F_{0}^j$, and physical magnetic field is expressed through the Maxwell tensor F_j^i as:

$$B_1 = F_{3}^2, \quad B_2 = -F_{3}^1, \quad B_3 = F_{2}^1, \tag{61}$$

or in compact form $B_i = \epsilon_{ijl}F_{\cdot m}^j\delta^{ml}$.

The first pair of Maxwell equation has the same form as in flat space-time:

$$\partial_{\lambda}F_{\mu\nu} + \partial_{\nu}F_{\lambda\mu} + \partial_{\mu}F_{\nu\lambda} = 0. \tag{62}$$

If the background electric field is absent, i.e., $F_{tj} = 0$, then

$$\partial_t F_{ij} = 0. \tag{63}$$

Hence F_{ij} remains constant in the process of cosmological expansion and correspondingly physical magnetic field behaves as:

$$F_i^{\cdot j} = g^{jk}F_{ik} = -F_{jk}/a^2. \tag{64}$$

In other words, physical magnetic field drops as $1/a^2$, the well known result.

If an electric field is absent and the only external magnetic field is non-zero, then the dual Maxwell tensor (34) has only space-time components. The quantity $D_{tj} = \tilde{F}_{tj}/\sqrt{-g} = (1/2)\epsilon_{tjlm}F^{lm}$ is expressed through magnetic field as

$$D_{tj} = -D_{jt} = B_j/a^4. \tag{65}$$

In flat space-time, varying the magnetic field induces an electric field according to

$$\nabla \times E = -\partial_t B. \tag{66}$$

In curved space-time, the analogue of this equation is Equation (62) with $\lambda = t$ or Equation (63), so if the original electric field was absent, it would not be induced by a time-varying magnetic field, in the case that the time variation is created by the cosmological expansion (64).

In terms of physical magnetic field \mathbf{B} the product $F_{\mu\nu}F^{\mu\nu}$ with indices lifted by the background metric $g^{\mu\nu}$ is

$$F_{\mu\nu}F^{\mu\nu} = F^2 = 2\mathbf{B}^2 \sim 1/a^4. \tag{67}$$

5.4. Scalar and Tensor Mode Mixing in External Magnetic Field

Using Equations (15)–(18), we rewrite Equation (14) for the case of the FLRW metric as:

$$\partial^2 h - 12 \frac{\ddot{a}}{a} h_{00} - 4 \left(\frac{\ddot{a}}{a} + 2H^2 \right) h_i^i + 6 \left(\frac{\ddot{a}}{a} + H^2 \right) h = 16\pi G T_\alpha^{\alpha(1)}. \tag{68}$$

The EMT perturbation originating from the Maxwell action is traceless, while that from the Heisenberg–Euler action has a non-zero trace. Indeed,

$$T_\alpha^{HE1} = C(T) \left[-hF^4 + 16F^2(Ff) - 8F^2(FFh) \right]. \tag{69}$$

Now, one could naively divide the source into a traceless part and a non-zero trace part (simply subtract the trace multiplied by the background metric). To this end, let us look at Equation (68) and explicitly substitute $T_\alpha^{EM(1)}$ into the right-hand side. We get

$$\begin{aligned} \partial^2 h - 12 \frac{\ddot{a}}{a} h_{00} - 4 \left(\frac{\ddot{a}}{a} + 2H^2 \right) h_i^i + 6 \left(\frac{\ddot{a}}{a} + H^2 \right) h \\ = 16\pi G C F^2 \left[-hF^2 + 16(Ff) - 8(F_{\alpha\beta} F^{\alpha\sigma} h_\sigma^\beta) \right]. \end{aligned} \tag{70}$$

We see that the equation contains both scalar and tensor parts. Thus, it is impossible to write a separate equation for each mode. To make this even more obvious, let us fix the coordinates so that the magnetic field is directed along the x -axis. The following components of the electromagnetic field tensor will then be non-zero:

$$F_{\cdot z}^y = -F_{\cdot y}^z = B_x. \tag{71}$$

$$F^{yz} = -F^{zy} = -\frac{B_x}{a^2}. \tag{72}$$

$$F_{yz} = -F_{zy} = -B_x a^2. \tag{73}$$

The trace from the correction to the EMT can then be rewritten taking into account the following relations:

$$F^2 = 2B^2, \tag{74}$$

$$Ff = F_\alpha^\beta f_{\cdot\beta}^\alpha = F_{\cdot z}^y f_{\cdot z}^y + F_{\cdot y}^z f_{\cdot y}^z = B \left(f_{\cdot z}^y - f_{\cdot y}^z \right) = 2B f_{\cdot z}^y, \tag{75}$$

$$FFh = h_\sigma^\alpha F_{\beta\alpha} F^{\beta\sigma} = B^2 \left(h_y^y + h_z^z \right), \tag{76}$$

and in Equation (70) we have

$$\begin{aligned} \partial^2 h - 12 \frac{\ddot{a}}{a} h_{00} - 4 \left(\frac{\ddot{a}}{a} + 2H^2 \right) h_i^i + 6 \left(\frac{\ddot{a}}{a} + H^2 \right) h \\ = 32\pi G C B^3 \left[-hB + 16f_{\cdot z}^y - 4B \left(h_y^y + h_z^z \right) \right]. \end{aligned} \tag{77}$$

The diagonal components can be written as the sum of scalar and tensor quantities of the helicity expansion

$$h_y^y = -2\Psi \delta_y^y + D_y^y, \tag{78}$$

$$h_z^z = -2\Psi \delta_z^z + D_z^z, \tag{79}$$

and, substituting the helicity expansion into the complete equation, we obtain the final equation, which shows the mixing of scalars Φ, Ψ and tensor D_{ij} :

$$\begin{aligned} \left(\partial^2 + 64\pi G C B^4 \right) (\Phi + 3\Psi) + 6(\Psi - \Phi) \left(\frac{\ddot{a}}{a} - H^2 \right) \\ = 32\pi G C B^3 \left[16f_{\cdot z}^y - 4B \left(4\Psi + D_y^y + D_z^z \right) \right], \end{aligned} \tag{80}$$

where $h = 2\Phi + 6\Psi$.

In addition, we note that there may also be implicit mixing through the term with $f_{\cdot z}^y$ in the above equation, since the equation for the electromagnetic wave contains various convolutions of tensors with tensor $h_{\mu\nu}$ (see below, Equation (148)).

As was noted in Section 4, the result is quite evident, since the external magnetic field gives, in addition to the GW propagation vector, another preferred direction in space. This leads to the loss of axial symmetry and to mixing of the scalar and tensor modes of metric perturbations.

6. Electromagnetic Wave Propagation in External Magnetic Field

In this section, we will derive the equation for the propagation of electromagnetic waves in curved space-time and in the presence of an external magnetic field, thereby completing the derivation of the system of differential equations (SoDE) for the metric-EMF perturbation system. We will briefly call this system $g - \gamma$, by g we mean a graviton with any possible polarization: 0, 1, 2.

6.1. Equation of Motion from the Maxwell Action

Variation in the Maxwell action from Equation (26) over δA_ν leads to the equation of motion $\bar{D}_\mu \bar{F}^{\mu\nu} = \bar{J}^\nu$, where \bar{D}_μ is the covariant derivative in the full metric $\bar{g}_{\mu\nu}$. Due to antisymmetry of $\bar{F}^{\mu\nu}$ this equation is reduced to:

$$\bar{D}_\mu \bar{F}^{\mu\nu} = \frac{1}{\sqrt{-\bar{g}}} \partial_\mu (\bar{F}^{\mu\nu} \sqrt{-\bar{g}}) = \bar{J}^\nu \tag{81}$$

Below we assume that neither electric charge density nor electric current are present, i.e., $\bar{J}^\nu = 0$.

Substituting expansions (5), (4), and (6) into Equation (81) we obtain

$$\begin{aligned} \frac{1}{\sqrt{-\bar{g}}} \partial_\alpha (\sqrt{-\bar{g}} \bar{F}^{\alpha\beta}) &= \frac{1}{\sqrt{-\bar{g}}} \partial_\alpha (\sqrt{-\bar{g}} \bar{g}^{\alpha\alpha'} \bar{g}^{\beta\beta'} \bar{F}_{\alpha'\beta'}) = \\ \frac{1}{\sqrt{-\bar{g}}} \partial_\alpha [\sqrt{-\bar{g}} (g^{\alpha\alpha'} - h^{\alpha\alpha'}) (g^{\beta\beta'} - h^{\beta\beta'}) (F_{\alpha'\beta'} + f_{\alpha'\beta'})] &= 0. \end{aligned} \tag{82}$$

The external electric field is supposed to be zero and only background magnetic field is present, so $F_{t\beta} = 0$. Thus, the zero-order term, which is the equation of motion for the background magnetic field, has the form;

$$\partial_\mu F^{\mu\nu} = \partial_\mu (g^{\mu\alpha} g^{\nu\beta} F_{\alpha\beta}) = 0. \tag{83}$$

This is the analogue of the equation $div \mathbf{B} = 0$ in flat space-time.

In FLRW metric the metric determinant is expanded as:

$$\sqrt{-\bar{g}} = \sqrt{-g}(1 + h/2) = a^3(1 + h/2). \tag{84}$$

and so Equation (82) takes the form:

$$\partial_\mu [(g^{\mu\alpha} - h^{\mu\alpha})(g^{\nu\beta} - h^{\nu\beta})(F_{\alpha\beta} + f_{\alpha\beta})] + F^{\mu\nu} \partial_\mu h/2 + 3H g^{\nu\beta} f_{t\beta} = 0, \tag{85}$$

where we took into account that $g^{t\alpha} = \delta^{t\alpha}$ and $F_{t\beta} = 0$. We also assume that $f_t = f^t = 0$ and impose the transversality condition on the propagating photon modes:

$$D_\mu f^\mu = \frac{1}{\sqrt{-g}} \partial_\mu (\sqrt{-g} f^\mu) = \partial_t f^t + 3H f^t - \partial_j f^j = 0, \tag{86}$$

which for $f^t = 0$ leads to $\partial_j f^j = 0$.

Thus, the first-order expansion of Equation (85) has the form:

$$\partial_\mu f^{\mu\nu} + 3H f^{t\nu} - \partial_\mu (h_\alpha^\mu F^{\alpha\nu} + h_\alpha^\nu F^{\mu\alpha}) + F^{\mu\nu} \partial_\mu h/2 + Q^\nu = 0. \tag{87}$$

where we introduced a new quantity Q^V to describe contributions from different additional terms such as Heisenberg–Euler corrections, matter effects, etc., to be considered below.

To derive the first-order equation for f_j , we multiply Equation (87) by $g_{vj} = -a^2\delta_{vj}$ (Latin indices are always supposed to be the space ones, e.g., $j = 1, 2, 3$) and recall that $F_{t\mu} = 0$ and $f_t = 0$. So, we finally obtain:

$$\partial_t^2 f_j - \frac{\Delta f_j}{a^2} + H\partial_t f_j - g_{vj}\partial_\mu \left(h^{\mu\alpha} g^{\nu\beta} F_{\alpha\beta} + g^{\mu\alpha} h^{\nu\beta} F_{\alpha\beta} \right) + F_{.j}^{\mu} \partial_\mu h / 2 + Q_j = 0, \tag{88}$$

where $Q_j = g_{vj}Q^V = -a^2\delta_{vj}Q^V$ and Δ is the flat space Laplacian.

To proceed further, we have to fix certain gauge conditions on metric perturbations $h_{\mu\nu}$. We will follow our paper [16], where it is shown that the following conditions can be imposed in arbitrary background metric:

$$D_\mu \psi_\nu^{\mu} \equiv D_\mu \left(h_\nu^{\mu} - h\delta_\nu^{\mu} / 2 \right) = 0, \quad h_{t\mu} = 0. \tag{89}$$

Since in FLRW metric the only non-zero components of the Christoffel symbols are:

$$\Gamma_{ti}^j = H\delta_{ti}^j, \quad \Gamma_{ij}^t = Ha^2\delta_{ij} \tag{90}$$

the covariant derivative of h^i_j is reduced to the ordinary derivative and

$$D_\mu h_\nu^{\mu} = \partial_\mu h_\nu^{\mu} - \Gamma_{\mu\nu}^{\lambda} h_\lambda^{\mu} + \Gamma_{\mu\lambda}^{\mu} h_\nu^{\lambda} = \partial_\mu h_\nu^{\mu}. \tag{91}$$

So using Equations (83) and (89), and the absence of an external electric field, $F_{tj} = 0$, we obtain:

$$\partial_t^2 f_j - \frac{\Delta f_j}{a^2} + H\partial_t f_j - h_i^m \partial_m F_{.j}^i - F_{.i}^m \partial_m h_j^i + Q_j \equiv \mathcal{M}[f_j] + Q_j = 0. \tag{92}$$

The terms proportional to $\partial_m h$ cancel out because $F_{.j}^i \partial_m h_i^m = F_{.j}^i \partial_i h / 2$.

Here, we have introduced the new notation:

$$\mathcal{M}_j[f] = \partial_t^2 f_j - \frac{\Delta f_j}{a^2} + H\partial_t f_j - h_i^m \partial_m F_{.j}^i - F_{.i}^m \partial_m h_j^i \tag{93}$$

to be used in what follows.

6.2. Equation of Motion from the Heisenberg–Euler Action

The variation of \mathcal{A}_{HE} (39) over δA_ν results in the following contribution to the electromagnetic field equation:

$$\bar{D}_\mu \bar{F}_{.j}^{\mu} + \bar{Q}_j^{(HE)} = 0, \tag{94}$$

where the first term originated from the variation of the Maxwell action (see previous subsection), while the second is the contribution from \mathcal{A}_{HE} (39) and has the following form

$$\begin{aligned} \bar{Q}_j^{(HE)} &= -g_{vj} D_\mu \left[C(T) \left(8\bar{F}^{\mu\nu} \bar{F}^2 + 14\bar{F}^{\mu\nu} (\bar{F}^{\alpha\beta} \bar{F}_{\alpha\beta}) \right) \right] \\ &= -\frac{g_{vj}}{\sqrt{-\bar{g}}} \partial_\mu \left[C(T) \sqrt{-\bar{g}} \left(8\bar{F}^{\mu\nu} \bar{F}^2 + 14\bar{F}^{\mu\nu} (F\bar{F}) \right) \right]. \end{aligned} \tag{95}$$

where $F^2 = F_{\mu\nu} F^{\mu\nu}$ and $(F\bar{F}) = \bar{F}_{\mu\nu} F^{\mu\nu}$.

We have shown in Section 5.3 that the free external magnetic field is not constant, but rises backward in time with the decreasing scale factor as $1/a^2$.

Let us return to Equation (95) and make perturbative expansion according to Equation (5). We start from consideration of the first term in square brackets, which with account of the zeroth- and first-order terms takes the form

$$g_{vj} \frac{\delta \mathcal{A}_{HE1}}{\delta \bar{A}_\nu} = g_{vj} \frac{(-1)}{\sqrt{-g(1+h)}} \partial_\mu \left\{ 8\sqrt{-g(1+h)} C \left[F^2 F^{\mu\nu} + F^2 f^{\mu\nu} + 2F^{\mu\nu} (fF) \right] \right\}$$

$$-2F^{\mu\nu}(FFh) - F^2\left(h_{\alpha}^{\mu}F^{\alpha\nu} + h_{\alpha}^{\nu}F^{\mu\alpha}\right)\Big], \quad (96)$$

where $fF = f_{\mu\nu}F^{\mu\nu}$, $(FFh) = h_{\sigma}^{\alpha}F_{\alpha\beta}F^{\beta\sigma}$, and indices are shifted up or down with the background metric.

The zero-order term in this equation somewhat changes the equation of motion of the background magnetic field in FLRW metric leading to:

$$\partial_j F^{j\nu} - 16C\partial_j(B^2 F^{j\nu}) = 0, \quad (97)$$

which is not of much importance for the evolution of B_j . The terms proportional to the time derivatives of $\sqrt{-g}$, C , and F^2 do not appear if $F^{t\mu} = 0$ and $h_{\alpha}^t = 0$.

The first-order part of expression (96) is equal to:

$$Q_j^{HE1} = -16g_{\nu j}C\partial_{\mu}\left[B^2 f^{\mu\nu} + F^{\mu\nu}(fF) + F^{\mu\nu}(FFh) - B^2\left(h_{\alpha}^{\mu}F^{\alpha\nu} + h_{\alpha}^{\nu}F^{\mu\alpha}\right)\right] - 16Cg_{\nu j}F^{\mu\nu}B^2\partial_{\mu}h/2 - 16B^2(\dot{C} + 3HC)f_{,j}^t. \quad (98)$$

The term proportional to B^2C in this expression, has the form:

$$-16CB^2g_{\nu j}\left(\partial_{\mu}f^{\mu\nu} + 3Hf^{t\nu} - h_{\alpha}^{\mu}\partial_{\mu}F^{\alpha\nu} - F^{\mu\alpha}\partial_{\mu}h_{\alpha}^{\nu}\right) \equiv -16CB^2\mathcal{M}_j[f], \quad (99)$$

where $\mathcal{M}_j[f]$ is defined in the Equations (92) and (93). The factor in the brackets in the left-hand side of the above equation coincides with the left-hand side of Equation (92), except for the last term Q_j , so it can be absorbed into Equation (92) changing the overall coefficient from 1 to $(1 - 16CB^2)$.

In addition to the terms proportional to B^2 , the first two terms in Equation (98) give the following contribution of the first part of the HE action to the photon propagation equation:

$$-16Cg_{\nu j}\left[f^{\mu\nu}\partial_{\mu}B^2 + F^{\mu\nu}\partial_{\mu}(fF)\right] = -16C\left[f_{,j}^{\mu}\partial_{\mu}B^2 + F_{,j}^{\mu}\partial_{\mu}(Ff)\right]. \quad (100)$$

So all the terms in Equation (98), except for those absorbed into Equation (92) and containing $h_{\mu\nu}$, turn into:

$$Q_j^{HE11} = -16B^2\dot{C}f_{ij} - 16C\left[f_{,j}^{\mu}\partial_{\mu}B^2 + F_{,j}^{\mu}\partial_{\mu}(Ff)\right]. \quad (101)$$

The contribution of the terms containing $h_{\mu\nu}$ in Equation (98) can be written as

$$Q_j^{HEh} = -16C\left[F_{,j}^{\mu}\partial_{\mu}(FFh) - (h^{\mu\alpha}F_{\alpha j} + h_{\alpha j}F^{\mu\alpha})\partial_{\mu}B^2\right]. \quad (102)$$

Finally, for the total Q_j^{HE1} we obtain

$$\begin{aligned} Q_j^{HE1} &= -16CB^2\mathcal{M}_j[f] + Q_j^{HE11} + Q_j^{HEh} \\ &= -16C\left[B^2\left(\mathcal{M}_j[f] + \frac{\dot{C}}{C}f_{ij}\right) + \left(f_{,j}^{\mu} - h^{\mu\alpha}F_{\alpha j} - h_{j\alpha}F^{\mu\alpha}\right)\partial_{\mu}B^2\right] \\ &\quad - 16CF_{,j}^{\mu}\partial_{\mu}(fF + FFh), \end{aligned} \quad (103)$$

where $\mathcal{M}_j[f]$ is defined in Equation (93).

It is convenient to introduce auxiliary vector field through the equation

$$F_{ij} = -\epsilon_{ijk}\mathcal{H}^k \quad (104)$$

Physical magnetic field is related to \mathcal{H} as $B_k = -\mathcal{H}^k/a^2 = -\mathcal{H}_ka^2$ (because $B_k \sim F_{,j}^i \sim g^{il}F_{lj} \sim \delta_{il}F_{lj}/a^2$).

To decipher the last term in Equation (103) we use the identity:

$$\epsilon_{abc}\epsilon^{ljm} = \delta_a^l\delta_b^j\delta_c^m + \delta_a^m\delta_b^l\delta_c^j + \delta_a^j\delta_b^m\delta_c^l - \delta_a^l\delta_b^m\delta_c^j - \delta_a^m\delta_b^j\delta_c^l - \delta_a^j\delta_b^l\delta_c^m. \quad (105)$$

and Equation (104). So FFh and $F_{,j}^{\mu}\partial_{\mu}(fF)$ turn into

$$FFh = F_{\alpha\beta}F^{\beta\sigma}h_{\sigma}^{\alpha} = -B^2h_i^i + h^{ij}B_iB_j, \tag{106}$$

$$\begin{aligned} F_{,j}^{\mu}\partial_{\mu}(fF) &= F_{,j}^m\partial_m(fF) = 2g_{nj}B_k\partial_m(f^{mn}B_k + f^{km}B_n + f^{nk}B_m) \\ &= 2B_k\partial_m(f_{,j}^mB_k + f^{km}B_j + f_j{}^k B_m), \end{aligned} \tag{107}$$

where summation over repeated indices is performed.

The variation of the second term in the HE action, Equation (95), is equal to:

$$\frac{\delta\mathcal{A}_{HE2}}{\delta\tilde{A}_{\nu}} = \frac{(-14)}{\sqrt{-\tilde{g}}}\partial_{\mu}\left[\sqrt{-\tilde{g}}C(T)\tilde{F}^{\mu\nu}(\tilde{F}^{\alpha\beta}\tilde{F}_{\alpha\beta})\right]. \tag{108}$$

In the case that the background electric field is absent and only magnetic field is non-zero, the right-hand side of the equation above vanishes in the zeroth-perturbation order because $F_{\alpha\beta}$ is non-zero only for space–space components, while $\tilde{F}_{\alpha\beta}$ is non-zero for space-time components. Hence $\tilde{F}_{\alpha\beta}F^{\alpha\beta} = 0$.

Accordingly, expression (108) multiplied by $g_{\nu\mu}$ can be expanded as

$$Q_j^{HE2} = -28\left[(\dot{C} + HC)\delta_{\mu}^t + C\partial_{\mu}\right]\tilde{F}_j^{\mu}(f\tilde{F}), \tag{109}$$

where

$$\tilde{F}_j^{\mu}(f\tilde{F}) = g_{\nu j}\tilde{F}^{\mu\nu}(f\tilde{F}) = \frac{1}{4}g_{\nu j}\epsilon^{\mu\nu\alpha\beta}F_{\alpha\beta}\epsilon_{\sigma\lambda\rho\gamma}F^{\sigma\lambda}f^{\rho\gamma}. \tag{110}$$

So using Equation (104) and contracting

$$\epsilon^{jkl}\epsilon_{mkl} = 2\delta_m^j \tag{111}$$

we obtain from Equation (109):

$$Q_j^{HE2} = -56C\left[\left(\frac{\dot{C}}{C} - 3H\right)B_jB_k\partial_t f_k + B_jB_k\partial_t^2 f_k\right], \tag{112}$$

where the summation over the repeated space indices is made with Kronecker delta and considers that $B_j \sim 1/a^2$.

So using Equations (92), (93), (103) and (109) we obtain:

$$\begin{aligned} \partial_t^2 f_j - \frac{\Delta f_j}{a^2} + H\partial_t f_j - h_i^m\partial_m F_{,j}^i - F_{,i}^m\partial_m h_j^i + Q_j^{HE1} + Q_j^{HE2} \equiv \\ \mathcal{M}_j[f] + Q_j^{HE1} + Q_j^{HE2} = 0 \end{aligned} \tag{113}$$

and come to the almost final equation for photons

$$\begin{aligned} (1 - 16CB^2)\mathcal{M}_j[f] - 16B^2\dot{C}f_{tj} - 16C\left(f_{,j}^t - h^{\mu\alpha}F_{\alpha j} - h_{j\alpha}F^{\mu\alpha}\right)\partial_{\mu}B^2 \\ - 16CF_{,j}^{\mu}\partial_{\mu}(fF + FFh) - 28\left[(\dot{C} + HC)\delta_{\mu}^t + C\partial_{\mu}\right]\tilde{F}_j^{\mu}(f\tilde{F}) = 0. \end{aligned} \tag{114}$$

We highlight that $\mathcal{M}_j[f]$ is defined in Equation (93).

6.3. Conformal Anomaly Effect

Quantum corrections to the energy–momentum tensor of electromagnetic field $T_{\mu\nu}^{(em)}$ in curved space-time background lead to the the well-known conformal anomaly, for a review see ref. [25], resulting in the nonzero trace of the electromagnetic energy–momentum tensor:

$$T_{\mu}^{\mu(anom)} = \frac{\alpha\beta}{8\pi}G_{\mu\nu}^{(a)}G^{\mu\nu(a)} \tag{115}$$

where $G_{\mu\nu}$ is the gauge field stress tensor, α is the fine structure constant and β is the first coefficient of the beta-function expansion for the gauge group of rank N :

$$\beta = \frac{11}{3}N - \frac{2}{3}N_F, \tag{116}$$

with N_F being the number of the fermion species.

There are additional contributions into the trace proportional to the products of the Riemann, Ricci tensors, and curvature scalar which are generally nonlocal [26,27]. We will not consider them in this work.

The trace anomaly allows for photon production by the conformally flat gravitational field [28,29] in contrast to the Parker theorem [30].

The Fourier transform of the amplitude of the photon propagation in the gravitational field has pole at $q^2 = 0$, where q is the four-momentum transfer to gravitational field. According to the result of paper [28] the anomalous part of the energy-momentum tensor has the form:

$$T_{\mu\nu}^{(anom)} \sim \frac{q_\mu q_\nu - g_{\mu\nu} q^2}{q^2} F_{\alpha\beta} F^{\alpha\beta}. \tag{117}$$

It is evidently conserved and has non-zero trace.

As is shown in Ref. [28], conformal anomaly (115) leads to an additional contribution to Equation (88) or, which is essentially the same, to Equation (92).

$$\alpha\beta \left(\partial_\mu F_{,\nu}^\mu \ln a - H F_{,\nu}^t \right). \tag{118}$$

The first term here is the usual charge renormalization and the second one is the anomaly giving rise to photon production in conformally flat metric. This metric allows for the transformation to the conformal time leading to the Minkowski metric proportional to the common scale factor. The canonical Maxwell equation, without the anomalous term, transforms in this metric into the free Maxwell equation in flat space-time, while the additional anomalous term does not allow this.

6.4. Plasma Interaction Effects

Photons propagating in the primeval plasma interact with plasma particles and as a result acquire an effective mass, the so-called plasma frequency, Ω_{pl} , so the relation between photon frequency, ω , and momentum, k , changes as $\omega^2 - k^2 = \Omega_{pl}^2$. Waves with $\omega < \Omega_{pl}$ do not propagate in plasma.

In the canonic theory, the effective action describing the plasma frequency term is usually written as

$$\mathcal{A}_{pl} = \frac{1}{2} \int d^4x \sqrt{-g} \Omega_{pl}^2 g_{\mu\nu} f^\mu f^\nu. \tag{119}$$

This term is proportional to the square of the small amplitude f^μ of the electromagnetic wave and seemingly should be neglected in our first order approximation. However, this is not so because to obtain the first-order equation one has to take the action in the second order in small quantities. The first-order terms are absent in the action since f^μ satisfies the equation of motion that are realised at the extreme value of action for which $\delta A / \delta f^\mu = 0$.

The corresponding energy-momentum tensor is

$$T_{\mu\nu} \sim f^2 \tag{120}$$

is quadratic in f and can be disregarded in our approximation. It is similar to a scalar field with small amplitude ϕ that has energy density proportional to $m_\phi^2 \phi^2$, so its energy-momentum tensor is quadratically small but non-zero mass, m_ϕ is essential for propagation of ϕ waves.

All electrically charged particles contribute to plasma frequency. If the particle mass is larger than the temperature of the relativistic cosmological plasma, $m > T$, the contribution to plasma frequency from such nonrelativistic charged particles is

$$\Omega_{pl}^{nr} = \frac{e^2 n}{m}, \tag{121}$$

where n is the number density of particles with charge e , $e^2 = 4\pi\alpha$. Note that the number density in this case is exponentially suppressed, $n \sim \exp(-m/T)$ [31].

On the other hand, relativistic particles, with $m < T$, contribute as:

$$\Omega_{pl}^{rel} = \frac{2T^2}{9} \sum_j e_j^2, \tag{122}$$

where the summation is done over all relativistic charged particles with charges e_j . The electric charge, e , depends on temperature due to radiative corrections [32].

Plasma frequency is determined by the photon Green’s function in the limit of vanishing photon momentum. More rigorous treatment of the problem of the photon propagation in plasma demands determination of the proper Green’s function. Simple derivation of these expression including the Green’s function can be found in ref. [33]. However, in this paper we will use simplified approximation describing the plasma effects by the plasma frequency only.

We need also take into account the loss of coherence of the photons produced by gravitons. We describe this phenomenon introducing a damping term into the equation of motion for photons in the form $\Gamma \dot{f}_j$, where we approximate Γ as

$$\Gamma = v s \sigma n, \tag{123}$$

where $n = 0.1 g_* T^3$ is the density of charged particles in plasma, $g_* = 10 - 100$ is the number of charged particle species, $v \sim 1$ is the relative velocity of “our” photon and the scatterer in plasma, and $\sigma = \alpha^2/T^2$ is the scattering cross-section.

Thus, the final equation for photons propagating in an arbitrary curved space-time background and external magnetic field in cosmic plasma accounting for photon collisions with plasma particles has the form:

$$\begin{aligned} & (1 - 16CB^2) \left[\partial_t^2 f_j - \frac{\Delta f_j}{a^2} + \frac{\partial_j \partial_k f_k}{a^2} + H \partial_t f_j - g_{vj} (h^{\mu\alpha} \partial_\mu F_{\alpha}^v + F_{\alpha}^\mu \partial_\mu h^{\nu\alpha}) \right] \\ & - 16B^2 \dot{C} f_{tj} - 16C \left[(f_j^\mu - h^{\mu\alpha} F_{\alpha j} - h_{j\alpha} F^{\mu\alpha}) \partial_\mu B^2 + F_{j\mu}^\mu \partial_\mu (fF - FFh) \right] \\ & - 28 \left[(\dot{C} + HC) \delta_\mu^t + C \partial_\mu \right] \tilde{F}_j^\mu (f\tilde{F}) + \alpha\beta \left[\ln a \left(\partial_t^2 f_j - \frac{\Delta f_j}{a^2} \right) - H \partial_t f_j \right] \\ & + \Omega_{pl}^2 f_j + \Gamma \dot{f}_j = 0. \end{aligned} \tag{124}$$

It is assumed that $f_t = 0$ and we used Equations (103), (109), (114), (118), (122) and (123).

7. Defining g and γ System of Differential Equations (SoDE)

In total, we have ten equations for the components of tensor $h_{\mu\nu}$ and three equations for the components of vector f_j . In fact, only six equations for gravitational waves are linearly independent.

In the case considered here, we assume that the vector modes do not arise. The first vector G_i in Equations (11)–(13) vanishes due to the gauge condition $h_{0i} = 0$. The second vector C_i is not zero because the corrections to EoM contain spacial derivative of electromagnetic potential $\partial_\mu f_\nu$. However, the vector modes decay as a^{-2} and thus they do not play an essential role in cosmology. It worth adding that an account of one more polarisation state would lead to a considerable complication of the system of equations. So, in this work we confine ourselves only to scalar and tensor modes.

Finally, let us mention that the solution for tensor h_j^i does not contain pure tensor mode, but a mixture of tensor and scalar modes. Nevertheless, the solution represents them qualitatively correctly, including the behaviour of the tensor mode that we are interested in.

Assuming an absence of vector mode, we obtain two components less in the EoM. More specifically, we have two scalars, Φ and Ψ (note that in the deal fluid model, i.e., without taking into account dissipation, $\Phi = \Psi$) and two polarisations of the tensor wave, that in total gives four independent equations for metric perturbations.

In the subsequent Sections 7.1 and 7.2, the SoDE is simplified for the specific choice of the reference frame, where an external magnetic field is directed along the x -axis. Next, one of two independent subsystems is solved numerically in Section 8.

7.1. Simplification of SoDE for Metric Perturbations

To derive the system of equations for the metric perturbations, that is solved below, it remains to simplify the right-hand side of Equation (24). Let us rewrite Equations (58)–(59) for an external magnetic field that is directed along the x -axis. For individual expressions, we get:

$$F^2 = 2B^2, \tag{125}$$

$$Ff = F_{\beta}^{\alpha} f_{\alpha}^{\beta} = F_{y,z}^z f_{z,y}^y + F_{z,y}^y f_{y,z}^z = B(f_{z,y}^y - f_{y,z}^z) = 2Bf_{z,y}^y, \tag{126}$$

$$FFh = h_{\sigma}^{\alpha} F_{\alpha\beta} F^{\sigma\beta} = B^2(h_y^y + h_z^z), \tag{127}$$

$$(f^{\mu\alpha} F_{\nu\alpha} + F^{\mu\alpha} f_{\nu\alpha}) = (f_{\alpha}^{\mu} F_{\nu}^{\alpha} + F_{\alpha}^{\mu} f_{\nu}^{\alpha}) = B(f_{z,y}^y \delta_{\nu y} - f_{y,z}^z \delta_{\nu z}) + B(f_{\nu}^z \delta^{\mu y} - f_{\nu}^y \delta^{\mu z}), \tag{128}$$

$$F^{\mu\alpha} F_{\nu\alpha} = 2B^2(\delta^{\mu z} \delta_{\nu z} + \delta^{\mu y} \delta_{\nu y}), \tag{129}$$

$$h^{\mu\sigma} F_{\sigma}^{\alpha} F_{\nu\alpha} = B^2(h_y^y \delta_{\nu y} + h_z^z \delta_{\nu z}), \tag{130}$$

$$h^{\alpha\lambda} F_{\alpha}^{\mu} F_{\nu\lambda} = B^2[-h_z^z(\delta^{\mu z} \delta_{\nu y} + \delta^{\mu y} \delta_{\nu z}) + h_y^y \delta^{\mu z} \delta_{\nu z} + h_z^z \delta^{\mu y} \delta_{\nu y}], \tag{131}$$

$$(f^{\alpha\beta} F_{\lambda\alpha} F^{\sigma\lambda} F_{\sigma\beta} - h_{\xi}^{\alpha} F_{\xi}^{\beta} F_{\lambda\alpha} F^{\sigma\lambda} F_{\sigma\beta}) = 2B^3 f_{z,y}^z + B^4(h_z^z + h_y^y). \tag{132}$$

In this section and in subsequent ones, for the sake of brevity, we will omit the signature EM in the correction to the EMT.

Using Equations (58) and (59) and Equations (126)–(137) we obtain the EMT components for 00 (remember that $F_{0\alpha} = 0, F_{z,y}^y \neq 0$):

$$\begin{aligned} T_{00}^{(1)} &= T_{00}^{Max(1)} + T_{00}^{HE(1)} = \frac{1}{2}(Ff - FFh) - C[F^4 h_{00} + 4F^2(Ff - FFh)] \\ &= \frac{1}{2}(1 - 16CB^2)[2Bf_{z,y}^z - B^2(h_y^y + h_z^z)] - 4CB^4 h_{00}. \end{aligned} \tag{133}$$

Similarly, we derive the expression for the component $0j$:

$$T_{0j}^{(1)} = (1 - 8CF^2)f_{0\alpha} F_{j}^{\alpha} = (1 - 16CB^2)B[f_{0y} \delta_{jz} - f_{0z} \delta_{jy}]. \tag{134}$$

The expression for the ij components is more cumbersome:

$$T_j^{i(Max1)} = \frac{1}{2}\delta_j^i[Ff - FFh] + h_{\sigma}^i F^{\sigma\alpha} F_{j\alpha} + h_{\lambda}^{\sigma} F^{i\lambda} F_{j\sigma} + (F_{\lambda}^i f_{j}^{\lambda} + f_{\lambda}^i F_{j}^{\lambda}), \tag{135}$$

$$\begin{aligned} T_j^{i(HE1)} &= -h_j^i 4CB^4 - 8CB^2 \delta_j^i (Ff - FFh) - 16B^2 C (F_{\lambda}^i f_{j}^{\lambda} + f_{\lambda}^i F_{j}^{\lambda}) \\ &\quad + 16CF^{i\lambda} F_{j\lambda} (Ff - FFh) - 16B^2 C h_{\lambda}^{\sigma} F^{i\lambda} F_{j\sigma} \end{aligned} \tag{136}$$

Let us regroup the terms

$$\begin{aligned} T_j^{i(1)} &= \left[\frac{1}{2}(1 - 16CB^2)\delta_j^i + 16CF^{i\lambda} F_{j\lambda} \right] (Ff - FFh) \\ &\quad + (1 - 16CB^2) [F_{\lambda}^i f_{j}^{\lambda} + f_{\lambda}^i F_{j}^{\lambda} + h_{\lambda}^{\sigma} F^{i\lambda} F_{j\sigma}] \\ &\quad - 4CB^4 h_j^i + h_{\sigma}^i F^{\sigma\alpha} F_{j\alpha} = \end{aligned}$$

$$\begin{aligned}
 &= \left[\frac{1}{2} (1 - 16CB^2) \delta_j^i + 16CB^2 (\delta^{iy} \delta_{jy} + \delta^{iz} \delta_{jz}) \right] \left[2B f_{.z}^y - B^2 (h_y^y + h_z^z) \right] \\
 &\quad + (1 - 16CB^2) B \left[f_{.j}^z \delta^{iy} - f_{.j}^y \delta^{iz} - f_{.z}^i \delta_{jy} + f_{.y}^i \delta_{jz} \right] \\
 &\quad + (1 - 16CB^2) B^2 \left[-h_z^y (\delta^{iz} \delta_{jy} + \delta^{iy} \delta_{jz}) + h_y^y \delta^{iz} \delta_{jz} + h_z^z \delta^{iy} \delta_{jy} \right] \\
 &\quad - 4CB^4 h_j^i + B^2 (h_y^i \delta_{jy} + h_z^i \delta_{jz}). \tag{137}
 \end{aligned}$$

It will now be useful to write down the spatial components separately. After reducing similar terms, we get

$$T_x^{x(1)} = \frac{1 - 16CB^2}{2} \left[2B f_{.z}^y - B^2 (h_y^y + h_z^z) \right] - 4CB^4 h_x^x, \tag{138}$$

$$T_y^{x(1)} = -B (1 - 16CB^2) f_{.z}^x + B^2 (1 - 4CB^2) h_y^x, \tag{139}$$

$$T_z^{x(1)} = B (1 - 16CB^2) f_{.y}^x + B^2 (1 - 4CB^2) h_z^x, \tag{140}$$

$$T_y^{y(1)} = B \left(-1 + 48CB^2 \right) f_{.z}^y + B^2 \frac{h_y^y + h_z^z}{2} - 12CB^4 (h_y^y + 2h_z^z), \tag{141}$$

$$T_z^{y(1)} = 12CB^4 h_z^y, \tag{142}$$

$$T_z^{z(1)} = B \left(-1 + 48CB^2 \right) f_{.z}^z + B^2 \frac{h_y^y + h_z^z}{2} - 12CB^4 (2h_y^y + h_z^z). \tag{143}$$

System of Equation (24) is now rewritten as Equations (133), (134), (138)–(143).

7.2. Simplification of SoDE for Electromagnetic Waves

Let us simplify the system of equations for an electromagnetic wave for the case when the external magnetic field is directed along the x -axis. For spatial components, Equation (124) was derived in general form. We assume that $C(T) = \text{const}$, so the time derivative is $\dot{C} = 0$. Also, to begin with, let us omit the last three terms in the left-side of the equation, that considers the interaction of photons with plasma. Now, let us write the convolutions with the background tensor of the electromagnetic field in terms of field \mathbf{B} :

$$\begin{aligned}
 -g_{vj} \left(h^{\mu\alpha} \partial_\mu F_{. \alpha}^v + F_{. \alpha}^\mu \partial_\mu h^{v\alpha} \right) &= g_{vj} \left[h^{0y} \delta^{vz} - h^{0z} \delta^{vy} \right] \dot{B} + g_{vj} B \left[\partial_z h^{vy} - \partial_y h^{vz} \right] \\
 &= \left[h_y^0 \delta_{jz} - h_z^0 \delta_{jy} \right] \dot{B} + B \left[\partial_z h_j^y - \partial_y h_j^z \right], \tag{144}
 \end{aligned}$$

$$\left(f_{.j}^\mu - h^{\mu\alpha} F_{\alpha j} - h_{j\alpha} F^{\mu\alpha} \right) \partial_\mu B^2 = \left(f_{.j}^t - h_y^0 \delta_{jz} B + h_z^0 \delta_{jy} B \right) 2B \dot{B}, \tag{145}$$

$$F_{.j}^\mu \partial_\mu (fF - FFh) = B^2 \left[\delta_{jz} \partial_y - \delta_{jy} \partial_z \right] \left[2f_{.z}^y - B (h_y^y + h_z^z) \right], \tag{146}$$

$$\left[(\dot{C} + HC) \delta_\mu^t + C \partial_\mu \right] \tilde{F}_{.j}^\mu (f\tilde{F}) = C \partial_m \tilde{F}_{.j}^m (f\tilde{F}) = 0. \tag{147}$$

The last equality follows from the fact that the only non-zero component of the dual electromagnetic tensor in cases where the magnetic field is directed along the x -axis is $\tilde{F}_{0x} = -aB/2 \neq 0$.

So, let us write the resulting Equation (we omit the terms from the interaction with the plasma):

$$\begin{aligned}
 &(1 - 16CB^2) \left[\partial_t^2 f_j - \frac{\Delta f_j}{a^2} + \frac{\partial_j \partial_k f_k}{a^2} + H \partial_t f_j + \left[h_y^0 \delta_{jz} - h_z^0 \delta_{jy} \right] \dot{B} + B \left[\partial_z h_j^y - \partial_y h_j^z \right] \right] \\
 &- 16C \left[\left(f_{.j}^t - h_y^0 \delta_{jz} B + h_z^0 \delta_{jy} B \right) 2B \dot{B} \right. \\
 &\left. + B^2 \left[\delta_{jz} \partial_y - \delta_{jy} \partial_z \right] \left[2f_{.z}^y - B (h_y^y + h_z^z) \right] \right] = 0. \tag{148}
 \end{aligned}$$

By analogy with the equations for gravitational waves, we write for x , y , and z components, respectively:

$$\begin{aligned} & (1 - 16CB^2) \left[\partial_t^2 f_x - \frac{\Delta f_x}{a^2} + \frac{\partial_x \partial_k f_k}{a^2} + H \partial_t f_x + B \left[\partial_z h_x^y - \partial_y h_x^z \right] \right] \\ & - 32CB \dot{B} f_x^t = 0, \end{aligned} \tag{149}$$

$$\begin{aligned} & (1 - 16CB^2) \left[\partial_t^2 f_y - \frac{\Delta f_y}{a^2} + \frac{\partial_y \partial_k f_k}{a^2} + H \partial_t f_y - h_z^0 \dot{B} + B \left[\partial_z h_y^y - \partial_y h_y^z \right] \right] \\ & - 16C \left[\left(f_y^t + h_z^0 B \right) 2B \dot{B} - B^2 \partial_z \left[2f_y^z - B \left(h_y^y + h_z^z \right) \right] \right] = 0, \end{aligned} \tag{150}$$

$$\begin{aligned} & (1 - 16CB^2) \left[\partial_t^2 f_z - \frac{\Delta f_z}{a^2} + \frac{\partial_z \partial_k f_k}{a^2} + H \partial_t f_z + h_y^0 \dot{B} + B \left[\partial_z h_z^y - \partial_y h_z^z \right] \right] \\ & - 16C \left[\left(f_z^t - h_y^0 B \right) 2B \dot{B} + B^2 \partial_y \left[2f_z^y - B \left(h_y^y + h_z^z \right) \right] \right] = 0. \end{aligned} \tag{151}$$

Similar ones can be given, taking into account that $B \sim 1/a^2$ (meaning $\dot{B} = -2HB$) and that $f_t = 0$. For x components we get:

$$(1 - 16CB^2) \left[\ddot{f}_x - \frac{\Delta f_x}{a^2} + \frac{\partial_x \partial_k f_k}{a^2} + H \dot{f}_x + B \left[\partial_z h_x^y - \partial_y h_x^z \right] \right] + 64CB^2 H \dot{f}_x = 0, \tag{152}$$

or

$$(1 - 16CB^2) \left[\ddot{f}_x - \frac{\Delta f_x}{a^2} + \frac{\partial_x \partial_k f_k}{a^2} + B \left[\partial_z h_x^y - \partial_y h_x^z \right] \right] + (1 + 48CB^2) H \dot{f}_x = 0. \tag{153}$$

For y component:

$$\begin{aligned} & (1 - 16CB^2) \left[\ddot{f}_y - \frac{\Delta f_y}{a^2} + \frac{\partial_y \partial_k f_k}{a^2} + H \dot{f}_y + 2HB h_z^0 + B \left[\partial_z h_y^y - \partial_y h_y^z \right] \right] \\ & + 16CB^2 \left[4H \left(\dot{f}_y + h_z^0 B \right) + \partial_z \left[2f_y^z - B \left(h_y^y + h_z^z \right) \right] \right] = 0, \end{aligned} \tag{154}$$

or

$$\begin{aligned} & (1 - 16CB^2) \left[\ddot{f}_y - \frac{\Delta f_y}{a^2} + \frac{\partial_y \partial_k f_k}{a^2} \right] + (1 + 48CB^2) H \dot{f}_y - 32CB^2 \frac{\partial_z f_{yz}}{a^2} \\ & - B \left(1 - 16CB^2 \right) \partial_y h_y^z - 16CB^3 \partial_z h_z^z + B \left(1 - 32CB^2 \right) \partial_z h_y^y = 0. \end{aligned} \tag{155}$$

For z component:

$$\begin{aligned} & (1 - 16CB^2) \left[\ddot{f}_z - \frac{\Delta f_z}{a^2} + \frac{\partial_z \partial_k f_k}{a^2} + H \dot{f}_z - 2HB h_y^0 + B \left[\partial_z h_z^y - \partial_y h_z^z \right] \right] \\ & + 16CB^2 \left[4H \left(\dot{f}_z - h_y^0 B \right) - \partial_y \left[2f_z^y - B \left(h_y^y + h_z^z \right) \right] \right] = 0, \end{aligned} \tag{156}$$

or

$$\begin{aligned} & (1 - 16CB^2) \left[\ddot{f}_z - \frac{\Delta f_z}{a^2} + \frac{\partial_z \partial_k f_k}{a^2} \right] + (1 + 48CB^2) H \dot{f}_z + 32CB^2 \frac{\partial_y f_{yz}}{a^2} \\ & + B \left(1 - 16CB^2 \right) \partial_z h_z^y + 16CB^3 \partial_y h_y^y - B \left(1 - 32CB^2 \right) \partial_y h_z^z = 0. \end{aligned} \tag{157}$$

Next, we would like to show the validity of the requirement $f_t = 0$. In general, due to the homogeneity of the magnetic field (depending only on time), we arrive at the following equation for the time component:

$$(1 - 16CB^2) \partial_\mu f^{\mu 0} = 0. \tag{158}$$

Now we need to select a calibration. If our problem can be called magnetostatic, in such cases the Coulomb gauge $\partial_\mu f^\mu = 0$ is usually introduced, where we then get:

$$\begin{aligned} \partial_\mu f^{\mu 0} &= \partial_\mu \partial^\mu f_0 + \partial_0 \partial_\mu f^\mu = \partial_\mu \partial^\mu f_0, \\ \partial_\mu \partial^\mu f_0 &= 0 \Rightarrow f_0 = \text{const.} \end{aligned} \tag{159}$$

From the initial conditions of electrical neutrality, we find that this constant is equal to zero.

8. Two Examples of Gravitational Wave Directions

For any initial direction of the gravitational (tensor) wave propagation, we can decompose it into a parallel and perpendicular component relative to the external magnetic field. Note that we consider the case when an initial pure tensor plane wave propagates from vacuum into a region with a magnetic field (and, in the future, with plasma).

It is shown below that, for $\mathbf{k} \parallel \mathbf{B}$ the scalar mode of metric perturbations is not excited, and the electromagnetic wave is not excited as well. For the perpendicular component $\mathbf{k} \perp \mathbf{B}$ the situation is different—the scalar mode of metric perturbations and both polarizations of the electromagnetic wave are excited. Until now, we have not taken into account dissipation and loss of coherence for photons due to their interaction with plasma. But even without taking these phenomena into account, it is already possible to detect a change in the amplitude of the initial tensor GW due to the transition to the scalar mode of metric disturbances and to an electromagnetic wave. We will consider both of these cases in more detail in the next two subsections.

8.1. $\mathbf{k} \parallel \mathbf{B}$

Let us write down the basic relations that allow us to simplify the system of differential equations for metric perturbations and for an electromagnetic wave (EMW):

$$\mathbf{k} = (k_x, 0, 0), \tag{160}$$

$$f^\mu = (0, 0, f^y, f^z), \tag{161}$$

$$f^\mu(t, x) \sim \exp(ik_x x), \tag{162}$$

$$h_{\mu\nu}(t, x) \sim \exp(ik_x x), \tag{163}$$

$$h_\nu^\mu = \begin{bmatrix} 0 & 0 & 0 & 0 \\ 0 & 0 & 0 & 0 \\ 0 & 0 & h_+ & h_\times \\ 0 & 0 & h_\times & -h_+ \end{bmatrix}, \tag{164}$$

$$h_y^y + h_z^z = 0. \tag{165}$$

Taking into account what was written above, we write the system of equations in terms of h_+, h_\times . From Equations (133), (134), (138)–(143) we obtain

$$T_{00}^{(1)} = 0, \tag{166}$$

$$T_{0j}^{(1)} = (1 - 16CB^2)B[\dot{f}_y \delta_{jz} - \dot{f}_z \delta_{jy}], \tag{167}$$

$$T_x^{x(1)} = 0, \tag{168}$$

$$T_y^{x(1)} = -B(1 - 16CB^2)\partial^x f_z, \tag{169}$$

$$T_z^{x(1)} = B(1 - 16CB^2)\partial^x f_y, \tag{170}$$

$$T_y^{y(1)} = 12CB^4 h_+, \tag{171}$$

$$T_z^{y(1)} = 12CB^4 h_\times, \tag{172}$$

$$T_z^{z(1)} = -12CB^4 h_+. \tag{173}$$

From Equations (152), (154) and (156) we obtain, respectively

$$(1 - 16CB^2) \left[\ddot{f}_x - \frac{\Delta f_x}{a^2} + \frac{\partial_x^2 f_x}{a^2} + H\dot{f}_x \right] + 64CB^2 H\dot{f}_x = 0, \tag{174}$$

$$(1 - 16CB^2) \left[\ddot{f}_y - \frac{\Delta f_y}{a^2} + H\dot{f}_y \right] + 64CB^2 H\dot{f}_y = 0, \tag{175}$$

$$(1 - 16CB^2) \left[\ddot{f}_z - \frac{\Delta f_z}{a^2} + H\dot{f}_z \right] + 64CB^2 H\dot{f}_z = 0. \tag{176}$$

In Equations (174)–(176), there are no terms related to the gravitational wave. Therefore, if the electromagnetic wave was not initially present, it does not arise for the case when the wave vector is parallel to the external magnetic field. Hence, we obtain that

$$T_{0j}^{(1)} = 0, \tag{177}$$

$$T_y^{x(1)} = 0, \tag{178}$$

$$T_z^{x(1)} = 0. \tag{179}$$

From the remaining non-zero components of EMT Equations (171)–(173), we see that the GW configuration is preserved: it remains tensorial and no scalar modes arise.

8.2. $\mathbf{k} \perp \mathbf{B}$

Similar to the previous subsection, we write down the main relations that will help to simplify the system of differential equations for perturbations of metric and for electromagnetic waves. Let us direct the wave vector along the z-axis (it is always possible to rotate the coordinate system so that $k_y = 0$).

$$\mathbf{k} = (0, 0, k_z), \tag{180}$$

$$f^\mu = (0, f^x, f^y, 0), \tag{181}$$

$$f^\mu(t, x) \sim \exp(ik_z z), \tag{182}$$

$$h_{\mu\nu}(t, x) \sim \exp(ik_z z), \tag{183}$$

$$h_\nu^\mu = \begin{bmatrix} 0 & 0 & 0 & 0 \\ 0 & h_+ & h_\times & 0 \\ 0 & h_\times & -h_+ & 0 \\ 0 & 0 & 0 & 0 \end{bmatrix}, \tag{184}$$

$$h_y^y + h_z^z = -h_+. \tag{185}$$

Taking into account what was written above, we will write the system of equations in terms of h_+, h_\times . From Equations (133), (134), (138)–(143) we obtain

$$T_{00}^{(1)} = \frac{1}{2} (1 - 16CB^2) \left[-2B\partial_z f^y + B^2 h_+ \right], \tag{186}$$

$$T_{0j}^{(1)} = (1 - 16CB^2) B\dot{f}_y \delta_{jz}, \tag{187}$$

$$T_x^{x(1)} = \frac{1}{2} (1 - 16CB^2) \left[-2B\partial_z f^y + B^2 h_+ \right] - 4CB^4 h_+, \tag{188}$$

$$T_y^{y(1)} = B (1 - 16CB^2) \partial_z f^x + B^2 (1 - 4CB^2) h_\times, \tag{189}$$

$$T_z^{z(1)} = 0, \tag{190}$$

$$T_y^{y(1)} = B (1 - 48CB^2) \partial_z f^y - \frac{B^2}{2} h_+ + 12CB^4 h_+ \tag{191}$$

$$T_z^{y(1)} = 0, \tag{192}$$

$$T_z^{z(1)} = B (1 - 48CB^2) \partial_z f^y - \frac{B^2}{2} h_+ + 24CB^4 h_+. \tag{193}$$

From Equations (152), (154) and (156), respectively

$$(1 - 16CB^2) \left[\ddot{f}_x - \frac{\Delta f_x}{a^2} + B\partial_z h_\times \right] + (1 + 48CB^2) H\dot{f}_x = 0, \tag{194}$$

$$(1 - 16CB^2) \left[\ddot{f}_y - \frac{\Delta f_y}{a^2} + H\dot{f}_y - B\partial_z h_+ \right] + 16CB^2 [4H\dot{f}_y + \partial_z(-2\partial_z f^y + Bh_+)] = 0, \tag{195}$$

$$(1 - 16CB^2) \left[\ddot{f}_z - \frac{\Delta f_z}{a^2} + H\dot{f}_z \right] + 64CB^2 H\dot{f}_z = 0. \tag{196}$$

In Equation (196), there are no terms associated with a gravitational wave. So, as expected, longitudinal EMW does not arise. From Equations (194) and (195), it follows that an electromagnetic wave with polarization along the x -axis is generated by the polarization h_\times of the GW, and an electromagnetic wave with polarization along the y axis—polarization h_+ of the gravitational wave. Also, from the Equations (186)–(193), we clearly see the emergence of a scalar mode from the equations for the 00 and zz components of the EMT (see Equation (24)).

It is important to note that the expressions for EMT in terms of h_+, h_\times are valid only at the moment of time immediately following the initial moment of GW entry into the region with a magnetic field. Further, the wave ceases to be purely tensorial, and it is impossible to assert that $h_x^x = -h_y^y$. To find a solution, it is necessary to express all the quantities precisely in terms of h_x^x and h_y^y (not in terms of h_+) or in terms of expansion in helicity, introducing Φ and Ψ .

9. System Solution in the Case $\mathbf{k} \perp \mathbf{B}$

Let us write out the system of equations completely, taking into account the conclusions of the previous section that f^z, h_x^z, h_y^z components that are absent at the beginning do not arise during the conversion of tensor GW into photons and scalar perturbations of the metric.

Let us draw the reader’s attention to the fact that we write the equations in terms of the electromagnetic potential with the superscript f^μ and the gravitational wave potential with mixed indices h_μ^ν . In this case, we use the following expansion in helicity states for perturbation of the metric

$$h_{tt} = 2\Phi(t, \mathbf{r}), \tag{197}$$

$$h_z^z = 2\Psi(t, \mathbf{r}), \tag{198}$$

$$h_x^x = 2\Psi(t, \mathbf{r}) + \mathbf{h}_+(t, \mathbf{r}), \tag{199}$$

$$h_y^y = 2\Psi(t, \mathbf{r}) - \mathbf{h}_+(t, \mathbf{r}), \tag{200}$$

$$h_y^x = h_\times(t, \mathbf{r}). \tag{201}$$

We also make the Fourier expansion in terms of momentum, and accept the law of the scale factor variation with time, corresponding to the stage of radiation dominance $a(t) \sim t^{\frac{1}{2}}$.

To further search for a numerical solution, it would be convenient to introduce dimensionless quantities. To do this, let us change the notation

$$f^x / m_{pl} \rightarrow f^x, \tag{202}$$

$$f^y / m_{pl} \rightarrow f^y, \tag{203}$$

and introduce τ_0 to make the scale factor dimensionless

$$a = \sqrt{\frac{t}{\tau_0}}. \tag{204}$$

Due to the last change, the tensor $h_{\mu\nu}$ also becomes dimensionless.

Let us assume that at the present-day Universe $a_0 = 1$. This is just a choice of reference point and this choice does not influence the solution, because the constant factor in front of the scale factor function has no physical meaning. The condition is convenient in our problem to recalculate magnetic field strength using the present day magnitude. Using the scale factor dependence during matter dominance epoch $a = (t/\tau_{tot})^{2/3}$ we obtain for the coefficient τ_0 :

$$\tau_0 = \tau_{tot} \left(\frac{\tau_{tot}}{t_{eq}} \right)^{1/3} \approx 35 \tau_{tot}, \quad (205)$$

where $\tau_{tot} = 13.8 \times 10^9$ years is the age of the Universe, $t_{eq} = 3.3 \times 10^5$ years is the moment when radiation and dust energy densities were equal.

We accept also that the scale factor a varies in the interval $10^{-9} \leq a \leq 10^{-4}$. The selected interval lies inside the radiation dominance epoch (from the hadronic to the recombination).

For the magnitude of the magnetic field B_0 in the system of equations, we take its value at the present time. There are bounds obtained from observations: $10^{-16} \leq B_0 \leq 10^{-9}$ Gs [34]. Therefore, let us put $B_0 = 10^{-9} \times 1.95 \times 10^{-14}$ MeV².

After the Fourier transform over momentum, it will be clear that the system of equations contains both imaginary and real terms. Therefore, to solve the SDE numerically, it will be necessary to decompose each of the required quantities into real and imaginary parts. For example, $h_+ = Re(h_+) + iIm(h_+)$ and so on. For brevity, we write down systems of equations without dividing into real and imaginary parts. To obtain a more universal result, it is convenient to write the system in terms of $a(t)$. The first independent system has the following form:

$$\begin{aligned} f^x : & a^2 H^2 f^{x''} + a H^2 \left[1 + a \frac{H'}{H} + 8 \frac{2B_0^2 C_0 - a^4}{16B_0^2 C_0 - a^4} + a H \Gamma \right] f^{x'} \\ & + \left[\frac{k^2}{a^2} + 2a H H' - 8H^2 \frac{4B_0^2 C_0 + a^4}{16B_0^2 C_0 - a^4} + 2\Gamma H + \omega_{pl}^2 \right] f^x - \alpha \beta H^2 (a f^{x'} + 2f^x) \\ & + \alpha \beta \ln a \left[a^2 H^2 f^{x''} + \left(\frac{k^2}{a^2} + 2a H H' \right) f^x + (5a H^2 + a^2 H H') f^{x'} \right] = -\frac{ikB_0}{a^4 m_{pl}} h_{\times}, \quad (206) \\ h_{\times}^y : & a^2 H^2 h_{\times}'' + (4a H^2 + a^2 H H') h_{\times}' + \left[\frac{k^2}{a^2} + \frac{16\pi G B_0^2}{a^4} \left(1 - \frac{4B_0^2 C_0}{a^4} \right) \right] h_{\times} \\ & = -\frac{16\pi G B_0 ik}{a^2} \left(1 - \frac{16B_0^2 C_0}{a^4} \right) m_{pl} f^x, \end{aligned}$$

where the prime denotes the derivative with respect to the scale factor, and we introduced the attenuation of the electromagnetic wave due to its interaction with the plasma using the damping factor $\Gamma \propto \alpha^2 T(a)$ and the plasma frequency $\omega_{pl}^2 \propto \alpha T(a)$. Let us recall that $T(a) \propto 1/a$.

All solution interval terms with the multiplier $\alpha \beta \ln a$ can be neglected. Therefore, the resulting system is

$$\begin{aligned} f^x : & a^2 H^2 f^{x''} + a H^2 \left[1 + a \frac{H'}{H} + 8 \frac{2B_0^2 C_0 - a^4}{16B_0^2 C_0 - a^4} + a H \Gamma \right] f^{x'} + \\ & + \left[\frac{k^2}{a^2} + 2a H H' - 8H^2 \frac{4B_0^2 C_0 + a^4}{16B_0^2 C_0 - a^4} + 2\Gamma H + \omega_{pl}^2 \right] f^x - \alpha \beta H^2 (a f^{x'} + 2f^x) = -\frac{ikB_0}{a^4 m_{pl}} h_{\times}, \quad (207) \\ h_{\times}^y : & a^2 H^2 h_{\times}'' + (4a H^2 + a^2 H H') h_{\times}' + \left[\frac{k^2}{a^2} + \frac{16\pi G B_0^2}{a^4} \left(1 - \frac{4B_0^2 C_0}{a^4} \right) \right] h_{\times} \\ & = -\frac{16\pi G B_0 ik}{a^2} \left(1 - \frac{16B_0^2 C_0}{a^4} \right) m_{pl} f^x, \end{aligned}$$

It can be seen that the initial conditions

$$\begin{aligned}
 h_{\times}(0) &= h_{\times}^0, \\
 f^y(0) &= 0, \\
 h'_{\times}(0) &= 0, \\
 f^{y'}(0) &= 0
 \end{aligned}
 \tag{208}$$

give nontrivial solution.

Let us stress here that the chosen initial conditions just allow us to formulate a simple problem to solve and to obtain the effect in order of magnitude, i.e., to obtain a representative result. That is the first step of the investigation. In future works, we are going to approach step-by-step more close to the real physics conditions.

It is important to note that there are poles at $a^4 = 16B_0^2C_0$ in the first equation. Let us remind the reader that the effective Heisenberg–Euler action Equation (32) is correct under the assumption of a weak external electromagnetic field. In our case, that means that $B_0/a^2 \ll m_e^2$. This restriction is valid in the selected interval of the variation of the scale factor: $a \in [10^{-9}, 10^{-4}]$. Indeed, for $B_0 = 1$ nGs inside the interval for the scale factor we obtain

$$B \in [10, 10^9] \text{Gs} = [1.95 \times 10^{-13}, 1.95 \times 10^{-3}] \text{MeV}^2.
 \tag{209}$$

All the values are less than the electron mass squared $m_e^2 \approx 0.25 \text{MeV}^2$. Using the definition (33), we can rewrite the term proportional to $B_0^2C_0/a^4$ as:

$$\frac{C_0B_0^2}{a^4} = \frac{\alpha^2}{90m_e^4}B^2.
 \tag{210}$$

On the other hand, we have shown that $B \ll m_e^2$ in the whole interval of solution variation. Therefore, after squaring and multiplying by $\alpha^2/90 \ll 1$, the condition remains the same

$$\frac{\alpha^2}{90m_e^4}B^2 \ll 1,
 \tag{211}$$

and means that the correction to the Maxwell action proportional to α^2 is sufficiently accurate for our consideration.

Another important question to be solved in future work is to what minimum value of the scale factor should the solution be expanded? The solution to this question should be sought in the theories of cosmological magnetogenesis, that study the epoch when the cosmological magnetic field was generated. We should also keep in mind that as the scale factor approaches the pole, higher order corrections will be excited [17], thereby removing any potential pole.

The second subsystem, which involves the quantities $\{\Phi, \Psi, f^y, h_{\times}\}$, is larger, more complex and requires solving many sub-problems. For example, the question of whether scalar metric perturbations propagate is quite nontrivial and requires careful analysis. In order to steer the article away from becoming excessively cumbersome, in this work we will concentrate on solving only the subsystem $\{f^x, h_{\times}\}$.

In order to numerically solve the system, we need to divide both parts of the equation by a^2H^2 and to introduce two new functions to lower the order of the equation in order to make it look like: $y' = f(x, y)$.

Two new functions and a system 4×4 to be solved:

$$f^{x'} = v_{f_x},
 \tag{212}$$

$$h'_{\times} = v_{h_{\times}},
 \tag{213}$$

$$\begin{aligned}
 f^x : v'_{f_x} &= -\frac{1}{a} \left[1 + a \frac{H'}{H} + 8 \frac{2B_0^2 C_0 - a^4}{16B_0^2 C_0 - a^4} + aH\Gamma \right] v_{f_x} + \frac{\alpha\beta}{a^2} (af^{x'} + 2f^x) \\
 &\quad - \frac{1}{a^2 H^2} \left[\frac{k^2}{a^2} + 2aHH' - 8H^2 \frac{4B_0^2 C_0 + a^4}{16B_0^2 C_0 - a^4} + 2\Gamma H + \omega_{pl}^2 \right] f^x - \frac{ikB_0}{a^6 H^2 m_{pl}} h_{\times} \\
 h_x^y : v'_{h_x} &= -\frac{(4aH^2 + a^2 HH')}{a^2 H^2} v_{h_x} - \frac{1}{a^2 H^2} \left[\frac{k^2}{a^2} + \frac{16\pi GB_0^2}{a^4} \left(1 - \frac{4B_0^2 C_0}{a^4} \right) \right] h_{\times} \\
 &\quad - \frac{16\pi GB_0 ik}{a^2} \left(1 - \frac{16B_0^2 C_0}{a^4} \right) \frac{m_{pl} f^x}{a^2 H^2}
 \end{aligned} \tag{214}$$

We use fifth-order implicit Runge–Kutta method, which is algebraically stable and allows solving stiff systems of differential equations, for more details see [35].

9.1. Method of Solution Validation

Before solving the system for a non-zero magnetic field strength, we must check whether the method for the SoDE solving works correctly for the case when it is absent. Equation of motion for tensor gravitational waves in the approximation $k\eta \sim 1$, where $\eta(t) = \int \frac{dt}{a(t)}$ is a conformal time, can be solved analytically. The solution has the form

$$h(\eta) = h_{init} \frac{\sin(k\eta + \phi_0)}{k\eta}, \tag{215}$$

where h_{init} is an initial magnitude of tensor perturbation, and ϕ_0 is a constant phase. The last two parameters are defined from the matching with the constant mode, obtained from the EoM solution in the approximation $k\eta \ll 0$ (see Section 3.2 in Ref. [15]).

In Figure 1a, the numerical and analytical solutions are presented for the two conformal time values $\eta_1 = 13.2, \eta_2 = 105.6$ and corresponding to them frequencies $k_1 = 0.076, k_2 = 0.0095$ Hz satisfying the condition $k\eta \sim 1$.

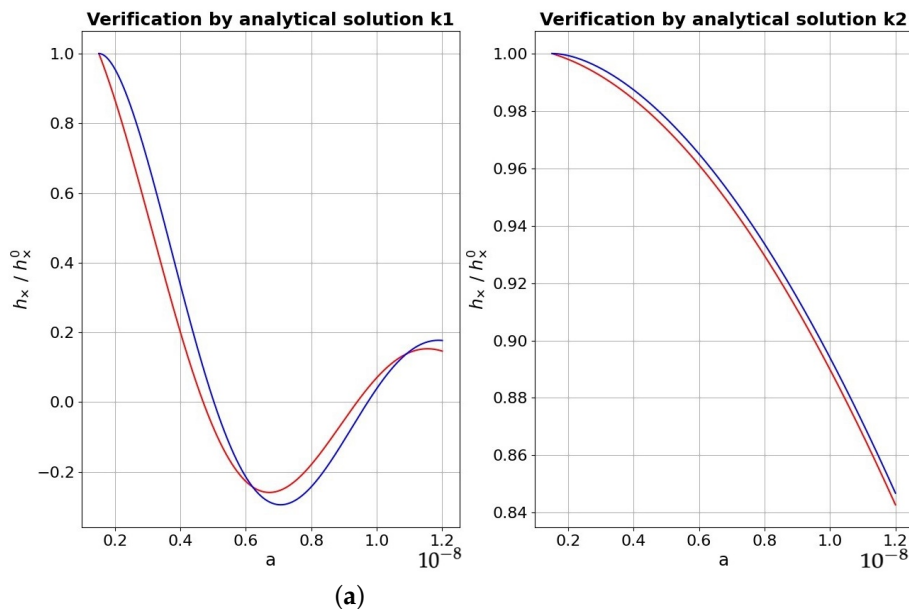


Figure 1. Cont.

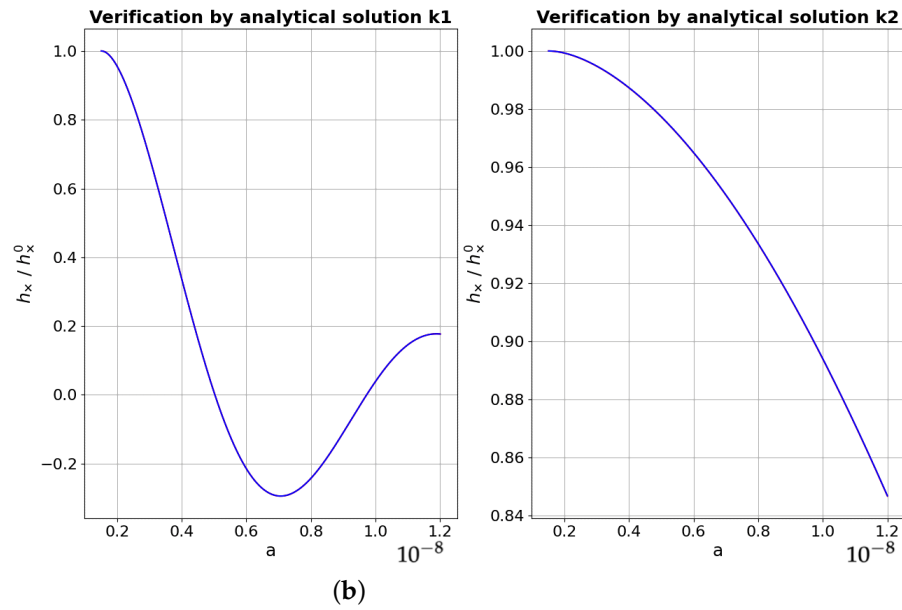


Figure 1. Verification of the numerical solution (blue line) by the analytical solution (red line) for two frequencies k_1 (left) and k_2 (right). (a) without phases; (b) with phases.

Here, we see a significant discrepancy, but after the correct phase selections, $\phi_0^1 = -0.22, \phi_0^2 = -0.00065$, we obtain a coincidence with an accuracy of four orders of magnitude (Figures 1b and 2). In Figure 2, an absolute difference between the numerical and the analytical solutions is presented for the two considered cases.

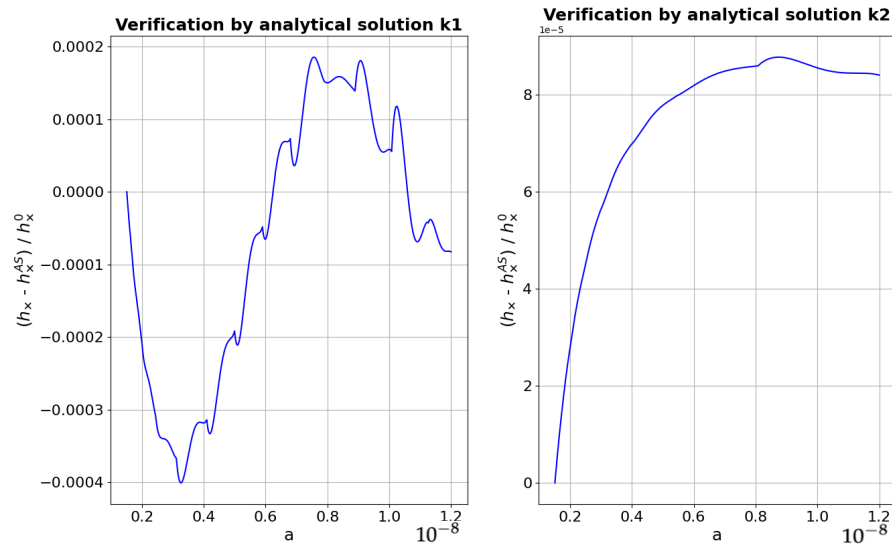


Figure 2. Absolute difference between the numerical solution and the analytical solution for two frequencies k_1 (left) and k_2 (right).

Eventually, we can conclude that the method of numerical solution works correctly, and the results obtained for a non-zero value of magnetic field strength are reliable.

9.2. Numerical Solution Results for the System $\{\mathbf{h}_x, \mathbf{f}^x\}$

Let us present the numerical solution results for the system of Equation (207) with the initial conditions according to the Equation (208). The code was written in Python using the solve-ivp package.

Of particular interest in the long-wave range are the wavelengths that have left their mark on the CMB. We found a solution for frequencies 10^{-18} – 10^{-16} Hz. We use an implicit

Runge–Kutta method of order five to solve the SoDE for $B_0 = 1$ nGs and for these frequencies. The scale factor interval is $[10^{-9}, 10^{-4}]$, and it lies within the radiation dominance (RD) epoch. For comparison, a solution to the system in the absence of a magnetic field was also found.

The results are as follows: by the end of the RD era, amplitude of GW with the selected frequencies is suppressed by about 0.01 percent. Thus, we can conclude that the considered effect of converting GWs into photons in a cosmological magnetic field has an extremely small effect on the amplitude of long-wavelength relic GWs.

It is instructive to say a few words about the physical reason for the suppression of the GW amplitude. In the problem we are considering, where the magnetic field is still not strong enough, the main contribution to the damping comes from the classical Maxwell action. Neglecting the loop correction in the equation of motion for the metric perturbation h_x^y in Equation (207), we obtain the second term in the brackets $\left[\frac{k^2}{a^2} + \frac{16\pi G B_0^2}{a^4} \right] h_x$, which works similarly to the plasma frequency for photons propagating in the plasma [36]. This term suppresses the low frequency end of the GW spectrum. Indeed, for the quantities $B_0 = 1$ nGs, $a_1 = 10^{-9}$ we obtain for the boundary value of the momentum less than the above mentioned analogue of the plasma frequency for GW:

$$k \lesssim \frac{\sqrt{16\pi} B_0}{m_{pl} a} \approx \frac{\sqrt{16\pi} 10^{-9} \times 1.95 \times 10^{-14} \text{ MeV}^2}{2.43 \times 10^{21} \text{ MeV} \times 10^{-9}} \approx \frac{5.7 \times 10^{-29} \text{ eV}}{6.6 \times 10^{-16} \text{ eV}^* \text{s}} \approx 10^{-13} \text{ Hz}. \quad (216)$$

10. Discussion

In the presented work, we have derived a coupled system of equations for gravitational and electromagnetic wave propagation in an external magnetic field. Subsequently, simplification of the differential equation system was performed for the FLRW background metric and for the case of homogeneous magnetic field directed perpendicularly to the initial gravitational wave vector. Finally, we have solved the system numerically for h_x —polarization putting $B_0 = 1$ nGs. The resulting estimate of the effect, without taking into account the inhomogeneity of the magnetic field, is about 0.01% suppression of the amplitude for a relic GW with a frequency of 10^{-18} Hz at the recombination.

It is worth noting that the results are obtained under a large list of simplifying assumptions and the research demands a deeper investigation (for example, the assumption about the magnetic field homogeneity is rather crude). Despite this, the results make sense and one can conclude that the considered phenomenon of GW conversion into photons in the intergalactic magnetic field cannot significantly suppress relic gravitational wave amplitude.

Let us emphasize that this result was not obvious at the beginning of the research. The smallness of the second-order corrections to the Maxwell action does not yet infer the smallness of the relic GW suppression effect. It is also necessary to take into account the interaction of the energy generated by GW photons with the primordial plasma, as well as the fact that the conversion occurs over a long period of time during the evolution of the Universe. A crucial point is also the dependence of the cosmological magnetic field amplitude on the scale factor according to the law $B = B_0/a^2$, which in the early stages of the evolution of the Universe could lead to a rather high magnetic field strength, and therefore to a noticeable conversion effect.

In future works, we plan to solve the second independent part of the SoDE, paying special attention to the following question: do the emerged scalar perturbations run? Subsequently, we want to expand the solution interval up to the end of the matter dominance epoch and to account for the magnetic field inhomogeneity.

It is worth stressing that the stochastic nature of the relic GW direction and the magnetic field direction should have a large impact on the magnitude of the suppression effect, and a more accurate analysis of this phenomenon is also very important. We plan to

perform such an analysis in order to present quantitatively the dependence of the full relic GW spectrum suppression on the intergalactic magnetic field strength.

Future research is not only of academic interest, but can also be applied to similar problems of converting gravitational waves into photons near astrophysical sources of strong magnetic fields. Of course, the background metric must be modified to suit the specific task conditions, but the inference structure and some of the qualitative findings discussed in this manuscript will remain valid and useful. In addition, the accuracy of future measurements of CMB polarization [37] will steadily increase, and may reach values of the order of the considered effect.

Author Contributions: Conceptualization, A.D.D.; methodology, A.D.D. and L.A.P.; software, L.A.P.; validation, A.D.D., L.A.P. and V.A.B.; formal analysis, L.A.P. and V.A.B.; investigation, A.D.D. and L.A.P.; writing—original draft preparation, L.A.P.; writing—review and editing, A.D.D. and V.A.B.; visualization, L.A.P.; supervision, A.D.D.; project administration, A.D.D.; funding acquisition, A.D.D. All authors have read and agreed to the published version of the manuscript.

Funding: The work was supported by the RSF grant number 23-42-00066.

Data Availability Statement: No new data were created or analysed in this study. Data sharing is not applicable to this article.

Conflicts of Interest: The authors declare no conflicts of interest. The funders had no role in the writing of the manuscript; or in the decision to publish the results.

Abbreviations

The following abbreviations are used in this manuscript:

GW	Gravitational Wave
FLRW space-time	Friedman–LeMaitre–Robertson–Walker space-time
EMT	Energy–Momentum Tensor
EMW	Electromagnetic Wave
HE Lagrangian	Heisenberg–Euler Lagrangian
SoDE	System of Differential Equations
EoM	Equation of Motion

References

- Gertsenshtein, M.E. Wave Resonance of Light and Gravitational Waves. *Zh. Eksp. Teor. Fiz.* **1961**, *41*, 113; Erratum in *Sov. Phys. JETP* **1960**, *14*, 84.
- Mitskevich, N.V. *Physical Fields in General Relativity*; Nauka: Moscow, Russia, 1970.
- Boccaletti, D.; De Sabbata, V.; Fortini, P.; Gualdi, C. Space-Time Curvature Mode Quanta. *Nuovo C.* **1970**, *70*, 129–146. [CrossRef]
- Dubrovich, V.K. Izvestiya Spetsial'noj Astroficheskoy Observatorii. *Zel'dovich Zh. Eksp. Teor. Fiz.* **1972**, *65*, 1311.
- Zel'dovich, Y.B. Electromagnetic and gravitational waves in a stationary magnetic field. *Zh. Eksp. Teor. Fiz.* **1973**, *65*, 1311; Erratum in *Sov. Phys. JETP* **1974**, *38*, 652.
- Fargion, D. *Gravitation and Cosmology*; Pleiades Publishing: New York, NY, USA, 1995; Volume 1, pp. 301–310.
- Raffelt, G.; Stodolsky, L. Mixing of the Photon with Low Mass Particles. *Phys. Rev. D* **1988**, *37*, 1237. [CrossRef] [PubMed]
- Dolgov, A.D.; Ejlli, D. Conversion of relic gravitational waves into photons in cosmological magnetic fields. *J. Cosmol. Astropart. Phys.* **2012**, *12*, 3. [CrossRef]
- Linde, A.D. Inflationary cosmology. *Phys. Rep.* **2000**, *333*, 17.
- Grishchuk, L.P. Amplification of gravitational waves in an isotropic universe. *Zh. Eksp. Teor. Fiz.* **1974**, *67*, 825; Erratum in *Sov. Phys. JETP* **1975**, *40*, 409.
- Lifshitz, E.M. On the gravitational stability of the expanding universe. *Zh. Eksp. Teor. Phys.* **1946**, *15*, 587.
- Lifshitz, E.M.; Khalatnikov, I.M. Problems of relativistic cosmology. *Uspekhi Fiz. Nauk* **1963**, *80*, 391. [CrossRef]
- Dolgov, A.D.; Ejlli, D. Resonant high energy graviton to photon conversion at post recombination epoch. *Phys. Rev. D* **2013**, *87*, 104007. [CrossRef]
- Misner, C.W.; Thorne, K.S.; Wheeler, J.A. *Gravitation*; Freeman and Company: San Francisco, CA, USA, 1973.
- Gorbunov, D.S.; Rubakov, V.A. *Introduction to the Theory of the Early Universe: Cosmological Perturbations and Inflationary Theory*; World Scientific: Hackensack, NJ, USA, 2011.
- Arbuzova, E.V.; Dolgov, A.D.; Panasenko, L.A. On graviton propagation in curved spacetime background. *J. Exp. Theor. Phys.* **2022**, *135*, 304–311. [CrossRef]

17. Heisenberg, W.; Euler, H. Folgerungen aus der Diracschen Theorie des Positrons. In *Zeitschrift für Physik*; Springer: Berlin/Heidelberg, Germany, 1936; Volume 98, pp. 714–732.
18. Fanizza, G.; Gasperini, M.; Pavone, E.; Tedesco, L. Linearized propagation equations for metric fluctuations in a general (non-vacuum) background geometry. *J. Cosmol. Astropart. Phys.* **2021**, *7*, 21. [CrossRef]
19. Maggiore, M. *Gravitational Waves: Theory and Experiments*; Oxford University Press: Oxford, UK, 2008; Volume 1.
20. Maggiore, M. *Gravitational Waves: Astrophysics and Cosmology*; Oxford University Press: Oxford, UK, 2018; Volume 2.
21. Mukhanov, V. *Physical Foundations of Cosmology*; Cambridge University Press: New York, NY, USA, 2005.
22. Weinberg, S. *Cosmology*; Oxford University Press: Oxford, UK, 2008.
23. Weinberg, S. *Gravitation and Cosmology: Principles and Applications of the General Theory of Relativity*; Wiley: Hoboken, NJ, USA, 1972.
24. Landau, L.D.; Lifshitz, E.M. *The Classical Theory of Fields*; Pergamon Press: New York, NY, USA, 1971; Volume 2
25. Duff, M.J. Twenty Years of the Weyl Anomaly. *Class. Quant. Grav.* **1994**, *11*, 1387. [CrossRef]
26. Bunch, T.S.; Davies, P.C.W. Stress Tensor and Conformal Anomalies for Massless Fields in a Robertson-Walker Universe. *Proc. R. Soc. Lond.* **1978**, *360*, 117.
27. Birrell, D.N.; Davies, P.C.W. *Quantum Fields in Curved Space*; Cambridge University Press: Cambridge, UK, 1982.
28. Dolgov, A.D. Conformal Anomaly and the Production of Massless Particles by a Conformally Flat Metric. *Sov. Phys. JETP* **1981**, *54*, 223; Erratum in *Zh. Eksp. Teor. Fiz.* **1981**, *81*, 417.
29. Dolgov, A.D. Breaking of conformal invariance and electromagnetic field generation in the universe. *Phys. Rev. D* **1993**, *48*, 2499–2501. [CrossRef]
30. Parker, L. Particle creation in expanding universes. *Phys. Rev. Lett.* **1968**, *21*, 562. [CrossRef]
31. Pitaevskii, L.P.; Lifshitz, E.M. *Physical Kinetic*; International Atomic Energy Agency: Vienna, Austria, 2012; Volume 10, ch. III
32. Kraemmer, U.; Rebhan, A.K.; Schulz, H. Resummations in Hot Scalar Electrodynamics. *Ann. Phys.* **1995**, *238*, 286. [CrossRef]
33. Dolgov, A.D.; Lepidi, A.; Piccinelli, G. Electrodynamics at non-zero temperature, chemical potential, and Bose condensate. *J. Cosmol. Astropart. Phys.* **2008**, *902*, 27. [CrossRef]
34. Barrow, J.D.; Ferreira, P.G.; Silk, J. Constraints on a Primordial Magnetic Field. *Phys. Rev. Lett.* **1997**, *78*, 3610. [CrossRef]
35. Burrage, K.; Butcher, J.C. Stability Criteria for Implicit Runge–Kutta Methods. *SIAM J. Numer. Anal.* **1979**, *16*, 46–57. [CrossRef]
36. Dolgov, A.D.; Postnov, K. Electromagnetic radiation accompanying gravitational waves. from black hole binaries. *J. Cosmol. Astropart. Phys.* **2017**, *9*, 18. [CrossRef]
37. Planck Collaboration. Planck 2018 results. VI. Cosmological parameters. *Astron. Astrophys.* **2020**, *641*, A6. [CrossRef]

Disclaimer/Publisher’s Note: The statements, opinions and data contained in all publications are solely those of the individual author(s) and contributor(s) and not of MDPI and/or the editor(s). MDPI and/or the editor(s) disclaim responsibility for any injury to people or property resulting from any ideas, methods, instructions or products referred to in the content.

Article

Nonrelativistic Quantum Mechanical Problem for the Cornell Potential in Lobachevsky Space

Laszlo Jenkovszky ¹, Yurii Andreevich Kurochkin ^{2,*}, N. D. Shaikovskaya ² and Vladimir Olegovich Soloviev ³

¹ Bogolyubov Institute for Theoretical Physics, National Academy of Sciences of Ukraine, Metrolohichna Str. 14b, 03143 Kiev, Ukraine; jenk@bitp.kiev.ua

² B.I. Stepanov Institute of Physics, National Academy of Sciences of Belarus, 68-2 Niezaliežnasci Av., 220072 Minsk, Belarus; n.shaikovskaya@dragon.bas-net.by

³ A.A. Logunov Institute for High Energy Physics, National Research Center Kurchatov Institute, Ploschad' Nauki, 1, 142281 Protvino, Russia; vladimir.soloviev@ihep.ru

* Correspondence: y.kurochkin@ifanbel.bas-net.by

Abstract: In Friedmann–Lobachevsky space-time with a radius of curvature slowly varying over time, we study numerically the problem of motion of a particle moving in the Cornell potential. The mass of the particle is taken to be a reduced mass of the charmonium system. In contrast to the similar problem in flat space, in Lobachevsky space the Cornell potential has a finite depth and, as a consequence, the number of bound states of the system is finite and motion with a continuum energy spectrum is also possible. In this paper, we study the bound states as well as the scattering states of the system.

Keywords: Cornell potential; Lobachevsky space; Friedmann universe; stationary bound states

PACS: 03.65.-w; 03.65.Ge; 02.40.Ky



Citation: Jenkovszky, L.; Kurochkin, Y.A.; Shaikovskaya, N.D.; Soloviev, V.O. Nonrelativistic Quantum Mechanical Problem for the Cornell Potential in Lobachevsky Space. *Universe* **2024**, *10*, 76. <https://doi.org/10.3390/universe10020076>

Academic Editor: Sergey V. Sushkov, Galina L. Klimchitskaya and Vladimir M. Mostepanenko

Received: 5 December 2023

Revised: 26 January 2024

Accepted: 28 January 2024

Published: 5 February 2024



Copyright: © 2024 by the authors. Licensee MDPI, Basel, Switzerland. This article is an open access article distributed under the terms and conditions of the Creative Commons Attribution (CC BY) license (<https://creativecommons.org/licenses/by/4.0/>).

1. Introduction

The centennial anniversary of the publication of the seminal paper by A.A. Friedmann [1], followed by related publications [2–4], motivated the present discussion on the role of geometrical ideas in particle physics and cosmology.

During 1922–1924, A. Friedmann derived his celebrated dynamical equations for the universe. Many details from Friedmann's biography can be found in the book [5]. He started from the General Relativity equations with arbitrary cosmological “constant” and opened the way to building models of a non-stationary universe. The non-stationary nature of the universe was brilliantly confirmed in astronomical observations by Hubble. Following Friedmann, a large number of models of the expanding universe were suggested (see, e.g., [6–8]).

In the beginning of the quark hypothesis of particle structure, composite models based on non-relativistic problems for various potentials demonstrated their effectiveness. Within the framework of that approach, the mass spectra of a number of mesons and hadrons and some of their static characteristics were successfully described. Examples of the use of such models are given in reviews [9–11]. In approaches in which particles are considered as consisting of quarks, a special role belongs to the Cornell potential, which ensures confinement of quarks (see, for example, [12]). As far as we know, the quantum-mechanical problem of a particle moving in the Cornell potential in Lobachevsky space has not yet been discussed in the literature, although coupled systems like the *b*-meson have been studied in a number of papers [13,14].

Now, more than 100 years after the creation of General Relativity, we may ask ourselves: what is its most unexpected and surprising prediction? There is no doubt that the answer should be the theory of an expanding universe, created by Alexander Friedmann [1–3].

This was also a triumph of non-Euclidean geometry, as proposed by J. Bolyai, C. F. Gauss, N. I. Lobachevsky (BGL), developed by Bernhard Riemann, and extended by Hermann Minkowski in a space-time manifold.

About 30 years later, George Gamow wrote in his book [15] “The Creation of the Universe”:

... the Russian mathematician A. Friedmann pointed out that the static nature of Einstein’s universe was the result of an algebraic mistake (essentially a division by zero) made in the process of its derivation. Friedmann then went on to show that the correct treatment of Einstein’s basic equations leads to a class of expanding and contracting universes...

In 1965, Erast B. Gliner [16] assumed that the pressure in Einstein–Friedmann equations for the very early universe is proportional to the energy density with a negative sign. This unusual relation between pressure and energy density was the first theoretical prediction of dark energy, now confirmed by observations. In subsequent papers [17,18], he found an exponentially increasing solution of these equations contributing to the development of cosmology with a rapid expansion phase, followed by a large number of inflationary cosmological models.

Simultaneously and independently of Gliner, a related activity preceding numerous papers on inflation took place in Kiev. The common feature in these papers was the exponential expansion of the universe, now called inflation, provided by negative pressure in the equation of state $p(T)$.

The relevant derivation is simple. In Friedmann’s homogeneous, isotropic and flat universe the scale factor ρ obeys the equations

$$\dot{\rho} - G\rho\sqrt{\epsilon} = 0, \tag{1}$$

$$\dot{\epsilon} + 3\dot{\rho}/\rho(\epsilon + p) = 0, \tag{2}$$

where p is pressure and $G = \sqrt{8\pi/3}/M_p$. From Equations (1) and (2),

$$\ddot{\rho} = -G^2\rho(\epsilon + 3p)/2 \tag{3}$$

follows, whence $3p + \epsilon < 0$ for inflationary solutions. As energy density is positive, the above inequality produces inflation only at negative pressure [19].

Historically, this was predicted in [7] from an equation of state of strongly interacting (nuclear) matter derived [7] in the framework of the S matrix formulation of statistical mechanics. It is interesting by itself and may have interesting consequences in nuclear and particle physics. Inflation resulting from this minimum was a bonus [19].

Here, several comments are in order. First, the rate of this kind of inflation is modest with respect to the popular scenarios. For this reason, it was also called [20,21] “tepid” compared to the alternative violent expansion. Furthermore, it may have occurred later with respect to those based on the Standard Theory. One cannot exclude a sequence of inflations of the early universe. The above “nuclear” one was the latest in time and it may have washed away the footprints of the earlier ones.

2. Quark–Antiquark Bound States in Lobachevsky Space

Einstein’s famous work [22], in which he introduced the cosmological constant and obtained the first cosmological solution, was the impetus for further research in the theory of relativity, quantum mechanics and theory for non-relativistic particles moving in curved spaces [23–30].

We will consider Friedmann-Lobachevsky space-time based on the assumption that the curvature radius $\rho(t)$ changes very slowly in time, and is considered as being constant, in particular, as it is in Einstein’s solution [22]. Taking into account the uncertainty of the

right side of Equation (3), we accept the assumption for a period of time δt satisfying the inequality $\rho'(t_0)\delta t \ll \rho(t_0)$ or $\delta t \ll H^{-1}$, where H is Hubble constant [31].

The Schrödinger equation for stationary states in Lobachevsky space with curvature radius ρ in spherical coordinates,

$$\begin{aligned} x_0 &= \rho \cosh \beta; & x_1 &= \rho \sinh \beta \sin \theta \cos \phi; \\ x_2 &= \rho \sinh \beta \sin \theta \sin \phi; & x_3 &= \rho \sinh \beta \cos \theta; \\ 0 &\leq \beta < \infty; & 0 &\leq \theta \leq \pi; & 0 &\leq \phi \leq 2\pi, \end{aligned} \tag{4}$$

has the form

$$-\frac{\hbar}{2m} \left(\frac{1}{\rho^2 \sinh^2 \beta} \frac{\partial}{\partial \beta} \left(\sinh^2 \beta \frac{\partial}{\partial \beta} \right) + \frac{1}{\rho^2 \sinh^2 \beta} \Delta_{\theta, \phi} \right) \psi + V\psi = E\psi, \tag{5}$$

where $\beta = r/\rho$.

Here, we use the embedding of Lobachevsky space into a four-dimensional pseudo-Euclidean space, in which the rectangular coordinates $x_\mu, \mu = 1, 2, 3, 4$ are introduced, and for points in Lobachevsky space the equality

$$x_\mu x_\mu = \mathbf{x}^2 + x_4^2 = \mathbf{x}^2 - x_0^2 = -\rho^2, \quad \mathbf{x} = (x_1, x_2, x_3), \quad x_4 = ix_0 \tag{6}$$

is valid.

In the case of a central symmetric potential $V = V(r)$, Equation (5) can be reduced to

$$-\frac{1}{2} \frac{d^2 u}{dr^2} + V_{eff}(r)u = \epsilon u, \tag{7}$$

where the effective potential is

$$V_{eff}(r) = mV(r) + \frac{l(l+1)}{2\rho^2 \sinh^2(r/\rho)} + \frac{1}{2\rho^2}, \tag{8}$$

and $\epsilon = mE$.

In this case, the wavefunction is written in terms of $u(r)$ and the spherical harmonics as

$$\psi(r, \theta, \phi) = \frac{u(r)}{\sinh(r/\rho)} Y_{lm}(\theta, \phi). \tag{9}$$

Here, a rational system of units has been chosen, in which $c = \hbar = 1$ and all physical quantities have units of measurement of powers of mass—namely, $(GeV)^a$, wherein $[r] = [\rho] = GeV^{-1}, [m] = GeV, [V(r)] = [E] = GeV, [\epsilon] = [V_{eff}] = GeV^2$.

Let us consider the motion of a particle whose mass is equal to the reduced mass of two c quarks (a system of a c quark and its anti-quark is called charmonium)—that is, let us take $m = 0.635 GeV$. Assume that such a particle moves in a field in which its potential energy is described by the Cornell potential, the expression for which in Lobachevsky space has the form

$$V(r) = \frac{a}{\rho} \coth \frac{r}{\rho} + b\rho \tanh \frac{r}{\rho}. \tag{10}$$

Note that the choice of the Cornell potential is generally ambiguous. We proceeded from the fact that the first term is a fundamental solution of the Laplace–Beltrami equation in three-dimensional Lobachevsky space, and we sought to preserve the symmetry inherent in the flat limit of this potential. In Formula (10), the first term corresponds to the Coulomb attraction and the second to the linearly increasing potential in flat space.

For parameters a and b we take the following values [11]:

$$a = -0.52; \quad b = 0.18 GeV^2.$$

In Lobachevsky space, the depth of the well of the effective potential is finite and it depends on the orbital quantum number l and the radius of curvature ρ . As l increases (keeping ρ constant) the well becomes more and more shallow, and at some high-enough value of l it disappears: no bound states are possible. On the contrary, as we increase ρ and keep l unchanged, the well becomes deeper and we can have more bound states. In the limit when $\rho \rightarrow \infty$ we are back to the flat space with an infinite number of bound states. The Cornell potential formula in Lobachevsky space also leads to that of the flat space in this limit. When ρ is small enough (which corresponds to the high curvature of the space, as it is supposed to take place in the early universe) the well again disappears and we do not have bound states. As the curvature radius increases in time (Friedmann’s solution for the open-universe model) a particle moving in the Cornell potential at first has no bound states; then, it has a larger and larger finite number of bound states and, as ρ approaches infinity (flat space), all states become bound.

When $r \rightarrow 0$ the asymptotic behavior of the solution to Equation (7) is

$$u \sim (\tanh (r / \rho))^{l+1}. \tag{11}$$

Indeed, at $r \rightarrow 0$ centrifugal energy makes the greatest contribution to the equation and the approximate equation has the form

$$-\frac{d^2 u}{d\beta^2} + \frac{l(l+1)}{\sinh^2(\beta)} u = 0.$$

The last equation has the following solution that is regular at zero:

$$u = (\tanh \beta)^{l+1} {}_2F_1\left(1 + \frac{l}{2}, \frac{1}{2} + \frac{l}{2}, \frac{3}{2} + l, \tanh^2 \beta\right) \approx (\tanh \beta)^{l+1}.$$

We will study Equation (7) using numerical methods: namely, we will find the energies of bound states. To do so, we apply the shooting method, at each step of which the differential Equation (7) is numerically solved under initial conditions specified by the asymptotic expressions

$$u(r_0) = [\tanh (r_0 / \rho)]^{l+1}; \quad u'(r_0) = \frac{(l+1)[\tanh (r_0 / \rho)]^l}{\rho \cosh^2 (r_0 / \rho)}, \tag{12}$$

where $r_0 = 0.001 GeV^{-1}$ —variable value close to zero.

Figure 1 shows a plot of the effective interaction potential at $\rho = 8 GeV^{-1}, l = 1$.

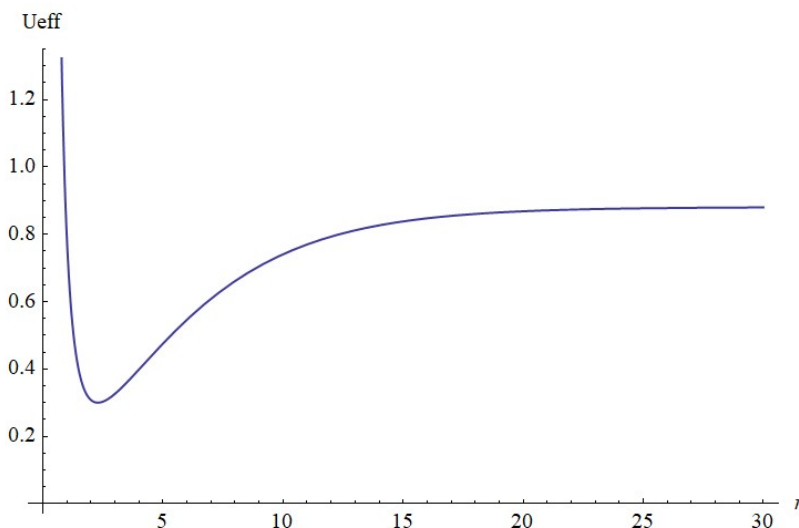


Figure 1. Effective potential plot.

It can be seen that in Lobachevsky space the effective interaction potential has the form of a potential well of finite depth, whereas in flat space for the Cornell potential we have an infinitely deep potential well. Let us denote

$$\epsilon_{max} = \lim_{r \rightarrow \infty} V_{eff}(r) = m \left(\frac{a}{\rho} + b\rho \right) + \frac{1}{2\rho^2}. \tag{13}$$

While scattering prevails at energies higher than ϵ_{max}/m , bound states are possible at lower energies.

Figure 2 shows numerical solutions for bound states and their corresponding energy levels for $\rho = 8\text{GeV}^{-1}$, $l = 1$. In this case, there are only four bound states.

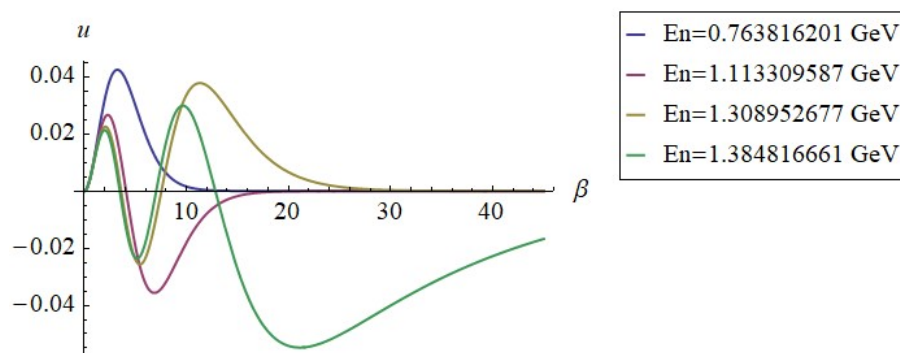


Figure 2. Numerical solutions for the bound states and corresponding energy levels.

As the depth of the well increases with increasing ρ and decreases with increasing l , we can expect that the number of bound states will be greater for the larger values of ρ and the smaller values of l . Figure 3 shows the results of the numerical calculation of the number of bound states for different values of ρ and l .

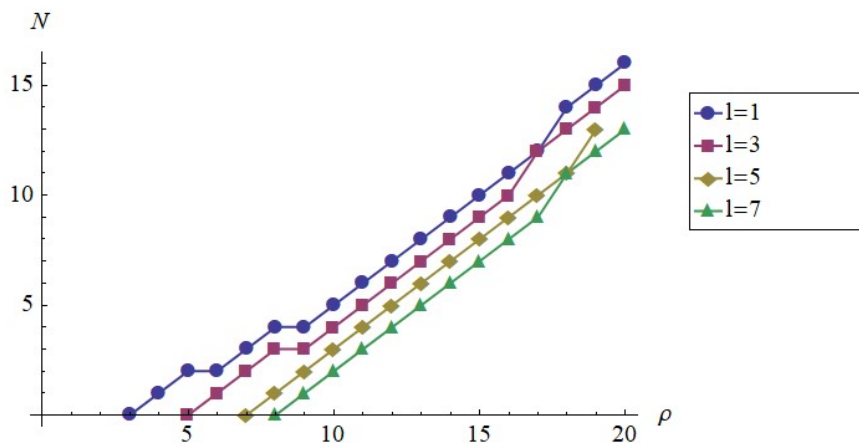


Figure 3. Number of bound states.

Using the numerically calculated values of energy levels at different l , Regge trajectories are constructed at $\rho = 10\text{GeV}^{-1}$ (see Figure 4). Here, we use the same approach as in [32,33]. It can be seen from the figure that as l increases the number of bound states decreases.

It should be noted that the above Regge trajectories differ from those resulting from analyticity and duality [34]. While the above are convex up and infinitely rising, those based on analyticity, unitarity and duality are concave down, with limited real parts, predicting a finite number of resonances (see [34]).

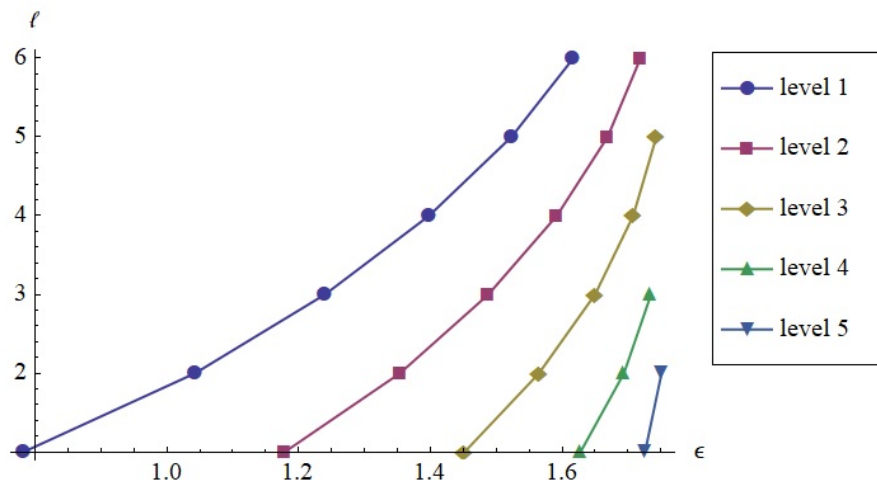


Figure 4. Regge trajectories.

3. Scattering in the Cornell Potential

Now, we consider the case when the particle energy exceeds the value ϵ_{max}/m (the case of scattering) and we determine the phase shifts $\delta_l(E)$ for given values of energy E and orbital quantum number l .

To do this, it is necessary to compare the numerical solution of Equation (7) at the end of the calculation segment with the solution of the approximate equation for $r \rightarrow \infty$. The approximate equation is

$$\frac{d^2u}{dr^2} + 2(\epsilon - \epsilon_{max})u = 0,$$

where ϵ_{max} is given by the Formula (13). In the case of scattering $\epsilon > \epsilon_{max}$ and under initial conditions (12), it has a solution of the form

$$u \sim \sin(\sqrt{2(\epsilon - \epsilon_{max})}r).$$

For the numerical solution of Equation (7), we will choose an interval from $r_0 = 0.001 GeV^{-1}$ to r_k , which is several times larger than r_c , where r_c is the distance from the origin at which $V_{eff}(x) \approx \epsilon_{max}$ with a given accuracy (we took $\Delta = |V - \epsilon_{max}| = 10^{-6} GeV^2$). Then, the numerical solution of Equation (7) under the same initial conditions (12) at the end of the computational segment will have the form

$$u \sim \sin(\sqrt{2(\epsilon - \epsilon_{max})}r + \delta_l(\epsilon)).$$

The phase shift can be determined from the numerical solutions as

$$\delta_l(\epsilon) = \sqrt{2(\epsilon - \epsilon_{max})}(r_{1max} - r_{2max}),$$

where r_{1max} and r_{2max} are the positions of the maxima in the last period of the first and second solutions, respectively. The integral partial cross-section is then determined by the formula

$$\sigma_l = \frac{4\pi}{(2\epsilon)}(2l + 1) \sin^2(\delta_l(\epsilon)), \tag{14}$$

Because in the selected units of measurement, $k^2 = 2\epsilon$. Figures 5 and 6 show the dependence of partial cross-sections on energy at $\rho = 10 GeV^{-1}$ for $l = 0$ and $l = 1$.

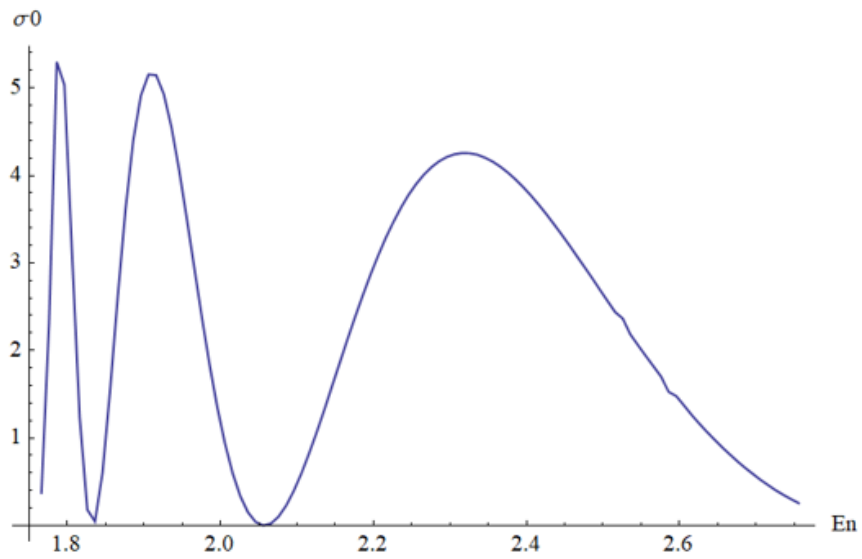


Figure 5. Partial cross-section $\sigma_0(E)$.

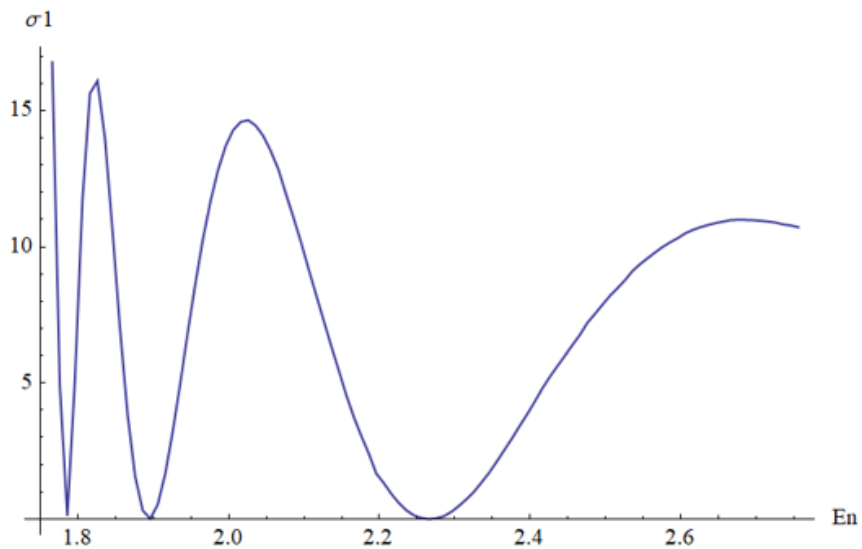


Figure 6. Partial cross-section $\sigma_1(E)$.

Let us also consider the case of low-energy scattering at $l = 0$. Let us study the dependence of the scattering length on the radius of curvature of Lobachevsky space. For each value of the radius of curvature, we will take an energy only slightly exceeding ϵ/m (we took $E = \epsilon/m + 0.01\text{GeV}$), which meets the condition $E \rightarrow \epsilon/m$. These values are different for different ρ (the energy that can be considered as “low” depends on the radius of curvature, i.e., it depends on the shape of the potential). Then, having determined the cross-section, using Formula (14), we find the scattering length as $L = \sqrt{\sigma_0/(4\pi)}$ and we study the dependence $L(\rho)$ (see Figure 7).

We see that the length of scattering varies significantly with the varying radius of curvature. For example, at $\rho \approx 2\text{GeV}^{-1}$ the low-energy scattering cross-section reaches its maximum, while at $\rho \approx 3.5\text{GeV}^{-1}$ it is zero (no scattering).

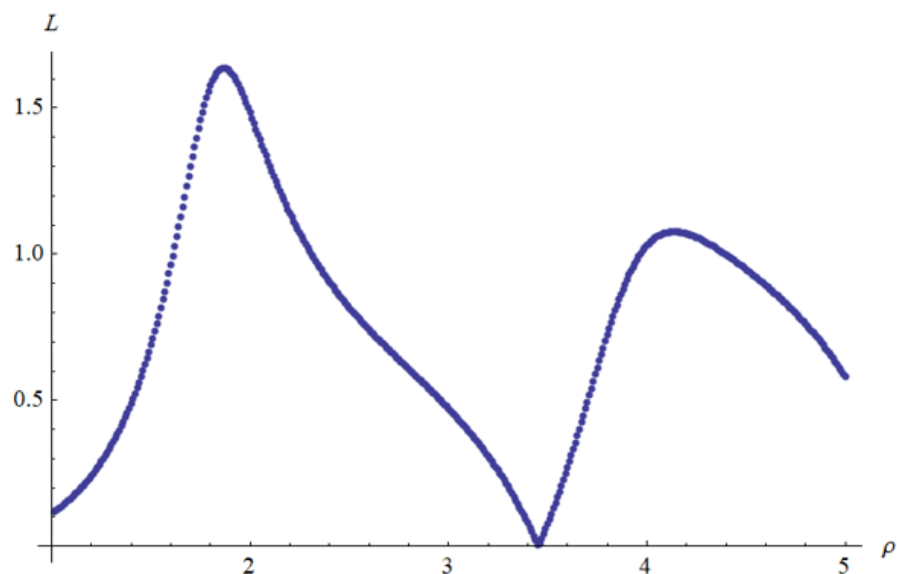


Figure 7. Scattering length.

4. Conclusions

This paper shows that the Cornell potential in Lobachevsky space, contrary to the case of flat space, is a potential well of finite depth. Therefore, for particles moving in such a potential, both bound states and scattering states are possible. In this case, the greater the radius of curvature of Lobachevsky space and the smaller the quantum number of the orbital momentum, the greater the depth of the potential well. For values of the potential parameters typical of charmonium and an arbitrarily chosen radius of curvature, numerical solutions corresponding to bound states and their corresponding energy levels were found. It was shown that the number of bound states of the system increases with an increasing radius of curvature and decreases with increasing orbital quantum numbers. For the scattering problem, energy dependences were obtained for the first few partial cross-sections, as well as the dependence of the scattering length on the radius of curvature of the space. It is interesting to note that for some values of ρ we had $\sigma_0 = 0$, which means that in Lobachevsky space with the particular radius of curvature a particle with zero angular momentum and with low energy is not scattered.

Author Contributions: Conceptualization, L.J. and Y.A.K.; Methodology, V.O.S.; Investigation, N.D.S.; Writing—original draft, V.O.S. All authors have read and agreed to the published version of the manuscript.

Funding: This research received no external funding.

Data Availability Statement: No new data were created or analyzed in this study. Date sharing is not applicable to this article.

Conflicts of Interest: The authors declare no conflicts of interest.

References

1. Friedman, A. Über die Krümmung des Raumes. *Z. Phys.* **1922**, *10*, 377–386. [CrossRef]
2. Friedmann, A. Über die Möglichkeit einer Welt mit konstanter negativer Krümmung des Raumes. *Z. Phys.* **1924**, *21*, 326–332. [CrossRef]
3. Friedmann, A. On the Curvature of Space. *Gen. Relativ. Gravit.* **1999**, *31*, 1991–2000. [CrossRef]
4. Friedmann, A. On the Possibility of a World with Constant Negative Curvature of Space. *Gen. Relativ. Gravit.* **1999**, *31*, 2001–2008. [CrossRef]
5. Tropp, E.A.; Frenkel, V.Y.; Chernin, A.D. *Alexander A. Friedmann. The Man Who Made the Universe Expand*; Dron, A., Burov, M., Translators; Cambridge University Press: Cambridge, MA, USA, 1993.
6. Gliner, E.B. Algebraic properties of the energy-momentum tensor and vacuum-like states of matter. *Sov. Phys. JETP* **1966**, *22*, 378–382.

7. Jenkovszky, L.L.; Trushevsky, A.A. Asymptotics of total cross-sections and ultimate temperature of hadronic systems. *Nuovo C. A* **1976**, *34*, 369–384.
8. Bugrij, A.I.; Trushevsky, A.A. Some cosmological consequences of high-temperature phase transition in hadron matter. *Astrofizika* **1977**, *13*, 361–374.
9. Kokkedee, J. *Theory of Quarks*; Mir: Moscow, Russia, 1971; 338p.
10. Shelest, A.P.; Zinoviev, G.M.; Miranskij, V.A. *Models of Strongly Interacting Particles*; Atomizdat: Moscow, Russia, 1975; 232p.
11. Bykov, A.A.; Dremin, I.M.; Leonidov, A.V. Potential models of quarkonium. *Sov. Phys. Uspekhi* **1984**, *27*, 321. [CrossRef]
12. Sergeenko, M.N. Masses and widths of Resonances for the Cornell Potential. *Adv. High Energy Phys.* **2013**, *2013*, 325431. [CrossRef]
13. Izmistiev, A.A. Exactly solvable potential model for quarkoniums. *Nucl. Phys.* **1990**, *52*, 1697–1710.
14. Kudryashov, V.V.; Murzov, V.I.; Tomilchik, L.M. *Triplet State of a Two-Fermion System with Homogeneous Relative Space*; Preprint No. 568; B.I. Stepanov Institute of Physics, Academy of Sciences of the BSSR: Minsk, Russia, 1969; 19p.
15. Gamow, G. *The Creation of the Universe*; Viking Press: New York, NY, USA, 1952.
16. Gliner, E.B. Algebraic Properties of the Energy-momentum Tensor and Vacuum-like States σ^+ Matter. *Sov. Phys. JETP* **1965**, *22*, 378.
17. Gliner, E.B. Vacuum-like state of a medium and Friedmann cosmology. *Dokl. Akad. Nauk USSR* **1970**, *192*, 771–774.
18. Gliner, E.B.; Dymnikova, I.G. Nonsingular Friedmann cosmology. *Sov. Astron. Lett. (Engl. Transl.)* **1975**, *1*, 7.
19. Bugrij, A.I.; Trushevsky, A.A. Some cosmological consequences of the high-temperature hadron phase transition. *Astrophysics* **1977**, *13*, 195–202. [CrossRef]
20. Jenkovszky, L.L.; Kämpfer, B.; Sysoev, V.M. On the expansion of the universe during the confinement transition. *Z. Phys. C* **1990**, *48*, 147. [CrossRef]
21. Jenkovszky, L.L.; Kaempfer, B.; Sysoev, V.M. Bubble-free energy during the confinement transition. *Phys. Atomic Nuclei* **1994**, *57*.
22. Einstein, A. Kosmologische Betrachtungen zur Allgemeinen Relativitätstheorie. *Sitzungsberichte Königlich Preuss. Akad. Wiss.* **1917**, *1*, 142.
23. Schrödinger, E. A method of determining quantum mechanical eigenvalues and eigenfunctions. *Proc. R. Irish. Acad. A* **1940**, *46*, 9–16.
24. Infeld, L. On a new treatment of some eigenvalue problems. *Phys. Rev.* **1941**, *59*, 737–747. [CrossRef]
25. Infeld, L.; Schild, A. A note on the Kepler problem in a space of constant negative curvature. *Phys. Rev.* **1945**, *67*, 121–122. [CrossRef]
26. Stevenson, A.F. A note on the Kepler problem in a spherical space, and the factorization method of solving eigenvalue problems. *Phys. Rev.* **1941**, *59*, 842–843. [CrossRef]
27. Higgs, P. Dynamical symmetries in a spherical geometry. *J. Phys. A Math. Gen.* **1979**, *12*, 309–323. [CrossRef]
28. Leemon, H. Dynamical symmetries in a spherical geometry. *J. Phys. A Math. Gen.* **1979**, *12*, 489–501. [CrossRef]
29. Kurochkin, Y.A.; Otchik, V.S. Analog of the Runge—Lenz vector and energy spectrum in the Kepler problem on a three-dimensional sphere. *Dokl. AN BSSR* **1979**, 987–990.
30. Bogush, A.A.; Kurochkin, Y.A.; Otchik, V.S. On the quantum-mechanical Kepler problem in a three-dimensional Lobachevsky space. *Dokl. AN BSSR*. **1980**, 19–22.
31. Kurochkin, Y.A.; Otchik, V.S.; Tereshenkov, V.I. Electron in a magnetic charge field in three-dimensional Lobachevsky space. *Proc. Acad. Sci. BSSR Phys. Math. Ser.* **1984**, 74–79.
32. Kurochkin, Y.A.; Shoukavy, D.V. Regge trajectories of the Coulomb potential in the space of constant negative curvature 1S_3 . *J. Math. Phys.* **2006**, *47*, 022103. [CrossRef]
33. Muradian, R. The Regge law for heavenly bodies. *Phys. Part. Nucl.* **1997**, *28*, 471.
34. Trushevsky, A.A. Asymptotic Behavior of Boson Regge Trajectories. *Ukr. J. Fiz.* **2021**, *97*, 66. [CrossRef]

Disclaimer/Publisher’s Note: The statements, opinions and data contained in all publications are solely those of the individual author(s) and contributor(s) and not of MDPI and/or the editor(s). MDPI and/or the editor(s) disclaim responsibility for any injury to people or property resulting from any ideas, methods, instructions or products referred to in the content.

Review

The Spectral Condition, Plane Waves, and Harmonic Analysis in de Sitter and Anti-de Sitter Quantum Field Theories

Ugo Moschella ^{1,2,3}¹ Università dell'Insubria, Via Valleggio 11, 21100 Como, Italy; ugo.moschella@uninsubria.it² CERN, Theory Department, 1211 Geneva, Switzerland³ INFN Sez. di Milano, Via Celoria 16, 20133 Milano, Italy

Abstract: We review the role of the spectral condition as a characteristic of Minkowski, de Sitter, and anti-de Sitter quantum field theories. We also discuss the role of plane waves which are compatible with the relevant analyticity domains linked to the spectral condition(s) and discuss harmonic analysis in terms of them.

Keywords: de Sitter; anti-de Sitter; spectral condition

1. The Birth of the de Sitter Model

After writing, in December 1915, his equations for the geometry of spacetime, Einstein turned his attention to cosmology and tried to apply them to the entire Universe, creating an entirely new science—modern scientific cosmology—whose founding idea is that a global exact solution of Einstein's equations corresponds somehow to a model for the Universe.

Einstein's concern was, at first, epistemological: the metric structure of the Universe must be entirely determined by the material content—this is more or less the so-called Mach principle. But general relativity still keep a remnant of absolute space in the boundary conditions that must be specified at spacelike infinity to determine the spacetime geometry. To solve this problem, or rather, to dispose of it, Einstein's "crazy idea" was to let the Universe be spherical, let it have spherical spatial sections.

A curved sphere should be imagined as a three-dimensional spherical hypersurface embedded in a Euclidean space of dimension four:

$$S_3 = \{x_1^2 + x_2^2 + x_3^2 + x_4^2 = r^2\}. \quad (1)$$

It obviously has no centre, or rather, it has its centre everywhere¹, and any point is equivalent to any other point. It has no boundary either; and therefore: no boundary, no conditions on boundary.

There was also a second guiding principle in Einstein's cosmological research: The Universe had to be static and its geometry should not change as time goes by. In 1917, the visible Universe still coincided with the Milky Way, the nebulae enigma had not yet been solved, and the hypothesis of a static Universe was perfectly reasonable. But, his General Theory of Relativity of 1915 does not allow for spherical static solutions.

Here came idea that would be remembered as his *biggest blunder*: to add to his equations a constant term Λ that acts repulsively and counteracts the gravitational attraction. This was, to quote Einstein,

an extension of the equations which is not justified by our real knowledge of gravitation [...] this term is necessary only for the purpose of making possible a quasi-static distribution of matter as required by the low speed of stars [1].

This commentary indicates that in his 1917 paper, Einstein was already aware of the fact that his original equations of 1915 implied a dynamical Universe, but that he had set aside this



Citation: Moschella, U. The Spectral Condition, Plane Waves, and Harmonic Analysis in de Sitter and Anti-de Sitter Quantum Field Theories. *Universe* **2024**, *10*, 199. <https://doi.org/10.3390/universe10050199>

Academic Editors: Galina L. Klimchitskaya, Vladimir M. Mostepanenko and Sergey V. Sushkov

Received: 18 March 2024

Revised: 23 April 2024

Accepted: 24 April 2024

Published: 28 April 2024



Copyright: © 2024 by the authors. Licensee MDPI, Basel, Switzerland. This article is an open access article distributed under the terms and conditions of the Creative Commons Attribution (CC BY) license (<https://creativecommons.org/licenses/by/4.0/>).

possibility. He kept adding Λ and found a perfectly Machian static spherical solution—his static model of 1917.

Shortly after the publication of Einstein's paper, de Sitter published a second solution of the new cosmological equations of 1917: an otherwise empty Universe made only by the cosmological constant. The astronomer found his model elaborating on the boundary condition problem. According to him, Einstein's solution still retained a trace of absolute space; a four-dimensional (complex) sphere could solve the problem in a more convincingly covariant way. As for the sphere (1), the de Sitter model can be better visualised as an embedded surface: it is the four-dimensional one-sheeted hyperboloid embedded in a five-dimensional Minkowski spacetime M_5

$$dS_4 = \{x_0^2 - x_1^2 - x_2^2 - x_3^2 - x_4^2 = -R^2\}. \quad (2)$$

Einstein was very unhappy with the new solution, but all his attempts to demonstrate that de Sitter's calculations were faulty consistently failed. Einstein finally surrendered: the de Sitter Universe was indeed a regular solution of his cosmological equations without matter, but, he said, it was nevertheless without physical interest because it was not globally static. Einstein was rejecting the possibility of a dynamical Universe, but other scientists simply did not know: until the early 1930s, the fundamental articles published in 1922 [2] and 1924 [3] by Friedmann, who made use of the original equations of general relativity to describe expanding universes, were substantially ignored. Lemaître's independent work in 1927 [4], based on the cosmological equations of 1917, was ignored too.

On a trip to Pasadena, Einstein learned of Hubble's latest observations and was persuaded of the advantages of dynamic models to describe the Universe. In two articles published shortly afterwards, Einstein asserted that the original reasons for introducing the cosmological constant no longer existed. Farewell to the cosmological constant.

In 1947, Einstein wrote to Lemaître:

The introduction of such a constant implies a considerable renunciation of the logical simplicity of the theory. . . . Since I introduced this term, I had always a bad conscience . . . I am unable to believe that such an ugly thing should be realized in nature.

Lemaître's answer in 1949 sounds like a prophecy.

The history of science provides many instances of discoveries which have been made for reasons which are no longer considered satisfactory. It may be that the discovery of the cosmological constant is such a case.

In fact, Einstein himself had been prophetic in 1917 in a letter to de Sitter.

In any case, one thing is clear. The theory of general relativity allows adding the term Λ in the equations. One day, our real knowledge of the composition of the sky of fixed stars, the apparent motions of the fixed stars and the position of spectral lines as a function of distance, will probably be sufficient to decide empirically whether or not Λ is equal to zero. Conviction is a good motive, but a bad judge.

In 1997, exactly eighty years after its discovery, the cosmological constant was observed [5,6]; or maybe, it was something similar that we now call "dark energy". These observations have upturned consolidated and rooted ideas, indicating that the gravitational effect of the greatest part of the energy of the Universe consists to producing an accelerated expansion, as in the case of Einstein's cosmological constant. Nowadays, almost every physicist believes that the dark component constitutes about seventy percent of the energy of the Universe and that its proportion, according to the standard cosmological Λ CDM (cold dark matter) model, is destined to increase. In the end, only the cosmological constant will remain, and the Universe will become a perfect de Sitter spacetime.

The de Sitter geometry seems therefore to assume the role of the reference geometry of the Universe. In other words, it is de Sitter's, and not Minkowski's, the geometry of spacetime when the latter is deprived of its content of matter and radiation.

Beyond the acceleration of the Universe at late times, the idea of inflation consists of a phase of accelerated quasi-exponential expansion, approximately described by de Sitter's geometry in the primordial Universe. A theoretical understanding of the structure of the Universe, which is observable today, is based on quantum field theory on de Sitter spacetime: quantum fluctuations of the vacuum at the epoch of inflation are thought to be responsible for the primordial density inhomogeneities that are at the origin of the structures existing in the Universe today.

Actually, once one admits that a cosmological constant may exist, it might also be negative, isn't it? The model of the Universe with a negative cosmological constant and nothing else is termed anti-de Sitter. It is a curious coincidence that in the very same year, 1997, the negative cosmological constant also took centre stage in theoretical physics [7] with the formulation of the by-now famous AdS/CFT (Anti-de Sitter/Conformal Field Theory) correspondence, a conjectured duality between two different physical theories—1997, the year of the two cosmological constants!

2. Quantum Field Theory: The Spectral Condition

The de Sitter and anti-de Sitter spacetimes thus have great importance in contemporary theoretical physics and cosmology, and both dS and AdS quantum field theory (QFT) also play a major role. The dS and AdS manifolds share the properties of having constant curvature and being maximally symmetric manifolds. Actually, in the general d -dimensional case, they are just different real submanifolds of one and the same complex manifold: the complex d -dimensional sphere

$$S_d^{(c)} = \{z \in \mathbf{C}^{d+1}; z_0^2 + z_1^2 + \dots + z_d^2 = R^2\}. \quad (3)$$

Otherwise, their geometries are radically different from each other. In particular, the (real) de Sitter manifold has no global timelike Killing vector field, while the (real) anti-de Sitter manifold is not globally hyperbolic and has closed timelike curves. One can get rid of these closed curves by moving to the universal covering of the real AdS manifold (even though this move might be just an illusion), but the universal covering remains not globally hyperbolic.

Global hyperbolicity is a basic property of quantum field theory on curved spacetimes, as it is usually formulated. Its absence renders AdS QFT a little more demanding from a technical viewpoint. But, as we will see, this is not a major difficulty since in AdS, there exists the possibility of identifying a global energy operator. It is precisely the lack of a global energy operator, which is a consequence of the absence of a global timelike Killing vector field, which renders dS QFT actually more difficult.

There is, however, a unifying characteristic that makes dS and AdS QFTs similar to each other and similar also to the standard zero-temperature Minkowski QFT: this is the analyticity of the correlation functions in suitable domains of the respective complexified manifolds. This unifying viewpoint is discussed in the following sections.

Here, to prepare the groundwork, we start by recalling that the fundamental theorem of Stone and Von Neumann, which states the uniqueness of the Hilbert space representation of the canonical commutation relations (CCRs), fails for infinite quantum systems. The distinction between observables and states, which is of no consequence for finitely many degrees of freedom, now becomes crucial, and there exist infinitely many Hilbert space realisations of the same algebra of the observables. In other words, knowing the Lagrangian of a quantum field theory is not enough. The Lagrangian just provides the commutation rules, but there are infinitely many inequivalent solutions of the field equations sharing the same commutation rules; one needs to specify some extra information to find the physically relevant ones. Only after this step has been taken can transition amplitudes may be computed and comparisons with the outcomes of the experiments may be done.

3. States and Two-Point Functions

This non uniqueness is true already at the level of free fields. What is unique is the commutator: on a globally hyperbolic manifold (\mathcal{M}, g) , the Klein–Gordon Lagrangian uniquely selects the (covariant) commutator $C(x_1, x_2)$, which is an *antisymmetric* bi-distribution solving the Klein–Gordon equation in each variable

$$(\square_{x_1} + m^2)C(x_1, x_2) = (\square_{x_2} + m^2)C(x_1, x_2) = 0 \tag{4}$$

with the precise initial condition given by the equal-time canonical commutation relations. The equal-time CCRs, in turn, imply that $C(x_1, x_2) = 0$ for any two events x_1, x_2 of \mathcal{M} , which are spacelike-separated with respect to the notion of locality inherent to \mathcal{M} .

For free fields, the smeared commutator is a multiple of the identity element of the field algebra (a *c-number*). Given two test functions f and g belonging to a suitable test function space $\mathcal{T}(\mathcal{M})$,

$$[\phi(f), \phi(g)] = C(f, g) = \int_{\mathcal{M} \times \mathcal{M}} C(x_1, x_2) f(x_1) g(x_2) \sqrt{-g(x_1)} dx_1 \sqrt{-g(x_2)} dx_2. \tag{5}$$

A quantisation is accomplished when the commutation relations (5) are represented by an operator-valued distribution in a Hilbert space \mathcal{H} . One should determine a linear map

$$\phi(f) \longrightarrow \hat{\phi}(f) \in Op(\mathcal{H}) \tag{6}$$

preserving the algebraic structures and such that

$$[\hat{\phi}(f), \hat{\phi}(g)] = C(f, g) \mathbf{1}. \tag{7}$$

As we stated, the Stone–Von Neumann theorem fails, and there are uncountably many solutions to this problem. How can we construct (at least some of) them?

A possible solution is completely encoded in the knowledge of a two-point function, i.e., a two-point distribution $\mathcal{W} \in \mathcal{T}'(\mathcal{M} \times \mathcal{M})$ that solves the Klein–Gordon equation in each variable

$$(\square_{x_1} + m^2)\mathcal{W}(x_1, x_2) = (\square_{x_2} + m^2)\mathcal{W}(x_1, x_2) = 0. \tag{8}$$

Because of Equation (7), $\mathcal{W}(x_1, x_2)$ is also required to be a solution of the functional equation

$$\mathcal{W}(x_1, x_2) - \mathcal{W}(x_2, x_1) = C(x_1, x_2) \tag{9}$$

in the sense of distributions.

Starting from $\mathcal{W}(x_1, x_2)$, the Hilbert space of the theory \mathcal{H} can be constructed using standard techniques [8]. The first step consists of giving a norm to the one-particle state Ψ_f corresponding to a given test function $f \in \mathcal{T}(\mathcal{M})$. The norm is computed using the two-point function:

$$\|\Psi_f\|^2 = \int_{\mathcal{M} \times \mathcal{M}} \mathcal{W}(x_1, x_2) f^*(x_1) f(x_2) \sqrt{-g(x_1)} dx_1 \sqrt{-g(x_2)} dx_2. \tag{10}$$

The squared norm (10) is positive (as it should be) if $\mathcal{W}(x_1, x_2)$ satisfies the *positive-definiteness condition*, which is nothing but the nonnegativity of the right-hand side of Equation (10). We assume that it does.

The norm (10) actually comes from a pre-Hilbert scalar product whose interpretation is that of providing the quantum transition amplitudes between two one-particle states:

$$\langle \Psi_f, \Psi_g \rangle = \int_{M_d} \mathcal{W}(x_1, x_2) f^*(x_1) g(x_2) \sqrt{-g(x_1)} dx_1 \sqrt{-g(x_2)} dx_2. \tag{11}$$

The one-particle Hilbert space $\mathcal{H}^{(1)}$ is obtained by quotienting out the subspace of zero-norm states and by taking the Hilbert completion. The full Hilbert space is the symmetric Fock space

$$\mathcal{H} = F_s(\mathcal{H}^{(1)}) = \mathcal{H}_0 \oplus [\oplus_n \text{Sym}(\mathcal{H}_1)^{\otimes n}]$$

(with Sym denoting the symmetrisation operation and $\mathcal{H}_0 = \{\lambda 1, \lambda \in \mathbf{C}\}$). In the final step, one introduces the field operator $\widehat{\phi}(f)$ decomposed into its “creation” and “annihilation” parts

$$\widehat{\phi}(f) = \widehat{\phi}^+(f) + \widehat{\phi}^-(f); \tag{12}$$

the latter are defined by their action on the dense subspace $\mathcal{H}^{(0)}$ of vectors having finitely many non-vanishing components $\Psi = (\Psi_0, \Psi_1, \dots, \Psi_k, \dots, 0, 0, 0, \dots)$:

$$(\widehat{\phi}^-(f)\Psi)_n = \sqrt{n+1} \int \mathcal{W}(x, x') f(x) \Psi_{n+1}(x', x_1, \dots, x_n) \sqrt{-g(x)} dx \sqrt{-g(x')} dx', \tag{13}$$

$$(\widehat{\phi}^+(f)\Psi)_n = \frac{1}{\sqrt{n}} \sum_{j=1}^n f(x_j) \Psi_{n-1}(x_1, \dots, x_j, \dots, x_n). \tag{14}$$

Equation (9) shows that these formulae imply the commutation relations (7) and that

$$\mathcal{W}(x, x') = \langle \Psi_0, \widehat{\phi}(x) \widehat{\phi}(x') \Psi_0 \rangle \tag{15}$$

where

$$\Psi_0 = (1, 0, 0, \dots) \tag{16}$$

is the cyclic reference state of the representation.

In the end, either in flat or curved spacetime, quantizing a free-field theory amounts to specifying its two-point function, which carries all the information about the Hilbert space and the field operators. Furthermore, the knowledge of the two-point function and the commutator allows us to determine the Green’s functions, modulo the necessary renormalisations; thus, the two-point function encodes not only the dynamics of the free field but also the possibility of studying interactions perturbatively.

But, how do we specify a criterion to choose among the infinitely many existing possibilities? Here comes the spectral condition.

4. Prelude: The Spectral Condition in Minkowski Space

This section contains material that may be found in (good) textbooks. The reason to recall it here is to better appreciate and understand the role of the spectral condition and plane waves in the de Sitter and anti-de Sitter contexts.

On page 97 of the classic book by R. Streater and A.S. Wightman, the following basic assumption about a relativistic quantum field theory is declared:

Axiom 0. Assumptions of Relativistic Quantum Theory.

The states of the theory are described by unit rays in a separable Hilbert space \mathcal{H} . The relativistic transformation law of the states is given by a continuous unitary representation of the inhomogeneous Lorentz group $\{a, A\} \rightarrow U(a, A)$. Since $U(a, 1)$ is unitary, it can be written as $U(a, 1) = \exp(ia_\mu P^\mu)$ where P^μ is an unbounded operator interpreted as the energy momentum operator of the theory. The eigenvalues of P^μ lie in or on the forward cone (*spectral condition*). There is an invariant state Ψ_0 , $U(a, 1)\Psi_0 = \Psi_0$ unique up to a constant phase factor (*uniqueness of the vacuum*).

Stated more succinctly:

The joint spectrum of the infinitesimal generators of $U(a, 1)$ lies in the closed forward cone \overline{V}_+ .

This is the spectral condition of standard (zero-temperature) QFT. It is its most important and characteristic feature. All the other axioms are of a kinematical character².

Here, we consider a general d -dimensional Minkowski spacetime M_d with metric

$$\eta_{\mu\nu} = \text{diag}(+, -, \dots, -) \tag{17}$$

and one scalar field. The open future cone of the origin (also called the forward cone) is the set

$$V_+ = \{x \in M_d : x \cdot x > 0, x^0 > 0\}. \tag{18}$$

Given the n -point vacuum expectation values of the field (in short, the n -point functions):

$$\mathcal{W}_n(x_1, \dots, x_n) = \langle \Psi_0, \hat{\phi}(x_1) \dots \hat{\phi}(x_n) \Psi_0 \rangle, \tag{19}$$

the spectral condition is immediately translated into a property of the support of their Fourier transforms $\tilde{\mathcal{W}}_n(p_1, \dots, p_n)$. The distribution

$$\tilde{\mathcal{W}}_n(p_1, \dots, p_n) = \int e^{ip_1 \cdot x_1 + \dots + ip_n \cdot x_n} \mathcal{W}_n(x_1, \dots, x_n) dx_1 \dots dx_n \tag{20}$$

vanishes unless all momenta are in the energy-momentum spectrum of the states

$$p_1 \in \bar{V}_+, p_1 + p_2 \in \bar{V}_+, \dots, p_1 + p_2 + \dots + p_n \in \bar{V}_+. \tag{21}$$

By Fourier–Laplace transform, support properties in one space give rise to analyticity properties in the dual space [8]. A fundamental theorem of this category shows that the n -point distributions are boundary values of n -point functions holomorphic in tubular domains of the complex Minkowski spacetime.

Theorem 1 (A.S. Wightman). *The distribution $\mathcal{W}_n(x_1, \dots, x_n)$ is the boundary value of a function $W_n(z_1, \dots, z_n)$ holomorphic in the tube*

$$T_n = \{(z_1, \dots, z_n) : \text{Im}(z_{j+1} - z_j) \in \bar{V}_+\}. \tag{22}$$

Wightman’s reconstruction theorem [8] finally states the *equivalence of the analyticity of the n -point function in the tubes T_n and the spectral condition*: starting from a set of Wightman functions having such analyticity properties, it is possible to reconstruct the Hilbert space of the theory, the representation of the inhomogeneous Lorentz group, and the infinitesimal generators of the translation group and verify that their joint spectrum is contained in the closed forward cone.

The above analyticity properties and the spectral condition have therefore one and the very same precise *physical meaning*: they assert that the states of the theory have positive energy in every Lorentz frame.

Focusing now on two-point functions, the spectral condition is equivalent to the following simpler property.

Corollary 1 (Normal analyticity property). *$\mathcal{W}(x_1, x_2)$ is the boundary value of a function $W(z_1, z_2)$ holomorphic in the tube $T_{12} = T_- \times T_+$:*

$$\mathcal{W}(x_1, x_2) = \langle \Psi_0, \hat{\phi}(x_2) \hat{\phi}(x_1) \Psi_0 \rangle = \underset{\substack{T_- \ni z_1 \rightarrow x_1 \\ T_+ \ni z_2 \rightarrow x_2}}{\text{b.v.}} W(z_1, z_2) \tag{23}$$

where

$$T_{\pm} = \{(z = x + iy : \pm y \in \bar{V}_+)\} \tag{24}$$

are the past and future tubes.

The tubes T_{\pm} are invariant under the action of the real inhomogeneous Lorentz group. Acting with the complex group, one discovers that every Lorentz invariant two-point function satisfying the spectral condition enjoys a much larger analyticity domain.

Theorem 2 (Maximal analyticity property). 1. The two-point function $W(z_1, z_2)$ depends only on the Lorentz-invariant variable $\lambda = (z_1 - z_2)^2$.

2. $W(z_1, z_2)$ can be continued to a function $\mathfrak{W}(z_1, z_2)$ analytic in the cut domain

$$\Delta_0 = \{(z_1, z_2); (z_1 - z_2)^2 \neq \rho, \rho \geq 0\} \tag{25}$$

that contains all pairs of complex events with the exception of all pairs of real events that are causally connected (the causal cut).

3. $\mathfrak{W}(z_1, z_2)$ is invariant in Δ_0 under the action of the complex inhomogeneous Lorentz group.

4. The permuted two-point function is the boundary value of $\mathfrak{W}(z_1, z_2)$ from the opposite tube $T_{21} = T_+ \times T_-$:

$$\mathcal{W}(x_2, x_1) = \langle \Psi_0, \hat{\phi}(x_2)\hat{\phi}(x_1)\Psi_0 \rangle = \underset{\substack{T_+ \ni z_1 \rightarrow x_1 \\ T_- \ni z_2 \rightarrow x_2}}{\text{b.v.}} \mathfrak{W}(z_1, z_2). \tag{26}$$

5. The cut domain Δ_0 contains all pairs of non-coinciding Euclidean points

$$\mathcal{E} = \{z_1, z_2 \in \Delta, \operatorname{Re} z_1^0 = \operatorname{Re} z_2^0 = 0, \operatorname{Im} z_1^i = \operatorname{Im} z_2^i = 0, i = 1, \dots, d - 1, z_1 \neq z_2\}. \tag{27}$$

The Schwinger function S (also called the Euclidean propagator) is the restriction of $\mathfrak{W}(z_1, z_2)$ to the non-coincident Euclidean points \mathcal{E} . S is analytic in \mathcal{E} and can be extended as a distribution to the whole Euclidean space \mathcal{E} , including the coinciding points.

Klein–Gordon Fields

Now, let us see how the spectral condition works in practice for Klein–Gordon fields. The first thing is to identify a suitable basis of solutions of the Klein–Gordon operator. In flat space, the exponential plane waves are almost always the convenient choice since they are also characters of the translation group:

$$\psi_{\vec{p}}^{(\pm)}(x) = \frac{1}{2\sqrt{(2\pi)^{d-1}\omega}} \exp(\pm ipx), \quad p^0 = \omega = \sqrt{|\vec{p}|^2 + m^2}. \tag{28}$$

The above plane waves extend to functions that are holomorphic in the whole complex Minkowski spacetime $M_d^{(c)}$. The important point to be noted is the following.

Remark 1. Positive frequency waves $\psi_{\vec{p}}^{(-)}(z)$ are exponentially decreasing in the past tube T_- ; negative frequency waves $\psi_{\vec{p}}^{(+)}(z)$ are exponentially decreasing in the future tube T_+ .

Let us now examine the two-point function. By translation invariance, it may depend only on the difference variable $\xi = x_1 - x_2$. Taking the Fourier transform of the Klein–Gordon equation with respect to ξ gives

$$(p^2 - m^2)\tilde{\mathcal{W}}_m(p) = 0. \tag{29}$$

The most general Lorentz invariant distributional solution has two disconnected components:

$$\tilde{\mathcal{W}}_m(p) = a\theta(p^0)\delta(p^2 - m^2) + b\theta(-p^0)\delta(p^2 - m^2) \tag{30}$$

and the spectral condition imposes $b = 0$. By Fourier anti-transforming, we obtain:

$$\mathcal{W}_m(x_1, x_2) = \frac{1}{2(2\pi)^{d-1}} \int \frac{e^{-i\omega(x_1^0 - x_2^0) + i\vec{p} \cdot (\vec{x}_1 - \vec{x}_2)}}{\sqrt{|\vec{p}|^2 + m^2}} d\vec{p} = \int \psi_{\vec{p}}^{(-)}(x_1)\psi_{\vec{p}}^{(+)}(x_2)d\vec{p}. \tag{31}$$

Remark 1 invites us to move the first point into the past tube T_- and the second point into the forward tube T_+ . This move greatly improves the convergence of the integral, as the function

$$W_m(z_1, z_2) = \int \psi_{\vec{p}}^{(-)}(z_1) \psi_{\vec{p}}^{(+)}(z_2) d\vec{p}, \quad z_1 \in T_-, \quad z_2 \in T_+ \tag{32}$$

is now an analytic function of $(z_1, z_2) \in T_- \times T_+$. The two-point distribution $\mathcal{W}(x_1, x_2)$ is recovered by taking the boundary value. The normalisation ensures that the CCRs hold with the correct coefficient.

Let us discuss the following elementary massless case in more detail:

$$W((t - is, 0 \dots, 0), 0) = \int \frac{e^{-i\omega(t-is)} k^{d-3}}{2(2\pi)^{d-1}} e^{-i\omega(t-is)} k^{d-3} dk d\Omega_{d-2} \tag{33}$$

$$= \frac{1}{(4\pi)^{\frac{d-1}{2}}} \frac{\Gamma(d-2)}{\Gamma\left(\frac{d-1}{2}\right)} \frac{1}{(it+s)^{d-2}}. \tag{34}$$

By restoring in this expression the Lorentz-invariant variable $(z_1 - z_2)^2$, we immediately obtain the maximally analytic two-point function:

$$\mathfrak{W}(z_1, z_2) = \frac{\Gamma\left(\frac{d-2}{2}\right)}{4\pi^{\frac{d}{2}}} [-(z_1 - z_2)^2]^{-\frac{d-2}{2}}. \tag{35}$$

Its boundary values from the relevant tubes give the two-point function $\mathcal{W}(x_1, x_2)$ and the permuted two-point function $\mathcal{W}(x_2, x_1)$. The covariant commutator is their difference (9):

$$C(x, y) = \frac{\Gamma\left(\frac{d-2}{2}\right)}{4\pi^{\frac{d}{2}}} \left([-(x-y)^2 + i\varepsilon(x^0 - y^0)]^{-\frac{d-2}{2}} - [-(x-y)^2 - i\varepsilon(x^0 - y^0)]^{-\frac{d-2}{2}} \right). \tag{36}$$

Using the notations of [9], we obtain

$$C(x, y) = \frac{1}{2\pi i} \frac{1}{\Gamma\left(2 - \frac{d}{2}\right)} \varepsilon(x^0 - y^0) [-(x-y)^2]_{-}^{-\frac{d-2}{2}}. \tag{37}$$

where $\varepsilon(x) = \theta(x) - \theta(-x)$. When the spacetime dimension d is even, the distribution $[-(x-y)^2]_{-}^{\lambda}$ has a simple pole at $\lambda = -\frac{d-2}{2}$ with residue

$$\text{Res}_{\lambda=-\frac{d-2}{2}} [-(x-y)^2]_{-}^{\lambda} = \frac{(-1)^{\frac{d}{2}-2}}{\Gamma\left(\frac{d}{2}-2\right)} \delta^{(\frac{d}{2}-2)} [(x-y)^2] \tag{38}$$

while $1/\Gamma\left(\frac{d}{2}-2\right)$ has a zero, and we obtain that the support of the commutator is the light cone (Huygens principle):

$$C(x, y) = \frac{1}{2\pi i} \varepsilon(x^0 - y^0) \delta^{(\frac{d}{2}-2)} [(x-y)^2]. \tag{39}$$

In particular, for $d = 4$, we obtain the well-known dominant term of the Pauli–Jordan function.

5. de Sitter

Let us consider now the d -dimensional de Sitter Universe (see Equation (2)):

$$dS_d = \{x \in M_{d+1} : x \cdot x = -R^2 = -1\}. \tag{40}$$

The future cone of the origin of the ambient spacetime in one dimension more is given by

$$V^+ = \{x \in M_{d+1} : x^2 > 0, x^0 > 0\} \tag{41}$$

which provides the causal ordering of the de Sitter manifold. An event x_2 is in the future of another event x_1 if the vector $(x_2 - x_1)$ belongs to the closed future cone \overline{V}^+ of the ambient spacetime. Two events $x_1, x_2 \in dS_d$ are spacelike separated if and only if

$$(x_1 - x_2)^2 = -2 - 2x_1 \cdot x_2 < 0. \tag{42}$$

A straightforward adaptation of the spectral condition of Wightman QFT is just not possible because there exists no global energy operator available in the de Sitter case. This is a consequence of the absence of a global timelike Killing vector field on the de Sitter manifold. Timelike Killing vector fields exist only on wedge-like submanifolds bordered by bifurcate Killing horizons, but there is no Killing vector field that remains timelike on the whole manifold.

Still, since the complexification of Minkowski space plays such a crucial role in Minkowski QFT, we may go on and consider the complex de Sitter spacetime, visualised here as a submanifold of the complex $(d + 1)$ -dimensional Minkowski space:

$$dS_d^{(c)} = \{z \in M_{d+1}^{(c)} : z \cdot z = -R^2 = -1\}. \tag{43}$$

Note that $z = x + iy \in dS_d^{(c)}$ if and only if $x^2 - y^2 = -R^2$ and $x \cdot y = 0$. On the complex manifold there acts the complex de Sitter group $G^{(c)}$ acts, which is the complexification of the restricted Lorentz group of the ambient space $G = SO_0(1, d)$.

$dS_d^{(c)}$ contains tuboids \mathcal{T}_\pm , which are very similar to the past and future tubes of Minkowski space. Actually, they can be described in the simplest way precisely as the intersections of the ambient tubes T_\pm with the complex de Sitter manifold:

$$\mathcal{T}_\pm = dS_d^{(c)} \cap T_\pm = \{x + iy \in dS_d^{(c)} : y \in \pm V_\pm\}. \tag{44}$$

The set of points with purely imaginary zero component $z^0 = iy^0$ and purely real spatial components $z^i = x^i, i = 1, \dots, d$, forms the Euclidean sphere of the complex de Sitter manifold:

$$S_d = \{z = (iy^0, x^1, \dots, x^d) \in \mathbf{C}^{1+d} : y^{0^2} + x^{1^2} + \dots + x^{d^2} = R^2 = 1\}. \tag{45}$$

Now, we come to de Sitter QFT. While it is impossible to formulate a true spectral condition, we may retain its most characteristic consequence: in the case of two-point functions, we may assume [10] there holds the following.

Assumption 1 (Normal analyticity property). $\mathcal{W}(x_1, x_2)$ is the boundary value of a function $W(z_1, z_2)$ holomorphic in the tube $\mathcal{T}_{12} = \mathcal{T}_- \times \mathcal{T}_+$,

$$\mathcal{W}(x_1, x_2) = \langle \Psi_0, \hat{\phi}(x_2)\hat{\phi}(x_1)\Psi_0 \rangle = \underset{\substack{\mathcal{T}_- \ni z_1 \rightarrow x_1 \\ \mathcal{T}_+ \ni z_2 \rightarrow x_2}}{b.v.} W(z_1, z_2) \tag{46}$$

where \mathcal{T}_- and \mathcal{T}_+ are the de Sitter past and future tubes (see Figure 1).

Of course, the physical interpretation of this property cannot be the positivity of the energy spectrum of the states. It turns out that the correct physical interpretation is thermodynamical [10–12].

The tubes \mathcal{T}_\pm are invariant under the action of the real de Sitter group. By acting with the complex group, a much larger analyticity domain appears, as before. The following theorem [10] is mutatis mutandis identical to Theorem 2 [10].

Theorem 3 (Maximal analyticity property). 1. The two-point function $W(z_1, z_2)$ depends only on the Lorentz-invariant variable $\zeta = z_1 \cdot z_2$.

2. $W(z_1, z_2)$ can be continued to a function $\mathfrak{W}(z_1, z_2)$ analytic in the cut domain

$$\Delta = \{(z_1, z_2); \zeta \neq \rho, \rho \leq -1\} \tag{47}$$

that contains all pairs of complex events minus the causal cut (42).

3. $\mathfrak{W}(z_1, z_2)$ is invariant under the action of the complex de Sitter group.

4. The permuted two-point function is the boundary value of $\mathfrak{W}(z_1, z_2)$ from the opposite tube $T_{21} = T_+ \times T_-$:

$$W(x_2, x_1) = \langle \Psi_0, \hat{\phi}(x_2) \hat{\phi}(x_1) \Psi_0 \rangle = \underset{T_+ \ni z_1 \rightarrow x_1}{\underset{T_- \ni z_2 \rightarrow x_2}{b.v.}} \mathfrak{W}(z_1, z_2). \tag{48}$$

5. The cut domain Δ contains all the non-coinciding Euclidean points

$$\mathcal{E} = \{z_1, z_2 \in \Delta, z_1 \in S_d, z_2 \in S_d, z_1 \neq z_2\}. \tag{49}$$

The Schwinger function S is the restriction of $\mathfrak{W}(z_1, z_2)$ to the non-coincident Euclidean points \mathcal{E} . S is analytic in \mathcal{E} and can be extended as a distribution to the whole Euclidean space \mathcal{E} , including the coinciding points.

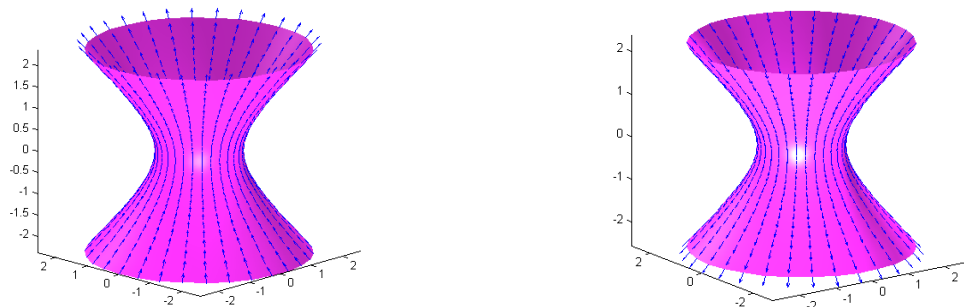


Figure 1. Sections of the forward and the backward tubes in the complex dS manifold. The arrows are the imaginary parts y of the vectors $z = x + iy$, represented as attached at the endpoint of their real parts x , which belong to the hyperboloid whose radius is $-R^2 + y^2$. Here is represented the section at a given fixed positive value of y^2 . Recall that $x \cdot y = 0$.

5.1. Klein–Gordon Fields and Plane Waves

Now we want to construct dS Klein–Gordon quantum fields starting from two-point functions (as in Equation (12)) that are *normal analytic* in the sense of Assumption 1. Following the paradigm of flat space, we should look for wave solutions of the Klein–Gordon equation analytic in the past, and respectively, in the future tube, and write a two-point function similar to Equation (32). When solving the Klein–Gordon equation, the normal strategy is to separate the variables; however, this would not be a good idea if the normal analyticity property has to appear manifestly, as in Equation (32).

One possibility comes from the study of geodesics [13]: a de Sitter timelike geodesic may be parametrised by the choice of two lightlike vectors belonging to the future light cone C_+ of the ambient Minkowski spacetime (see Figure 2), as follows:

$$x^\mu(\tau) = \frac{R}{\sqrt{2\tilde{\zeta} \cdot \eta}} (\tilde{\zeta}^\mu e^{\frac{\tau}{R}} - \eta^\mu e^{-\frac{\tau}{R}}). \tag{50}$$

The two null vectors parametrising the geodesics point towards its asymptotic directions. In fact, the conformal compactification of the Sitter manifold has a boundary at timelike infinity, and the light cone of the ambient spacetime is, in a precise sense, equivalent to it [14].

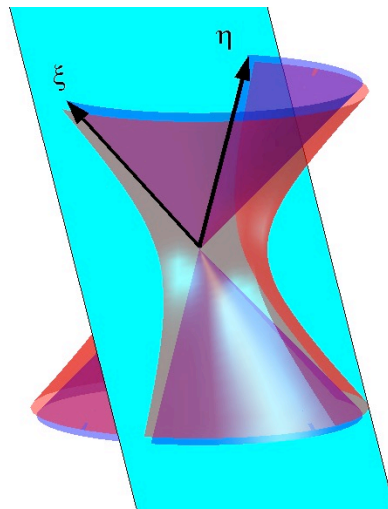


Figure 2. Timelike geodesics can be parametrised by the choice of two null vectors in the ambient space; they have the physical interpretation of asymptotic momentum directions.

A natural basis of the solutions of the de Sitter Klein–Gordon equation

$$\square_{dS}\psi(z) + m^2\psi(z) = 0 \tag{51}$$

can thus be parametrised by the choice of a lightlike vector $\xi \in C^+$ and a complex number λ , as follows:

$$\psi_\lambda(z, \xi) = (z \cdot \xi)^\lambda = e^{\lambda \log(z \cdot \xi)}. \tag{52}$$

In this definition, the scalar product is in the sense of the ambient spacetime. The functions (52) are plane waves, as their phase is constant on the planes $z \cdot \xi = \text{const}$. As required, they are well defined and analytic in each of the tubes \mathcal{T}^+ and \mathcal{T}^- [10].

It is useful to introduce a new complex parameter ν with the following definition:

$$\lambda = -\frac{d-1}{2} + i\nu. \tag{53}$$

The parameters λ and ν are related to the complex mass squared and the complex dimension as follows:

$$m^2 = -\lambda(\lambda + d - 1) = \frac{(d-1)^2}{4} + \nu^2. \tag{54}$$

Of course, m^2 is real and positive only under the following conditions:

1. ν is real. This corresponds, in a group-theoretical language, to the principal series of unitary representations of the Lorentz group;
2. ν is purely imaginary and $|\nu| < \frac{d-1}{2}$. This corresponds to the complementary series of unitary representations of the Lorentz group.

But, in the de Sitter Universe, there is also room for negative mass squared at certain discrete values [15,16].

5.2. Construction of the Two-Point Function

We can now mimic Equation (32) and consider the two-point function:

$$\int_\gamma (\xi \cdot z_1)^{-\frac{d-1}{2} - i\nu} (\xi \cdot z_2)^{-\frac{d-1}{2} + i\nu} d\mu_\gamma, \quad z_1 \in \mathcal{T}_-, \quad z_2 \in \mathcal{T}_+ \tag{55}$$

where

$$d\mu_\gamma(\xi) = \alpha(\xi)|_\gamma = (\xi^0)^{-1} \sum_{j=1}^d (-1)^{j+1} \xi^j d\xi^1 \dots \widehat{d\xi^j} \dots d\xi^d|_\gamma. \tag{56}$$

γ denotes any $(d - 1)$ -dimensional integration cycle in C^+ . To fix the ideas, we can integrate over the spherical basis S_{d-1} of the cone C^+ equipped with its canonical orientation:

$$\gamma_0 = S_{d-1} = C^+ \cap \{\zeta : \zeta^0 = 1\} = \{\zeta \in C^+ : \zeta^1^2 + \dots + \zeta^d^2 = 1\}. \tag{57}$$

In this case, $\alpha(\zeta)|_\gamma$ coincides with the rotation-invariant measure $d\mu_{\gamma_0}$ on S_{d-1} , normalised as follows:

$$\omega_d = \int_{\gamma_0} d\mu_{\gamma_0} = \frac{2\pi^{\frac{d}{2}}}{\Gamma\left(\frac{d}{2}\right)}. \tag{58}$$

The following is self-evident.

Property 1. *The two-point function (55) solves by construction the Klein–Gordon equation by construction in each variable and is manifestly holomorphic in $\mathcal{T}_- \times \mathcal{T}_+$.*

Since the integrand is a homogeneous function of ζ of degree $(1 - d)$, the integral (55) is actually the integral of a closed differential form and, as such, does not depend on the integration cycle. This immediately implies the following property.

Property 2. *The two-point function (55) is de Sitter-invariant and depends only on the invariant $\zeta = z_1 \cdot z_2$.*

To compute it explicitly, we may, therefore, choose the two arbitrary points z_1 in \mathcal{T}^- and z_2 in \mathcal{T}^+ in the way that most pleases us. Interestingly, different choices produce different integral representations of the same function. A useful choice is

$$z_1 = (-i, 0, \dots, 0, 0), \quad z_2(s) = (\sinh(is), 0, \dots, 0, \cosh(is)), \quad \zeta = (1, \vec{n} \sin \theta, \cos \theta),$$

so that

$$\zeta = z_1 \cdot z_2(s) = \sin(s), \quad (\zeta^2 - 1)^{\frac{1}{2}} = i \cos s. \tag{59}$$

The condition z_2 in \mathcal{T}^+ means $0 < s < \pi$. We obtain [17], Equation (7), p. 156

$$\begin{aligned} & \int_{S_{d-1}} (\zeta \cdot z_1)^{-\frac{d-1}{2}-iv} (\zeta \cdot z_2)^{-\frac{d-1}{2}+iv} d\zeta = \\ &= \omega_{d-1} \int_0^\pi e^{-\frac{i\pi}{2}(-\frac{d-1}{2}-iv)} (i \sin s - \cos s \cos \theta)^{-\frac{d-1}{2}+iv} \sin^{d-2} \theta d\theta \\ &= (2\pi)^{\frac{d}{2}} e^{-\pi v} (\zeta^2 - 1)^{-\frac{d-2}{4}} P_{-\frac{1}{2}+iv}^{-\frac{d-2}{2}}(\zeta). \end{aligned} \tag{60}$$

Imposing the normalisation of the CCRs gives the plane-wave expansion of the two-point function, valid for any complex value of ν that is not a pole of $\Gamma\left(\frac{d-1}{2} + iv\right)\Gamma\left(\frac{d-1}{2} - iv\right)$.

Main formula: The canonically normalised (so-called Bunch–Davis) Wightman function of a Klein–Gordon de Sitter scalar field has the following expressions:

$$\begin{aligned} W_\nu(z_1, z_2) &= w_\nu(z_1 \cdot z_2) \\ &= \frac{\Gamma\left(\frac{d-1}{2} + iv\right)\Gamma\left(\frac{d-1}{2} - iv\right)e^{\pi\nu}}{2^{d+1}\pi^d} \int_\gamma (\zeta \cdot z_1)^{-\frac{d-1}{2}-iv} (\zeta \cdot z_2)^{-\frac{d-1}{2}+iv} \alpha(\zeta) \end{aligned} \tag{61}$$

$$= \frac{\Gamma\left(\frac{d-1}{2} + iv\right)\Gamma\left(\frac{d-1}{2} - iv\right)}{2(2\pi)^{d/2}} (\zeta^2 - 1)^{-\frac{d-2}{4}} P_{-\frac{1}{2}+iv}^{-\frac{d-2}{2}}(\zeta). \tag{62}$$

Equation (61) is only valid in the normal domain of analyticity, with z_1 in \mathcal{T}^- and z_2 in \mathcal{T}^+ . On the other hand, the right-hand side of Equation (62) is maximally analytic, that is, entire in the cut plane Δ .

The discontinuity of the Wightman function on the cut provides the commutator. The retarded propagator function is obtained by (carefully) multiplying the commutator with the relevant step function:

$$C_\nu(x_1, x_2) = \mathcal{W}_\nu(x_1, x_2) - \mathcal{W}_\nu(x_2, x_1), \tag{63}$$

$$R_\nu(x_1, x_2) = i\theta(x_2, x_1)C_\nu(x_1, x_2). \tag{64}$$

To compute the retarded propagator, let us choose x_2 in the future cone of the origin:

$$x_0 = (0, 0, \dots, 0, 1) \quad x_2(t) = (\sinh t, 0, \dots, 0 \cosh t), \quad t > 0, \quad \zeta = -\cosh t.$$

The retarded discontinuity ($x_2 > x_1$) is, therefore,

$$\begin{aligned} r_\nu(u) &= \frac{i\Gamma\left(\frac{d-1}{2} + i\nu\right)\Gamma\left(\frac{d-1}{2} - i\nu\right)}{2(2\pi)^{d/2}} (u^2 - 1)^{-\frac{d-2}{4}} \left(P_{-\frac{1}{2}+i\nu}^{-\frac{d-2}{2}}(\zeta - i\epsilon) - P_{-\frac{1}{2}+i\nu}^{-\frac{d-2}{2}}(\zeta + i\epsilon) \right) \\ &= \cosh(\pi\nu) \frac{\Gamma\left(\frac{d-1}{2} + i\nu\right)\Gamma\left(\frac{d-1}{2} - i\nu\right)}{(2\pi)^{d/2}} (\zeta^2 - 1)^{-\frac{d-2}{4}} P_{-\frac{1}{2}+i\nu}^{-\frac{d-2}{2}}(-\zeta). \end{aligned} \tag{65}$$

The Schwinger function is the restriction of the maximally analytic two-point function to the Euclidean sphere. Given any two points of the Euclidean sphere, their invariant product may be parametrised as follows: $z_1 \cdot z_2 = -\cos(s)$. The choice of sign is because at coincident points, $z^2 = -1$. Thus,

$$G_\nu(-\cos s) = \frac{\Gamma\left(\frac{d-1}{2} + i\nu\right)\Gamma\left(\frac{d-1}{2} - i\nu\right)}{2(2\pi)^{d/2}} (\sin s)^{-\frac{d-2}{2}} e^{\frac{i\pi}{2}(d-2)} P_{-\frac{1}{2}+i\nu}^{-\frac{d-2}{2}}(-\cos s). \tag{66}$$

At this point, we are fully equipped to begin studying perturbative quantum field theory on the de Sitter Universe. Of course, we do not do it here, but we want to discuss one remarkable success of the above formalism.

5.3. Linearisation and the Källén–Lehmann Representation

In Minkowski space, any scalar two-point function $W(z_1, z_2)$ satisfying the properties described in Section 4 admits a Källén–Lehmann representation of the form

$$W(z_1, z_2) = \int_0^\infty \rho(m^2) W_m(z_1, z_2) dm^2 \tag{67}$$

where $W_m(z_1, z_2)$ is given in Equation (32) and the weight $\rho(m^2)$ is a positive measure of tempered growth. In particular, given two masses m_1 and m_2 , computing the weight for the bubble

$$W_{m_1}(z_1, z_2)W_{m_2}(z_1, z_2) = \int_{(m_1+m_2)^2}^\infty \rho(m^2 : m_1, m_2)W_m(z_1, z_2)dm^2 \tag{68}$$

is an easy exercise of Fourier transformation.

The corresponding de Sitter case is much more difficult. To obtain the Källén–Lehmann weight of the corresponding integral

$$W_\lambda(z_1, z_2)W_\nu(z_1, z_2) = \int_{-\infty}^\infty \rho(\lambda, \nu, \kappa)W_\kappa(z_1, z_2)\kappa d\kappa, \tag{69}$$

one should compute the Mehler–Fock transform of $W_\lambda(\zeta)W_\nu(\zeta)$. This amounts to the following integral:

$$h_d(\lambda, \nu, \kappa) = \int_1^\infty P_{-\frac{1}{2}+i\lambda}^{-\frac{d-2}{2}}(u)P_{-\frac{1}{2}+i\nu}^{-\frac{d-2}{2}}(u)P_{-\frac{1}{2}+i\kappa}^{-\frac{d-2}{2}}(u)(u^2-1)^{-\frac{d-2}{4}} du \tag{70}$$

and the Källén–Lehmann weight is

$$\rho(\lambda, \nu, \kappa) = \frac{\Gamma\left(\frac{d-1}{2} + i\nu\right)\Gamma\left(\frac{d-1}{2} - i\nu\right)\Gamma\left(\frac{d-1}{2} + i\lambda\right)\Gamma\left(\frac{d-1}{2} - i\lambda\right) \sinh(\pi\kappa) h_d(\lambda, \nu, \kappa)}{2(2\pi)^{1+\frac{d}{2}}}. \tag{71}$$

The evaluation of $h_d(\lambda, \nu, \kappa)$ is very far from obvious. In the particular case where the two masses are equal, $h_d(\lambda, \lambda, \kappa)$ may be evaluated by Mellin transform techniques, used for the first time in the de Sitter context in [18,19]. The same idea of using Mellin techniques was used a few years later to compute the Källén–Lehmann weight in the case of two equal masses [20] in AdS QFT³.

The general case of two independent masses cannot be dealt with by Mellin transformation techniques, and something more similar to the Fourier transform of flat space is needed. It is precisely at this point that the plane-wave representation (61) makes a substantial difference.

An especially important Fourier-type representation is obtained by evaluating (61) at the purely imaginary events in the tubes [22]: $z = -iy \in \mathcal{T}^-$ and $z = +iy' \in \mathcal{T}^+$. y and y' can be visualised as points belonging to a Lobachevsky space, modelled as the upper sheet of a two-sheeted hyperboloid:

$$H_d = \{y \in \mathbb{M}_{1,d} : y^2 = y \cdot y = R^2, y^0 > 0\}. \tag{72}$$

It follows that

$$\begin{aligned} w_\nu(-iy, iy') &= \frac{\Gamma\left(\frac{d-1}{2} + i\nu\right)\Gamma\left(\frac{d-1}{2} - i\nu\right)}{2^{d+1}\pi^d} \int_\gamma (y \cdot \xi)^{-\frac{d-1}{2}+i\nu} (\xi \cdot y')^{-\frac{d-1}{2}-i\nu} d\mu_\gamma(\xi) \\ &= \frac{\Gamma\left(\frac{d-1}{2} + i\nu\right)\Gamma\left(\frac{d-1}{2} - i\nu\right)}{2(2\pi)^{\frac{d}{2}}} \left((y \cdot y')^2 - 1\right)^{-\frac{d-2}{4}} P_{-\frac{1}{2}+i\nu}^{-\frac{d-2}{2}}(y \cdot y'). \end{aligned} \tag{73}$$

By choosing, in particular, $\gamma = \gamma_0$ and $y' = (1, 0, \dots, 0)$ so that $y \cdot y' = y^0 = u \geq 1$, we then obtain the following integral representation:

$$(u^2 - 1)^{-\frac{d-2}{4}} P_{-\frac{1}{2}+i\nu}^{-\frac{d-2}{2}}(u) = \frac{1}{(2\pi)^{\frac{d}{2}}} \int_{\gamma_0} (y \cdot \xi)^{-\frac{d-1}{2}-i\nu} d\mu_{\gamma_0}. \tag{74}$$

This formula is of crucial importance for computing $h_d(\lambda, \nu, \kappa)$: it allows us to rewrite the one-dimensional integral (70) as the following multiple integrals over the manifold $H_d \times S_{d-1} \times S_{d-1} \times S_{d-1}$:

$$h_d(\lambda, \nu, \kappa) = \frac{(2\pi)^{-\frac{3d}{2}}}{\omega_{d-1}} \int_{\gamma_0} \int_{\gamma_0} \int_{\gamma_0} \int_{H_d} (y \cdot \xi_1)^{-\frac{d-1}{2}-i\lambda} (y \cdot \xi_2)^{-\frac{d-1}{2}-i\nu} (y \cdot \xi_3)^{-\frac{d-1}{2}-i\kappa} dy d\mu_{\gamma_0} d\mu_{\gamma_0} d\mu_{\gamma_0} \tag{75}$$

where dy is the Lorentz-invariant measure on H_d . The above integral may be computed, and the final result is [22]

$$\rho(\lambda, \nu, \kappa) = \frac{1}{2^d \pi^{\frac{d-1}{2}} \kappa \Gamma\left(\frac{d-1}{2}\right)} \frac{\prod_{\epsilon, \epsilon', \epsilon'' = \pm 1} \Gamma\left(\frac{d-1}{4} + \frac{i\epsilon\lambda + i\epsilon'\nu + i\epsilon''\kappa}{2}\right)}{\prod_{\epsilon = \pm 1} \Gamma\left(\frac{i\epsilon\kappa}{2}\right) \Gamma\left(\frac{1}{2} + \frac{i\epsilon\kappa}{2}\right) \Gamma\left(\frac{d-1}{4} + \frac{i\epsilon\kappa}{2}\right) \Gamma\left(\frac{d+1}{4} + \frac{i\epsilon\kappa}{2}\right)}. \tag{76}$$

The application of this formula and its AdS twin to loop calculations are discussed in [23,24].

6. Anti-de Sitter

The anti-de Sitter spacetime can also be visualised as a hypersurface embedded in an ambient flat space, which is \mathbf{R}^{d+1} with two timelike directions and metric mostly minus, as follows:

$$AdS_d = \{x \in \mathbf{R}^{d+1} : x^2 = x \cdot x = R^2\}, \tag{77}$$

$$x \cdot y = x^0 y^0 - x^1 y^1 - \dots - x^{d-1} y^{d-1} + x^d y^d. \tag{78}$$

The AdS manifold has a boundary at spacelike infinity and, therefore, is not globally hyperbolic. This feature gives AdS QFT a little extra complication with respect to the standard globally hyperbolic case.

We also have to consider the complexification of the AdS manifold, which is defined as before by an embedding:

$$AdS_d^{(c)} = \{z = x + iy \in \mathbf{C}^{d+1} : z^2 = R^2\}. \tag{79}$$

While $AdS_d^{(c)}$ is simply connected, the real manifold AdS_d is not and admits a nontrivial universal covering space \widetilde{AdS}_d . Here, we focus mainly on the uncovered manifold AdS_d .

The symmetry group of the anti-de Sitter spacetime is the pseudo-orthogonal group of the ambient space $SO(2, d - 1)$. This group may also be regarded as the conformal group of transformations of the boundary, represented as the null cone of the ambient space

$$C_d = \{\xi \in \mathbf{R}^{d+1} : \xi^2 = \xi \cdot \xi = 0\}. \tag{80}$$

This simple geometrical fact lies at the basis of the AdS/CFT correspondence. The null cone of the ambient space also plays the role of giving a causal order to the AdS spacetime, which is, however, only *local* due to the existence of closed timelike curves. Two events are spacelike separated if

$$(x_1 - x_2)^2 = 2 - 2x_1 \cdot x_2 < 0. \tag{81}$$

The covering manifold is globally causal but remains non-globally hyperbolic (see Figures 3 and 4).

It is possible to identify in the complex manifold $AdS_d^{(c)}$ an analogue of the Euclidean subspace of the complex Minkowski spacetime: it is the real submanifold H_d of $AdS_d^{(c)}$ defined by

$$H_d = \{z \in \mathbf{C}^{d+1} : z \cdot z = R^2, z(y) = (y^0, \dots, y^{d-1}, iy^d), y^\mu \in \mathbf{R}, y^0 > 0\}. \tag{82}$$

This is indeed the same Lobachevsky space we met before in (72) at the end of the de Sitter tubes, but it has, of course, a different interpretation in the AdS context, and, more importantly, AdS correlation functions have singularities at coincident Euclidean points of H_d , while dS correlation functions do not.

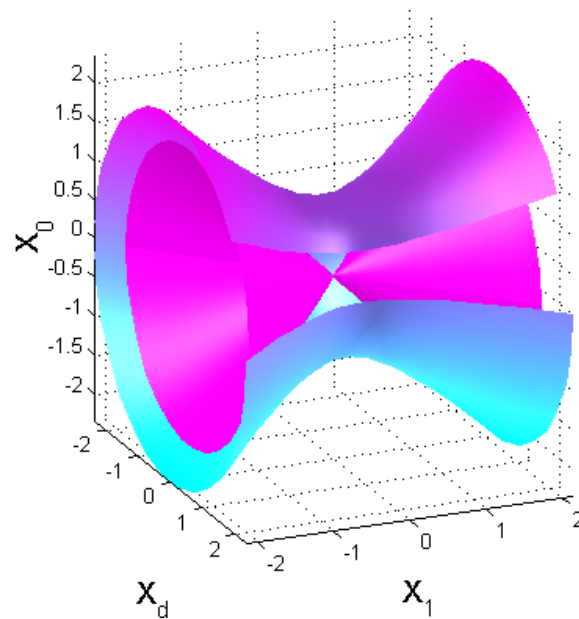


Figure 3. The AdS manifold and the null cone of the ambient space, which models its boundary at spacelike infinity.

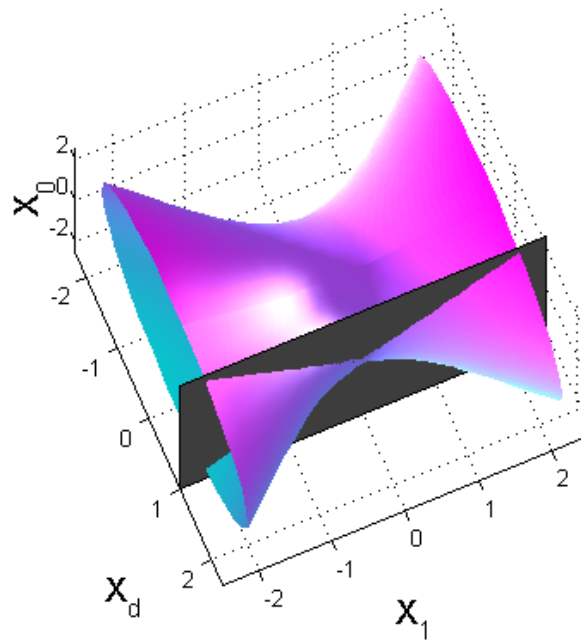


Figure 4. The null cone of the ambient space induces a causal order on the AdS manifold, which is only local.

6.1. The Analytic Structure of Two-Point Functions

The status of AdS QFT is more similar to that of Minkowski space, and it is possible to formulate a true spectral condition. This question was studied in full generality in [25]. A simplified account can be found in [26]. The point is that the parameter of the group of rotations in the $(0, d)$ -plane may be interpreted as a global time variable: the AdS spectral condition is thus formulated by requiring that the corresponding generator M_{0d} be represented in the Hilbert space of the theory by a self-adjoint operator whose spectrum is positive. As in flat space, this requirement is equivalent to the precise analyticity properties of the n -point functions [25].

In particular, there are two distinguished complex domains of $AdS_d^{(c)}$, invariant under real AdS transformations [25,26], defined as follows (see Figure 5)

$$\mathcal{Z}_+ = \{z = x + iy \in AdS_d^{(c)}; y^2 > 0, \epsilon(z) = +1\}, \tag{83}$$

$$\mathcal{Z}_- = \{z = x + iy \in AdS_d^{(c)}; y^2 > 0, \epsilon(z) = -1\}, \tag{84}$$

where

$$\epsilon(z) = \text{sign}(y^0 x^d - x^0 y^d). \tag{85}$$

The tubes \mathcal{Z}_+ and \mathcal{Z}_- have a definite chirality and wrap the real AdS manifold in opposite directions. The spaces \mathcal{Z}_+ , \mathcal{Z}_- , and AdS_d have the same homotopy type. Their universal coverings are denoted as $\tilde{\mathcal{Z}}_+$ and $\tilde{\mathcal{Z}}_-$.

The AdS spectral condition implies that a general two-point function satisfies the following property [25].

Normal analyticity property: $\mathcal{W}(x_1, x_2)$ is the boundary value of a function $W(z_1, z_2)$ holomorphic in the domain $\mathcal{Z}_- \times \mathcal{Z}_+$

$$\mathcal{W}(x_1, x_2) = \langle \Psi_0, \hat{\phi}(x_1) \hat{\phi}(x_2) \Psi_0 \rangle = \underset{\substack{\mathcal{Z}_- \ni z_1 \rightarrow x_1 \\ \mathcal{Z}_+ \ni z_2 \rightarrow x_2}}{\text{b.v.}} W(z_1, z_2). \tag{86}$$

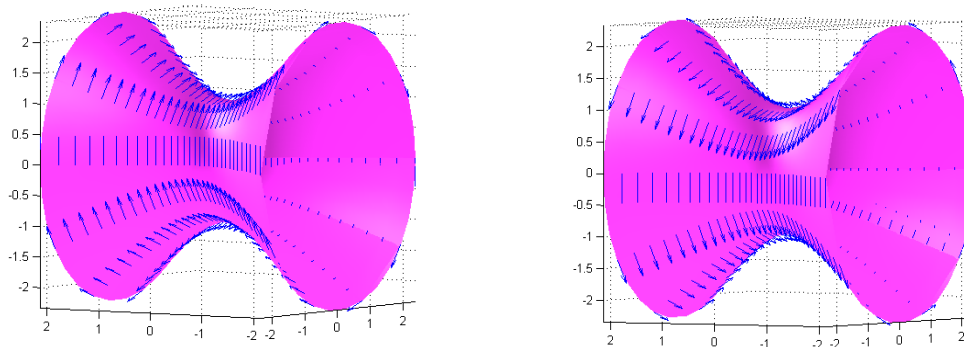


Figure 5. Sections of the backward and forward tubes in the complex AdS manifold. The tubes wrap the real manifold in opposite directions. The arrows are the imaginary parts y of the vectors $z = x + iy$ parts attached at the end of the real parts x , which varies on the hyperboloid whose radius is $R^2 + y^2$. Here is represented the section at a fixed positive value of y^2 . Recall that $x \cdot y = 0$.

AdS invariance and normal analyticity imply the following.

- Theorem 4** (Maximal analyticity property). 1. The two-point function $W(z_1, z_2)$ depends only on the AdS-invariant variable $\zeta = z_1 \cdot z_2$.
 2. $W(z_1, z_2)$ can be continued to a function $\mathfrak{W}(z_1, z_2)$ analytic in the cut domain

$$\Delta_1 = \{\mathbf{C} \setminus [-1, 1]\}. \tag{87}$$

3. $\mathfrak{W}(z_1, z_2)$ is invariant under the action of the complex de Sitter group.
 4. The permuted two-point function is the boundary value of $\mathfrak{W}(z_1, z_2)$ from the opposite tube $\mathcal{Z}_{21} = \mathcal{Z}_+ \times \mathcal{Z}_-$.
 5. The cut domain Δ_1 contains all the non-coinciding Euclidean points

$$\mathcal{E} = \{z_1, z_2 \in \Delta, z_1 \in S_d, z_2 \in H_d, z_1 \neq z_2\}. \tag{88}$$

The Schwinger function S is the restriction of $\mathfrak{W}(z_1, z_2)$ to the non-coincident Euclidean points \mathcal{E} . S is analytic in \mathcal{E} and can be extended as a distribution to the whole Euclidean space \mathcal{E} , including the coinciding points.

Regarding the global hyperbolicity issue, the maximal analytic structure completely determines the two-point functions for Klein–Gordon fields and, consequently, selects the boundary behaviour of the modes.

6.2. Klein–Gordon Fields and Plane Waves

Klein–Gordon fields display the simplest example of the previous analytic structure. For a given mass m , the two-point function $\mathcal{W}(x_1, x_2)$ must satisfy the equation

$$(\square_{x_i} + m^2)\mathcal{W}(x_1, x_2) = 0, \quad i = 1, 2, \tag{89}$$

with respect to both variables, where \square_{x_i} is the Laplace–Beltrami operator relative to the AdS metric. The two-point functions are labelled by the (complex) dimension d and a (complex) parameter ν as follows:

$$W_\nu^d(z_1, z_2) = w_\nu^d(\zeta) = \frac{1}{(2\pi)^{\frac{d}{2}}} (\zeta^2 - 1)^{-\frac{d-2}{4}} e^{-i\pi\frac{d-2}{2}} Q_{-\frac{1}{2}+\nu}^{\frac{d-2}{2}}(\zeta) = \tag{90}$$

$$= \frac{\Gamma\left(\frac{d-1}{2} + \nu\right)}{2\pi^{\frac{d-1}{2}} (2\zeta)^{\frac{d-1}{2}+\nu} \Gamma(\nu+1)} {}_2F_1\left(\frac{d-1}{4} + \frac{\nu}{2}, \frac{d+1}{4} + \frac{\nu}{2}; \nu+1; \frac{1}{\zeta^2}\right) \tag{91}$$

where the various parameters are related as follows:

$$m^2 = \nu^2 - \frac{(d-1)^2}{4}. \tag{92}$$

There are two possible cases:

1. For $\nu > 1$, the spectrum condition uniquely selects one field theory for each given value of mass parameter ν ;
2. For $|\nu| < 1$, there are two acceptable theories for each given mass.

The difference between the two theories lies in their large distance behaviour. More precisely, in view of [17], Equation (3.3.1.4), one has

$$w_{-\nu}^d(\zeta) = w_\nu^d(\zeta) + \frac{\sin \pi\nu \Gamma\left(\frac{d-1}{2} - \nu\right) \Gamma\left(\frac{d-1}{2} + \nu\right)}{(2\pi)^{\frac{d}{2}}} (\zeta^2 - 1)^{-\frac{d-2}{4}} P_{-\frac{1}{2}-\nu}^{-\frac{d-2}{2}}(\zeta). \tag{93}$$

The last term in this relation is *regular on the cut* $\zeta \in [-1, 1]$ and, therefore, does not contribute to the commutator. By consequence, the two theories represent the same algebra of local observables at short distances. But since the second term at the right-hand side grows faster as $|\nu|$ increases (see [17], Equation (3.9.2)), the two theories have drastically different long-range behaviours.

Let us now proceed to the harmonic analysis in plane waves for the AdS correlation functions. Here, to keep the discussion as simple as possible, we limit ourselves to the two-dimensional uncovered anti-de Sitter spacetime AdS_2 [27]. A full analysis will be presented elsewhere.

As for the de Sitter case, the wave solutions of the anti-de Sitter Klein–Gordon equation may also be parameterised by the choice of a null vector $\zeta \in C_2$ and a complex number λ , as follows:

$$\psi_\lambda(z, \zeta) = (z \cdot \zeta)^\lambda = e^{\lambda \log(z \cdot \zeta)}. \tag{94}$$

Since we are considering the uncovered manifold, the parameter λ must be an integer:

$$\lambda = \ell. \tag{95}$$

Now, we observe that while Equation (50) maintains its validity in the present context, for real ξ, η belonging to the null cone C_2 , it describes spacelike geodesics. Timelike geodesics would correspond to vectors ξ belonging to the complex cone

$$C_2^{(c)} = \{\xi \in \mathbb{C}^3 : \xi^2 = \xi \cdot \xi = 0\}. \tag{96}$$

This suggests that the harmonic analysis of the AdS correlation function should also be made in terms of waves parametrised by null complex vectors ξ .

The complex cone $C_2^{(c)}$ admits the partition $C_2^{(c)} = C_{2+} \cup C_{2-}$, where

$$C_{2+} = \{\xi \in C^{(c)}; \epsilon(\xi) = +\}, \tag{97}$$

$$C_{2-} = \{\xi \in C^{(c)}; \epsilon(\xi) = -\}; \tag{98}$$

and as before,

$$\epsilon(z) = \text{sign}[(\text{Im } \xi^0)(\text{Re } \xi^2) - (\text{Re } \xi^2)(\text{Im } \xi^2)]. \tag{99}$$

The bases for the cones C_{2+} and C_{2-} are

$$(\gamma_0^{(c)})_+ = \{\xi = \xi(\Phi) = (\sin \Phi, 1, \cos \Phi); \Phi = \phi + i\eta, \eta > 0\}, \tag{100}$$

$$(\gamma_0^{(c)})_- = \{\xi = \xi(\Phi) = (\sin \Phi, 1, \cos \Phi); \Phi = \phi + i\eta, \eta < 0\}. \tag{101}$$

Let us now consider the integral

$$\int_{\gamma(z_1)} [z_1 \cdot \xi]^\ell [\xi \cdot z_2]^{-\ell-1} d\mu_{\gamma^{(c)}}(\xi), \quad z_1 \text{ in } \mathcal{Z}_-, \quad z_2 \text{ in } \mathcal{Z}_+. \tag{102}$$

For each z_1 in \mathcal{Z}_- , $\gamma(z_1)$ is a relative cycle in $H^1(C_2^{(c)}, \{\xi; [z \cdot \xi] = 0\})$ with support contained in C_{2-} and end points belonging, respectively, to the two linear generatrices of the cone $C_2^{(c)}$ defined by $[z_1 \cdot \xi] = 0$. Being the integral of a closed differential form, (102) does not depend on the choice of $\gamma(z_1)$ inside its homology class.

There is no loss of generality in defining the integration cycle $\gamma(z_1)$ only for points of the form

$$z_1 = z_v = (i \sinh v, 0, \cosh v), \quad v < 0. \tag{103}$$

We choose the path

$$\phi \rightarrow \xi(\phi + iv) = (\sin(\phi + iv), 1, \cos(\phi + iv)), \quad -\frac{\pi}{2} < \phi < \frac{\pi}{2}. \tag{104}$$

The support of $\gamma(z_v)$ does belong to C_{2-} , and $[z_v \cdot \xi(\phi + iv)] = \cos(\phi)$ vanishes, as required, at the boundaries of the cycle.

Since $z_2 \in \mathcal{Z}_+$, the factor $[\xi \cdot z_2]^{-\ell-1}$ never becomes singular on the integration cycle $\gamma(z_v)$. This may be seen by explicitly giving coordinates to \mathcal{Z}_+ [27]. This suffices to show the AdS invariance of the integral (102), which is, therefore, a function of the invariant variable $\zeta = z_1 \cdot z_2$, holomorphic in the cut domain Δ_1 .

To actually compute (102), we choose the second point at the origin $x_0 = (0, 0, 1)$ so that $z_1 \cdot z_2 = z_v \cdot x_0 = \cosh v$. With a few self-explanatory changes of variables, we obtain [17], Equation (2), p. 155:

$$\begin{aligned} & \int_{\gamma(z_v)} [z_v \cdot \xi]^\ell [\xi \cdot x_0]^{-\ell-1} d\mu_\gamma(\xi) = \\ & = \int_{-\frac{\pi}{2}}^{\frac{\pi}{2}} \cos^\ell \phi \cos^{-(\ell+1)}(\phi + iv) \, d\phi = \int_{-\infty}^{\infty} (\cosh v - it \sinh v)^{-(\ell+1)} \frac{dt}{(1+t^2)^{\frac{1}{2}}} \\ & = 2 \int_0^\infty (\cosh v + \cosh u \sinh v)^{-(\ell+1)} du = 2Q_I(\cosh v). \end{aligned} \tag{105}$$

Therefore, we can write the following plane-wave expansion of the two-point function:

$$W_{l+\frac{1}{2}}^2(z_1, z_2) = \frac{1}{\pi} \int_{\gamma(z_v)} [z_v \cdot \xi]^\ell [\xi \cdot x_0]^{-\ell-1} d\mu_\gamma(\xi). \quad (106)$$

7. Conclusions and Outlook

There is a unifying feature that connects Minkowski, de Sitter, and anti-de Sitter quantum field theories: the analyticity properties of the correlation functions of the quantum fields in the relevant tubular domains of the corresponding complex manifolds [10,12,25]. These analyticity properties are, in the Minkowski and the anti-de Sitter cases, a consequence of the spectral condition, i.e., a consequence of the requirement that the Hamiltonian operator has a positive spectrum in every Lorentz frame. The reconstruction procedures actually show that the analyticity properties are equivalent to the spectral condition [8,25]. In the de Sitter case, the analyticity of the correlation functions may be taken as a replacement of the spectral condition since there exists no globally defined conserved energy operator in the de Sitter geometry. Taking seriously the analyticity properties of correlation functions seriously has produced valuable nontrivial results, which, at the moment, seem to be out of reach of other methods, such as the Källén–Lehmann representations of two-point functions [10,21,22] and the calculation of one- and two-loop Feynman diagrams for both the de Sitter and anti-de Sitter cases. There are many opportunities opened by this formalism and lots of things to do. This review is also an invitation to readers interested in either dS or AdS quantum field theory to join the effort.

Funding: This research received no external funding.

Data Availability Statement: Data are contained within the article.

Acknowledgments: I would like to thank the Department of Theoretical Physics of CERN and its director Gian F. Giudice for their warm hospitality and support while writing this paper.

Conflicts of Interest: The authors declare no conflicts of interest.

Notes

- ¹ *Sphaera infinita cuius centrum est ubique, circumferentia tamen nullibi* is the second definition of God that can be read in the Liber XXIV philosophorum, an anonymous medieval treatise attributed to Hermes Trismegistus. Nicolas de Cues applied this definition to the Universe: The world machine has, so to speak, its centre everywhere and its circumference nowhere (La Docte Ignorance, 1440). Giordano Bruno later adopted this definition in various works. Einstein's novelty was that his sphere was not infinite but rather finite and curved.
- ² Apart from the nonlinear (and hard to verify) positivity condition of the correlation functions necessary to reconstruct a Hilbert space.
- ³ At the very same time, however, a general Källén–Lehmann formula for AdS fields with two different masses was for the first time published and available [21]. But many subsequent authors seem to have ignored it.

References

1. Einstein, A. *Cosmological Considerations in the General Theory of Relativity*; Sitzungsber. Preuss. Akad. Wiss. Berlin (Math. Phys.); 1917; Volume 6, pp. 142–152.
2. Friedmann, A.A. Über die Krümmung des Raumes. *Z. Phys.* **1922**, *10*, 377–386. [CrossRef]
3. Friedmann, A.A. Über die Möglichkeit einer Welt mit konstanter negativer Krümmung des Raumes. *Z. Phys.* **1924**, *21*, 326–332. [CrossRef]
4. Lemaître, G. Un univers homogène de masse constante et de rayon croissant, rendant compte de la vitesse radiale des nébuleuses extra-galactiques. *Ann. Soc. Sci. Brux. A* **1927**, *47*, 49–59.
5. Riess, A.G.; Filippenko, A.V.; Challis, P.; Clocchiatti, A.; Diercks, A.; Garnavich, P.M.; Gilliland, R.L.; Hogan, C.J.; Jha, S.; Kirshner, R.P.; et al. Observational Evidence from Supernovae for an Accelerating Universe and a Cosmological Constant. *Astron. J.* **1998**, *116*, 1009–1038. [CrossRef]
6. Perlmutter, S.; Aldering, G.; Goldhaber, G.; Knop, R.A.; Nugent, P.; Castro, P.G.; Deustua, S.; Fabbro, S.; Goobar, A.; Groom, D.E.; et al. Measurements of Ω and Λ from 42 High-Redshift Supernovae. *Astron. J.* **1999**, *517*, 565. [CrossRef]
7. Maldacena, J.M. The Large N limit of superconformal field theories and supergravity. *Adv. Theor. Math. Phys.* **1998**, *2*, 231–252. [CrossRef]

8. Streater, R.F.; Wightman, A.S. *PCT, Spin and Statistics, and All That*; Benjamin: New York, NY, USA, 1964.
9. Gelfand, I.M.; Shilov, G.E. *Generalized Functions*; Academic Press: New York, NY, USA, 1964.
10. Bros, J.; Moschella, U. Two point functions and quantum fields in de Sitter universe. *Rev. Math. Phys.* **1996**, *8*, 327–392. [CrossRef]
11. Gibbons, G.W.; Hawking, S.W. Cosmological event horizons, thermodynamics, and particle creation. *Phys. Rev. D* **1977**, *10*, 2738–2751. [CrossRef]
12. Bros, J.; Epstein, H.; Moschella, U. Analyticity properties and thermal effects for general quantum field theory on de Sitter space-time. *Commun. Math. Phys.* **1998**, *196*, 535–570. [CrossRef]
13. Cacciatori, S.; Gorini, V.; Kamenshchik, A.; Moschella, U. Conservation laws and scattering for de Sitter classical particles. *Class. Quant. Grav.* **2008**, *25*, 075008. [CrossRef]
14. Bros, J.; Epstein, H.; Moschella, U. The Asymptotic symmetry of de Sitter space-time. *Phys. Rev. D* **2002**, *65*, 084012. [CrossRef]
15. Bros, J.; Epstein, H.; Moschella, U. Scalar tachyons in the de Sitter universe. *Lett. Math. Phys.* **2010**, *93*, 203–211. [CrossRef]
16. Epstein, H.; Moschella, U. de Sitter tachyons and related topics. *Commun. Math. Phys.* **2015**, *336*, 381–430. [CrossRef]
17. Erdélyi, A. (Ed.) *The Bateman Project: Higher Transcendental Functions*; McGraw-Hill Book Company: New York, NY, USA, 1953; Volume I.
18. Bros, J.; Epstein, H.; Moschella, U. Lifetime of a massive particle in a de Sitter universe *J. Cosmol. Astropart. Phys.* **2008**, *2008*, 003. [CrossRef]
19. Bros, J.; Epstein, H.; Moschella, U. Particle decays and stability on the de Sitter universe. *Ann. Henri Poincaré* **2010**, *11*, 611–658. [CrossRef]
20. Fitzpatrick, A.L.; Kaplan, J. Analyticity and the Holographic S-Matrix. *J. High Energy Phys.* **2012**, *10*, 127. [CrossRef]
21. Bros, J.; Epstein, H.; Gaudin, M.; Moschella, U.; Pasquier, V. Anti de Sitter quantum field theory and a new class of hypergeometric identities. *Commun. Math. Phys.* **2012**, *309*, 255–291. [CrossRef]
22. Bros, J.; Epstein, H.; Gaudin, M.; Moschella, U.; Pasquier, V. Triangular invariants, three-point functions and particle stability on the de Sitter universe. *Commun. Math. Phys.* **2010**, *295*, 261–288. [CrossRef]
23. Cacciatori, S.L.; Epstein, H.; Moschella, U. Loops in de Sitter space. *arXiv* **2024**, arXiv:2403.13145.
24. Cacciatori, S.L.; Epstein, H.; Moschella, U. Loops in Anti de Sitter space. *arXiv* **2024**, arXiv:2403.13142.
25. Bros, J.; Epstein, H.; Moschella, U. Towards a general theory of quantized fields on the anti-de Sitter space-time. *Commun. Math. Phys.* **2002**, *231*, 481–528. [CrossRef]
26. Bertola, M.; Bros, J.; Moschella, U.; Schaeffer, R. A general construction of conformal field theories from scalar anti-de Sitter quantum field theories. *Nucl. Phys.* **2000**, *587*, 619–644. [CrossRef]
27. Bros, J.; Moschella, U. Fourier analysis and holomorphic decomposition on the one-sheeted hyperboloid. In *Géométrie Complexe II. Aspects Contemporains dans les Mathématiques et la Physique*; Norguet, F., et Ofman, S., Szczeciniarz, J.-J., Eds.; Hermann: Paris, France, 2003; Volume II, pp. 100–145.

Disclaimer/Publisher’s Note: The statements, opinions and data contained in all publications are solely those of the individual author(s) and contributor(s) and not of MDPI and/or the editor(s). MDPI and/or the editor(s) disclaim responsibility for any injury to people or property resulting from any ideas, methods, instructions or products referred to in the content.

DeWitt Boundary Condition in One-Loop Quantum Cosmology

Giampiero Esposito ^{1,2}

¹ Dipartimento di Fisica "Ettore Pancini", Complesso Universitario di Monte S. Angelo, Via Cintia Edificio 6, 80126 Napoli, Italy; gesposito@na.infn.it

² INFN Sezione di Napoli, Complesso Universitario di Monte S. Angelo, Via Cintia Edificio 6, 80126 Napoli, Italy

Abstract: DeWitt's suggestion that the wave function of the universe should vanish at the classical Big Bang singularity is considered here within the framework of one-loop quantum cosmology. For pure gravity at one loop about a flat four-dimensional background bounded by a 3-sphere, three choices of boundary conditions are considered: vanishing of the linearized magnetic curvature when only transverse-traceless gravitational modes are quantized; a one-parameter family of mixed boundary conditions for gravitational and ghost modes; and diffeomorphism-invariant boundary conditions for metric perturbations and ghost modes. A positive $\zeta(0)$ value in these cases ensures that, when the three-sphere boundary approaches zero, the resulting one-loop wave function approaches zero. This property may be interpreted by saying that, in the limit of small three-geometry, the resulting one-loop wave function describes a singularity-free universe. This property holds for one-loop functional integrals, which are not necessarily equivalent to solutions of the quantum constraint equations.

Keywords: quantum cosmology; boundary conditions; strong ellipticity; spectral ζ -function



Citation: Esposito, G. DeWitt Boundary Condition in One-Loop Quantum Cosmology. *Universe* **2023**, *9*, 187. <https://doi.org/10.3390/universe9040187>

Academic Editors: Galina L. Klimchitskaya, Vladimir M. Mostepanenko and Sergey V. Sushkov

Received: 9 March 2023

Revised: 11 April 2023

Accepted: 13 April 2023

Published: 14 April 2023



Copyright: © 2023 by the author. Licensee MDPI, Basel, Switzerland. This article is an open access article distributed under the terms and conditions of the Creative Commons Attribution (CC BY) license (<https://creativecommons.org/licenses/by/4.0/>).

1. Introduction

After the birth of relativistic cosmology thanks to Friedmann's work [1], and the subsequent proof of the singularity theorems of Penrose, Hawking, and Geroch [2–7], it became well-accepted by the scientific community that classical general relativity leads to the occurrence of cosmological singularities (a spacetime being singular if it is timelike or null geodesically incomplete) in a generic way. Since then, several developments occurred, and in particular, we here mention what follows.

- (i) At the classical level, the work of Christodoulou and Klainerman [8] led to the discovery of asymptotically flat spacetimes, which are timelike geodesically complete.
- (ii) At the quantum level, DeWitt [9] proposed to look at the behavior of the wave function of the universe in correspondence with the classical Big Bang singularity. Such a proposal was assessed in the outstanding work in Ref. [10].
- (iii) Over many years, various concepts of singularity have been conceived, as can be seen in an important review of Kamenshchik [11].

Moreover, in the literature on quantum gravity and quantum cosmology, several approaches were developed to study the possible quantum origin of spacetime geometry. One-loop effects in the early universe were investigated in detail, especially with the help of ζ -function methods. It is the aim of our review to describe them and then discuss their relevance for the singularity issue in cosmology. The structure of the paper is as follows.

Section 2 presents in detail a $\zeta(0)$ calculation when only transverse-traceless perturbations are considered, with boundary conditions requiring the vanishing of linearized magnetic curvature on the three-sphere boundary. Section 3 discusses a one-parameter family of $\zeta(0)$ values obtained with mixed boundary conditions for metric perturbations and ghost fields. Sections 4–7 outline the basic steps of the $\zeta(0)$ calculation with diffeomorphism-invariant boundary conditions. Open problems are discussed in Section 8.

2. Linearized Magnetic Curvature Vanishing on S^3

We study pure gravity at one loop about flat Euclidean four-space with a three-sphere boundary of radius a , because when $a \rightarrow 0$, this is the limiting case of a four-sphere geometry bounded by a three-sphere [12]. The prefactor of the semiclassical wave function is given by the following (with I_2 denoting the part of the action quadratic in metric perturbations)

$$P(a) = \int e^{-I_2[\gamma]} D\gamma, \tag{1}$$

which is a functional integral over all metric perturbations γ_{ab} that are regular at the origin $\tau = 0$ and satisfy a given boundary condition at $\tau = a$. Integration is here restricted to the physical degrees of freedom, which are found by using the Hamiltonian formulation with the following transverse-traceless choice of gauge condition:

$$\sum_i (D^i \gamma)_{ij} = 0, \quad \sum_k \gamma_k^k = 0. \tag{2}$$

These relations pick out the transverse-traceless tensor hyperspherical harmonics $G_{ij}^{(n)}(\phi^k)$ multiplied by functions of the radial coordinate τ . Hence, we write

$$\gamma_{ij} = \gamma_{ij}^{TT} = \sum_{n=3}^{\infty} q^n(\tau) G_{ij}^{(n)}(\phi^k). \tag{3}$$

Our work in Ref. [13] studied the Breitenlohner–Freedman–Hawking [14,15] local boundary conditions for fields of spin $0, \frac{1}{2}, 1, \frac{3}{2}, 2$. For gravity, these imply that the linearized magnetic curvature should vanish at the boundary. Our detailed analysis in Section 7.3 of Ref. [13] never appeared in any journals, and hence it is of interest to our review article.

The action that is quadratic in metric perturbations involves a second-order elliptic operator A with eigenvalues λ_n , for which one can define a spectral ζ -function

$$\zeta_A(s) = \text{Tr}_{L^2} A^{-s} = \sum_n (\lambda_n)^{-s}. \tag{4}$$

Eventually, as was shown by Schleich [12], the prefactor of the semiclassical wave function of Equation (1), with γ having the form (3), can be expressed as

$$P(a) = \frac{1}{\sqrt{\det\left(\frac{-\nabla_f \nabla^f}{4\pi l_p^2 \mu^2}\right)}} = D a^{\zeta(0)}, \tag{5}$$

where $-\nabla_f \nabla^f$ is the Laplacian acting on transverse-traceless metric perturbations, and $\zeta(0)$ is the value at $s = 0$ of the analytic continuation of the spectral ζ -function (4) (for further details, see now the Appendix A on the one-loop approximation). Thus, within a functional-integral framework, the wave function of the universe may fulfill the DeWitt boundary condition if and only if $\zeta(0)$ is positive.

The linearized magnetic curvature for gravity is defined from the Weyl tensor C and from the normal n to the boundary according to the rule (with summation over repeated tensor indices)

$$B_{ij} \equiv \frac{1}{2} \epsilon_{j\mu}{}^{kl} C_{kliv} n^\mu n^\nu,$$

and it can only vanish on S^3 if [13]

$$\sum_{n=3}^{\infty} \frac{dq^n}{d\tau}(a) \epsilon_j{}^{kl} \left(G_{il|k}^{(n)} - G_{ik|l}^{(n)} \right) = 0. \tag{6}$$

The only condition on the modes that ensures the validity of (6) is

$$\frac{dq^n}{d\tau}(a) = 0, \forall n \geq 3. \tag{7}$$

We are now interested in evaluating $\zeta(0)$ using (7). Thus, after setting $\tau = t$, we study the kernel of the heat equation for the operator

$$P_n \equiv -\left(\frac{d^2}{dt^2} - \frac{1}{t} \frac{d}{dt} - \frac{(n^2 - 1)}{t^2}\right), \forall n \geq 3, \tag{8}$$

which results from studying the Laplacian on transverse-traceless metric perturbations. On denoting by $E > 0$ the eigenvalues of P_n , we find that its eigenfunctions regular at the origin are (up to a multiplicative constant)

$$u_n(t) = tJ_n(\sqrt{Et}) = q^n(t). \tag{9}$$

Thus, the boundary condition (7) implies the eigenvalue condition

$$J_n(\sqrt{Ea}) + \sqrt{Ea}J'_n(\sqrt{Ea}) = 0, \forall n \geq 3. \tag{10}$$

This equation is of the general kind studied in Ref. [16]. Setting now $a = 1$ for simplicity, we define the function

$$F_n(z) \equiv J_n(z) + zJ'_n(z), \forall n \geq 3. \tag{11}$$

Of course, the consideration of such $F_n(z)$ is suggested by (10). It only has real simple zeros apart from $z = 0$ (page 482 of Ref. [17]). The basic idea is now the following [16]. Given the zeta-function at large x

$$\zeta(s, x^2) \equiv \sum_n (\lambda_n + x^2)^{-s}, \tag{12}$$

one has, in four dimensions (see Theorem 2 on page 6 of Ref. [18]),

$$\Gamma(3)\zeta(3, x^2) = \int_0^\infty t^2 e^{-x^2 t} G(t) dt \sim \sum_{n=0}^\infty B_n \Gamma\left(1 + \frac{n}{2}\right) x^{-n-2}, \tag{13}$$

where we have used the asymptotic expansion of the heat kernel for $t \rightarrow 0^+$, i.e.,

$$G(t) \sim \sum_{n=0}^\infty B_n t^{\frac{n}{2}-2}. \tag{14}$$

Strictly speaking, since we have not proved general results on the existence of the asymptotic expansion of the heat kernel, our Formula (14) could be initially regarded as an assumption. However, existence theorems hold for the problems studied in this paper [19,20].

On the other hand, one also has the identity

$$\Gamma(3)\zeta(3, x^2) = -\sum_{p=0}^\infty N_p \left(-\frac{1}{2x} \frac{d}{dx}\right)^3 \log\left((ix)^{-p} F_p(ix)\right), \tag{15}$$

where N_p is the degeneracy of the problem. Thus the comparison of (13) and (15) can yield the coefficients B_n and in particular $\zeta(0) = B_4$, provided we carefully perform a uniform Debye expansion of $F_p(ix)$. It should be emphasized that this technique seems to be the most efficient. In fact, by using this algorithm, Moss [16] was able to compute $\zeta(0)$ for a real scalar field subject to Robin boundary conditions, whereas the technique of Kennedy

based on charge layers on the plane tangent to S^3 failed to provide such a value [21,22]. Indeed, the eigenvalue condition (10) is of the Robin type (just set $\beta = 1$ in Equation (22) of Ref. [16]). Thus, on passing to the variable $x \rightarrow ix$ and then defining $\alpha_p \equiv \sqrt{p^2 + x^2}$, $C \equiv -\log(\sqrt{2\pi})$, we can write

$$\log\left((ix)^{-p}F_p(ix)\right) \sim C - p \log(p + \alpha_p) + \frac{1}{2} \log(\alpha_p) + \alpha_p + \sum_{n=1}^{\infty} \sum_{r=0}^n a_{nr} p^{2r} \alpha_p^{-n-2r}. \tag{16}$$

The coefficients a_{nr} in (16) can be computed by comparison using the formula

$$\sum_{n=1}^{\infty} \sum_{r=0}^n a_{nr} t^{2r} = \sum_{m=1}^{\infty} a_m(t), \tag{17}$$

because the $a_m(t)$ values are known polynomials in t arising from uniform asymptotic expansions of Bessel functions and their first derivatives. Thus, setting $\beta = 1$ in the Formulae (29)–(31) of Ref. [16] for the $a_m(t)$, we find in our case that

$$a_{10} = \frac{5}{8}, \quad a_{11} = \frac{7}{24}, \tag{18}$$

$$a_{20} = -\frac{3}{16}, \quad a_{21} = \frac{1}{8}, \quad a_{22} = -\frac{7}{16}, \tag{19}$$

$$a_{30} = \frac{17}{384}, \quad a_{31} = \frac{389}{640}, \quad a_{32} = -\frac{203}{128}, \quad a_{33} = \frac{1463}{1152}, \tag{20}$$

plus infinitely many other coefficients that we do not strictly need here. We can now insert (16)–(20) into (15), apply three times the differential operator $-\frac{1}{2x} \frac{d}{dx}$, and finally use the contour formula for positive integer values of k [16]

$$\sum_{p=0}^{\infty} p^{2k} \alpha_p^{-2k-m} = \frac{\Gamma\left(k + \frac{1}{2}\right)\Gamma\left(\frac{m}{2} - \frac{1}{2}\right)}{2\Gamma\left(k + \frac{m}{2}\right)} x^{1-m}, \quad \forall k = 1, 2, 3, \dots, \tag{21}$$

and the known properties of the Γ -function [23]. Now, writing the asymptotic expansion of the right-hand side of (15) in the form

$$\Gamma(3)\zeta(3, x^2) \sim \sum_{n=0}^{\infty} b_n x^{-n-2}, \tag{22}$$

the comparison with (15) shows that

$$\zeta(0) = B_4 = \frac{b_4}{2} = \zeta^I(0) + \zeta^{II}(0), \tag{23}$$

since it is well-known that the asymptotic expansion, if it exists, is unique. The two contributions to $\zeta(0)$ are obtained from the following formulae:

$$\Gamma(3)\zeta(3, x^2) \sim [\sigma_1 + \sigma_2] \sim \sum_{n=0}^{\infty} b_n x^{-n-2}, \tag{24}$$

$$\sigma_1 \sim - \sum_{p=0}^{\infty} N_p \left(-\frac{1}{2x} \frac{d}{dx}\right)^3 \left[-p \log(p + \alpha_p) + \frac{1}{2} \log(\alpha_p) + \alpha_p\right], \tag{25}$$

$$\sigma_2 \sim - \sum_{p=0}^{\infty} N_p \left(-\frac{1}{2x} \frac{d}{dx}\right)^3 \sum_{n=1}^{\infty} \sum_{r=0}^n a_{nr} p^{2r} \alpha_p^{-n-2r}. \tag{26}$$

Bearing in mind (15) and (16), we write (24)–(26) because we can apply Theorem 3 on page 7 of Ref. [18], concerning the differentiation of asymptotic expansions.

Thus, $\zeta^I(0)$ (respectively, $\zeta^{II}(0)$) is half the coefficient of x^{-6} in the asymptotic expansion of σ_1 (respectively, σ_2). We first study the asymptotic expansion of σ_2 , since it is easier to perform this calculation. In our problem, the degeneracy N_p is [12]

$$N_p = 0 \quad \forall p = 0, 1, 2, \quad N_p = 2(p^2 - 4) \quad \forall p \geq 3. \tag{27}$$

This is why we find

$$\sigma_2 \sim - \sum_{n=1}^{\infty} \sum_{r=0}^n a_{nr} \left(r + \frac{n}{2}\right) \left(r + \frac{n}{2} + 1\right) \left(r + \frac{n}{2} + 2\right) [(G - H)(r, x, n)], \tag{28}$$

where, setting $A = -8$, $B = 2$ (cf. (27)), we have, using also (21),

$$\begin{aligned} G(r, x, n) &= \sum_{p=0}^{\infty} (A + Bp^2) p^{2r} \alpha_p^{-n-2r-6} = O(x^{-n-6}) \\ &+ \frac{A}{2} \frac{\Gamma\left(r + \frac{1}{2}\right) \Gamma\left(\frac{n}{2} + \frac{5}{2}\right)}{\Gamma\left(r + \frac{n}{2}\right)} \frac{x^{-5-n}}{\left(r + \frac{n}{2}\right) \left(r + \frac{n}{2} + 1\right) \left(r + \frac{n}{2} + 2\right)} \\ &+ \frac{B}{2} \frac{\Gamma\left(r + \frac{3}{2}\right) \Gamma\left(\frac{n}{2} + \frac{3}{2}\right)}{\Gamma\left(r + \frac{n}{2}\right)} \frac{x^{-3-n}}{\left(r + \frac{n}{2}\right) \left(r + \frac{n}{2} + 1\right) \left(r + \frac{n}{2} + 2\right)}, \end{aligned} \tag{29}$$

$$\begin{aligned} H(r, x, n) &= \sum_{p=0}^2 2(p^2 - 4) p^{2r} \alpha_p^{-n-2r-6} = -6x^{-n-2r-6} \left(1 + \frac{1}{x^2}\right)^{-\frac{n}{2}-r-3} \\ &- 8\delta_{r0} x^{-n-6}. \end{aligned} \tag{30}$$

Thus, $H(r, x, n)$ gives rise to terms in (28) that contain x^{-k} with $k \geq 7$, and it does not contribute to $\zeta^{II}(0)$. This is why (28) and (29) lead to

$$\zeta^{II}(0) = \frac{1}{2} \left[-A(a_{10} + a_{11}) - B(a_{30} + a_{31} + a_{32} + a_{33}) \right]. \tag{31}$$

The insertion of (18), (20) and (27) into (31) finally yields

$$\zeta^{II}(0) = \frac{11}{3} - \frac{121}{360} = \frac{1199}{360}. \tag{32}$$

The calculation of (25) is more involved. By performing the three derivatives and using the identity $\frac{1}{2x} \frac{d\alpha_p}{dx} = \frac{1}{2\alpha_p}$, we find

$$\left(\frac{1}{2x} \frac{d}{dx}\right)^3 \log\left(\frac{1}{p + \alpha_p}\right) = (p + \alpha_p)^{-3} \left[-\alpha_p^{-3} - \frac{9}{8} p \alpha_p^{-4} - \frac{3}{8} p^2 \alpha_p^{-5}\right]. \tag{33}$$

This intermediate step is very important because it proves that by summing over all integer values of p from 0 to ∞ , we obtain a convergent series. However, to be able to perform the $\zeta(0)$ calculation, it is convenient to use the identity

$$(p + \alpha_p)^{-3} = \frac{(\alpha_p - p)^3}{x^6}. \tag{34}$$

Upon inserting (34) into (33) and re-expressing p^2 as $\alpha_p^2 - x^2$, we obtain

$$\left(\frac{1}{2x} \frac{d}{dx}\right)^3 \left[-p \log(p + \alpha_p)\right] = -px^{-6} + p^2x^{-6}\alpha_p^{-1} + \frac{p^2}{2}x^{-4}\alpha_p^{-3} + \frac{3}{8}p^2x^{-2}\alpha_p^{-5}$$

$$\equiv M(x, \alpha_p, p), \tag{35}$$

which implies

$$\sigma_1 \sim \left[\sum_{p=0}^{\infty} N_p M(x, \alpha_p, p) \right] + \sigma_1'' \sim [\sigma_1' + \sigma_1''], \tag{36}$$

where

$$\begin{aligned} \sigma_1'' &= - \sum_{p=0}^{\infty} N_p \left(-\frac{\alpha_p^{-6}}{2} - \frac{3}{8}\alpha_p^{-5} \right) \\ &= \sum_{p=0}^{\infty} (A + Bp^2) \left(\frac{\alpha_p^{-6}}{2} + \frac{3}{8}\alpha_p^{-5} \right) \\ &\quad + \sum_{p=0}^2 (A + Bp^2) \left(-\frac{\alpha_p^{-6}}{2} - \frac{3}{8}\alpha_p^{-5} \right). \end{aligned} \tag{37}$$

The infinite sum on the right-hand side of (37) contributes to $\zeta(0)$ only through the following part:

$$\sum_{p=0}^{\infty} \frac{A}{2} \alpha_p^{-6} = \frac{A}{2} \left[\frac{x^{-6}}{2} + \frac{\pi}{2} \frac{3!!}{4!!} x^{-5} \right]. \tag{38}$$

The result (38) is proved by applying the Euler–Maclaurin formula [18] to the calculation of $\sum_{p=0}^{\infty} (p^2 + x^2)^{-3}$, and then using the Formula (3.249.1) on page 294 of Ref. [24]. In addition, the finite sum on the right-hand side of (37) contributes to $\zeta(0)$. In fact, one finds (we have $x \rightarrow \infty$) that

$$\begin{aligned} &\sum_{p=0}^2 (A + Bp^2) \left(-\frac{\alpha_p^{-6}}{2} - \frac{3}{8}\alpha_p^{-5} \right) = -\left(\frac{A}{2} + \frac{B}{2}\right)x^{-6} \left[1 - \frac{3}{x^2} + \frac{6}{x^4} + \dots \right] \\ &- \frac{A}{2}x^{-6} - \frac{3}{8}Ax^{-5} \\ &- \frac{3}{8}(A + B)x^{-5} \left[1 - \frac{5}{2x^2} + \frac{35}{8x^4} + \dots \right], \end{aligned} \tag{39}$$

which implies that the total contribution of σ_1'' to $\zeta(0)$ is given by

$$\zeta^{Ib}(0) = \frac{1}{2} \left(-A - \frac{B}{2} \right) + \frac{A}{8} = \frac{7}{2} - 1 = \frac{5}{2}. \tag{40}$$

Thus, we have so far

$$\zeta(0) = \zeta^I(0) + \zeta^{II}(0) = \zeta^{Ia}(0) + \zeta^{Ib}(0) + \zeta^{II}(0), \tag{41}$$

where

$$\zeta^{Ib}(0) + \zeta^{II}(0) = \frac{5}{2} + \frac{1199}{360}. \tag{42}$$

It now remains to compute $\zeta^{Ia}(0)$, i.e., the contribution to $\zeta(0)$ due to σ_1' in (36). Indeed, one has

$$\sigma_1' \sim \left[A \sum_{p=0}^{\infty} M(x, \alpha_p, p) + B \sum_{p=0}^{\infty} p^2 M(x, \alpha_p, p) - \sum_{p=0}^2 (A + Bp^2) M(x, \alpha_p, p) \right]. \tag{43}$$

Let us now denote by $\Sigma^{(a)}$, $\Sigma^{(b)}$ and $\Sigma^{(c)}$ the three sums on the right-hand side of (43). Both $\Sigma^{(a)}$ and $\Sigma^{(b)}$ contain divergent parts in view of (35). These fictitious divergences may be regularized by dividing by α_p^{2s} and then taking the limit as s tends to zero, as shown in Ref. [16]. It might not appear a priori obvious that this technique leads to unambiguous results, since the limit $s \rightarrow 0$ is a delicate mathematical point. However, a fundamental consistency check is presented in Section 7.4 of Ref. [13] for all one-loop calculations involving only physical degrees of freedom of bosonic fields, showing that the method is correct. In performing the calculation, we must use the contour Formula (21) and also the following asymptotic expansion [16]:

$$\sum_{p=0}^{\infty} p \alpha_p^{-1-n} \sim \frac{x^{1-n}}{\sqrt{\pi}} \sum_{r=0}^{\infty} \frac{2^r}{r!} \tilde{B}_r x^{-r} \frac{\Gamma\left(\frac{r}{2} + \frac{1}{2}\right) \Gamma\left(\frac{n}{2} - \frac{1}{2} + \frac{r}{2}\right)}{2\Gamma\left(\frac{1}{2} + \frac{n}{2}\right)} \cos\left(\frac{r\pi}{2}\right), \tag{44}$$

where $\tilde{B}_0 = 1, \tilde{B}_1 = -\frac{1}{2}, \tilde{B}_2 = \frac{1}{6}, \tilde{B}_4 = -\frac{1}{30}$ etc., are Bernoulli numbers. Thus, using the label R for the regularized quantities, we define

$$\begin{aligned} \Sigma_R^{(a)} \equiv & A \left[-x^{-6} \left(\lim_{s \rightarrow 0} \sum_{p=0}^{\infty} p \alpha_p^{-1-(2s-1)} \right) + x^{-6} \left(\lim_{s \rightarrow 0} \sum_{p=0}^{\infty} p^2 \alpha_p^{-2-(2s-1)} \right) \right. \\ & \left. + \frac{x^{-4}}{2} \left(\lim_{s \rightarrow 0} \sum_{p=0}^{\infty} p^2 \alpha_p^{-2-(2s+1)} \right) + \frac{3}{8} x^{-2} \left(\lim_{s \rightarrow 0} \sum_{p=0}^{\infty} p^2 \alpha_p^{-2-(2s+3)} \right) \right]. \end{aligned} \tag{45}$$

In view of (44), the first limit in (45) gives the following contribution to $\zeta(0)$:

$$\delta_1 = -\frac{A}{2} \left(-\frac{\tilde{B}_2}{\sqrt{\pi}} \Gamma\left(\frac{3}{2}\right) \right) = \frac{A}{24} = -\frac{1}{3}, \tag{46}$$

whereas the other limits in (45) do not contribute to $\zeta(0)$ in view of (21), because one only obtains terms proportional to x^{-4} .

Moreover, bearing in mind the identity

$$\sum_{p=0}^{\infty} p^3 \alpha_p^{-2s} = \sum_{p=0}^{\infty} p \alpha_p^{-1-(2s-3)} - x^2 \sum_{p=0}^{\infty} p \alpha_p^{-1-(2s-1)}, \tag{47}$$

we also define

$$\begin{aligned} \Sigma_R^{(b)} \equiv & B \left[-x^{-6} \left(\lim_{s \rightarrow 0} \sum_{p=0}^{\infty} p^3 \alpha_p^{-2s} \right) + x^{-6} \left(\lim_{s \rightarrow 0} \sum_{p=0}^{\infty} p^4 \alpha_p^{-4-(2s-3)} \right) \right. \\ & \left. + \frac{x^{-4}}{2} \left(\lim_{s \rightarrow 0} \sum_{p=0}^{\infty} p^4 \alpha_p^{-4-(2s-1)} \right) + \frac{3}{8} x^{-2} \left(\lim_{s \rightarrow 0} \sum_{p=0}^{\infty} p^4 \alpha_p^{-4-(2s+1)} \right) \right]. \end{aligned} \tag{48}$$

In view of (44) and (47), the first limit in (48) gives the following contribution to $\zeta(0)$:

$$\delta_2 = -\frac{B}{2} \left(-\frac{\tilde{B}_4}{4} \right) = -\frac{B}{240} = -\frac{1}{120}. \tag{49}$$

Note that the second sum in (47) does not contribute to δ_2 because its only constant term contains $\frac{\Gamma(s+1)}{\Gamma(s)}$, which tends to 0 as $s \rightarrow 0$. The other limits in (48) do not contribute to $\zeta(0)$ in view of (21), because they only yield terms proportional to x^{-2} .

Last, the sum $\Sigma^{(c)}$ in (43) has the following asymptotic behavior as $x \rightarrow \infty$:

$$\Sigma^{(c)} \sim \left[(3A + 9B)x^{-6} + \sum_{k=0}^{\infty} (AC_k + BD_k)x^{-7-k} \right], \tag{50}$$

which yields the following contribution to $\zeta(0)$:

$$\delta_3 = \frac{(3A + 9B)}{2} = -3. \tag{51}$$

To sum up, we find

$$\zeta^{Ia}(0) = \delta_1 + \delta_2 + \delta_3 = -\frac{1}{3} - \frac{1}{120} - 3, \tag{52}$$

Therefore, the full $\zeta(0)$ for physical degrees of freedom is given by (cf. (41) and (42))

$$\zeta(0) = \zeta^{Ia}(0) + \frac{5}{2} + \frac{1199}{360} = \frac{112}{45}. \tag{53}$$

3. First Example of Mixed Boundary Conditions on the Whole Set of Metric Perturbations and Ghost Modes

The previous example is very instructive, but of course it would be desirable to compute the effect of boundary conditions on the whole set of metric perturbations and Feynman–DeWitt–Faddeev–Popov ghost fields [25–27]. For this purpose, the work in Ref. [28] studied the following one-parameter family of mixed boundary conditions (with λ being a freely specifiable real parameter):

$$\left[\frac{\partial h_{ij}}{\partial \tau} + \frac{\lambda}{\tau} h_{ij} \right]_{\partial M} = 0, \tag{54}$$

$$\left[h_{0i} \right]_{\partial M} = 0, \tag{55}$$

$$\left[h_{00} \right]_{\partial M} = 0, \tag{56}$$

$$\left[\frac{\partial \varphi_i}{\partial \tau} + \frac{\lambda}{\tau} \varphi_i \right]_{\partial M} = 0, \tag{57}$$

$$\left[\frac{\partial \varphi_0}{\partial \tau} + \frac{(\lambda + 1)}{\tau} \varphi_0 \right]_{\partial M} = 0. \tag{58}$$

With our notation, τ lies in the closed interval $[0, a]$; h_{ij}, h_{0i}, h_{00} are the components of metric perturbations; and φ_i and φ_0 are covariant components of the ghost field of quantum gravity. One therefore deals with transverse-traceless modes, scalar modes, vector modes, decoupled scalar modes, decoupled vector modes, scalar ghost modes, vector ghost modes, and decoupled ghost modes.

A one-parameter family of full $\zeta(0)$ values is therefore obtained [28]:

$$\zeta_\lambda(0) = \frac{89}{90} + \frac{\lambda}{3}(\lambda^2 - 9\lambda - 3). \tag{59}$$

The λ -dependent part of (59) is always positive, either for all

$$\lambda > \frac{9 + \sqrt{93}}{2}, \tag{60}$$

or for all

$$\lambda \in \left] \frac{9 - \sqrt{93}}{2}, 0 \right[. \tag{61}$$

Equations (60) and (61) are sufficient conditions for the positivity of the full $\zeta_\lambda(0)$, and other suitable values of λ can be computed numerically.

This model is more complete than the one in Section 2, since it deals with all perturbative modes in the one-loop functional integral. However, it still suffers from a non-trivial drawback: the whole set of boundary conditions (54)–(58) is not completely invariant under infinitesimal diffeomorphisms on metric perturbations. For this reason, we resort to the boundary conditions of Section 4.

4. Completely Diff-Invariant Boundary Conditions

The boundary conditions that we study are part of a unified scheme for Maxwell, Yang–Mills, and Quantized General Relativity at one loop, i.e., [29,30]

$$\left[\pi \mathcal{A} \right]_{\mathcal{B}} = 0, \tag{62}$$

$$\left[\Phi(A) \right]_{\mathcal{B}} = 0, \tag{63}$$

$$[\varphi]_{\mathcal{B}} = 0. \tag{64}$$

With our notation, π is a projector acting on the gauge field \mathcal{A} , Φ is the gauge-fixing functional, and φ is the full set of ghost fields. Both Equations (62) and (63) are preserved under infinitesimal gauge transformations provided that the ghost obeys homogeneous Dirichlet conditions as in (64). For gravity, we choose Φ so as to have an operator P of Laplace type on metric perturbations in the one-loop Euclidean theory.

5. Eigenvalue Conditions for Scalar Modes

On the Euclidean four-ball, we expand metric perturbations $h_{\mu\nu}$ in terms of scalar, transverse vector, and transverse-traceless tensor harmonics on S^3 . For the vector, tensor, and ghost modes, boundary conditions reduce to Dirichlet or Robin. For scalar modes, one finds eventually the eigenvalues $E = x^2$ from the roots x of [31,32]

$$J'_n(x) \pm \frac{n}{x} J_n(x) = 0, \tag{65}$$

$$J'_n(x) + \left(-\frac{x}{2} \pm \frac{n}{x} \right) J_n(x) = 0. \tag{66}$$

Note that both x and $-x$ solve the same equation.

6. Four Spectral ζ -Functions for Scalar Modes

From Equations (65) and (66), we obtain the following integral representations of the resulting ζ -functions upon exploiting the Cauchy theorem and rotation of contour:

$$\zeta_{A,B}^\pm(s) \equiv \frac{(\sin \pi s)}{\pi} \sum_{n=3}^\infty n^{-(2s-2)} \int_0^\infty dz z^{-2s} \frac{\partial}{\partial z} \log F_{A,B}^\pm(zn), \tag{67}$$

where (here $\beta_+ \equiv n, \beta_- \equiv n + 2$)

$$F_A^\pm(zn) \equiv z^{-\beta_\pm} \left(zn I'_n(zn) \pm n I_n(zn) \right), \tag{68}$$

$$F_B^\pm(zn) \equiv z^{-\beta_\pm} \left(zn I'_n(zn) + \left(\frac{(zn)^2}{2} \pm n \right) I_n(zn) \right), \tag{69}$$

with I_n being the modified Bessel functions of the first kind. Regularity at the origin is easily proved in the elliptic sectors, corresponding to $\zeta_A^\pm(s)$ and $\zeta_B^\pm(s)$.

7. Regularity of ζ_B^+ at $s = 0$

We now define $T \equiv (1 + z^2)^{-1/2}$ and consider the uniform asymptotic expansion (away from $T = 1$)

$$z^{\beta+} F_B^+(zn) \sim \frac{e^{n\eta(T)}}{h(n)\sqrt{T}} \frac{(1 - T^2)}{T} \left(1 + \sum_{j=1}^{\infty} \frac{r_{j,+}(T)}{n^j} \right), \tag{70}$$

the functions $r_{j,+}$ being obtained from the Olver polynomials for the uniform asymptotic expansion of I_n and I'_n . On splitting $\int_0^1 dT = \int_0^\mu dT + \int_\mu^1 dT$ with small μ , we obtain an asymptotic expansion of the l.h.s. by writing, in the first interval on the r.h.s.,

$$\log \left(1 + \sum_{j=1}^{\infty} \frac{r_{j,+}(T)}{n^j} \right) \sim \sum_{j=1}^{\infty} \frac{R_{j,+}(T)}{n^j}, \tag{71}$$

and then computing

$$C_j(\tau) \equiv \frac{\partial R_{j,+}}{\partial T} = (1 - T)^{-j-1} \sum_{a=j-1}^{4j} K_a^{(j)} T^a. \tag{72}$$

The integral $\int_\mu^1 dT$ is instead found to yield a vanishing contribution in the $\mu \rightarrow 1$ limit. Remarkably, by virtue of the spectral identity

$$g(j) \equiv \sum_{a=j}^{4j} \frac{\Gamma(a+1)}{\Gamma(a-j+1)} K_a^{(j)} = 0, \tag{73}$$

which holds $\forall j = 1, \dots, \infty$, we find

$$\lim_{s \rightarrow 0} s \zeta_B^+(s) = \frac{1}{6} \sum_{a=3}^{12} a(a-1)(a-2) K_a^{(3)} = 0, \tag{74}$$

and

$$\zeta_B^+(0) = \frac{5}{4} + \frac{1079}{240} - \frac{1}{2} \sum_{a=2}^{12} \omega(a) K_a^{(3)} + \sum_{j=1}^{\infty} f(j) g(j) = \frac{296}{45}, \tag{75}$$

where

$$\begin{aligned} \omega(a) \equiv & \frac{1}{6} \frac{\Gamma(a+1)}{\Gamma(a-2)} \left[-\log(2) - \frac{(6a^2 - 9a + 1) \Gamma(a-2)}{4 \Gamma(a+1)} \right. \\ & \left. + 2\psi(a+1) - \psi(a-2) - \psi(4) \right], \end{aligned} \tag{76}$$

$$f(j) \equiv \frac{(-1)^j}{j!} \left[-1 - 2^{2-j} + \zeta_R(j-2)(1 - \delta_{j,3}) + \gamma \delta_{j,3} \right]. \tag{77}$$

The spectral cancellation (73) achieves three goals: (i) vanishing of the log 2 coefficient in Equation (75); (ii) vanishing of $\sum_{j=1}^{\infty} f(j) g(j)$ in Equation (75); and (iii) regularity at the origin of ζ_B^+ .

To cross-check our analysis, we evaluate $r_{j,+}(T) - r_{j,-}(T)$ and hence obtain $R_{j,+}(T) - R_{j,-}(T)$ for all j . Only $j = 3$ contributes to $\zeta_B^\pm(0)$, and we find

$$\begin{aligned} \zeta_B^+(0) &= \zeta_B^-(0) - \frac{1}{24} \sum_{l=1}^4 \frac{\Gamma(l+1)}{\Gamma(l-2)} \left[\psi(l+2) - \frac{1}{(l+1)} \right] \kappa_{2l+1}^{(3)} \\ &= \frac{206}{45} + 2 = \frac{296}{45}, \end{aligned} \tag{78}$$

in agreement with Equation (75), where $\kappa_{2l+1}^{(3)}$ are the four coefficients on the right-hand side of

$$\frac{\partial}{\partial T}(R_{3,+} - R_{3,-}) = (1 - T^2)^{-4} (80T^3 - 24T^5 + 32T^7 - 8T^9). \tag{79}$$

Within this framework, the spectral cancellation reads as

$$\sum_{l=1}^4 \frac{\Gamma(l+1)}{\Gamma(l-2)} \kappa_{2l+1}^{(3)} = 0, \tag{80}$$

which is a particular case of

$$\sum_{a=a_{\min}(j)}^{a=a_{\max}(j)} \frac{\Gamma((a+1)/2)}{\Gamma((a+1)/2-j)} \kappa_a^{(j)} = 0. \tag{81}$$

Interestingly, the full $\zeta(0)$ value for pure gravity (i.e., including the contribution of tensor, vector, scalar, and ghost modes) is then found to be positive [31,32]:

$$\zeta(0) = \frac{142}{45}, \tag{82}$$

which suggests in light of (5) a quantum avoidance of the cosmological singularity driven by full diffeomorphism invariance of the boundary-value problem for one-loop quantum theory.

8. Open Problems

The DeWitt boundary condition lies at the very heart of deep issues in quantum gravity. As far as we can see, the main open problems are as follows.

- (1) Among the three schemes studied in our Sections 2– 7, the latter, i.e., the choice of completely diff-invariant boundary conditions on all perturbative modes, might seem the most satisfactory, but unfortunately, the strong ellipticity of the boundary-value problem is not fulfilled in such a case [30,33–37]. However, our analysis shows that, in the particular case of flat Euclidean four-space bounded by a three-sphere boundary, peculiar cancellations occur, and the resulting $\zeta(0)$ value can be defined and is positive. The deeper underlying reason might be that, in order to define a spectral ζ -function, it is sufficient to find a sector of the complex plane free of eigenvalues of the leading symbol of the elliptic operator under consideration (we are grateful to Professor Gerd Grubb for correspondence about this property a long time ago). An alternative approach might consist in considering non-local boundary conditions in Euclidean quantum gravity [38–40], or the normalizability criterion for the wave function of the universe [41].
- (2) The outstanding work in Ref. [10] looked for solutions of the quantum constraint equations in order to check the validity of DeWitt’s proposal. However, although one can obtain under suitable assumptions a formal proof of the equivalence of canonical and functional-integral approaches [42], DeWitt himself provided an enlightening example of a sum over histories that does not solve the Wheeler–DeWitt equation [43].

This remark might therefore account for the inequivalence between our conclusions and the results in Ref. [10].

The fascinating question of whether our universe can be non-singular in a semiclassical theory of quantum gravity [44] is therefore still waiting for a fully satisfactory answer.

Funding: This research received no external funding

Data Availability Statement: All calculations were done by hand, hence there are no data stored

Conflicts of Interest: The author declares no conflict of interest

Appendix A. The One-Loop Approximation

We are here interested in the approach to quantum field theory in terms of Feynman functional integrals. Hence, we study the amplitudes of going from data on a spacelike surface Σ_1 to data on a spacelike surface Σ_2 . For example, in the case of real scalar fields ϕ in a curved background M , the data are the induced three-metric h and a linear combination of ϕ and its normal derivative: $a\phi + b\frac{\partial\phi}{\partial n}$. The latter reduces to homogeneous Dirichlet conditions if $b = 0$, and Neumann conditions if $a = 0$. Otherwise, it is a Robin boundary condition. The quantum amplitudes are functionals of these boundary data. On making a Wick rotation and using the background-field method, we may expand both the four-metric g and the field ϕ about solutions to the classical field equations as $g = g_0 + \bar{g}$ and $\phi = \phi_0 + \bar{\phi}$. However, the more general possibility remains to consider background fields that are not solutions to any field equations, or which are (approximate) solutions in the asymptotic regions. The logarithm of the one-loop functional integral Z for a scalar field (in the main body of our paper, we study pure gravity, but here we focus on scalar fields for simplicity) has an asymptotic expansion

$$\log(Z) \sim \log \int \mu[\bar{\phi}] e^{-I_2[\bar{\phi}]/\hbar} + O(\hbar^2), \tag{A1}$$

where μ is a suitable measure of the space of scalar-field perturbations. The part $I_2[\bar{\phi}]$ of the action that is quadratic in scalar-field perturbations involves a second-order elliptic operator \mathcal{B} . Assuming completeness of the set $\{\varphi_n\}$ of eigenfunctions of \mathcal{B} , with eigenvalues λ_n , the corresponding contribution to one-loop quantum amplitudes involves an infinite product of Gaussian integrals, i.e.,

$$\prod_{n=n_0}^{\infty} \int \mu dy_n e^{-\frac{\lambda_n}{2} y_n^2} = \frac{1}{\sqrt{\det\left(\frac{1}{2}\pi^{-1}\mu^{-2}\mathcal{B}\right)}}. \tag{A2}$$

In order to make sense of this infinite product of eigenvalues, one can use ζ -function regularization. This is a rigorous mathematical tool that relies on the spectral theorem, according to which for any elliptic, self-adjoint, and positive-definite operator B , its complex powers B^{-s} can be defined. Hence, its spectral ζ -function is defined as in Equation (4), and the analytic continuation of the ζ -function to the whole complex- s plane takes the form

$$\zeta_B(s) = \sum_{k=-n}^N \frac{a_k}{\left(s + \frac{k}{m}\right)} + \phi_N(s), \quad k \neq 0. \tag{A3}$$

Thus, on using analytic continuations, $\zeta_B(0)$ is actually finite, and its value gives information about scaling properties of quantum amplitudes. We can now be more precise and describe in detail some key properties. The relation

$$\det B = e^{-\zeta'(0)} \tag{A4}$$

becomes a possible way to define the determinant of the elliptic operator B upon the analytic continuation of $\zeta_B(s)$. If B is a second-order operator, its eigenvalues λ_n have dimension $(\text{length})^{-2}$. Under conformal rescaling of the metric according to $\hat{g} = k^2g$, one has $\hat{\lambda}_n = \lambda_n/k^2$, and the new spectral ζ -function is $\hat{\zeta}(s) = k^{2s}\zeta(s)$. This leads to

$$\log \det \hat{B} = \log \det B - \log(k^2)\zeta(0), \tag{A5}$$

and hence the partition function scales as

$$\log(\hat{Z}) = \log(Z) + \frac{1}{2} \log(k^2)\zeta(0) + \log(\hat{\mu}/\mu)\zeta(0). \tag{A6}$$

The parameter μ is the one occurring in the one-loop semiclassical evaluation of the functional integral. This formula allows for the more general case when the normalization parameter μ changes under scale transformations. One can avoid this complication by assuming that the measure in the functional integral is defined on scalar densities of weight $\frac{1}{2}$.

Equation (A5) can also be used to deduce that the one-loop effective action (for the scalar field) reads as

$$\Gamma^{(1)} = \frac{1}{2} \log \det \hat{B} = -\frac{1}{2}\zeta'(0) - \frac{1}{2}\zeta(0) \log(k^2). \tag{A7}$$

Note that the resulting one-loop $\langle \text{out} | \text{in} \rangle$ amplitude is measure-dependent unless $\zeta(0) = 0$. This is why $\zeta(0)$ is frequently called the anomalous scaling factor.

References

1. Friedmann, A. Über die krümmung des raumes. *Z. Phys.* **1922**, *10*, 377. [CrossRef]
2. Penrose, R. Gravitational collapse and space-time singularities. *Phys. Rev. Lett.* **1965**, *14*, 57. [CrossRef]
3. Hawking, S.W. The occurrence of singularities in cosmology. *Proc. R. Soc. Lond. A* **1966**, *294*, 511.
4. Hawking, S.W. The occurrence of singularities in cosmology. II. *Proc. R. Soc. Lond. A* **1966**, *295*, 490.
5. Geroch, R.P. Singularities in closed universes. *Phys. Rev. Lett.* **1966**, *17*, 445. [CrossRef]
6. Hawking, S.W. The occurrence of singularities in cosmology. III. Causality and singularities. *Proc. R. Soc. Lond. A* **1967**, *300*, 187.
7. Hawking, S.W.; Penrose, R. The singularities of gravitational collapse and cosmology. *Proc. R. Soc. Lond. A* **1970**, *314*, 529.
8. Christodoulou, D.; Klainerman, S. *The Global Nonlinear Stability of Minkowski Space*; Princeton University Press: Princeton, NJ, USA, 1993.
9. DeWitt, B.S. Quantum theory of gravity. I. The canonical theory. *Phys. Rev.* **1967**, *160*, 1113. [CrossRef]
10. Matsui, H.; Mukoyama, S.; Naruko, A. DeWitt boundary condition is consistent in Horava-Lifshitz gravity. *Phys. Lett. B* **2022**, *833*, 137340. [CrossRef]
11. Kamenshchik, A.Y. Quantum cosmology and late-time singularities. *Class. Quantum Grav.* **2013**, *30*, 173001. [CrossRef]
12. Schleich, K. Semiclassical wave function of the universe at small three-geometries. *Phys. Rev. D* **1985**, *32*, 1889. [CrossRef] [PubMed]
13. Esposito, G. *Quantum Gravity, Quantum Cosmology and Lorentzian Geometries*; Lecture Notes in Physics Monographs; Springer: Berlin/Heidelberg, Germany, 1994; Volume 12.
14. Breitenlohner, P.; Freedman, D.Z. Stability in gauged extended supergravity. *Ann. Phys.* **1982**, *144*, 249. [CrossRef]
15. Hawking, S.W. The boundary conditions for gauged supergravity. *Phys. Lett. B* **1983**, *126*, 175. [CrossRef]
16. Moss, I.G. Boundary terms in the heat kernel expansion. *Class. Quantum Grav.* **1989**, *6*, 759. [CrossRef]
17. Watson, G.N. *A Treatise on the Theory of Bessel Functions*; Cambridge University Press: Cambridge, UK, 1966.
18. Wong, R. *Asymptotic Approximations of Integrals*; Academic Press: New York, NY, USA, 1989.
19. Greiner, P. An asymptotic expansion for the heat equation. *Arch. Rat. Mech. Anal.* **1971**, *41*, 163. [CrossRef]
20. Branson, T.P.; Gilkey, P.B. The asymptotics of the Laplacian on a manifold with boundary. *Commun. Part. Diff. Eqs.* **1990**, *15*, 245. [CrossRef]
21. Kennedy, G. Boundary terms in the Schwinger-DeWitt expansion: Flat-space results. *J. Phys. A* **1978**, *11*, L173. [CrossRef]
22. Kennedy, G. Some Finite-Temperature Quantum-Field-Theory Calculations in Manifolds with Boundaries. Ph.D. Thesis, University of Manchester, Manchester, UK, 1979.
23. Abramowitz, M.; Stegun, I.A. *Handbook of Mathematical Functions*; Dover: New York, NY, USA, 1964.
24. Gradshteyn, I.S.; Ryzhik, I.M. *Table of Integrals, Series and Products*; Academic Press: New York, NY, USA, 1965.
25. Feynman, R.P. Quantum theory of gravitation. *Acta Phys. Pol.* **1963**, *24*, 697.
26. DeWitt, B.S. Quantum theory of gravity. II. The manifestly covariant theory. *Phys. Rev.* **1967**, *162*, 1195. [CrossRef]
27. Faddeev, L.D.; Popov, V. Feynman diagrams for the Yang-Mills field. *Phys. Lett. B* **1967**, *25*, 29. [CrossRef]

28. Esposito, G.; Kamenshchik, A.Y. Mixed boundary conditions in Euclidean quantum gravity. *Class. Quantum Grav.* **1995**, *12*, 2715. [CrossRef]
29. Esposito, G.; Kamenshchik, A.Y.; Pollifrone, G. *Euclidean Quantum Gravity on Manifolds with Boundary*; Fundamental Theories of Physics; Kluwer: Dordrecht, The Netherlands, 1997; Volume 85.
30. Avramidi, I.G.; Esposito, G. Gauge theories on manifolds with boundary. *Commun. Math. Phys.* **1999**, *200*, 495. [CrossRef]
31. Esposito, G.; Fucci, G.; Kamenshchik, A.Y.; Kirsten, K. Spectral asymptotics of Euclidean quantum gravity with diff-invariant boundary conditions. *Class. Quantum Grav.* **2005**, *22*, 957. [CrossRef]
32. Esposito, G.; Fucci, G.; Kamenshchik, A.Y.; Kirsten, K. A non-singular one-loop wave function of the universe from a new eigenvalue asymptotics in quantum gravity. *J. High Energy Phys.* **2005**, *9*, 063. [CrossRef]
33. Avramidi, I.G.; Esposito, G. Lack of strong ellipticity in Euclidean quantum gravity. *Class. Quantum Grav.* **1998**, *15*, 1141. [CrossRef]
34. Witten, E. A note on boundary conditions in Euclidean gravity. *Rev. Math. Phys.* **2021**, *33*, 2140004. [CrossRef]
35. Witten, E. A note on the canonical formalism for gravity. *arXiv* **2022**, arXiv:2212.08270.
36. Park, I.Y. Holographic quantization of gravity in a black hole background. *J. Math. Phys.* **2016**, *57*, 022305. [CrossRef]
37. Park, I.Y. Foliation, jet bundle and quantization of Einstein gravity. *Front. Phys.* **2016**, *4*, 25. [CrossRef]
38. Esposito, G. Non-local boundary conditions in Euclidean quantum gravity. *Class. Quantum Grav.* **1999**, *16*, 1113. [CrossRef]
39. Esposito, G. New kernels in quantum gravity. *Class. Quantum Grav.* **1999**, *16*, 3999. [CrossRef]
40. Schröder, M. On the Laplace operator with non-local boundary conditions. *Rep. Math. Phys.* **1989**, *27*, 259. [CrossRef]
41. Barvinsky, A.O.; Kamenshchik, A.Y. One-loop quantum cosmology: The normalizability of the Hartle-Hawking wave function and the probability of inflation. *Class. Quantum Grav.* **1990**, *7*, L181. [CrossRef]
42. Halliwell, J.J.; Hartle, J.B. Wave functions constructed from an invariant sum over histories satisfy constraints. *Phys. Rev. D* **1991**, *43*, 1170. [CrossRef] [PubMed]
43. DeWitt, B.S. The quantum and gravity: The Wheeler-DeWitt equation. In *Relativity, Particle Physics and Cosmology, Proceedings of the Richard Arnowitt Fest, College Station, TX, USA, 5–8 April 1998*; World Scientific: Singapore, 1999; pp. 70–92.
44. Hawking, S.W. A non-singular universe. *Phys. Scripta T* **2005**, *117*, 49.

Disclaimer/Publisher’s Note: The statements, opinions and data contained in all publications are solely those of the individual author(s) and contributor(s) and not of MDPI and/or the editor(s). MDPI and/or the editor(s) disclaim responsibility for any injury to people or property resulting from any ideas, methods, instructions or products referred to in the content.

No-Boundary Wave Functional and Own Mass of the Universe

Natalia Gorobey ^{1,†}, Alexander Lukyanenko ^{1,†} and Alexander V. Goltsev ^{2,*,†} 

¹ Department of Physics, Physical-Mechanical Institute, Peter the Great Saint Petersburg Polytechnic University, Polytekhnicheskaya 29, 195251 St. Petersburg, Russia; alex.lukyan@mail.ru (A.L.)

² Ioffe Physical-Technical Institute, Polytekhnicheskaya 26, 195251 St. Petersburg, Russia

* Correspondence: goltsev@ua.pt

† These authors contributed equally to this work.

Abstract: An alternative formulation of the no-boundary initial state of the universe in the Euclidean quantum theory of gravity is proposed. Unlike the no-boundary Hartle–Hawking wave function, in which time appears together with macroscopic space–time in the semiclassical approximation, in the proposed formalism, time is present from the very beginning on an equal footing with spatial coordinates. The main element of the formalism is the wave functional, which is defined based on the world histories of the universe. This ensures formal 4D covariance of the theory. The wave functional is defined independently of the wave function as an eigenvector of the action operator. The shape of the Origin region, together with the boundary conditions, is determined by the structure of the total energy of the universe, which includes a 3D-invariant contribution of the expansion energy. The own mass of the universe arises as a non-zero value of the expansion energy in the Origin.

Keywords: universe; time; own mass; quantum; Euclidean instanton

1. Introduction

The question of the origin of the universe has been and remains central to cosmology. In this work, we will focus on the idea of the quantum birth of the universe from “nothing” [1–6]. This theory was most consistently developed within the framework of the Euclidean quantum theory of gravity (QTG) in the works of Hartle, Hawking, and Hertog [7]. The main object in this approach is the representation of the no-boundary wave function of the universe in the form of a functional integral

$$\psi = \int \prod J d g d \varphi \exp \left(-\frac{1}{\hbar} \tilde{I}_{GR} \right), \quad (1)$$

where \tilde{I}_{GR} is the action of General Relativity in Euclidean signature; see also [8]. Integration is carried out over all Euclidean 4D metrics and configurations of matter fields with given values on a single 3D boundary, and J is the Faddeev–Popov determinant. However, in practice, when using polar coordinates in the Origin [7], integral Equation (1) is considered as a representation of the Green’s function for the Wheeler–De Witt (WDW) equation with two boundary surfaces, one of which is contracted to a point—a pole. In this case, it is not possible to completely get rid of the boundary conditions for the fundamental dynamic variables at the pole. In particular, the initial value of the scalar field remains a free parameter [7]. A more aggravating circumstance is the fact that integral Equation (1) diverges and the no-boundary wave function can be given meaning only within the framework of the semiclassical approximation. Therefore, in subsequent work [9], the authors considered it reasonable to state the problem in the semiclassical approximation without using a functional integral, directly for the WDW equation, or through the holographic principle [10]. The reason for the divergence of integral Equation (1) is the uncertainty of the sign of the Hilbert–Einstein action. This problem is closely related to the problem of



Citation: Gorobey, N.; Lukyanenko, A.; Goltsev, A.V. No-Boundary Wave Functional and Own Mass of the Universe. *Universe* **2024**, *10*, 101. <https://doi.org/10.3390/universe10020101>

Academic Editors: Sergey V. Sushkov and Lorenzo Iorio

Received: 5 December 2023

Revised: 25 January 2024

Accepted: 16 February 2024

Published: 19 February 2024



Copyright: © 2024 by the authors. Licensee MDPI, Basel, Switzerland. This article is an open access article distributed under the terms and conditions of the Creative Commons Attribution (CC BY) license (<https://creativecommons.org/licenses/by/4.0/>).

the positivity of the gravitational field energy [11]. The latter was solved thanks to the proof of the positive energy theorem for the case of asymptotically flat geometry [12,13]. A modification of this theorem for the case of a closed universe is considered in [14]. Here, there is an irremovable negative contribution to energy, which is entirely related to the expansion of the universe.

This paper proposes a formalism alternative to the functional integral Equation (1) on the basis of the invariant wave functional $\Psi[g(x, t), \varphi(x, t)]$, which is defined based on the space of 4D world histories of the universe. To avoid terminological confusion, we immediately emphasize that the wave function $\psi(g_{ik}(x), \varphi(x), N, N^k, t)$ is a functional of the functions $g_{ik}(x), \varphi(x)$ on a 3D spatial section at a given time t and a functional of the given lapse and shift functions N, N^k [15]. To determine the wave functional, the work [16] formulated the quantum principle of least action, according to which the wave functional is an eigenvector of the action operator.

In the new formalism, the integration over N, N^k is initially absent. In the covariant quantum theory, based on the Batalin–Fradkin–Vilkovysky theorem [17,18], the integration over the lapse function N is equivalent to the integration over proper time (see [19]), so in the new formalism, time remains a free parameter. This makes it possible to formulate a boundary value problem for the wave functional in the “subpolar” region (Euclidean instanton), in which the pole is an internal point, without any additional conditions for the fundamental dynamic variables in it. To fix time in an instanton, one additional parameter will be required—the own mass of the universe.

The next section formulates the basic concepts of the canonical formalism and a new description of the dynamics in the quantum theory of gravity. The second section gives a representation of the energy of a closed universe using spin variables. In the third section, the boundary value problem for the Euclidean instanton is considered in the case of a homogeneous isotropic model of the universe, in which the concept of its own mass arises. In the fourth section, a new canonical representation of the action of the theory of gravity is introduced, based on the energy structure of a closed universe, in which the own mass is realized in the form of a mass spectrum of individual 3D-invariant dynamic modes.

2. Wave Functional in the Quantum Theory of Gravity

Let us start our consideration with the classical action of general relativity

$$I_{GR} = -\frac{1}{16\pi G} \int \sqrt{-g} d^4x R + I_m[g, \varphi]. \tag{2}$$

Using 3 + 1 splitting of the metric

$$ds^2 = (Ndt)^2 - g_{ik} (dx^i + N^i dt) (dx^k + N^k dt), \tag{3}$$

let us write it in the canonical form of Arnovitt, Deser, and Misner (ADM) [20]:

$$I_{ADM} = \int dt \int_{\Sigma} d^3x (g_{ik} \pi^{ik} - N\mathcal{H} - N_i \mathcal{H}^i), \tag{4}$$

$N_i = g_{ik} N^k$, where

$$\mathcal{H}(\pi^{ik}, g_{ik}, \pi_{\varphi}, \varphi) = -\frac{1}{\sqrt{g}} [Tr \pi^2 - (Tr \pi)^2] + \sqrt{g} R, + \mathcal{H}_m, \tag{5}$$

$$\mathcal{H}^i(\pi^{ik}, g_{ik}, \pi_{\varphi}, \varphi) = 2\pi^i_k + \mathcal{H}_m^i \tag{6}$$

are Hamiltonian and momentum constraints and the canonical momenta conjugated to the 3D metric tensor g_{ik} have the form

$$\pi^{ik} = \sqrt{g^{(3)}} \left(g^{ik} \text{Tr} \mathbf{K} - K^{ik} \right), \tag{7}$$

$$K_{ik} = \frac{1}{2N} \left(N_{|i|k} + N_{k|i} - \frac{\partial g_{ik}}{\partial t} \right). \tag{8}$$

The last terms in Equations (5) and (6) are the energy and momentum density of the matter fields, respectively.

In order to describe the evolution of the universe in QTG in terms of world histories, we introduce the state functional Ψ . We define it as the product of wave functions $\psi(g_{ik}(x), \varphi(x), N, N^k, t)$ on spatial sections Σ_n for each time $t_n = \varepsilon n, \varepsilon = T/n$. We suppose that the time dependence of the wave function is determined by the Schrödinger equation

$$i\hbar \frac{\partial \psi}{\partial t} = \int_{\Sigma} d^3x \left(N \hat{\mathcal{H}} + N_k \hat{\mathcal{H}}^k \right) \psi. \tag{9}$$

Consequently, the wave function ψ is also a functional of N, N_k , and the WDW wave equations

$$\hat{\mathcal{H}}\psi = \hat{\mathcal{H}}^i \psi = 0 \tag{10}$$

are not initially postulated in our approach, which means they may not be fulfilled. For the wave functional Ψ , the normalization condition is assumed to be satisfied:

$$\langle \Psi | \Psi \rangle = \int \prod J dg d\varphi \bar{\Psi} \Psi. \tag{11}$$

It should be assumed that, being a functional of 4D geometry (including the lapse and shift functions N, N_k), the wave functional is an invariant of general covariant transformations. The assumption is based on the fact that the basic equation of motion—the Schrödinger equation Equation (9)—for the wave function ψ can be equivalently replaced by the corresponding equation for the wave functional Ψ . The latter is a secular equation for the action operator, which is obtained by directly quantizing the action of ADM Equation (4) [16]. This means that we have the opportunity to calculate, for example, the average values of expressions containing the first and second derivatives with respect to time, in particular,

$$\langle \Psi | R_{\mu\nu} | \Psi \rangle, \tag{12}$$

where $R_{\mu\nu}$ is the 4D Ricci tensor. Based on the above, we should expect that expression Equation (12) forms a tensor of the second rank with respect to arbitrary transformations of space–time coordinates, as in the classical theory. This follows from the fact that it is an eigenvector of the action operator. The action operator contains, in particular, the following contribution:

$$\int_{\Sigma} d^3x \int_0^T N dt \left[\dots + 2\hat{\pi}^{ik} \frac{1}{2N} \left(\frac{\partial g_{ik}}{\partial t} - N_{|i|k} - N_{k|i} \right) + \dots \right], \tag{13}$$

where $\hat{\pi}^{ik}$ is the momentum operator, i.e., derivatives with respect to coordinate time and spatial coordinates (together with the lapse and shift functions N and N^m) “gathered” into an expression equal to the tensor of the external curvature of the hypersurface Σ , as was the case in classical general relativity. Since the quantum principle of least action formulated in previous works is equivalent to the Schrödinger equation, we conclude that the latter is also fine with respect to covariance. Formally, this means that arbitrary transformations of time and spatial coordinates, with corresponding transformations of the lapse and shift functions N and N^m , provide the necessary transformation properties of all observables. The quantum principle of least action will allow us to determine the structure

of space–time at the beginning of the universe without a priori conditions in the form of the WDW equations. Let us also pay attention to another formulation of dynamics in terms of Heisenberg’s operator formalism [21].

3. The Energy of a Closed Universe

The lapse and shift functions N, N_k in the new formalism remain arbitrary. Their integration is carried out only under the normalization condition Equation (11). Next, we will introduce a special spin parametrization of these functions, and at the same time, the Ashtekar [22] complex representation of canonical variables of the gravitational field ($\tilde{\sigma}_{AB}^k, A_{kAB}, A, B = 0, 1$ —spin indices). We immediately take into account the so-called reality condition for the Ashtekar connection, setting

$$A_{kAB} = \Gamma_{kAB}(\sigma) + \frac{i}{\sqrt{2}}M_{kAB}, \tag{14}$$

where $\Gamma_{kAB}(\sigma)$ are components of the real spin-connection, and M_{kAB} are the canonical momenta conjugated to the spin variables $\tilde{\sigma}_{AB}^k$ in the real representation, in which we can also immediately put

$$M_{kAB} = \frac{\pi_{kl}\sigma_{AB}^l}{\sqrt{g^{(3)}}} \tag{15}$$

(Gaussian constraint \mathcal{P}^{AB} of Ashtekar). Let us introduce the 3D Dirac operator on a spatial section Σ :

$$\mathcal{D}\eta \equiv i\sqrt{2}\begin{pmatrix} n_{A'}^A \tilde{\sigma}_{B'}^{kA'} \nabla_k \bar{\mu}^{B'} \\ n_{A'}^A \sigma_B^{kA} \nabla_k \lambda^B \end{pmatrix}, \tag{16}$$

where η is the bispinor Dirac field on the spatial section Σ ,

$$\eta = \begin{pmatrix} \lambda^A \\ \bar{\mu}^{A'} \end{pmatrix}, \tag{17}$$

and $n_{A'}^A$ is an arbitrary unitary matrix (spin-tensor) in the spin space. The complex covariant derivative of a spinor field is defined as follows:

$$\nabla_k \lambda_A \equiv \partial_k \lambda_A + A_{kA}^B \lambda_B. \tag{18}$$

Let us introduce anti-involution in the spin space,

$$\lambda_A^+ \equiv \sqrt{2}n_{A'}^A \bar{\lambda}^{A'}, (\lambda_A^{++} = -\lambda_A). \tag{19}$$

We assume that $\sigma_{AB}^{k+} = \sigma_{AB}^k$. Let us also introduce the Hermitian scalar product in the spin space:

$$(\eta_1, \eta_2) \equiv \int_{\Sigma} \sqrt{g^{(3)}} d^3x n_{AA'} (\lambda_1^A \bar{\lambda}_2^{A'} + \bar{\mu}_1^{A'} \mu_2^A). \tag{20}$$

It is easy to verify that the Dirac operator Equation (16) is Hermitian with respect to this scalar product. Our constructions are based on the Witten identity, which relates the difference of two positive definite quadratic forms of the bispinor η with a linear combination of gravitational constraints in the Ashtekar representation (see [16]),

$$\begin{aligned} (\eta, W\eta) &\equiv -\frac{11}{9}(\eta, \mathcal{D}^2\eta) + (\eta, (-\Delta + \mathcal{T})\eta) \\ &\equiv \mathcal{L}(\tilde{C}, \tilde{C}_k, \tilde{\mathcal{P}}^{AB}), \end{aligned} \tag{21}$$

The coefficients of the linear combination are the lapse and shift functions, as well as the zero components of the Ashtekar connection of the form [23]:

$$N = \frac{1}{8} n_{AA'} (\lambda^A \bar{\lambda}^{A'} + \bar{\mu}^{A'} \mu^A), \tag{22}$$

$$N^k = -\frac{i}{4} \sigma_{AB}^k (\lambda^A \lambda^{+B} + \mu^{+A} \mu^B), \tag{23}$$

$$A_{0AB} = -\frac{1}{16\sqrt{2}} \sigma_{(A|C|}^m (\nabla_m \lambda_B) \lambda^{+C} + \nabla_m \mu_B) \mu^{+C}. \tag{24}$$

The second term in Equation (21) has the form

$$\begin{aligned} & (\eta, (-\Delta + \mathcal{T})\eta) \\ = & \frac{1}{2} \int_{\Sigma} \sqrt{g^{(3)}} d^3x n_{AA'} n_{MM'} n_{NN'} (\bar{\xi}^{AMN} \bar{\xi}^{A'M'N'} \\ & + \chi^{AMN} \bar{\chi}^{A'M'N'}) + (\eta, \mathcal{T}\eta), \end{aligned} \tag{25}$$

where

$$\chi^{MNA} \equiv \sigma^{mMN} \nabla_m \mu^A + \frac{2}{3} \epsilon^{A(M} \sigma_P^{mN)} \nabla_m \mu^P, \tag{26}$$

$$\bar{\xi}^{MNA} \equiv \sigma^{mMN} \nabla_m \lambda^A + \frac{2}{3} \epsilon^{A(M} \sigma_P^{mN)} \nabla_m \lambda^P, \tag{27}$$

where ϵ^{AB} is a completely antisymmetric unit spin tensor. Spin tensors Equations (26) and (27) are completely symmetric. The last term on the right side of Equation (25) is a positive definite form of the energy–momentum tensor of matter fields. Thus, identity Equation (21) gives a representation of the Hamilton function of the theory of gravity (right-hand side of Equation (21)) as the difference of two positive definite quadratic forms of the bispinor η . The fact that we thus obtain the Hamilton function in an arbitrary gauge follows from counting the number of real constraints of the theory of gravity (seven pieces) and the number of independent real parameters of the bispinor η (eight pieces). The presence of a redundant parameter leads to the degeneracy of the quadratic form of the operator

$$W = -\frac{11}{9} D^2 + (-\Delta + \mathcal{T}), \tag{28}$$

i.e., the existence of a zero eigenvalue for this operator.

In the representation of the Hamilton function of a closed universe Equation (21), separation of the contributions of energy components with different signs has been achieved. The quadratic form $(\eta, D^2\eta)$ contains the kinetic energy $(Tr\pi)^2$ (together with the corresponding potential energy), it describes the dynamics of the 3D geometry scale factor $\sqrt{g^{(3)}}$. Therefore, we will call it the energy of space. The quadratic form $(\eta, \Delta\eta)$ does not contain $(Tr\pi)^2$, and describes the dynamics of the “transverse” components of the gravitational field that describe gravitational waves. We will call this, together with $(\eta, \mathcal{T}\eta)$, the energy of matter. The explicit separation of these two components in Equation (21) is a version of the positive energy (of matter) theorem for the case of a closed universe. The combination of signs in Equation (21) also determines the signature of the configuration space of the theory of gravity (superspace).

We can now discuss the issue of regularizing the convergence of the functional integral representation of the kernel of the evolution operator for the Schrödinger equation Equation (9). For the functional integral to converge, it is necessary that the total energy of the universe have a certain sign. This can be achieved by introducing a variable value e instead of the minus sign in Equation (21), which is equal to +1 at the calculation stage. In the previously identified wave function, along with the return to real time, the sign of

e should also be changed. At the same time, a natural gauge condition would be to take the eigenvector of the 3D Dirac operator as the bispinor η . In this case, one can use the Heisenberg formalism [21] in the case of a closed universe.

4. Euclidean Beginning of a Homogeneous Isotropic Model of the Universe

The transition to describing the quantum evolution of the universe in terms of world histories and the wave functional allows us to take a fresh look at the problem of initial data for this evolution. In the classical theory of gravity, the timelines of the universe begin at one point, which is the Big Bang singularity. In Euclidean QTG, these lines simply serve as meridians of the “polar” coordinate system [7]. The pole itself has no features other than a coordinate singularity. Therefore, in [24], the state of the universe in the “subpolar” region (with one boundary along the “polar” circle) was proposed to be sought in a non-singular coordinate system using the generalized canonical De Donder-Weyl formalism. And although to introduce time, we return to the usual 3 + 1 ADM splitting of the metric in polar coordinates, at the pole itself, as an equal point, we place not the initial data for the fundamental dynamic variables (g, φ) , but their distribution in terms of the wave functional $\Psi[g, \varphi]$. In this sense, we refer to the wave functional of the universe as no-boundary.

Let us consider in more detail the initial stage of evolution of the homogeneous isotropic Friedmann–Lemaître universe with the metric

$$ds^2 = N^2(t)dt^2 - a^2(t)d\Omega_3^2, \tag{29}$$

where $d\Omega_3^2$ is an element of length on a 3D sphere of unit radius, with a real scalar field and zero cosmological constant. Its dynamics are described by the action (Lorentzian signature)

$$I_{FL}[a, \phi] = \frac{1}{2} \int_0^T dt \left[-\frac{a}{\gamma} \left(\frac{\dot{a}}{N} - N \right) + 2\pi^2 a^3 \left(\frac{\dot{\phi}}{N} - V(\phi)N \right) \right], \tag{30}$$

where $\gamma = 2G/3\pi$. The Hamilton function and the corresponding Schrödinger equation for this model are

$$h_{FL} = N\mathcal{H}_{FL} = N \frac{1}{2} \left[-\left(\frac{\gamma p_a^2}{a} + a \right) + \left(\frac{p_\phi^2}{2\pi^2 a^3} + 2\pi^2 a^3 V(\phi) \right) \right], \tag{31}$$

$$i\hbar \frac{\partial \psi}{\partial s} = \hat{\mathcal{H}}_{FL} \psi, s = \int_0^t N(t) dt. \tag{32}$$

We will further restrict ourselves to the semiclassical approximation; therefore, we do not consider the problem of ordering noncommuting factors in $\hat{\mathcal{H}}_{FL}$ here. We also do not consider the problem of convergence of the Euclidean functional integral, which represents the kernel of the evolution operator for equation Equation (32). The extremum conditions for the Euclidean action, which is obtained from Equation (30) after the transition to imaginary time $s = -i\tau$, have the form

$$\ddot{a} + \frac{1}{2} \left(\frac{\dot{a}}{a} - 1 \right) - 3\pi^2 a^2 \gamma \left(\frac{\dot{\phi}}{a} + V \right) = 0 \tag{33}$$

is the extremum condition in a and

$$\ddot{\phi} + 3\frac{\dot{a}}{a}\dot{\phi} - \frac{1}{2}V'(\phi) = 0 \tag{34}$$

is the extremum condition with respect to ϕ , where the dot denotes the derivative with respect to $\tau, \tau \in [0, T]$. Let us immediately note that the constraint equation $\mathcal{H}_{FL} = 0$ is not among the extremum conditions, since the lapse function N is not considered as a dynamic variable, and the integral of it is the proper time s .

Now, let us consider the problem of boundary conditions for differential Equations (33) and (34). In [7], the Euclidean functional integral of the form Equation (1) is observed in a compact region of 4D Riemannian space with a single boundary on which the values of the scale factor $a(T) = b$ and the scalar field $\phi(T) = \chi$ are given. At the ‘‘pole,’’ ‘‘natural’’ initial conditions are chosen

$$a(0) = 0, \phi(0) = 0. \tag{35}$$

However, the composition of the equations–extremum conditions in the work [7] differs from that of Equations (33) and (34). Since integral Equation (1) contains additional integration over proper time, the constraint equation also arises under extremum conditions. And since the constraint is also the first integral of the equations of motion Equations (33) and (34), one of them, namely equation Equation (34), can be considered redundant. With this formulation of the boundary value problem, the free parameter turns out to be the value of the scalar field at the pole $\phi(0) = \phi_0$. But this contradicts the very idea of constructing a no-boundary wave function, which assumes the absence of any initial data for fundamental dynamic variables in the polar region. This does not apply to conditions Equation (35), which arise precisely as a result of the choice of a polar coordinate system in a homogeneous isotropic model of the universe.

Let us see how the second of the ‘‘natural’’ conditions, Equation (35), arises if we consider it as the primary representation of the evolution operator in non-singular coordinates in the subpolar region. Moving along the meridian to the pole (one of the timelines in polar coordinates), beyond the pole, we will smoothly continue this movement along the opposite (at an angle 180^0) meridian, connecting them into one timeline of a non-singular coordinate grid. Let us divide this time axis into small sections of length ϵ and write the contribution of the scalar field to the functional integral for the evolution operator of the pole and neighboring points located symmetrically:

$$\int \dots d\phi_0 \dots \exp \left\{ -\frac{1}{\hbar} \pi^2 \left[\left(\frac{a_{-1}}{2} \right)^3 \times \left(\frac{(\phi_0 - \phi_{-1})^2}{\epsilon} + V \left(\frac{\phi_0 + \phi_{-1}}{2} \right) \right) \epsilon + \left(\frac{a_1}{2} \right)^3 \left(\frac{(\phi_0 - \phi_1)^2}{\epsilon} + V \left(\frac{\phi_0 + \phi_1}{2} \right) \right) \epsilon \right] \right\} \tag{36}$$

To calculate this integral using the steepest descent method, we find the extremum of the exponent in ϕ_0 , which (in the limit $\epsilon \rightarrow 0$) gives: $\phi_0 = \phi_1$. Here, we also take into account the symmetry of the model under consideration, $\phi_1 = \phi_{-1}, a_1 = a_{-1}$. Thus, the second condition in Equation (35) arises as a consequence of estimating the integral over ϕ_0 in the functional integral representation of the propagator. The presence of this integral also means that the initial condition for the wave function at the pole (at $\tau = 0$) should be taken

$$\psi_0 = A\delta(a). \tag{37}$$

Thus, natural initial conditions mean that initially, $a = 0$, and the field ϕ can take on any value with equal probability.

To complete the formulation of the boundary problem, we define the boundary conditions at $\tau = T$. Equations (33) and (34) determine the initial instanton in the Euclidean region if its right boundary point on the a -axis is a cusp point, i.e.,

$$\dot{a}(T) = 0. \tag{38}$$

Thus, the history of the scale factor $a(\tau)$ in the instanton is completely determined. For a given T , the history of the scalar field $\phi(\tau)$, including its initial ϕ_0 (as well as final $\phi(T)$) value, also becomes completely determined, since the shape of the potential well for the instanton $a(\tau)$ is determined by the function $\phi(\tau)$. There remains one undefined parameter T , fixed by us. We can still calculate the first integral of the equations of motion, which in the general case is constant, but not equal to zero:

$$\mathcal{H}_{FL}(\tau) = -M^2 \neq 0. \tag{39}$$

As we remember, the constraint equation $\mathcal{H}_{FL} = 0$ serves to precisely determine the time of movement T in the generally accepted approach. However, here, this constraint equation, in the presence of a free time parameter, does not follow from anywhere, and we are forced to accept as an additional possibility the presence of a non-zero own mass of the universe M^2 in Equation (39). The result can be formulated differently: if the own mass of the universe is given, the shape of the initial instanton in the Euclidean QTG with its own time is completely determined. The minus sign in Equation (39) follows from the analysis of the asymptotic behavior of the scale factor at the pole. It is easy to check that

$$a \sim \left(\frac{9}{2}\right)^{1/3} M^{2/3} \tau^{2/3} + \frac{9}{20M^{2/3}} \left(\frac{2}{9}\right)^{1/3} \tau^{4/3} + \dots \tag{40}$$

at $\tau \rightarrow 0$. Thus, the spatial part of the energy of the universe dominates in the beginning, and this serves as a source of its expansion. The simple asymptotic behavior demonstrated in Equation (40) and the entire expansion picture will change if we also take into account the dynamics of anisotropy near the beginning [15]. However, the main term in asymptotics Equation (40) will be preserved, as well as the meaning of the constant M . The proper mass remains constant only in a homogeneous isotropic model of the universe. In general, this is not the case, and the dynamics of one's own mass can be directly related to the universe's own time.

5. Own Mass and Proper Time in an Inhomogeneous Universe

To establish the connection between proper mass and proper time in the general case, let us consider the new canonical representation of the theory of gravity, which is naturally induced by the representation of the Hamilton function Equation (21). If we consider the bispinor η as an independent dynamic variable, then the corresponding Euler–Lagrange equation has the form:

$$W\eta = 0. \tag{41}$$

Taking into account that η is initially considered as an arbitrary bi-spinor, we obtain a representation of the system of gravitational connections in the form of an operator equation

$$W = 0. \tag{42}$$

The operator W is Hermitian on the space of bispinors and its spectrum is real. The operator itself is equal to zero if and only if all its eigenvalues w_n are equal to zero. The eigenval-

ues, as well as the eigenvectors η_n , are functions of the fundamental canonical variables. The eigenvalues w_n form a closed algebra with respect to Poisson brackets:

$$\{w_n, w_m\} = C_{nm}^p w_p, \tag{43}$$

in which the structural “constants” C_{nm}^p are determined by the eigenvectors η_n , i.e., are also functions of canonical variables. Going forward, we will refer to eigenvalues w_n as dynamic modes. Expanding an arbitrary bispinor η over a complete (orthonormal) set of eigenfunctions,

$$\eta = \sum_n \zeta^n \eta_n, \tag{44}$$

we can represent the Hamilton function of gravity theory as a linear combination of a new set of constraints:

$$(\eta, W\eta) = \sum_n L^n w_n, L^n = |\zeta^n|^2. \tag{45}$$

Arbitrary Lagrange multipliers L^n under infinitesimal general covariant transformations generated by w_n constraints,

$$\delta A = \delta s^m \{A, w_m\}, \tag{46}$$

where A is an arbitrary function of canonical variables, must be transformed as follows

$$\delta L^n = \delta \dot{s}^n - C_{mp}^n L^m \delta s^p \tag{47}$$

to ensure action invariance. These infinitesimal transformations are generated by infinitesimal shifts of the proper time parameters s^n , and the generators of these shifts are the eigenvalues w_n . To determine the Lagrange multipliers corresponding to finite values of the proper time parameters, equation Equation (47) can be solved iteratively, and the solution can be represented as a power series:

$$L^m = \Lambda_n^m(s) \dot{s}^n, \tag{48}$$

$$\begin{aligned} \Lambda_n^m(s) &= \delta_n^m - C_{np}^m s^p \\ &+ \frac{1}{2!} C_{rp}^m C_{nq}^r s^p s^q + \dots \end{aligned} \tag{49}$$

The proper time parameters introduced in this way are integrals of the Lagrange multipliers:

$$\int_0^T dt L^m(t) = \int_0^{S^n} \Lambda_n^m(s, C) ds^n. \tag{50}$$

The values of the canonical variables in the structure functions C_{np}^m are taken at the same moment of coordinate time t as the proper time parameters s^p . The time evolution of the eigenvalues w_n is determined by the equations

$$\begin{aligned} \frac{dw_n}{dt} &= \frac{\partial w_n}{\partial s^p} \dot{s}^p = \{w_n, L^m w_m\} \\ &= \{w_n, \Lambda_p^m\} \dot{s}^p + \Lambda_p^m C_{nm}^q w_q \dot{s}^p, \end{aligned} \tag{51}$$

i.e.,

$$\frac{\partial w_n}{\partial s^p} = \{w_n, \Lambda_p^m\} + \Lambda_p^m C_{nm}^q w_q. \tag{52}$$

In quantum theory, all these relations should be considered in the form of average values in the state described by the wave functional Ψ . It follows that if the eigenvalues w_n are zero at the beginning (classical constraints), they always remain so. In this case, we can

talk about preserving the 4D covariance of the theory. If at first there is a non-zero intrinsic mass in some dynamic mode,

$$w_n = -m_n^2 \neq 0, \tag{53}$$

the distribution of own masses over modes will change over time, and this change itself can be considered as a measure of proper time.

Thus, the Euclidean instanton in the general case has the following structure in polar coordinates (radial coordinate—time axis). At the pole (approaching the pole), the approximation of a homogeneous, isotropic model of the universe with a single dynamic mode described by the Hamilton function \mathcal{H}_{FL} is valid. This will happen when choosing polar coordinates in a small neighborhood of any interior point of a smooth manifold. Accordingly, this dynamic mode can be associated with its own mass M as the only parameter of the universe model. The Euclidean “evolution” of the instanton along the radial axes is given by the equation

$$\frac{d}{dt} \sqrt{g^{(3)}} = \left\{ \sqrt{g^{(3)}}, L^m w_m \right\}. \tag{54}$$

We actually have an infinite set of equations (one for each point of the spatial section). The spatial boundary of the Euclidean instanton is determined by the condition that the derivative of $\sqrt{g^{(3)}}$ with respect to time is equal to zero at all spatial points. This provides a system of equations for determining the complete set of proper time parameters at the boundary, and the system of equations Equation (52) allows us to find the resulting distribution of proper mass over modes.

6. Conclusions

The generally accepted formulation of the covariant quantum theory of gravity, based on the WDW equations, as well as using the formalism of the invariant functional integral, gives rise to the problem of time (more precisely, its absence). Along with time, the possibility of introducing any additional quantities, in addition to the set of fundamental dynamic variables and associated parameters of the original Lagrangian, is excluded. However, the observed evolution of the universe (or the generally accepted interpretation of observational data) and the idea of the Big Bang as the beginning of this evolution, one way or another, require the introduction of time. This can be achieved by identifying the time parameter with a suitable fundamental dynamic variable [25]. In this case, time acquires a material character in the literal sense of the word, if one of the fields of matter is taken as such a variable. In this paper, an alternative option is proposed—the preservation of the coordinate time parameter of the classical theory of gravity in quantum theory. This is achieved by transition from the description of the quantum state of the universe from a 3D distribution on a spatial section Σ to a description in terms of the wave functional on 4D world histories. With this modification, the formal covariance of quantum theory is preserved in the same form as in the classical one, when time and spatial coordinates were equal. However, this equality is actually violated in the case of a closed universe by the signature of the configuration space: the negative contribution in it is clearly highlighted by the 3D-invariant quadratic form of the expansion energy, corresponding to the degrees of freedom of the scale factor $\sqrt{g^{(3)}}$. This energy structure of the universe determines the shape of the initial Euclidean instanton in the semiclassical approximation. This 3D-invariant energy structure is also associated with the spectrum of parameters of the proper time and the canonically conjugate spectrum of parameters of the own mass of the universe. If the proper mass, the distribution and motion in space can be associated with a selected reference frame, which is assumed to be equal to zero, there is no physical reason for the violation of the 4D covariance of the theory. General covariance can be preserved even with a non-zero own mass if it is a constant of motion. But this is possible when the structure constants in Equation (43) are equal to zero, i.e., the dynamic modes in the theory of gravity

are completely independent. This possibility is not excluded, but a detailed analysis of the new canonical representation of the theory is required.

Author Contributions: Investigation, N.G. and A.L.; Draft review and editing, N.G., A.L. and A.V.G. All authors have read and agreed to the published version of the manuscript.

Funding: This research received no external funding.

Data Availability Statement: Data are contained within the article.

Acknowledgments: We would like to thank V.A. Franke for the useful discussions.

Conflicts of Interest: The authors declare no conflicts of interest.

References

1. Vilenkin, A. Creating of the Universe from Nothing. *Phys. Lett. B* **1982**, *117*, 25–28. [CrossRef]
2. Hartle, J.B.; Hawking, S.W. Wave function of the Universe. *Phys. Rev. D* **1983**, *28*, 2960. [CrossRef]
3. Linde, A.D. Quantum creation of the inflationary universe. *Lett. Nuovo C.* **1984**, *39*, 401–405. [CrossRef]
4. Rubakov, V.A. Quantum mechanics in the tunneling universe. *Phys. Lett. B* **1984**, *148*, 280–286. [CrossRef]
5. Vilenkin, A. Quantum creation of universes. *Phys. Rev. D* **1984**, *30*, 509. [CrossRef]
6. Zeldovich, Y.B.; Starobinsky, A.A. Quantum creation of a universe in a nontrivial topology. *Sov. Astron. Lett.* **1984**, *10*, 135.
7. Hartle, J.B.; Hawking, S.W.; Hertog, T. Classical universes of the no-boundary quantum state. *Phys. Rev. D* **2008**, *77*, 123537. [CrossRef]
8. Gibbons, G.W.; Hawking, S.W. (Eds.) *Euclidean Quantum Gravity*; World Scientific: Singapore, 1993.
9. Halliwell, J.J.; Hartle, J.B.; Hertog, T. What is the no-boundary wave function of the Universe? *Phys. Rev. D* **2019**, *99*, 043526. [CrossRef]
10. Hartle, J.B.; Hawking, S.W.; Hertog, T. Quantum Probabilities for Inflation from Holography. *J. Cosmol. Astropart. Phys.* **2014**, *2014*, 015. [CrossRef]
11. Hawking, S.W. *General Relativity; An Einstein Centenary Survey*; Hawking, S.W., Israel, W., Eds.; Cambridge University Press: Cambridge, UK, 1980.
12. Witten, E. A new proof of the positive energy theorem. *Commun. Math. Phys.* **1981**, *80*, 381–402. [CrossRef]
13. Faddeev, L.D. The energy problem in Einstein's theory of gravitation (Dedicated to the memory of V. A. Fock). *UFN* **1982**, *136*, 435–457. [CrossRef]
14. Gorobey, N.N.; Lukyanenko, A.S. Three-dimensional volume of a closed universe as a canonical time parameter. *TMF* **1992**, *95*, 541–548. [CrossRef]
15. Misner, C.W.; Thorne, K.S.; Wheeler, J.A. *Gravitation*; W. H. Freeman and Company: San Francisco, CA, USA, 1973.
16. Gorobey, N.; Lukyanenko, A.; Goltsev, A.V. Wave Functional of the Universe and Time. *Universe* **2021**, *7*, 452–461. [CrossRef]
17. Fradkin, E.S.; Vilkovisky, G.A. Quantization of relativistic systems with constraints. *Phys. Lett. B* **1975**, *55*, 224–226. [CrossRef]
18. Batalin, I.A.; Vilkovisky, G.A. Relativistic S-matrix of dynamical systems with boson and fermion constraints. *Phys. Lett. B* **1977**, *69*, 309–312. [CrossRef]
19. Govaerts, J. A note on the Fradkin-Vilkovisky theorem. *Int. J. Mod. Phys. A* **1989**, *4*, 4487–4504. [CrossRef]
20. Arnowitt, R.; Deser, S.; Misner, C.W. The dynamics of general relativity. In *Gravitation: An Introduction to Current Research*; Witten, L., Ed.; Wiley: New York, NY, USA, 1962; p. 227.
21. Vereshkov, G.; Marochnik, L. Quantum gravity in Heisenberg representation and self-consistent theory of gravitons in macroscopic spacetime. *J. Mod. Phys.* **2013**, *4*, 285–297. [CrossRef]
22. Ashtekar, A. New Hamiltonian formulation of general relativity. *Phys. Rev. D* **1987**, *36*, 1587. [CrossRef]
23. Ashtekar, A. On the Hamiltonian of general relativity. *Phys. (Utrecht) A* **1984**, *124*, 51–60. [CrossRef]
24. Gorobey, N.N.; Lukyanenko, A.S.; Goltsev, A.V. On the Birth of the Universe and Time. *Universe* **2022**, *8*, 568. [CrossRef]
25. Ashtekar, A.; Pawłowski, T.; Singh, P. Quantum nature of the big bang. *Phys. Rev. Lett.* **2006**, *96*, 141301. [CrossRef] [PubMed]

Disclaimer/Publisher's Note: The statements, opinions and data contained in all publications are solely those of the individual author(s) and contributor(s) and not of MDPI and/or the editor(s). MDPI and/or the editor(s) disclaim responsibility for any injury to people or property resulting from any ideas, methods, instructions or products referred to in the content.

MDPI AG
Grosspeteranlage 5
4052 Basel
Switzerland
Tel.: +41 61 683 77 34

Universe Editorial Office
E-mail: universe@mdpi.com
www.mdpi.com/journal/universe



Disclaimer/Publisher's Note: The statements, opinions and data contained in all publications are solely those of the individual author(s) and contributor(s) and not of MDPI and/or the editor(s). MDPI and/or the editor(s) disclaim responsibility for any injury to people or property resulting from any ideas, methods, instructions or products referred to in the content.



Academic Open
Access Publishing

mdpi.com

ISBN 978-3-7258-2281-2